

**“Molecular manipulation and
new antimicrobial identification
in *Acanthamoeba spp.*”**

**Alemao Gustavo Carpinteyro Sanchez
(BSc, MSc)**

Thesis submitted in partial fulfilment of the
requirements of the University of Strathclyde for the
award of Doctor of Philosophy.

November 2021

Declaration of authenticity and author's rights

This thesis is the result of the author's original research. It has been composed by the author and has not been previously submitted for examination which has led to the award of a degree.

The copyright of this thesis belongs to the author under the terms of the United Kingdom Copyright Acts as qualified by University of Strathclyde Regulation 3.50. Due acknowledgment must always be made of the use of any material contained in, or derived from, this thesis.

Signed: Alemao Gustavo Carpinteyro Sanchez

Date: November 5th, 2021

General abstract

Acanthamoeba spp. are causative agents of a painful and severe sight-threatening corneal infection that can lead to blindness known as *Acanthamoeba* keratitis and a subacute disease in the brain which is usually fatal known as granulomatous amoebic encephalitis. Over the last few years, there has been a notorious increase in the number of infections due to *Acanthamoeba* spp. Poor diagnosis, problems of side effects, toxicity of the current drug treatment and the lack of gene editing tools as potential future therapy contribute to a high mortality rate. Strathclyde Minor Groove Binders (S-MGBs), compounds that bind to the minor groove of the DNA that designed and synthesised at University of Strathclyde were evaluated as potential alternative inhibitors against *Acanthamoeba* infections. Through cell viability microplate alamarBlue assays 42 S-MGBs were screened from which S-MGB 235 showed the most potent inhibitory effect with IC_{50} in the nanomolar range against five *Acanthamoeba* isolates after 24 h and 96 h incubation. Confocal microscopy of trophozoites labelled with fluorescent S-MGB 363 (analogue of S-MGB235) showed this compound in the nucleus, nucleolus and distributed over the granuloplasm causing cell lysis, supporting the potent effect observed *in vitro* by S-MGB 235. Furthermore, conditions were standardised to establish *Galleria mellonella* larvae as a new *in vivo* infection model for *A. castellanii* Neff infections to assess the efficacy and toxicity of voriconazole, miltefosine and S-MGB 235. Voriconazole and miltefosine did not protect larvae from trophozoite infection, however S-MGB 235 significantly protected larvae when compared with the negative control. It was attempted to establish a CRISPR-Cas9 system for gene editing in *Acanthamoeba*. The plasmids pBRFPT7NeoCas9 and pBRFPT7PhleoCas9 (containing genes for the red fluorescent protein, T7 RNA polymerase, Cas9 along with the neomycin and phleomycin resistance genes, respectively, were constructed and transfected into *A. castellanii* Neff trophozoites using Xfect. Expression of RFP was confirmed by fluorescence microscopy and fluorescence-activated cell sorting.

Contents

General abstract	i
List of Figures	viii
List of Tables	xiii
List of Appendix.....	xv
List of Abbreviations	xvi
Acknowledgments	xxii
Chapter 1. Introduction	1
1.1 Free-Living Amoeba	2
1.2 <i>Acanthamoeba</i> spp.....	3
1.2.1 Opening remarks	3
1.2.2 Discovery of pathogenic <i>Acanthamoeba</i>	3
1.3 Cell Biology	5
1.4 The <i>Acanthamoeba</i> genome.....	6
1.5 Life cycle	9
1.5.1 Trophozoite and Cyst stage	9
1.5.2 Encystment process	10
1.5.3 Excystment process	12
1.6 Amoebic infections	12
1.6.1 <i>Acanthamoeba</i> keratitis (AK)	13
1.6.1.1 Clinical features.....	14
1.6.1.2 Epidemiology.....	15
1.6.1.3 Pathogenesis	16
1.6.1.4 Immune response.....	19
1.6.1.5 Laboratory Diagnosis.....	22
1.6.2 Granulomatous Amoebic Encephalitis (GAE).....	23
1.6.2.1 Clinical features.....	24
1.6.2.2 Epidemiology.....	24
1.6.2.3 Pathogenesis	25
1.6.2.4 Immune Response	27
1.6.2.5 Laboratory diagnosis	28
1.7 Treatment for <i>Acanthamoeba</i> spp. infections: AK, GAE and cutaneous lesions.....	29
1.7.1 Biguanides.....	30
1.7.2 Diamidines.....	31

1.7.3 Antifungal agents	32
1.7.4 Azoles.....	33
1.7.5 Antiseptics	36
1.7.6 Phospholipid analogues.....	37
1.7.7 Antibiotics and detergents.....	37
1.7.8 Photodynamic agents	38
1.7.9 Repurposed drugs	39
1.7.10 Natural compounds.....	40
1.7.11 Synthetic experimental agents	40
1.7.12 Other experimental agents that target biochemical pathways absent in humans.....	41
1.8 Aims and Objectives.....	46
Chapter 2. Material & Methods.....	47
2.1 Materials	48
2.1.1 Chemicals.....	48
2.1.2 Media and Buffers.....	50
2.1.3 Molecular Biology Kits.....	51
2.1.4 Antibiotics	51
2.1.5 DNA/Protein Molecular Weight Markers.....	52
2.1.6 Enzymes.....	52
2.1.6 Bacterial Strain	53
2.1.7 Plasmids.....	54
2.1.8 Oligonucleotides	55
2.1.9 Strathclyde Minor Groove Binders (S-MGBs).....	56
2.2 Methods	61
2.2.1 <i>Acanthamoeba</i> spp. seeding, harvesting and preparation of S-MGBs.....	61
2.2.1.1 <i>Acanthamoeba</i> spp. and isolates.....	61
2.2.1.2 Cultivation, harvesting and passage of <i>Acanthamoeba</i> spp. trophozoites.	61
2.2.1.3 Preparation of Strathclyde Minor Groove Binders (S-MGBs)	61
2.2.2 <i>In vitro</i> alamarBlue™ Assays	62
2.2.2.1 Calculating alamarBlue™ Reduction Compared to Control.....	62
2.2.2.2 alamarBlue™ Drug sensitivity assay	62
2.2.2.3 Optimal seeding density standardisation	63
2.2.3 Microscopy	63
2.2.3.1 Fluorescence Microscopy.....	63

2.2.3.2 Confocal Microscopy	64
2.2.4 <i>Galleria mellonella</i> larvae as new <i>in vivo</i> infection model	64
2.2.4.1 <i>Galleria mellonella</i> larvae test injection procedure	64
2.2.4.2 Determination of the infective dose of trophozoites.	65
2.2.4.3 Antibiotic efficacy testing	65
2.2.5 Molecular Biology	65
2.2.5.1 Analytical Plasmid Restriction Cleavage.....	65
2.2.5.2 Preparative Plasmid Restriction Cleavage.....	66
2.2.5.3 Analytical Agarose Gel Electrophoresis	66
2.2.5.4 Preparative Agarose Gel Electrophoresis	66
2.2.5.5 Gel Agarose Band Purification.....	66
2.2.5.6 Klenow treatment protocol.....	67
2.2.5.7 Shrimp Alkaline Phosphatase (SAP) treatment protocol	67
2.2.5.8 Ligation	67
2.2.5.9 Heat-shock transformation	67
2.2.5.10 Plasmid DNA purification	68
2.2.5.11 Plasmid DNA Mini preparation: TENS method.....	68
2.2.5.12 Plasmid DNA Mini preparation: ISOLATE II Plasmid Mini Kit.....	68
2.2.5.13 Plasmid DNA Midi-preparation: NucleoBond Xtra Midi kit.....	69
2.2.6 PCR.....	70
2.2.6.1 Generation of repair cassettes for CRISPR.	70
2.2.6.2 PCR-amplification of sgRNA templates	70
2.2.7 Sequencing.....	71
2.2.7.1 Sequencing of pRFPSV40 plasmid construction.....	71
2.2.8 Transfections	71
2.2.8.1 Transfection of pRFPSV40 with Xfect in <i>Acanthamoeba castellanii</i> Neff strain trophozoites.	71
2.2.8.2 Transfection of pBRFPNeoCas9 with Xfect and Polyplus in <i>Acanthamoeba castellanii</i> Neff strain trophozoites.	72
2.2.8.3 Transfection of pBRFPNeoCas9 and pBRFPPhleoCas9 with Xfect in <i>Acanthamoeba</i> Neff strain trophozoites.....	72
2.2.9 Fluorescence-Activated Cell Sorting (FACS) and flow cytometry analysis.	73
Chapter 3. <i>In vitro</i> screening of Strathclyde Minor Groove Binders (S-MGBs) against <i>Acanthamoeba</i> spp.	74
3.1 Abstract.....	75
3.2 Background.....	76

3.2.1 Minor Groove Binders	76
3.2.2 Classification.....	76
3.2.3 Minor groove binders as antibacterial drugs.....	78
3.2.4 MGBs as antiparasitic drugs	79
3.2.5 MGBs against <i>Acanthamoeba</i> diseases.....	81
3.2.6 Strathclyde Minor Groove Binders (S-MGBs).....	81
3.3 Aims and Objectives.....	83
3.4 Results	84
3.4.1 Optimal Seeding Density of <i>Acanthamoeba</i> spp.	84
3.4.2 Effect of S-MGBs against <i>Acanthamoeba</i> Neff strain trophozoites at 96 hours.	86
3.4.3 Potent effect of S-MGB-235 <i>in vitro</i> against <i>Acanthamoeba</i> spp. at 24 hours and 96 hours.....	98
3.4.4 Fluorescent S-MGB-363 binds to nucleus, nucleolus and granulooplasm causing cell wall disruption in <i>A. castellanii</i> Neff trophozoites as observed by Confocal microscopy analysis.....	101
3.4.5 Fluorescent S-MGB-245 weakly binds to nucleus and do not cause cell wall disruption in <i>A. castellanii</i> Neff trophozoites as observed by Confocal microscopy analysis.....	109
3.5 Discussion.....	111
Chapter 4. Use of wax moth <i>Galleria mellonella</i> larvae as new <i>in vivo</i> infection model for <i>Acanthamoeba castellanii</i> Neff strain trophozoites.	116
4.1 Abstract.....	117
4.2 Background.....	118
4.2.1 Biology.....	118
4.2.2 <i>G. mellonella</i> immune system	118
4.2.3 Use of <i>G. mellonella</i> as an alternative <i>in vivo</i> infection model.....	120
4.2.4 <i>In vivo</i> infection models for parasites	122
4.2.5 <i>In vivo</i> Infection models to assess <i>Acanthamoeba</i> infections	125
4.3 Aims and Objectives.....	126
4.4 Results	127
4.4.1 <i>G. mellonella</i> larvae infected with <i>A. castellanii</i> Neff strain show melanisation, generalised inflammation, and stiffness.	127
4.4.2 <i>G. mellonella</i> larvae survival is inoculum-dependent over time when infected with <i>A. castellanii</i> Neff strain trophozoites.....	130
4.4.3 Voriconazole and miltefosine treatment of <i>G. mellonella</i> larvae infected with <i>A. castellanii</i> Neff trophozoites does not protect from death	132
4.4.4 S-MGB 235 Treatment of <i>G. mellonella</i> larvae infected with <i>A. castellanii</i> Neff trophozoites does provides some protection against death	133

4.5 Discussion.....	143
Chapter 5. Construction of pBRFPT7NeoCas9 for the development of a new CRISPR-Cas9 system for <i>Acanthamoeba castellanii</i> Neff strain.....	148
5.1 Abstract.....	149
5.2 Background.....	150
5.2.1 Use of Green and Red Fluorescent proteins (GFP, RFP) as transfection reporters in <i>Acanthamoeba</i> spp.....	150
5.2.2 General features of genome-editing tools	155
5.2.3 CRISPR-Cas9 as genome-editing technology.....	155
5.2.4 Chorismate synthase as target for gene deletion by CRISPR-Cas9 in <i>Acanthamoeba</i> spp.....	161
5.3 Aims and Objectives.....	163
5.4 Results	164
5.4.1 General overview: Development of the CRISPR-Cas9 system for <i>Acanthamoeba castellanii</i> Neff strain.....	164
5.4.2 Standardisation of drug selection markers against <i>A. castellanii</i> Neff strain using alamarBlue assays.....	169
5.4.3 Generation of pBBXSV40RFP	171
5.4.4 Generation of pRFPSV40	175
5.4.6 <i>Acanthamoeba castellanii</i> Neff strain trophozoites expressed the Red Fluorescent Protein when transfected with pRFPSV40.....	181
5.4.7 Generation of pBRFPNeoCas9 and pBRFPPhleCas9	183
5.4.8 Analysis of <i>Acanthamoeba castellanii</i> trophozoites transfected with pBRFPNeoCas9 using Xfect and Polyplus.	196
5.4.9 <i>Acanthamoeba castellanii</i> trophozoites transfected with pBRFPNeoCas9 utilising Polyplus.	201
5.4.10 Change of Neo resistance gene to Phleo resistance gene in pBRFPNeoCas9.	206
5.4.11 Addition of T7 RNA polymerase gene sequence to pBRFPNeoCas9 and pBRFPPhleCas9 to generate pBRFPT7NeoCas9 and pBRFPT7PhleoCas9.	214
5.4.12 PCR amplification of CS-Neo-CS, CS-Phleo-CS, and CS-Hyg-CS	224
5.4.13 Single-guide RNA template construction.....	227
5.4.14 Robust fluorescence of <i>A. castellanii</i> Neff strain trophozoites transfected with pBRFPT7NeoCas9 compared to trophozoites transfected with pBRFPT7PhleoCas9.	228
5.4.15 Red fluorescent protein (RFP) expression in <i>A. castellanii</i> Neff trophozoites transfected with pBRFPT7NeoCas9 and pBRFPPhleCas9 confirmed by Flow Cytometry.	242

5.4.16 Different level of red fluorescent protein (RFP) expression in <i>A. castellanii</i> Neff trophozoites transfected with pBRFPT7NeoCas9 observed in Fluorescence microscopy after Fluorescence-activated cell sorting (FACS) .	246
5.4.17 Red fluorescent protein (RFP) expression in <i>A. castellanii</i> Neff trophozoites transfected with pBRFPT7NeoCas9 confirmed by Flow Cytometry post-FACS	250
5.5 Discussion.....	255
Chapter 6. General Discussion	259
6.1 Overview	260
6.2 New anti-amoebic Strathclyde Minor Binding Groove <i>in vitro</i> screening	260
6.3 Novel <i>in vivo</i> infection model	261
6.4 Gene editing tools as therapeutic options.....	263
6.5 Future work	264
References	266
Appendix	300

List of Figures

Figure 1. Comparison of papers published on <i>Acanthamoeba</i> spp. in journals of major biomedical importance since 1958. _____	5
Figure 2. Life cycle of <i>Acanthamoeba</i> spp. _____	10
Figure 3. DNA minor and major groove. _____	77
Figure 4. Structural representative example of a Strathclyde MGB (S-MGBs) derived from the prototype structure of Distamycin. _____	82
Figure 5. Reduction of alamarBlue by five different isolates of <i>Acanthamoeba</i> spp. trophozoites at 24 hours and 96 hours. _____	85
Figure 6. No active inhibitory effect of S-MGBs against <i>A. castellanii</i> Neff strain through alamarBlue assays. _____	90
Figure 7. Mild active effect of S-MGBs against <i>A. castellanii</i> Neff strain through alamarBlue assays. _____	93
Figure 8. Robust effect of S-MGBs against <i>A. castellanii</i> Neff strain through alamarBlue assays. _____	94
Figure 9. Efficacy of S-MGB-235 against <i>Acanthamoeba</i> spp. trophozoites through alamarBlue assays. _____	99
Figure 10. Cellular effect of fluorescent S-MGB-363 against <i>Acanthamoeba</i> Neff strain trophozoites. _____	104
Figure 11. Time-laps confocal imaging of the effect of fluorescent S-MGB-363 against <i>A. castellanii</i> Neff trophozoites. _____	107
Figure 12. Confocal fluorescence imaging of S-MGB-363 bound to nucleus and nucleolus in <i>Acanthamoeba</i> Neff strain trophozoites. _____	108
Figure 13. Cellular effect of fluorescent S-MGB-245 against <i>A. castellanii</i> Neff strain trophozoites. _____	110
Figure 14. Infection signs on <i>Galleria mellonella</i> larvae inoculated with <i>A. castellanii</i> Neff strain _____	128
Figure 15. <i>Galleria mellonella</i> pupae formation. _____	129
Figure 16. Kaplan-Meier survival curves of <i>G. mellonella</i> larvae after infection with <i>A. castellanii</i> Neff strain at different inoculum concentrations. _____	131
Figure 17. Kaplan-Meier survival curves of <i>Galleria mellonella</i> larvae infected with <i>Acanthamoeba castellanii</i> Neff strain and treated with voriconazole. _____	135

Figure 18. Kaplan-Meier survival curves of <i>Galleria mellonella</i> larvae infected with <i>Acanthamoeba castellanii</i> Neff strain and treated with miltefosine. _____	136
Figure 19. Kaplan-Meier survival curves of <i>Galleria mellonella</i> larvae infected with <i>Acanthamoeba castellanii</i> Neff strain and treated with S-MGB 235. _____	138
Figure 20. Kaplan-Meier survival curves of <i>Galleria mellonella</i> larvae infected with <i>Acanthamoeba castellanii</i> Neff strain and treated with S-MGB 235 diluted with DMSO 11%. _____	142
Figure 21. CRISPR-Cas9 Adaptive Immune System process representation occurring in bacteria and archaea. _____	157
Figure 22. Deletion of CS using CRISPR-Cas9 in <i>A. castellanii</i> Neff strain. _____	166
Figure 23. Wild type chorismate synthase (CS) gene locus in <i>A. castellanii</i> Neff strain. _____	167
Figure 24. Genomic situation after replacement of CS gene by CS-Neo-CS. _____	168
Figure 25. Efficacy of drug selection markers against <i>A. castellanii</i> Neff strain using alamarBlue assays. _____	170
Figure 26. Plasmid map of pBBsdRFPCSV40 (5249 bp). _____	171
Figure 27. Restriction cleavage of pBBsdRFPCSV40 with BgIII. _____	171
Figure 28. Gel Purification of SV40 promoter and restriction cleavage of pBBsdRFPCSV40 with XbaI. _____	172
Figure 29. Plasmid map of pBSV40 (3393 bp) _____	173
Figure 30. Shrimp Alkaline Phosphatase (SAP) treatment of SV40 promoter fragment. _____	173
Figure 31. Miniprep restriction cleavage with EcoRV+HindIII. _____	174
Figure 32. Plasmid map of pBBXSV40RFP (4051 bp). _____	174
Figure 33. Plasmid map of pBASV40GFP (6002 bp). _____	175
Figure 34. Restriction cleavage of pBASV40GFP with NotI. _____	176
Figure 35. Restriction analysis of pBBXSV40RFP with Pme, HindIII and Xba I. _	176
Figure 36. Preparative restriction cleavage of linear pBASV40GFP and linearisation of pBBXSV40RFP with BgIII. _____	177
Figure 37. Preparative restriction cleavage of linearised pBBXSV40RFP with PmeI. _____	177

Figure 38. Gel purification of fragments derived from pBASV40GFP and pBBXSV40RFP. _____	178
Figure 39. Plasmid map of pRFPSV40 (5948 bp). _____	179
Figure 40. Restriction analysis of pRFPSV40 with XbaI and EcoRI. _____	179
Figure 41. Confocal microscopy analysis of the expression of the red fluorescent protein (RFP) in <i>A. castellanii</i> Neff strain trophozoites transfected with pRFPSV40. _____	182
Figure 42. Plasmid map of pBSKII(+) (2961 bp). _____	183
Figure 43. Agarose gel showing linearised pBSKII(+) and pRFPSV40 cleaved with Kpn+ClaI. _____	184
Figure 44. Plasmid map of pBKCTBPpNeo (4034 bp) _____	184
Figure 45. Restriction analysis of pBKCTBPpNeo with EcoRI, KpnI, NcoI and HindIII. _____	185
Figure 46. Restriction cleavage of pBKCTBPpNeo with AvrII. _____	186
Figure 47. Restriction cleavage of pBKCTBPpNeo with AvrII and NcoI. _____	186
Figure 48. Purified and SAP-treated pBKCTBPpNeo AvrII/NcoI-fragment. _____	187
Figure 49. Plasmid map of pT007_Cas9_T7_Tub (15446 bp) _____	187
Figure 50. Restriction cleavage of pT007_Cas9_T7_Tub with EcoRI+NcoI. _____	188
Figure 51. Isolated EcoRI/NcoI fragment of pT007_Cas9_T7_Tub fragment. _____	188
Figure 52. Plasmid map of pBTBPpCas9 (7512 bp). _____	189
Figure 53. Restriction cleavage of pBTBPpCas9 with EcoRI, EcoRV and HindIII. _____	190
Figure 54. Restriction cleavage of pBTBPpCas9 with Acc65I. _____	191
Figure 55. Restriction cleavage of pBTBPpCas9 with Acc65I and ClaI. _____	191
Figure 56. Agarose gel showing purified pBTBPpCas9 fragment and linearised pRFPSV40 _____	192
Figure 57. Agarose gel showing purified pBTBPpCas9 fragment (4582 bp). _____	193
Figure 58. Plasmid map of pBRFPNeoCas9 (10536 bp). _____	194
Figure 59. Restriction cleavage of pBRFPNeoCas9 with BamHI, EcoRV, EcoRI and BglII _____	194

Figure 60. Transfection efficiency of pBRFPNeoCas9 using Xfect reagent. ____	196
Figure 61. Efficiency of pBRFPNeoCas9 expression in <i>A. castellanii</i> trophozoites using Xfect reagent. _____	200
Figure 62. Transfection efficacy of pBRFPNeoCas9 using Polyplus reagent. ____	201
Figure 63. Transfection efficiency of pBRFPNeoCas9 expression in <i>A. castellanii</i> trophozoites utilising Polyplus reagent. _____	205
Figure 64. Restriction cleavage of pBRFPNeoCas9 with ClaI and KpnI _____	207
Figure 65. Agarose gel showing purified pBRFPNeoCas9 (9436 bp) fragment. _	207
Figure 66. Plasmid map of pCR2.1phleo (4298 bp). _____	208
Figure 67. Restriction cleavage of pCR2.1Phleo and pBKCTBPpNeo with NcoI and AvrII. _____	208
Figure 68. Agarose gel showing purified pCR2.1Phleo and pBKCTBPpNeo fragments and Shrimp Alkaline Phosphatase (SAP) treatment to pBRFPNeoCas9 fragment. _____	209
Figure 69. Plasmid map of pBTBPPhleopolyA (3611 bp). _____	210
Figure 70. Restriction cleavage of pBTBPPhleopolyA _____	210
Figure 71. Restriction cleavage of pBTBPPhleopolyA with ClaI and KpnI. ____	211
Figure 72. Plasmid map of pBRFPPhleocas9 (10113 bp) _____	212
Figure 73. Restriction cleavage of pBRFPPhleocas9 with ClaI, NcoI, EcoRI ____	213
Figure 74. Restriction cleavage of pBRFPNeoCas9 and pBRFPPhleocas9 with MfeI _____	214
Figure 75. Plasmid map of pUCSV40T7PolyA (6544 bp) _____	215
Figure 76. Restriction cleavage of pUCSV40T7PolyA. _____	215
Figure 77. Agarose gel showing Shrimp Alkaline Phosphatase (SAP) treated fragments of pBRFPNeoCas9 and pBRFPPhleocas9 and purified pUCSV40T7PolyA fragment. _____	216
Figure 78. Plasmid map of pBRFPT7sNeoCas9 (13928 bp). _____	217
Figure 79. Restriction cleavage of pBRFPT7sNeoCas9 with XbaI and XhoI, NdeI and KpnI _____	217
Figure 80. Plasmid map of pBRFPT7sPhleocas9 (13505 bp). _____	218

Figure 81. Restriction cleavage of pBRFPT7sPhleoCas9 with XbaI and XhoI, NdeI and KpnI. _____	219
Figure 82. Restriction cleavage of pUCSV40T7PolyA with NdeI and KpnI and purified fragment. _____	219
Figure 83. Restriction cleavage of pBRFPT7NeoCas9 and pBRFPT7PhleoCas9 with NcoI and NdeI, EcoRI, ApaLI and EcoRV. _____	220
Figure 84. Plasmid map of pBRFPT7sNeoCas9 (13283 bp) _____	221
Figure 85. Plasmid map of pBRFPT7sPhleoCas9 (12860 bp) _____	222
Figure 86. Agarose gel showing CS-Neo-CS, CS-Phleo-CS, and CS-Hyg-CS DNA repair cassettes amplicons. _____	224
Figure 87. Sequence of donor DNA repair cassettes CS-Neo-CS, CS-Phleo-CS and CS-Hyg-CS. _____	226
Figure 88. Agarose gel showing sgRNA templates for CRISPR-Cas9 system. ____	227
Figure 89. Transfection efficiency of <i>A. castellanii</i> Neff trophozoites with pBRFPT7NeoCas9 _____	232
Figure 90. Transfection efficiency of <i>A. castellanii</i> Neff trophozoites with pBRFPT7PhleoCas9 _____	235
Figure 91. Transfection efficiency of pBRFPT7NeoCas9 and pBRFPPPhleoCas9 expression in <i>A. castellanii</i> trophozoites utilising Xfect reagent analysed by confocal microscopy _____	241
Figure 92. Flow cytometry analysis of trophozoites transfected with pBRFPT7NeoCas9 and pBRFPT7PhleoCas9 _____	245
Figure 93. Analysis of FACS-sorted <i>A. castellanii</i> Neff trophozoites transfected with pBRFPT7NeoCas9 analysed by fluorescence microscopy _____	249
Figure 94. FACS profile of <i>Acanthamoeba</i> Neff trophozoites transfected with pBRFPT7NeoCas9 _____	251
Figure 95. Flow cytometry analysis of trophozoites transfected with pBRFPT7NeoCas9 expressing plasmids post-fluorescence-activated cell sorting (FACS) _____	254

List of Tables

Table 1. Summary of agents used against <i>Acanthamoeba</i> spp. diseases. _____	43
Table 2. Chemicals _____	48
Table 3. Media and Buffers _____	50
Table 4. Molecular biology kits _____	51
Table 5. Antibiotics _____	51
Table 6. DNA/Protein Molecular Weight Markers _____	52
Table 7. Enzymes _____	52
Table 8. Bacterial strain _____	53
Table 9. Plasmids _____	54
Table 10. Oligonucleotides _____	55
Table 11. Strathclyde Minor Groove Binders _____	56
Table 12. Summary of optimal seeding density of <i>Acanthamoeba</i> spp. _____	84
Table 13. Relative activity of 42 S-MGBs examined against <i>Acanthamoeba castellanii</i> Neff strain _____	95
Table 14. Library of potent active S-MGBs against <i>Acanthamoeba castellanii</i> Neff trophozoites _____	97
Table 15. Anti-amoebic activity of S-MGB-235 against <i>Acanthamoeba</i> spp. at 24 h and 96 h evaluated <i>in vitro</i> _____	100
Table 16. Description of voriconazole, miltefosine and S-MGB 235 efficacy testing procedure in <i>Galleria mellonella</i> larvae groups infected and non-infected with <i>Acanthamoeba castellanii</i> Neff strain trophozoites _____	134
Table 17. Description of S-MGB 235 efficacy testing procedure in <i>Galleria mellonella</i> larvae groups infected and non-infected with <i>Acanthamoeba castellanii</i> Neff strain trophozoites _____	140
Table 18. Overview of transfections in <i>Acanthamoeba</i> spp. _____	152
Table 19. Current reports of genome editing via CRISPR-Cas9 in protozoan parasites. _____	160
Table 20. Drug concentrations used to select pBRFPT7NeoCas9 and pBRFPT7PhleoCas9 after transfection using Xfect. _____	169

Table 21. Restriction analysis of pBBXSV40RFP _____	175
Table 22. Restriction cleavage of pBASV40GFP, pBBXSV40RFP and pRFPSV40 _____	180
Table 23. Restriction analysis of pBSKII(+), pRFPSV40, and pBKCTBPpNeo. ___	185
Table 24. Restriction cleavage of pT007_Cas9_T7_Tub, pBKCTBPpNeo and pBTBPpCas9 _____	190
Table 25. Restriction cleavage of pBTBPpCas9, pRFPSV40 and pBRFPNeoCas9 _____	195
Table 26. Restriction cleavage of pBRFPNeoCas9, pCR2.1Phleo and pBKCTBPpNeo _____	211
Table 27. Restriction cleavage of pBTBPPhleopolyA and pBRFPPhleocas9 ____	213
Table 28. Restriction analysis of pBRFPNeoCas9, pBRFPPhleocas9, pUCSV40T7PolyA, pBRFPT7sNeoCas9, pBRFPT7sPhleocas9, pBRFPT7NeoCas9, and pBRFPT7Phleocas9 _____	223

List of Appendix

Appendix 1. Electropherograms of wild-type and S-MGB 235 treated *Acanthamoeba* spp. trophozoites RNA extracted. _____ 301

List of Abbreviations

°C	Degree Celsius
µg	Microgram(s)
µl	Microliter(s)
AA	Arachidonic acid
AcAtg	Autophagy-related proteins
AcPHS	<i>Acanthamoeba</i> phosphatase transporter
ADP	Adenosine diphosphate
AIDS	Acquired immunodeficiency syndrome
AK	<i>Acanthamoeba</i> keratitis
AMP	Ampicillin resistant gene
AMP	Antimicrobial peptides
aPa	<i>Acanthamoeba</i> plasminogen activator
ATCC	American type culture collection
ATP	Adenosine triphosphate
BALB	Bagg albino mouse
BBB	Blood-brain barrier
BLAST	Basic Local Alignment Search Tool
bp	Base pair(s)
cAMP	Cyclic adenosine monophosphate
CASCADE	CRISPR-associated complex for antiviral defence
CD	Chagas disease
CD54	Cluster of differentiation 54
CDC	Centre for disease control
cDNA	Complementary deoxyribonucleic acid
CFDA	Carboxyfluorescein diacetate
CFSE	Carboxyfluorescein succinimidyl ester
CL	Contact lenses
CL	Cutaneous leishmaniasis

CNS	Central nervous system
COI	Cytochrome oxidase
CPA	Cation proton antiporter
CRD	Carbohydrate recognition domain
CRISPR	Clustered regularly interspaced short palindromic repeats
CS	Chorismate synthase
CSF	Cerebrospinal fluid
CSP21	Cyst-specific protein 21
CT	Computed tomography
CXCL	C-X-C motif chemokine ligand
DAG	Diacylglycerol
DAHP	3-Deoxy-D-Arabino-Heptulosonate 7-Phosphate
DALK	Deep anterior lamellar keratoplasty
ddH ₂ O	Double distilled water
DH	3-dehydroquinate dehydratase
DHQS	3-dehydroquinate synthase
DMSO	Dimethyl sulfoxide
DNA	Deoxyribonucleic acid
dNTP	Deoxyribonucleotide triphosphate
DPBS	Dulbecco's phosphate-buffered saline
DSB	Double strand break
DTH	Delayed-type hypersensitivity
EC ₅₀	Half maximal effective concentration
ECM	Extracellular matrix
EDTA	Ethylenediamine tetra-acetic acid
EDU	Efficacy of drug usage
EEA	Encystment-enhancing activity
EPSP	5-enolpyruvateshikimate-3-phosphate
EPSPS	Enolpyruvylshikimate-3-phosphate synthase
ERK	Extracellular-signal-regulated kinase

EST	Expressed sequence tag
EtBr	Ethidium bromide
FACS	Fluorescence-activated cell sorting
FDA	The food and drug administration
FDU	Frequency of drug usage
F-GAP	phenylalanyl-glycyl-glycyl-alanyl-prolyl
FITC	Fluorescein isothiocyanate
FLA	Free-living amoeba
FMN	Flavin mononucleotide
FU	Fluorescence units
FW	Formula weight
g	grams
GAE	Granulomatous amoebic encephalitis
GAPDH	Glyceraldehyde-3-phosphate dehydrogenase
GFP	Green fluorescent protein
GPCR	G protein-coupled receptor
GTPase	Guanosine triphosphatase
H	Hour(s)
HAT	Human African trypanosomiasis
HBMEC	Human microvascular endothelial cells
HDR	Homology-directed repair
HEPES	4-(2-hydroxyethyl)-1-piperazineethanesulfonic acid
HF	High-fidelity
HIV	Human immunodeficiency virus
HSR	Hypersensitivity reaction
IC ₅₀	Half maximal inhibitory concentration
ICAM-1	Intercellular Adhesion Molecule 1
ID	Identity number
IF	Interferon
IFA	Indirect fluorescent antibody test

Ig	Immunoglobulin
IIF	Indirect immunofluorescence
IL	Interleukin
IPA	Indirect immunoperoxidase assay
IVCM	<i>in vivo</i> tandem confocal microscopy
kDa	kilodaltons
kg	kilograms
L	litre
LB	Lysogeny broth
LBP	Laminin binding-protein
LGT	Lateral gene transfer
M	molar
MAPK	Mitogen-activated protein kinase
MBP	Mannose-binding protein
mg	Milligram
MIC	Minimum inhibitory concentration
MIP	Mannose-induced protein
MMEJ	Microhomology-mediated end joining
MMP	Metalloprotease
MRI	Magnetic resonance imaging
mtDNA	Mitochondrial deoxyribonucleic acid
MyD	Myeloid differentiation protein
nt	Nucleotide(s)
NADH	Nicotinamide adenine dinucleotide reduced
NADPH	Nicotinamide adenine dinucleotide phosphate reduced
NCBI	National centre for biotechnology information
NEM	Neff's encystment medium
NHEJ	Non-homologous end joining
NPF motif	Asparagine-Proline-Phenylalanine motifs
OD	Optical density

ORF	Open reading frame
PAM	Primary amoebic meningoencephalitis
PAM	Protospacer adjacent motif
PAMP	Pathogen-associated molecular pattern
PAR	Protease-activated receptor
PCR	Polymerase chain reaction
PEP	Phosphoenolpyruvate
PG	Peptone-protease glucose medium
pH	Potential of hydrogen
PHMB	Poly hexamethylene biguanide
PKC	Protein kinase C-like
PMN	Polymorphonuclear leukocytes
PMSF	Phenylmethylsulphonyl fluoride, a serine protease inhibitor
PO	Phenol oxidase
PPR	Pentatricopeptide repeat proteins
pRB	Retinoblastoma protein
PRR	Pattern recognition receptor
PTKS	Phosphotyrosine kinase
pTyr	Phosphotyrosine system
PYG	Peptone Yeast Glucose medium
qRT-PCR	Real time quantitative reverse transcription PCR
rDNA	Ribosomal deoxyribonucleic acid
RFLP	Restriction fragment length polymorphism
RFP	Red fluorescent protein
RIN	RNA integrity number
RNA	Ribonucleic acid
RNase	Ribonuclease
ROS	Reactive oxygen species
RT	Room temperature
s	second(s)

SAP	Shrimp Alkaline Phosphatase
SAR	Structure-activity relationship
SD	Shikimate dehydrogenase
SEM	Standard error of mean
sgRNA	Single-guide ribonucleic acid
SH2	src homology 2
SK	Shikimate kinase
S-MGB	Strathclyde minor groove binder
SPR	Surface plasmon resonance
SV40	Simian virus 40 promoter
TBE	Tris/Borate/EDTA buffer
TBP	TATA box binding protein
TEMED	Tetramethyl ethylenediamine
TENS	Tris-EDTA sodium hydroxide SDS buffer
Th	T helper cell
THC	Tetrahydrocannabinol
TLR	Toll-like receptor
TNF	Tumour necrosis factor
TRIF	Toll/interleukin receptor that induces interferon
tRNA	Transfer ribonucleic acid
UK	United Kingdom
USA	United States of America
WT	Wild type
ZO	Zona occludens

Acknowledgments

All my appreciation and sincere gratitude to the Mexican National Council for Science and Technology (CONACYT) for awarding me with a scholarship to carry out this tough and incredible experience.

To my parents, Maria del Carmen Sanchez Dorado, and Gustavo Carpinteiro Trujillo for all your love, support, and motivation. You were always on my mind and heart in every positive and negative moment. To my auntie, Maria de los Angeles Sanchez Dorado for listening to me in the most fragile moments. To my cousin MSc Laura Caba for your affection and best wishes.

There are not enough words to express all my deepest gratitude to Prof Craig W. Roberts. During the last 4 years he has been not only a supervisor, but he has also been a mentor of life. I am delighted and so honoured to have worked with such an expert and quite genuine person. Thanks for all your consistent guide, knowledge, patience, kindness, and attention to me. It is a real dream come true to belong to your professional team.

All my admiration to my second supervisor Dr Martin Wiese, such a professional who motivated me every time I was committing any mistake in the lab. He is such an exemplaire of discipline and critical thinking. Thanks a lot!

I owe all my gratitude to Roberts's lab for all your support, advice, and corrections, especially to Dr Scott Thomson, for all his meticulous guidance and training. To Dr. Margaret Cunningham for all the assistance in the confocal microscopy sessions.

To all the University of Stathclyde staff that most of the time are "behind the curtains", especially to the stores and sterilisation personnel. You are a fundamental part of the proper performance of these experiments.

To all my friends that during the last four years motivated me and gave me the most enjoyable and rewarding experiences in Glasgow: Carola, Thalia, Paz, Violeta, Esmee, Rachel, Dr Toni, Dr Gustavo, Pablo, Ionut, Amlan, Basem.

To my Biomedical souls Tania, Era, Liliana, and Estela Scott for your friendship, encouragement, and support. Love ya!

To my Brazilian girls Debora, Rafa, Jo and Dr Veridiana, despite the distance I felt you close, and your kind words were useful during the writing of this thesis.

“Only those who attempt the absurd...will achieve the impossible. I think ...I think it's in my basement...Let me go upstairs and check.”

— Maurits Cornelis Escher

Chapter 1. Introduction

1.1 Free-Living Amoeba

The Free-Living Amoebae (FLA) are aerobic microorganisms with mitochondria that can complete life cycles with or without a host (amphizotic). FLA, often known as “Limax Amoebae”, are ubiquitous in a lot of wet habitats forming part of biocenosis such as water, soil, and dust (Scheid, 2014). They are mobile and use phagocytosis for getting food from bacteria, algae, fungi and protozoa or other organic particles. They are also capable of pinocytosis as an alternative way of feeding (Marciano-Cabral and Cabral, 2003; Greub and Raoult, 2004). Several studies have reported their prevalence in extreme environments such as desert, arctic and Antarctic soils but their abundance was reported to be higher in wastewater as these environments are enriched in organic material and bacteria, which serve as food (Salvador and Soledad, 1997; Ramirez *et al.*, 2005; Rodriguez-Zaragoza, Mayzlish and Steinberger, 2005; Ramirez *et al.*, 2014; Tysl *et al.*, 2016).

As FLA feed on other microorganisms, they affect the microbial communities and strengthen the return of nutrients to soil. FLA participate in these ecological community dynamics contributing to nutrient recycling and have a considerable impact on biofilm formation (Thomas *et al.*, 2010).

The most important genera of FLA are *Acanthamoeba*, *Naegleria*, *Balamuthia*, *Sappinia*, *Vermamoeba*, *Valkampfia* and *Leptomyxa* (Visvesvara, Moura and Schuster, 2007; Lorenzo-Morales *et al.*, 2010; De Obeso Fernandez Del Valle, Lorenzo-Morales and Maciver, 2017). The taxonomy of FLA has been revised several times because of the availability of genomic sequence data. Regarding morphological, biochemical, and molecular data, a new taxonomic classification was proposed by the International Society of Protozoologists. According to this classification, *Acanthamoeba*, *Balamuthia* and *Sappinia* have been classified under the super group Amoebozoa and *Naegleria* under Excavata (Adl *et al.*, 2005).

For a long time, FLA were considered harmless protozoa of soil and water. Nevertheless, scientific research since the 1960's has demonstrated that FLA can be pathogenic to humans and animals, especially *Acanthamoeba*, *Naegleria*, *Balamuthia* and *Sappinia* (Trabelsi *et al.*, 2012). When FLA are in intimate contact with humans, they can provoke localised diseases (skin, eyes, sinuses, lungs, and kidneys) as well as fatal infections of the central nervous system (CNS). New cases are constantly being reported worldwide and occur both in immunocompetent and

immunocompromised individuals, including patients with AIDS (Visvesvara, 2010). Even though FLA have been spread from pole to equator cases of these pathogens are scarcely reported due to lack of understanding and awareness from the medical staff resulting in misdiagnosis (Visvesvara, Moura and Schuster, 2007; Yousuf *et al.*, 2013; Onichandran *et al.*, 2014; Retana-Moreira *et al.*, 2015).

1.2 *Acanthamoeba* spp.

1.2.1 Opening remarks

From all FLA, *Acanthamoebae* are among the most prevalent parasites occurring in natural environments such as soil, fresh or marine water, but also thrive in in man-made habitats such as air conditioning units, domestic tap water, dental treatment units, hospital and dialysis units (Fanselow *et al.*, 2021). The life cycle of *Acanthamoeba* spp. comprises two stages, an infective trophozoite stage that feeds and multiplies, and a dormant resistant cyst stage, which allows the amoeba not only to withstand harsh conditions but also resist disinfection and drug therapy. *Acanthamoeba* is one of the most versatile protozoans being able to feed on bacteria, algae, and yeasts. It can live under extreme conditions concerning pH, level of oxygen, salinity, and temperature. It is an amphizoic microorganism but is the causative agent of a painful sight-threatening infection known as *Acanthamoeba* keratitis (AK) occurring mostly in contact lens wearers and granulomatous amoebic encephalitis (GAE), which is a fatal disseminated disease generally occurring in immunodeficient patients. *Acanthamoeba* is also the cause of cutaneous infections that manifest as reddish nodules, ulcers, or abscesses (Walia *et al.*, 2007; Galarza *et al.*, 2009; Morrison *et al.*, 2016). Despite all these infections being rare, they are progressive. Cases are increasing due to a lack of awareness in the clinic, the deficiency of rapid diagnostic tools and increased numbers of people wearing contact lenses. The lack of reliably effective treatments is further cause for concern (Marciano-Cabral and Cabral, 2003).

1.2.2 Discovery of pathogenic *Acanthamoeba*

Puschkarew in 1913 elucidated the first evidence ever of *Acanthamoeba* in dust, which at that period was named *Amoeba polyphagus*. Afterwards, in 1930 a free-living amoeba growing in a yeast culture of *Cryptococcus pararoseus* was isolated by Aldo Castellani in Oxford, England. This amoeba was placed in the genus

Hartmanella and named as *Hartmanella castellanii*, but later was reclassified as *Acanthamoeba castellanii* (Visvesvara, Moura and Schuster, 2007). Volkonsky in 1931 developed a classification based on morphology, locomotion and appearance of the cyst stage that recognised the genus *Acanthamoeba* (Visvesvara, 1991). Three morphological groups comprise the genus based on the polygonal morphologies and the number of opercula in cysts but intraspecific polymorphism is rather usual in *Acanthamoeba* (Pussard, 1977). Close to 25 species have been described and validated by molecular analyses and 23 genotypes (T1-T23) have been established according to 18S rDNA sequences with T4 being the most common and abundant genotype in human *Acanthamoeba* infections (Page, 1987; Moura, Wallace and Visvesvara, 1992; Nerad *et al.*, 1995; Putaporntip *et al.*, 2021).

The first notion of an *Acanthamoeba* infection was in 1957 when Jahnes, Fullmer and Li reported a contaminant of the control in monkey kidney cell cultures. This parasite, currently known as *Acanthamoeba culbertsoni*, was isolated and inoculated in mice treated with corticosteroid and monkeys where it caused an encephalitis syndrome resulting in death. Consequently, Culbertson described the infection and hypothesised that humans might be a potential host of this lethal infection. Years later, in 1972, the very first case of brain abscesses was detailed in a patient with Hodgkin's disease (Jager and Stamm, 1972) while the first infection case in the eye occurred in 1974; both diseases were caused by *Acanthamoeba* (Jager and Stamm, 1972; Nagington *et al.*, 1974). The scientific research interest in these infections has increased all over the world ever since (Figure 1).

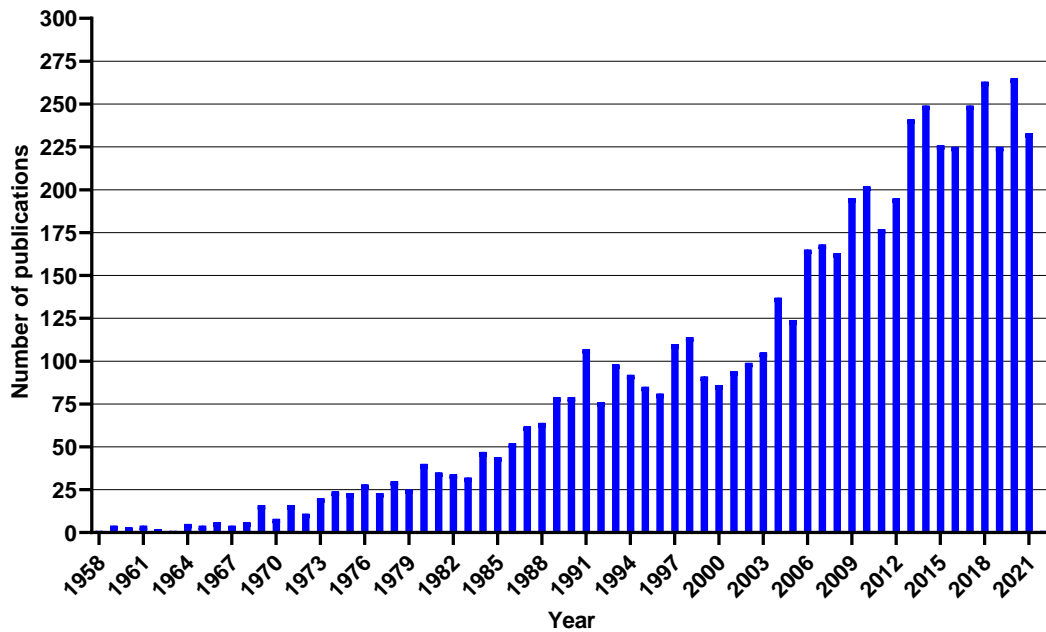


Figure 1. Comparison of papers published on *Acanthamoeba* spp. in journals of major biomedical importance since 1958.

The data was collected on 03/11/2021 from PubMed website <https://www.ncbi.nlm.nih.gov/pubmed/> with the search term “acanthamoeba”. Bar graph was generated with Graphpad Prism 9.0.

1.3 Cell Biology

Acanthamoeba is a word formed from the prefix “acanth” (meaning ‘spikes’ in Greek) and amoeba (meaning ‘to change’ in Greek) with the view to indicate the presence of spine-like structures (acanthopodia) on the surface of this protozoan with the ability to change shape. The spikes are important in adhesion to surfaces (biological or inert), movement and capturing prey. These structures are cytoskeletal structures that protrude from the body of the parasite.

The plasma membrane is formed of proteins, phospholipids, sterols and lipophosphoglycans, with sugars exposed on both sides of the membrane (Dearborn and Korn, 1974). Interestingly, *Acanthamoeba* produces prostaglandins, however *in vivo* studies have suggested that their biosynthesis is activated when this amoeba is in the presence of tissue or body fluids, which facilitates the invasion and penetration to the host (Hadas and Mazur, 1997).

The cytoplasm is finely granular and hyaline and contains ribosomes, fibrils, glycogen, lipid droplets, lysosomes, peroxisomes, food vacuoles, and a contractile vacuole whose function is to expel water for maintaining hydrostatic homeostasis. Most of the cellular activities such as cellular respiration and growth are carried out in the cytoplasm. The cytoplasm is a translucent fluid composed of water, salts, and organic molecules. The granuloplasm (endoplasm) is referred to as the inner and granular fluid portion of the cytoplasm. Inclusion bodies are present in the cytosol and are important for storage of nutrients such as polysaccharides and lipids, pigment granules and secretory products. Similar to other eukaryotic cells, *Acanthamoeba* presents membrane systems including the rough endoplasmic reticulum (concerned with protein synthesis and transport), a small amount of smooth endoplasmic reticulum (which synthesises and transports lipids and steroids), free ribosomes and a Golgi complex (Chlapowski and Band, 1971). The ribosome contains large subunit rRNAs (5S, 5.8S, 28S) and small subunit rRNA (18S). In addition, the *Acanthamoeba* mitochondrial rRNA molecule consists of a large subunit (5S, 23S) and a small subunit (16S). The trophozoite stage normally possesses a big single nucleus, however amoebas with more than one nucleus have been observed (Siddiqui and Khan, 2012a). The nuclear envelope (consisting of two membranes made up of a lipid bilayer and pores) encloses the nucleus and separates the cell genetic material from the cytoplasm. Inside the nucleus is the nucleolus, a prominent organelle without membrane. The *Acanthamoeba* nucleus contains RNA precursors confirming that RNA synthesis is a main function of this structure (Prescott, 1959). *Acanthamoeba* owns a substantial number of mitochondria, producing the energy required for metabolic activities involved in feeding, movement, reproduction, and other cellular purposes (Siddiqui and Khan, 2012a).

1.4 The *Acanthamoeba* genome

Most studies on the genome of *Acanthamoeba* have been undertaken with the Neff strain of *Acanthamoeba castellanii*, genotype T4, which is the strain also used in the *Acanthamoeba* genome project. This strain has the advantage of being very well characterised concerning its cell biology. This strain is a non-pathogenic environmental isolate that has been grown under laboratory conditions since 1957 and, moreover, seems to be rather exceptional, as similar strains have rarely been isolated. Early studies estimated a total cellular DNA content of uni-nucleate *Acanthamoeba* during log phase of 1-2 pg and a haploid genome size of 40-50 Mb

(Bohnert and Herrmann, 1974; Jantzen, Schulze and Stohr, 1988; Byers, Hugo and Stewart, 1990). A whole first genome assembly approach has been undertaken, revealing a 45 Mb genome encoding 15,455 compact genes with an average of 6.2 introns per gene, which is among the highest known in eukaryotes (Clarke *et al.*, 2013b). The ploidy level and the number of chromosomes of *Acanthamoeba* spp. is suggested to be extremely variable (Byers, 1986). The number of chromosomes, previously assumed to be in the range of several dozens, has been estimated to lie between 9 and 25 (Byers, Hugo and Stewart, 1990; Matsunaga *et al.*, 1998). The genome has a significant number of genes presumably acquired by lateral gene transfer, and it has a rather complex cell communication repertoire; however, the genetics of *Acanthamoeba* spp. is far from being elucidated. *Acanthamoeba* generally multiplies by binary fission and there still no convincing evidence for genetic recombination, nevertheless *Acanthamoeba* owns several genes similar to eukaryotes that are implicated in meiosis (Khan and Siddiqui, 2015; Speijer, Lukeš and Eliáš, 2015).

The nuclear genome has revealed that *Acanthamoeba* possesses extensive metabolic networks and great environmental capacities for adaptation; these include the Chorismate synthesis pathway (for the synthesis of aromatic amino acids and folate), purine and pyrimidine biosynthetic pathways and the synthesis of ribonucleotides and deoxyribonucleotides. Other important enzymes are involved in processes like phagocytosis (NADPH and lysozyme), pathogenicity (proteases) and even glycosylation (Schiller *et al.*, 2012; Henriquez *et al.*, 2015).

One of the important findings during the genome assembly project was the identification of several serine, threonine, tyrosine, and histidine protein kinases allowing the amoeba to sense and respond to environmental changes and stress conditions (Clarke *et al.*, 2013b). Interestingly, *Acanthamoeba* can rearrange its biosynthetic machinery during a stress response. This was shown when a homologue of trehalose-6-phosphate synthase produced the disaccharide trehalose, which is involved in the protection from desiccation, osmotic stress and extreme temperature all related with the induction of encystment (Anderson *et al.*, 2005).

The mitochondrial proteome of *Acanthamoeba* is one of the most complex in composition and function (Gawryluk *et al.*, 2014). The genome is circular, approximately 41 kb, and encodes two rRNAs, 16 tRNAs and 41 proteins (Burger *et al.*, 1995; Fučíková and Lahr, 2016). The diversity in mtDNA among different strains

is high as shown by restriction enzyme digests (Byers, Hugo and Stewart, 1990). It was suggested that tRNAs are imported from the cytosol into mitochondria to support mitochondrial protein synthesis since the *Acanthamoeba* mitochondrial genome encodes less than the minimal number of rRNA to support this process (Burger *et al.*, 1995). The translation process in the mitochondria uses a genetic code different from the one used in the cytosol, in particular TGA codons appear to specify Trp instead of termination codons and nearly all of the proteins produced have functions associated with respiration and translation (Gawryluk *et al.*, 2014). Proteins involved in respiration include cytochrome oxidase, apocytochrome b, the NADH dehydrogenase and ATP synthase complex; both last mentioned are interestingly extra-encoded by *Acanthamoeba* compared to other animal or fungi mtDNAs. This situation is similar to the unusual production of mitochondrion-targeted pentatricopeptide repeat proteins (PPR) thought to be participating in processes such as RNA editing, intron splicing, transcript stabilisation and translational control (Gawryluk *et al.*, 2014).

Genetic exchange is an important process that has facilitated genome and transcriptome evolution in *Acanthamoeba*. One of the most remarkable genetic exchange processes due to *Acanthamoeba* capacity to harbour endosymbionts and hence picking up foreign DNA is Lateral Gene Transfer (LGT). This process is hypothesised to take place for the colonisation of many ecologic niches driven by selective pressure with trophic purposes. The genome sequence of *Acanthamoeba* spp. suggests that 450 genes may have arisen through LGT (Clarke *et al.*, 2013b). Although the precise function of G protein-coupled receptors (GPCRs) is not yet established, *Acanthamoeba* encodes 35 GPCRs suggesting a role in detecting endosymbiont bacterial molecules and possibly in encystment induction. Altogether, 377 protein kinases were identified, out of which 48 are sensor histidine kinases involved in environmental sensing processes, 2 green algae rhodopsin homologues might represent possible light sensors and a primitive but functional phosphotyrosine system (pTyr) composed of 22 phosphotyrosine kinases (PTKS), 12 tyrosine phosphatases (PTPs) and 48 Src homology 2 (SH2) domain-containing proteins were distinguished despite of being considered absent in amoebozoan lineages (Clarke *et al.*, 2013b).

1.5 Life cycle

1.5.1 Trophozoite and Cyst stage

The *Acanthamoeba* life cycle consists of two stages: infective and mobile trophozoite (15-45 μm in size) and dormant-resistant cyst with minimal metabolic activity (12-32 μm in size) (Figure 2). Trophozoites feed on bacteria, algae, yeast, and organic particles through phagocytosis as well as pinocytosis, where it absorbs liquid nutrients. Ingestion presents the typical phagocytic cell-cell contact with consecutive invagination of the cell membrane feeding of any particle of adequate size, including non-organic particles (Korn and Weisman, 1967). Trophozoites divide mitotically, in which the nucleolus and the nuclear membrane disappear during cell division and is capable of sluggish locomotion (approximately 0.8 μm per second) via a pseudopodium (lobopodium) with hyaline sub-pseudopodia (acanthopodia) (Bowers and Korn, 1968). The proteins responsible for the movement are actin (constitutes around 20% of the total protein) and myosin together with more than 20 cytoskeletal proteins (Gordon, Eisenberg and Korn, 1976). Fibres and networks of actin are extended beyond cytoplasmic structures, being found in various endocytic structures (González-Robles *et al.*, 2008). Intracellular transport and cell division is also accomplished by actin polymerisation and breakdown (Preston and King, 1984). The multiplication is fast in a favourable environment with a growth rate depending on the species. Under optimal temperature conditions (30°C) they divide every 6-8 h. When the trophozoite is exposed to harsh conditions such as lack of nutrients, extreme temperatures (cold or heat), hyper- or hypo-osmolarity, extreme levels of pH and desiccation lead to the double-layered cyst formation stage. The ectocyst (outer layer) is composed of polysaccharides and the endocyst (inner layer) is a fibril layer made up of cellulose and acid insoluble proteins. This stage is resistant to germicides, biocides, chlorination and antibiotics (Guimaraes *et al.*, 2016). The cysts are highly resistant to repeated cycles of freeze-thawing and also remarkably high doses of ultraviolet and gamma radiation (Marciano-Cabral and Cabral, 2003). Despite being metabolically inactive, the cysts can remain viable for up to 20 years *in vitro* (Sriram *et al.*, 2008). Trophozoite and cyst are immunogenic but both forms can evade the immune system (McClellan *et al.*, 2002). Eventually, when the environmental conditions are ideal, the trophozoite emerges from the cyst completing the process of

excystment. It is known that during the summer months the trend towards disease increases (McAllum *et al.*, 2009; Chew *et al.*, 2011).

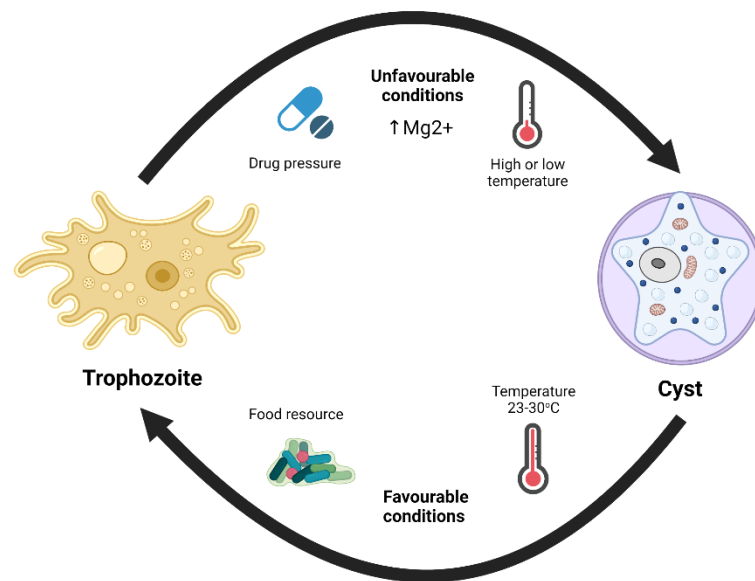


Figure 2. Life cycle of *Acanthamoeba* spp.

The diagram displays the change of a trophozoite to a cyst and vice versa due to harsh or favourable conditions. Taken and adapted from (Roberts and Henriquez, 2010). Created with Biorender® by Alemao Sanchez.

1.5.2 Encystment process

Encystment is accompanied by morphological changes, the end of cell growth and biochemical alterations. At first, the amoeba become rounded and then, the cyst walls are synthesised (Weisman, 1976). This synthesis goes with the decrease of metabolic functions and macromolecules, particularly the cytoplasmic mass through dehydration, thereby causing a shrinkage of the protoplast (Bowers and Korn, 1969). This is caused naturally when starvation, extreme temperatures or osmotic stress are present but under laboratory conditions, catecholamines (epinephrine, norepinephrine), magnesium and taurine can be used to induce encystment (Verma *et al.*, 1974; Köhler *et al.*, 2008). Interestingly, quorum-sensing molecules and an encystment-enhancing activity (EEA) are involved in correlating high cell densities with higher encystment rates (Akins and Byers, 1980; Fouque *et al.*, 2012). As stated above, 35 GPCRs act as sensors for extracellular stimuli, hence they constitute possible candidates for the first step in signal transduction in the start of encystment (Clarke *et al.*, 2013b). Precise mechanisms for the regulation of signal transduction

are far from being understood; however, the family of β -adrenergic receptors are important for the encystment process and its inhibition reduces this process (Murti and Shukla, 1984; Aqeel *et al.*, 2015). GPCRs activate the small GTPase Ras, which commonly activates the mitogen-activated protein kinase (MAPK) pathway but this has not been observed in *Acanthamoeba* (Dudley, Jarroll and Khan, 2009). Adenylate cyclase is also activated via GPCRs converting adenosine triphosphate (ATP) to cyclic adenosine monophosphate (cAMP), the latter plays an important role in encystment converting glycogen phosphorylase to the active form for glycogen degradation producing cellulose for cyst wall formation (Siddiqui and Khan, 2012a). Silencing of glycogen phosphorylase results in incomplete assembly of the cellulose-containing inner cyst (Lorenzo-Morales *et al.*, 2008). Inhibition of phosphodiesterase (enzyme that degrades cAMP into AMP) strongly causes encystation involving a tenfold increase of cellular cAMP levels (Du *et al.*, 2014). Additionally, xylose isomerase appears to be crucial, highlighting the important role of xylose together with cellulose in cyst wall formation (Aqeel, Siddiqui and Khan, 2013). A large set of sensor histidine and tyrosine kinases with potential receptor function are involved in encystment confirmed by the genome sequence assembly (Anderson *et al.*, 2005; Dudley, Jarroll and Khan, 2009; Clarke *et al.*, 2013a). Other signalling molecules, protein kinase C-like genes (PKC) are highly expressed during the early stage of encystment and have been identified as primitive because they lack a Ca^{+2} binding domain and a diacylglycerol (DAG) binding domain; nevertheless, PKCs have been detected amongst expressed sequence tags (ESTs) of *Acanthamoeba* cysts (Moon *et al.*, 2011).

Certainly, there are changes on DNA and RNA levels over this stage. DNA synthesis continues during this process but at a significantly reduced rate meanwhile RNA levels decrease by 50% and rRNA production is completely stopped after 7 h of encystment (Weisman, 1976; Byers *et al.*, 1991). Activity of the RNA polymerase II is significantly increased indicating that additional genes, which might be repressed in the trophozoite, are active and transcribed during encystment, meanwhile activities of the RNA polymerase type II and III decrease (Orfeo and Bateman, 1998). In some way, it was shown that chromatin remodelling occurs during encystment (Köhler *et al.*, 2008). Moreover, the cyst-specific protein 21 (CSP21) is actively repressed during the infective stage but is related to cyst wall formation during the early stages of encystment, however the mode of action needs to be clarified (Chen *et al.*, 2004). Rho kinase plays an important role in the cytoskeletal rearrangement because it is

involved in actin polymerisation and gelation factor hydrolysis, thus is an important factor in the course of differentiation (Bouyer *et al.*, 2009; Dudley, Jarroll and Khan, 2009). Similarly, proteases such as subtilisin-like serine protease (promoting autolysis), cysteine protease (promoting significant roles for serine proteases) and cyst-specific cysteine proteases (participating in mitochondrial autolysis) have an important role for building up the cyst walls (Moon *et al.*, 2008a; Moon *et al.*, 2012). Although encystment shows an interplay of many molecules, it is still far from being totally understood. Other important molecules related to the process of differentiation are P-type ATPases, proteasome, heat shock proteins, cullin 4 and ubiquitin-conjugating enzymes (Moon *et al.*, 2008a). Components of the autophagic machinery named autophagy-related proteins (AcAtg) have been identified in this process: AcAtg8 (participates in the formation of the autophagosomal membrane), AcAtg3 (participates in AcAtg8 lipidation) and AcAtg16 (found in vesicular structures co-localised with autophagolysosomes) (Moon *et al.*, 2009; Song *et al.*, 2012). A recent study using quantitative real-time PCR (qRT-PCT) indicates AcSir2, a Sir2-like class-IV sirtuin as an important regulatory protein with transcriptional activity that promotes the encystment process in *A. castellanii* (Joo *et al.*, 2020).

1.5.3 Excystment process

The process happens when the trophozoite finds favourable conditions, however, few details are known about this pathway. Excystment takes 12 h, the cyst hatches through the ostioles leaving behind the operculum (Mattar and Byers, 1971). *Acanthamoeba* uses the cellulose as a food from their own cyst wall in natural conditions, on the other hand under lab conditions the nutrients are supplied by the media where undamaged and empty cyst walls are commonly observed (Anderson *et al.*, 2005). The role of ion transport pumps in the formation of cysts and excystment has been explored. A study using tenatoprazole (proton pump inhibitor), cariporide (Na⁺-proton exchanger) and both stevioside and lanthanum oxide (K⁺ channel modulators) showed to hamper the excystment process, suggesting an important role in the sensory perception to lead the trophozoites to emerge (Siddiqui *et al.*, 2019).

1.6 Amoebic infections

Free-living amoebae occur as worldwide distributed protists which cause serious clinical infections in hosts such as humans and animals. Despite low morbidity, patients infected with *Acanthamoeba* diseases result in a high mortality rate, hence

the diagnosis and treatment outcome are challenging. The eyes, skin, and kidneys are predilected sites by *Acanthamoeba* trophozoites and cysts, however infections of CNS leading to brain damage are eventually fatal and occur in immunocompromised (patients with diabetes or AIDS) or immunocompetent. *Acanthamoeba* spp. are the causative agents of *Acanthamoeba* keratitis (AK), granulomatous amoebic encephalitis (GAE) and disseminated infection which typically shows as skin infection or inflammation of the lungs and sinuses (Zhang and Cheng, 2021).

1.6.1 *Acanthamoeba* keratitis (AK)

AK is a rare but sight-threatening disease with an infiltrative corneal ulceration caused by at least 8 *Acanthamoeba* pathogenic strains: *A. castellanii*, *A. culbertsoni*, *A. polyphaga*, *A. hatchetti*, *A. rhyodes*, *A. lugdunensis*, *A. quina* and *A. griffin*. The first registered case of AK was described in 1974 in the UK (Jones, Visvesvara and Robinson, 1975). Contact lens (CL) wear is the main risk factor with >80 percent of the cases of AK, however, this infection occurs even in non-contact lens wearers where exposure to contaminated sources such as water or soil, trauma and poor socioeconomic conditions accounts for the most important factors in these cases (Garg, Kalra and Joseph, 2017; Neelam and Niederkorn, 2017). Around 80-85% cases in the UK, USA and other developed countries show a high prevalence of infection in CL users, however, in Asian countries the majority of the AK happened in non-CL users (Ertabaklar *et al.*, 2007; Watt and Swarbrick, 2007; Buerano *et al.*, 2014; Juárez *et al.*, 2017). Nonetheless, surgical trauma in the eye like penetrating keratoplasty (PK), radial keratotomy and laser refractive surgery also have been reported as infection factors (Garg, Kalra and Joseph, 2017). Nonetheless, aging is becoming one more factor in recent years where a high rate of infections has been detected in people older than 53 possibly due to corneal changes (Fanselow *et al.*, 2021). Both stages trophozoite and cyst are the causative agents of this infection where trophozoites bind to the eye and produce several enzymes that help to penetrate and destroy the eye tissue as well as the cysts adhere to the soft or rigid CL (Juárez *et al.*, 2017). Moreover, it was established that 90 to 100% of the adult population has serum antibodies specific for *Acanthamoeba* antigens without previous AK; this indicates the close exposure to this parasite, yet the infection is rare (Brindley, Matin and Khan, 2009).

As mentioned before, T4 is the most pathogenic genotype and clinical isolates from both keratitis and non-keratitis samples are related with this type; but others have also been found to be associated including T2a, T3, T5, T6, T10, T11 and T15 (Visvesvara *et al.*, 2007; Risler, Coupat-Goutaland and Pélandakis, 2013). Specifically, the genotype T13 has been reported as etiological agent of keratitis (Grün, Stemplewitz and Scheid, 2014). It should be pointed out that non-T4 genotypes produce worse symptoms with the poorest response to therapy compared to T4 (Arnalich-Montiel *et al.*, 2014).

1.6.1.1 Clinical features

Commonly literature describe pain, radial keratoneuritis and ring infiltrate as the classic symptoms in AK infection. However, the presentation is highly variable suggesting that corneal signs vary according to the duration of the disease and habitually progresses slowly depending on the inoculum size. Garg, Karla, and Joseph in 2017 have described a case series where the classical initial symptoms are not prominent because pain was seen in only 1-4 (n=52, 23%) of patients, radial keratoneuritis was seen in 6 (2.7%) cases while ring infiltrate was seen in 74 (33%) cases. Early symptoms include severe pain, punctuate eye epithelial erosion, anterior stromal haze, stromal oedema, nummular keratitis and low corneal sensation in one single eye but CL wearers can manifest the infection in both eyes (Juárez *et al.*, 2017). During the first month the infection could be misdiagnosed as *Herpes simplex* because manifestations such as pseudo dendrites, subepithelial and perineural infiltration are common in both infections. Radial keratoneuritis has been described as a pathognomonic standard sign since *Acanthamoeba* trophozoites invade corneal nerves causing extreme pain, this is presented in up 63% of cases diagnosed within the first 6 weeks, which should be used as evidence of AK infection (Dart, Saw and Kilvington, 2009). The generation of incomplete or double and concentric ring-shaped stromal infiltrates is possibly caused by collagenolytic enzymes and could be identified using a slit-lamp (Illingworth *et al.*, 1995).

If it is not diagnosed and immediately treated, clinical symptoms such as the classical ring infiltrates, marked ulceration, necrotizing or diffuse infiltrative keratitis, uveitis, hypopyon and in some patients, corneal oedemas set the advanced stage of the disease. Vascularisation is present if a secondary infection takes place. Inflammation in the sclera (scleritis) is observed as a secondary immunological reaction and not as

a direct invasion of the amoeba (Illingworth and Cook, 1998). In the case series carried out by (Garg, Kalra and Joseph, 2017), 74 (33%) patients presented ring infiltration while 141 (64%) presented diffuse infiltration. Severe forms of AK are relatively common and may include abscess formation, glaucoma, cataracts, corneal melt, optic nerve oedema, neuropathy and atrophy leading to blindness. Lamentably, sclerokeratitis is a common feature when AK infection process leads to negative clinical outcomes, producing inflamed lesions at this level as a consequence of a T-cell dependent immune response to trophozoite and cyst antigens (Iovieno *et al.*, 2014a).

1.6.1.2 Epidemiology

Despite being relatively uncommon, the epidemiological characteristics of AK vary according to geographic regions, weather conditions and environments. It has been established that there is an association between hot or rainy weather and a marked increase in the number of AK infection cases; this explains peaks of infection during the summertime with activities involving swimming pools (McAllum *et al.*, 2009; Lalitha *et al.*, 2012; Page and Mathers, 2013).

According to Centre for Disease Control (CDC), storing lenses for long time frames and topping off the lens case with care solution increases four-fold the risk to get infected followed by the non-hygienic use, contamination of lenses with dirty hands as well as rinsing the CL cases with tap water before keep them back in the lens case (Cope, 2014). The type of water supplied in the UK, such as soft and hard water, is associated with the incidence of 0-42 cases per million inhabitants hypothesising hard water provides an advantageous environment for *Acanthamoeba* reducing the efficacy of chlorine disinfection systems (Radford, Minassian and Dart, 2002). In India, 2% of all cases with culture-positive corneal ulcers are due to AK at eye care clinic centres (Garg, Kalra and Joseph, 2017).

The impact of factors such as the hygiene of lenses, care solutions and correct usage of storage lens cases are decisive on the rate of AK (Joslin *et al.*, 2006; Thebpatiphat *et al.*, 2007; Por *et al.*, 2009). Several studies of CL care solutions have been conducted showing incapacity in the protection against bacterial contamination and *Acanthamoeba* strains making them a real risk factor (Joslin *et al.*, 2007; Johnston *et al.*, 2009). It has been observed pseudo-cyst formation produced by the use of ophthalmic contact lens solution containing demulcents such as propylene glycol,

raising the risk of infection due to reversibility of pseudo-cysts to viable and infective trophozoites (Kliescikova, Kulda and Nohynkova, 2011). Susceptibility studies of multi-purpose solutions has been conducted using different genotypes with T3, T5 and T11 being the most resistant compared to T4 genotype (Shoff *et al.*, 2007). Interestingly, a case of AK infection in a young girl without, contact lenses use and inappropriate management of the infection has been reported, inferring that non-specific and diverse clinical manifestations of early stages could challenge the proper diagnosis of AK (Cristina, Cristina and Mihaela, 2016).

1.6.1.3 Pathogenesis

Despite all the information about the pathogenic mechanisms used by *Acanthamoeba* in keratitis, it is not clear if this pathogenesis depends on the characteristics of a specific strain or if all the strains are potentially pathogenic. Frequently the studies conducted to evaluate the pathogenic mechanisms use animal inoculation. Interestingly, trophozoites have demonstrated specific predilection to bind to the corneal epithelium of human, pig and Chinese hamster but failed to adhere in mice, rats, cotton rats and rabbits where cytopathic evaluation is done intranasally into the brain in these classical laboratory animals (Clarke and Niederkorn, 2006b). Important to mention is key virulence factors such as high growth rate and temperature tolerance are epigenetically regulated in trophozoites (Griffin, 1972; Walochnik, Obwaller and Aspöck, 2000; Köhler *et al.*, 2008; Pumidonming, Koehler and Walochnik, 2010). In general terms, the pathogenic process can be defined by adhesion to the corneal epithelium, cytopathic effects, and the immune response of the host.

The first step in AK infection is the contact mediated by trophozoite adhesins to the membrane of the corneal epithelium (González-Robles *et al.*, 2008). The binding is primarily mediated by the mannose-binding protein (MBP) of *Acanthamoeba*, a lectin that recognises mannosylated glycoproteins such as methyl- α -D-mannopyranoside and α -1-3-D-mannobiose with high affinity, leading to cytolysis (Cao, Jefferson and Panjwani, 1998). Previously, it was believed that CL was a kind of vector for trophozoites, however, not only CLs deliver infectious *Acanthamoeba* to the cornea, but they modify the ocular surface by means of upregulation in the expression of mannosylated glycoproteins on the eye, making the corneal epithelium an easy target to be invaded and infected (Hurt *et al.*, 2003). Garate *et al.*, in 2004 detailed MBP as

a protein of 400 kDa composed of several 130 kDa subunits consisting of an N-terminal extracellular domain, transmembrane domain and a short C-terminal cytoplasmic domain showing the common characteristics of cell surface receptor. The C-terminal domain carries phosphorylation sites and an NPLF motif, which participates in cell signalling leading to cellular shape change. It has been recognised as a novel carbohydrate recognition domain (CRD), which is also used for adhesion in the initiation of AK leading to a cascade of signal transduction inducing cytopathic effects on the eye (Panjwani, 2010).

It is reasonable to think that MBP is not the only molecule involved in the complex process of *Acanthamoeba* binding to corneal cells. Another 207 kDa protein that does not bind to mannose was discovered using monoclonal antibodies blocking the binding of trophozoites to corneal epithelial cells (Kennett *et al.*, 1999). Sixteen glycoproteins also were identified: eight with mannose and eight with N-acetylglucosamine residues (Soto-Arredondo *et al.*, 2014). Certain *Acanthamoeba* strains have shown a special affinity to components of the host extracellular matrix (ECM): laminin, collagen IV and fibronectin are essential for the binding of *A. polyphaga* while pathogenic *A. culbertsoni* expressed a 54 kDa laminin-binding protein (LBP) showing that the actual involvement of other proteins than MBP are indispensable (Gordon *et al.*, 1993; Rocha-Azevedo *et al.*, 2010).

The next step after adhesion to mannosylated glycoproteins is the release of a 133-kD protein named mannose-induced protein (MIP-133), right after the interaction with mannose receptors which provokes apoptosis of corneal epithelial cells facilitating the penetration to corneal stroma (Leher *et al.*, 1998b). MIP-133 is directly related to the pathogenic cascade since this protein is only expressed in clinical but not in soil isolates producing stromal melting and degradation of the collagen matrix as well as degradation of collagen types I and IV making possible the induction of apoptosis via the caspase 3 dependent pathway (Hurt *et al.*, 2003; Clarke and Niederkorn, 2006c). Apoptosis is achieved by the interaction of phospholipids on the plasma membrane of corneal cells with MIP-133 activating cytosolic phospholipase A_{2α} (cPLA_{2α}) and the release of arachidonic acid (AA) making cells losing its viability (Taketo and Sonoshita, 2002; Tripathi *et al.*, 2012). Straight after, activation of matrix metalloproteases (MMP) by corneal cells is carried out in response to external pathogenic microorganisms (Fini, Girard and Matsubara, 1992). MIP-133 upregulates the expression from 2 to 4-fold of MMP-2 and MMP-3, making the invasion of

trophozoites easier (Alizadeh *et al.*, 2008). MIP-133 has been employed in mucosal immunisation blocking the enzymatic degradation of corneal cells in Chinese hamster producing secretory IgA and anti MIP-133 antibodies that are found in the tears (Alizadeh, Neelam and Niederkorn, 2007). Surprisingly, a specific bacterium has been categorised as a “co-factor” in the infection of AK. *Corynebacterium xerosis* exacerbates AK inducing MIP-133 because of the high content of mannose present in its cell walls (Badenoch *et al.*, 1990; Alizadeh *et al.*, 2005).

Acanthamoeba not only depends on the production of proteins for inducing apoptosis. An interesting strategy depends on the release of adenosine diphosphate (ADP), which causes a rise of the concentration of cytosolic free-calcium and then apoptosis (Mattana *et al.*, 2001). Moreover, ADP together with other not yet identified soluble compounds stimulate the secretion of pro-inflammatory cytokines such as TNF- α , IL-1 β and IL-6 (Mattana *et al.*, 2001; Mattana *et al.*, 2002). Ecto-ATPases are glycoproteins anchored in the plasma membrane that hydrolyse extracellular ATP to ADP involved in the infection mechanism of trophozoites in AK since pathogenic and non-pathogenic strains show different classes of ecto-ATPases; as matter of fact, it has been observed that the inhibition of these ecto-ATPases reduces the host cell cytotoxicity and the presence of mannose boosts the ecto-ATPase function in pathogenic strains (Sissons *et al.*, 2004).

Another molecule with a high pathogenic potency is the *Acanthamoeba* plasminogen activator (aPa), a serine protease of 40 kDa, which facilitates the penetration of trophozoites through the basement membrane (Alizadeh, Neelam and Niederkorn, 2007). aPa activates a protease-activated receptor type 2 (PAR-2) cleaved by a protease leading to expression and production of IL-8 (Tripathi, Abdi and Alizadeh, 2014).

Specific pore-forming proteins in *Acanthamoeba* have been identified and named acanthaporins, which are involved in the process of tissue destruction. These proteins form oligomeric pores through the shift from an inactive dimer to an active monomer via the protonation of histidine residues within the carboxy-terminal helix. It has also been proven that acanthaporins have cytotoxic effects in human neurons and for several bacterial strains combating its growth inside phagosomes (Michalek *et al.*, 2013).

Proteases produced by pathogenic strains of *Acanthamoeba* have been widely described during the last years; these use their proteolytic properties to penetrate and

dissolve the host tissue. Two proteases, a serine protease and a metalloprotease of 97 and 80 kDa, respectively, are upregulated until contact to host cells; but both of them depend on the mannose-binding (Cao, Jefferson and Panjwani, 1998).

During recent years, the close association between the microbiome of the ocular surface and *Acanthamoeba* has brought new updates for the development of AK. Intriguingly, a clinical study of *Acanthamoeba* trophozoites isolates from corneal biopsies, scrapings, buttons, CLs, and lens cases showed that the same patients harboured different bacterial endosymbionts such as *Pseudomonas* and *Mycobacterium* collected at different time points while *Acanthamoeba* isolated from different patients has similar endosymbionts. *Acanthamoeba* trophozoites that harbour endosymbionts show higher levels of cytopathic effects *in vitro* compared to isolates without any endosymbionts, so it was speculated that endosymbionts cell wall plays an important role stimulating the strong increase of proteases (Iovieno *et al.*, 2010). It is also believed that *Acanthamoeba* protects these endosymbionts from drugs and the adverse host environment for using them as possible pathogenic mechanisms, food supply or transfer of virulence genes. (Schmitz-Esser *et al.*, 2008; Henriquez *et al.*, 2020).

1.6.1.4 Immune response

Not only the damage to the corneal epithelium is responsible for AK, it has been proposed that the host immune system plays an important role influencing the development and severity of this infection (Nieder Korn, 2002). The wide-spread exposure of humans to this parasite was demonstrated by the frequency of anti-*Acanthamoeba* antibody titres in healthy populations and AK patients. 50 to 100 % of individuals with no clinical infection or AK showed specific antibodies against *Acanthamoeba* in a serological analysis of IgG and tear IgA (Clarke and Nieder Korn, 2006a). Curiously, the levels of these immunoglobulins were lower in patients that presented with AK compared to the healthy patients (Nieder Korn *et al.*, 1999; Nieder Korn *et al.*, 2002). The presence of tear IgA and the activation of the innate immune apparatus (macrophages, neutrophils and complement system) are known as the first defence line against AK (Cursons *et al.*, 1980; Walochnik *et al.*, 2001). The important role of macrophages was demonstrated in Chinese hamsters treated with liposomes containing clodronate to ablate their macrophages which were found to be unable to clear AK (van Klink *et al.*, 1996). An *in vitro* study showed a similar scenario

in neutrophils where these were depleted by the use of anti-neutrophil antibodies (Hurt *et al.*, 2001). Another *in vitro* study showed that trophozoites are killed by macrophages and neutrophils in the early stage of the infection, a situation that is enhanced with specific antibodies (Marciano-Cabral and Toney, 1998).

Oral immunization with *Acanthamoeba* antigens and a mucosa adjuvant in animal models has demonstrated the importance of mucosal immunity, especially the role of secretory IgA. During initial stages of AK, secretory IgA antibodies prevents the adhesion of trophozoites on the corneal surface, however this protection is unsuccessful after trophozoites have penetrated the corneal surface (Alizadeh *et al.*, 2001). This makes it clear that the IgA defence depends on the stage of the AK infection where diverse protective functions such as prevention of adhesion, interaction with neutrophils Fc α -receptors or complement cascade activation via alternative/lectin pathways are evoked (Feng *et al.*, 2015). Studies have been unsuccessful immunisation of pigs and Chinese hamsters against AK (Alizadeh *et al.*, 1995; Leher *et al.*, 1998a).

Acanthamoeba mostly causes clinical infections in the eye and the brain which both exhibit immune privilege meaning that they lack certain aspects or have reduced levels of the immune functions that operate in other anatomical sites. For example, the complement system is active but in low levels (Bora, Jha and Bora, 2008; Woodruff *et al.*, 2010). Activation of this system in AK infections is by specific antibodies against antigens on the surface of the trophozoites (classical pathway) or via mannosylated glycoproteins (alternative pathway). Elements of the alternative pathway such as C5, C6, C7, C8 and C9 damage the membrane causing lysis of the parasite (Ferrante and Rowan-Kelly, 1983). Furthermore, *Acanthamoeba* lacks of sialic acid in the membrane supporting the effective effect of alternative pathway against this amoeba since it has been proven that many pathogen microorganisms have sialic acid on its plasma membrane, which prevents the activation of alternative pathway immune response by the host (Ulsamer *et al.*, 1971). By contrast, pathogenic *Acanthamoeba* strains are able to express complement regulatory proteins that impair the complement cascade (Toney and Marciano-Cabral, 1998). The latter study was supported by the use of cytochalasin D (metabolic inhibitor) and PMSF (serine protease inhibitor), which blocked the expression of complement regulatory proteins increasing the vulnerability to lysis mediated via the complement pathway (Clarke and Niederkorn, 2006a).

Toll-like receptors (TLRs) are involved in the recognition of pathogen-associated molecular patterns (PAMPs) expressed in the infective forms of *Acanthamoeba*. For trophozoites, specifically TLR4 has been identified and when it is activated it leads to the release of cytokines and chemokines using two different signalling pathways: MyD88 (a signal transducing adaptor protein of myeloid differentiation protein 88) and TRIF (a Toll/Interleukin-1 receptor domain adaptor that induces IFN- β) (Ren and Wu, 2011). IL-6, 8, TNF α and other chemokines are activated by MyD88; while IFN- β and induced genes by IFN are activated by TRIF (Medzhitov *et al.*, 1998; Yamamoto *et al.*, 2002). A marked difference is the response time between the next two pathways: TLR4-MyD88 is activated during the early adhesion between *Acanthamoeba* and the human corneal cells; meanwhile TLR4-ERK1/2 (extracellular signal-regulated kinase pathways1/2) is activated some time afterwards (Ren and Wu, 2011). Clinical but not soil strains upregulate TLR4 producing chemokines such as TNF- α , CXCL2, and IL-8, the last two chemoattract polymorphonuclear leukocytes (PMN) to the infection site for protection, however, PMN inflict certain damage to corneal cells (Alizadeh *et al.*, 2014).

Studies in animal models showed that the adaptive response is induced in the form of delayed-type hypersensitivity (DTH) and IgG antibodies when immunised subcutaneously with trophozoites and cysts of *Acanthamoeba* (Clarke and Niederkorn, 2006a). Recently, an important role for Th17 cells in adaptive protection in AK has been proposed as high levels of IL-17 and neutrophils were found in a murine model diminishing the symptoms and severity of the infection (Suryawanshi *et al.*, 2015).

Persistent stages of AK showed ischemic inflammation in the retina of four patients with absence of trophozoites or cysts giving rising to an interesting molecular mimicry theory known as epitope spreading (Awwad *et al.*, 2007). On these kind of events, subpopulations of T and B cells diversify multiple epitopes in order to obtain higher antigen specificity than those that induced the first antigen exposure in chronic autoimmune diseases or inflammatory responses (Cornaby *et al.*, 2015). Histopathologic samples of the four patients supported this theory revealing inflammatory retinal lesions such as thrombosis of the retinal arteries, perivascular lymphocytic infiltration, and ischemia, all of them classical features of DTH injuries. Ultimately, a recent report in murine models infected with the pathogenic strain *A. castellanii* showed cross-reactive T cells process that recognized myelin antigens

resulting in a CNS autoimmune disease developed on the mice, confirming the potential *Acanthamoeba* antigens molecular mimicry which suggests that a normal process of AK infection might culminate with a strong T cell-dependent immune-mediated process of the retina and potentially in the brain (Awwad *et al.*, 2007; Massilamany *et al.*, 2014).

1.6.1.5 Laboratory Diagnosis

Appropriate diagnosis in AK infection is eventually delayed due to the lack of suspicion and familiarity by clinicians, in addition it is an infection that present similar symptoms to those caused by bacteria, virus or fungus, making AK infection frequently misdiagnosed (Sánchez *et al.*, 2016). If the infection is not diagnosed within 3 weeks, the prognosis exacerbates; therefore, it is recommended to consider AK infection in patients with corneal trauma associated with recent aquatic or soil activities and chronic history of keratitis that failed to respond to bacterial, viral or fungal keratitis first- line treatment (Dart, Saw and Kilvington, 2009).

It has been established that the definitive diagnosis of AK infection is using culture media or histology as well as the identification of *Acanthamoeba* DNA by PCR (Bouheraoua *et al.*, 2014). The standard protocol for the identification of bacterial and fungal keratitis has been applied to *Acanthamoeba* with some minor modifications including microscopic analysis of eye smears and inoculation of scraped samples in culture media or on *Escherichia coli*-seeded non-nutrient agar (Sharma *et al.*, 2002; Duarte *et al.*, 2013). It is important to maintain incubated the collected specimen samples at least 3 weeks before to set a negative infection verdict (Dart, Saw and Kilvington, 2009). The sensitivity is relatively low from 7 to 52% and sometimes it needs longer incubation times (Kokot *et al.*, 2012).

Sometimes a corneal biopsy is needed in patients with profound infiltrate and negative results in corneal scrapings. The most common staining procedures use Giemsa, fluorescein-conjugated lectin, haematoxylin, and eosin (Robin, Chan and Andersen, 1988; Byers, Hugo and Stewart, 1990). For cysts it is suggested to use smears stained with calcofluor-white or Gram stain (Wilhelmus *et al.*, 1986). Use of indirect fluorescent antibody test (IFA) or indirect immunoperoxidase assay (IPA) are the most described immunostaining procedures on corneal tissues (Garg, Kalra and Joseph, 2017).

PCR identification of *Acanthamoeba* showed 84% sensitivity and 100% specificity; although it suggested that statistical results have been equivalent between culture and PCR (Page and Mathers, 2013; Kowalski *et al.*, 2015).

The use of the 18S rDNA gene in a molecular method of diagnosis of AK has been tested. This method is called Loop-mediated isothermal amplification and is fast (2-3 hours less than PCR), highly specific, sensitive and affordable, especially in situations where time is critical (Mewara *et al.*, 2017).

One of the non-invasive diagnostic imaging techniques occasionally used during the last decade is confocal microscopy (CM), which is considered by the American academy of ophthalmology as a potent resource of immediate diagnosis; especially in cases of fungal or *Acanthamoeba* keratitis with 90% of specificity and sensitivity (Kaufman *et al.*, 2004). Trophozoites are visualised as ovoid structures reflecting their roundness and cysts clearly show the double-wall (Winchester *et al.*, 1995). *In vivo* tandem-scanning CM (IVCM) using corneal smear and corneal culture showed 91% sensitivity and 100% specificity; even so, it is only recommended for the detection of *Acanthamoeba* in deep corneal infiltrates that are inaccessible by scraping (Tu *et al.*, 2008). To achieve an accurate diagnosis, the patient should remain calm, which is difficult to accomplish in severe painful AK. In addition, the observer needs to be experienced (Hau *et al.*, 2010). Another diagnostic technique is specular microscopy, which is an *in vitro* non-invasive photographic technique assisted by a computer that analyses the cell density, morphology and population of the corneal endothelium where refractile granular aspects of *Acanthamoeba* can be observed (Illingworth and Cook, 1998).

1.6.2 Granulomatous Amoebic Encephalitis (GAE)

Amoebic encephalitis is a fatal disease of the CNS caused by pathogenic FLA commonly in immunocompromised individuals (post transplantation, HIV infection), but cases in immunocompetent have also been described (Aparicio *et al.*, 2021; Lee *et al.*, 2021). *Naegleria fowleri* accounts for Primary Amoebic Meningoencephalitis (PAM) and *Acanthamoeba* or *Balamuthia* are the causative agents of Granulomatous Amoebic Encephalitis (GAE) (Callicott *et al.*, 1968). Both diseases are distinguished by their risk factors, route of entrance, clinical features and lab diagnosis but the differential feature is the duration of the illness: PAM is a sharp infection that is able to kill the host within 48-72 h while GAE is subacute to chronic disease that can last

months and has a 90% of mortality (Ong, Khan and Siddiqui, 2017; Duggal *et al.*, 2018). (Jager and Stamm, 1972) analysed the first case of GAE by *Acanthamoeba* in 1972 in a patient with Hodgkin's disease. In general, *Acanthamoeba* goes through the brain via the bloodstream, it is able to cross the blood-brain barrier (BBB) targeting the tight junction proteins, then cause a great damage to the brain by the release of parasite-derived toxins and proteases (Khan and Siddiqui, 2009; Kristensson, Masocha and Bentivoglio, 2013).

1.6.2.1 Clinical features

Clinical symptoms of GAE are similar to the viral, bacterial infections, neurocysticercosis or tuberculosis meningitis: headache, fever, personality changes (confusion, irritability, hallucinations, dizziness), hemiparesis, fatigue, visual disturbances, neck pain, aphasia, ataxia, nausea and vomiting, cranial nerves paralysis, seizures and eventually death (Carter *et al.*, 1981; Martinez and Janitschke, 1985; Martinez, 1991). Post-mortem examination shows severe oedema and haemorrhagic necrosis in the occipital, parietal, temporal, or frontal lobes. The classical lesion in the parenchyma of CNS it's a subacute necrotizing encephalitis or a chronic granulomatous where the trophozoites or the cysts are usually found in association with giant cells (Naveed, 2015).

1.6.2.2 Epidemiology

There are several reasons that makes uncertain the accurate number of cases reported in GAE infections. This is due to lack of diagnostic experience, proper healthcare equipment, monitoring, lack of awareness about this disease in clinicians, low autopsy rates and underrecognized globally (Visvesvara, Moura and Schuster, 2007). The period of incubation is hypothesized to be around 10 days, most of the cases have occurred between the 20 and 40 years and 10 times more in men (Vyas *et al.*, 2013).

Globally, more than 400 cases of GAE have been reported with only 2-3% of survival. The relation GAE-HIV/AIDS helped in the past to indicate and set an statistic approach to yield a rate of 1.57 encephalitis deaths per 10,000 HIV/AIDS deaths in USA (Naveed, 2015). A recent update that displays the predilection sites in the brain by FLA examined 86 cases from 1968 to 2016 available in PubMed, where 46 cases were GAE due to *Acanthamoeba* spp. reviewed in 35 publications and up to 90%

were generated in USA. In summary, the frontal lobe, parietal lobe, temporal lobe, and occipital lobe were damaged most in cases of GAE. A report of protozoan coinfection that involves a neurotoxoplasmosis case complicated for GAE of *Acanthamoeba* and *B. mandrillaris* in a HIV patient supports that these infections take advantage of the immunocompromised nature of the host (Pietrucha-Dilanchian *et al.*, 2012). A fatal report in a kidney transplanted case clearly shows a disseminated infection of GAE which made *Acanthamoeba* a subcategory 1c as emerging disease (Chua and Gubler, 2013; Salameh *et al.*, 2015).

Corticosteroids have a harmful impact on the treatment of GAE since not only reduce the inflammation but is able to decrease the immune system response, facilitating infections and diseases. In fact, people with autoimmune diseases such as lupus erythematosus previously treated with corticosteroids have been reported with *Acanthamoeba* coinfections (Duggal *et al.*, 2018).

1.6.2.3 Pathogenesis

Until now the precise pathogenic mechanisms by which *Acanthamoeba* reach the brain are still unclear but has been suggested that great damage is principally caused by the amplified host immune response rather than own *Acanthamoeba* factors (Baig, 2015). Generally, trophozoites enter to the extracellular spaces taking advantage of wounds in the skin or via the nose, air sinuses lungs, nasal olfactory mucosal as well as the corneal epithelium followed by hematogenous spread reaching the BBB reaching the CNS, which finally leads to neural damage and brain dysfunction (Khan, 2015).

Trophozoites MBP has also a role in GAE infection binding to human brain microvascular endothelial cells which activates Rho-associated intracellular signalling leading to phosphorylation of myosin light chains which causes disturbances on the tight junctions and cause an elevated permeability of BBB (Alsam *et al.*, 2003). Liberation of serine proteases induce the degradation of the zona occludens type 1 (ZO-1) and occludin, collagen type I, III, IV, elastin, fibronectin, antibodies such as IgG, IgA, Hb which increases permeability of the basement membrane (Khan and Siddiqui, 2009). Additional factors are ecto-ATPases and caspase-3 activation. The neuraminidase activity has been associated with modifications in glycolipids being relevant in the colonization of the amoeba. Specific dismutases were identified: 50 kDa iron superoxide dismutase helps in antioxidant defence and a 38 kDa copper-

zinc superoxide dismutase. Plasmin generated from aPa activates the production of metallo-proteinases yielding degradation of the basement membrane. Hydrolytic enzymes (elastases, phospholipases, glycosidases) and metalloproteases (serine, cysteine) produce tissue degradation and invasion, migration, cytoadherence and evasion of host responses. Cell cycle arrest has also been observed when pRB phosphorylation is inhibited in human brain microvascular endothelial cells. Phagocytosis and digestion of the nervous tissue are done by the amebostomes and proteases, respectively (Visvesvara, Moura and Schuster, 2007). It is feasible that *Acanthamoeba* promote the increase of intracellular calcium ions in host nervous cells (Naveed, 2015).

Two proposed routes based on histopathological findings might answer the puzzle on why the systemic and neurological symptoms appear long after the infection occurs. These routes are trans endothelial route and the rete vasorum. In the trans endothelial route, trophozoites begin a contact with endothelial glycocalyx, common site where the amoebas come across with platelets, hence the potential formation of thrombi and the development of vasculitis. The trophozoite contact uses MBP and LBP to ligand endothelial cells adhesion molecules such as P-selectin/L selectin, intercellular adhesion molecule-1 (ICAM-1 or CD54) which binds to human leukocytic alpha integrins (CD11a/CD11b). CD11a/CD11b integrins are known to promote the trans-endothelial migration through the veins. Analysis *in silico* have revealed an integrin- α FG-GAP repeat containing protein surface alpha integrin homologous on *Acanthamoeba spp.* supporting the fact that trophozoites might use this integrin opportunely when a wound is provoked, next the amoebas cross and have access to blood vessel walls. On this stage, the leukocytes build up a wall-off against trophozoites. *Acanthamoeba* counterattack evading the immune response by means of its particular ameboid locomotion, the production of extracellular toxins or cytotoxic enzymes, metalloproteinases or pore-forming toxins (Baig and Khan, 2015).

Following a tropism targeting oxygen-rich areas and neuronal tissue; it is hypothesized that *Acanthamoeba* take advantage of the rete-vasorum, the small vascular channels into the thick vessel walls of the brain. On this way, trophozoites would not damage the BBB and would end up in an external area to the endothelium very close to neurons. On this site *Acanthamoeba* evades the complement immune response, however leukocytes halt them forming aggregations which is consistent with the lesions of these type observed in the biopsies. It is possible that

Acanthamoeba is restrained in the halfway of the cerebral artery when selects the rete vasorum route which would explain why long-time lapses between the onset of the disease and the manifestation of clinical symptoms since the halfway cerebral artery is far away from the brain (Baig, 2015).

1.6.2.4 Immune Response

As we know, it is established that previous exposure to *Acanthamoeba* appears to be usual since the presence of antibodies in serum samples have been demonstrated in asymptomatic healthy people (Cerva, 1989). This is supported with the activation of the type IV hypersensitivity reaction (HSR) against the amoeba which is a classical pattern for antigens that have been previously exposed (Baig, 2015). Immune response succumbs to *Acanthamoeba* mainly because its big size (around 12-25 μm) leading to the inability of being phagocytized by the host leukocytes as well as opsonization is not another option (Cerva, 1989). The immune response among *Naegleria*, *Balamuthia* and *Acanthamoeba* as a cause of CNS infection is completely different. In *Acanthamoeba* spp. macrophages, monocytes, eosinophils, and lymphocytes encircle the blood vessels walls which develop a granulomatous inflammatory injury in 2-3 weeks. An effort of the body to contain the dissemination of these protists known as “substantial tissue destruction” is started: the immune cells wall-off trophozoites lead to epithelioid cells and produce lytic enzymes trying to halt and kill these infective cells in immunodeficient hosts. In the case of immunocompetent hosts, this response is driven by the T-cell immunity (Baig, 2014). Several *in vitro* studies have showed the severe damage caused by enzymes in tissue and BBB co-culturing FLA with different cell lineages such as human microvascular endothelial cells (HBMEC), macrophages and leukocytes (Cerva, 1989; Marciano-Cabral and Cabral, 2003). Suppressing the immune system with Tetrahydrocannabinol (THC) in animals previously treated with corticosteroids, methylprednisolone, tetracycline and then infected via nasal route with *A. castellanii* showed a high rate of mortality compared with untreated ones (Marciano-Cabral and Cabral, 2003). Important parameters such as sluggish movement and chemokine driven specific ligand-receptor in the deeper cerebral tissue helps to combat the circulation and attach to endothelium which reacts with an apparent movement of “retraction-contraction” which let to trophozoites invade the vessel walls. To emphasize, the parasitic infection, the strong immune response caused by cytokines, and the high

pressure of the circulating blood act together to let the amoebas breach the BBB and reach the brain (Baig, 2015).

1.6.2.5 Laboratory diagnosis

Computed tomography (CT) commonly generates single or multiple lesions in the cerebral cortex, basal ganglia, subcortical white matter, cerebellum, and pons. Conversely magnetic resonance imaging (MRI) may show multifocal lesions, intense ring like pattern in diencephalon, thalamus, brain stem, and posterior fossa structures. Necrotizing angiitis produces haemorrhagic lesions which are important signs in the identification of severe cases of GAE (Duggal *et al.*, 2018). The microscopy findings in cerebrospinal fluid (CSF) are not specific which frequently show a high number of PMN leukocytes, elevated protein or glucose concentration and a reduced cloudiness as well as the amoeba is often mistaken for monocytes, PMN leukocytes and especially macrophages. In order to avoid the death of trophozoites or cysts and make possible the microscopy observations, is important to centrifuge specifically at 250 f for 10 minutes (Naveed, 2015). Whether it is possible to obtain CSF or cerebral biopsy material, inoculation on solid media is recommended with substrate (bacteria, yeasts, or other protozoa) to promote the parasites growth which can be observed after 12 h to up to 7 days depending on the quantity of amoebae present in the sample. Interestingly, blood and chocolate agar are useful media for culturing *Acanthamoeba* spp. trophozoites since AK has shown important symbiosis with many pathogenic bacteria (List *et al.*, 2021). The classical medium for growth of *Acanthamoeba* spp. axenically is done from Peptone-Yeast-Glucose media (PYG) or Nelson's media added with foetal calf serum or brain extract. This should not be used for purposes of virulence studies, conversely the amoebas have been passed to lab animal models such as mice, monkeys, *Locusta*, *Drosophila*, or mammalian cells lines like E6 monkey kidney cells, human embryonic lung cells, etc. It is important to know that only the detection of antibodies is not enough to guarantee a GAE diagnosis since as mentioned before, healthy population may react to this disease even with low titres of antigen. Therefore, high levels of antibodies are expected in serum patients where the use of indirect immunofluorescence (IIF) assays is an important diagnostic tool based in the incubation with fluorescein isothiocyanate (FITC)-labelled antihuman antibody with the consequent visualization under fluorescence microscope (Duggal *et al.*, 2018).

Histopathological samples examination has been key in the detailed description of GAE since the first reports of this fatal disease. Lesion in basal ganglia, midbrain, brainstem, and cerebral hemiparesis are common. Additionally, necrosis and haemorrhage, encephalomalacia, fibrinoid necrotizing panarteritis, thrombosis, perivascular centrifugal granulomas, PMN, lymphoplasmacytic inflammatory infiltrate, foamy macrophages, and multinucleated giant cells are observed in sections of the brain embedded in paraffin or frozen. Stains like Giemsa-Wright, acridine or calcofluor white stain make easier the identification of *Acanthamoeba*. A specific diagnostic tool is immunohistochemistry but the chromogen anti-*acanthamoeba* are not readily available (Khan, 2006b).

PCR and real-time PCR are useful molecular techniques when the amoeba is difficult to identify, however, a novel modality real time fast duplex TaqMan® PCR is able to find out and discern between 10 different genotypes of *Acanthamoeba* ATCC strains (Goldschmidt *et al.*, 2009). Further interest in the identification of the relation among isolates is carried on with isoenzyme electrophoresis or restriction fragment length polymorphism (RFLP). Sometime long ago the metabolic gene cytochrome oxidase (COI-gene) has been used to determine the genus and the genotype with only using a single primer (Crary, 2012). Multiple samples and assays are needed to differentiate GAE from neurocysticercosis, toxoplasmosis, fungal granuloma, emboli, abscesses, among others. In summary, microscopy and culture remain as the gold standards methods of GAE diagnostic (Duggal *et al.*, 2018).

1.7 Treatment for *Acanthamoeba* spp. infections: AK, GAE and cutaneous lesions.

Elimination of trophozoites/viable cysts and rapid resolution of the symptoms caused by *Acanthamoeba* spp. infections are the main goals of the medical therapy. Nonetheless, management of patients with AK, cutaneous amoebic lesions and GAE still remain challenging due to the limitations with the current therapeutic drugs. Until now, no commercial drug has been approved by the U.S. Food and Drug Administration (FDA) to treat *Acanthamoeba* infections, but a wide variety of therapeutic agents are used as monotherapy or combinatory therapy to treat these infections (Rice *et al.*, 2020a). The current treatment for AK comprises combinational therapy of 0.1% propamidine isethionate plus chlorhexidine (0.02%-0.2%) or polyhexamethylene biguanide 0.02%-0.06% (topical) with or without any antibiotics (neomycin), azoles or other amidines (Rice *et al.*, 2020a). In the case of GAE, different

combinatory therapies have been proposed, however rifampicin, trimethoprim-sulfamethoxazole and fluconazole are the basis (Taravaud *et al.*, 2021). For cutaneous lesions the treatment that has been proved to be efficacious is the combination of amphotericin B, pentamidine isethionate, chlorhexidine gluconate, 5-fluorocytosine, fluconazole, itraconazole, ketoconazole, azithromycin, clarithromycin, sulfadiazine, and pyrimethamine (Rice *et al.*, 2020a). Many of these combinations have been derived empirically and their efficacies are poor especially in treating GAE which is almost always fatal.

A substantial number of chemotherapeutics have shown their potential effect against specific targets in *Acanthamoeba* spp., among which gene products, processes such as DNA transcription or translation and cell components like cell membrane have been previously described (Roberts and Henriquez, 2010). In this context, a classification of chemotherapeutics employed clinically or experimentally so far against *Acanthamoeba* spp. is feasible based on the drug target and its mechanism of action against AK, GAE or cutaneous amoebic lesions. These drugs consist of biguanides, diamidines, azoles, antiseptics, antibiotics, alphaphosphocolines, photodynamic agents, etc (Table 1). Most of the drugs included in the antiacanthamoebic groups have been tested *in vitro* or *in vivo* yielding discrepant results among research groups caused by the lack of standardisation in experimental features such as the strains and assay conditions (Ahmed *et al.*, 2021). Considering the aforementioned, herein the most updated clinical findings and *in vitro/in vivo* results for drug efficacy against *Acanthamoeba* infections are presented:

1.7.1 Biguanides

Biguanides derivatives such as polyhexamethylene biguanide (PHMB) and chlorhexidine gluconate are cationic compounds generally used as disinfectants, antiseptics, and preservatives. It is believed that the great biocidal activity of PHMB is due to its long chain length which make it non-volatile and chemically stable which produces a long-term effect (Kenawy, Worley and Broughton, 2007). In the case of clorhexidine, the activity depends on the pH and concentration (Carrijo-Carvalho *et al.*, 2017). These compounds target and disintegrate membrane of *Acanthamoeba* spp., hence internalisation occurs with consequent dense precipitates on the cellular surface and eventually leakage of intracellular content (Khunkitti *et al.*, 1998; Lee *et al.*, 2007). Swelling in the wall of cysts followed by internalisation via the opercula,

appearance of lipid vesicles, denaturation of α -helix proteins and nuclear fragmentation have also been observed by microspectroscopy (Rusciano *et al.*, 2013). Biguanides have been used as first-line therapy for AK as an eye drop solution with an initial dosing for both PHMB and chlorhexidine gluconate of 0.02% with a potential increase in refractory cases to 0.06% for PHMB and 0.2% for chlorhexidine gluconate (Maycock and Jayaswal, 2016; Carrijo-Carvalho *et al.*, 2017). Commonly PHMB and chlorhexidine gluconate are prescribed together while other clinicians choose PHMB plus hexamidine (diamidine) because their synergy is more effective and non-toxic (Seal, 2003). Reports have shown both PHMB and CLX to have potent biocide effects against trophozoites and cysts *in vitro*. PHMB has shown to be trophocidal at 3.9 $\mu\text{g/ml}$ and a minimum cysticidal concentration at 2.37 $\mu\text{g/ml}$ (Lee *et al.*, 2007; Heaselgrave *et al.*, 2019). Chlorhexidine gluconate was identified as trophocidal at a concentration of 10 $\mu\text{g/ml}$ and a minimum cysticidal concentration of 7.02 $\mu\text{g/ml}$ (Lee *et al.*, 2007; Alizadeh, Neelam and Cavanagh, 2009). A comparative clinical study between PHMB 0.2% and chlorhexidine gluconate 0.02% eye drops as monotherapies in 56 eyes infected with AK of 55 patients concluded that both agents acting alone produce good outcomes (78% and 85.7 % keratitis cases resolved with PHMB and chlorhexidine gluconate, respectively) with few of them requiring surgical procedures, specifically those treated with PHMB (Lim *et al.*, 2008).

Alexidine is another biguanide present in contact-lenses solutions with an inhibitory effect against pathogenic strains of *Acanthamoeba*, nevertheless it requires higher concentrations than chlorhexidine gluconate to achieve cysticidal effects as further investigations against other isolates are suggested (Alizadeh, Neelam and Cavanagh, 2009).

1.7.2 Diamidines

Aromatic diamidines are a class of compounds with broad antimicrobial spectrum. Propamidine and hexamidine are the most representative diamidines that have been proven to be effective against *Acanthamoeba* infections (Maycock and Jayaswal, 2016). It has been proposed that biocide activity of diamidines involves electrostatic interaction with lipids in plasma membrane which leads to increased permeability and consequently leakage of cell content and denaturation of intracellular proteins (Perrine *et al.*, 1995). Additionally, propamidine binds reversibly to rich Adenine-Thymine (AT) regions in the DNA minor groove (Jenkins and Lane, 1997)

and inhibits the enzyme S-adenosyl-L-methionine decarboxylase affecting the polyamine metabolism leading to encystment (Hugo and Byers, 1993). Other biomolecules are suspected to be targeted by diamidines such as ion channels, enzymes, DNA/RNA/protein-protein interactions, etc (Huang, Mayence and Vanden Eynde, 2014).

To treat AK, the diamidines propamidine isethionate (Brolene, Patheon UK Ltd., Swindon, UK or hexamidine (Desomedine, Chauvin Laboratory, Montpellier, France) infections (Maycock and Jayaswal, 2016) are commonly used. *In vitro* and clinical reports suggest propamidine is highly effective as trophocidal and cysticidal. Trophocidal concentration range for propamidine is reported to be as low as 15.6 µg/ml and as high as 1000 µg/ml in various *in vitro* assays. The minimum *in vitro* cysticidal concentration has been reported to be as low as 250 µg/ml and as high as 421 µg/ml (Pérez-Santonja *et al.*, 2003; Heaselgrave *et al.*, 2019). Clinically, it is best used synergistically in conjunction with PHMB where it has been shown to improve the visual acuity of the total of AK cases ($\geq 79\%$) (Duguid *et al.*, 1997) and as propamidine in solution at 0.1% with neomycin achieving a successful AK resolution of AK in 50 of 60 eyes (83%) of patients (Hargrave, McCulley and Hussein, 1999). Hexamidine has previously been used as trypanocidal agent. Hexamidine was successfully used for the first time as topical 0.1% against *Acanthamoeba* due to recalcitrant AK treated with propamidine (Brasseur *et al.*, 1994). Hexamidine have shown trophocidal (7.5 µg/ml to 31.3 µg/ml) and cysticidal (222 µg/ml and 250 µg/ml) effects *in vitro* (Alizadeh *et al.*, 1997; Pérez-Santonja *et al.*, 2003; Heaselgrave *et al.*, 2019). Pentamidine is also used to treat trypanosomiasis, leishmaniasis and pneumonia caused by *Pneumocystis* in immunocompromised patients (Miller *et al.*, 1996; Barrett and Croft, 2012). Despite the lack of clinical evidence of pentamidine isethionate as treatment against AK, *in vitro* studies suggest a potent effect against trophozoites ATCC 50492 when used with liposomal carriers (Siddiqui *et al.*, 2009).

1.7.3 Antifungal agents

Amphotericin B is a polyene antifungal agent commonly used for AK management, however clinical data and case reports are limited. It binds irreversibly to ergosterol in pathogens which causes the formation of a transmembrane channel leading to ion leakage with consequent cell death (Siddiqui, Aqeel and Khan, 2016). *In vitro* evidence has elucidated *Acanthamoeba* spp. tend to be resilient to

amphotericin B allowing the amoebas to return to an initial level of susceptibility over time (Taravaud, Loiseau and Pomel, 2017). It was reported that Amphotericin B has an inhibitory concentration ranging from 1-100 µg/ml against *A. castellanii* and *polyphaga* (Nagington and Richards, 1976). The similarity between fungal and *Acanthamoeba* cell membrane components, specifically ergosterol was the main reason this compound have been used to resolve AK; however, its use is limited due to toxicity (Austin, Lietman and Rose-Nussbaumer, 2017). Despite the successful treatment of fungal keratitis or CNS infections such as *Arthrographis* keratitis, *C. albicans* meningoencephalitis or cryptococcal meningitis using amphotericin B, its efficacy against *Acanthamoeba* is questionable. Clinically patients treated with Amphotericin B in combination with other agents for GAE survived had only a 23% survival, however it is difficult to deconvolute the contribution of each of the drugs used in these multi-drug treatments (Taravaud *et al.*, 2021). Amphotericin B also has poor penetration to the BBB (Shing *et al.*, 2021; Taravaud *et al.*, 2021). Furthermore some laboratories have routinely propagated *Acanthamoeba in vitro* in the presence of Amphotericin B as an antifungal (McBride *et al.*, 2005).

Natamycin is an antifungal agent that also binds to ergosterol which prevents membrane fusion and fission due to the inhibition of ergosterol-dependant fusion of vacuoles (Siddiqui, Aqeel and Khan, 2016). The effect of both amphotericin B and natamycin is amoebostatic rather than amoebicidal, therefore higher concentrations are required resulting in side effects and drug resistant strains. However, natamycin 5% and 0.5% have been demonstrated as cysticidal against 56 *Acanthamoeba* non-axenic isolates *in vitro* (Sunada *et al.*, 2014). Additionally, natamycin 1% has been used as an ointment as part of combinatory therapy with 0.02% chlorhexidine gluconate where AK cases were gradually improved in a week (Kitagawa *et al.*, 2003). The role of natamycin is again difficult to establish when used in combination with other drugs.

1.7.4 Azoles

Azoles are a type of antifungal agents that target 14- α demethylase (CYP51), which is an essential cytochrome P450 enzyme that converts lanosterol to ergosterol which is an important constituent of *Acanthamoeba* membranes (Sheehan Daniel, Hitchcock Christopher and Sibley Carol, 1999). These azole compounds have been widely used as treatments against *Acanthamoeba* infections since the amoeba 14- α

demethylase shares 31-35% of sequence identity to fungal enzyme and are well tolerated (Lamb *et al.*, 2015). Imidazoles e.g., clotrimazole, miconazole and ketoconazole and triazoles e.g., itraconazole, fluconazole and voriconazole have been shown to have effective amoebicidal and cysticidal properties against *Acanthamoeba* spp., notwithstanding they should be required to be topically applied since poor penetration in the corneal epithelium has been demonstrated (Moiseev *et al.*, 2019). Hence, it has been reported that these compounds have improved bioavailability when used as adjunctive to surgical interventions where the cornea has been disrupted (Shing *et al.*, 2021).

Clotrimazole has been proven to be trophocidal and cysticidal as monotherapy, however its clinical efficacy in clearing AK cases is noted in combination with other drug agents. Regarding *in vitro* evidence, this compound impacted the trophozoites motility with concentrations ranging 50-100 µg/ml and high concentration of the drug are required to reach the minimum cysticidal concentration (>500 µg/ml) (Duma and Finley, 1976). Clotrimazole in combination with propamidine has been reported to be used as primary therapy against AK. Following this, in a study reporting four cases of patients with AK treated with 1% clotrimazole with topical neomycin sulphate-polymyxin B sulphate-gramicidin and propamidine isethionate, clotrimazole was well tolerated (Driebe *et al.*, 1988; Lin *et al.*, 2009).

Miconazole is an antifungal agent with unclear efficacy *in vitro* and clinical effects against AK. This compound was reported to display a trophocidal effect ranging from 10-100 µg/ml and a minimum cysticidal concentration of 1000 µg/ml *in vitro* (Nagington and Richards, 1976). However, in contrast more recently it was reported that 1% miconazole did not have any substantial effect against cysts (Saunders *et al.*, 1992). Patients infected with AK have been successfully treated with a combinatory therapy including miconazole 0.1% and 150 mg oral itraconazole (Ishibashi *et al.*, 1990).

Ketoconazole is a common prescribed azole to treat AK. The effectiveness of ketoconazole has been proven as part of combinatory therapy with 50 mg administered orally in conjunction with 0.02% chlorhexidine gluconate, which also resolved corneal inflammation (Demirci *et al.*, 2006). Another combinatory therapy consisting of 200 mg daily oral ketoconazole, topical 0.02% chlorhexidine gluconate hourly, ciprofloxacin every 4 h and 1% atropine cleared AK in patients within a week, however recurrent infection was recorded (Wynter-Allison *et al.*, 2005). In rabbits, the

bioavailability reached high concentrations of ketoconazole when administered either topical or orally with potential improvement following debridement or keratoplasty (Hirst *et al.*, 1984; Hemady, Chu and Foster, 1992).

Itraconazole is considered a new azole with a broad-spectrum antimicrobial, however it has shown minimal inhibitory effects *in vitro* but promising clinical effects against AK (Shing *et al.*, 2021). *A. castellanii* was minimally susceptible to itraconazole with an IC₅₀ 20.14±4.93 µM compared with *A. polyphaga* and *A. palestinensis* displaying IC₅₀ 3.311±0.69 µM and 0.502±0.11 µM, respectively. Despite poor bioavailability when applied topically, 150 mg oral itraconazole in conjunction with 0.1% topical miconazole and debridement improved 3 patients with AK with no apparent recurrent infection (Ishibashi *et al.*, 1990; Kaur, Rana and Singh, 2008).

Fluconazole is a common azole with broad-spectrum antimicrobial that have shown minimal activity against *Acanthamoeba* but with high bioavailability in the cornea. This compound has been reported as a weakly trophocidal with a minimum inhibitory concentration of 64 µg/ml (Lamb *et al.*, 2015). To note, fluconazole improved the antiamebic effect when conjugated with gold nanoparticles compared but not silver nanoparticles (Anwar *et al.*, 2018; Anwar *et al.*, 2019). The corneal bioavailability has been assessed in rabbit models (20 mg/kg via oral) and humans (0.2% via topical), showing considerable concentrations in ocular tissues and aqueous humour (O'Day *et al.*, 1990; Abbasoglu *et al.*, 2001). In a case report, 300 mg of fluconazole administered orally daily over 8 weeks with cryosurgery resolved AK in a woman patient (Amoils and Heney, 1999).

Voriconazole is considered an alternative antifungal agent to be prescribed when patients with fungal infections when these are not resolved with other antifungal therapies. There are conflicting data regarding its trophocidal and cysticidal *in vitro* effects. However, it has been successfully used in patients as part of combinatory therapy. Bioavailability in animal and human cornea have been demonstrated (Shing *et al.*, 2021). The minimum inhibitory concentration of voriconazole against trophozoites ranged 1-2 µg/ml. Initially, minimum cysticidal concentrations of voriconazole were reported for clinical isolates (33.13 ± 22.83 µg/mL) and cell culture strains (46.25 ± 23.26 µg/mL), however, another study reports 200 µg/mL or even an antagonistic effect when used with chlorhexidine gluconate and propamidine (Iovieno *et al.*, 2014a; Gueudry *et al.*, 2018; Talbott *et al.*, 2019). Efficacious corneal

penetration has been reported for rabbit models (10 µg/mL topical) and for humans (1% eye drops) (Sponsel *et al.*, 2006; Lau *et al.*, 2008).

Isavuconazole and Posaconazole are new generation azoles that have been proven to be cysticidal against *Acanthamoeba* spp. (Shing *et al.*, 2021). Isavuconazole is trophocidal with an IC₅₀ of 4.65 nM and a minimum cysticidal concentration of 70 µM, additionally excystation was not observed making this antifungal an important alternative for recurrent AK cases (Shing *et al.*, 2021). Amoebicidal effect was further confirmed testing the prodrug isavuconazonium displaying an IC₅₀ of 0.09±0.02 µM (Rice *et al.*, 2020b). Although these results seem promising, another study found isavuconazole just amoebostatic and not cysticidal (Brunet *et al.*, 2020). Conflicting results *in vitro* for posaconazole have also been demonstrated. Recently, potent inhibitory effects of posaconazole were estimated as 3 - 7.5 nM depending upon strain of *Acanthamoeba* examined. However, cysticidal effect of this drug at 200 µM could not be reproduced from another study reporting 43.75 ± 25.04 µg/mL for clinical strains and 52.5 ± 23.75 µg/mL for cell culture strains (Iovieno *et al.*, 2014b; Shing *et al.*, 2021). No clinical evaluations about the bioavailability or corneal penetration of isavuconazole and posaconazole to treat AK have been reported.

1.7.5 Antiseptics

Povidone-iodine is an iodophor that penetrates pathogens and oxidize cell components such as intracellular proteins and inhibits synthesis of nucleic acids leading to death (Lepelletier *et al.*, 2020). Due to its adaptation in CL, this agent has been characterised as trophocidal and cysticidal in recent years. PI 0.1% was reported to be cysticidal against 56 different *Acanthamoeba* spp. clinical isolates. A further study showed ~80% cysticidal inhibition and totally trophocidal with PI 0.25% (Sunada *et al.*, 2014; Shing *et al.*, 2021). Other reports conflict with these results, however this is likely due to strain differences and testing conditions (Lim, Coster and Badenoch, 2000; Pelletier *et al.*, 2011). Still, efficacy of this agent should be standardised among research groups and in the clinic to eventually validate this agent as a potential AK treatment.

Acriflavine and proflavine are anionic biocides that bind to nuclear and cellular membrane, perturbing the membrane associated proteins compromising its integrity (Khan, 2015). Both have shown an apparent activity against *Acanthamoeba* spp.

trophozoites and cysts. Acriflavine hydrochloride and proflavine hemisulphate were trophocidal and cysticidal at 100 µg/ml and 1000 µg/ml, respectively (Nagington and Richards, 1976).

1.7.6 Phospholipid analogues

Miltefosine is a heterocyclic alkyl phosphocholine agent previously used for topical treatment of skin metastases and anti-leishmaniasis which has displayed cytotoxic effects against AK and GAE (Shing *et al.*, 2021). This compound induces apoptosis-like cell death by inhibiting proteinase kinase B (Siddiqui, Aqeel and Khan, 2016). An early *in vitro* study revealed a weak active effect at 24 h with minimal trophocidal concentration for *A. castellanii* and *A. lugdunensis* of 62.5 and 500 µM, respectively (Mrva *et al.*, 2011). Conversely, a recent report elucidated miltefosine as cysticidal at a minimal concentration 2.42 mM for genotypes T4 and T5, although for T3 the MCC was 38.72 mM (Chao *et al.*, 2020). In the clinic, miltefosine has been demonstrated to resolve AK cases when administered orally at 50 mg (Tavassoli *et al.*, 2018; Heaselgrave *et al.*, 2019; Hirabayashi, Lin and Ta, 2019; Naranjo *et al.*, 2020; Avdagic *et al.*, 2021; Thulasi *et al.*, 2021), however systemic administration has previously shown toxicity and teratogenicity (Carrijo-Carvalho *et al.*, 2017). Other phospholipid analogues including octadecylphosphocoline, elaidylphosphocoline, erucylphosphocoline and edelfosine have been tested against *Acanthamoeba* with varying degrees of efficacy established. Notably none tested had better efficacy than miltefosine (McBride *et al.*, 2005; McBride *et al.*, 2007).

1.7.7 Antibiotics and detergents

Many antibiotics from the groups of aminoglycosides (neomycin and paramomycin) and macrolides (rokytamicin, spiramycin and corifungin) have been used to complement treatments for patients presenting AK and GAE because a bacterial co-infection is commonly found in the cornea (Shing *et al.*, 2021). Particularly neomycin and the detergent polymyxin B have been used together in the management of AK where sometimes a cyclic peptide bacitracin is also used which in conjunction are known as Neosporin. Neomycin is a broad-spectrum antibiotic that binds to the ribosomal subunit 16S rRNA to inhibit translation and protein synthesis. It has been shown to have trophocidal and cysticidal effects in high concentrations 250 and 500 µg/ml, respectively (Siddiqui, Aqeel and Khan, 2016). Polymyxin B is a cationic detergent that disrupts cell membranes. In the clinic, several cases have

described the combinatory therapy using neomycin-polymyxin B and propamidine isethionate with good results (Skarin *et al.*, 1996; Sharma *et al.*, 2013). Another clinical trial using the binomial neomycin-polymyxin B with gramicidin reported favourable outcomes for patients infected with AK (Hargrave, McCulley and Hussein, 1999). The combination neomycin and paramomycin have been proved to be cysticidal when cryotherapy is performed (Elsheikha, Siddiqui and Khan, 2020). Polymixin E (colistin) is another polycationic compound that interacts with the cell membrane, modifying its permeability leading to lytic effects. *In vitro* data has shown colistin as trophocidal with a minimum concentration of 62.5 µg/ml and cysticidal with >500 µg/ml both at 48 h, however variations on these concentrations depend on the isolates, species, and genotypes of *Acanthamoeba* spp. The use of colistin has been limited since it has been proven to be toxic in human cells (Khan, 2015).

Macrolides such as rokitamycin spiramycin and corifungin inhibit protein biosynthesis by binding to the ribosome. Rokitamycin was found to be amoebastatic, trophocidal and cysticidal in a dose and time dependant manner at high concentrations. Additionally, rokitamycin when combined with chlorpromazine and amphotericin B enhanced its trophocidal and cysticidal activity and in low concentrations this macrolide alone or in combination inhibited the cytophatic effect of *A. castellanii* against human corneal cells (Mattana *et al.*, 2004). Spiramycin is another macrolide that has been tested against *Acanthamoeba*, however the trophocidal and cysticidal effects are reached in high concentrations at 250 and 500 µg/ml, respectively (Duma and Finley, 1976; Nagington and Richards, 1976). Corifungin is a water-soluble polyene macrolide which reduced 73% trophozoites growth at 100 µM with apparent swollen mitochondria, damage cytoplasm architecture, presence of granules and degradation of nuclear chromatin structure (Debnath *et al.*, 2014).

1.7.8 Photodynamic agents

Alternative approaches to conventional drug treatment against *Acanthamoeba* spp. infections have been explored, especially for AK. Photodynamic chemotherapy (PDT) relies on the stimulation of photosensitizers by light to kill specific target cells. In this way, this therapy has been used to treat various diseases (Kwiatkowski *et al.*, 2018). Despite there being a substantial number of studies that highlight PDT as potential treatment for AK using tetracationic phthalocyanine RLP068, hypocrellin B, tin porphyrin, methylene blue, riboflavin, titanium dioxide, chorin derivative

TONSS504 and rose bengal, most of the studies are restricted to *in vitro* results against *Acanthamoeba* isolates (Shing *et al.*, 2021).

RLP068 was reported to be trophocidal causing nuclear damage with consequent cell death of *A. palestenensis* (Kassab *et al.*, 2003). Hypocrellin B was trophocidal (0.23 µg/ml) and cysticidal (3.8 µg/ml), however toxic effects were observed in rabbit corneas (Chen *et al.*, 2008). Tin porphyrin was found as a potent amoebostatic against *A. castellanii* T4 inhibiting the amoeba to bind to human corneal epithelial cells (Siddiqui and Khan, 2012b). Methylene blue was reported to suppress the respiratory activity of *A. castellanii* ATCC 50370 trophozoites and displayed synergism with PHMB and amphotericin B, but not with voriconazole (Mito *et al.*, 2012). A single dose of cross-linking with riboflavin could not eradicate two strains of *Acanthamoeba*. A further study increased tenfold the concentration of riboflavin to explore a synergistic effect with PHMB or chlorhexidine gluconate without success (del Buey *et al.*, 2012; Lamy *et al.*, 2016). Evaluation of titanium dioxide reported this photosensitiser as trophocidal and cysticidal besides a synergistic effect with chlorhexidine gluconate on cysts (Gomart *et al.*, 2018). TONS504 suppressed trophozoites viability by 77% inducing necrosis and attenuated cyst survival by 42% causing apoptosis (Pertiwi *et al.*, 2019). A further *in vivo* study with TONS504 showed 58% of infected rabbits with AK clinical signs were markedly reduced (Dwia Pertiwi *et al.*, 2021). A similar assessment on rabbit corneas was carried out using rose Bengal where parasite loads were significantly decreased (Atalay *et al.*, 2020). Clinically, both riboflavin and rose Bengal have been proved to be effective in patients with AK (Morén *et al.*, 2010; Khan *et al.*, 2011; Price Marianne *et al.*, 2012; Naranjo *et al.*, 2019).

1.7.9 Repurposed drugs

Drugs that have been clinically approved and are effective against other diseases have shown anti-amoebic inhibitory effects *in vitro*. Interestingly, amlodipine (calcium channel blocker), loperamide (antidiarrheal), haloperidol (dopamine receptor blocker), procyclidine (anti-parkinsonian), and digoxin (inhibitor of active transport of potassium and sodium) have some trophocidal effects. Prochlorperazine (antipsychotic) has been reported to have both trophocidal and cysticidal effects (Baig, Iqbal and Khan, 2013; Elsheikha, Siddiqui and Khan, 2020). The mild effect that exerts corifungin (macrolide) and tigecycline (3rd generation tetracycline) at 100 µM showed degeneration of the cytoplasm and damage in mitochondria in *A.*

castellanii trophozoites (Debnath *et al.*, 2014; Jha *et al.*, 2015). The relatively high concentrations of the drugs used in these *in vitro* studies make their mode of action questionable and are likely to preclude their use *in vivo*. A widely drug used against malaria, chloroquine, and a group of drugs to control cholesterol levels such as atorvastatin, fluvastatin and simvastatin have been able to induce autophagy (programmed cell death) which decreased the survival in *A. castellanii* (Jha *et al.*, 2014; Martín-Navarro *et al.*, 2015). Notably these drugs also target sterol biosynthesis, via inhibition of HMG-CoA reductase and might therefore work in a similar manner to azoles (Thomson, 2020).

1.7.10 Natural compounds

A plethora of plant-based natural products have shown to be efficacious due to their bio-active molecules against *Acanthamoeba* spp. Some recent representative examples are quercetin (QT), kolavenic acid extracted from the plant *Polyalthia longifolia var pendula* (PGEA) and the crude plant methanolic extract of *Caesalpinia pulcherrima* (CPFLM) exhibited inhibitory effect since the number of *A. castellanii* was significantly reduced from 5×10^5 to 2.3×10^5 , 2.18×10^5 and 8.12×10^4 when conjugated with silver nanoparticles without any toxic effect in human cells (Anwar *et al.*, 2020). Oakmoss which is a natural fragrance ingredient whose antibacterial inhibitory effect is well established in *L. pneumophila*, showed amoebicidal effect at 48 h against *A. castellanii* ATCC 30234 (Nomura *et al.*, 2015). Plant extracts from *Rubus chamaemorus*, *Pueraria lobata*, *Solidago virgaurea* showed chemotherapeutic properties *in vitro* with concentrations ranging 0.01-0.05 mg extract/ml and BALB/c mice survived 2.5-3 times longer with no apparent toxic effects (Derda, Hadaś and Thiem, 2008). Animal-based natural products such as magainins (MSI-103 and MSI-94) which are self-defence peptides with antimicrobial activity secreted by *Xenopus laevis* induced amoebistatic and amoebicidal effects at concentrations from 20 to 40 µg/ml (Schuster and Jacob, 1992). Crude extracts as described above are unlikely to be used in the clinic and identification of active components within these is required to progress these.

1.7.11 Synthetic experimental agents

Due to the limitations to finance the discovery of new drugs by pharmaceuticals or side effects caused by the current treatment against *Acanthamoeba* infections, many synthetic compounds and their derivatives have

been assessed for their potential anti-amoebic effect. These compounds are still on experimental stages and could be complementary to the current treatment. Among these, heterocyclic compounds have been proved to exhibit diverse inhibitory biological effects. Some of the “new generation” groups of synthetic drugs that have been tested against *Acanthamoeba* spp. are quinazolinones, quinolinones derivatives, dihydropyridine compounds, tetrazoles, benzimidazoles and benzotriazoles, thiazoles, benzothiazoles, imidazolium salts, carbonyl thiourea derivatives, phenalenones, porphyrins, hexadecylphosphocolines and their analogues, ursolic acid derivatives, rosmarinic acid derivatives, samarium and terbium complexes, phosphane-gold(I) thiolates, thioureidic derivatives, agelasine and their analogues (Ahmed *et al.*, 2021).

Multiple anti-amoebic agents are prescribed for patients to ameliorate AK and GAE, however early diagnosis and the implementation of a strict non-toxic treatment system it is of utmost importance to prevent relapses or resistant infections especially as cysts are very difficult to eradicate and toxic side effects in patients (Elsheikha, Siddiqui and Khan, 2020; Ahmed *et al.*, 2021; Shing *et al.*, 2021). Thus, further studies are necessary to analyse new synthetic compounds with enhanced activity which become a safe complement therapy for *Acanthamoeba* spp. infections.

1.7.12 Other experimental agents that target biochemical pathways absent in humans.

Studies have also identified and targeted biochemical pathways that are absent in humans including the shikimate pathway and histidine biosynthesis. Glyphosate is a broad-spectrum systemic herbicide and crop desiccant commonly used for agricultural weed control. This herbicide was found to be amoebastatic for *A. castellanii* Neff and a clinical strain when grown in defined medium lacking aromatic compounds with IC_{50} ranging 17.5-35 μ M and 70-140 μ M, respectively. Additionally, glyphosate was found to be non-toxic at concentrations 17.5-1130 μ M when assessed to rabbit corneal epithelial (RCE) cells (Henriquez *et al.*, 2015).

Another study has demonstrated *Acanthamoeba* spp. growth is restricted by 3-amino-1,2,4-triazole (3AT) *in vitro* at concentrations of 105 μ M for *A. castellanii* Neff, 113 μ M for *A. castellanii* and a Clinical T4 strain, 125 μ M for *A. castellanii* ATCC 50370 and 55 μ M for *A. polyphaga* ATCC 50371. Also, the structure of *Acanthamoeba* Imidazoleglycerol-Phosphate Dehydratase (IGPD), which is the main target of 3AT in

the histidine biosynthetic pathway was also determined. Furthermore, a novel compound C-348 that also targets IGPD was found to inhibit *Acanthamoeba* growth at nM concentrations and co-crystalised with IGPD to reveal its interaction with the active site (Rice *et al.*, 2018).

Table 1. Summary of agents used against *Acanthamoeba* spp. diseases.

Group of agents	Type of drug	Drug target	Mechanism of action	Examples	<i>Acanthamoeba</i> spp. disease target	Reference
	Biguanides	Cell membrane	Disruption of negatively charged cell membranes causing cell lysis	Chlorhexidine gluconate	AK Cutaneous	Rice <i>et al.</i> , 2020a
				Polyhexamethylene-biguanide (PHMB)	AK GAE	Shing <i>et al.</i> , 2021 Taravaud <i>et al.</i> , 2021
	Diamidines	Cell membrane, Cytosolic proteins, Nucleic acids	Disruption of cell membrane resulting in cell death, denaturation of cytosolic proteins and inhibition of DNA synthesis	Propamidine isethionate, Hexamidine isethionate	AK	Shing <i>et al.</i> , 2021 Taravaud <i>et al.</i> , 2021
		DNA and RNA synthesis	Interferes with polyamine synthesis, RNA polymerase activity and binds to tRNA preventing the synthesis of proteins, nucleic acids, phospholipids, and folate	Pentamidine isethionate	GAE Cutaneous	Rice <i>et al.</i> , 2020a Hafiz and Kyriakopoulos, 2021 Taravaud <i>et al.</i> , 2021
	Polyene	Cell membrane	Binds to ergosterol causing cell instability leading to cell death	Amphotericin B	AK GAE Cutaneous	Rice <i>et al.</i> , 2020a Shing <i>et al.</i> , 2021 Taravaud <i>et al.</i> , 2021
Antifungals	Echinocandins	Endocyst (β 1,3-glucan)	Inhibiting β 1,3-glucan synthase enzyme	Caspofungin	AK	Carrijo-Carvalho <i>et al.</i> , 2017 Elsheikha, Siddiqui and Khan, 2020 Taravaud <i>et al.</i> , 2021

				Ketoconazole	AK GAE Cutaneous	Rice <i>et al.</i> , 2020a Taravaud <i>et al.</i> , 2021
				Voriconazole	AK	Carrijo-Carvalho <i>et al.</i> , 2017 Shing <i>et al.</i> , 2021
				Clotrimazole	AK	Shing <i>et al.</i> , 2021
				Miconazole	AK	Shing <i>et al.</i> , 2021
				Itraconazole	AK Cutaneous	Rice <i>et al.</i> , 2020a Shing <i>et al.</i> , 2021
				Fluconazole	AK GAE Cutaneous	Rice <i>et al.</i> , 2020a Shing <i>et al.</i> , 2021 Taravaud <i>et al.</i> , 2021
				Isavuconazole	AK	Shing <i>et al.</i> , 2021
				Posaconazole	AK	Shing <i>et al.</i> , 2021
	Antiseptic	Cell key structures	Free form iodine penetrates microbial cell membrane and oxidises key proteins, nucleotides, and fatty acids, leading to cell death.	Povidone-iodine, acriflavine and proflavine	AK	Carrijo-Carvalho <i>et al.</i> , 2017 Shing <i>et al.</i> , 2021
	α -phosphocholines	Mitochondria, lipid metabolism and membrane composition	Inhibition of proteinase kinase B Suppressing phospholipid biosynthesis, disruption of cellular membranes and intracellular signalling, inducing apoptosis	Miltefosine	AK GAE	Carrijo-Carvalho <i>et al.</i> , 2017 Shing <i>et al.</i> , 2021 Taravaud <i>et al.</i> , 2021
Antiparasitics	Nitroimidazole	DNA	Inhibits protein synthesis by interacting with DNA and causing loss of helical DNA structure and strand breakage	Metronidazole	GAE	Taravaud <i>et al.</i> , 2021 Weir and Le, 2021
Antibiotics	Aminoglycosides	Ribosomes	Binds to ribosomal subunit to inhibit translation and protein synthesis	Neomycin paromomycin Neosporin (neomycin, polymyxin B and bacitracin)	AK	Shing <i>et al.</i> , 2021

Macrolides	Bacterial 50S ribosomal subunit	Inhibition of bacterial protein synthesis	Rokitamycin, spiramycin, corifungin	AK	Siddiqui, Aqeel and Khan, 2016 Elsheikha, Siddiqui and Khan, 2020
			Azithromycin	Cutaneous	Rice <i>et al.</i> , 2020a
			Clarithromycin	Cutaneous	Rice <i>et al.</i> , 2020a
	Fungal cell membrane	Binds to sterols causing cell permeabilization leading to cell death.	Natamycin	AK	Siddiqui, Aqeel and Khan, 2016 Shing <i>et al.</i> , 2021
Sulphonamides	Dihydropteroate synthase	Inhibition of folate synthesis, needed for DNA synthesis and cell replication	Trimethoprim-sulfamethoxazole	GAE	Taravaud <i>et al.</i> , 2021
			Sulfadiazine	Cutaneous	Rice <i>et al.</i> , 2020a
Anti-mycobacterial	DNA-dependent RNA polymerase	Inhibits RNA synthesis	Rifampicin	GAE	Suresh, Rosani and Wadhwa, 2021 Taravaud <i>et al.</i> , 2021
	Cell wall	Inhibits bacterial cell wall synthesis by preventing the dephosphorylation of P-P-phospholipid carrier that attaches the cell wall peptidoglycan	Bacitracin Gramicidin	AK	Nguyen <i>et al.</i> , 2021 Shing <i>et al.</i> , 2021
Detergents	Cell membrane	Disruption of cell membrane	Polymyxin B Polymyxin E (Colistin)	AK	Elsheikha, Siddiqui and Khan, 2020 Shing <i>et al.</i> , 2021
Photodynamic therapy	Cell key structures	Chemotherapy leading to cell death	Tetracationic phthalocyanine, RLP068, hypocrellin B, tin porphyrin, methylene blue, riboflavin, titanium dioxide, chorin derivative, TONS504, rose bengal	AK	Elsheikha, Siddiqui and Khan, 2020 Shing <i>et al.</i> , 2021

Abbreviations: AK: *Acanthamoeba* keratitis, GAE: Granulomatous amoebic encephalitis, DNA: deoxyribonucleic acid; RNA: ribonucleic acid

1.8 Aims and Objectives

During the past years, numerous studies have identified the potential of drugs to target *Acanthamoeba* trophozoites at different cellular levels, however their inability to be efficient or high toxicity are main challenges on the quest to eradicate AK and GAE.

DNA from parasites continues to be an important pharmacological target in clinical application. Distamycin A is one of the first natural aromatic oligoamide to bind to the minor groove of double strand DNA. This compound has shown to be a molecular template due to its major suitability to be modified and synthesized to further generate derivatives that have been widely used against pathogens, showing important and potent antibacterial, antifungal and antiparasitic activities. Meanwhile advanced gene-editing tool technologies such as CRISPR-Cas9 allows for gene deletions, insertion or mutations which have shown promising results in the appropriate management of diseases caused by bacteria and fungi, scarce studies have been exploited against parasites, especially in amoeba field.

The work developed on this thesis aims to characterise *in vitro* a considerable number of Distamycin A derivative minor groove binders against *Acanthamoeba* spp. trophozoites by means of viability alamarBlue assays at different point times, furthermore the most effective compound will be chosen to elucidate through confocal imaging technique its specific cellular target. Equally important, the next chapter will evaluate the effective activity and toxicity of the hit compound using for the very first time the wax moth *Galleria mellonella* as a new *in vivo* infection model. Additionally, a novel approach to introduce the CRISPR-Cas9 system in *A. castellanii* Neff strain trophozoites is explored. This chapter aims to analyse the possibility to engineer and integrate a fast and reliable cloning free CRISPR-Cas9 method to develop stable cell lines with Chorismate synthase gene mutated by virtue of expressing Cas9 protein and T7 RNA polymerase to trigger sgRNA *in vivo* transcription from the addition of DNA repair templates generated by PCR reactions. Because of the previous potent effect observed of S-MGBs against parasites such as *Trypanosoma* spp. and the recent successful application of CRISPR-Cas9 in *Entamoeba histolytica*, we hypothesised that such compounds and genetic edition tool might provide new and effective possibilities of potential therapeutics to overcome health complications and current limitations due to neglected *Acanthamoeba* infections.

Chapter 2. Material & Methods

2.1 Materials

2.1.1 Chemicals

Table 2. Chemicals

All the chemicals that were used throughout experimental proceedings in every chapter are depicted.

Chemical	Manufacturer	Location of Headquarters
alamarBlue®	Biorad	Hercules, USA
Acrylamide	Carl Roth GmbH & Co	Karlsruhe, Germany
Agar	Thermo Fisher Scientific	Waltham, USA
Agarose	Bioline	London, UK
B12	Sigma-Aldrich	St. Louis, USA
Biotin	Sigma-Aldrich	St. Louis, USA
Boric Acid	Severn Biotech Ltd	Kidderminster, UK
Calcium Chloride Monohydrate (CaCl ₂ ·H ₂ O)	Thermo Fisher Scientific	Waltham, USA
Carboxyfluorescein succinimidyl ester (CFSE)	Sigma-Aldrich	St. Louis, USA
Chloroform	Carl Roth GmbH & Co	Karlsruhe, Germany
Deoxyribonucleotide Triphosphate (dNTP) Mix	Roche Diagnostics	Basel, Switzerland
Dimethyl Sulfoxide (DMSO)	Sigma-Aldrich	St. Louis, USA
Dulbecco's phosphate-buffered saline (DPBS)	Thermo Fisher Scientific	Waltham, USA
Ethanol	Thermo Fisher Scientific	Waltham, USA
Ethidium Bromide (EtBr)	Sigma-Aldrich	St. Louis, USA
Ethylenediamine Tetra-Acetic Acid (EDTA)	Carl Roth GmbH & Co	Karlsruhe, Germany
Glucose	Alfa Aesar	Haverhill, USA
Glycerol	Melford, Biolaboratories Ltd	Ipswich, UK
HEPES	Carl Roth GmbH & Co	Karlsruhe, Germany
Hoechst	Thermo Fisher Scientific	Waltham, USA
Hydrochloric Acid (HCl)	Thermo Fisher Scientific	Waltham, USA

L-methionine	Sigma-Aldrich	St. Louis, USA
Magnesium sulphate heptahydrate (MgSO ₄ ·7H ₂ O)	Sigma-Aldrich	St. Louis, USA
Immersion Oil	Cargille laboratories	Cedar Grove, USA
Iron Chloride (FeCl ₃)	Sigma-Aldrich	St. Louis, USA
Isopropanol	Thermo Fisher Scientific	Waltham, USA
Magnesium sulphate (MgSO ₄)	Thermo Fisher Scientific	Waltham, USA
Methanol	VWR	Radnor, USA
Potassium chloride (KCl)	VWR	Radnor, USA
Potassium dihydrogen phosphate (KH ₂ PO ₄)	Sigma-Aldrich	St. Louis, USA
Protease Peptone	Sigma-Aldrich	St. Louis, USA
Sodium acetate (NaAC)	Sigma-Aldrich	St. Louis, USA
Sodium bicarbonate (NaHCO ₃)	VWR	Radnor, USA
Sodium chloride (NaCl)	Fisher Chemical	Waltham, USA
TEMED	Melford, Biolaboratories Ltd	Ipswich, UK
Thiamine	Sigma-Aldrich	St. Louis, USA
Trizma (Tris)	Sigma Life Science	Gillingham, UK
Tryptone	Melford, Biolaboratories Ltd	Ipswich, UK
Vectashield Plus Antifade Mounting Medium with DAPI	Vector	Burlingame, USA
Yeast Extract	Melford, Biolaboratories Ltd	Ipswich, UK

2.1.2 Media and Buffers

Table 3. Media and Buffers

Composition of media and buffers employed in this thesis are described.

Media/Buffer	Constituents
Agarose gel (0.8%)	0.8% (w/v) Agarose 0.5 µg/ml Ethidium bromide In 0.5x TBE
Agarose gel (1.5%)	1.5% (w/v) Agarose 0.5 µg/ml Ethidium bromide In 0.5x TBE
LB agar	1.5% (w/v) Agar In autoclaved LB medium
LB medium	1% (w/v) Tryptone 1% (w/v) NaCl 0.5% (w/v) Yeast Extract In autoclaved ddH ₂ O Antibiotics added if required
Neff's encystment medium (NEM)	20 mM Tris-HCl pH 8.8 100 mM KCl 8 mM MgSO ₄ 0.4 mM CaCl ₂ ·H ₂ O 1 mM NaHCO ₃ In autoclaved ddH ₂ O
Peptone-Protease Glucose (PG) medium	15 g/l Glucose 15 g/l Protease Peptone 0.3 g/l KH ₂ PO ₄ 0.001 g/l Thiamine 0.0149 g/l L-methionine 0.1 mg/ml B12 0.2 mg/ml Biotin 0.15 g/100ml CaCl ₂ ·H ₂ O ^{***} 0.02 g/100 ml FeCl ₃ ^{***} 2.46 g/100 ml MgSO ₄ ·7H ₂ O ^{***}

TBE (5x)	1.1 M Trizma/Tris Base 900 mM Boric Acid 25 mM EDTA Adjusted to pH 8.3
TBE (0.5x)	90% ddH ₂ O 10% 5x TBE

*** indicates agents that are part of the Salt Solution. Prior to autoclaving, 1 ml/L of Salt Solution is added.

2.1.3 Molecular Biology Kits

Table 4. Molecular biology kits

A table to depict all the kits that were employed throughout experimental proceedings on this thesis. The manufacturer and the location from which item was acquired are also mentioned.

Molecular biology kit	Manufacturer	Location of Headquarters
ISOLATE II Plasmid Mini Kit	Bioline	London, UK
M&N NucleoSpin Plasmid	Macherey & Nagel	Düren, Germany
M&N NucleoSpin Extract II	Macherey & Nagel	Düren, Germany
M&N Nucleo bond Xtra Midi	Macherey & Nagel	Düren, Germany

2.1.4 Antibiotics

Table 5. Antibiotics

All the antibiotics used throughout experimental proceedings on this thesis are depicted. The manufacturer and the location from which item was acquired are also mentioned.

Antibiotic	Manufacturer	Location of Headquarters
Amphotericin B (1% 125 µg)	Sigma-Aldrich	St. Louis, USA
Blasticidin (10 mg/ml)	InVivoGen	Toulouse, France
Carbenicillin disodium (100 mg/ml)	Thermo Fisher Scientific	Waltham, USA
G418 (14.7 mg/ml)	InVivoGen	Toulouse, France

Hygromycin B (100 mg/ml)	InVivoGen	Toulouse, France
Miltefosine (10 mg/ml)	Sigma-Aldrich	St. Louis, USA
Voriconazole (20 mg/ml)	Sigma-Aldrich	St. Louis, USA
Penicillin/Streptomycin (P/S) (1% 125 µg)	Sigma-Aldrich	St. Louis, USA
Phleomycin (5 mg/ml)	InVivoGen	San Diego, USA
Puromycin (10 mg/ml)	InVivoGen	San Diego, USA

2.1.5 DNA/Protein Molecular Weight Markers

Table 6. DNA/Protein Molecular Weight Markers

All molecular weight markers employed through all experimental proceedings are depicted including manufacturer and location, from which each item was acquired.

DNA/Protein Molecular Weight Marker	Manufacturer	Location of Headquarters
1kb Plus DNA ladder	New England BioLabs	Ipswich, UK
1 kb DNA ladder	New England BioLabs	Ipswich, UK
Quick-Load® Purple 100 bp DNA Ladder	New England BioLabs	Ipswich, UK
1 kb HyperLadder	Bioline	London, UK
1 kb DNA Ladder	Promega	Madison, USA
1 kb Plus DNA ladder	Thermo Fisher Scientific	Waltham, USA

2.1.6 Enzymes

Table 7. Enzymes

All enzymes, restriction enzymes and any associated buffers employed through all experimental proceedings are depicted including manufacturer and location, from which each item was acquired.

Enzyme	Manufacturer	Location of Headquarters
ACC65I	New England BioLabs	Ipswich, UK
ApaLI	New England BioLabs	Ipswich, UK
AvrII	New England BioLabs	Ipswich, UK

BamHI-HF	New England BioLabs	Ipswich, UK
BglII	New England BioLabs	Ipswich, UK
Buffer 2.1	New England BioLabs	Ipswich, UK
Buffer 3.1	New England BioLabs	Ipswich, UK
Clal	New England BioLabs	Ipswich, UK
CutSmart Buffer	New England BioLabs	Ipswich, UK
DNA Polymerase I, Large (Klenow)	New England BioLabs	Ipswich, UK
EcoRI-HF®	New England BioLabs	Ipswich, UK
EcoRV	New England BioLabs	Ipswich, UK
HindIII	New England BioLabs	Ipswich, UK
KpnI HF®	New England BioLabs	Ipswich, UK
MfeI (isoschizomer of MunI)	New England BioLabs	Ipswich, UK
MyTaq Buffer	Bioline	Nottingham, UK
NcoI	New England BioLabs	Ipswich, UK
NdeI	New England BioLabs	Ipswich, UK
NotI	New England BioLabs	Ipswich, UK
PmeI	New England BioLabs	Ipswich, UK
Q5 High Fidelity Enzyme	New England BioLabs	Ipswich, UK
RNase A (Bovine Pancreas)	Roche Diagnostics	Basel, Switzerland
SAP Buffer	New England BioLabs	Ipswich, UK
SAP Enzyme	New England BioLabs	Ipswich, UK
SacI	New England BioLabs	Ipswich, UK
SmaI	New England BioLabs	Ipswich, UK
T4 Ligase Buffer	Roche Diagnostics	Basel, Switzerland
T4 Ligase Enzyme	Roche Diagnostics	Basel, Switzerland
XbaI	New England BioLabs	Ipswich, UK
XhoI	New England BioLabs	Ipswich, UK

2.1.6 Bacterial Strain

Table 8. Bacterial strain

A table to depict the bacterial strain utilised throughout experimental proceedings is depicted, including the genotype, manufacturer, and location, from which each item was acquired.

Bacterial description	Genotype	Manufacturer	Location of Headquarters
DH5 α	F- ϕ 80lacZ Δ M15 Δ (lacZYAargF)U169recA1endA1 hsdR17(rK-,mK+) phoA supE44 λ - thi1 gyrA96 relA	Thermo Fisher Scientific	Waltham, USA

2.1.7 Plasmids

Table 9. Plasmids

All the plasmids generated in conjunction with the source from which they originated are depicted.

Plasmid description	Size (bps)	Source
pBASV40GFP	6002	Sanchez, A., PhD student (2018)
pBBsdRFPCSV40	5249	Wiese, M., University of Strathclyde
pBSV40	3397	Sanchez, A., PhD student (2019)
pBBXSV40RFP	4051	Sanchez, A., PhD student (2019)
pBKCTBpNeo	4034	Sanchez, A., PhD student (2019)
pBRFPNeoCas9	10536	Sanchez, A., PhD student (2019)
pBRFPPhleCas9	10113	Sanchez, A., PhD student (2019)
pBRFPT7NeoCas9	13283	Sanchez, A., PhD student (2020)
pBRFPT7PhleoCas9	12860	Sanchez, A., PhD student (2020)
pBRFPT7sNeoCas9	13928	Sanchez, A., PhD student (2020)
pBRFPT7sPhleoCas9	13505	Sanchez, A., PhD student (2020)
pBSKII(+)	2961	Wiese, M., University of Strathclyde
pBTBPpCas9	7512	Sanchez, A., PhD student (2019)
pCR2.1Phleo	4298	Wiese, M., University of Strathclyde
pRFPSV40	5948	Sanchez, A., PhD student (2018)
pT007_Cas9_T7_Tub	15446	Wiese, M., University of Strathclyde
pUCSV40T7PolyA	6544	Wiese, M., University of Strathclyde
TBPpPhleoPolyAAmp	3611	Sanchez, A., PhD student (2019)

2.1.8 Oligonucleotides

Table 10. Oligonucleotides

A table to depict the oligonucleotides utilised throughout experimental proceedings, including the genotype, manufacturer, and location, from which each item was acquired.

Oligonucleotide description	Nucleotide sequence	Manufacturer
G00	5'AAAAGCACCGACTCGGTGCCACTTTT TCAAGTTGATAACGGACTAGCCTTATTT TAACTTGCTATTTCTAGCTCTAAAC3'	Invitrogen life Technologies (Loughborough, UK)
sgRNACSds	5'gaaattaatacgaactcactataggTCGAGAGAA ACGAGGGCGTCgtttagagctagaaatagc3'	
sgRNACSup	5'gaaattaatacgaactcactataggAAGCACCGG TGCAGGCGACAgtttagagctagaaatagc3'	
CSCRupphleo.for	5'GGCGTTAGAGCTTGAAGAAGACGCG ACATCTTCGGCTTAGATCACCATGG3'	
CSCRdsphleo.rev	5'CAGCGCGCTTCTTGCTCTGTTTGGCG CACGTTTCGGCTTCGGCCTAGGTCA3'	
CSCRuphyg.for	5'GGCGTTAGAGCTTGAAGAAGACGCG ACATCATTGGGCCCTCTAGATGCAT3'	
CSCRdshyg.rev	5'CAGCGCGCTTCTTGCTCTGTTTGGCG CACGCGGCTTCGGCAGCTAGCCTA3'	
CSCRupneo.for	5'GGCGTTAGAGCTTGAAGAAGACGCG ACATCAATTCGGCTTGCCATCATGA3'	
CSCRdsneo.rev	5'CAGCGCGCTTCTTGCTCTGTTTGGCG CACGCGGCTTTGCCGGCTAGCTCA3'	
pBArev	5'-TACAAATAAAGCAATAGCAT-3'	
M13R	5'-CAG GAA ACA GCT ATG ACC-3'	
ColE1 (F)	5'-GGTCCGCCACCTCTGACTT-3'	
T7NeoCas9.for	5'-GAAAGTATCCATCATGGC-3'	
T7NeoCas9.rev	5'-GCACCTTGAATTTCTTGC-3'	
T7PhleoCas9.for	5'-CGACGTGACCCTGTTTCAT-3'	

2.1.9 Strathclyde Minor Groove Binders (S-MGBs)

Table 11. Strathclyde Minor Groove Binders

A table to show the S-MGBs utilised throughout experimental proceedings is shown, including the given identity number (ID), batch number, formula weight (FW) and chemical structure. The compounds were diluted with DMSO to reach a stock concentration of 40mM. All the compounds were synthesized and donated by Dr Fraser J. Scott. Details of compounds with ID 375, 449, 495, 496 and 505 are not shown due to intellectual property reasons.

S-MGB ID	Formula Weight	Chemical structure
1	724.28	
2	839.27	
146	744.29	
171	809.26	
227	650.6	
228	636.6	

229	602.6	
230	288.5	
231	559.5	
233	607.5	
234	796.24	
235	681.67	
236	545.5	
237	593.5	
238	622.6	

240	574.7	
241	608.6	
242	560.5	
245	852.79	
300	816.25	
306	662.54	
359	701.26	
360	693.64	
363	809.73	

502	759.26	
503	719.27	
504	699.63	
506	716.23	

2.2 Methods

2.2.1 *Acanthamoeba* spp. seeding, harvesting and preparation of S-MGBs

2.2.1.1 *Acanthamoeba* spp. and isolates.

The amoeba species and strains used throughout this thesis for comparative results were (i) *Acanthamoeba castellanii* environmental Neff strain donated by Keith Vickerman (Glasgow, United Kingdom), (ii) *Acanthamoeba polyphaga* environmental gently donated by Professor Tony Page (Glasgow, United Kingdom), (iii) *Acanthamoeba* Clinical T4 gently donated by Dr Antonella Mattana (Sassari, Italy) and both (iv) ATCC50370 and (v) ATCC50371 were bought from the American Type Culture Collection belonging to *A. castellanii* and *A. polyphaga*, respectively.

2.2.1.2 Cultivation, harvesting and passage of *Acanthamoeba* spp. trophozoites.

All *Acanthamoeba* spp. were cultured in PG (Peptone-Glucose) medium supplemented with 1% 125 µg penicillin/streptomycin (Sigma, Poole, United Kingdom) and 1% 125 µg amphotericin B (Sigma, Poole, United Kingdom), and maintained as axenic cultures at room temperature in 75 cm² tissue culture flasks (Corning, Amsterdam, The Netherlands). Unless stated otherwise, a cycle period of 3-4 days was the time where trophozoites reached a confluence of 95-100%, they were harvested via mechanical detachment and collected in 50 ml centrifugations tubes (Corning, Amsterdam, The Netherlands) by centrifugation at 2500 rpm 4°C for 5 minutes to prepare a cell pellet. When the cell pellet is formed, the medium is discarded, and the cell pellet is re-suspended in 1 ml of new medium PG. 10 µl are taken and added to new tissue culture flask containing 10 ml to develop a new culture.

2.2.1.3 Preparation of Strathclyde Minor Groove Binders (S-MGBs)

The S-MGBs were prepared using organic Dimethyl sulfoxide (DMSO) to have a stock concentration of 40 mM. Before the dilution preparations, all the drugs were sterilised via filtration or gamma ray radiation. Afterwards, 5 µl of every S-MGB are taken and mixed with 995 µl of PG medium to reach a starting point dilution concentration of 200 µM; afterwards 10 serial dilutions are prepared on a 96 well plate and tested against the optimal seeding density cell number. All S-MGBs were

synthesised and gently donated by Dr Fraser J. Scott to be screened against *Acanthamoeba* spp. (Table 11).

2.2.2 *In vitro* alamarBlue™ Assays

2.2.2.1 Calculating alamarBlue™ Reduction Compared to Control

The percentage reduction of alamarBlue™ compared to the control was calculated using the following equation:

$$(Y \cdot T1) - (X \cdot T2) / (Y \cdot C1) - (X \cdot C2) * 100$$

Whereby X is the molar extinction coefficient (E) of oxidized alamarBlue™ at 570nm (80568); Y is the E of oxidized alamarBlue™ at 600nm (117216); T1 is the absorbance of the test wells at 570nm; T2 is the absorbance of the test wells at 600nm; C1 is the absorbance of the control wells at 570nm; C2 is the absorbance of the control wells at 600nm. The results obtained were then multiplied by 100 and averaged to give the percentage difference in reduction from test wells to control. Background reduction caused by the medium was accounted for by subtracting the average reduction of alamarBlue caused by the medium from all results and then dividing the new results of the test wells by those of the control. For clarity purposes the positive control, trophozoites with medium alone unless stated otherwise, was set to 100% with all other results compared.

2.2.2.2 alamarBlue™ Drug sensitivity assay

Once the S-MGBs are prepared according to section 2.2.1.2., a colorimetric microtiter plate assay based on alamarBlue (Biorad, UK) reaction developed by McBride *et al.*, 2005 with some modifications was carried out. The drug is serially diluted 10-fold adding 50 µl in triplicate on a 96 well tissue culture plate (TPP, SigmaAldrich UK). Then, the appropriate number of trophozoites for the isolate and time-point (96 h or 24 h) is added as follows: add 1 ml of new PG medium to cell pellet, mix and take 10 µl of this stock to 990 µl of new PG medium. From this new 1ml dilution, take 10 µl and pour it in Neubauer haemocytometer chamber (Blaubrand) for cell counting. The total cell number of the quadrants is divided in 4 and the result number represent the millions of cells in the flask. This number is divided with the optimal density number to generate the dilution factor. Once the optimal seeding density is prepared, 50 µl are mixed with the previously added 50 µl of S-MGB.

Controls consisted of a PG blank, trophozoites with medium alone, trophozoites with the highest concentration of DMSO solvent and trophozoites with the highest concentration of S-MGB (200 μ M). The final volume for all wells is 100 μ l. The plates are incubated at 23°C until 6 hours before the time-point was being measured. 10 μ l of alamarBlue reagent is added to every triplicate, including controls except the PG blank, the plate was incubated at 23°C for a further 6 hours in dark conditions. Finally, the absorbance was then read on a Spectromax (Molecular devices, US) spectrophotometer at OD₅₇₀ and OD₆₀₀.

2.2.2.3 Optimal seeding density standardisation

Trophozoites were grown and harvested according to section 2.2.1.2. The harvested cells from each isolate were diluted in PG medium to reach a starting concentration of 32x10⁴ cells/ml or 16x10⁴ cells/ml for 24 h and 96 h standardisation assays, respectively. This suspension was 8-fold serially diluted down. 50 μ l of each dilution was then seeded in triplicate on a 96 well tissue culture plate, with an additional 50 μ l of PG media then added to each well, the control consisted of a 100 μ l PG media blank. The plates were incubated at 23°C. Six hours before the plate reached its time of initial incubation the plate was removed from the incubator and 10 μ l of alamarBlue™ reagent was aseptically added to all wells except the blank. The plate was then incubated again at 23.3°C for 6 hours in low light conditions. The plate was read on a Spectromax spectrophotometer at OD₅₇₀ and OD₆₀₀, results were calculated using the equation from section 2.2.2.1.

2.2.3 Microscopy

2.2.3.1 Fluorescence Microscopy

To observe the expression of pBRFPT7NeoCas9 and pBRFPT7PhleoCas9 transfected trophozoites were spun down at 2,500 rpm for 5 minutes, and the media was removed. The cells were resuspended in 1 ml of PG media, and 25 μ l of cells was placed on a microscope slide. The cells were examined on a Nikon Eclipse 600 Epifluorescent Upright Microscope (Nikon, USA) under DAPI filter with Ex_{max.} 340-380 nm/DM 400 and Em_{max.} 435-485 nm and TRITC filter with Ex_{max.} 540 nm/DM 565 and Em_{max.} 605/55 nm.

2.2.3.2 Confocal Microscopy

Acanthamoeba castellanii Neff trophozoites were harvested according to section 2.2.1.2. For observation, samples with a total number of 1×10^6 cells/ml were labelled altogether or separately. Cells untreated were used as control. The observation and analysis were carried out on multiphoton Leica SP8 Confocal microscope under DAPI (exc 360/40, em 425 LP), FITC (exc 470/40, em 515 LP). The labelling was performed as follows: (i) Vectashield Plus Antifade Mounting Medium with DAPI (Vector Laboratories, Burlingame CA) one drop incubated with cells for 5 minutes at room temperature. (ii) Hoechst (ThermoFischer Scientific, UK) to reach a final concentration of 1 $\mu\text{g/ml}$, the mix was incubated during 5 - 30 min at room temperature. (iii) CFSE (Sigma-Aldrich, UK) as follows: cells thoroughly resuspended in 1 ml were placed in the bottom of a fresh (non-wetted) 10 ml conical tube. The tube was laid horizontally in which 110 μl of DPBS (ThermoFischer Scientific, UK) were added to the non-wetted portion of the plastic at the top of the tube to avoid the contact with the cell solution. 1.1 μl of 5 mM CFDA stock (non-fluorescent molecule of CFSE) are resuspended in 110 μl of DPBS to start the conversion reaction to CFSE. The tube was quickly capped and mixed initially via inversion, then it was well vortexed until a uniform mix was obtained. The cells were incubated in dark conditions for 5 minutes at room temperature. Finally, the cells are washed twice with DPBS (adapted from Quah and Parish, 2010). (iv) Fluorescent S-MGB-363 and S-MGB-245. The compounds were down diluted to 100 μM from the stock prepared as described in section 2.2.1.3 and well mixed.

2.2.4 *Galleria mellonella* larvae as new *in vivo* infection model

2.2.4.1 *Galleria mellonella* larvae test injection procedure.

Five larvae around 250-340 mg (Livefood UK, Ltd) uniformly cream coloured were chosen randomly, discarding any larva with presence of dark plaques or dark cuticle. To inject the larvae, an "injection station" is set up inside the microbiological safety cabinet involving taping a P1000 blue tip onto the filter paper, then a larva was gently held with the index and thumb finger over the tip exposing the prolegs visible. The needle is carefully inserted angled to the head of the larvae and the pressure was reduced on the larvae just before the inoculation. 5-10 μl of DPBS or sterile ddH₂O were administered through the first right proleg using a sterile 1ml 30Gx1/2" (0.3mm x 12mm) insulin syringe (Omnican, BRAUN). Once injected, larvae were moved into

the petri dish containing a filter paper and placed on their side or pro legs down to reduce potential leakage.

2.2.4.2 Determination of the infective dose of trophozoites.

An infective dose of *A. castellanii* Neff strain was determined by injecting groups of 10 larvae (as described on section 2.2.4.1) with 5 different trophozoites concentrations ranging 1×10^7 cells/ml to 1×10^3 cells/ml. Once injected, the larvae were incubated during 20 days at room temperature and mortality was recorded daily.

2.2.4.3 Antibiotic efficacy testing

To determine the antibiotic efficacy testing, 14 groups of five larvae were properly injected as described in section 2.2.4.1 with a pre-determined infective dose of trophozoites suspension. The groups infected were incubated during 2 hours at room temperature. After the incubation, the larvae were injected on the left first proleg with a different dose of drug. The drugs used on different tests were voriconazole (125 mg/ml, 25 mg/ml, and 5 mg/ml), miltefosine (43.8, 8.75, 1.75 mg/kg) and S-MGB-235 (125 mg/ml, 25 mg/ml, 5 mg/ml, and 1 mg/ml). Each step in the procedures included three different control groups: non-infected and untreated control, infected and untreated control, and vehicle-injected control (DMSO or ddH₂O). The values were compared and assigned to values recommended for human use. A new sterile syringe was used per every group to avoid contamination and cross-reaction. The tests were screened in duplicate per every drug. The mortality was recorded daily for 14 days, and therapeutic dose was assigned.

2.2.5 Molecular Biology

2.2.5.1 Analytical Plasmid Restriction Cleavage

To produce a proper analysis of plasmid restriction enzyme digest, all the components were mixed in a 1.5 ml microcentrifuge tube as follows: 1 µl of plasmid, 1.5 µl of 10x enzyme buffer, 0.4 µl of each restriction enzyme and up to 15 µl sterile ddH₂O. The mixed sample was generally placed in a shaking incubator during 3 h (unless stated otherwise) at 37°C prior to analytical gel resolution.

To conduct a Mini-preparation test digest, 4 µl of the mini-preparation sample were mixed with 0.2 µl of each restriction enzyme and 0.1 µl of RNase A, where on sterile

ddH₂O added was adjusted accordingly. In the case of a Midi-preparation test digest, the sample mix was prepared on a similar with the difference residing in 2 µl of the Midi-preparation sample volume added.

2.2.5.2 Preparative Plasmid Restriction Cleavage

When setting up a plasmid restriction enzyme digest, all the components were combined in a 1.5 ml microcentrifuge tube as follows: 15 µl of plasmid, 10 µl of 10x enzyme buffer, 2 µl of each restriction enzyme and up to 100 µl sterile ddH₂O. The mixed sample was generally placed in a shaking incubator during 3 h (unless stated otherwise) at 37°C prior to analytical gel resolution.

2.2.5.3 Analytical Agarose Gel Electrophoresis

Following a proper analytical plasmid restriction cleavage, 5 µl of the restriction cleavage samples are combined with 1.5 µl AP loading dye and 10 µl ddH₂O, afterwards they are run on a 0.8% (or 1.5%) analytical gel agarose submerged in 0.5x TBE buffer in an electrophoretic chamber. DNA marker is also run along the samples at 120V for 45 min.

2.2.5.4 Preparative Agarose Gel Electrophoresis

After a proper plasmid restriction cleavage and confirmed via analytical gel electrophoresis, the remaining sample (95 µl) were mixed with 10 µl of AP loading dye. The sample was run on a 0.8% preparative gel agarose submerged in 0.5x TBE buffer in an electrophoretic chamber. DNA marker is also run along the samples at 60V for 15 min, followed by 100V for 1 hour to ensure the fragments are clearly separated and discernible.

2.2.5.5 Gel Agarose Band Purification

The plasmid DNA bands were gel extracted according to M&N NucleoSpin Extract II protocol. A clean scalpel was used to excise the DNA fragment from a preparative agarose gel and any gel potential excess was removed. The weight of the gel slice was determined and transferred to a clean 1.5 ml microcentrifuge tube. 200 µl NTI binding buffer per 100 mg gel band were combined. The sample was placed in a shaking incubator for 5-10 min at 50°C. Then, 700 µl of the sample were loaded onto the spin column and centrifugated for 30 s at 11 000 x *g*. Any potential flow-

through was discarded and repeated until no DNA sample remained. 700 µl of NT3 (washing buffer) were loaded onto the spin column and centrifuged as previously. The flow-through was discarded again. The spin column was dry spun for 1 min at 11 000 x g to remove any buffer remain. The collection tube was replaced. Finally, 30 µl of NE (elution buffer) were loaded onto the spin column. The sample was incubated at room temperature and centrifugated as previously. A further 30 µl NE were loaded and the process repeated as previously to have a final volume of 60 µl.

2.2.5.6 Klenow treatment protocol

Protocol for blunting ends by 5' overhang fill in and 3' recessed end removal. In a 1.5 ml microcentrifuge tube were combined 40 µl DNA in dH₂O, 6 µl NEB buffer 2.1, 1 µl dNTPs (0.22 mM) and 3 µl of 1-unit DNA Polymerase I Large (Klenow) fragment. The mix was placed in a shaking incubator for 15 minutes at 25°C then, 1 µl 0.5M EDTA was added to stop the reaction, finally the mix was incubated at 75°C for 20 minutes. To corroborate a correct treatment, 5 µl of the final mix were run on an analytical gel.

2.2.5.7 Shrimp Alkaline Phosphatase (SAP) treatment protocol

Protocol used to dephosphorylate 5'- and 3'-phosphate groups from DNA, RNA, and nucleotides. After gel extraction, the resulting 60 µl were combined with 1.5 µl SAP enzyme, 7 µl 10x SAP buffer, 1.5 µl SAP enzyme and top up to 70 µl sterile ddH₂O. The mix was firstly incubated 2 hours at 37°C after, secondly it was incubated at 65°C for 30 minutes. Finally, to corroborate 5 µl were tun in an analytical gel.

2.2.5.8 Ligation

Standard reactions were carried out in a 0.5 µl PCR Eppendorf tube. A ratio 3:1 insert:vector, 0.8 µl of T4 ligase enzyme, 1.5 µl of 10X ligase buffer and top up 15 µl of ddH₂O. Ligation mix was short vortexed and given a short-spin, then was incubated at 65°C for 30 min or 13°C overnight. To confirm a successful ligation, 5 ul of the sample was run in 0.8% on an analytical agarose gel.

2.2.5.9 Heat-shock transformation

5 µl of ligation were mixed with 100 µl of *E. coli* DH5α competent cells. The competent cells tube was vortexed and incubated on ice for 1 hour. Afterwards these

cells were exposed to a heat-shock in a water bath during 90 seconds at 42°C and immediately placed back on ice for 10 minutes. 900 µl of LB liquid media were added, well mixed and vortexed. Afterwards, the competent cells were transferred in a shaking incubator for 1 hour at 37°C. 100 µl and 200 µl of transformed cells were plated to two different LB solid agar plates with selection antibiotics. Finally, both plates were incubated upside down overnight at 37°C and potential transformants were analysed the following day.

2.2.5.10 Plasmid DNA purification

Following ligation-transformation processes, different colonies were randomly taken from LB solid plates and every single bacterial colony was cultured in 3 ml or 6 ml LB medium for Mini-preparation or 100 ml for Midi-preparation with selection antibiotics and incubated overnight at 37°C. Before the purification, every sample is taken and streaked on LB solid agar plate which is dried on a safety cabinet 10 minutes and incubated overnight at 37°C. Afterwards, the plasmid DNA was purified as follows:

2.2.5.11 Plasmid DNA Mini preparation: TENS method

The remaining sample was centrifuged at 11 363 x g for 30 s to obtain a pellet. The supernatant was discarded, and liquid was removed as much as possible. 300 µl TENS buffer were combined with the sample and vortexed for 4 seconds, upon which the samples immediately placed on ice. Next, 150 µl 3M NaOAc (pH 5.2) were added to the sample and vortexed for 3 seconds. Once more, the sample was immediately on ice. Then, the sample was centrifuged at 11 363 x g for 15 minutes at 4°C. The supernatant was transferred to a new 1.5 ml microcentrifuge tube and centrifugation rounds are repeated until the supernatant is white particle-free. 900 µl ice-cold 100% ethanol are added to the sample and centrifugation is repeated as previously. The supernatant is removed and replaced with 500 µl ice-cold 70% ethanol. Again, the sample was centrifuged as previously. The pellet was air-dried for 15 minutes and re-suspended in 40 µl sterile ddH₂O.

2.2.5.12 Plasmid DNA Mini preparation: ISOLATE II Plasmid Mini Kit

To harvest the bacterial cells, 6 ml were pelleted from a saturated LB culture (containing antibiotics for selectivity) at 11 000 x g for 30 seconds. The supernatant

was discarded, and any remaining liquid was removed as much as possible. The pellet was resuspended with 250 µl of P1 buffer via vortex, after this 250 µl of P2 lysis buffer was added whereupon the samples were gently mixed inverting the tube 6-8 times. The sample was incubated at room temperature for up to 5 min or until lysate appeared clear. Then, 300 µl of P3 neutralization buffer were added, the sample was thoroughly mixed by inversion 6-8 times. The mix sample was centrifuged at 11 000 x g for 5 min at room temperature. 750 µl of clear lysate supernatant was transferred to a spin column placed in a 2 ml collection tube to bind plasmid DNA and centrifuged at 11000 x g for 1 min, thereupon the flow-through was discarded. 600 µl of PW2 wash buffer previously supplemented with ethanol 100% was added and centrifuged as previously, the flow-through is once more discarded and the collection tube reused. The spin column was centrifuged at 11000 x g for 2 min to dry silica membrane and transferred onto a 1.5 ml microcentrifuge tube. 50 µl of P elution buffer were added onto the centre of silica membrane. The sample was incubated for 1 minute at room temperature and lastly centrifuged at 11000 x g for 1 min to elute the plasmid DNA.

2.2.5.13 Plasmid DNA Midi-preparation: NucleoBond Xtra Midi kit

Near flame sterilisation environment, 500 µl of bacterial culture were mixed with 500 µl of glycerol in a 1.5 ml cryogenic tube. The sample was vortexed and immediately placed on ice for 10 minutes before stored at -80°C. The remaining culture was split in two 50 ml tubes, thereupon the samples were centrifuged at 3500 x g for 15 minutes at 4°C, then the supernatant was discarded. Both pellets were re-suspended in 8 ml of RES buffer added with RNase A by pipetting up and down to avoid clumps in the suspension. 8 ml of LYS buffer were added to the suspension and softly inverted 5 times. The suspension was incubated for 5 min at room temperature. 12 ml of EQU buffer are added onto the rim of filter inserted on a column, whereupon the column is allowed to be emptied by gravity flow. 8 ml of NEW buffer are added to the suspension and immediately the lysate was gently mixed by inversion 10-15 times until the blue sample turns to colourless. The homogeneous suspension is carefully loaded onto the filter column to avoid potential clogs in the filter. The forecited was repeated until the lysate sample was completely loaded, and the column was emptied by gravity flow. 5 ml of EQU were added in the column to wash out any remains of lysate in the filter. The filter was removed, and 8 ml of WASH buffer were added in the column. The plasmid DNA was eluted adding 5 ml of ELU buffer and collected in a new sterile 50 ml tube. The elution is aliquoted transferring 833 µl into six 1.5 µl

microcentrifuge tubes and mixed with 583 μl of room temperature Isopropanol. The tubes were thoroughly vortexed and centrifuged at 15 000 x g for 30 minutes at 4°C. The supernatant was carefully discarded. 333 μl of room temperature 70% ethanol per tube were added to the pellet, upon which the samples were vortexed and centrifuged at 15 000 x g for 5 min at room temperature. The remaining supernatant was carefully discarded by pipetting, then the pellets were air-dried for 15 min at room temperature in sterile conditions. Finally, the plasmid DNA is resuspended in 30 μl of TE buffer or sterile ddH₂O.

2.2.6 PCR

2.2.6.1 Generation of repair cassettes for CRISPR.

In a 200 μl PCR tube previously cooled on ice were combined 36.5 μl sterile ddH₂O, 10 μl MyTaq buffer, 1 μl pCR2.1neo/phleo/hyg plasmid (0.02 to 0.04 $\mu\text{g}/\mu\text{l}$), 1 μl forward oligomer (2 μM), 1 μl reverse oligomer (2 μM) and 0.5 μl Q5 polymerase. The samples were placed in a PCR machine (Gene Amp PCR Cycler, PE Applied Biosystems, Weiterstadt, Germany) using the conditions outlined next:

Denaturation at 94°C for 2 minutes.
Denaturation at 94°C for 10 seconds.
Annealing at 60°C for 40 seconds.
Elongation at 72°C for 1 minute 20 seconds.
Elongation at 72°C for 2 minutes.
Infinity to 4°C

} 40 cycles

2.2.6.2 PCR-amplification of sgRNA templates

In a 200 μl PCR tube previously cooled on ice were combined 37.5 μl sterile ddH₂O, 10 μl 5x MyTaq buffer, 1 μl G00 (2 μM), 1 μl upstream oligomer (2 μM) or 1 μl downstream oligomer (2 μM) and 0.5 μl Q5 polymerase. The samples were placed in a PCR machine (Gene Amp PCR Cycler, PE Applied Biosystems, Weiterstadt, Germany) using the conditions outlined next:

Denaturation at 94°C for 30 seconds.
Denaturation at 94°C for 10 seconds.
Annealing at 60°C for 30 seconds.
Elongation at 72°C for 15 seconds.
Elongation at 72°C for 7 minutes.
Infinity to 4°C

} 35 cycles

2.2.7 Sequencing

2.2.7.1 Sequencing of pRFPSV40 plasmid construction

The new pRFPSV40 plasmid construction was sent to Source Bioscience to be sequence analysed. The plasmid construction and the primer were both sent at a concentration of 100 ng/μl and 3.2pmol/ul respectively, with a minimum of 5μl per reaction.

2.2.8 Transfections

2.2.8.1 Transfection of pRFPSV40 with Xfect in *Acanthamoeba castellanii* Neff strain trophozoites.

On day 1, *A. castellanii* Neff trophozoites were cultured, harvested, and counted to reach 5×10^5 cells/ml were pelleted, washed with 10 ml of Neff encystment medium (NEM) and then re-suspended in 500 μl of NEM, before being transferred to a six-well culture plate. The reaction mix was prepared as follows: 5 μg/μl of the plasmid pBRFPNeoCas9 were added to a 1.5 ml microcentrifuge tube, Xfect (TakaraBio) Reaction Buffer was then added to give a total volume of 100 μl and vortexed for 5 seconds. Then, Xfect polymer was vortexed for 5 seconds and 1.5 μl was added to the mixed sample, whereupon vortexed for 10 seconds. The solution was briefly centrifuged to collect the contents, and then incubated for 10 minutes at room temperature. The entirety of the reaction mix was added to the cell culture, the plate was gently rocked for 1 minute to mix the contents. 700 ul of fresh NEM was then added to the cell culture for a total volume of 1300 μl. The reaction mix was left for 24 hours at room temperature. On day 2, the mixed sample was carefully removed by pipetting and replaced with 4 ml of PG medium. The cells were given 24 hours to recover. On day 3, 1 ml of PG media were added followed by 6.25 μM G418 to act as a selection marker. The cells were incubated at room temperature until ~70% confluence before being transferred to a T75 containing 10ml of PG media supplemented with 6.25 μM G418 to maintain the plasmid construction. Two different culture flasks containing trophozoites adding only the plasmid without the Xfect polymer and buffer as well as another one containing non-transfected trophozoites worked as controls.

2.2.8.2 Transfection of pBRFPNeoCas9 with Xfect and Polyplus in Acanthamoeba castellanii Neff strain trophozoites.

The previous method was used for the transfection of pBRFPNeoCas9 using both Xfect and Polyplus reagents. The conditions for Polyplus for the reaction mix were 10 µg/µl of plasmid DNA, 200 µl of Reaction buffer and 5 µl Polymer reagent. Additionally, on day 2 the reaction mix was carefully removed via pipette and replaced with 3 ml of PG medium for Xfect, and 1 ml of PG medium for Polyplus.

2.2.8.3 Transfection of pBRFPNeoCas9 and pBRFPPhleoCas9 with Xfect in Acanthamoeba Neff strain trophozoites.

On the preparative day, *A. castellanii* Neff trophozoites were grown, harvested, washed with PBS, and counted to reach 4×10^5 cells/ml. The cells were added to a 6-well culture plate containing 3 ml of PYG medium and incubated at 25°C for 24 h. On the transfection day, 5 µg/µl of pBRFPT7NeoCas9 or pBRFPT7PhleoCas9 were added to a microcentrifuge tube containing 100 µl of Xfect reaction buffer and vortexed for 5 s. The Xfect polymer was vortexed for 5 s and 1.5 µl was added to the microcentrifuge tube to complete the transfection complex. The mix was vortexed for 10 s, centrifuged to collect all the contents, and then incubated for 10 minutes at RT. PG medium on 6-well plate previously prepared was gently aspirated and the remaining amoebas attached to the well were washed once with 3 ml of PBS at RT. 1 ml of PG medium was added to the microcentrifuge tube containing the transfection complex and mixed via pipetting. The mix is immediately added dropwise to the attached cells and incubated for 3 h at 25°C. Three hours later, PYG medium was removed, and cells were washed with PBS. The cells were incubated to with 3 ml of PG medium for 48 h at 25°C. The transfected cells were transferred to T75 flasks containing 10 ml of PG medium supplemented with high dose, optimal dose, and low dose of G418 or phleomycin for 2-3 weeks until cell growth is apparent. Transfection of pBRFPNeoCas9 was used as positive control. Cultures of wild type trophozoites supplemented with G418 or phleomycin were used as negative control. A total of 15 transfections were performed.

2.2.9 Fluorescence-Activated Cell Sorting (FACS) and flow cytometry analysis.

Fluorescence activated cell sorting (FACS) was performed using MoFlo XDP Cell Sorter (Beckman Coulter Life Sciences) with 488 nm blue excitation laser and data collected with Summit Software V5.0. Flow cytometry analysis was performed using AttuneNxt (Invitrogen) with 488 nm blue excitation laser, 574/26 nm emission filter and channel BL2. *Acanthamoeba castellanii* positive transfected trophozoites with pBRFPT7NeoCas9 and pBRFPT7PhleoCas9 were treated with the higher dose of G418 and phleomycin, respectively. Wild type amoebas were also treated with the same conditions as the positive transfectants and used to define the analysis gate. Data was analysed using AttuneNxt Software V4.2

Chapter 3. *In vitro* screening of Strathclyde Minor Groove Binders (S-MGBs) against *Acanthamoeba* spp.

3.1 Abstract

Minor groove binders are molecules that form strong bonds with DNA of pharmaceutical interest because have shown before significant anti-infective activity against a wide range of pathogenic microorganisms. At University of Strathclyde, the minor groove binder Distamycin A has served as major template for molecular manipulation to design and synthesise prominent drug candidates (S-MGBs) for potential therapeutic use. In this chapter, a substantial number of S-MGBs were screened *in vitro* against *Acanthamoeba* spp. trophozoites utilising the colorimetric microtiter plate alamarBlue assay. From 42 S-MGBs, a library of 6 showed potent active inhibitory effect with half maximal inhibitory concentration (IC_{50}) below 1 μ M. S-MGB 235 showed the most potent activity at 24 h and 96 h against *A. castellanii* Neff, *A. polyphaga*, *A. castellanii* Clinical T4, ATCC50370 and ATCC50371 isolates generating IC_{50} values in the range of nanomolar. Moreover, the intrinsic fluorescence properties of S-MGB 363 and S-MGB 245 allowed for Confocal microscopy visualisations. These compounds bound to nucleus, nucleolus and were distributed through *Acanthamoeba* granuloplasm, however only the former caused disruption of the cell membrane leading to trophozoite cell lysis.

3.2 Background

Protists are eukaryotes that have metabolic processes with similarities to the human host opposed to those of prokaryotic pathogens. Consequently, infections caused by some protists are more difficult to treat than bacterial infections. Regrettably, anti-protist drugs exhibit unwanted or toxic side effects and the acquisition of drug resistance is a real challenge in developing novel drugs (Khan, 2015). Most of antiprotozoal drugs currently in clinical use act by as-yet-unknown modes of action, as a result this impacts our ability to optimize treatment strategies, understand parasite resistance mechanisms, and monitor drug efficacy and toxicity. Unfortunately, there is still a dearth of validated targets for parasitic diseases due to the lack of detailed information concerning of modes of action currently used as antiprotozoal drugs (Giannangelo *et al.*, 2016).

3.2.1 Minor Groove Binders

A particular set of compounds known as Minor Groove Binders (MGBs) have the characteristic of sequence-specific binding to the minor groove of a B-DNA duplex (Figure 3) forming hydrogen bonds (often with N3 of adenine and O2 of thymine). Their main effects are inhibiting DNA synthesis, interfering with transcription machinery, as well as inhibiting DNA topoisomerases, achieving apoptosis and then cell death. These molecules are often cations due to the complementary negative electrostatic potential of the DNA minor groove facilitating strong binding interactions. Moreover, this negative electrostatic potential is more prevalent in regions of high AT content, due to the presence of amino N6 and the carbonyl O4. Consequently, MGBs often possess a degree of specificity to AT-rich sequences rather than GC-rich sequences. Furthermore, the iso-helical topology of many MGBs is a complementary match to DNA, as this shape appropriately fits to the minor groove. MGBs have received great attention for drug design since they have a strong affinity to cellular DNA and are therefore potentially able to target multiple diseases including cancers and bacterial, fungal, viral, and parasitic infections. Therefore, they are still widely considered by many researchers as effective therapeutic treatments (Tyagi, 2017).

3.2.2 Classification

MGBs can be classified according to their interactions with DNA:

- I. Non-alkylating MGBs: These compounds interact with the minor groove through hydrogen bonding and hydrophobic interactions. In this group are included Distamycin A, diarylamidines (DAPI, berenil, pentamidine), and bis-benzimidazoles like Hoechst 33258 dye.

- II. Alkylating MGBs: These compounds bind irreversibly to DNA, through formation of covalent bonds. In this group are included CC-1065 (Carzelising and Adozelesin as synthetic analogs), anthramycin, mitomycin C, enedyne antibiotics (e.g. neocarzinostatin, esperamicin A₁, calicheamicin γ₁), ET-743 (an ecteinascidine derivative), and bleomycins (Baraldi *et al.*, 2004).

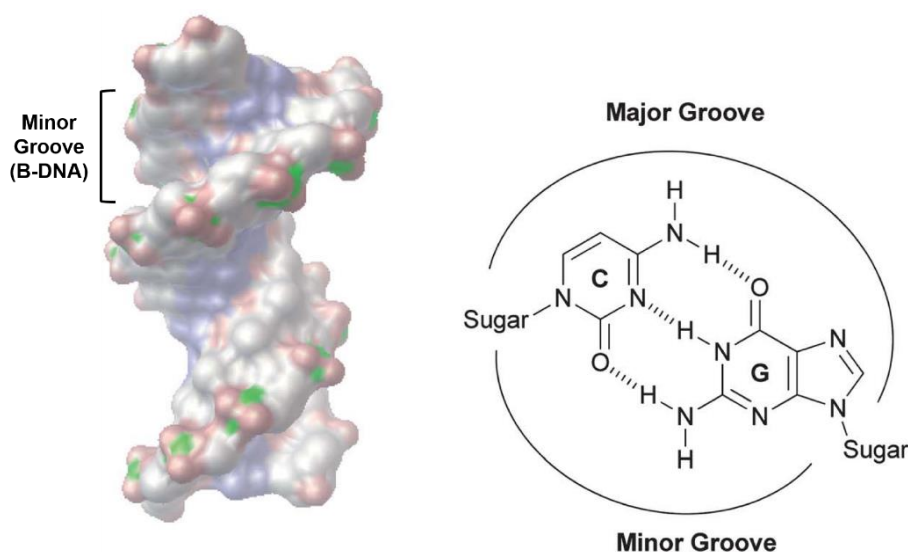


Figure 3. DNA minor and major groove.

Representation of B-DNA duplex highlighting the minor groove (left) and a line-bond structural formula of the hydrogen bond donor-acceptor in the major and minor grooves found in the DNA base pairs. Modified from Hamilton and Arya, 2012.

Natural MGBs such as distamycin, netropsin, CC1065 and anthramycin possess affinity to adenine-thymine (AT) rich regions of the minor groove. Specifically, Netropsin binds to four AT base pairs and one single molecule is bound in the minor groove, on the other hand, distamycin (also named Distamycin A or Stallimycin) binds to five AT base pairs and is usually binds as two antiparallel molecules within the minor groove (Khalaf, 2009). Both distamycin and netropsin are composed of several pyrrole units joined by amide bonds.

The binding of duocarmycins and anthramycins to DNA is through covalent binding to DNA nucleophilic groups depending overall in the modifications. CC1065 uses an aromatization reaction where the cyclopropane ring opens at the moment with the amino group contact of a G base; anthramycin also uses the amino group in a reaction that takes place in the double bond of the carbon-nitrogen of the diazepine ring, this is common in DNA sequences where GC base pairs is mostly found (Rahman *et al.*, 2009). Modifications in the structure of MGBs are carried out with the objective of improving the molecular recognition for DNA and the activity against pathogens; such changes are in different levels of the molecule like the head group, the tail group (which often contains the cationic groups), the heterocyclic rings (antimicroorganism activity) and the amide linkages. Commonly, distamycin A or netropsin natural MGBs include at least one pyrrole ring which are replaced for heterocyclic thiazole, imidazole, furan, oxazole or thiophene to obtain synthetic derivatives for testing in biological systems. Olefinic double bonds or diazo groups are common replacements of amide linkages in synthetic MGBs. To exemplify the former, Trabectidin (also known as Yondelis®) is a MGB isolated from marine tunicates and widely used as a treatment for soft tissue sarcoma that overcomes the “common” linear structure of MGBs because is composed of two substructures arc-like that bind to DNA by hydrogen binding and non-polar interactions whose activity apparently depends upon two sulphide-linked substituted isoquinoline rings with the right hand ring projected from the minor groove (D'Incalci and Galmarini, 2010). This complex agent causes disarrangement of DNA structure preventing protein binding, double strand breaks and interferes with nucleoside excision repair machinery (Suckling, 2012). Nevertheless, other intrinsic factors need to be considered to be validated for clinical use: safe measures of MIC and MBC, to show potent activity against diverse clinical strains, effective -cidal/-static activity, to prevent potential resistance and physicochemical factors such as low pKa, solubility and stability (Barrett, Gemmell and Suckling, 2013).

3.2.3 Minor groove binders as antibacterial drugs

Efforts in creating antibacterial MGBs have been emphasised and in-depth development because of extensive antimicrobial drug resistance. Some important considerations are the recognition and binding to DNA, parameters such as mechanism of action, recognition of a specific target in infectious pathogens, interactions, and toxic effects in the host. Hydrophobic interactions might improve the

binding to bacterial cells through the modification in N-alkyl groups than methyl, thiazoles in place of imidazoles, aromatic head groups, basic tails, and amides isosteres. Historically GSQ 1530, a derivative of Distamycin A and created and marketed by Genesoft, is a potent inhibitor of bacterial DNA function and DNA-dependant RNA transcription in *S. aureus* (both methicillin sensitive and resistant strains), *S. epidermis* and *S. haemolyticus*. It was bactericidal in *S. aureus* and *S. pneumoniae* but bacteriostatic against *Enterococcus faecalis* (Ge *et al.*, 2002). Not all effects of MGBs are due to interaction with DNA. The antibacterial activity shown by two head pyrrole tetramide with two cationic tail groups inhibiting MRSA at 1.4-2.8 μM and vancomycin-resistant enterococci at 1.4-5.7 μM was found to be due to targeting the bacterial cell membrane (Dyatkina *et al.*, 2002). Khalaf in 2004 have rearranged several MGBs molecules making substitutions of thiazoles and thiophenes which enhanced significant antibacterial effects towards gram-positive bacteria, fungi (*Aspergillus nidulans*), and yeasts (*Candida albicans*) (Khalaf *et al.*, 2004). At the University of Strathclyde more than 500 compounds have been developed with the significant results obtained against Gram-positive such as *Staphylococcus aureus*, and *Mycobacteria*, although little activity against Gram-negative bacteria has been found (Suckling, 2012).

3.2.4 MGBs as antiparasitic drugs

Investigations into the efficacy of MGBs against protozoal diseases started as early as the 1930's with works based in the main aromatic diarylamidine Pentamidine against Human African Trypanosomiasis (HAT) and *Leishmania* (Soeiro *et al.*, 2013). After these, the development of new synthesized derivatives such as DAPI and Berenil have been elucidated (Baraldi *et al.*, 2004). In addition to their antiparasitic activities, diamidines have also been found to be effective *in vitro* and *in vivo* against fungi, distinctive examples are *Candida* spp., *Fusarium* and *Cryptococcus neoformans* (Barchiesi *et al.*, 1994; Del Poeta *et al.*, 1998; Miletto and Leibowitz, 2000; Lionakis *et al.*, 2003).

Pentamidine isethionate (Pentacarinat ®, Rhodia) is a derivative agent of synthalin (analogue of insulin) developed in 1937 that has been used widely in clinic against the early-stage of HAT, antimony resistant strains of *Leishmania* and infections caused by *Pneumocystis jiroveci* in AIDS patients (Obaji *et al.*, 2003; Soeiro *et al.*, 2005). However, it has been somewhat restricted due to its high toxicity and poor

bioavailability. Important to mention, pentamidine needs to be administered and monitored in hospital for possible modifications in blood glucose and blood decompensation as well as possible damage in liver and kidneys. Another parasite target of pentamidine is *Toxoplasma* spp. where it has been shown to inhibit the growth of tachyzoites in culture suggesting a possible role as a treatment (Lindsay *et al.*, 1991).

Berenil (known as diminazene) originally created for treating trypanosomiasis in cattle during the 50's, has activity against *Leishmania* and *Trypanosoma* both *in vitro* and *in vivo*. This MGB inhibits promastigotes of *L. donovani* and *L. tarentolae* in a dose-dependent manner as well as healing ulcers in children presenting cutaneous manifestations when applied topically. A variation of Berenil containing procaine and antipyrine (Trypan®) was shown to decrease the development and multiplication of *Leishmania* promastigotes and the resulting cutaneous lesions in BALB/c mice; in *L. major* strain the effect impacted after the infection when applied topically, but such effectiveness was not produced in human trials. Negative and severe relapses were obtained when around 50-60% of rats infected with *T. brucei* were treated with Trypan (Soeiro *et al.*, 2005).

Furamide or DB75 is a MGB with important antiparasitic effects against a number of organisms including *Pneumocystis jiroveci*, *Giardia lamblia*, *Plasmodium falciparum*. However, due Furamide's cationic nature similar to its analogues, it offers very low oral bioavailability. In clinical trials a prodrug of Furamide (DB289) has shown activity against HAT and pneumonia caused by *P. jiroveci*. When this prodrug is metabolized inside the host, the active form of this diamidine shows impressive antiparasitic activity avoiding toxicity. Another prodrugs (DB820) have reached an ideal oral bioavailability, but efforts for improving this feature in future compounds continue (Soeiro *et al.*, 2005).

One of the dicationic molecules that has exhibited excellent *in vitro* activity based on IC₅₀ (around 4.5 nM) against HAT is CPG4015A. Even *in vivo* experiments, cure is established in murine models with trypanosomiasis with only three intraperitoneal doses. When used in combination with eflornithine it can also stop CNS infection. With this result, the significance of this MGB was advanced to study its pharmacological effects in African green monkeys but, lamentably this molecule was unable to cross the BBB therefore further research was ceased (Soeiro *et al.*, 2005).

Representative active MGB antiparasitic compounds are bis-heterocyclic amidines, whereas anticancer agents tend to possess alkylating groups. One of the first MGBs used as an anticancer is Tallimustine, where distamycin was modified with a β -chloroethylamine (nitrogen mustard) substituent. Brostallicin is a compound where the α , β -unsaturated bromoamide was included that reached Phase II of the clinical trials for soft tissue sarcoma. Another example is Centanamycin, an alkylating drug which is a derivative of CC1065 with *in vivo* anticancer activity in ovarian xenografts (Sato *et al.*, 2005). This MGB has also been proved to be highly cytotoxic *in vitro* (IC_{50} = 1.8 nM/L) and DNA damage was detected in *Plasmodium* isolated from mice 24 h after mice treated with this compound (Yanow *et al.*, 2008). In spite of its low aqueous solubility, the anthramycin derivative SJG136 showed a clear effect against solid tumours in a phase I trials; the molecular mechanism has not been detailed, but it possibly creates stable purine-GATC-pyrimidine binding sites (Rahman *et al.*, 2009; Janjigian *et al.*, 2010). Not long ago, a new group of N-phenylbenzamide derivatives showed *in vitro* effects as a potential drug for Human African Trypanosomiasis (HAT) and effectively healed mice. Clear damage to the kinetoplast was identified via surface plasmon resonance (SPR)-biosensor (Millan *et al.*, 2017).

3.2.5 MGBs against *Acanthamoeba* diseases

Only few studies about the application and analysis of MGBs against *Acanthamoeba* spp. in the literature are found. As established above, Brolene is a close related diamidine commonly used against AK and in combination with other drugs is effective and non-toxic showing *in vitro* higher effect. However, prolonged use leads to corneal damage and scleral inflammation causing invasion of viable parasites (Pérez-Santonja *et al.*, 2003). Another derivate of diamidines, hexamidine di-isethionate (DesomedineTM) has shown amebicide effect against *Acanthamoeba* *in vitro* and *in vivo* (Brasseur *et al.*, 1994).

3.2.6 Strathclyde Minor Groove Binders (S-MGBs)

The Scott research group at the University of Strathclyde has recently led important studies in the development, synthesis, and analysis of Strathclyde MGBs (S-MGBs) against parasites that cause neglected tropical diseases with promising results. In this work, modifications of the structure of Distamycin A to create novel S-MGBs included the introduction of less basic functional groups to replace the amidine at the C-terminus, larger alkyl side chains instead methyl groups and thiazole rings

have been added to the body (Figure 4). Four of 32 S-MGBs tested showed significant effects against *Trypanosoma brucei*, and it was found that the head group moiety was a main modulator of the antiparasitic effect (Scott *et al.*, 2016b). In a different study of S-MGBs, the effects of different physicochemical properties and modifications in the head group to an isosteric alkene were also explored for activity against *Plasmodium falciparum*. This study used two different strains of the pathogen, one being chloroquine resistant (3D7 and Dd2), and IC₅₀s ranging 30-500 nM were found against both strains. The lack of observed resistance suggests that these MGBs may be candidates for future development (Scott *et al.*, 2016a).

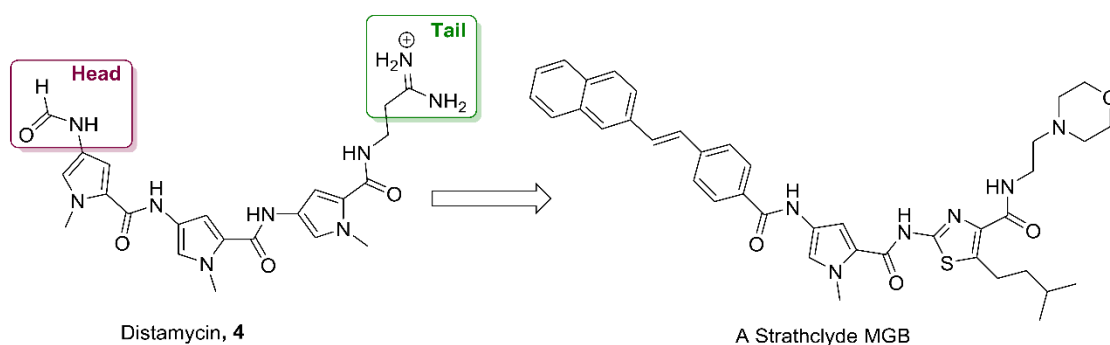


Figure 4. Structural representative example of a Strathclyde MGB (S-MGBs) derived from the prototype structure of Distamycin.

Taken from Scott *et al.*, 2016b.

3.3 Aims and Objectives

New effective and non-toxic drug treatments for *Acanthamoeba* diseases are needed. MGB derivatives of Distamycin A are a group of compounds poorly explored against this amoeba, despite their potent and prior proven antiparasitic effects against tropical diseases such as trypanosomiasis and malaria. Therefore, a new series of S-MGBs designed and synthesised at University of Strathclyde by the Scott research group offer the possibility to elucidate potential inhibitors against *Acanthamoeba* spp.

Thus, this chapter aims to standardize the optimal seeding density of *Acanthamoeba* spp. trophozoites to be screened with a substantial collection of S-MGBs *in vitro* against *Acanthamoeba* Neff strain to find out potential inhibitory effects. The most effective S-MGB will be tested against four additional *Acanthamoeba* strain/species to discriminate and describe any significant difference on the inhibitory effect among them and lastly make the most of some S-MGBs with fluorescent properties to investigate the intracellular distribution in the amoeba.

Objectives of this chapter are (i) to determine the sensitivity and viability of *Acanthamoeba* spp. trophozoites to S-MGBs by means of alamarBlue assays. Additionally, (ii) the mode of action and cellular impact will be evaluated in *Acanthamoeba* Neff strain trophozoites through Confocal microscopy analysis using selected fluorescent analogues S-MGBs.

3.4 Results

3.4.1 Optimal Seeding Density of *Acanthamoeba* spp.

The seeding densities for *A. castellanii* Neff strain, *A. polyphaga*, ATCC50371, Clinical T4 and ATCC50370 trophozoites that achieved the highest possible rate of alamarBlue reduction (without risking over-reduction) were determined at 96 h and 24 h in three independent experiments. The plates were incubated at 23°C. The seeding densities that achieved 80%-100% of alamarBlue reduction varied depending upon time-point with 24 h ranging from 16×10^3 – 0.125×10^3 cells/well and 96 h ranging from 32×10^3 – 0.025×10^3 cells/well (Figure 5). A correlation for every given seeding concentration was found between the high trophozoites number due to parasite proliferation and the metabolization of resazurin to resorufin which increased with the length of incubation periods. The optimal seeding density was chosen according to the cell concentration found in the log phase which caused a maximum potential reduction of alamarBlue just before the high concentration of trophozoites caused over-reduction. A complete summary of the optimal seeding densities for every *Acanthamoeba* species is shown in Table 12.

Table 12. Summary of optimal seeding density of *Acanthamoeba* spp.

The selected seeding densities for the alamarBlue assays for 96 hours and 24 hours are displayed for all five isolated of *Acanthamoeba* spp. In black is shown the initial cell concentration in the assay, in red is shown the final cell concentration per well.

<i>Acanthamoeba</i> specie/strain	96 h standardised cell density	24 h standardised cell density
<i>Castellanii</i> Neff	4x10 ⁴ cells/ml	32x10 ⁴ cells/ml
	2x10 ³ cells/ml (per well)	16x10 ³ cells/ml (per well)
<i>Polyphaga</i> (environmental)	16x10 ⁴ cells/ml	64x10 ⁴ cells/ml
	8x10 ³ cells/ml (per well)	32x10 ³ cells/ml (per well)
<i>Polyphaga</i> ATCC50371	4x10 ⁴ cells/ml	64x10 ⁴ cells/ml
	2x10 ³ cells/ml (per well)	32x10 ³ cells/ml (per well)
<i>Castellanii</i> Clinical T4	4x10 ⁴ cells/ml	64x10 ⁴ cells/ml
	2x10 ³ cells/ml (per well)	32x10 ³ cells/ml (per well)
<i>Castellanii</i> ATCC50370	4x10 ⁴ cells/ml	64x10 ⁴ cells/ml
	2x10 ³ cells/ml (per well)	32x10 ³ cells/ml (per well)

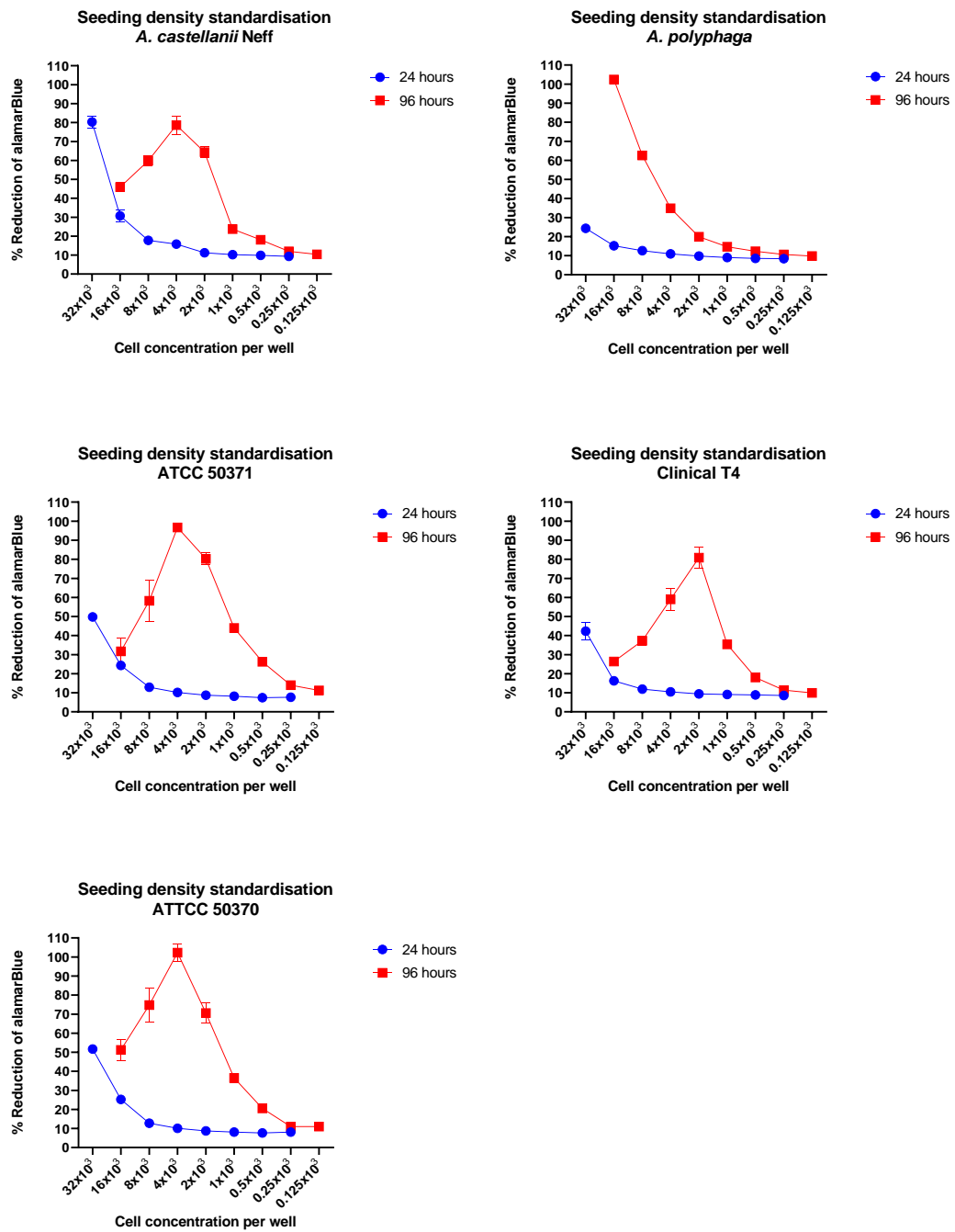


Figure 5. Reduction of alamarBlue by five different isolates of *Acanthamoeba* spp. trophozoites at 24 hours and 96 hours.

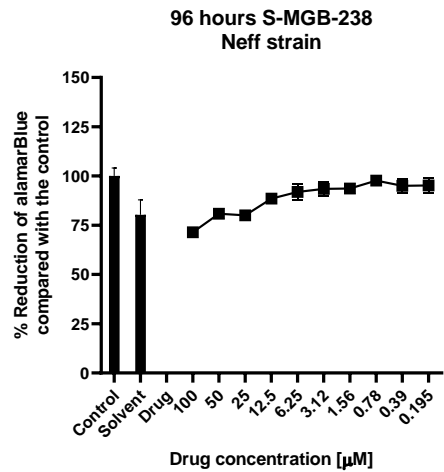
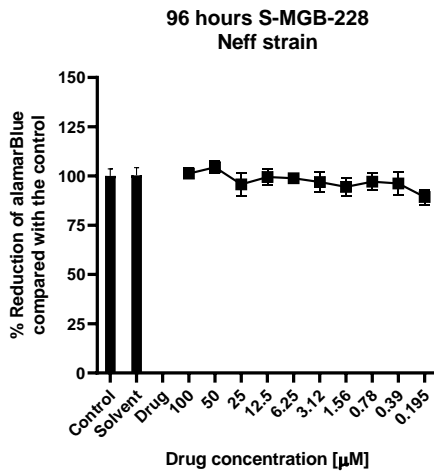
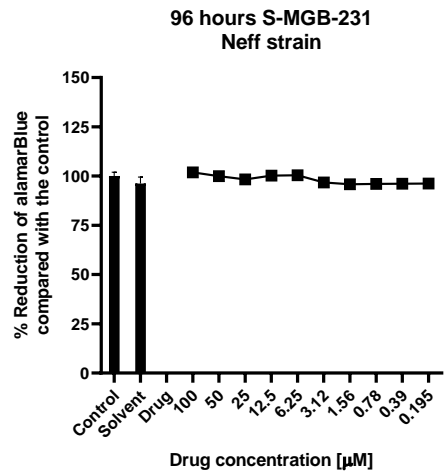
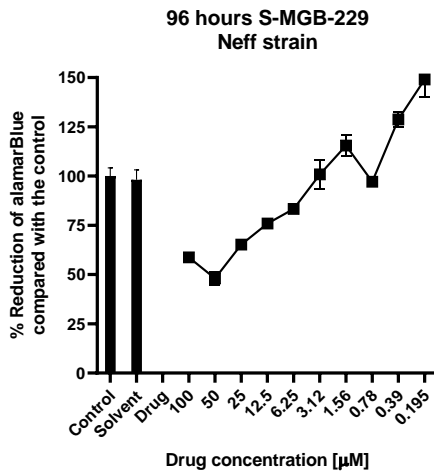
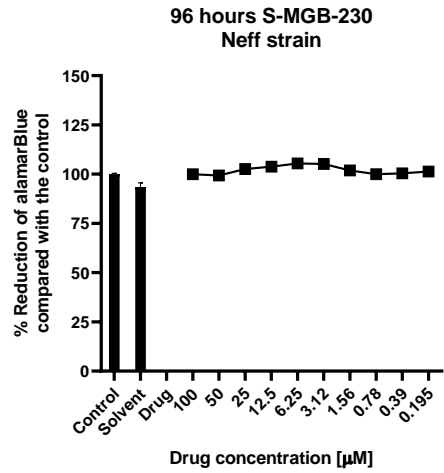
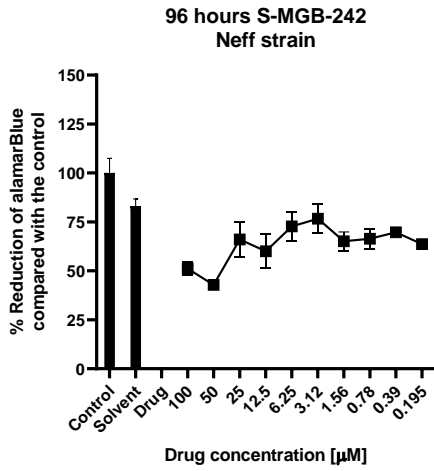
The assays were carried out in 96-well plates, incubated at 23°C, and read in SpectraMax spectrophotometer. The results represent the mean of triplicate wells ±SEM, and each assay was repeated in three independent experiments with a single representative run shown for clarity.

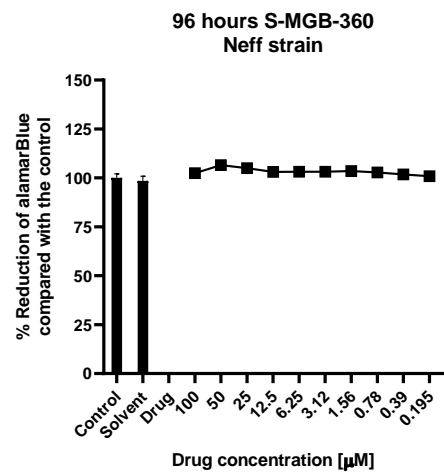
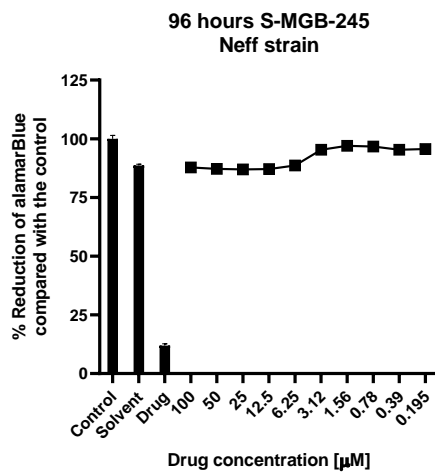
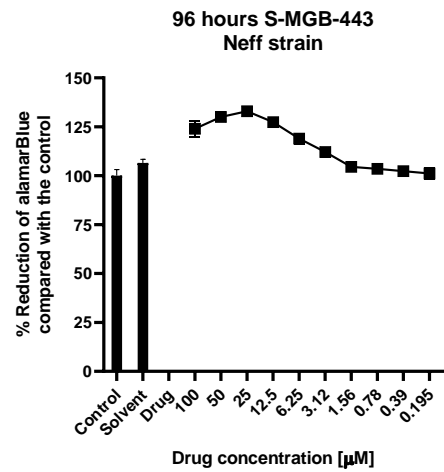
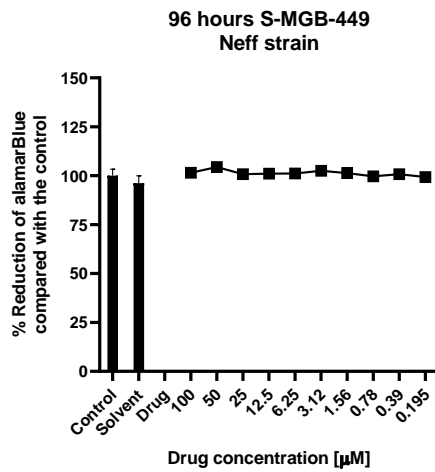
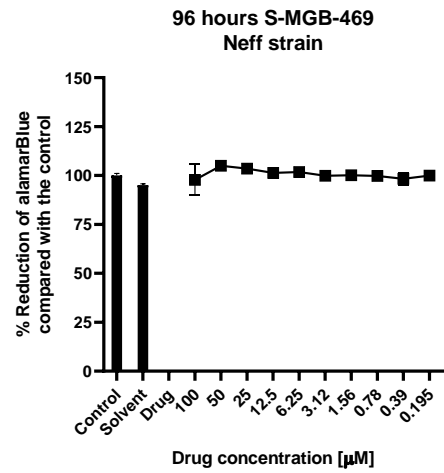
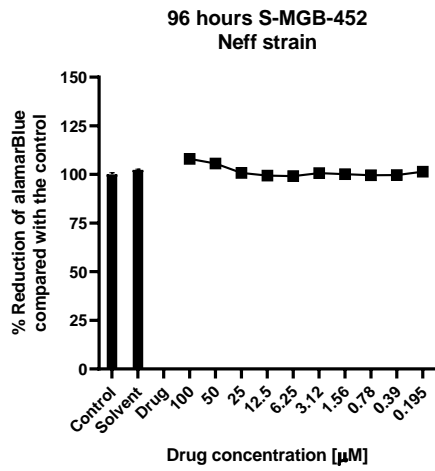
3.4.2 Effect of S-MGBs against *Acanthamoeba* Neff strain trophozoites at 96 hours.

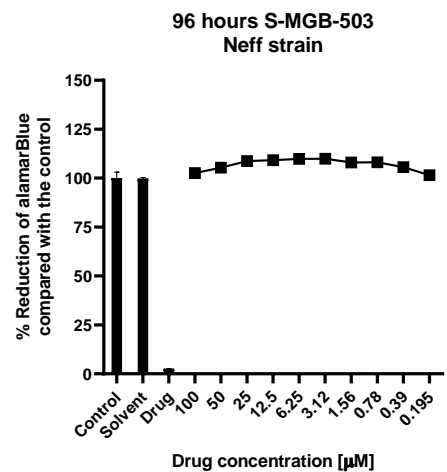
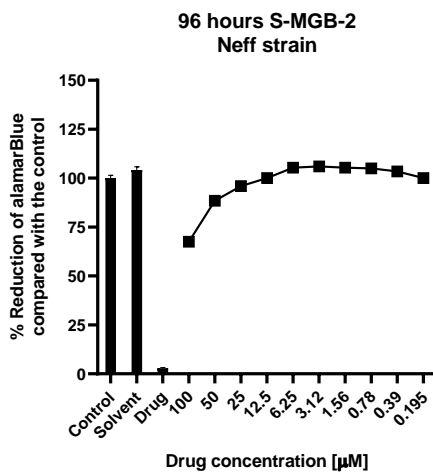
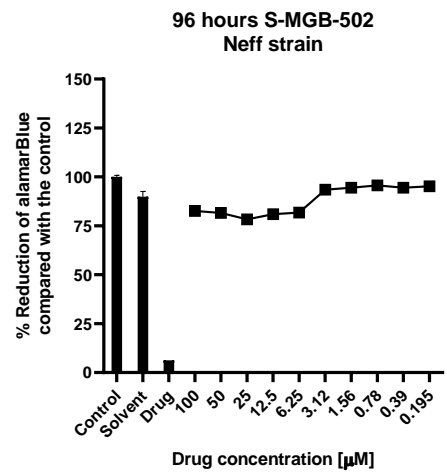
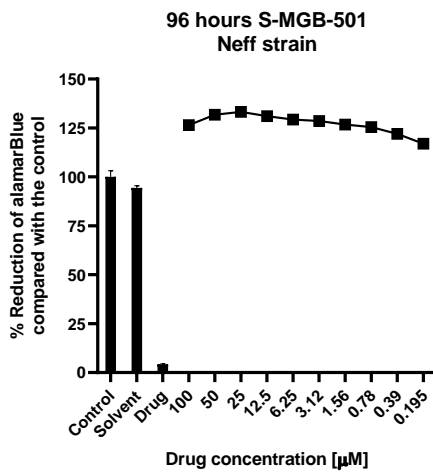
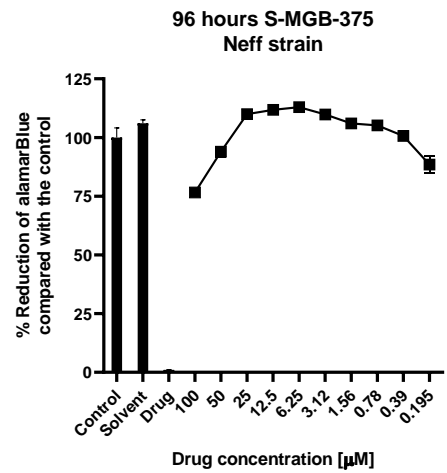
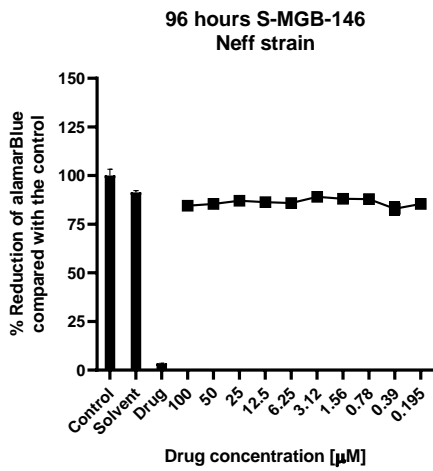
The effect of S-MGBs were screened against *Acanthamoeba* Neff trophozoites, based on the assay developed by McBride *et al.*, 2005. The half maximal inhibitory concentration (IC_{50}) effect of 42 S-MGBs against *A. castellanii* Neff trophozoites is summarized in Table 13.

Twenty-three S-MGBs did not produce any considerable inhibitory effect within the concentration range investigated, generating IC_{50} values $>100 \mu\text{M}$ (Figure 6). Thirteen S-MGBs showed a wide variation of inhibitory effect generating IC_{50} s in the range of $93.72 \mu\text{M} - 2.42 \mu\text{M}$ (Figure 7). S-MGBs: 410, 300, 504, 363, 234 and 235 showed high inhibitory effect generating IC_{50} s below $1 \mu\text{M}$ (Figure 8). All these S-MGBs in this 'hit library' contain an amidinylethyl tail group in their structure, with variations in the head group (Table 14). Light microscopic observations of cultures confirmed the effects of these S-MGBs on amoeba with trophozoites changing their appearance from ameboid to rounded (data not shown).

The most potent effect evident in the alamarBlue was displayed by S-MGB-235 with an IC_{50} 75.4 nM.







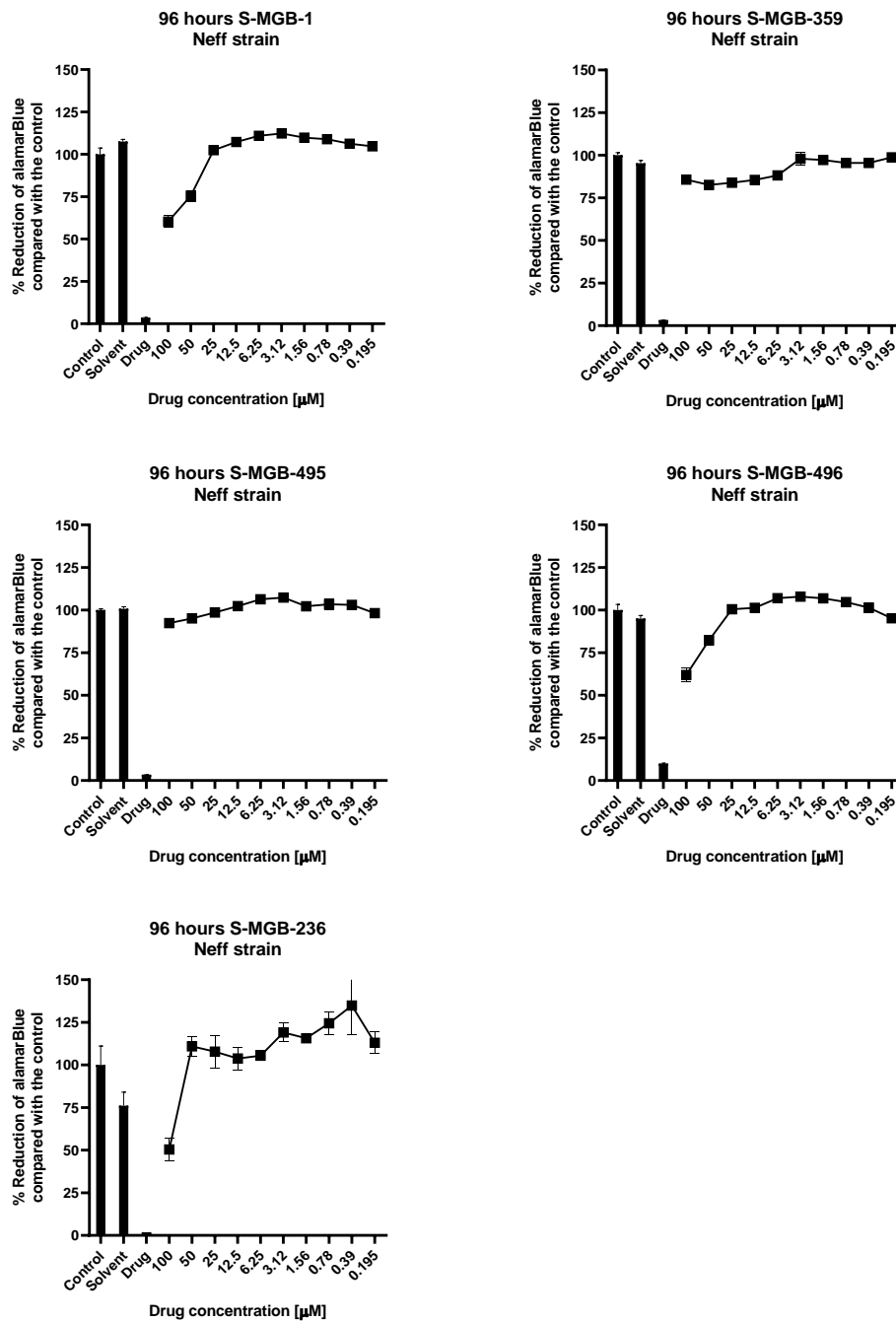
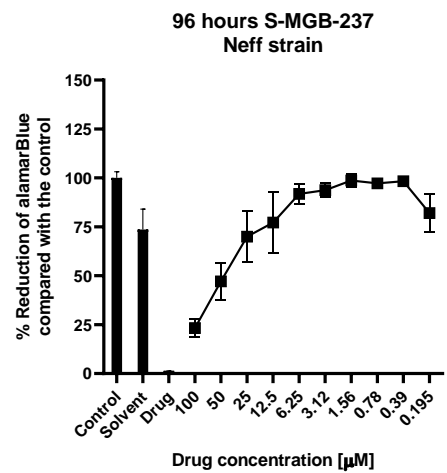
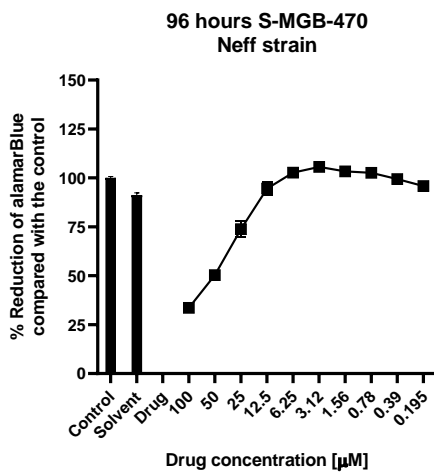
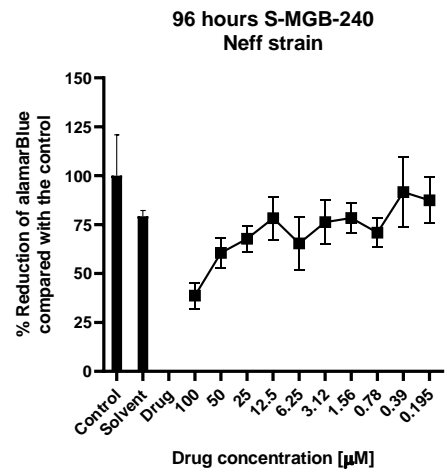
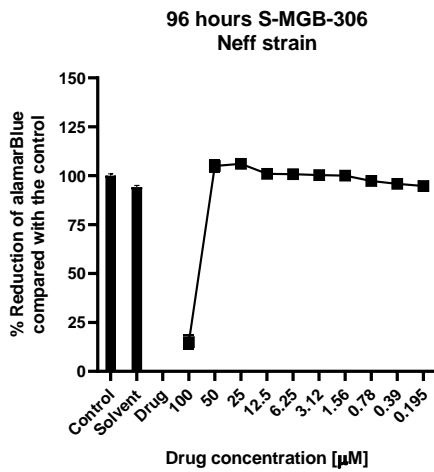
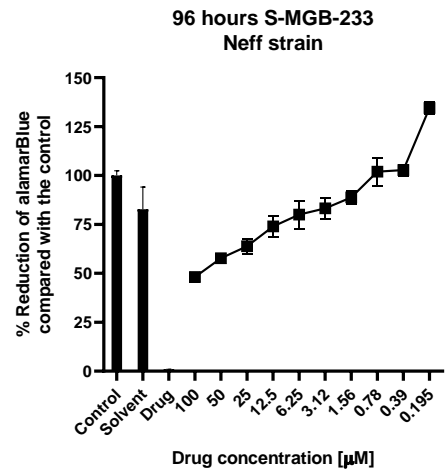
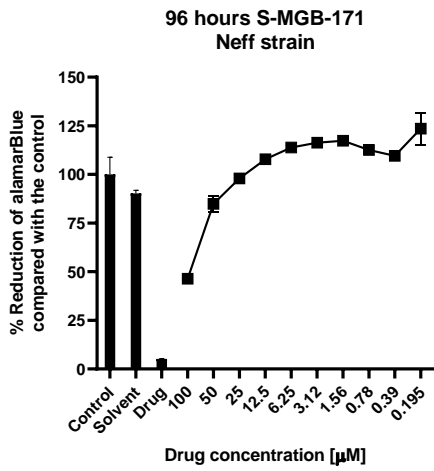
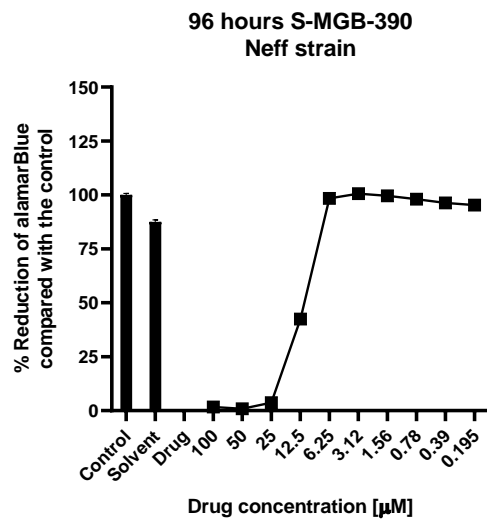
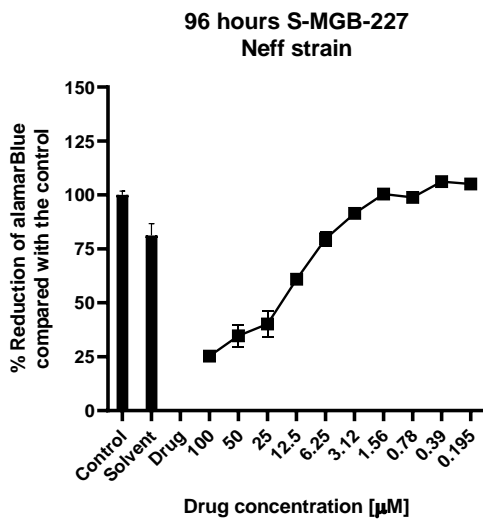
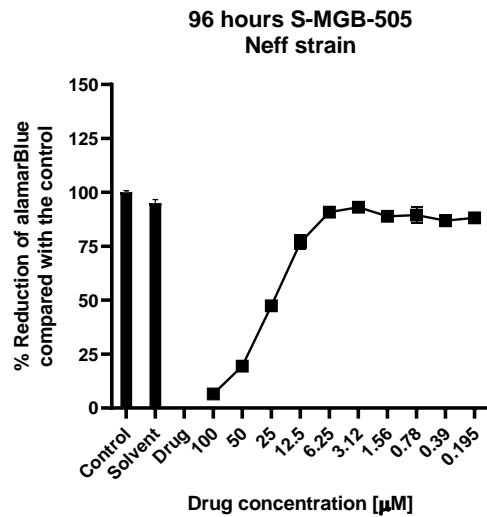
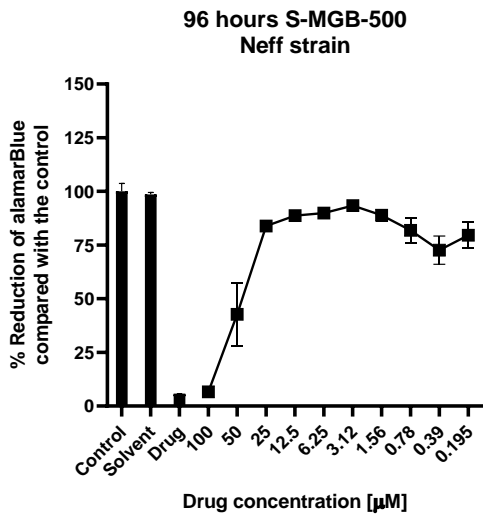


Figure 6. No active inhibitory effect of S-MGBs against *A. castellanii* Neff strain through alamarBlue assays.

Twenty-one S-MGBs showed IC₅₀s above 100 µM. 2x10³ trophozoites per well were seeded in PG media with 10 serial dilutions of S-MGBs. Trophozoites and PG medium (control), a DMSO (solvent) and PG medium with the highest concentration of S-MGB (100µM) (drug) were used as controls. The alamarBlue reduction percentage was read in a SpecMax spectrophotometer at 96 h, 23°C. Each value represents the mean of duplicate or triplicate wells ±SEM, the screening was carried out in three independent experiments of which single representative run shown for clarity.





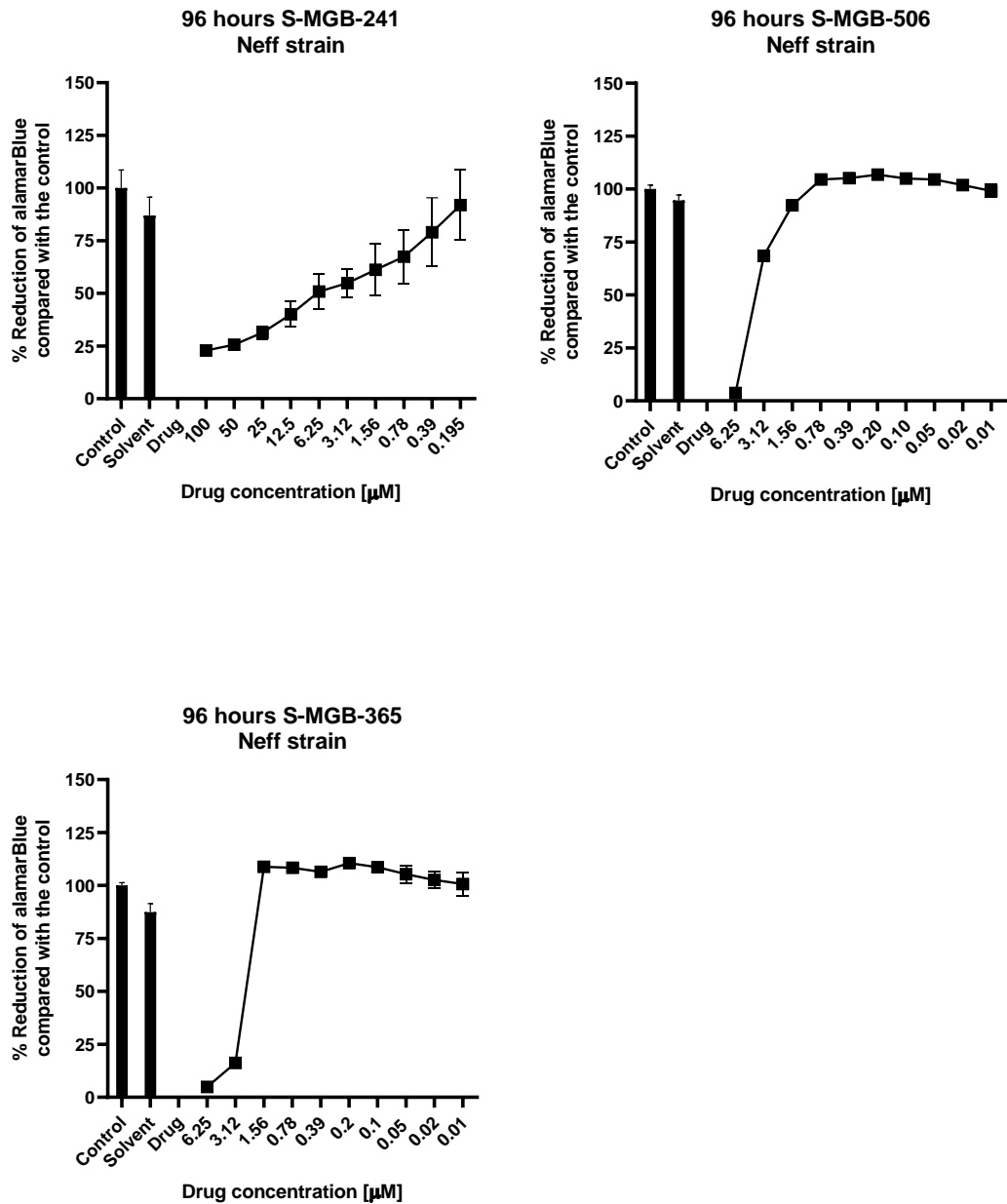


Figure 7. Mild active effect of S-MGBs against *A. castellanii* Neff strain through alamarBlue assays.

Fourteen S-MGBs showed IC₅₀s in the range of 100.46 µM – 2.42 µM. 2x10³ trophozoites per well were seeded in PG media with 10 serial dilutions of S-MGBs. Trophozoites and PG medium (control), a DMSO (solvent) and PG medium with the highest concentration of S-MGB (100 µM or 6.25 µM) (drug) were used as controls. The alamarBlue reduction percentage was read in a SpecMax spectrophotometer at 96 h, 23°C. Each value represents the mean of triplicate wells ±SEM, the screening was carried out in three independent experiments of which single representative run shown for clarity.

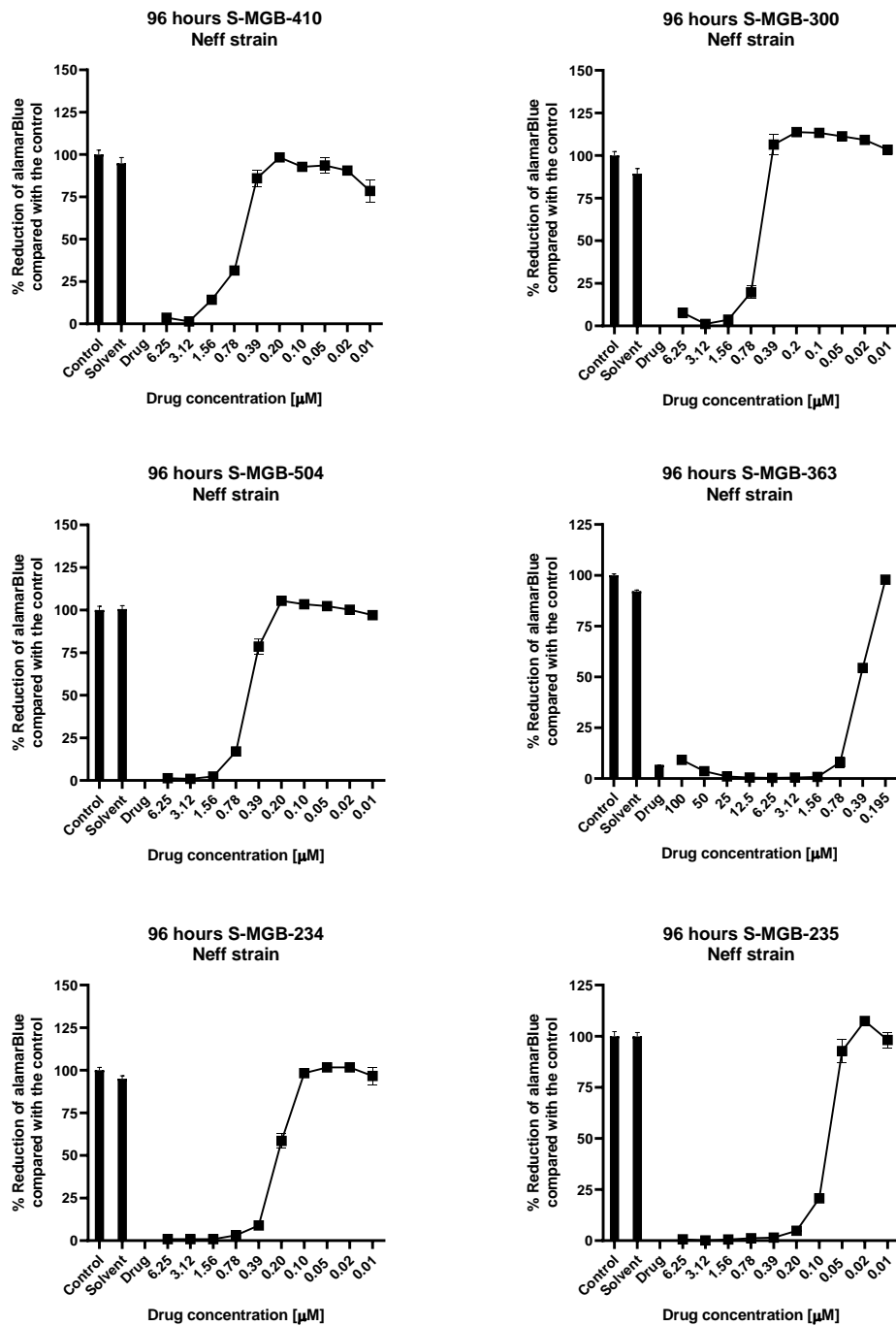


Figure 8. Robust effect of S-MGBs against *A. castellanii* Neff strain through alamarBlue assays.

Six S-MGBs showed IC₅₀s below 1 µM. 2x10³ trophozoites per well were seeded in PG media with 10 serial dilutions of S-MGBs. Trophozoites and PG medium (control), a DMSO (solvent) and PG medium with the highest concentration of S-MGB (100 µM) (drug) were used as controls. The alamarBlue reduction percentage was read in a SpecMax spectrophotometer at 96 h, 23°C. Each value represents the mean of triplicate wells ±SEM, the screening was carried out in three independent experiments of which single representative run shown for clarity.

Table 13. Relative activity of 42 S-MGBs examined against *Acanthamoeba castellanii* Neff strain

S-MGBs are ordered by activity and half maximal inhibitory concentration (IC₅₀), and Standard Error (SE) are shown where less than 100uM.

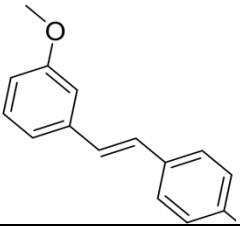
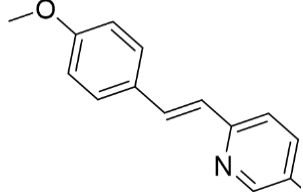
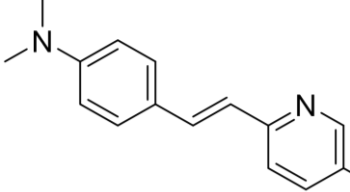
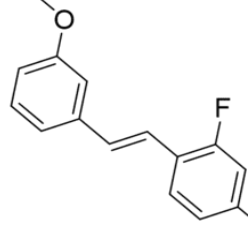
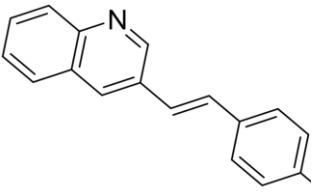
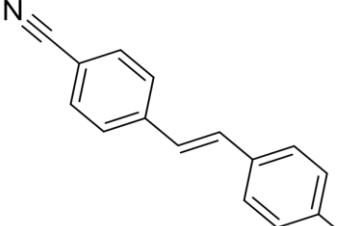
No.	S-MGB ID	IC ₅₀ (µM) at 96 h	SE
1	242	>100	N/A
2	230	>100	N/A
3	229	>100	N/A
4	231	>100	N/A
5	228	>100	N/A
6	238	>100	N/A
7	452	>100	N/A
8	469	>100	N/A
9	449	>100	N/A
10	443	>100	N/A
11	245	>100	N/A
12	360	>100	N/A
13	146	>100	N/A
14	375	>100	N/A
15	501	>100	N/A
16	502	>100	N/A
17	2	>100	N/A
18	503	>100	N/A
19	1	>100	N/A
20	359	>100	N/A
21	495	>100	N/A
22	496	>100	N/A
23	236	>100	N/A
24	171	93.72	2.15
25	233	87.35	3.84
26	306	76.35	6.93
27	240	69.93	1.35
28	470	50.73	2.70
29	237	45.83	1.18
30	500	44.22	0.69
31	505	23.89	1.47
32	227	18.01	3.16

33	390	11.39	1.11
34	241	6.6	0.40
35	506	3.81	0.61
36	365	2.43	0.18
37	410	0.62	0.63
38	300	0.61	0.53
39	504	0.54	0.24
40	363	0.42	0.11
41	234	0.22	0.14
42	235	0.08	0.02

Each value represents the mean of triplicate wells \pm SEM, assays were carried out in duplicate or triplicate according to the drug supplies. Single representative run shown for clarity. Abbreviations: ID: identification number, N/A: Not applicable.

Table 14. Library of potent active S-MGBs against *Acanthamoeba castellanii* Neff trophozoites

The variations in the head and second ring on the chemical structure of S-MGBs that displayed a strong effect with IC₅₀s below 1 μM against Neff trophozoites are depicted.

S-MGB ID	Modification in the chemical structure	IC ₅₀ (μM)
235	 m-Methoxybenzyl+Phenyl	0.08
234	 p-Methoxybenzyl+Pyridine	0.22
363	 N, N-dimethylbenzylamine +Pyridine	0.42
504	 m-Methoxybenzyl + fluorobenzene	0.54
300	 Quinoline+Phenyl	0.61
410	 Benzonytrile+Phenyl	0.62

3.4.3 Potent effect of S-MGB-235 *in vitro* against *Acanthamoeba* spp. at 24 hours and 96 hours.

S-MGB-235 showed an IC₅₀ value of 75.4 nM for *A. castellanii* Neff strain trophozoites, the most potent effect of all S-MGBs screened in the alamarBlue assays. The chemical structure of S-MGB-235 possess the typical heterocycles required for DNA binding and shared through all the S-MGBs presented in this chapter, a *m*-methoxybenzyl head group and amidinyl ethyl tail group. Further alamarBlue assays on S-MGB-235 were carried out using four additional strains: *A. polyphaga*, *A. castellanii* Clinical T4, *A. castellanii* ATCC 50370 and *A. castellanii* ATCC 50371 isolates, at 24 h and 96 h. A summary of the results is shown in Table 15.

S-MGB-235 showed a robust inhibitory effect in all *Acanthamoeba* species, with IC₅₀s values in the range of nanomolar (nM). A potent effect by S-MGB-235 is still observed *in A. castellanii* Neff strain at 24 h, with an IC₅₀ of 181.9 nM. Still substantial, *A. polyphaga* displayed the lowest inhibitory effect with an IC₅₀ of 295.5 nM at 24 h. *A. castellanii* ATCC 50371 isolate was the strain with the highest inhibition effect, with IC₅₀ of 55.3 nM and 13 nM at 24 h and 96 h, respectively (Figure 9). As expected, the inhibitory activity is correlated to time, with the highest activity observed at 96 h compared with 24 h effect.

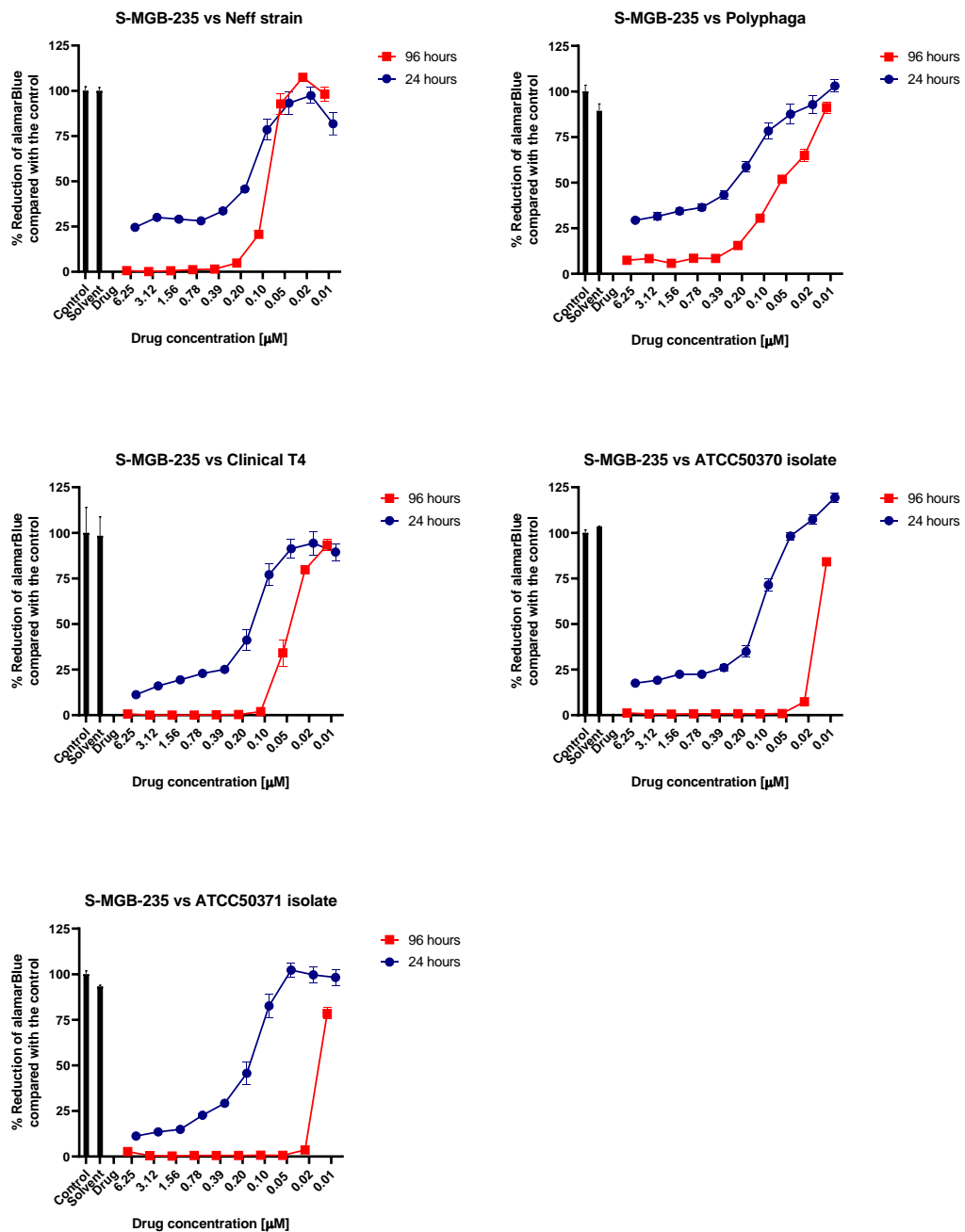


Figure 9. Efficacy of S-MGB-235 against *Acanthamoeba* spp. trophozoites through alamarBlue assays.

A strong inhibitory effect of S-MGB-235 is observed against five different *Acanthamoeba* species/strain: Neff, environmental Polyphaga, Clinical T4, ATCC 50370 and ATCC 50371. Different concentrations of trophozoites according to specie/strain per well were seeded in PG media with 10 serial dilutions of S-MGBs. Trophozoites and PG medium (Control), a DMSO (solvent) and PG medium with the highest concentration of S-MGB (6.25 µM) (Drug) were used as controls. The alamarBlue reduction percentage was read in a SpecMax spectrophotometer at 24 h and 96 h, 23°C. Each value represents the mean of triplicate wells ±SEM, the screening was carried out in three independent experiments of which single representative run shown for clarity.

Table 15. Anti-amoebic activity of S-MGB-235 against *Acanthamoeba* spp. at 24 h and 96 h evaluated *in vitro*.

S-MGB-235 vs <i>Acanthamoeba</i> spp.	IC₅₀ (nM) 24 h	SE	IC₅₀ (nM) 96 h	SE
Neff	181.9	0.01	75.4	0.02
Polyphaga	295.5	0.10	53	0.08
Clinical T4	168.6	0.21	36.4	0.22
ATCC50370	150	0.02	13.6	0.03
ATCC50371	55.3	0.02	13	0.01

Abbreviations. nM: nanomolar

3.4.4 Fluorescent S-MGB-363 binds to nucleus, nucleolus and granuloplasm causing cell wall disruption in *A. castellanii* Neff trophozoites as observed by Confocal microscopy analysis.

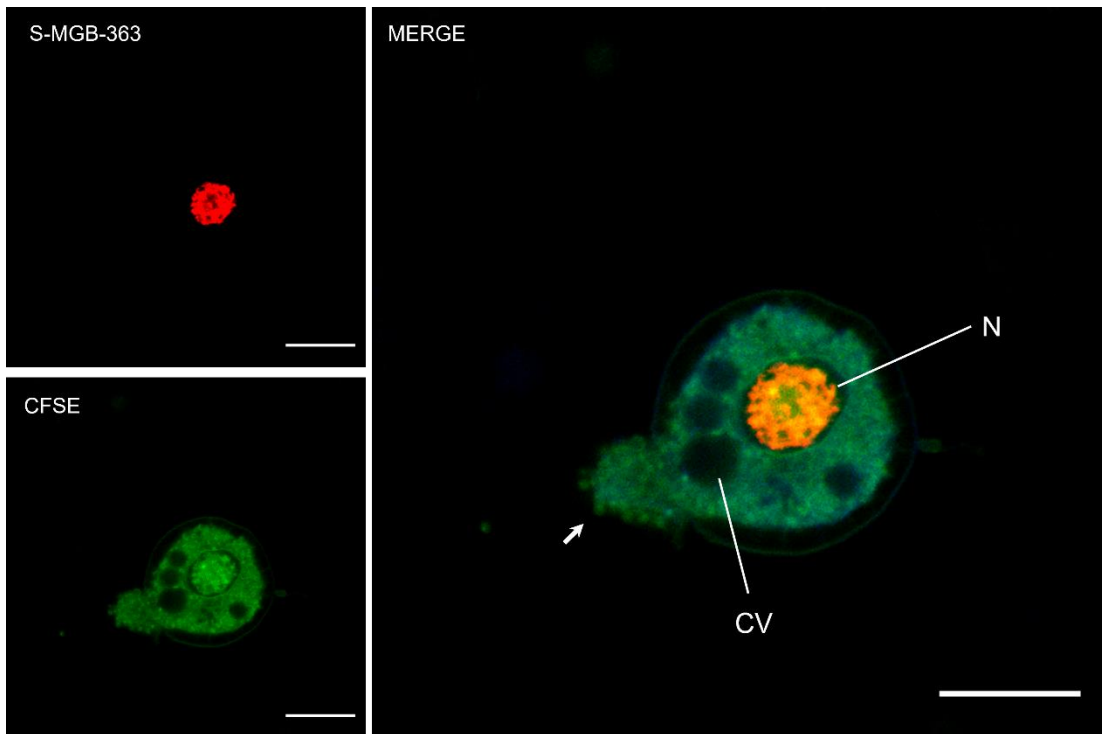
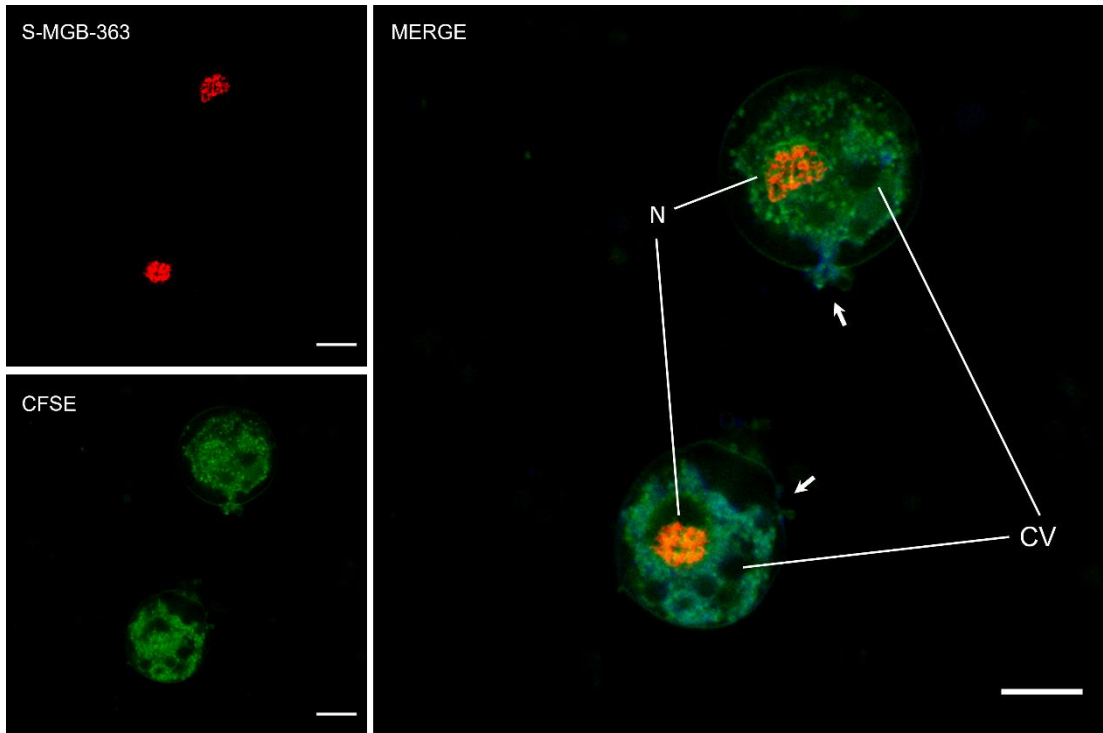
Two of the S-MGBs examined in the inhibition studies (S-MGB-245 and S-MGB-363) have intrinsic fluorescence. Importantly, these molecules are identical except from their tails. S-MGB-245 has an morpholinoethyl tail and is not active against the amoeba, whereas S-MGB-363 has an amidinylethyl tail and is active against the amoeba. Therefore, the ability of these 2 compounds to enter and bind structures within *A. castellanii* were investigated.

Acanthamoeba castellanii Neff strain trophozoites were harvested, counted, and labelled as described in section 2.2.2.2 and 2.2.3.2 in Material and Methods. S-MGB-363 specifically was found to bind the nucleus, resulting in an intense red fluorescence. This is in line with the proposed mechanism of action of these compounds, which involves binding to the minor groove of the nuclear DNA. CFSE dye, used here as a contrast dye was observed in nucleus, cytoplasm, granuloplasm and cell wall membrane. The cytotoxic effect of S-MGB-363 caused substantial cell morphological changes such as rounded shape of the amoebas with evident loss of acanthopodia, blebbing which eventually resulted in cytolysis (Figure 10).

As Hoechst is a commonly used dye in microscopy and is also a MGB, studies were undertaken to investigate if S-MGB-363 and Hoechst show a similar intracellular distribution and if S-MGB-363 might displace Hoechst from the nucleus. Thus, *Acanthamoeba* trophozoites were first stained with Hoechst (1 µg/ml) for 5-30 min, which was then followed by the addition of S-MGB-363 (100 µM). Time lapse confocal imaging was performed to monitor the distribution of each dye.

Figure 11 shows three different trophozoites observed at 63x for a total time of 53 m 23 s. Figure 11, C. clearly shows that at approximately 6 minutes the S-MGB is taken up and begins to occupy the granuloplasm and nucleus. Five minutes later, a slight increase of S-MGB (red) fluorescence is observed in the granuloplasm accompanied with intense S-MGB fluorescence (red) in the nucleus. A further twenty minutes later, the nucleus shows a robust increase of red fluorescence, larger than the Hoechst signal. At this time-point, the cytoplasmic membrane was disrupted and disintegrated confirming the cytolysis effect previously observed. During the last 15 minutes, the trophozoite appeared damaged with fragmented nucleus. The other two cells followed the same process previously described; however, it was the cytolysis effect was not

observed during the time the analysis was carried out (Figure 11 A. and B.). During the same time-lapse imaging process, zoom visualisation of another different trophozoite confirmed S-MGB-363 bound with significant localisation in the nucleus and nucleolus. However, these experiments demonstrate that S-MGB-363 and Hoechst bind similar intracellular locations, however, S-MGB-363 is unable to displace Hoechst previously bound to the nuclear DNA at the concentrations used (Figure 12). However, the fact both compounds have occupied similar intracellular locations, specifically the nucleus, suggest that they both interact with nuclear DNA.



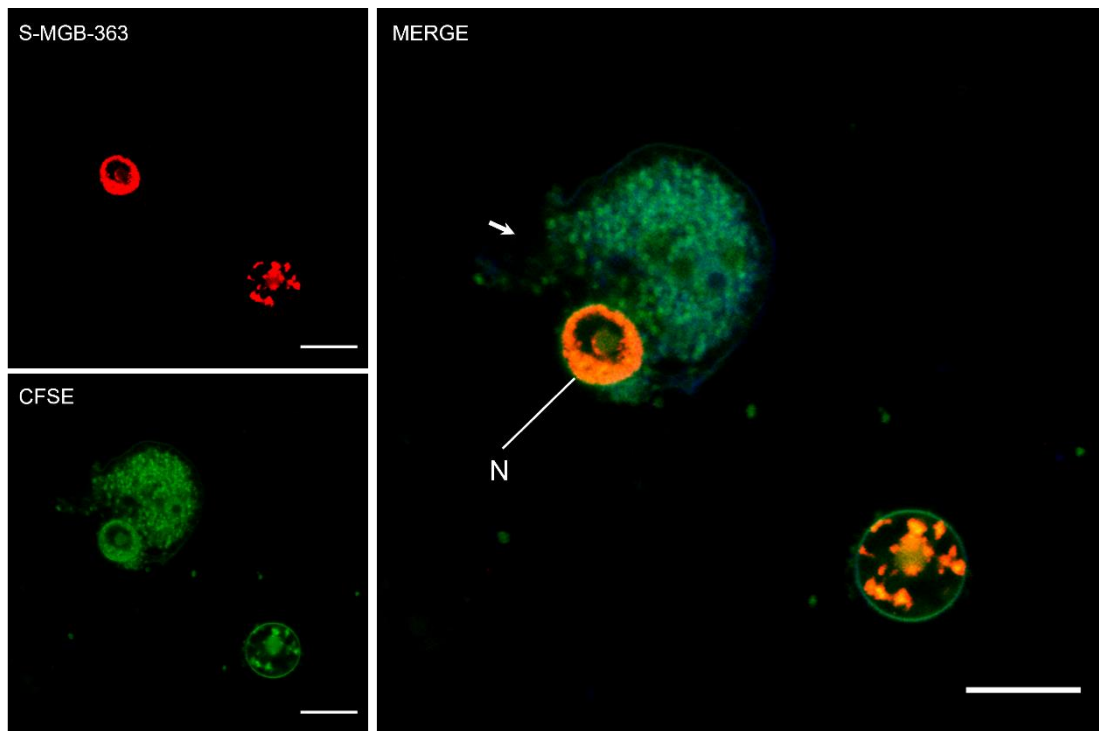


Figure 10. Cellular effect of fluorescent S-MGB-363 against *Acanthamoeba* Neff strain trophozoites.

Confocal fluorescence microscopy was performed in trophozoites labelled with fluorescent S-MGB-363 and CFSE for 10-30 min at RT. S-MGB 363 only binds to nucleus as shown by the red fluorescence. The stress caused by the effect S-MGB-363 in trophozoites cause a loss of its pleomorphic shape to develop a rounded pre-cyst wall whereupon cytolysis occur, triggering leak of cellular components (indicated with white arrows). Analysis was carried out with Leica TCS SP8 multiphoton confocal microscope under FITC (exc 470/40, em 515 LP) with Magnification: 63x. Scale bar= 10 μ m.

Abbreviations: N= nucleus, CV= contractile vacuole, CFSE= carboxyfluorescein succinimidyl ester.

A)

00:06:37

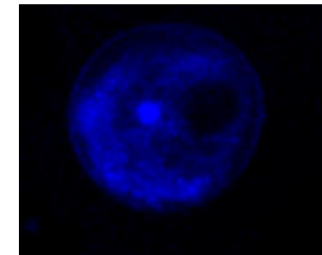
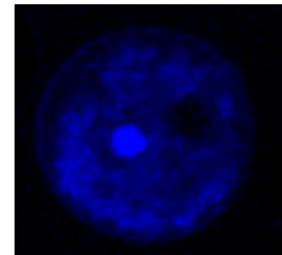
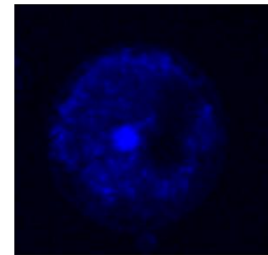
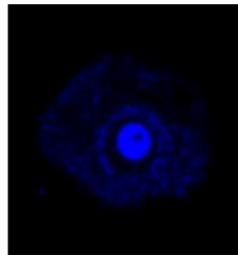
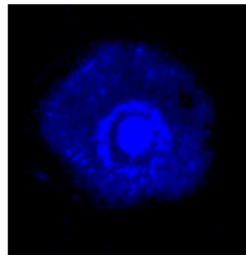
00:11:03

00:31:02

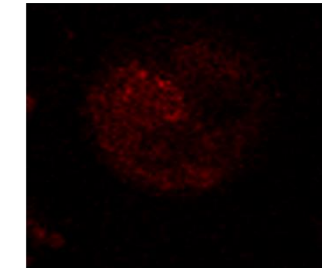
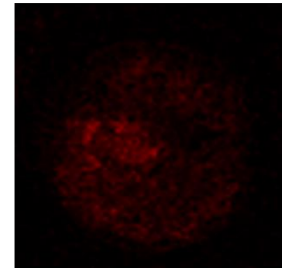
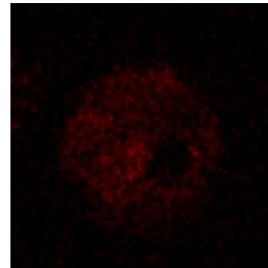
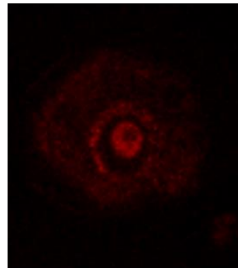
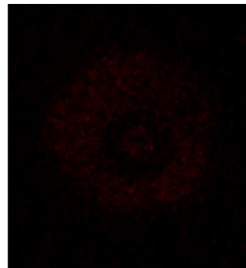
00:41:41

00:46:57

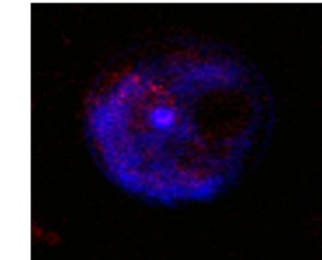
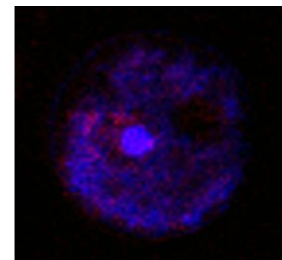
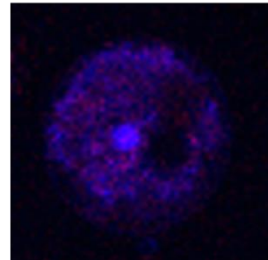
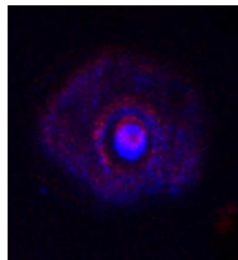
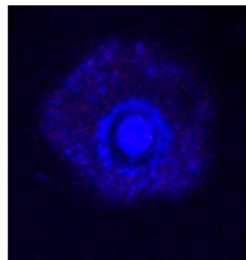
Hoechst



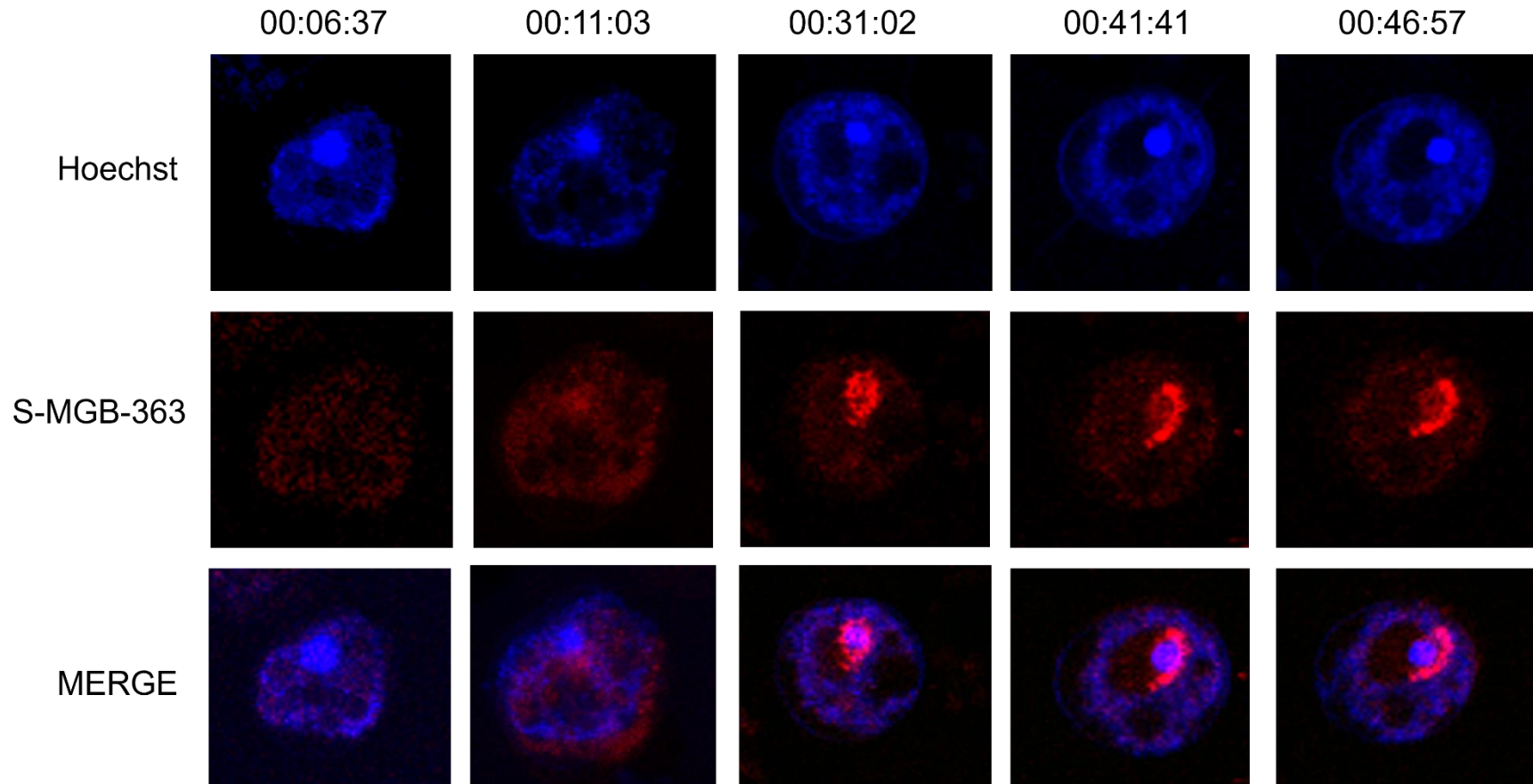
S-MGB-363



MERGE



B)



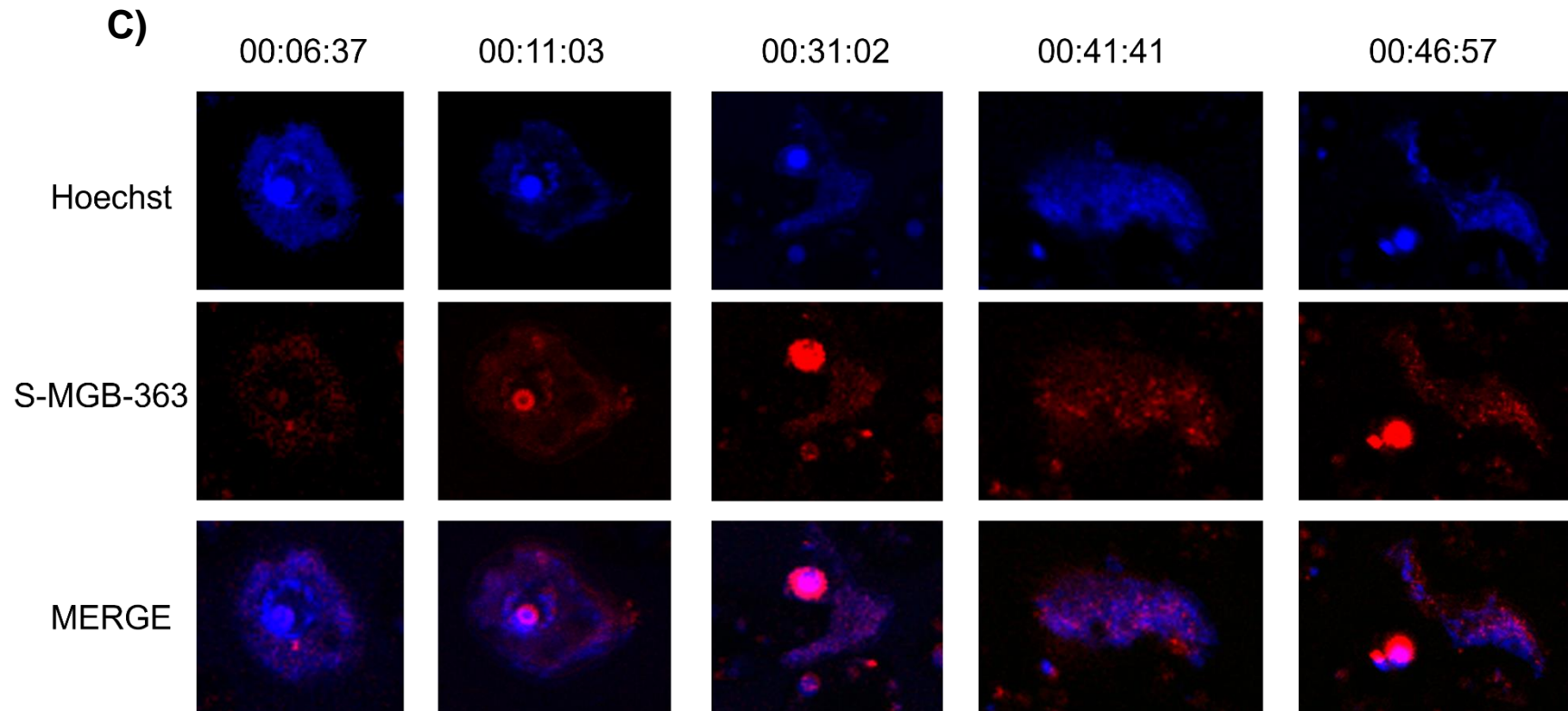


Figure 11. Time-laps confocal imaging of the effect of fluorescent S-MGB-363 against *A. castellanii* Neff trophozoites.

Three different trophozoites previously stained with Hoechst during 5-30 min were immediately stained with S-MGB-363 and its effect was observed during 53 min 23 s. **A.** and **B.** show accumulation of S-MGB-363 in nucleus and nucleolus, in **C.** is evident the cell lysis around minute 31. Analysis was carried out with Leica TCS SP8 multiphoton confocal microscope under DAPI (exc 360/40, em 425 LP) and FITC (exc 470/40, em 515 LP). Magnification: 63x. Images were scrapped manually from an original image with scale bar= 10 μ m.

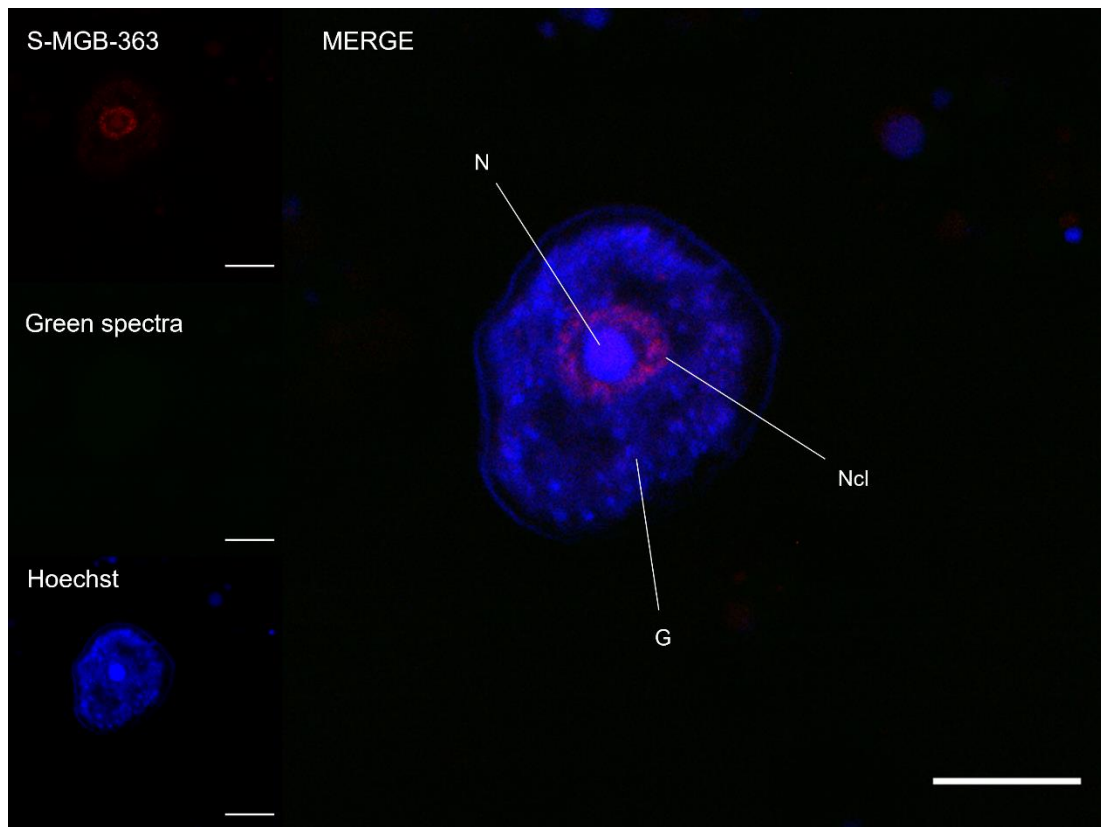


Figure 12. Confocal fluorescence imaging of S-MGB-363 bound to nucleus and nucleolus in *Acanthamoeba Neff* strain trophozoites.

Confocal fluorescence microscopy was performed in trophozoites labelled initially with Hoechst for 10-30 min at RT; soon after labelled with S-MGB-363. S-MGB-363 binds to nucleus and nucleolus. Hoechst binds to nucleus and granuloplasm. Analysis was carried out with Leica TCS SP8 multiphoton confocal microscope under DAPI (exc 360/40, em 425 LP), FITC (exc 470/40, em 515 LP). Magnification: 63x. Scale bar= 10 μ m.

Abbreviations: N= nucleus; Ncl= nucleolus; G: granuloplasm.

3.4.5 Fluorescent S-MGB-245 weakly binds to nucleus and do not cause cell wall disruption in *A. castellanii* Neff trophozoites as observed by Confocal microscopy analysis.

Trophozoites samples prepared as previously described on section 2.2.3.2 of Material and Methods were labelled with Hoechst (1 µg/ml) for 5-30 min whereupon 100 µM of S-MGB-245 were added just before confocal imaging was performed. The analysis was performed 1h after S-MGB-245 was added.

Figure 13 depicts a trophozoite displaying robust Hoechst blue fluorescence in the nucleus. S-MGB-245 red fluorescence in the nucleus is minimal compared with previous observations to S-MGB-363 and is not visualised in the nucleolus. The granuloplasm shows the same low-level pattern of red fluorescence. These results are consistent with the inability of this S-MGB to inhibit *Acanthamoeba* growth.

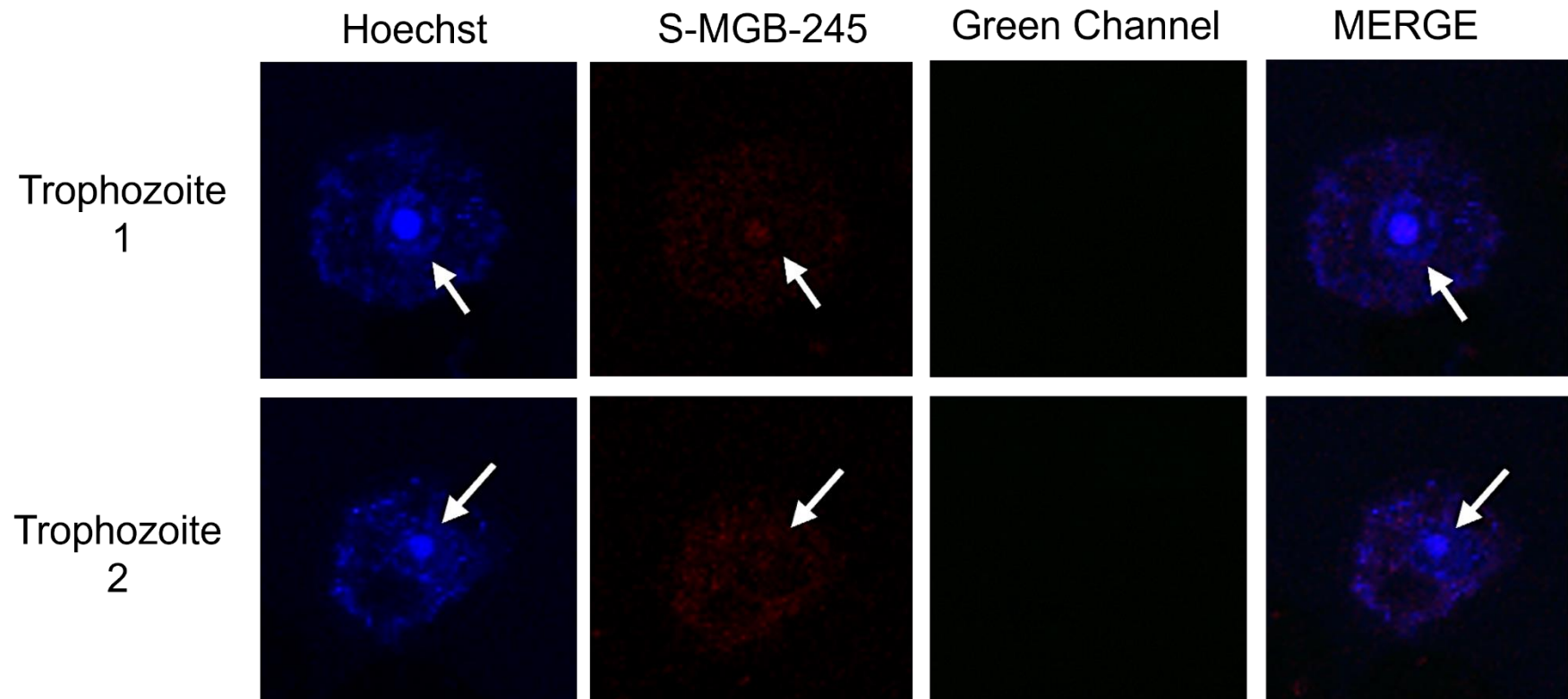


Figure 13. Cellular effect of fluorescent S-MGB-245 against *A. castellanii* Neff strain trophozoites.

Confocal fluorescence microscopy was performed in trophozoites labelled with Hoechst for 10-30 min at RT, then 100 μ M fluorescent S-MGB-245 was added. S-MGB-245 bound to nucleus, led changes in the cell structure, however it did not trigger cytolysis as compared with S-MGB-363. The nucleus is indicated by a white arrow. Analysis was carried out with Leica TCS SP8 multiphoton confocal microscope under DAPI (exc 360/40, em 425 LP), FITC (exc 470/40, em 515 LP). The original images were cropped manually, with a magnification 63x and a scale bar of 30 μ m.

3.5 Discussion

Acanthamoeba spp. are causative agents of severe sight-threatening AK infection and chronic progressive disease of CNS known as GAE. The medical treatment for these diseases is challenging due to the high selectivity of BBB which hinders a proper delivery of the drug and most of the current compounds used to treat these diseases cause undesirable side effects (Elsheikha, Siddiqui and Khan, 2020).

Drug agents that bind to the minor groove of double-helical DNA sequences have potential for therapeutic development since they properly fit into the narrow shape of the DNA minor groove, they selectively interact with specific sequences inhibiting the binding of regulatory proteins to DNA. Furthermore, potential drug resistance is less likely than it might be compared with other highly specifically targeted drugs due to the many sites MGBs can in theory occupy (Bhaduri, Ranjan and Arya, 2018). Strathclyde Minor Groove Binders (S-MGBs) are DNA-binding compounds based upon the polyamide natural product Distamycin A. Over recent years, the variations in the head group and specific linker moiety, the alkyl substituents in the heterocycles and the tail group have yielded a wide range of S-MGBs with effective activity against various diverse groups of microorganisms such as Gram-positive bacteria, fungi, and parasites (Giordani *et al.*, 2019).

In this chapter the seeding densities for alamarBlue inhibition assays to test S-MGBs by alamarBlue assays were optimised at 24 h and 96 h for five different species/strains of *Acanthamoeba* (Neff, Polyphaga environmental, Clinical T4, ATCC50370 and ATCC50371) trophozoites. Forty-two S-MGBs were screened at 96 h against *A. castellanii* Neff from which six compounds showed a significant amoebicidal effect with IC_{50s} below 1 μ M. The most effective compound of this library, S-MGB-235, was chosen to carry out alamarBlue assays with the remaining isolates of *Acanthamoeba* at 96 h and 24 h. S-MGB-235 demonstrate high activity in the range of nanomolar (IC_{50s} = 291.32 nM – 13.02 nM) across all strains. ATCC50370 and ATCC50371 were the most sensitive strains to S-MGB-235, exhibiting IC_{50} values of 150.03 nM at 24 h, 13.60 nM at 96 h and 112.13 nM at 24 h, 13.02 nM at 96 h, respectively. This demonstrates that the activity of S-MGB-235 is consistent across a wide range of *Acanthamoeba* isolates, including ATCC50370 and ATCC50371 which are used in the ISO14534 for development of contact lens solutions.

To investigate the intracellular accumulation of S-MGBs and explore the importance of the tail group to the compounds' activities, two S-MGBs with intrinsic fluorescence were investigated. S-MGB-363 is a fluorescent analogue of S-MGB-235 with robust effect against *A. castellanii* Neff generating an IC_{50} of 0.42 μ M at 96 h whereas S-MGB-245, a fluorescent analogue of S-MGB-1 did not have any significant effect in alamarBlue assays. Confocal microscopy imaging confirmed S-MGB-363 strongly bound to nucleus and nucleolus in a similar manner to DAPI and Hoechst. A weak distribution of the compound was also observed in the granuloplasm. Additionally, presence of this compound around 1 hour led to aberrant cell modifications in trophozoites such as loss of acanthopodia, rounded morphology, blebbing and eventual disruption of the cell wall allowing all the cell contents to leak which finally resulted in cell death. These observations suggest S-MGB-363 had a strong cytotoxic effect. In contrast with S-MGB-245 which was found only to weakly bind the nucleus and nucleolus without any cytotoxic effect. These microscopy results confirmed the results obtained *in vitro* using the alamarBlue assay for these two compounds.

To note, a structure-activity relationship (SAR) was conceived based on the lethal effects displayed by our substantial library of six S-MGBs screened against *Acanthamoeba* Neff strain. All S-MGB-410, S-MGB-300, S-MGB-504, S-MGB-363, S-MGB-234 and S-MGB-235 displayed IC_{50s} values below 1 μ M and all of them contained the amidinylethyl tail group compared with analogues that have morpholine as a tail groups such as S-MGB-503, S-MGB-171 S-MGB- 500, S-MGB-245, S-MGB-2, and S-MGB-1 that generated IC_{50s} values higher than 100 μ M. Specifically, S-MGB-235 has also shown significant inhibition effect against *T. congolense* IL3000 EC_{50} = 0.08 μ M and *T. vivax* EC_{50} = 1.15 μ M (Giordani *et al.*, 2019) and *T. brucei brucei* EC_{50} = 0.36 μ M (unpublished data). It is well established that early MGBs such as pentamidine and diminazene (which contain amidines in their chemical structure) have been widely used against both trypanosomes and plasmodia and are actively taken up via membrane transports. These MGBs achieve elevated intracellular concentrations and bind strongly to AT-rich sites of the minor groove of DNA, leading to cell destruction (Scott *et al.*, 2016b). The microscopy results, that show the MGB binding the nucleus before any obvious disruption of the *Acanthamoeba* membrane suggest that their amoebicidal effect of S-MGB-235 in *Acanthamoeba* spp. is likely due to its strong DNA binding. This is consistent with what has previously been demonstrated for *Trypanosoma brucei* and *Leishmania* spp. However, other mechanisms of action cannot be ruled out as other drugs with amidine groups have

been shown to be active against *Acanthamoeba*. For example, one compound belonging to the diamidine family, propamidine-isethionate (PD), was the first cure for AK reported and it is still part of the current treatment used along with biguanides, although there are reports of *Acanthamoeba* resistance to this compound (Wright, Warhurst and Jones, 1985). Since then, the only study on amoebicidal and cysticidal effects of various diamidines analogues of propamidine such as hexamidine and octamidine have been proven through diffusion kinetic studies the best amoebicidal effect of this family of compounds *in vitro* (Perrine *et al.*, 1995). The lethal effect of diamidine analogues on *Acanthamoeba* spp. is related to the contact of protonated amidines groups attached to each benzene ring with the amphipathic lipids of the plasma membrane bilayer of trophozoites, inducing aberrant morphological changes that led modifications in the permeability which could be responsible for the leakage of biomolecules such as ions and water. The lipophilic properties of these type of agents due to the multiple alkyl groups makes them easier to be incorporated into the lipid bilayer of the amoebic plasma membrane, which enables to reach the lethal concentration required to generate amoebicidal effects. Additionally, when compounds containing amidine groups have penetrated the amoebic cytoplasm, lethal effects such as coagulation and denaturation of cytoplasmic proteins and enzymes occur due to the basicity environment provided by these groups. Interestingly, in this current study similar effects were observed in the confocal microscopy sessions showing trophozoites with aberrant morphology, blebbing and cytolysis which clearly led to leakage of all the cellular content due to the presence of S-MGB-363, a compound with amidinylethyl tail group.

The mechanism by which S-MGBs are taken up into trophozoites, is unknown. Food and solutes uptake in *Acanthamoeba* occurs via phagocytosis and pinocytosis, the former a receptor-dependant process and the latter occurs through the creation of membrane invaginations (Bowers and Olszewski, 1972). It is potentially feasible that S-MGBs uptake in *Acanthamoeba* spp. occurs through either or both these processes. On the other hand, the description of *Acanthamoeba* spp. passive transport or membrane transports is a field poorly explored, except for the last reports of a cation proton antiporter (CPA) and a phosphate transporter (AcPHS) (Carvalho-Kelly *et al.*, 2020; Weber-Lima *et al.*, 2020).

S-MGB-234 which has a similar chemical structure to S-MGB-235 with slightly different head groups, have been previously assessed against *T. congolense* IL3000

and *T. vivax* STIB 719 generating significant IC₅₀ values of 0.09 µM and 0.45 µM, respectively (Giordani *et al.*, 2019). Such potent effect was also obtained in our results, displaying the second best IC₅₀ value of 0.22 µM against *A. castellanii* Neff trophozoites.

The efficacy displayed by S-MGB-235 or S-MGB-234 in *Trypanosoma* spp. and in our results *in vitro* against *Acanthamoeba* spp., are also observed in some Gram-positive bacteria and fungi. S-MGB-235 has a strong effect against *C. neoformans*, *C. glabrata* and *A. fumigatus* (MIC₉₉= 0.78 µg /ml, 1.56 µg /ml, and 12.5 µg /ml, respectively), *S. aureus* (MIC₈₀= 4 µg/ml) but not for *E. coli* (MIC₈₀= NA) (unpublished results) and *Mycobacterium tuberculosis* H37RvMtb-GFP (MIC₉₉= >25 µM) (Hlaka *et al.*, 2017). It has been suggested that such change in the efficacy is related to the function of efflux pumps and outer Gram-negative bacterial cell wall, which apparently functions as a fence to naturally hamper the penetration of S-MGBs (Suckling and Scott, 2017).

On the other hand, SAR was also developed *in vitro* for S-MGB-363 (containing amidinylethyl tail group) versus 245 (containing morpholine tail group) for the results reported here in *Acanthamoeba* Neff strain. Although not active for *Acanthamoeba*, S-MGB-245 had better efficacy against *Trypanosoma brucei brucei* (IC₅₀=0.17 µM) and a similar inhibitory concentration effect for *Mycobacterium tuberculosis* H37RvMtb-GFP (MIC₉₉=>25 µM) when compared with our results (Scott *et al.*, 2016b; Hlaka *et al.*, 2017).

In AK, the current treatment is applied in eye drops containing diamidines and biguanides. The most common diamidines used are 0.1% propamidine-isethionate (Brolene); hexamidine-diisethionate (Hexacyl) and dibromopropamidine (Golden eye). As biguanides, polyhexamethylene-biguanide (Lavasept) and chlorhexidine (Curasept) (Fanselow, 2021). Regarding GAE, at least three drug combinations are used, however the combination of rifampicin + cotrimoxazole + fluconazole or ketoconazole are the most used according to efficacy of drug usage (EDU > 30%) as a function of the frequency of drug usage (FDU ≥ 25%) (Taravaud *et al.*, 2021). The efficacy of these drugs against *Acanthamoeba* isolates is controversial, due to the lack of standardized methods which generates different inhibition concentrations among research groups, and it has been observed their effects differ when compared *in vitro* versus *in vivo* (Shi *et al.*, 2020).

An *in vitro* evaluation of antimicrobial drugs effects used as current treatment against *A. castellanii* Neff ATCC 30010 trophozoites through alamarBlue method reported

IC_{50s} values at 72 h, 96 h, and 120 h, which is quite useful to compare our results reported on this chapter (Taravaud, Loiseau and Pomel, 2017). Of particular significance, our hit compound S-MGB-235, containing a functional amidinylethyl tail group with IC₅₀ of 0.08 µM at 96 h against *A. castellanii* Neff trophozoites showed superior IC₅₀ value when compared with the diamidine propamidine-isethionate (8.96 ± 1.45 µM) at the same time point. The IC₅₀ values are as follow for chlorhexidine (1.10 ± 0.01 µM), hexamidine-diisethionate (0.04 ± 0.01 µM), both rifampicin and Cotrimoxazole (IC_{50s} not determined at 96h but >100 µM at 72 h) and ketoconazole (7.91 ± 3.78 µM). Voriconazole has been scarcely used during the last years on the treatment against GAE but still a considerable substitute of gluconazole or ketoconazole. On this study, voriconazole showed an IC₅₀ value of 0.40 ± 0.14 µM; miltefosine, a compound infrequently used for GAE but with an important capacity to penetrate the BBB showed an IC₅₀ value of 11.22 ± 2.65 µM; both at 96 h (Taravaud, Loiseau and Pomel, 2017). Similar IC₅₀ of 0.54 and 0.98 values for voriconazole were obtained by our research group in *Acanthamoeba* ATCC 50370 and ATCC 50371 respectively at 96 h (Thomson *et al.*, 2017). In the case of Neff, an IC₅₀ value of 2.1 µM. This is the same strain that was used to be tested against S-MGB 235 in which a robust effect was generated.

Given the above, we suggest S-MGB-235 as a relevant novel compound that might complement aromatic diamidines in the current combination therapies for *Acanthamoeba* spp. diseases.

Chapter 4. Use of wax moth *Galleria mellonella* larvae as new *in vivo* infection model for *Acanthamoeba castellanii* Neff strain trophozoites.

4.1 Abstract

A substantial number of researchers have adopted insects as a new model system for the study of microbial pathogenesis that cause human diseases. The suitability of wax moth *Galleria mellonella* larvae to reproduce bacterial and fungal infections and evaluate new antimicrobial agents have been well-established because the immune response of this insect displays many structural and functional similarities to the innate immune response of mammals. On the contrary, this insect model has not been applied to evaluate parasitic infections so far. In this chapter, we investigate *Galleria mellonella* larvae as a novel *in vivo* infection model of *Acanthamoeba castellanii* Neff infections. Initial studies compared the ability of different infectious doses of *A. castellanii* to induce lethal infection of *G. mellonella*. Larvae infected with *A. castellanii* Neff trophozoites showed systemic melanisation, inflammation, and stiffness. An infective dose of 1×10^7 trophozoites was determined to induce 100% lethality by day 10 post infection and was used for antibiotic efficacy testing. Both voriconazole and miltefosine failed to protect larvae at concentrations of 125, 25, 1 mg/kg and 43.8, 8.75, 1.75 mg/kg, respectively. A dose of 25 mg/kg of S-MGB 235 was found to be non-toxic and offered significant protection against infection with *A. castellanii* Neff, confirming its activity previously exhibited *in vitro*.

4.2 Background

4.2.1 Biology

Galleria mellonella is a cosmopolitan wax moth from the order Lepidoptera which larva is predominantly found as nest parasite in beehives and bee nests. Despite not directly damaging the bees, they are considered a plague since they can spread virus diseases to honeybees. The life cycle lasts approximately six to eight weeks and divides in four main stages: egg, larva, pupa, and adult (Kwadha *et al.*, 2017). The larva is about 25-30 mm in length and 5-7 mm in diameter prior to the pupa stage. There is no sexing on larvae, since on this stage they lack specific external morphological features. The anatomy of larvae is composed of six thoracic legs and 8 prolegs over the abdomen segment, their cuticle is a creamy-white colour when healthy. In the head is present antennae that are only visible under light microscopy and apical teeth with well-established destructive nature (Smith, 1965). The metamorphosis of the great wax moth varies from 8 – 12 weeks depends mainly on diet quality to boost its immune system and it requires a relatively humid and warm temperature to develop into adult (Firacative *et al.*, 2020). Mating is an interesting process that depends on acoustic signaling. Part of male moths stimulate the females with the aid of their wings crawling producing nonanal, a sexual pheromone that is found in the wax and may indicate the ideal crevice to spawn (Kwadha *et al.*, 2017; Singkum *et al.*, 2019).

4.2.2 *G. mellonella* immune system

The wax moth *Galleria mellonella* possesses an outstanding immune system akin to vertebrates to counterattack any potential injury and hence infection. The worm-like body consists of a harden cuticle composed of chitin which extends until the base membrane and acts as a first barrier. The second barrier is the trachea, which is a completely dry and low-level nutrient zone where any microbial colonization or growth is not viable. However, if the infection goes through the oral cavity, the stomach harsh conditions such as low pH and digestive enzymes will stop the penetrating pathogens.

Galleria mellonella immune system relies exclusively on an innate immune response since the lack of an adaptive immune response is well established in this organism.

The innate immune system of this insect is based on two major parts (Tsai, Loh and Proft, 2016):

- I. Cellular immune system: response mediated by six different types of hemocytes: prohemocytes, plasmatocytes, granular cells, coagulocytes, spherulocytes and oenocytoids. Specifically, plasmatocytes and granular cells are involved in defense important processes such as phagocytosis, nodular formation and encapsulation, the aforementioned is a primary immune defense against the invasion of protozoa and nematodes (Boman and Hultmark, 1987). Curiously, several homologous elements between the human and *G. mellonella* phagocytosis process have been discovered: hemocytes express proteins that resemble calreticulin in human neutrophils for non-self-recognition of external pathogens defense reactions. In addition, homologous p47 and p67 proteins responsible for the formation of NADPH complex involved in oxidative burst processes against pathogen microbes after phagocytosis were also identified in both wax moth and human systems (Bergin *et al.*, 2005; Renwick *et al.*, 2007).
- II. Humoral immune system: this type of defense includes a wide range of elicitor effector molecules able to kill the pathogens like opsonins, antimicrobial peptides (AMP), melanisation and extracellular nucleic acid traps. Study of AMPs in *G. mellonella* elucidated at least 18 known or putative peptides which are antimicrobials mainly produced in the fat body (a biosynthetic organ analogous to human liver), hemocytes, digestive and reproductive tracts, and salivary glands. *G. mellonella* lysozyme also owns the same hydrolytic function on wall peptidoglycan as well as a cationic defense role synergistically assisted by the anionic peptide 2 (Sowa-Jasitek *et al.*, 2016). Cecropins, moricins, gailomycin, gallerimycin, gloverin and moricins are AMPs well identified with important selective antimicrobial activity against Gram-negative and Gram-positive bacteria, fungi, and yeast (Wojda, 2017). Encapsulation of pathogens through the synthesis and deposition of melanin is known as melanisation. Hemocytes are responsible for the production of pro-phenoloxidase (ProPO), which is an inactive zymogen that is cleaved into active phenoloxidase (PO) form which the Serine-Protease cascade is triggered after pattern recognition receptors (PRRs) find their target in pathogen surface. Phenols and monophenols are converted to quinines from

hemolymph circulating PO; whereupon quinine 'walls off' invading pathogens. Production of PO is highly regulated by protease inhibitors and some AMPs, since PO can produce reactive oxygen species (ROS) (Lu *et al.*, 2014; Zdybicka-Barabas *et al.*, 2014).

4.2.3 Use of *G. mellonella* as an alternative *in vivo* infection model

In vivo experimentation has an integral role in biomedical research making remarkable contributions to medical advancements such as new therapies, new models for drug discovery/delivery and toxicological studies. It is well known that antimicrobial resistance, new or emerging and neglected diseases are causing serious economic losses and millions of deaths, leading a big challenge for the clinical and biomedical communities in the next decades. Therefore, discovery and development of alternative efficacious treatments and vaccines are utmost priority, which generally are first screened *in vitro* to measure their effectiveness, potential toxicity, and viability and subsequently to be tested in *in vivo* infection models (Swearengen, 2018).

Animal *in vivo* infection models have been historically crucial since they reproduce similar physiological or behavioral conditions observed in humans, many infection animal models have their genome completely sequenced, boosting the possibility of environmental standardization and genetic manipulation to address specific scientific challenges. Alternative nematodes or some invertebrate for *in vivo* infection model experimentation such as worms (*Caenorhabditis elegans*), flies (*Drosophilla melanogaster*), yeasts (*Saccharomyces cerevisiae*) or fish (Zebra fish) are required to overcome scientific limitations in terms of ethical, logistic, and financial issues currently present in murine models (Romero and Vela, 2014).

Interestingly, during the last years *Galleria mellonella* is getting attention for antimicrobial studies since similar observations in the virulence of pathogens between *G. mellonella* and mice have been established. Furthermore, some of the advantages that make the great wax moth caterpillar larvae to be used as model infection in the laboratory compared with mammalian model hosts are: (i) Similar innate immune system response but no adaptive, (ii) able to grow around 15°-37°C which is the common temperature where pathogens develop in human body, so virulence factors and pathogenic mechanisms could be analysed, (iii) size of larvae (2-3 cm) is easy to handle and apply accurate dosing assays, (iv) no requirement of special lab devices,

(v) easy to rear, (vi) ideal short life period for complex experimentation (i.e. high-throughput studies) (Kamal *et al.*, 2019).

Several similar experimental methods to use *G. mellonella* as an animal model in biomedical research have been proposed in literature, nevertheless there is no determined standard method. Scientific literature data coincide in using populations (n) of 10-20 larvae maintained with the ideal environmental conditions in sterile petri dishes. Before any infection screening, larvae feeding should be stopped at least 24 h prior to infection (Ramarao, Nielsen-Leroux and Lereclus, 2012).

Delivery of pathogenic microorganism into the larvae might be through three different techniques:

- I. *Topical*: absorption of pathogens via larvae cuticle.
- II. *Feeding*: via oral when pathogens are mixed with pollen. e.g., force-feeding method.
- III. *Injection*: Inoculation via intra-haemocoel through the first or last proleg.

The injection method is the most used in literature since the number of pathogens is controlled. In addition, it is recommended to use specific syringes such as Hamilton syringe or 26-gauge needle because bigger needles cause a lethal trauma in larvae (Fuchs *et al.*, 2010). Washing the pathogens inoculum before injection is suggested with the purpose of avoiding secondary factors that contribute to decrease or boost the infection screening. In addition, it is important to set up controls using placebos to monitor any trauma caused to the larvae during the injection process (Desbois and Coote, 2011). The ideal temperature to maintain the larvae post-infection is 37°C in microbial infections (Konkel and Tilly, 2000; Smoot *et al.*, 2001).

Post-infection visible features are based on a recent well-standardised health index scoring system assessing larvae mobility, cocoon formation, melanisation and survival. These features should be cautiously monitored since they describe the larvae health status and hence the infection process. Signs of an ongoing infection process include appearance of black spots on healthy cream-colour cuticle indicating the beginning of melanisation process along with loss of motility or sensitiveness in response to touch larvae with a pipette tip or shaking the petri dish (Tsai, Loh and Proft, 2016). Finally, larvae are considered dead when cuticle becomes completely black (Kamal *et al.*, 2019). Proliferation of pathogens inside the larvae during the

infection is a useful enumeration method to screen microbial virulence which is typically carried out plating larvae on agar or via biophotonic imaging (La Rosa *et al.*, 2012; La Rosa *et al.*, 2013; Loh *et al.*, 2013; Wand *et al.*, 2013).

Most of the scientific studies using the great wax moth as model infection have only focused in studying novel therapeutic compounds against bacterial or fungal infections, few viruses, and even phages (Tsai, Loh and Proft, 2016; Singkum *et al.*, 2019). *G. mellonella* infection has been used to analyse a wide variety of Gram-positive bacteria, including *Streptococcus pyogenes*, *pneumoniae*; *Enterococcus faecalis*, *faecium*; *Staphylococcus aureus* and *Listeria monocytogenes*; Gram-negative such as *Pseudomonas aeruginosa*, *Burkholderia cepacia*, *Acinetobacter baumannii*, *Bacillus cereus*, *Francisella tularensis*, *Legionella pneumophila*, *Listeria monocytogenes*, *Mycobacterium strains*, *Proteus mirabilis*, *Salmonella typhimurium* and *Vibrio parahaemolyticus* (Tsai, Loh and Proft, 2016; Kamal *et al.*, 2019). Immune response of *G. mellonella* has also been analysed to fungi infections. Studies analysed the virulence of *Candida* spp.; assessed the infection, virulence factors and resistance to Amphotericin B of *Aspergillus terreus* and the characterised pathogenic features in *Histoplasma capsulatum* and *Paracoccidioides lutzii* (Thomaz *et al.*, 2013; Maurer *et al.*, 2015; Borman, Szekely and Johnson, 2016).

4.2.4 *In vivo* infection models for parasites

Current scientific research in parasitic diseases have aimed host-parasite interactions, pathogenic mechanisms/factors, significance of biochemical pathways in their metabolism, *in vivo* maintenance of parasites and clinical evaluation of drug candidates (Mears *et al.*, 2015). A wide variety of animal models have been the most common source of *in vivo* experimentation in parasitic diseases, however, none of them have emerged so far as an absolute infallible model since the selection of infection models is complex due to intrinsic parasite factors such as parasite strain, specific stage in the life cycle and host factors.

Mice have been the most common animal chosen for drug analysis to fight Chagas disease (CD) caused by *Trypanosoma cruzi*, however, larger mammals such as dogs and primates are reliable animal models since they are able to develop the chronic phase of CD in a comparable way produced in humans (Chatelain and Konar, 2015). In fact, benznidazole is a drug that is similarly effective in both dogs and human with parasitic charge recovery in acute and chronic stages of 68.75% and 37.50%

respectively, however cardiomyopathy was unable to be avoided in the chronic phase. The preceding shows that the canine model is suitable to antichagasic prototypes because it is comparable to human parasitemia levels, clinical manifestations, immune responses, and drug effectiveness (Guedes *et al.*, 2002). It has been observed that non-human primates like Rhesus monkeys (*Macaca mulatta*) and baboons (*Papio spp.*) exhibit comparable cardiac alterations (electrocardiogram changes), megacolon and megaesophagus during the process of CD or even death, which opens a viable possibility to make them a potential animal model to explore new antitrypanosomal agents (Teixeira *et al.*, 2006). New world primates for instance, *Callithrix penicillata*, *Cebus apella*, and *Saimiri sciureus* have been used as natural reservoirs to develop at times *T. cruzi* infections (Fonseca-Berzal *et al.*, 2018).

A similar scenario where the animal models show a low validity profile due to remarkable differences in the presentation of cutaneous leishmaniasis (CL) between animal and human is a reality. These *in vivo* models should resemble the transmission to develop the diseases the most accurate possible (Mears *et al.*, 2015). Currently, there is a wide range of animal models used after a successful transmission and development of CL infection such as hamster, rat (primary stage), dogs (secondary stage) and nonhuman primates (tertiary stage), these models assure reproducibility to screen new experimental drugs according to their appropriate use defined by clinical trial phases (Grimaldi, 2008). Indeed, different inbred mice strains are the most frequent animal to develop and analyse CL infections on the grounds that previous analysis have achieved better development of histopathological and immunological patterns in contrast to nonhuman primates (Charret *et al.*, 2013). Moreover, rodents have been a perfect model to elucidate pathogenic mechanisms based in different recovery models because they are very susceptible to infection caused by different strains and species of *Leishmania* (Indiani de Oliveira *et al.*, 2004).

Validation and search for animal models that display the spectrum and complexity features produced by malaria disease have been a challenge and have given rise to meetings and discussions among experts (Craig *et al.*, 2012). Birds, nonhuman primates (splenectomised chimpanzees), mice and bats are model organisms that have contributed to malaria research, but they cannot be affordable by many laboratories in the world, hence inbred and outbred mice have been a reference model due to its genetic and immunological similarities to human, the possibility of generating transgenic strains, and humanized/xenografted samples. Balb/c, C57BL/6

and DBA/2 are the main African rodents used to be infected for four *Plasmodium* species where these models have provided important insights in protein export related to sequestration and the link between nutrient sensing and parasite virulence (De Niz *et al.*, 2018).

Toxoplasma gondii disease has also been deeply analysed in warm-blooded superior mammals such as the sheep and goat, even chickens but mice remain as the cost-effective animal model (Saraf *et al.*, 2017; Geuthner *et al.*, 2019; Stelzer *et al.*, 2019). The use of any of this model depends on the nature of the research since *Toxoplasma* displays a complex life cycle, the route by which *Toxoplasma* is inoculated, the chosen life stage to be analysed and each animal might develop different characteristics during the development of the disease.

In contrast to the previous parasites, mice are naturally resistant to both *Cryptosporidium parvum* and *hominis*, but immunosuppression has led an insight about the resistance of innate mechanisms and the importance of T cells function (Borad and Ward, 2010; Mead, 2014). *Cryptosporidium muris* has been used to infect immunocompetent mice although differences between the species infecting humans are remarkable, especially in the anatomical site of infection. Despite requiring sophisticated and specialized facilities, large animals such as piglets and calves have successfully showed susceptibility to *C. hominis* and *C. parvum*, respectively. Vaccination is ideal to prevent the development of cryptosporidiosis in humans, especially in children and old people. A recent study of *C. tyzzeri*, a phylogenetically similar strain to *C. hominis* and *C. parvum* was able to cause live immunity protection in mice C57BL/6 displayed by the resistance acquired through vaccination with attenuated parasites opening the possibility to evaluate the rationale for vaccine development (Sateriale *et al.*, 2019).

Significant contributions in the knowledge of amoebiasis have been achieved using resistant and susceptible *in vivo* animal models, especially mice. However, besides the human, there is no specific *in vivo* model to reproduce *Entamoeba histolytica* life cycle and the production of both intestinal and extra intestinal amoebic lesions, which leads to experimental analysis in either intestinal or hepatic models (Tsutsumi and Shibayama, 2006). Recently, was elucidated that serum of Wistar rats is toxic for the *E. histolytica* trophozoites, making them resistance to the generation of hepatic abscesses lesions (Cortes *et al.*, 2019). Several studies show guinea pigs as models to study intestinal amoebiasis but the production of the lesions, especially amoebic

ulcers is doubtful (Diamond, Tanimoto Weki and Martínez-Palomo, 1978; Anaya-Velázquez *et al.*, 1985). Gerbils are rodents highly susceptible to hepatic damage and the lesions are produced in similar way to those observed in hamsters, however trophozoites are less virulent and the evolution of the amoebiasis is slower and death might take long periods of time (Shibayama *et al.*, 1997).

4.2.5 *In vivo* Infection models to assess *Acanthamoeba* infections

The understanding of the pathogenic mechanisms and pathophysiology displayed by AK and GAE disease produced by *Acanthamoeba* clinical and environmental strains is a challenge to overcome in the *in vivo* experimentation through animal models. One of the main problems to study AK in animal models is the host specificity adhesion, since in previous studies *Acanthamoeba* trophozoites showed predilection for binding to corneal epithelium only in humans, pigs and Chinese hamsters which has failed to reproduce in common lab animals such as mice, rabbit, rats (Neelam and Niederkorn, 2017). Additionally, one of the common problems found in the screening of new potential anti-amoebic compounds against AK is the complex structure of the eye, which hinders a successful penetration of the drugs through the ocular cell layers until the stroma (Morgan *et al.*, 2020). In the case of GAE, transmigration of the trophozoites into de CNS is a goal that has not been mimicked in *in vivo* models as occur in humans. The ease of inoculation in mice has set up this animal as the most used in experimental research of AK and GAE, nonetheless they are required to be immunosuppressed with steroids or antibiotics to develop disease analogous to humans (Mortazavi *et al.*, 2010).

4.3 Aims and Objectives

In the previous chapter, it was established S-MGB 235 as the most potent amoebicidal compound from all the S-MGBs analysed *in vitro*. However, to complete this important milestone and confirm its biological effect, it is fundamental to determine its toxicity and efficacy over *A. castellanii* Neff trophozoites *in vivo*.

The primary aims of this chapter is to establish and adapt for the first time in the literature the wax moth *G. mellonella* larvae as a new and appropriate *in vivo* infection model for *A. castellanii* infection and to determine the efficacy of currently used drugs (voriconazole and miltefosine) and S-MGB 235 in this model.

This chapter objectives are (i) to delimit *G. mellonella* larvae survival over time when injected with different densities of trophozoites and (ii) to describe the signs developed in the course of amoebic infection. Furthermore, (iii) test the efficacy and toxicity of voriconazole, miltefosine and S-MGB 235 in non-infected and infected larvae.

4.4 Results

4.4.1 *G. mellonella* larvae infected with *A. castellanii* Neff strain show melanisation, generalised inflammation, and stiffness.

Acanthamoeba castellanii Neff strain trophozoites were seeded, harvested, and counted according to sections 2.2.1.2 and 2.2.2.2 in Material and Methods. Larvae were purchased from Live Foods United Kingdom (Rooks Bridge, UK) and infected through inoculation as described in sections 2.2.4.1 and 2.2.4.2 in Material and Methods.

Inoculation via haemocoel in wax moth *G. mellonella* larvae of *A. castellanii* Neff strain trophozoites resulted in severe disease. Figure 14 show larvae that exhibited from day 6 post-infection difficulty to crawl (paralysis), permanent upside-down position, different degrees of melanisation (particularly in the dorsal midline, systemic) generalised inflammation (potential encapsulation or nodulation), most of them showed twitching or stiffness, eventually death, which suggest amoebas activate a strong immune reaction through the phenol oxidase pathway and damage of CNS.

In our studies, the instar larvae in the control group (non-infected and without treatment or vehicle) started the process of pupation around day 6 showing apparent “loss of the head” and attachment of the cocoon and pupate (Figure 15). Furthermore, the obtect process was observed in these larvae (this is the process in which legs and wings are attached immovably against the body changing the colour from white, yellow and brown during the next 4 days). Pupation is considered a sign of “healthy” status in control groups of larvae analysed in pathogenicity screenings.

A



B



C



Figure 14. Infection signs on *Galleria mellonella* larvae inoculated with *A. castellanii* Neff strain

Images display physical symptoms observed in larvae through the infection assays with trophozoites. Infected larvae presented different degrees of melanisation through the body, such as **A.** melanin deposits (left central larva), systemic melanisation (right central larva) and **B.** systemic melanisation with increased inflammation (encapsulation or nodulation). **C.** Larvae showing marked arched abdomen (stiffness) with noticeable twitching (indicated by black arrows) preventing a proper crawl. Images taken by Alemao Sanchez.



Figure 15. *Galleria mellonella* pupae formation.

Image depicts the pupa stage development found in control groups around 6-10 day in pathogenicity screenings. Features such as loss of head, immobilisation and body changing colour were observed. Image taken by Alemao Sanchez.

4.4.2 *G. mellonella* larvae survival is inoculum-dependent over time when infected with *A. castellanii* Neff strain trophozoites.

Acanthamoeba castellanii Neff strain trophozoites were cultured, harvested, and counted as previously described on section 2.2.1.2. Wax moth *G. mellonella* larvae were purchased from Live Foods United Kingdom (Rooks Bridge, UK). Only healthy-looking larvae with no signs of melanisation were picked up and placed in 90 mm Petri dishes with filter paper until infected.

To examine the effect of *Acanthamoeba* Neff trophozoites in *Galleria mellonella*, larvae in groups of 10 were treated identically and inoculated with 10^3 , 10^4 , 10^5 , 10^6 , and 10^7 cells. The control group was injected with 10 μ l of PG medium. Following the injections, larvae were incubated at RT for the following 25 days to allow the progression of infection caused by trophozoites. Every 24 h larvae were scored as dead when immobility was observed despite external stimuli using tweezers and when larvae showed systemic melanisation. The assay was repeated in duplicate.

Figure 16 shows a Kaplan-Meier graph displaying *G. mellonella* larvae survival is dose-dependent over time ($p < 0.0001$, Survival analysis, Log-rank Mantel-Cox test) where lower survival correlated with higher inoculum doses. All the concentrations produced 100% of mortality. More than 80% mortality occurred within 9 days testing 1×10^7 , and this increased to 100% by next day. The highest rates of mortality were observed by days 10, 15, 20 and 24 post-inoculation for 10^3 , 10^4 , 10^5 , 10^6 , and 10^7 cells, respectively. By contrast, larvae infected with 10^3 cells had 80% of mortality by day 23 and this increased to 100% by next day. Interestingly, a similar trend of mortality was observed in most of the groups, since all the five larvae died with a gap of five days among every group infected with different parasitic burden, except for 10^5 and 10^6 cells. All larvae in the control group inoculated with PG medium survived 25 days, with the first larva transforming in pupa at day 6.

The parasitic burden 1×10^7 cells was chosen to carry out further antibiotic efficacy tests since was sufficient to kill all the larvae in the shortest time.

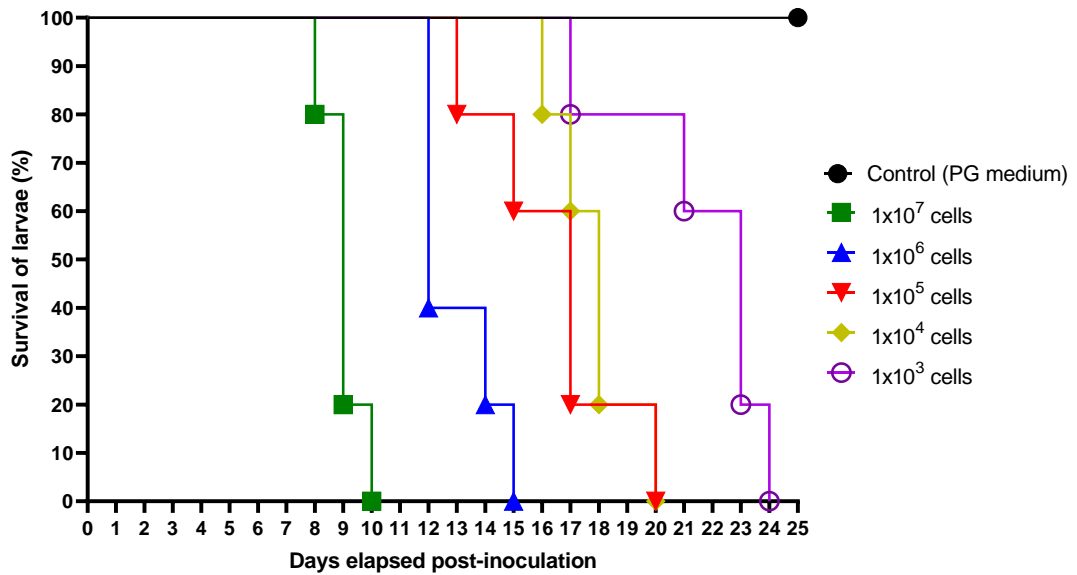


Figure 16. Kaplan-Meier survival curves of *G. mellonella* larvae after infection with *A. castellanii* Neff strain at different inoculum concentrations.

Ten larvae were infected with *A. castellanii* Neff strain. All the larvae (100%) in every group died at day 10, 15, 17, 20, 20 and 24 when inoculated with 10^3 , 10^4 , 10^5 , 10^6 , and 10^7 cells, hence survival of larvae depends on inoculum over time. Control group represents larvae only inoculated with PG medium. The survival curves are significantly different ($p < 0.0001$, Survival analysis, Log-rank Mantel-Cox test). The data is representative of two independent experiments.

4.4.3 Voriconazole and miltefosine treatment of *G. mellonella* larvae infected with *A. castellanii* Neff trophozoites does not protect from death

Acanthamoeba castellanii Neff strain trophozoites were cultured, harvested, and counted as previously described on section 2.2.1.1 on Chapter 2. Wax moth *G. mellonella* larvae were purchased from Live Foods United Kingdom (Rooks Bridge, UK). Only healthy-looking larvae with no signs of melanisation were picked up (n=5) and placed in 90 mm Petri dishes with filter paper until infected into the hindmost right proleg with lethal inoculum of 1×10^7 cells. After two hours of incubation at RT, groups of larvae infected and non-infected were treated with antibiotics Voriconazole (125, 25, 5 mg/kg), miltefosine (43.8, 8.75 and 1.75 mg/kg) and S-MGB 235 (125, 25, 5 and 1 mg/kg) or vehicles (DMSO or sterile ddH₂O), these groups were inoculated into the hindmost left proleg. Doses were based on human equivalent doses in terms of mg/kg. After treatment, larvae were scored as dead or alive as described previously. Two independent experiments per antibiotic were performed and pooled data is presented. Distribution of groups used on antibiotic efficacy testing are described in Table 16.

The effect of single doses of voriconazole, miltefosine and S-MGB 235 in *G. mellonella* larvae treated post-infection with *A. castellanii* trophozoites are shown in Figures 17, 18 & 19.

Voriconazole and miltefosine at any concentration used did not offer protection when compared with the non-treated control group that died at day 10. Voriconazole was somewhat toxic to larvae at each concentration used. At the concentration of 125 mg/kg voriconazole killed 50% of non-infected larvae by day 14 (Figure 17). On the other hand, all the larvae in non-infected groups but treated with each concentration of miltefosine (43.8, 8.75 and 1.75 mg/kg) survived demonstrating that this drug is non-toxic to the larvae (Figure 18).

4.4.4 S-MGB 235 Treatment of *G. mellonella* larvae infected with *A. castellanii* Neff trophozoites does provides some protection against death

S-MGB 235 was found to be toxic when administered at 125 mg/kg with 100% of larva succumbing to death by day 7. This toxicity could also be due to the high concentration of DMSO required to dissolve S-MGB 235 at this concentration as larva given 55% DMSO as a vehicle control suffered 80% mortality by day 11. In contrast none of the non-infected larva given a 25 mg/kg died and all larvae given the appropriate 11% DMSO control inoculation survived.

Three larvae were found dead on days 1, 4 and 6 in the group of larvae infected with *Acanthamoeba* trophozoites and administered S-MGB at 25 mg/kg. These deaths are likely a result of experimental error or poor initial health status in the larvae as this concentration of S-MGB is non-toxic and deaths due to *Acanthamoeba* infection are not normally observed until day 15 post infection. A dose of 25 mg/kg S-MGB did not significantly protect larvae from infection relative to control untreated larvae (Mann–Whitney U test, $p=0.12924$). In addition, DMSO alone was also found to provide no significant protection relative to control untreated larva (Mann–Whitney U test, $p=0.18141$). Furthermore, no obvious protection was offered for larvae treated with 5mg/kg of S-MGB 235 (Figure 19).

Table 16. Description of Voriconazole, miltefosine and S-MGB 235 efficacy testing procedure in *Galleria mellonella* larvae groups infected and non-infected with *Acanthamoeba castellanii* Neff strain trophozoites

Voriconazole and miltefosine

Group (5 larvae each)	Infected with <i>A. castellanii</i> Neff (1x10⁷ cells/ml)	Treatment	
G1 (Positive control)	No	No	
G2	No	55% DMSO	ddH ₂ O
G3	No	11% DMSO	ddH ₂ O
G4	No	2.2% DMSO	ddH ₂ O
G5	No	125 mg/kg voriconazole	43.8 mg/kg miltefosine
G6	No	25 mg/kg voriconazole	8.75 mg/kg miltefosine
G7	No	5 mg/kg voriconazole	1.75 mg/kg miltefosine
G8 (Negative control)	Yes	No	
G9	Yes	55% DMSO	ddH ₂ O
G10	Yes	11 % DMSO	ddH ₂ O
G11	Yes	2.2 % DMSO	ddH ₂ O
G12	Yes	125 mg/kg voriconazole	43.8 mg/kg miltefosine
G13	Yes	25 mg/kg voriconazole	8.75 mg/kg miltefosine
G14	Yes	5 mg/kg voriconazole	1.75 mg/kg miltefosine

S-MGB 235

Group (5 larvae each)	Infected with <i>A. castellanii</i> Neff (1x10⁷ cells/ml)	Treatment
G1 (Positive control)	No	No
G2	No	55% DMSO
G3	No	11% DMSO
G4	No	2.2% DMSO
G5	No	0.44% DMSO
G6	No	125 mg/kg S-MGB 235
G7	No	25 mg/kg S-MGB 235
G8	No	5 mg/kg S-MGB 235
G9	No	1mg/kg S-MGB 235
G10 (Negative control)	Yes	No
G11	Yes	55% DMSO
G12	Yes	11% DMSO
G13	Yes	2.2% DMSO
G14	Yes	0.44% DMSO
G15	Yes	125 mg/kg S-MGB 235
G16	Yes	25 mg/kg S-MGB 235
G17	Yes	5 mg/kg S-MGB 235
G18	Yes	1 mg/kg S-MGB 235

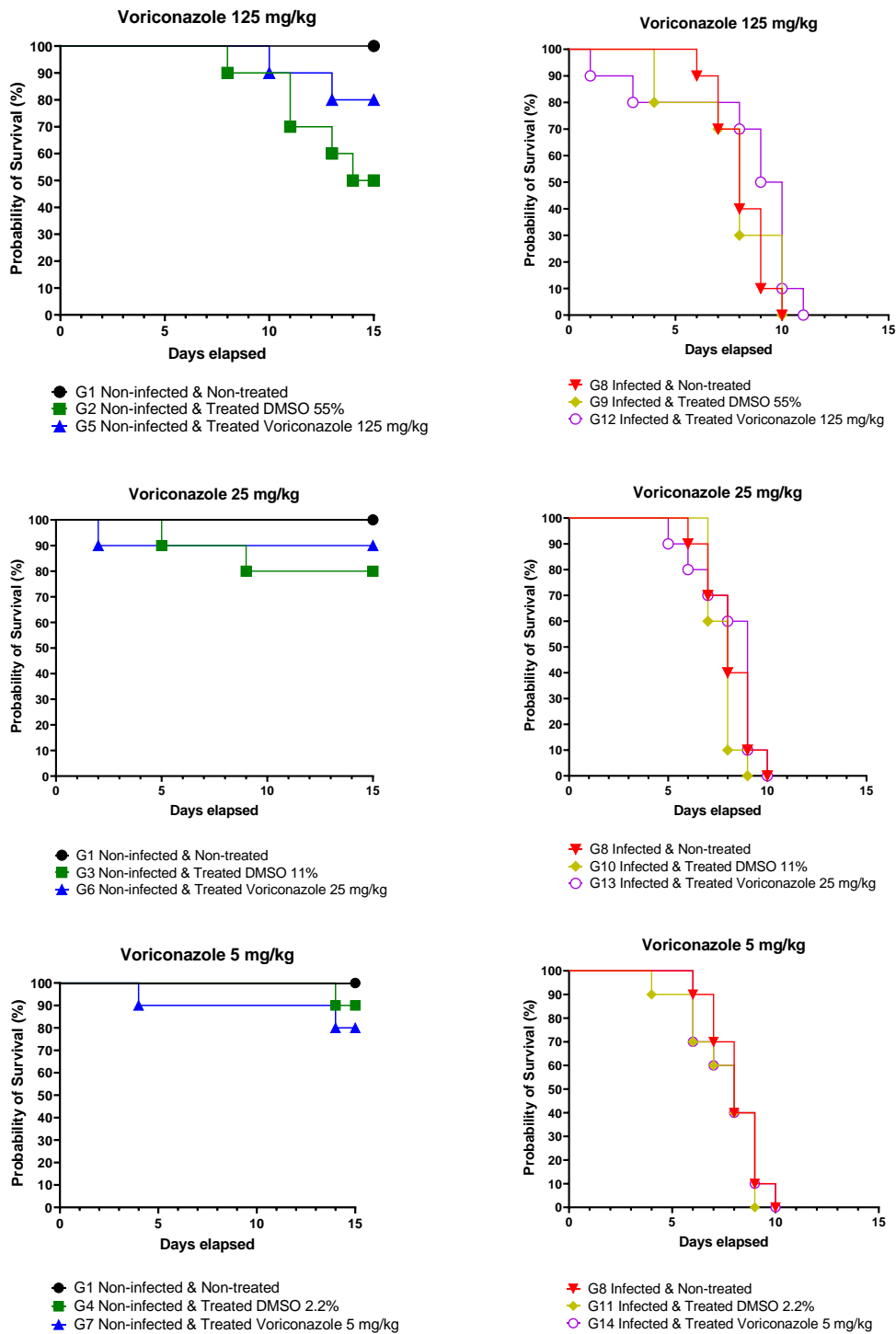


Figure 17. Kaplan-Meier survival curves of *Galleria mellonella* larvae infected with *Acanthamoeba castellanii* Neff strain and treated with voriconazole.

Larvae (n= 5 per group) were infected with 1×10^7 cells/ml of *A. castellanii* Neff strain trophozoites. Following infection, larvae were treated with 10 μ l of voriconazole 125, 25 and 5 mg/kg; and DMSO 55%, 11%, 2.2% and 0.44%. Two control groups consisted of non-infected, and non-treated, infected, and non-treated. Survival was monitored every 24 h over a period of 14 days. Data are pooled from two independent experiments.

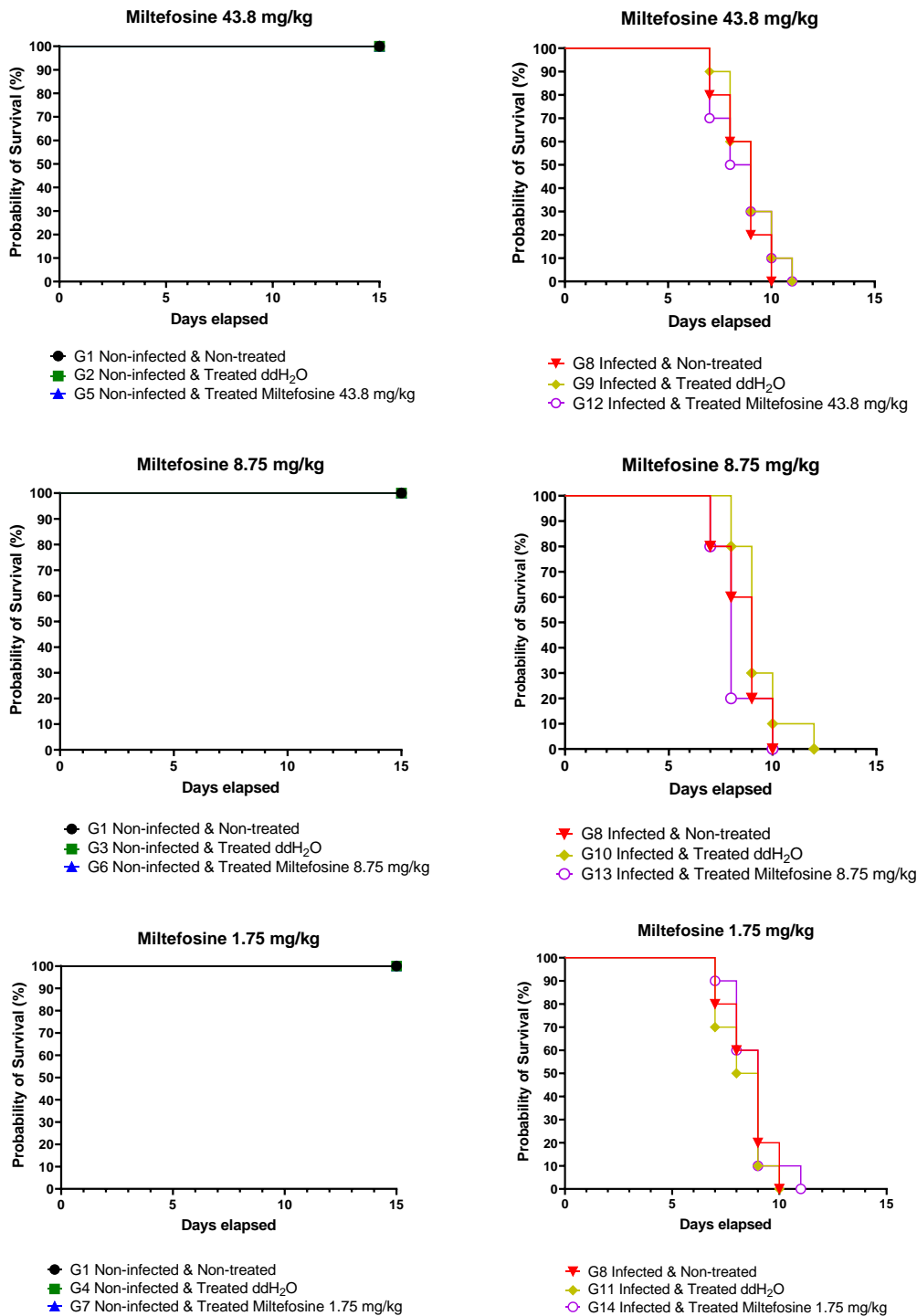
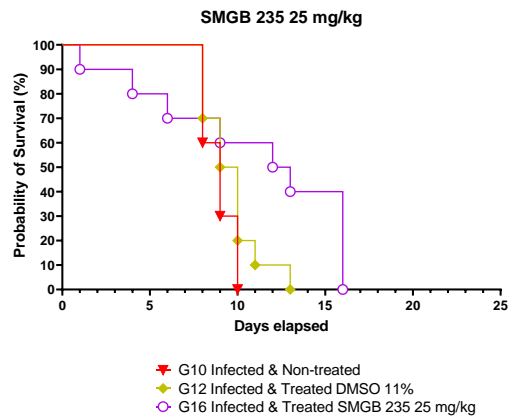
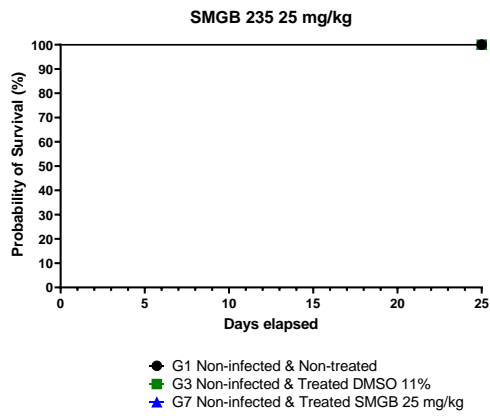
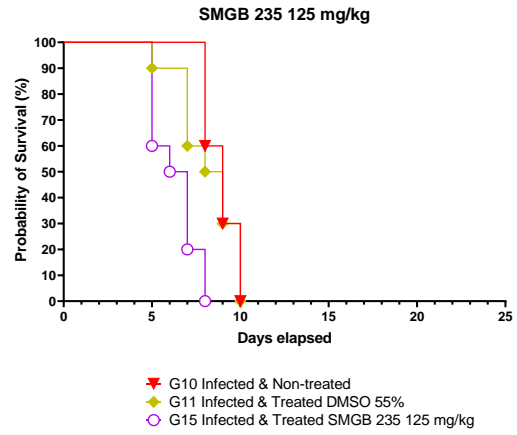
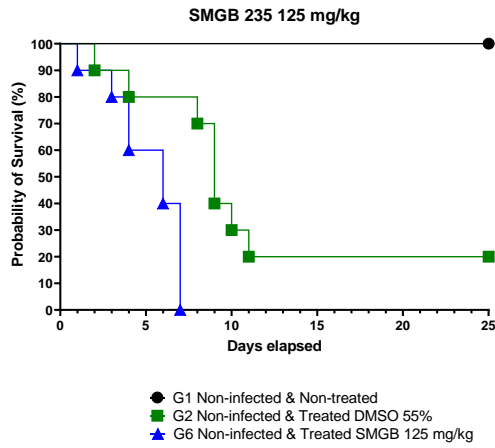


Figure 18. Kaplan-Meier survival curves of *Galleria mellonella* larvae infected with *Acanthamoeba castellanii* Neff strain and treated with miltefosine.

Larvae (n= 5 per group) were infected with 1×10^7 cells/ml of *A. castellanii* Neff strain trophozoites. Following infection, larvae were treated with 10 μ l of miltefosine 43.8, 8.75 and 1.75 mg/kg; and ddH₂O. Two control groups consisted of non-infected, and non-treated, infected, and non-treated. Survival was monitored every 24 h over a period of 14 days. Data are pooled from two independent experiments.



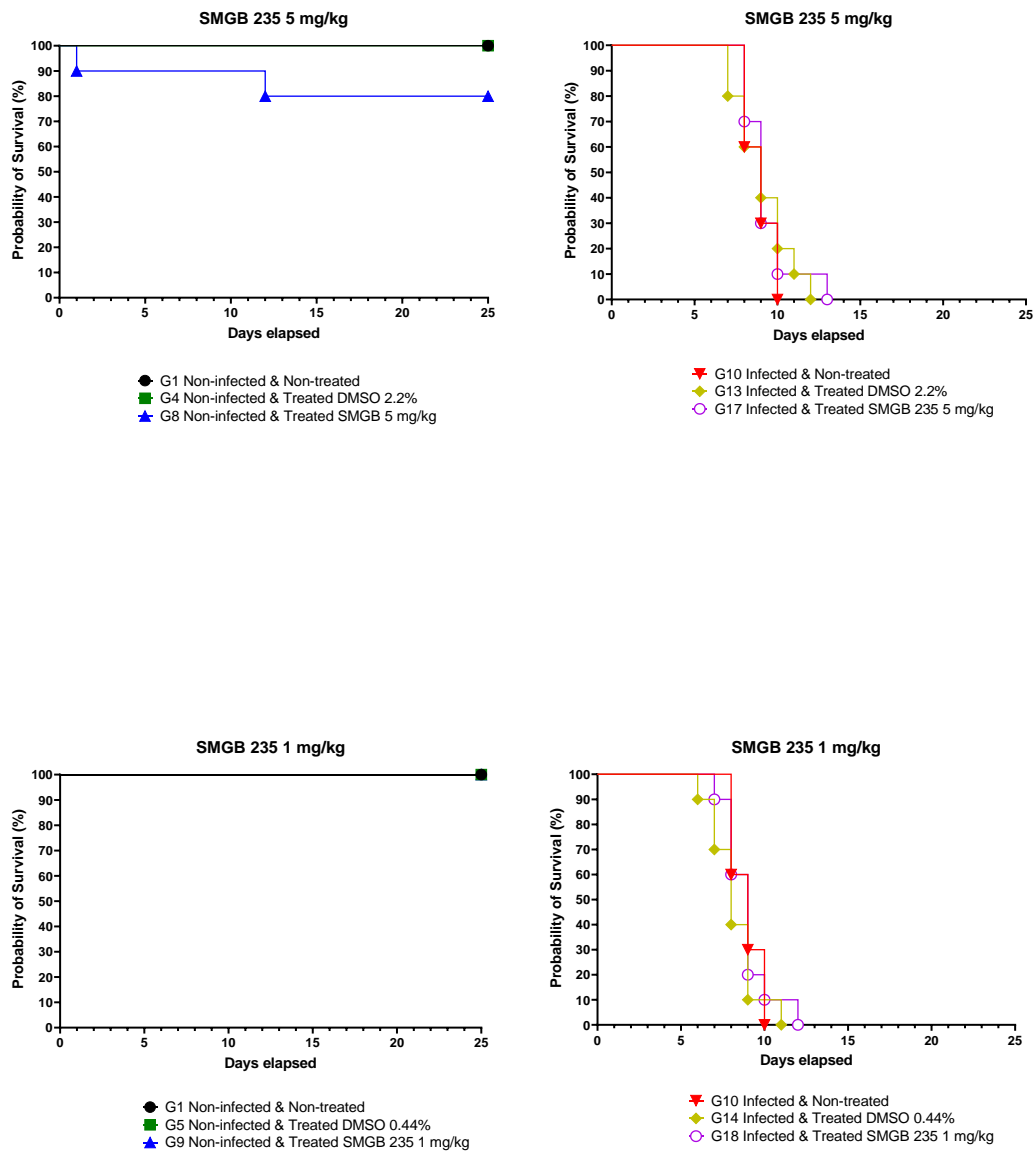


Figure 19. Kaplan-Meier survival curves of *Galleria mellonella* larvae infected with *Acanthamoeba castellanii* Neff strain and treated with S-MGB 235.

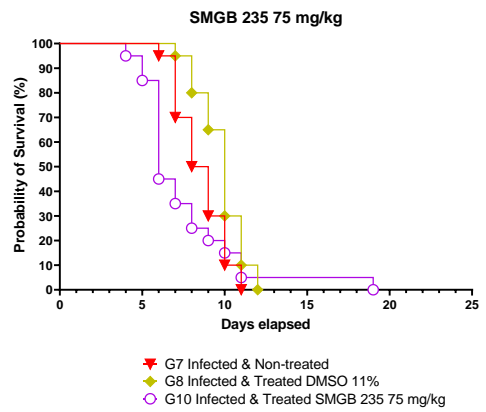
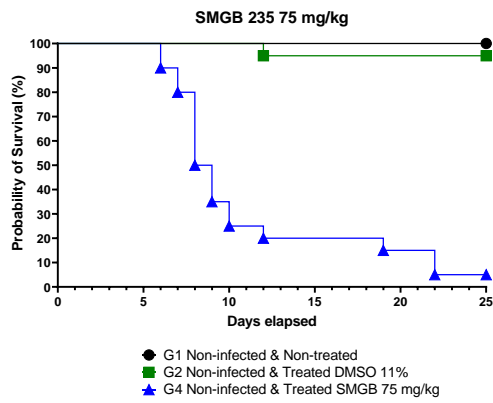
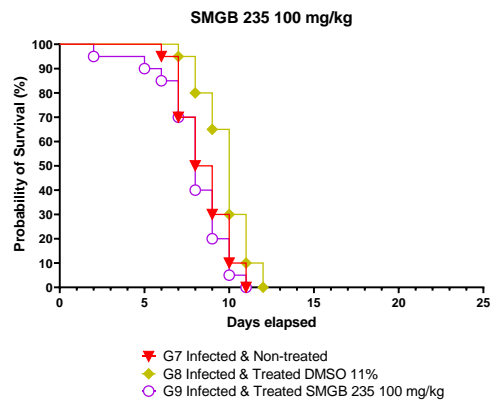
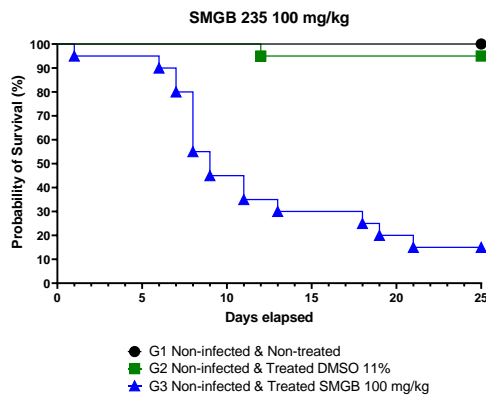
Larvae (n= 5 per group) were infected with 1×10^7 cells/ml of *A. castellanii* Neff strain trophozoites. Following infection, larvae were treated with 10 μ l of S-MGB 125, 25, 5 and 1 mg/kg. Two control groups consisted of non-infected, and non-treated, infected, and non-treated. Survival was monitored every 24 h over a period of 25 days. Data are pooled from two independent experiments.

Given the unexpected early deaths in the previous experiment a second experiment was performed. As 125mg/kg of S-MGB was known to be toxic to larvae this experiment excluded this dose and instead including doses of 100, 75 and 50 mg/kg. Moreover, to potentially reduce the possibility of any detrimental effects of DMSO, a constant concentration 11% DMSO was used in all doses of S-MGB. Previous studies by Giordani *et al.*, 2019 have demonstrated that S-MGBs are generally soluble at this concentration of DMSO. In addition, the number of larvae was increased to 10 per group. Two independent experiments were performed, and the pooled data is presented. Distribution of groups used on antibiotic efficacy testing are described in Table 17.

Similar to the previous experiments, doses of S-MGB above 25mg/kg (50, 75 and 100mg/kg) were also toxic to non-infected larvae. On this second assay, 25 mg/kg of S-MGB 235 protected 50% infected larvae until day 11, which is a similar result with the previous assay in which 50% of infected larvae were alive on day 12 (Figure 20). This protection was statistically significant compared with control untreated, infected larva which all died by day 11 (Mann–Whitney U test, $p=0.00126$) (Figure 20). In addition, 25 mg/kg of S-MGB 235 was non-toxic with 95% of non-infected larvae treated with this concentration of the drug surviving for 25 days. Larvae treated with DMSO were also significantly protected against infection (Mann–Whitney U test, $p=0.00695$).

Table 17. Description of S-MGB 235 efficacy testing procedure in *Galleria mellonella* larvae groups infected and non-infected with *Acanthamoeba castellanii* Neff strain trophozoites

Group (10 larvae each)	Infected with <i>A. castellanii</i> Neff (1x10⁷ cells/ml)	Treatment or Vehicle
G1 (Positive control)	No	No
G2	No	DMSO 11%
G3	No	100 mg/kg S-MGB 235
G4	No	75 mg/kg S-MGB 235
G5	No	50 mg/kg S-MGB 235
G6	No	25 mg/kg S-MGB 235
G7 (Negative control)	Yes	No
G8	Yes	DMSO 11%
G9	Yes	100 mg/kg S-MGB 235
G10	Yes	75 mg/kg S-MGB 235
G11	Yes	50 mg/kg S-MGB 235
G12	Yes	25 mg/kg S-MGB 235



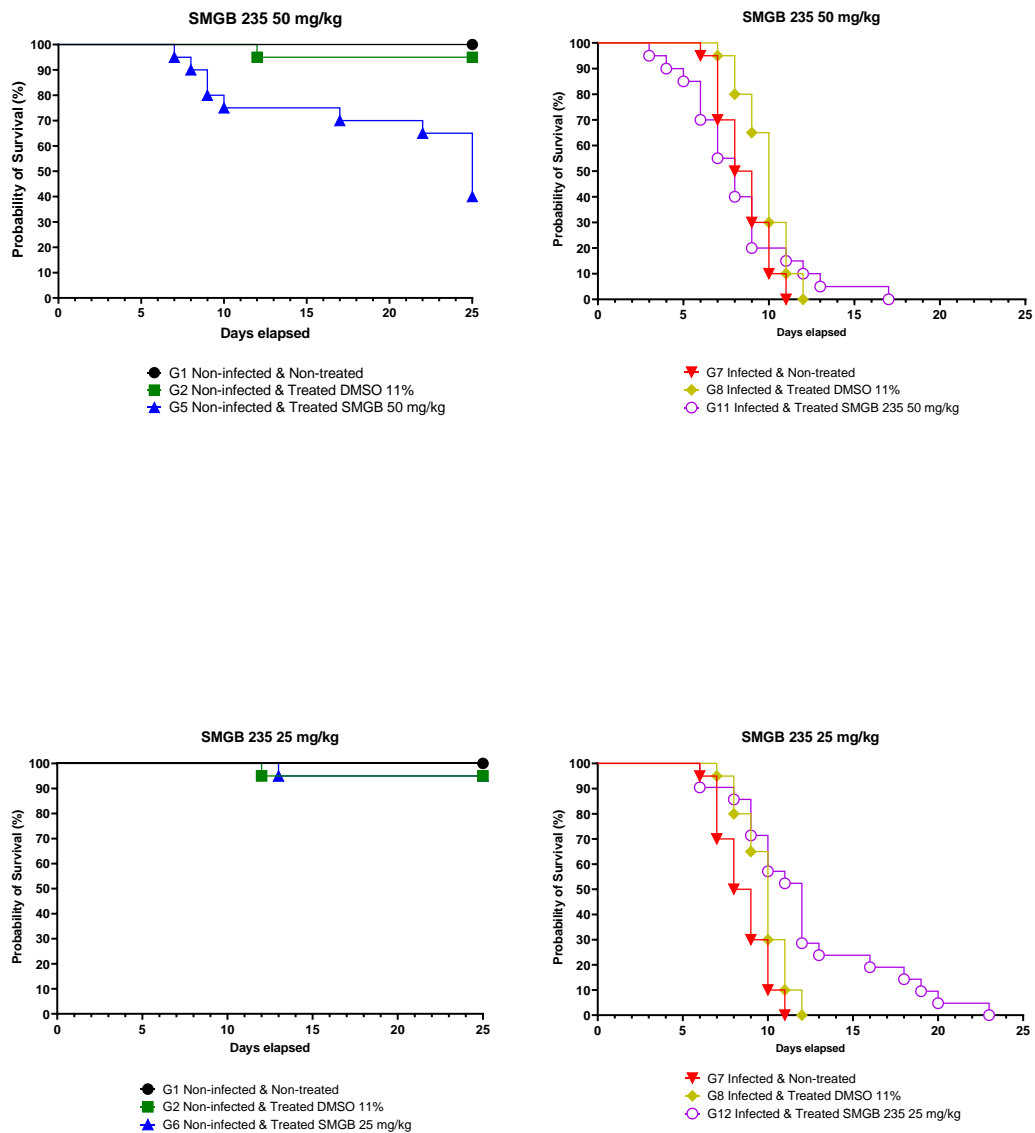


Figure 20. Kaplan-Meier survival curves of *Galleria mellonella* larvae infected with *Acanthamoeba castellanii* Neff strain and treated with S-MGB 235 diluted with DMSO 11%.

Larvae (n= 10 per group) were infected with 1×10^7 cells/ml of *A. castellanii* Neff strain trophozoites. Following infection, larvae were treated with 10 μ l of S-MGB 100, 75, 50 and 25 mg/kg. Two control groups consisted of non-infected, and non-treated; infected, and non-treated. Survival was monitored every 24 h over a period of 25 days. Data are pooled from two independent experiments.

4.5 Discussion

Insects represent an important alternative model to circumvent the employment of mammals, in testing the *in vivo* efficacy and toxicity of antimicrobial compounds. Development and validation of insect models also encourage efforts to adopt the 3Rs (Replace, Reduce and Refine) policy operative in the UK and other countries around the world to reduce the suffering of and number of higher animals in research. Therefore, development of novel scientifically competent screening systems is an important endeavour. Wax moth *Galleria mellonella* larvae has been widely used as a *in vivo* infection model to evaluate microbial and fungi virulence in recent years because it displays functional similarities with certain aspects of mammals as well as convenient features. This includes their innate immune response, which is comparable to mammalian models, smooth handling and inexpensive to purchase. Furthermore, there are less ethical concerns and legal restrictions (Piatek, Sheehan and Kavanagh, 2020).

In the present chapter it has been demonstrated that *G. mellonella* larvae survival is inoculum-dependent over time when different groups are infected with 10^3 - 10^7 cells/ml of *A. castellanii* Neff trophozoites. Physical changes due to infection are observed such as systemic melanisation, robust inflammation, stiffness, and twitching which suggest severe CNS damage of the insect. An infective dose of 1×10^7 cells was chosen to perform antibiotic efficacy tests for two reasons: (i) to explore the possibility of any of the drugs tested was able to protect the infected larvae with such high concentration of trophozoites and (ii) to reduce the time to carry out as many tests as possible and minimise the potential interference of pupation which starts around day 6. All the larvae infected with this cell density and not treated died by day 10 post-infection.

In order to explore the utility of this model, 2 drugs currently used in the treatment of human infection, voriconazole and miltefosine were first tested. *G. mellonella* larvae infected with 1×10^7 cells were treated with varying concentrations of voriconazole (125, 25 and 5 mg/kg) or miltefosine (43.8, 8.75 and 1.75 mg/kg). Voriconazole and miltefosine did not induce any significant protection since most of *G. mellonella* larvae in these treated groups died on day 11 post-infection. It is worth remembering that both of these drugs have only limited utility in the clinic and the results obtained here might also reflect their limited efficacy (Shing *et al.*, 2021).

With the above in mind the efficacy of S-MGB 235 was investigated in this model. Due to the relatively low cost and less ethical concerns of using this model toxicity and efficacy studies were able to proceed in parallel. Over the course of two sets of experiments S-MGB 235 was found to be toxic at doses of greater than 25mg/kg. However, S-MGB-235 was non-toxic at doses of 25 mg/kg. S-MGB-235 at 25 mg/kg was found to lower mortality in infected *G. mellonella* larvae in 2 sets of experiments, but this protection was only statistically significant in one of these sets. The first experiment had some spurious larvae deaths in the S-MGB treated larvae at the early stages of the experiment that would seem likely to be responsible for the lack of statistical significance. In addition, in the second set of experiments, the DMSO vehicle control also afforded some protection. Clearly, additional experiments are required to determine the consistency of the protection afforded by S-MGB-235. These experiments should minimise the final concentration of DMSO used to dissolve the drug. In addition, in the future, the infectious dose of *Acanthamoeba* could be reduced to perhaps provide a greater sensitivity to detect protective effects of drugs.

S-MGB-235 had previously been shown to be the best inhibitory compound from a group of three S-MGBs tested in a murine model of *Trypanosoma congolense* disease. In this study, five groups of four mice each were infected intraperitoneally with *T. congolense* STIB 736/IL1 180 and infection was allowed to develop before three different concentrations of the compound (50, 10 or 5 mg/kg) were administered on day 7 and 8 post infection or days 7-10 post infection. The mice were monitored for 2 months and considered cured when parasites were no longer detected in their blood. The highest dose 50 mg/kg was toxic for all the mice. However, at a dose of 10 mg/kg, all mice were fully cured by a minimum of 2 applications. One single application per day at this dose cured 3 of 4 mice. Lastly, the lowest dose 5 mg/kg cured 3 out of 4 mice when administered twice per day (Giordani et al., 2019). These data demonstrate that this S-MGB can be tolerated in mice at concentrations effective against at least this pathogen.

Other S-MGBs have also been shown to be efficacious *in vivo* against pathogenic microorganisms such as bacteria and fungi. MGB-BP-3 is an anti-infective with robust effect against *Clostridium difficile* improving the survival of hamsters challenged with this pathogen. In this study, six hamsters per group were infected with *C. difficile* and treated with vehicle, vancomycin (25 mg/kg), MGB-BP-3 (10 mg/kg) in two different formulations (suspension or microparticles) and compared with the untreated groups.

Interestingly, this S-MGB in a microparticle formulation was found to be as effective as oral vancomycin with the 100% of hamsters surviving 13 days post-infection compared with the suspension formulation where 5 hamsters died by day 11 and one survived until the end of the test. In addition, the microparticle formulation was remarkable in reducing the recovery of *C. difficile* by ten-fold as measured by colony forming units (cfu)/g from small intestine, colon, and caecum. MGB-BP-3 was recently found to be safe and effective during the Phase II clinical trials and thus could become a potential first-line treatment against *C. difficile* infection (Biopharma, 2013). Further confidence can be taken if the potential of S-MGBs as two members of this family, S-MGB-363 and S-MGB-364, have shown to be effective *in vivo* in mice against *A. fumigatus* and *M. tuberculosis*, respectively (Scott *et al.*, unpublished). Overall, these data support that S-MGBs are non-toxic, effective, and protective compounds against diseases caused by different pathogenic microorganisms *in vivo*.

There is no other analysis reported in the literature so far using *G. mellonella* as an *in vivo* infection model for parasites and let alone *Acanthamoeba*. However, the African migratory *Locusta migratoria* has been used as an insect model to study *Acanthamoeba* pathogenesis *in vivo* (Mortazavi *et al.*, 2010). Insect mortality was determined following injecting groups of 8-10 locusts (15-30 days old) into the haemocoel between two abdominal terga with 1×10^6 of *Acanthamoeba* T1 (ATCC50494) and T4 (ATCC 50492) genotypes. The number of dead locusts was recorded every 24 h post-infection. More than 80% of mortality in locusts infected with 10^6 parasites occurred by day 9, in our study, the group of larvae infected with the same concentration of *A. castellanii* Neff (also a T4 genotype) died by day 14. Notably, by day 11, 100% of the locusts were dead regardless of the genotype, whereas *G. mellonella* larvae were dead by day 15 when given this dose of parasites. Curiously, the non-infected control group in the locust model injected with PYG medium alone showed around 15% mortality by day 11 post-injection, in our group control no dead larva were reported and no illness or melanisation (as sign of illness) was generally observed by day 14 (when pupation could be observed). This indicates the healthy status of the larvae. Thus, our data suggests that somehow *G. mellonella* larvae shows better long immune protection to succumb *Acanthamoeba* infection compared with the locust model. Nonetheless, stiffness was also an effect observed on the locust model through the course of the infection. Histopathological sections revealed that both T1 and T4 genotypes were able to invade the locust brain. Similar

histological studies would be necessary to determine if *Acanthamoeba* also invade the ganglia of *G. mellonella* larvae.

Several animals or have been used as *in vivo* models for the pathogenic potential of AK and GAE infections (Khan, 2010). Other studies have used organs harvested from animals as alternative models of infection (He *et al.*, 1992; Morgan *et al.*, 2020). However, the lack of similar symptoms to human in animal models infected with AK or GAE and the ethical constraints have halted the analysis of important treatment options.

The lack of efficacy afforded by voriconazole and miltefosine in *G. mellonella* is puzzling. Voriconazole is a second generation of drugs derived from fluconazole which mainly affects the integrity and permeability of fungi membrane by inhibiting the cytochrome P-450 enzyme lanosterol 14- α -demethylase (Shing *et al.*, 2021). *Acanthamoeba* spp. is phylogenetically proximal to fungi and metazoans, and it has been established that the major component of its sterol biosynthesis is ergosterol, the main target of voriconazole. This compound has proven effective in the combination treatment using biguanides and diamidines against AK caused by both *A. castellanii* and *polyphaga* which provokes disruption of the cell membrane leading to lysis (Thomson *et al.*, 2017). Voriconazole has been scarcely analysed *in vivo* for its amoebicidal activity. A recent study on rat cornea showed poor bioavailability of voriconazole regardless of whether the drug was applied via eye drops or given orally. (Guedry *et al.*, 2018). In the current *in vivo* study, voriconazole did not induce protection of larvae from *A. castellanii* Neff infection. The drug was in fact toxic at the highest concentration used and killed non-infected larva, which indicates that it is likely to benefit in examining higher doses of drug in this model.

Initially implemented as an experimental antineoplastic agent for breast cancer, miltefosine started to be recommended by the CDC in 2013 for the treatment of PAM caused by *Naegleria fowleri*. It was previously shown to be effective against *Acanthamoeba in vitro* (Walochnik *et al.*, 2002; McBride *et al.*, 2007). This drug belongs to the class of alkyl phosphocholine drug family and despite the fact the precise mechanism of action against *Naegleria* or *Acanthamoeba* is poorly understood, the phospholipid and alkyl phosphocholine structure allow the drug to reach the BBB and be active in brain tissue (Alli *et al.*, 2021). Just like voriconazole, few studies have examined the *in vivo* efficacy of miltefosine. One *in vivo* study infected the corneas of Syrian hamsters with 1 μ l of 1×10^6 amoeba/ml of

Acanthamoeba hatchetti strain 2HH trophozoites, a human corneal isolate. The effect of topical miltefosine (160 μ M) vs 0.1% propamidine isethionate plus 0.02% polyhexanide was evaluated. Grades of infection (G0, G1, G2 or G3) were established after the fifth day of incubation. The therapy lasted one month with eight applications a day during the first week and three applications during the last 3 weeks of the therapeutic agents. Cornea treated with miltefosine reached the last day of treatment with 85% of the eyes scored as G0 compared with the 65% of the eyes treated with propamidine isethionate (Polat et al., 2012). Miltefosine has also been shown to have some efficacy in humans with GAE. In six case reports, from patients treated with miltefosine, four patients survived and two died (Alli et al., 2021). In addition, a recent case described the successful treatment with a young male that developed acanthamoebic encephalitis, after immunosuppression due to infection by COVID-19 (Siripurapu et al., 2021). In contrast, the studies described herein found that miltefosine did not protect infected larvae at any of the concentrations used in this *in vivo* assay. Of note, none of the concentration used were found to be toxic in this model leaving the possibility to further investigate higher doses of this drug.

Overall, the studies described in this chapter demonstrate that *Acanthamoeba* Neff trophozoites are capable of infecting *G. mellonella* and establish infectious doses and timelines of mortality for future studies. S-MGB 235 would appear to provide a degree of protection in this model, but future studies are required to corroborate the results obtained.

Chapter 5. Construction of pBRFPT7NeoCas9 for the development of a new CRISPR-Cas9 system for *Acanthamoeba castellanii* Neff strain.

5.1 Abstract

The availability of genetic tools to manipulate genomes opens new possibilities to decipher the biology of pathogenic microorganisms. *Acanthamoeba* has been used for gene expression analysis and methods for stable or transient transfection systems have been reported, however, the CRISPR-Cas9 technology has not been adapted for this free-living amoeba. This chapter represents the first effort to develop a complete CRISPR-Cas9 system for *Acanthamoeba*. To validate the method these tools were developed to delete the *chorismate synthase* gene of the Shikimate pathway and hence, to inhibit the biosynthesis of folates and aromatic amino acids. Two expression plasmids, pBRFPT7NeoCas9 and pBRFPT7PhleoCas9 were constructed carrying the genes for Cas9, T7 RNA Polymerase and Red Fluorescent Protein (RFP). pBRFPT7NeoCas9 transfection in *Acanthamoeba* Neff trophozoites with Xfect polymer was confirmed by fluorescence microscopy and by fluorescence-activated cell sorting (FACS). DNA templates for the expression of single guide RNAs (sgRNAs) and DNA constructs containing the gene for a drug selectable marker surrounded by 30 nucleotides homology flanks identical to the target locus were generated. The completion of this chapter was interrupted due to Covid-19 constraints; however, it is highly recommended to further investigate this new gene editing tool to allow the functional analysis of genes and proteins in *Acanthamoeba*.

5.2 Background

5.2.1 Use of Green and Red Fluorescent proteins (GFP, RFP) as transfection reporters in *Acanthamoeba* spp.

The first observation in 1962 by Shimomura of the Green Fluorescent Protein (GFP) in the jellyfish *Aequorea victoria* led to further work that ultimately resulted in the Nobel Prize awarded to Chalfie and Tsien in 2008. GFP has had a major contribution to present day understanding of cellular and molecular biology of numerous organisms (Misteli and Spector, 1997). The GFP-technology has many advantages over other reporter systems. Mainly, when expressed, these proteins do not need additional cofactors or substrates other than molecular oxygen that supplies the necessary energy to form a chromophore and emit light (Shcherbakova *et al.*, 2012). GFP is also resistant to numerous physicochemical parameters and compounds and furthermore the fusion of GFP to a particular protein scarcely affects the function, activity, or mobility. Importantly it is also non-toxic. Different colour variants of GFP such as blue, cyan and yellowish-green were described in the late 1990s and this variety was expanded by the addition of red variants now available for scientific research (Miyawaki, Shcherbakova and Verkhusha, 2012).

Red Fluorescent Protein (RFP) is attractive because its fluorescence can be modulated at specific excitation wavelengths. Although it shares structural organisation with GFP it has lower susceptibility to light-scattering and its emission spectra penetrates tissues better than that given off by green variants. The emission spectra are also less likely to overlap with autofluorescence and is less likely to result in phototoxicity (Müller *et al.*, 2007; Shcherbakova *et al.*, 2012). A wide array of laboratory applications has employed GFP or RFP. Transgenic animals, plants, fungi, bacteria engineered to express these proteins have been important in numerous applications including understanding cell structure, protein dynamics in living cells, function of genes and gene products, signalling pathways and embryo development. GFP-based reported systems have also been useful in the discovery of markers for tumours and in drug discovery (Zimmer, 2002). The introduction of transgenes is achieved through the construction of plasmid vectors that include GFP. GFP expression can be used for the identification of transfected cells that have successfully taken up the plasmid and show fluorescence and therefore are distinguishable from wild type cells. GFP-based systems can even be used as a selectable marker, in

combination with fluorescence-activated cell sorting, to assist the isolation of successfully transfected cells and thus generation of stably transfected cell lines. (Liu, 2013).

Use of GFP as a reporter in living parasites has been described in Apicomplexa. This promoted the development of experimental protocols to elucidate cellular activities such as protein trafficking, organelle biogenesis and cell division in *Toxoplasma gondii* and *Plasmodium falciparum* (Gubbels and Striepen, 2004).

There have been some studies that have reported transient or stable plasmid transfection carrying GFP/EGFP or RFP in *Acanthamoeba* spp. (Table 18). One pioneer study that developed a reliable enhanced GFP (EGFP) transfection method for *Acanthamoeba* was used in the early 2000s to describe the cellular localisation and dynamics of different myosin isoforms (Kong and Pollard, 2002). Subsequently, the method was standardised using GFP or EGFP as reporter gene in different *Acanthamoeba* species mainly by Moon et al. describing several members and regulators involved in the encystment process (Moon et al., 2006; Moon et al., 2008b; Moon et al., 2009; Moon et al., 2016; Moon et al., 2017). Furthermore, there is only one study up to now in the literature describing the stable transfection of a plasmid carrying a monomeric red fluorescent protein that was transfected into *A. castellanii* MEEI0184 strain isolated from an infected human cornea. The authors used this transfected cell line to visualise *Acanthamoeba* in the eyes of infected mice demonstrating the essential role of IL-17A expression for host protection in the AK infection process (Suryawanshi et al., 2015).

Table 18. Overview of transfections in *Acanthamoeba* spp.

<i>Acanthamoeba</i> specie/strain	Plasmid transfected	Plasmid backbone	Drug resistance marker	Transfection reagent or method	Transfection type	Transfection efficiency	Reference
Isolate 1B6 <i>Polyphaga</i>	pOPSBU	pOP13CAT	G418	Calcium phosphate	Stable	40% 10%	Yin and Henney Jr, 1997
Isolate 1B6	pOPSBU	pOP13CAT	-	Electroporation	Transient	45% (enhanced by DEAE-dextran)	Hu and Henney, 1997
<i>Castellanii</i> Neff	pUbPG, pUbGMII _t , pUbGMII, pUbGMII _m , pUbGMIC _h , pUbGMIC _b , pUbGMIC _g , pUbGMIC _s , pUbGMIC _f , pUbGMIC _t ,	pGL3	-	Superfect	Transient	3% for smaller plasmids 0.5% for larger plasmids	Kong and Pollard, 2002
<i>Castellanii</i> (strain NA)	p-110Neo, p-110EGFP(Neo), p-50EGFP(Neo), pCSP21EGFP, p-110EGFPFHTBP(Neo)	pAgTFIID, pCI-EGFP, pCSP-FL, pET3AFHTBP	G418	Superfect	Stable	-	Peng, Omaruddin and Bateman, 2005
<i>Healyi</i> (strain NA)	-	pUb-EGFP	-	Superfect	-	-	Baldo <i>et al.</i> , 2005
<i>Healyi</i> OC-3A strain ATCC 30866	pUbAhSub(f)g, pUbAhSub(pre)g, pUbAhSub(pre-pro)g, pUbAhSub(pro-m)g, pUbAhSub(m)g, pUbAhSub(pro)g, pUbAhCP(f)g, pUbAhCP(pre-pro)g, pUbAhCP(pro)g, pUbAhCP(m)g, pUbAhCP(pre)g	pUbg	-	Superfect	Transient	1.5 to 2.2%	Moon <i>et al.</i> , 2006

<i>Healyi</i> OC-3A strain ATCC 30866	AhABP-F, AhABP Δ EF, AhABP Δ AS, AhABP Δ CT	pUb-EGFP	-	Superfect	Transient	0.5 to 3%	Alafag <i>et al.</i> , 2006
<i>Healyi</i> OC-3A strain (ATCC 30866) and <i>Castellanii</i> ATCC 30011	<i>EMSP</i> gene + pUb-EGFP	pUb-EGFP	-	Superfect	Transient	99% by FACS	Moon <i>et al.</i> , 2008b
<i>Castellanii</i> ATCC 30011	<i>AcAtg8</i> gene + pUb-EGFP	pUb-EGFP	-	Superfect	Transient	1.7% by FACS	Moon <i>et al.</i> , 2009
<i>Castellanii</i> (strain NA)	pEBMCS, pEBMCSTBP, pEBMCSTPBF, pEBMCSGAPDH, pGAPDH-EGFP, pTPBF- EGFP	p-110EGFP	G418	Superfect	Stable	-	Bateman, 2010
<i>Castellanii</i> ATCC 30011	<i>AcAtg3</i> gene + pUb-EGFP	pUb-EGFP	-	Superfect	Transient	-	Moon <i>et al.</i> , 2011
<i>Castellanii</i> ATCC 30011	<i>CSCP</i> gene + pUb-EGFP	pUb-EGFP	-	Superfect	Transient	-	Moon <i>et al.</i> , 2012
<i>Castellanii</i> ATCC 30011	<i>AcStefin</i> gene + pUb-EGFP	pUb-EGFP	-	Superfect	Transient	-	Lee <i>et al.</i> , 2013

<i>Castellani</i> MEEI 0184	p-475TBP-mRFP	-	G418	Superfect	Stable	100% by fluorescence microscopy	Suryawanshi <i>et al.</i> , 2015
<i>Castellani</i> ATCC 30011	pGAPDHgPRMT5	pGAPDH- EGFP	G418	Superfect	Stable	-	Moon <i>et al.</i> , 2016
<i>Castellani</i> ATCC 30011	pGAPDH-AcSir2-EGFP	pGAPDH- EGFP	G418	Superfect	Stable	-	Joo <i>et al.</i> , 2020

Abbreviations: (E)GFP= (enhanced) green fluorescent protein; RFP: red fluorescent protein; DEAE= Diethylaminoethyl; - information not described.

5.2.2 General features of genome-editing tools

Gene editing approaches to produce accurate modifications in the genome of living cells have led to a wide array of possibilities to probe the functionality of a gene by modifying it (mutating or deleting) and observing a phenotype. This is important in approaches to develop effective drugs against a specific disease in which specific genes are involved. Many tools have been developed during the last decades to enable changes in genomic loci with minimal off-effects; such changes are achieved with programmable nucleases, enzymes that cause double-stranded breaks (DSB) in DNA (Harrison and Hart, 2018). Repair of defective endogenous DSBs in eukaryotes is carried out either by non-homologous end joining (NHEJ) or homology-directed repair (HDR). NHEJ is an error-prone system, it uses a homologous DNA template to repair the damaged strand using protein factors to insert or delete nucleotides (indels). On the other hand, HDR uses the same homologous repair template for precise repair (Lino *et al.*, 2018).

The introduction of site-specific DNA DSBs has led to engineered molecular tools such as mobile genetic elements, mega-nucleases, zinc finger nucleases, transcription activator-like effectors and the most recently, Clustered Regularly-Interspaced Palindromic Repeats (CRISPR), a bacterial immune system using a DNA endonuclease known as Cas9 guided to its target cleavage site by guide RNA (Doudna and Charpentier, 2014).

5.2.3 CRISPR-Cas9 as genome-editing technology

Clustered Regularly Interspaced Palindromic Repeats (CRISPR) is a highly adaptive and heritable immune system typical of bacteria and archaea to defend against the incorporation of foreign phage (virus) or plasmid DNA into their own genome (Doudna and Charpentier, 2014). Through different phases: adaptation, biogenesis and interference (Figure 21), this system generates a “memory” and in this way is able to degrade the next invader sequence attack (Thurtle-Schmidt and Lo, 2018). Found for the first time in the *E. coli* genome by (Ishino *et al.*, 1987), CRISPR loci have been reported approximately in 40% of bacteria and 90% of archaea genomes sequenced (Hryhorowicz *et al.*, 2017).

In **adaptation**, acquisition or immunisation, a Cas nuclease protein cuts the phage DNA in short sequences named *protospacers*, which then are incorporated in the CRISPR locus of the bacteria/archaea genome in a highly-variable fashion: non-contiguous repetitions separated by continuous *spacers*, term used for the invader

phage sequences once integrated in an orderly fashion (Thurtle-Schmidt and Lo, 2018). A distinct feature of this system is the capacity to preserve and inherit these spacers in a Lamarckian evolutive trend, however, they also can lose them (Bhaya, Davison and Barrangou, 2011). Integrated invader phage sequences are transcribed into a long transcript known as *pre-crRNA* followed by endonucleolytic cleavage of into mature *crRNA* by Cas proteins. Along with *pre-crRNA*, the antisense strand upstream inside the CRISPR locus is also transcribed generating the trans-activating CRISPR (*tracrCRISPR*), defined as a complementary region of the repeat region that hybridises with a *precrRNA* which is cleaved by an RNAase type III generating the *crRNA:tracrRNA* flanked by one single repetition. The processed complex is bound to a specific Cas protein endonuclease forming an activated ribonucleoprotein multisubunit known as CASCADE (CRISPR-associated complex for antiviral defence). This sequence of events is also referred to in the literature as **biogenesis** or expression phase.

Interference or immunity is the final stage where the CASCADE complex is ready to recognise and cleave further foreign phage invader sequences (Bhaya, Davison and Barrangou, 2011; Thurtle-Schmidt and Lo, 2018). The *crRNA* is often referred to as “guide RNA” since the CASCADE complex contains a mature *crRNA* with a specific base sequence that will base pair with the corresponding further invasive phage DNA sequence through the Cas9 protein. The recognition occurs with a short motif of conserved nucleotides next to the protospacer named as Protospacer Adjacent Motif (PAM). Cas proteins from different bacteria recognise different PAM sites, with *S. pyogenes* Cas9 using PAM 5'-NGG-3', which is the most common motif used for genome editing (Thurtle-Schmidt and Lo, 2018). Two main nuclease domains belonging to Cas9 HNH (named after the histidine and asparagine residues) nicks the complementary DNA strand to *crRNA* and RuvC (*E. coli* protein implicated in DNA repair) nicks the non-complementary DNA strand to *crRNA* introducing double-strand breaks 3 bp upstream of the PAM generating a blunt-end. PAM is crucial to distinguish the invading DNA and the CRISPR loci (Shah *et al.*, 2013).

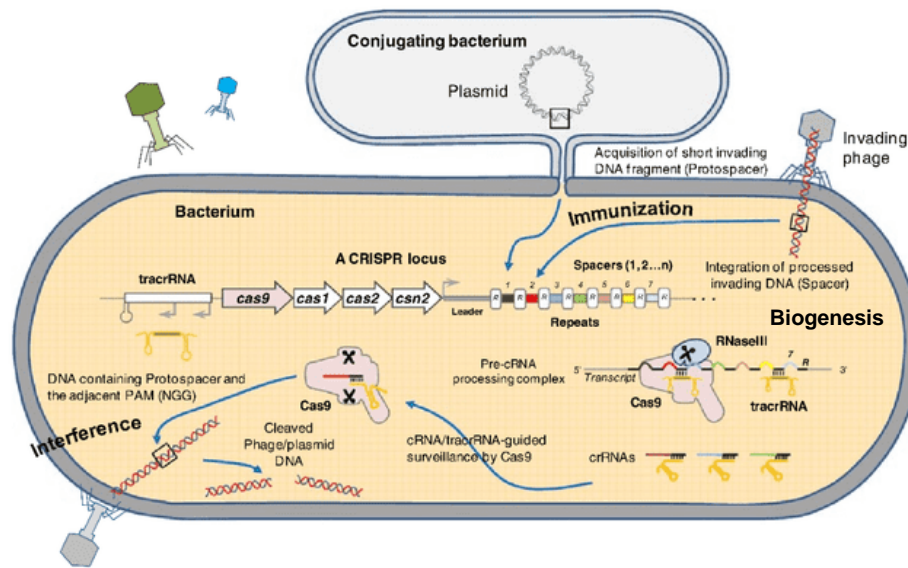


Figure 21. CRISPR-Cas9 Adaptive Immune System process representation occurring in bacteria and archaea.

The three stages are depicted: Immunisation, Biogenesis, and Interference. Modified from (Fichtner, Urrea Castellanos and Ülker, 2014).

The CRISPR-Cas9 system has been exploited over the last years as a powerful tool for genome editing unravelling its full potential. The system has been engineered since 2013 to include: (i) targeted mutations through DSBs where the bacterial cells will employ their own error prone repair DNA system pathway through NHEJ meaning that the damage is repaired imperfectly yielding insertions, deletions or single-nucleotide substitutions or HDR where a homologous DNA sequence is used as template to repair the break and (ii) regulation of gene expression (Bikard *et al.*, 2013; Jiang *et al.*, 2013).

With the purpose of generating and introducing proper CRISPR-Cas9 mutations, certain steps are recommended and outlined next:

1. Target and guide selection

When the gene target has been selected it is important to create a guide RNA. The target region composed of approximately 20 nucleotides must be immediately close to a PAM site. The generation of the *single guide RNA* (sgRNA) can be carried out using computational online tools focusing on the specificity for the target region in order to decrease the potential off-targets. It has not been elucidated what affects the sgRNA efficiency but the presence of a purine base, either G or A, at the 3'-end of the 20 nucleotides target has

shown to be effective (Farboud and Meyer, 2015; Gagnon *et al.*, 2014; Ren *et al.*, 2014; Ahmad and Amiji, 2018).

2. Generation and delivery of the CRISPR-Cas9 system components

Once generated, the sgRNA and the whole CRISPR-Cas9 system can be introduced and expressed mainly in two modes:

- a) *DNA*: two plasmids encoding the sgRNA and the Cas9 sequence are required. Additionally, it is recommended to codon-optimize Cas9, 5' and 3' untranslated regions (UTR) must be included for an improved translation of Cas9 as well as an appropriate promoter needs to be present to transcribe the gene.
- b) *RNA & CASCADE complex*: This mode avoids the sgRNA and Cas9 transcription and transcription-translation process, respectively. sgRNA and mRNA encoding Cas9 might be delivered to the target cell. Appropriate expression is assured when the mRNA is post-transcriptionally modified adding both a 5' cap and a 3' poly-A tail or as a CASCADE complex (crRNA:tracrRNA:Cas9).

For both modes described above, the introduction is carried out using microinjection (worms, fruit flies and zebrafishes), electroporation or transfection (commonly in eukaryotic cells such as mammalian cells or protists) (Thurtle-Schmidt and Lo, 2018).

3. Identification of the desired mutation

The identification of a genome edit is carried out by different strategies, the most useful are screens and selections. The screen looks for a phenotypic change associated with the desired mutation, then the cell progeny can be selected. Different fluorescent proteins such as GFP or RFP are inserted to tag a protein of interest through HDR, fluorescence expression is expected as a marker (Paix *et al.*, 2014). Genetic changes can also be screened, especially when the genetic repair pathway such as NHEJ generates insertions or deletions.

In genetic selection the “survival strategy” is the most used through the addition of a specialised template for repair, which introduces a gene for a drug resistance. Only the cells that successfully introduced the repair template at the desired locus

due to DNA double strand break induced by Cas9 will survive after exposure to the drug (Thurtle-Schmidt and Lo, 2018).

A type II CRISPR-Cas9 system has been applied in different cell lines and organisms such as plants, insects, mice, rabbits, pigs, monkeys and human cells (Hryhorowicz *et al.*, 2017). Over the last years, this system has been the most applied gene editing tool, offering benefits to satisfy current complex interests in industry such as the crop industry or in biomedical science such as regenerative medicine, oncology, genetics, drug discovery and infectious diseases (Ahmad and Amiji, 2018; Loureiro and da Silva, 2019).

Over the past few years, a small number of studies using CRISPR-Cas9 in bacteria to elucidate cellular pathways that manifest pathogenic factors and resistance genes have been carried out in *Mycobacterium tuberculosis*, *Francisella novicida*, *Pseudomonas aeruginosa*, *Klebsiella pneumoniae*, *Escherichia coli*, *Staphylococcus aureus*, enterohemorrhagic *E. coli*, *Bacillus subtilis*, *Clostridium septicum*, *Vibrio parahaemolyticus*, *Clostridium difficile* toxin B, etc. (Bikard *et al.*, 2014; Citorik, Mimee and Lu, 2014; Koike-Yusa *et al.*, 2014; Choudhary *et al.*, 2015; Blondel *et al.*, 2016; Peters *et al.*, 2016; Singh *et al.*, 2016; Tao *et al.*, 2016; Wu and Li, 2016; Sampson *et al.*, 2019).

Relatively slow progress on the application of this genome editing tool can be observed in protozoan parasites. First reports of successful genome editing via CRISPR-Cas9 were published in 2014 in *Plasmodium falciparum*. Since then significant findings are glimpsing the importance of this tool that also has been applied in *Toxoplasma* spp., *Cryptosporidium parvum*, *Trypanosoma* spp., *Leishmania* spp. and recently *Trichomonas vaginalis* (Grzybek *et al.*, 2018) (Ghorbal *et al.*, 2014; Grzybek *et al.*, 2018; Bryant *et al.*, 2019) (Table 19).

Table 19. Current reports of genome editing via CRISPR-Cas9 in protozoan parasites.

Updated and adapted from Grzybek et al., 2018.

Organism	Purpose	Strategy	Repair mechanism	References
<i>P. falciparum</i>	Gene knockout	2 vectors	HDR	Ghorbal <i>et al.</i> , 2014
<i>P. falciparum</i>	Gene knockout	2 vectors	HDR	Wagner <i>et al.</i> , 2014
<i>P. yoelii</i>	Gene knockout, C-terminal tagging, and insertion of point mutations	1 vector	HDR	Zhang <i>et al.</i> , 2014
<i>T. gondii</i>	Gene knockout and knock-in	1 vector	NHEJ, HDR	Shen <i>et al.</i> , 2014 Behnke Michael, Khan and Sibley, 2015 Rugarabamu <i>et al.</i> , 2015 Wang <i>et al.</i> , 2016
<i>T. gondii</i>	Gene knockout, C-terminal tagging and insertion of point mutations	1 vector	NHEJ, HDR	Sidik <i>et al.</i> , 2014
<i>T. gondii</i>	Gene tandem replacement	1 vector	HDR	Behnke <i>et al.</i> , 2015
<i>T. gondii</i>	Gene knockout	1 vector	NHEJ	Zheng, Jia and Zheng, 2015
<i>C. parvum</i>	Gene knockout and knock-in	1 vector	HDR	Vinayak <i>et al.</i> , 2015
<i>T. cruzi</i>	Gene knockout	1 vector and 2 vectors	MMEJ, HDR	Lander <i>et al.</i> , 2015
<i>T. cruzi</i>	Gene disruption (single, multi), exogenous gene swapping	1 vector	MMEJ, HDR	Peng <i>et al.</i> , 2014
<i>T. brucei</i>	Gene knock-in	1 vector	MMEJ	Beneke <i>et al.</i> , 2017
<i>L. major</i>	Replacement of a gene tandem	2 vectors	HDR	Sollelis <i>et al.</i> , 2015 Beneke <i>et al.</i> , 2017 Zhang <i>et al.</i> , 2017
<i>L. mexicana</i>	Gene knock-in	1 vector and 2 vectors	MMEJ, HDR	Beneke <i>et al.</i> , 2017 Zhang <i>et al.</i> , 2017
<i>L. donovani</i>	Gene knockout and C-terminal tagging	2 vectors	IHR, MMEJ, HDR	Zhang, Matlashewski and Sibley, 2015 Zhang <i>et al.</i> , 2017
<i>T. vaginalis</i>	Gene knockout and knock-in	1 vector and 2 vectors	NHEJ, HDR	Janssen <i>et al.</i> , 2018
<i>Dictyostelium</i>	Gene knockout	1 vector and 2 vectors	NHEJ, HDR	Muramoto <i>et al.</i> , 2019
<i>Entamoeba histolytica</i>	Gene reparation by insertion	2 vectors	HDR	Kangussu-Marcolino <i>et al.</i> , 2021
<i>Giardia intestinalis</i>	Gene knockout	RNP complex	HDR	Horáčková <i>et al.</i> , 2021
<i>Babesia spp.</i>				
<i>Eimeria spp.</i>				
<i>Isospora spp.</i>				
<i>Cystoisospora spp.</i>				
<i>Sarcocystis spp.</i>				
<i>Naegleria fowleri</i>				
<i>Acanthamoeba spp.</i>				
<i>Pentatrichomonas hominis</i>				
<i>Balantidium coli</i>				
<i>Spironucleus spp.</i>				

?

Abbreviations: HDR: homologous direct repair, NHEJ: non-homologous end joining, MMEJ: microhomology-mediated end joining, IHR: interhomolog recombination.

5.2.4 Chorismate synthase as target for gene deletion by CRISPR-Cas9 in *Acanthamoeba* spp.

The Shikimate pathway is an ancestral common pathway related to primary metabolism found in plants, algae, bacteria, fungi, and protozoans including apicomplexans. In this metabolic pathway, the phosphoenolpyruvate (PEP) and D-erythrose 4-phosphate are converted through seven enzymatic reactions into chorismate, a precursor of important aromatic amino acids required for protein biosynthesis such as L-Phenylalanine (Phe), L-Tryptophan (Trp) and L-Tyrosine (Tyr). Existing data suggests significant differences in the genetic organisation and regulators of this pathway among plants, bacteria and fungi which define the mode of regulation and inhibition (Bentley, 1990; Herrmann, 1995; Derrer, Macheroux and Kappes, 2013).

In plants, this vital pathway carries out its activity in the plastids, leading to proper growth, development and reproduction, defence, and secondary metabolites production (Maeda and Dudareva, 2012). In pathogenic bacteria this biosynthetic pathway is in the cytosol in order to grow *in vivo* and preserve the infection (Payne *et al.*, 2000). Mutations or deletions generated in genes related to the shikimate pathway in pathogenic bacteria (e.g., *Salmonella*, *Shigella* and *Aeromonas*) have completely blocked the growth and attenuated their pathogenic capacity to cause an infection.

Inhibition of the 5-enolpyruvateshikimate-3-phosphate (EPSP) synthase in the Shikimate pathway using glyphosate inhibited the growth of *T. gondii*, *P. falciparum*, and *Cryptosporidium parvum*. This elucidated the importance of this metabolic pathway as a potential target for the development of new antimicrobials in apicomplexan parasites responsible for a variety of important diseases to humans and animals (Roberts *et al.*, 2002).

A similar study demonstrated *Acanthamoeba* spp. possess the Shikimate pathway (Henriquez *et al.*, 2015). The effectiveness of glyphosate to inhibit the growth of *A. castellanii* Neff and ATCC50370 trophozoites was assessed through alamarBlue assays. This was confirmed by the addition of essential amino acids such as phenylalanine and tryptophan in cultures with trophozoites previously treated with glyphosate, which rescued trophozoites and ablated any inhibitory effect of glyphosate. Moreover, *in silico* analysis and computational models revealed that *Acanthamoeba* contain 3-deoxy-D-arabino-heptulosonate 7-phosphate (DAHP) synthases type I and II, a tetrafunctional fused gene cluster comprising 3-

dehydroquinase synthase (DHQS), 5-enolpyruvylshikimate-3-phosphate synthase (EPSPS), shikimate kinase (SK) and 3-dehydroquinase dehydratase (DH) and a trifunctional fused gene cluster comprising shikimate dehydrogenase (SD), phosphoribosyl anthranilate isomerase and indole-3-glycerol-phosphate synthase which were confirmed by PCR using cDNA in both strains. Similarly, a putative chorismate synthase (CS) gene, coding for the enzyme that converts EPSP into chorismate was confirmed by hot-start PCR (Henriquez *et al.*, 2015).

The reaction mechanism to convert EPSP to chorismate via CS is unique considering that the cofactor flavin mononucleotide (FMN) is required to eliminate *anti*-1,4 of the 3-phosphate and C(6*proR*) hydrogen. Two different types of CS have been described so far depending on the way they obtain the cofactor FMN: (i) from cellular environmental resources and (ii) the presence of reduced nicotinamide adenine dinucleotide phosphate (NADPH) (Arcuri and Palma, 2011).

The current knowledge of the chemical structure and mechanism of action has led the development of inhibitors of CS; first attempts have used fluorine for the synthesis of two new analogues considering the loss of C(6*proR*) hydrogen: (6R)-6-fluoro and (6S)-6-fluoro shikimate which have been screened against *Neurospora crassa* and *E. coli* showing antimicrobial activity (Ramjee *et al.*, 1992; Dias *et al.*, 2007). Further *in vivo* infection studies with *S. aureus* and *Salmonella dublin* in mice were also performed with (6S)-6-fluoro shikimate inhibiting the growth of these pathogenic bacteria (Davies *et al.*, 1994).

This chapter reports the results of the construction, transfection, and expression of plasmids as an approach to introduce the CRISPR-Cas9 system with the aim to target the *chorismate synthase* gene in *Acanthamoeba castellanii* Neff strain trophozoites.

5.3 Aims and Objectives

The development of new gene editing tools has been crucial during the last years for genome manipulation of various pathogenic microorganisms. The versatility and programmability of CRISPR-Cas9 has been useful for the study of parasite biology which provides a powerful molecular genetic toolbox to identify new drug targets or vaccine candidates to prevent lethal parasitic diseases that are considered a major public health concern. To date, a complete CRISPR-Cas9 gene editing system has not been established for free-living amoebas.

The main aim of this chapter is to develop a fast and reliable CRISPR-Cas9 system for *Acanthamoeba* spp. and exploit its efficiency based on the approach generated for *Leishmania* spp. by Beneke *et al.*, 2017.

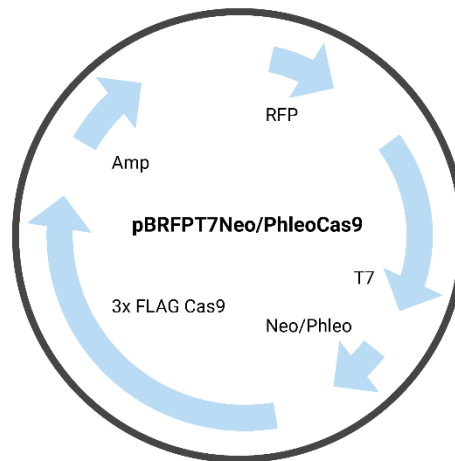
The objectives are (i) to generate an expression plasmid carrying the genes for Cas9, T7 RNA polymerase and red fluorescent protein (RFP) as a reporter to confirm gene expression from the plasmid. In addition, to generate single guide RNAs (sgRNAs) and donor DNA templates with antibiotic resistance markers and 30 nucleotides homology flanks specific to the *chorismate synthase* (CS) gene; (ii) to transfect the plasmid, sgRNAs and donor DNA templates into *Acanthamoeba*; (iii) to confirm successful CS replacement by using PCR, fluorescence microscopy and immunoblot analysis.

5.4 Results

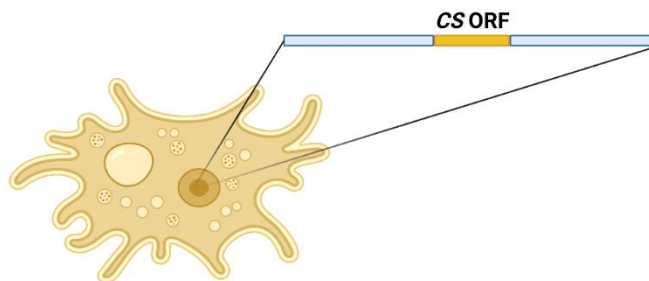
5.4.1 General overview: Development of the CRISPR-Cas9 system for *Acanthamoeba castellanii* Neff strain.

To achieve the project's aim, a rapid and scalable CRISPR-Cas9 method toolkit applied in *Leishmania* spp. (Beneke et al., 2017) was applied in *Acanthamoeba castellanii* Neff strain. As part of the strategy (Figure 22), it was necessary to construct pBRFPT7NeoCas9 (13283 bp) and pBRFPT7PhleoCas9 (12860 bp). In addition, a double-stranded template, formed by annealing and filling-in of G00 (sgRNA scaffold) and sgRNA oligomers, is transcribed into a single guide RNA in *A. castellanii* Neff and directs the Cas9 enzyme to cleave upstream (5') and downstream (3') of the targeted *chorismate synthase* (CS) gene (Figure 23 and 24). Amplicons pCR7.1-Neo/Phleo/HygB carrying flanking fragments of the CS gene will be inserted in place of the wild-type CS gene. RFP will express fluorescence as a potential indicator of successful transfection and expression of Cas9 and T7 RNA polymerase which will be assessed by fluorescence microscopy.

A. Construction of plasmid constructs



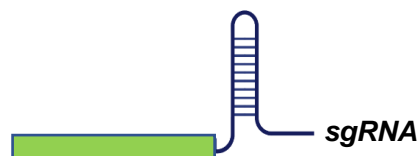
B. WT *A. castellanii* Neff genome situation



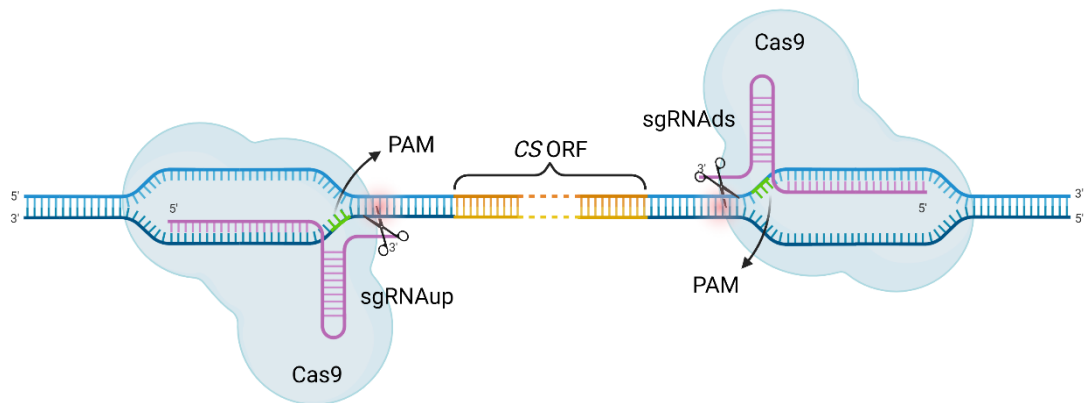
C. Strategy for sgRNA formation



Fill-in product



D. CS gene deletion by CRISPR-Cas9



E. Genomic situation after CRISPR-Cas9 deletion

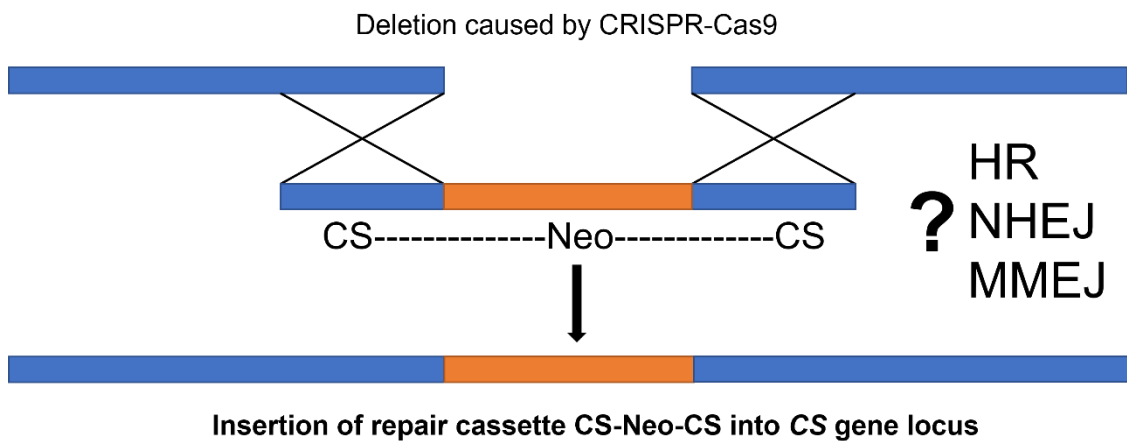


Figure 22. Deletion of CS using CRISPR-Cas9 in *A. castellanii* Neff strain.

(A), Schematic of pBRFPT7NeoCas9/pBRFPT7PhleoCas9 showing the machinery required for CRISPR-Cas9; (B), WT *A. castellanii* Neff genome situation; (C), sgRNA delivery: the template is produced by PCR fill-in reaction utilising an oligo encoding the T7 promoter (T7) and the target site defined by 20 nt, and a second oligo with a sequence complementary at the 3'-end which includes the G00 sgRNA scaffold; (D), Cas9 protein is expressed, deletion of CS gene is targeted via two sgRNAs (sgRNACSup/ds). Repair cassettes containing drug selection marker genes (Neomycin/Phleomycin/Hygromycin B) and 30 nucleotide homology flanks specific to the CS target gene are PCR-amplified from pCR2.neo/phleo/hygB utilising oligomers CSCRupneo/phleo/hygB.for and CSCRupneo/phleo/hygB.rev to generate CS-Neo-CS, CS-Phleo-CS and CS-HygB-CS; (E), the PCR-amplified fragment is inserted into the CS gene locus in place of the deleted gene. It is unknown if the repair mechanism in *A. castellanii* Neff strain uses homologous recombination (HR), non-homologous end joining (NHEJ) or microhomology-mediated end joining (MMEJ). Figures A, B and D were created with BioRender.com.

GATCTTTGCTTCGCTTTTTTTCGACCTCCGGTCCCAGAATGCGAGGAATGTCCCAGACCTCCGCGCC
 ACGCATAGTTTCGCAATCCACGAACTATAAATTGAAATAAACAAAAAGAAGATAAAAAGATAACGGC
 GTTAGAGCTTGAAGAAGACGCGACATCAAGCACCGGTGCAGGCGACAAGGCAACACTGAAGAGAAG
 AG**ATG**AGCAGCTTTGGCAGAGCGTTTCGAGTGACCACCTTCGGTGAATCGCACGGCGCGGAGTGG
 GATGCATTATCGGTGCGTGCTGCGAGATACAACAATCAGTTTTTTATCTGTCTAATCGGGCAGATT
 GCACACTCGATCTCGCTCGTCCATCCATCCATCCATCTACTTTGTTTCATCTTGTGTGCGTTCCGT
 GGAATACCTGCTCACAGCGCTCCATCTCTACTCTTCTTCTTCTTCTTTCCTTTCGAGATGGAGTGCCGCC
 TGCCTGCCCTCACCGAAGCCGACATCCAGCCGAGCTCAGCCGTCGCCGCCCGGCCAGAGCTCC
 CTCACCACCCCGTTCCGCCCTTCGCTCTCCTCCCTCCCTTCTTCTTTCGCTGACCGTGTATGT
 GCGGTGCTGTGCCGTGTGCCGTGTGCCGTGTGCCGTGTGCCGTGTGCCGTGTGCCGTGTGCCGTGT
 GCCGTGTGCCGTGTGCCGTGTGCCGTGTGTGTGCTGTCTGATCAGAGGAATGAGGCGGACCAGGTG
 AAGATCCAGGCTGGCACGGAGAACGGGTACACGCTGGGCTCGCCGATCAGCCTCTTCGTGGCCAAC
 CAGGACCAGCGGCCCGTTCGACTACTCGGACATGTCCAAGATCCCGCGGCCCTCGCACGCCGACTAC
 ACCTACGCGGCCAAGTACAACATCAAGTCTCCTCGGGCGGCGGCCGCTCCTCCGCGGAGAGACC
 ATCGGCCGAGTCGGCGCCGGCGCCGTCGCTGAGAAGTGGCTCAAGCTCAAGGTACCCAGGCTCGCG
 CGTGTGCTGTCATTGGTGTGCGCGTGTGCGCGTGTGCCGTGTGCCGTGTGTGTGGTGTGCTGA
 TGACGATTGGCCGCGTGCACAGTACGGTGTGAGATCGTGGCGTGGGTGAGCTCGATCGGCCGACCA
 GGAGATCGAGAGGGAGCTCGACCTGGACACCATTTTCGCGGAGGACGTCGACAAGTCGCTCGTTTCG
 CTGCCCCGACGAGGCCGCCACGGCCAAGATGATTGAGGTTCCCCCACCACCACAACGCCAACGAT
 TCATCGGCCTGGTCTCACACACGACACACACGACACACACGACACACACGACACCACGACACACGA
 CACCACGACACCACGACACGTACCATAGATCATTTGAGGCGGCAAAAGGCTGACAAGGACAGCATCGG
 CGGCGTGGTGTGCGTGTGCCGTAACGTACCGACGGGCTGGGCGAGCCCTGCTTCGACAAGCT
 CGAGGCCATGCTCGCCACGCCATGCTCTCCATCCCGGCCACGAAGGGGTTTCGAGATCGGCAGCGG
 CTTTCGCGGGCACGCGGATGCGGGGACGAAGCACAAACGACCCCTTCGTGGTCAAGACCGGGGCCGA
 CGGCAAGAAGCGGCTCGGTACCACTACCAACCACAGCGGCGGCATCCAGGGCGGAATCACCAACGG
 CGAACACGTCGCTTCAAGGTCTGCCCCTGTTGTGTGTGTCGTTGTGTGTCGTTGTGCTGA
 TGGAATGTGGAATGTGTAGGTGGCGTTCAAGCCCGGCCACGATTAGCCAGGCGCAGAAGACGAG
 CGAGTACGGCGGCGGAGGCGGTGCTGGAGGCCAGGGGAGACACGACCCGTGCGTGGTGGCGCG
 GGCCATCGCTATCGTTCGAGGCCATGGCAGCCCTGGTTCATCGCCGACGCGGCCCTGCTCCAGCTCGC
 ACGCCAAGGCTCCCTCGTCTCCGAGCCCATCGTTCGCTGGCAGATT**TGA**ACGGGAGGTTGTGCTG
 ACAGCTCCAGAAAAAGTACTTAAAGTGGCTAAATGTGCGTGTCTCGAACACTATCATGCA**CCTGAC**
GCCCTCGTTTCTCTCGACGTGCGCCAAACAGAGCAAGAAGCGCGCTGCTCCAGAGTGTGCCACATC
 ACGGGCCTGTGTTGGGTGAAGAAAAGCTGTAGTTGATGTGGGCGAAACGCC

Figure 23. Wild type chorismate synthase (CS) gene locus in *A. castellanii* Neff strain.

Chorismate synthase (ACA1_283500) locus map to indicate the 30 nucleotide homology
 flanks highlighted in **blue** used to PCR-generate the repair cassettes containing drug
 selection marker genes, in **red** the sequences of sgRNACSup that targets the 5'-end of the
 donor DNA to an upstream site of the CS ORF and sgRNACSDs that targets the 3'-end of
 the donor DNA to a downstream site of the CS ORF. PAM sites are highlighted in **green**;
 the CS ORF is highlighted in **yellow** and start/stop codons are in **bold**. Insertion of the
 donor DNA will result in replacement of the CS gene.

GATCTTTGCTTCGCTTTTTTTCGACCTCCGGTCCCAGAATGCGAGGAATGTCCCAGACCTCCGCGCC
ACGCATAGTTTCGCAATCCACGAACATAAAATTGAAATAAACAAAAAGAAGATAAAAGATAACGGC
GTTAGAGCTTGAAGAAGACCGGACATCAATTCCGGCTTGCCATC**ATG**AGCTCGGCCATTGAACAAGA
TGGATTGCACGCAGGTTCTCCGGCCGCTTGGGTGGAGAGGCTATTCCGGCTATGACTGGGCACAACA
GACAATCGGCTGCTCTGATGCCGCCGTGTTCCGGCTGTCAGCGCAGGGGCGCCGGTCTTTTTTGT
CAAGACCCGACCTGTCCGGTGCCCTGAATGAACTGCAGGACGAGGCAGCGCGGCTATCGTGGCTGGC
CACGACGGGCGTTCCCTTGCGCAGCTGTGCTCGACGTTGTCACTGAAGCGGGAAGGGACTGGCTGCT
ATTGGGCGAAGTGCCGGGGCAGGATCTCCTGTCATCTCACCTTGCTCCTGCCGAGAAAAGTATCCAT
CATGGCTGATGCAATGCGGGCGGCTGCATACGCTTGATCCGGCTACCTGCCATTCGACCACCAAGC
GAAACATCGCATCGAGCGAGCACGTACTCGGATGGAAGCCGGTCTTGTCGATCAGGATGATCTGGA
CGAAGAGCATCAGGGGCTCGCGCCAGCCGAACTGTTCCGCCAGGCTCAAGGCGCGCATGCCCGACGG
CGAGGATCTCGTTCGTGACCCATGGCGATGCCTGCTTGCCGAATATCATGGTGGAAAAATGGCCGCTT
TTCTGGATTTCATCGACTGTGGCCGGCTGGGTGTGGCGGACCGCTATCAGGACATAGCGTTGGCTAC
CCGTGATATTGCTGAAGAGCTTGGCGGCGAATGGGCTGACCGCTTCTTCGTGCTTTACGGTATCGC
CGCTCCCGATTTCGACGCGCATCGCCTTCTATCGCCTTCTTGACGAGTTCTT**TGA**GCTAGCCGGCA
AAGCCG**CGTGCGCCAAACAGAGCAAGAAGCGCGCTG**CTCCAGAGTGTGCCACATCACGGGCCTGTG
TTGGGTGAAGAAAAGCTGTAGTTGATGTGGGCGAAACGCC

Figure 24. Genomic situation after replacement of CS gene by CS-Neo-CS.

Insertion of Neomycin gene sequence highlighted in **orange** after deletion of CS gene which is located between the 30 nucleotide homology flanks highlighted in **blue**. Start/stop codons are in **bold**.

5.4.2 Standardisation of drug selection markers against *A. castellanii* Neff strain using alamarBlue assays

A set of drug selection markers commonly used against *Leishmania spp.* were screened against *Acanthamoeba castellanii* Neff strain to investigate a killing effect for later use as drug selection marker (Figure 25). Phleomycin produced a potent inhibitory effect against trophozoites, followed by G418 and Hygromycin B. Hence, G418 and Phleomycin were chosen as selection markers to construct the plasmids containing the T7 RNA polymerase and Cas9 sequences. The concentrations of G418 and Phleomycin used throughout transfections to select pBRFPT7NeoCas9 and pBRFPT7PhleoCas9 are depicted on Table 20. Hygromycin B gene sequence was used to construct DNA repair cassettes (see section 5.4.12).

Table 20. Drug concentrations used to select pBRFPT7NeoCas9 and pBRFPT7PhleoCas9 after transfection using Xfect.

Toxicity dose	Final Concentration				Culture volume [ml]	Volume of drug (µl)	
	G418		Phleomycin			G418	Phleomycin
	IC50 [µM]	IC50 [µg/ml]	IC50 [µM]	IC50 [µg/ml]			
High dose	12.5	6.2	0.40	0.53	10	4.21	1.06
Optimal dose	6.25	3.1	0.20	0.26	10	2.1	0.52
Low dose	3.12	1.55	0.10	0.13	10	1.05	0.26

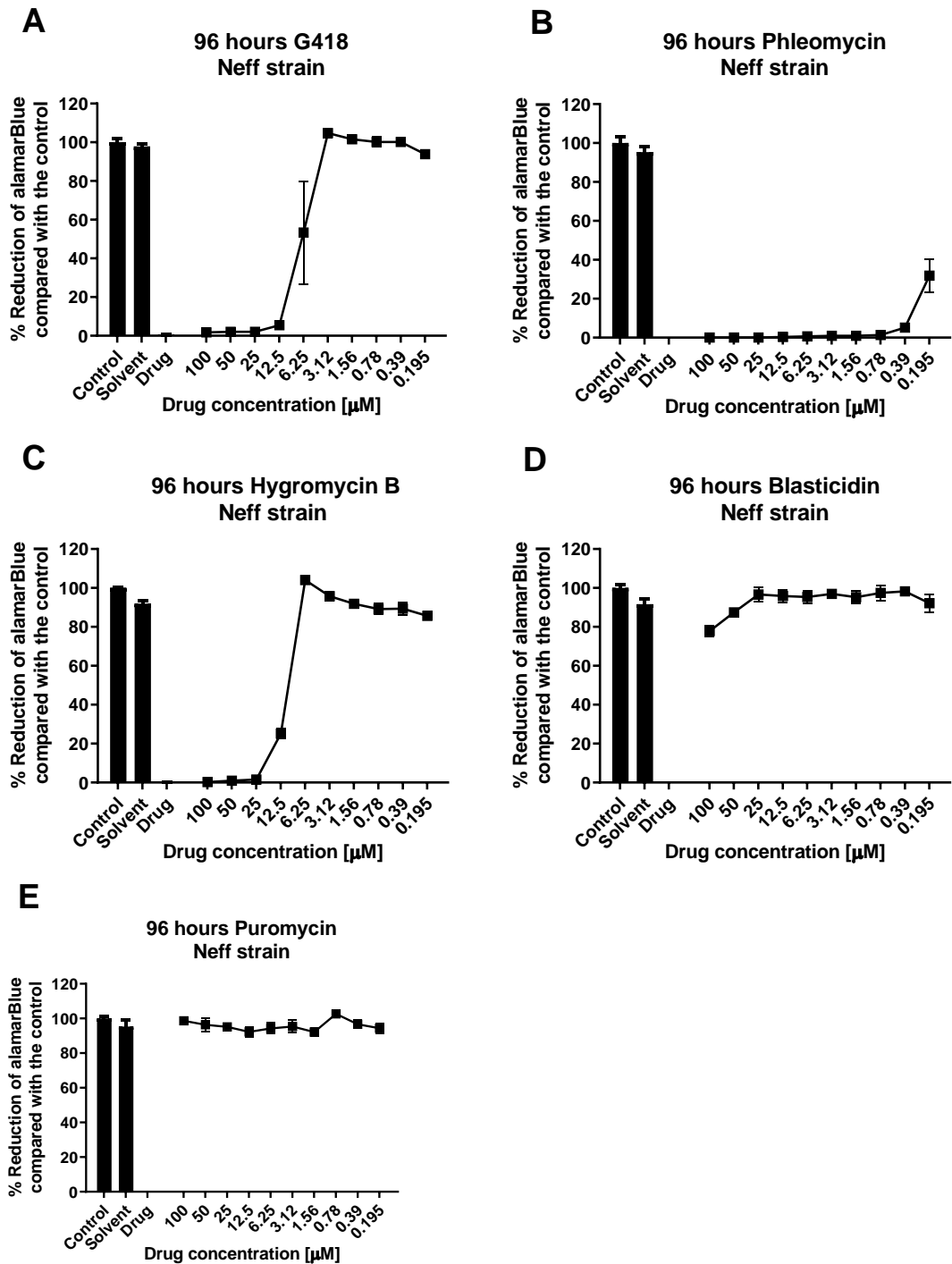


Figure 25. Efficacy of drug selection markers against *A. castellanii* Neff strain using alamarBlue assays.

Half maximal inhibitory (IC_{50}) concentrations of **(A)** G418= 6.25 μM , $\pm\text{SEM}$ = 0.45; **(B)** Phleomycin= 0.20 μM $\pm\text{SEM}$ = 0.17; **(C)** Hygromycin B= 10.05 μM ; **(D)** Blastidicin= >100 μM ; **(E)** Puromycin= >100 μM . Each value represents the mean of triplicate wells $\pm\text{SEM}$, the screening was performed in three independent experiments. Only for G418 and Phleomycin single representative assays are shown for clarity.

5.4.3 Generation of pBBXSV40RFP

To generate pBRFPT7NeoCas9 and pBRFPPhleCas9 as part of the CRISPR-Cas9 system, the formation of pBBXSV40RFP was required. The plasmid pBBsdRFPCSV40 (5249 bp) (Figure 26) was cleaved with BglIII to generate two fragments: 3397 bp and 1852 bp (Figure 27). The 3397 bp band containing the SV40 promoter was isolated and purified.

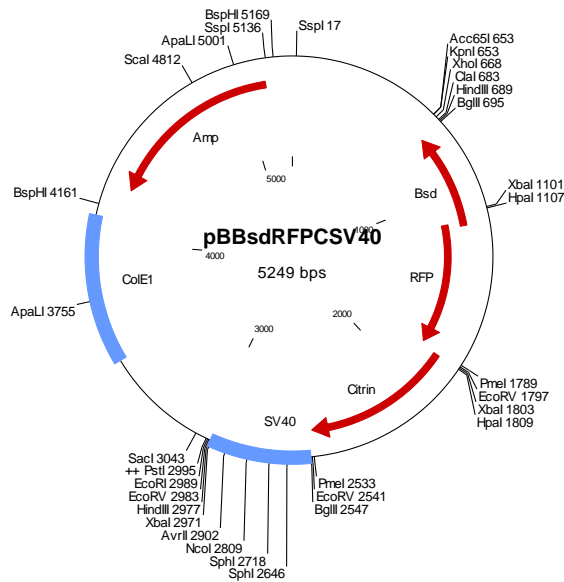


Figure 26. Plasmid map of pBBsdRFPCSV40 (5249 bp).

AMP, ampicillin resistant gene; Bsd, Blasticidin resistance gene; RFP, red fluorescent protein, Citrin, yellow fluorescent protein; SV40, simian virus 40 promoter; ColE1, origin of replication. The plasmid map was generated in Clone Manager 9.

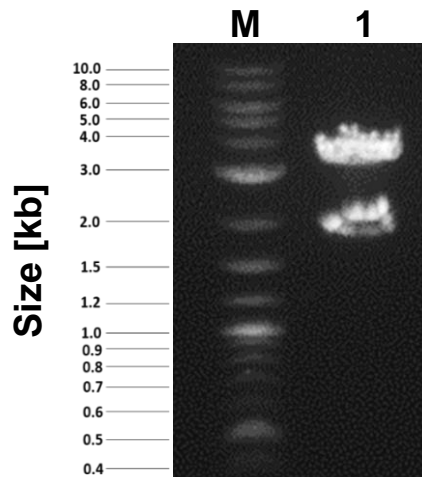


Figure 27. Restriction cleavage of pBBsdRFPCSV40 with BglIII.

M, 1 kb Plus DNA ladder; lane 1, plasmid cleaved with BglIII generating 3397 bp (SV40 promoter) and 1852 bp DNA fragments. 0.8% agarose gel prepared with 0.5x TBE after electrophoresis stained with ethidium bromide.

Afterwards, pBBsdRFPCSV40 was cleaved with XbaI to generate three fragments: 3379 bp, 1168 bp and 702 bp; the latter containing the RFP sequence was isolated (Figure 28).

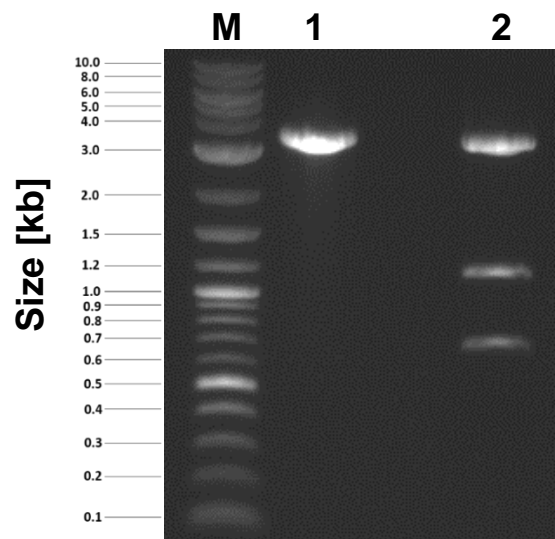


Figure 28. Gel Purification of SV40 promoter and restriction cleavage of pBBsdRFPCSV40 with XbaI.

M, 1 kb Plus DNA ladder; lane 1, gel purification of SV40 fragment (3397 bp); lane 2, pBBsdRFPCSV40 cleaved with XbaI: (3379 bp, 1169 bp and 702 bp). The RFP fragment (702 bp) was gel isolated. 0.8% agarose gel prepared with 0.5x TBE after electrophoresis stained with ethidium bromide.

The isolated 3397 bp fragment generated with BglII was self-ligated and transformed into *E. coli* DH5 α to generate pBSV40 (3397 bp) (Figure 29). pBSV40 was linearised with XbaI, purified and SAP-treated to prevent self-ligation (Figure 30) to be used for ligation with the 702 bp RFP fragment (see above).

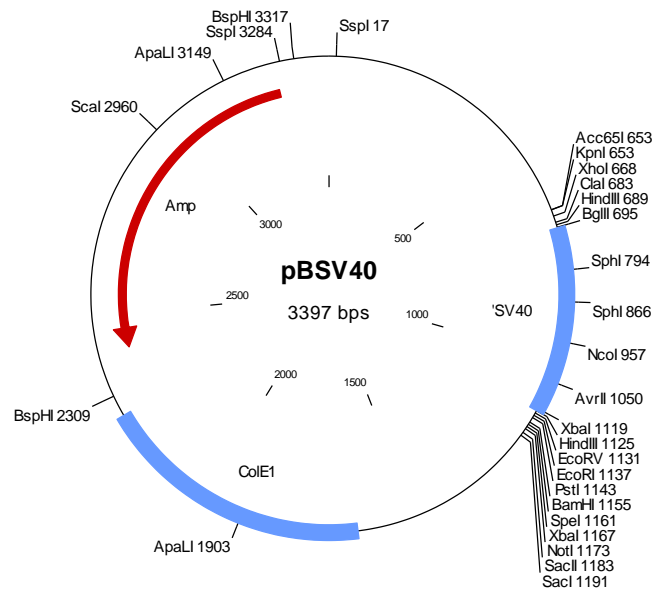


Figure 29. Plasmid map of pBSV40 (3393 bp)

AMP, ampicillin resistant gene; SV40, simian virus 40 promoter; ColE1, origin of replication. The plasmid map was generated in Clone Manager 9.

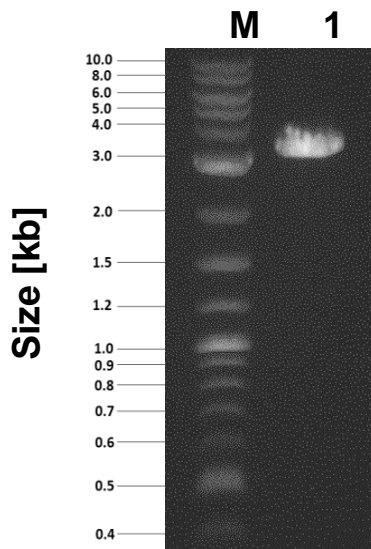


Figure 30. Shrimp Alkaline Phosphatase (SAP) treatment of SV40 promoter fragment.

M, 1 kb Plus DNA ladder; lane 1, the 3397 bp SV40 promoter carrying fragment after dephosphorylation of 5'- and 3'-ends. 0.8% agarose gel prepared with 0.5x TBE after electrophoresis stained with ethidium bromide.

The SV40 promoter fragment (3397 bp) and the RFP fragment (702 bp) were ligated, transformed into *E. coli* and plasmid DNA isolated from seven colonies ("miniprep"). After cleavage with EcoRV + HindIII positive clones showed the expected band sizes of 2923 bp and 1128 bp. Some plasmids produced 3613 bp and 438 bp indicating the wrong orientation of the insert (Figure 31). The new plasmid pBBXSV40RFP has a size of 4051 bp (Figure 32) (Table 21).

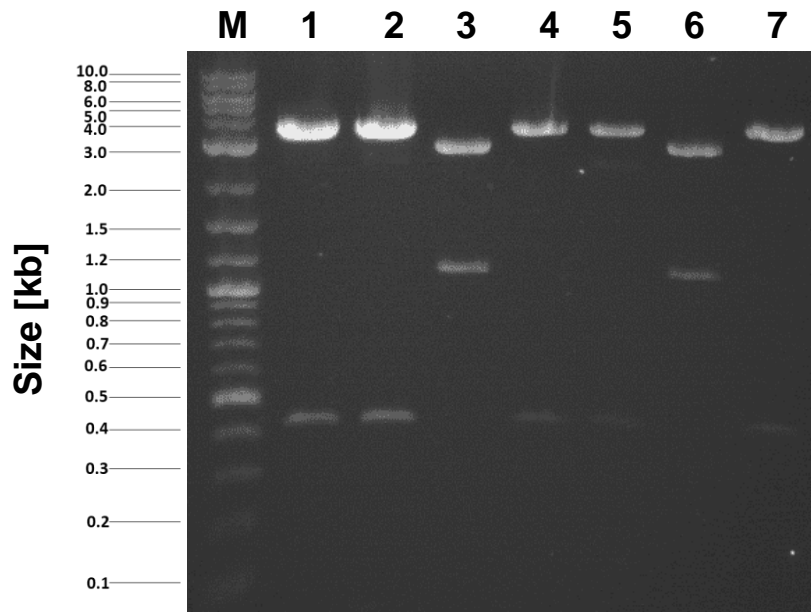


Figure 31. Miniprep restriction cleavage with EcoRV+HindIII.

M, 1 kb Plus DNA ladder; lanes 1, 2, 4, 5 and 7 show 3613 bp and 438 bp DNA fragments indicating the wrong orientation of the insert; lanes 3 and 6 show the expected pBBXSV40RFP generating 2923 bp and 1128 bp DNA fragments. 0.8% agarose gel prepared with 0.5x TBE after electrophoresis stained with ethidium bromide.

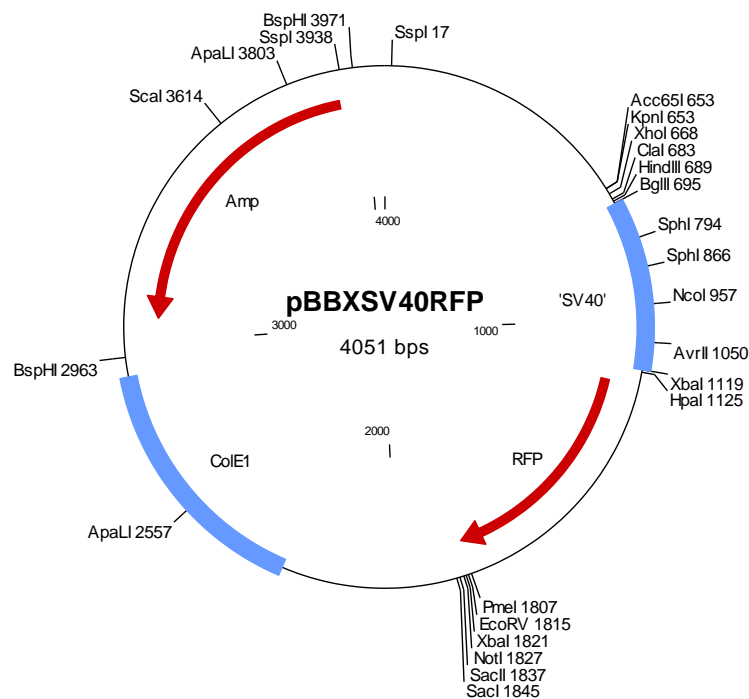


Figure 32. Plasmid map of pBBXSV40RFP (4051 bp).

AMP, ampicillin resistance gene; SV40, simian virus 40 promoter; RFP, red fluorescent protein; ColE1, origin of replication. The plasmid map was generated in Clone Manager 9.

Table 21. Restriction analysis of pBBXSV40RFP

A table to illustrate the expected fragment sizes, in base pairs, after pBBXSV40RFP cleavage utilising various restriction enzymes.

Plasmid	Restriction enzymes	Fragment sizes [bp]
pBBXSV40RFP	PmeI+HindIII	2930 and 1121
	XbaI	3349 and 702
	HindIII	4051

5.4.4 Generation of pRFPSV40

pBASV40GFP (6002 bp) (Figure 33) was used to isolate the neomycin phosphotransferase antibiotic resistance gene Neo. The plasmid was cleaved with NotI for linearisation followed by a fill-in reaction using Klenow polymerase (Figure 34).

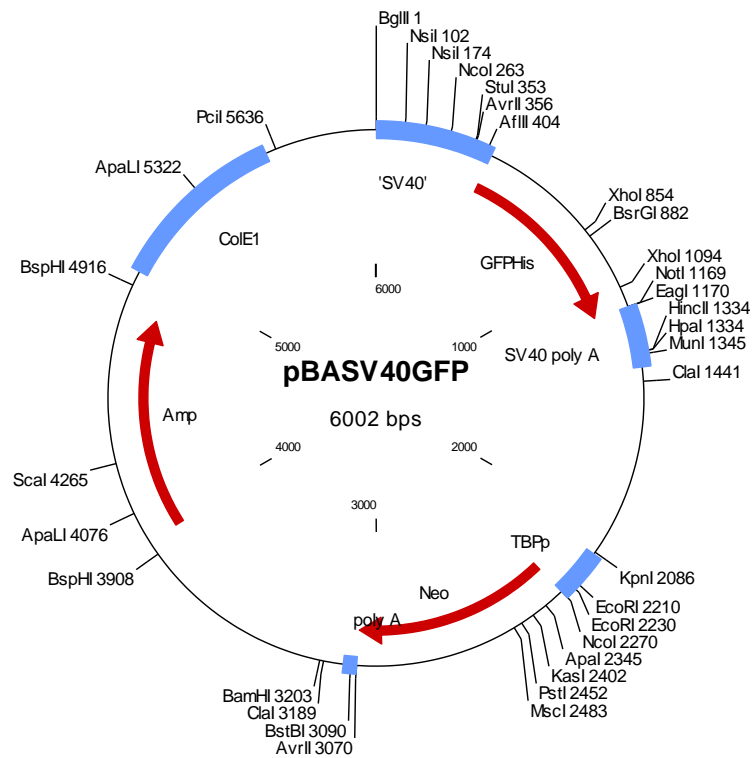


Figure 33. Plasmid map of pBASV40GFP (6002 bp).

AMP, ampicillin resistance gene; ColE1, origin of replication; SV40, simian virus 40 promoter; GFPHis, Green Fluorescent Protein with C-terminal His-tag; SV40 poly A; SV40 poly A tail addition site; TBPp, TATA box binding-protein promoter; Neo, Neomycin resistance gene; poly A, poly A tail addition site. The plasmid map was generated in Clone Manager 9.

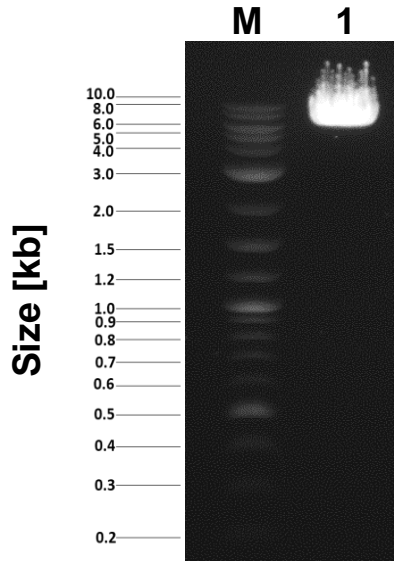


Figure 34. Restriction cleavage of pBASV40GFP with NotI.

M, 1 kb Plus DNA ladder; lane 1, linearised plasmid after cleavage with NotI. 0.8% agarose gel prepared with 0.5x TBE after electrophoresis stained with ethidium bromide.

DNA of one of the positive colonies containing pBBXSV40RFP was isolated and analysed by restriction cleavage as follows: PmeI + HindIII resulting in DNA fragments 2930 bp and 1121 bp; XbaI resulting in DNA fragments 3349 bp and 702 bp and HindIII resulting in a linear fragment of 4051 bp (Figure 35).

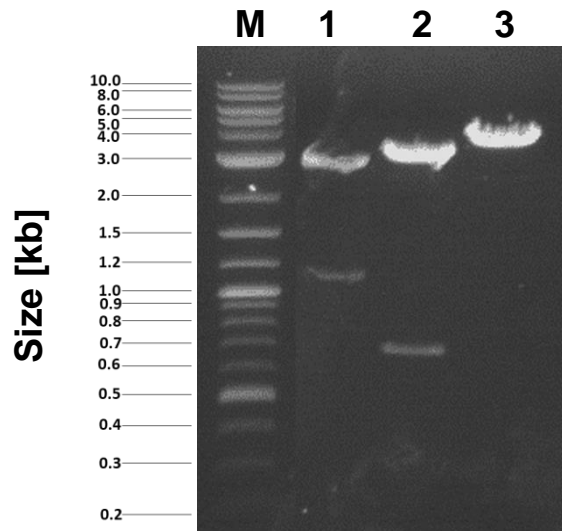


Figure 35. Restriction analysis of pBBXSV40RFP with Pme, HindIII and Xba I.

M, 1 kb Plus DNA ladder; lane 1, cleavage of pBBXSV40RFP with PmeI+HindIII resulting in 2930 bp and 1121 bp; lane 2, XbaI resulting in resulting in DNA fragments 3349 bp and 702 and lane 3, HindIII linearised plasmid. 0.8% agarose gel prepared with 0.5x TBE after electrophoresis stained with ethidium bromide.

pBBXSV40RFP and linearised pBASV40GFP were cleaved with BglIII in a preparative assay (Figure 36).

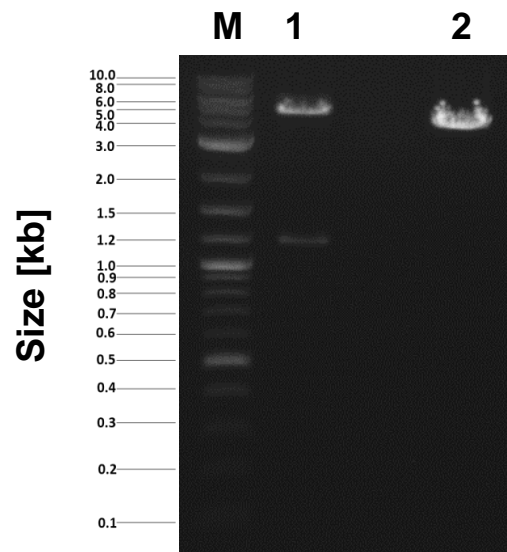


Figure 36. Preparative restriction cleavage of linear pBASV40GFP and linearisation of pBBXSV40RFP with BglIII.

M, 1 kb Plus DNA ladder; lane 1, pBASV40GFP cleaved with NotI + BglIII resulting in 4833 bp and 1169 bp DNA fragments; lane 2, pBBXSV40RFP cleaved with BglIII resulting in a 4051 bp DNA fragment. 0.8% agarose gel prepared with 0.5x TBE after electrophoresis stained with ethidium bromide.

Following the linearisation of pBBXSV40RFP with BglIII, the open plasmid was further cleaved with PmeI. The resulting bands were 2936 bp and 1115 bp (Figure 37).

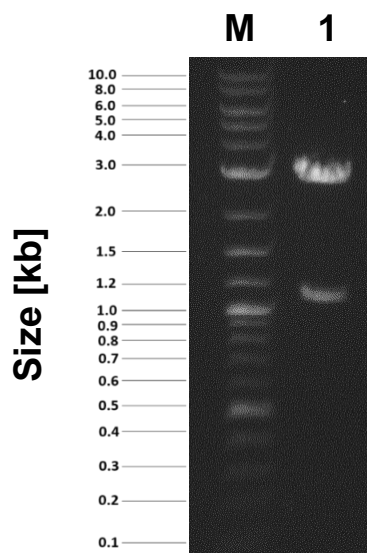


Figure 37. Preparative restriction cleavage of linearised pBBXSV40RFP with PmeI.

M, 1 kb Plus DNA ladder; lane 1, linear pBBXSV40RFP was cleaved with PmeI resulting in 2936 and 1115 bp DNA fragments. 0.8% agarose gel prepared with 0.5x TBE after electrophoresis stained with ethidium bromide.

The pBASV40GFP 4833 bp fragment contains the antibiotic resistance gene Neo that will be used as drug selection marker and the pBBXSV40RFP 1115 bp fragment contains the SV40 promoter + RFP gene (Figure 38).

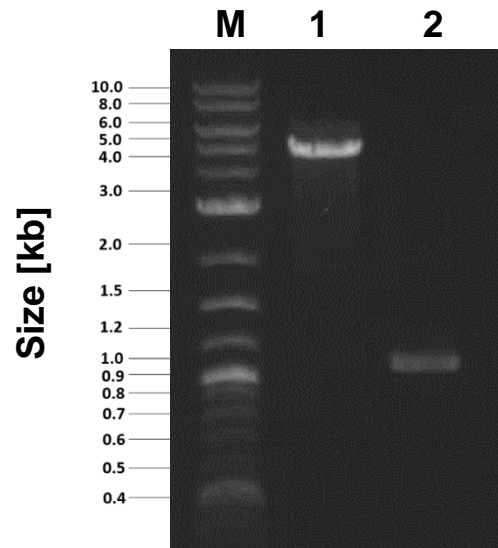


Figure 38. Gel purification of fragments derived from pBASV40GFP and pBBXSV40RFP.

M, 1 kb Plus DNA ladder; lane1, 4833 bp DNA fragment from pBASV40GFP; lane 2, 1115 bp DNA fragment from pBBXSV40RFP. 0.8% agarose gel prepared with 0.5x TBE after electrophoresis stained with ethidium bromide.

The isolated fragments were ligated, transformed into *E. coli* DH5 α to generate pRFPSV40 (5948 bp) (Figure 38). Following on from analysing plasmid DNA from 7 individual colonies more DNA was isolated in a "MIDIPREP" and the identity of the plasmid was confirmed by restriction cleavage with XbaI+EcoRI which generated the expected fragments of 4197 bp, 1731 bp and 20 bp (Figure 40) followed by DNA sequencing of the region containing the SV40 promoter followed by the RFP open reading frame (sequence determined from position 5510 bp to 1067 bp on the plasmid map shown in figure 40). All the restriction cleavage process to generate pRFPSV40 is summarised in table 22.

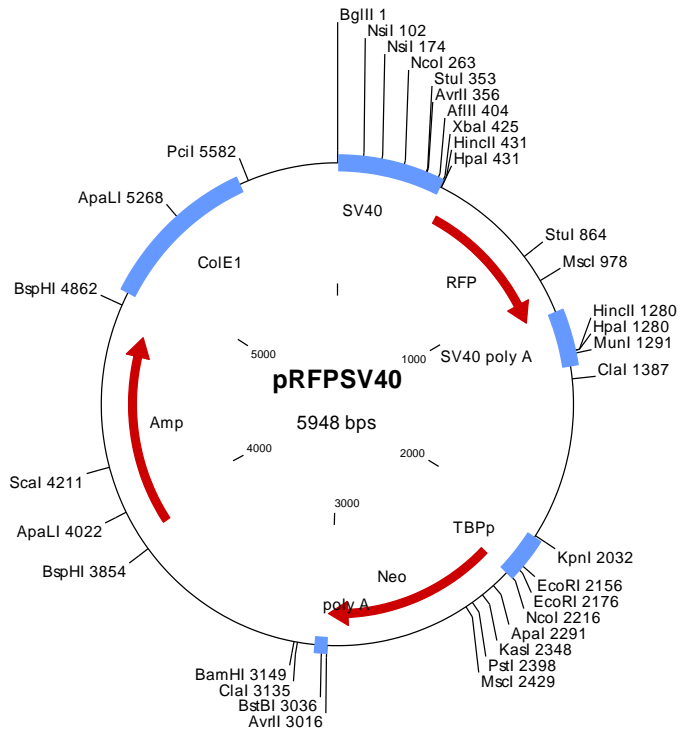


Figure 39. Plasmid map of pRFPSV40 (5948 bp).

Amp, ampicillin resistance gene; ColE1, origin of replication; SV40, simian virus 40 promoter; RFP, Red Fluorescent Protein gene; SV40 poly A, poly A tail addition site; TBPp, TATA box binding-protein promoter; Neo, Neomycin resistance gene; poly A, poly addition site. The plasmid map was generated in Clone Manager 9.

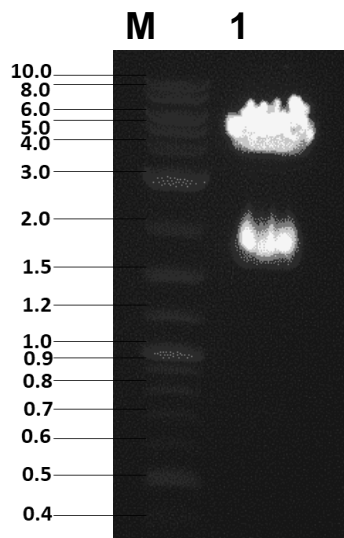


Figure 40. Restriction analysis of pRFPSV40 with XbaI and EcoRI.

M, 1 kb Plus DNA ladder; lane 1, pRFPSV40 cleaved with XbaI+EcoRI generating 4197 bp and 1731 bp DNA fragments. 0.8% agarose gel prepared with 0.5x TBE after electrophoresis stained with ethidium bromide.

Table 22. Restriction cleavage of pBASV40GFP, pBBXSV40RFP and pRFPSV40

A table to illustrate the expected fragment sizes, in base pairs, after pBASV40GFP, pBBXSV40RFP, and pRFPSV40 cleavage utilising various restriction enzymes.

Plasmid	Restriction enzymes	Fragment sizes [bp]
pBASV40GFP	NotI	6002
	BglII	4833 and 1169
pBBXSV40RFP	PmeI+HindIII	2930 and 1121
	XbaI	3349 and 702
	HindIII	4051
	BglII	4051
	PmeI	2936 and 1115
pRFPSV40	XbaI+EcoRI	4197, 1731 and 20

5.4.6 *Acanthamoeba castellanii* Neff strain trophozoites expressed the Red Fluorescent Protein when transfected with pRFPSV40.

A. castellanii Neff trophozoites were transfected with pRFPSV40 and grown in medium with 6.25 μ M G418. Immediately after adding the drug the cells became rounded due to the drug pressure compared with the pleomorphic and translucent cells observed in the control. Additionally, slow growth in the transfected cells was observed spanning two to three weeks until reaching a confluence of 90%. This was a first clue suggesting a stable transfection indicating expression of the neomycin resistance gene. Expression of the second reporter gene was determined by confocal fluorescence microscopy analysis (Figure 41).

Confocal microscopy observations showed potent and bright red fluorescence in the trophozoite population transfected with the highest concentration of Xfect polymer compared with the lower concentrations (1 μ l and 0.5 μ l). The control group, WT cells treated with Xfect did not show any trophozoite fluorescence. These results also determine the efficacy of two different promoters (SV40 and TBP) to be able to express two different proteins (Neo and RFP) from the same plasmid.

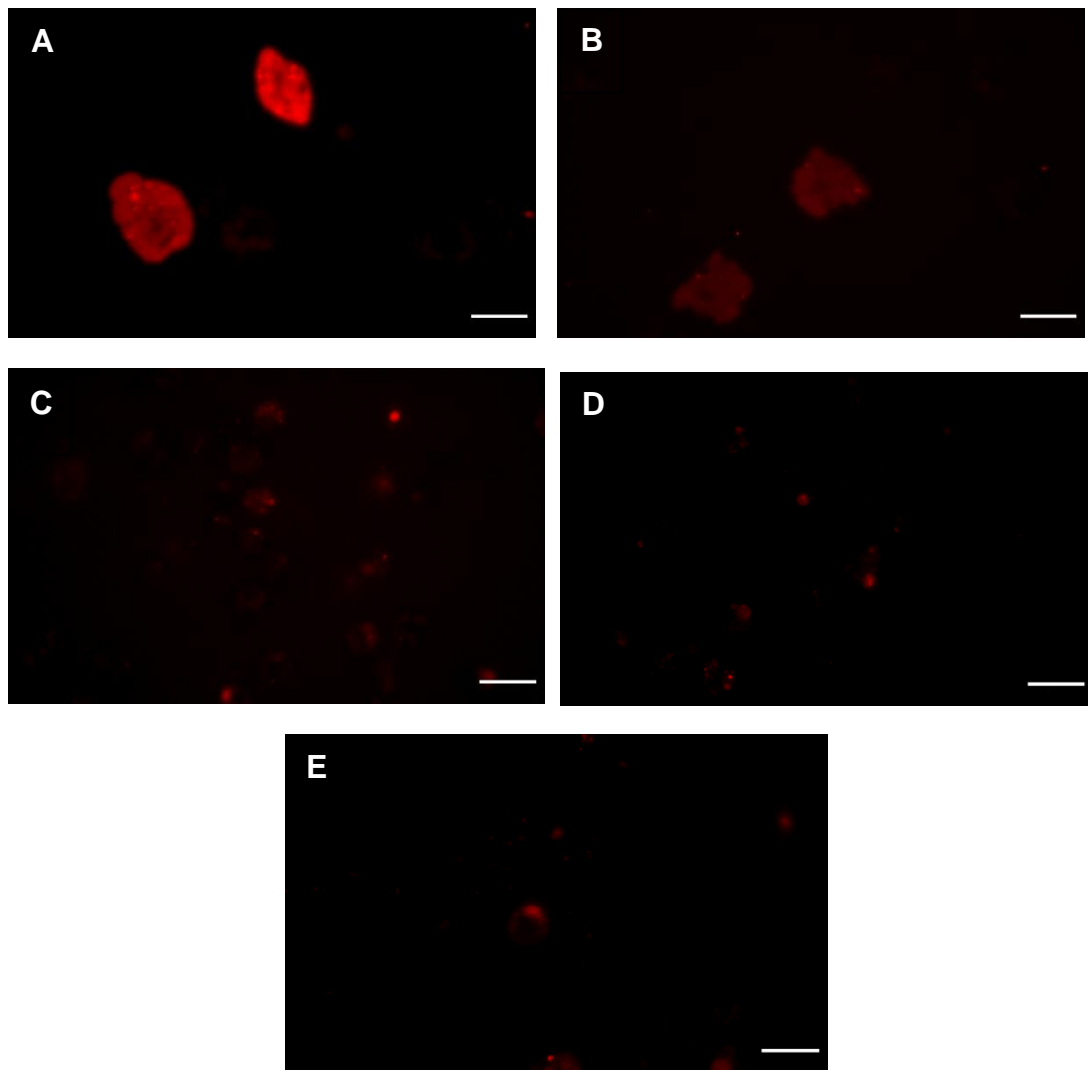


Figure 41. Confocal microscopy analysis of the expression of the red fluorescent protein (RFP) in *A. castellanii* Neff strain trophozoites transfected with pRFPSV40.

Photomicrographs of trophozoites transfected with pRFPSV40 using different volumes of Xfect polymer (Takara Bio): **A.** 1.5 μ l, **B.** 1 μ l and **C.** 0.5 μ l. **D.** Positive control: Wild type trophozoites non-transfected and **E.** Negative control: Trophozoites mixed with pRFPSV40 without Xfect polymer. Fluorescent images were obtained using a Nikon Eclipse 600 Epifluorescent Upright Microscope (Nikon, USA) under TRITC filter with Ex_{max} . 540 nm/DM 565 and Em_{max} . 605/55 nm. using 300 ms exposure with 100 \times objective. Scale bar: 20 μ M. No brightfield images were taken for this group of images.

5.4.7 Generation of pBRFPNeoCas9 and pBRFPPhleoCas9

To generate pBRFPT7NeoCas9 and pBRFPT7PhleoCas9 as part of the CRISPR-Cas9 system, the formation of pBRFPNeoCas9 was required. The parent plasmid pBSKII(+) (2961 bp)(Figure 42) was cleaved with KpnI+Clal to generate two DNA fragments of 27 bp and 2934 bp. Then, the 2934 bp DNA fragment was isolated using an agarose gel, purified and SAP-treated (Figure 43).

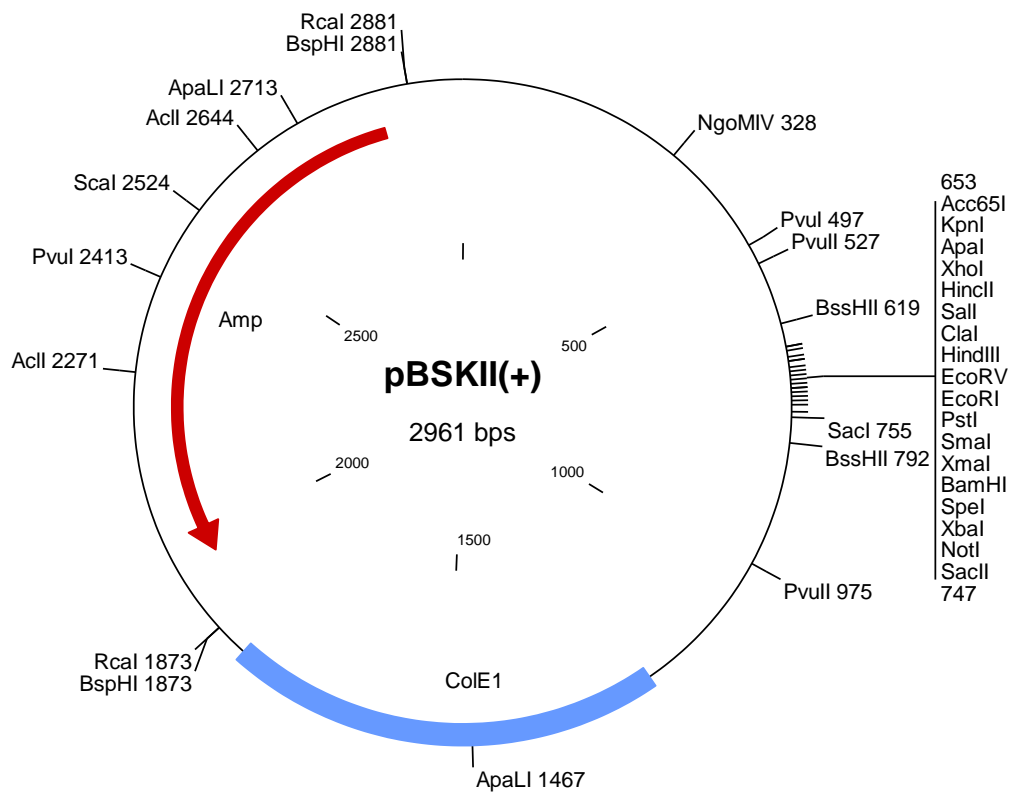


Figure 42. Plasmid map of pBSKII(+) (2961 bp).

AMP, ampicillin resistance gene, ColE1, origin of replication. The plasmid map was generated in Clone Manager 9.

pRFPSV40 (5948 bp) was also cleaved with Kpn+Clal to generate DNA fragments of 1100 bp and 4848 bp (Figure 43), the 1100 bp DNA fragment was isolated and the isolated DNA fragments were ligated (2934 bp and 1100 bp) to generate the new construct pBKCTBpNeo (4034 bp) (Figure 44). The ligation was transformed in *E. coli* DH5 α and plated on LB agar plates with Carbenicillin according to Chapter 2, section 2.2.5.9.

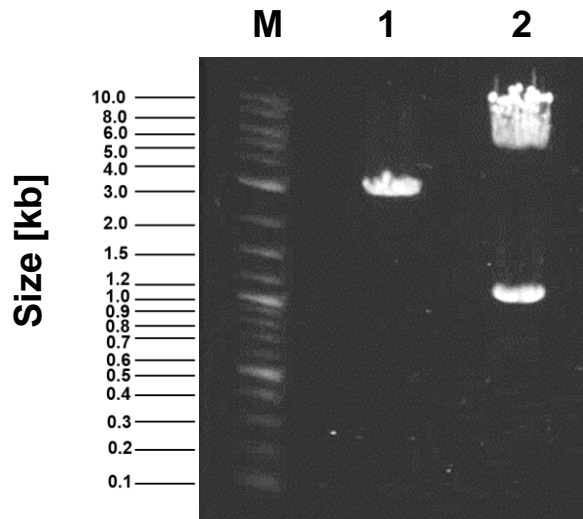


Figure 43. Agarose gel showing linearised pBSKII(+) and pRFPSV40 cleaved with Kpn+Clal.

M, 1 kb Plus DNA ladder; lane 1, pBSKII(+) 2934 bp DNA fragment; lane 2, pRFPSV40 4848 bp and 1100 DNA fragments, both plasmids were cleaved with KpnI+Clal. 0.8% agarose gel prepared with 0.5x TBE after electrophoresis stained with ethidium bromide.

DNA of one of the positive colonies containing pBKCTBPpNeo was isolated and analysed by restriction cleavage as follows: EcoRI, 3037 bp, 977 bp and 20 bp; KpnI, 4034 (plasmid linearisation); NcoI+HindIII, 3109 bp and 925 bp (Figure 45 and Table 23).

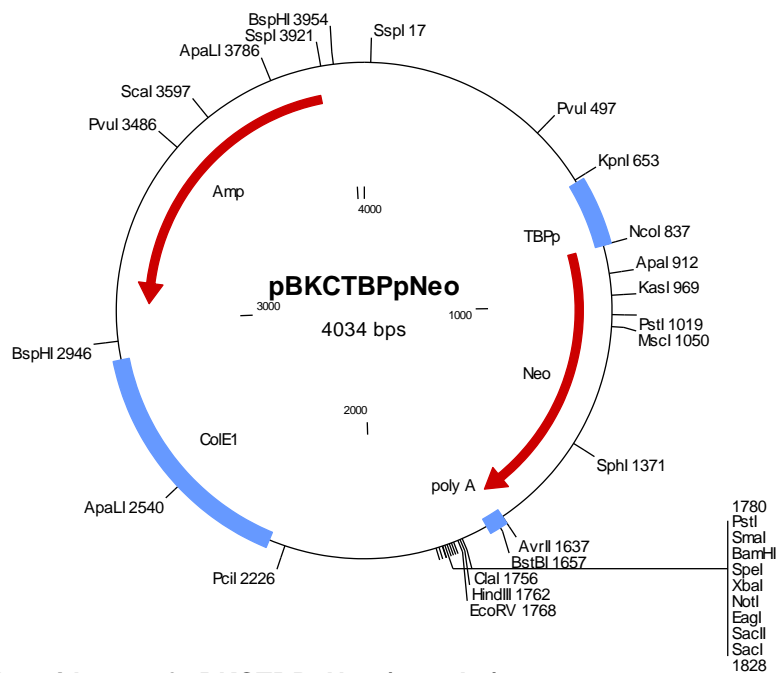


Figure 44. Plasmid map of pBKCTBPpNeo (4034 bp)

AMP, ampicillin resistance gene; TBPp, TATA box binding-protein promoter; Neo, Neomycin resistance gene; poly A, poly A tail addition site; ColE1, origin of replication. The plasmid map was generated in Clone Manager 9.

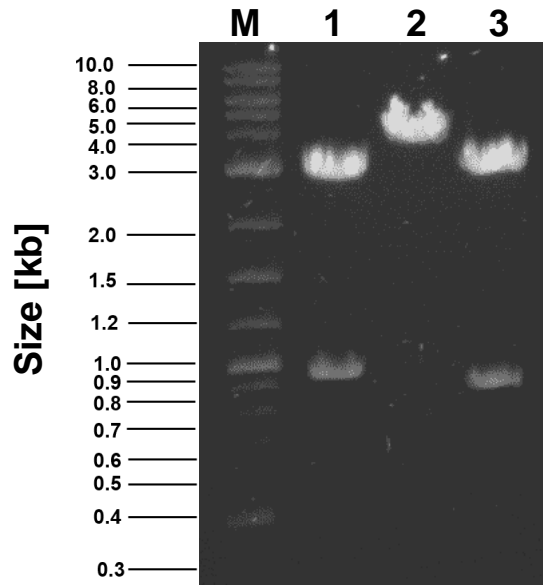


Figure 45. Restriction analysis of pBKCTBPpNeo with EcoRI, KpnI, NcoI and HindIII.

M, 1 kb Plus DNA ladder; lane 1, EcoRI, 3037 bp, 977 bp and 20 bp (not visible as too small); lane 2, KpnI, 4034; lane 3, NcoI and HindIII, 3109 bp and 925 bp. 0.8% agarose gel prepared with 0.5x TBE after electrophoresis stained with ethidium bromide.

Table 23. Restriction analysis of pBSKII(+), pRFPSV40, and pBKCTBPpNeo.

A table to illustrate the expected fragment sizes, in base pairs, after pBSKII(+), pRFPSV40, and pBKCTBPpNeo cleavage utilising various restriction enzymes.

Plasmid	Restriction enzymes	Fragment sizes [bp]
pBSKII(+)	KpnI+Clal	2934 and 27
pRFPSV40	Kpn+Clal	4848 and 1100
pBKCTBPpNeo	EcoRI	3037, 977 and 20
	KpnI	4034
	NcoI+HindIII	3109 and 925

pBKCTBPpNeo was cleaved with AvrII to be linearised (Figure 46) and purified the via PCR-clean up method, Klenow polymerase fill-in, and a last purification were performed. The linearised construct was cleaved with NcoI to generate 800 bp and 3234 bp fragments (Figure 47).

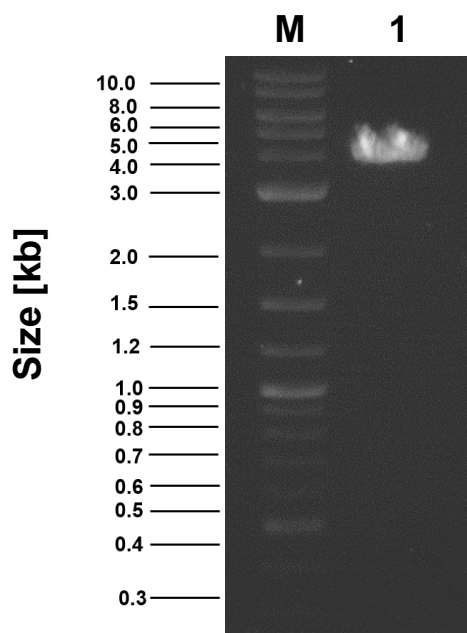


Figure 46. Restriction cleavage of pBKCTBpNeo with AvrII.

M, 1 kb Plus DNA ladder; lane 1, pBKCTBpNeo cleaved with AvrII resulting in DNA fragment 4032 bp to linearise the construct. 0.8% agarose gel prepared with 0.5x TBE after electrophoresis stained with ethidium bromide.

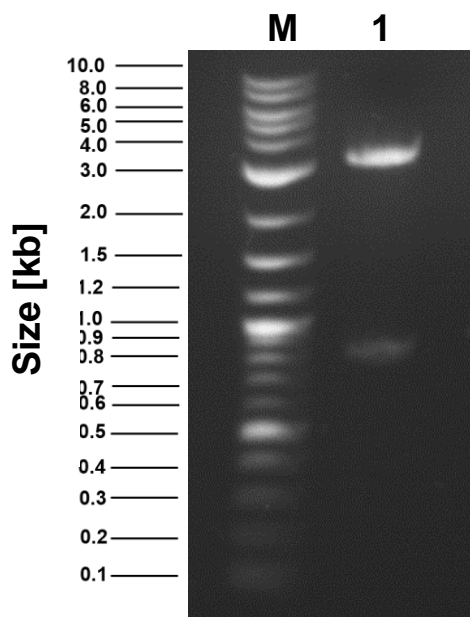


Figure 47. Restriction cleavage of pBKCTBpNeo with AvrII and NcoI.

M, 1 kb Plus DNA ladder, lane 1, pBKCTBpNeo linearised with AvrII was cleaved with NcoI resulting in 3234 bp and 800 bp DNA fragments. 0.8% agarose gel prepared with 0.5x TBE after electrophoresis stained with ethidium bromide.

The 3234 bp fragment was gel isolated and SAP-treated (Figure 48).



Figure 48. Purified and SAP-treated pBKCTBpNeo AvrII/NcoI-fragment.

M, 1 kb Plus DNA ladder; lane 1, 3234 bp DNA fragment containing Neo gene was isolated using an agarose gel and SAP-treated. 0.8% agarose gel prepared with 0.5x TBE after electrophoresis stained with ethidium bromide.

The parent plasmid pT007_Cas9_T7_Tub (15446 bp) (Figure 49) was cleaved with EcoRI, purified, filled-in, purified again and cleaved with NcoI (10184 bp, 4274 bp, 890 bp, 36 bp, 33 bp and 29 bp) (Figure 50).

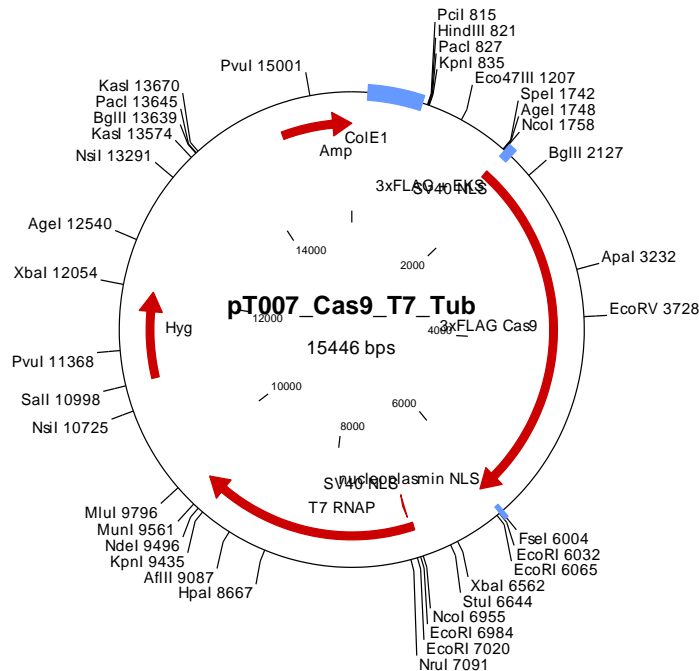


Figure 49. Plasmid map of pT007_Cas9_T7_Tub (15446 bp)

AMP, ampicillin resistance gene; ColE1, origin of replication; SV40, simian virus 40 promoter; poly A, poly A tail addition site; 3xFLAG Cas9, three FLAG tandem peptides (DYKDHD-G-DYKDHD-I-DYKDDDDKRFP) fused to Cas9; NLS, nuclear localisation signal/sequence; T7

RNA polymerase sequence, Hyg, Hygromycin B resistance gene. The plasmid map was generated in Clone Manager 9.

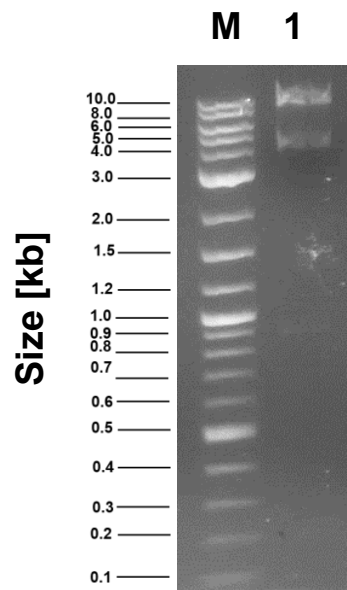


Figure 50. Restriction cleavage of pT007_Cas9_T7_Tub with EcoRI+NcoI.

M, 1 kb Plus DNA ladder; lane 1, pT007_Cas9_T7_Tub was cleaved with EcoRI+NcoI generating 10184 bp, 4274 bp, 890 bp, 36 bp, 33 bp and 29 bp DNA fragments. 0.8% agarose gel prepared with 0.5x TBE after electrophoresis stained with ethidium bromide.

The 4274 bp fragment was gel isolated (Figure 51).

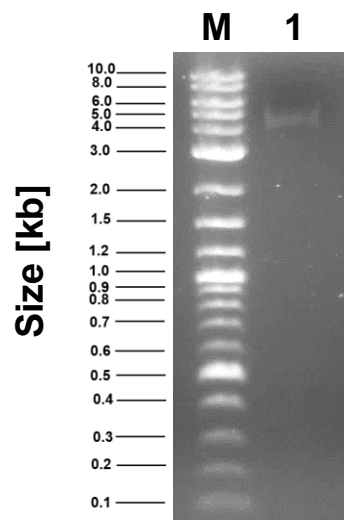


Figure 51. Isolated EcoRI/NcoI fragment of pT007_Cas9_T7_Tub fragment.

M, 1 kb Plus DNA ladder; lane 1, pT007_Cas9_T7_Tub 4274 bp DNA fragment was gel isolated. 0.8% agarose gel prepared with 0.5x TBE after electrophoresis stained with ethidium bromide.

The isolated 3234 bp (pBKCTBPpNeo) and 4274 bp (pT007_Cas9_T7_Tub) DNA fragments were ligated, transformed into *E. coli* DH5 α to generate pBTBPpCas9 (7512 bp) (Figure 52). Following on from analysing plasmid DNA from 6 individual colonies more DNA was isolated in a “MIDIPREP” and the identity of the plasmid was confirmed by restriction cleavage with i) EcoRI: 4314 bp, 3037 bp, 141 bp and 20 bp, ii) EcoRV: 5073 bp and 2439 bp, and HindIII 7512 bp (Figure 53 and Table 24).

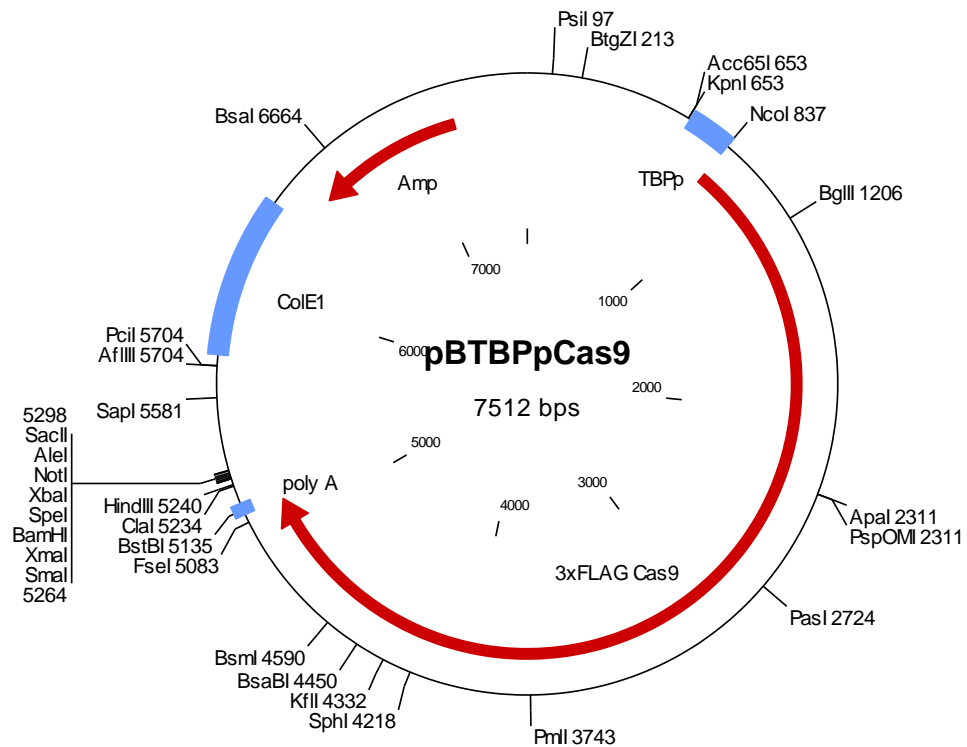


Figure 52. Plasmid map of pBTBPpCas9 (7512 bp).

AMP, ampicillin resistance gene; TBPp, TATA box binding-protein promoter; 3xFLAG Cas9, three FLAG tandem peptides (DYKDHD-G-DYKDHD-I-DYKDDDDKRFP) fused to Cas9; poly A, poly A tail addition site. The plasmid map was generated in Clone Manager 9.

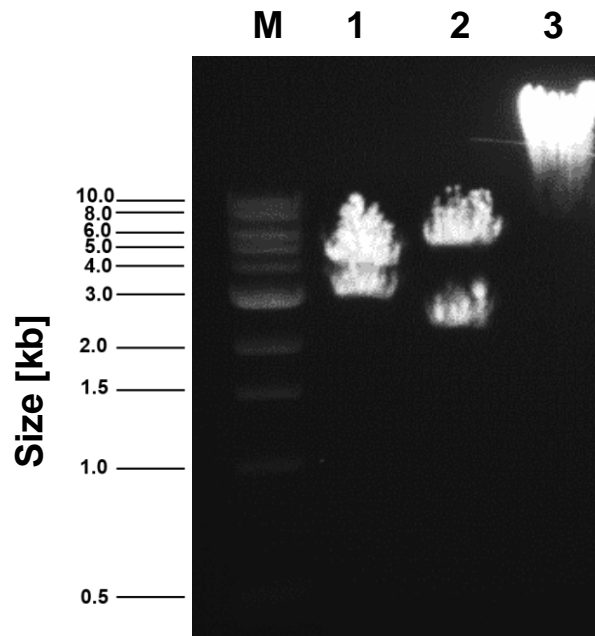


Figure 53. Restriction cleavage of pBTBPPCas9 with EcoRI, EcoRV and HindIII.

Restriction cleavage to confirm the generation of pBTBPPCas9. M, 1 kb DNA ladder; lane 1, EcoRI: 4314 bp and 3031 bp; lane 2, EcoRV: 5073 bp and 2439 bp, lane 3, HindIII: 7512 bp. 0.8% agarose gel prepared with 0.5x TBE after electrophoresis stained with ethidium bromide.

Table 24. Restriction cleavage of pT007_Cas9_T7_Tub, pBKCTBpNeo and pBTBPPCas9

A table to illustrate the expected fragment sizes, in base pairs, after pT007_Cas9_T7_Tub, pBKCTBpNeo and pBTBPPCas9 cleavage utilising various restriction enzymes.

Plasmid	Restriction enzymes	Fragment sizes [bp]
pT007_Cas9_T7_Tub	EcoRI + NcoI	10184, 4274, 890, 36, 33 and 29
pBKCTBpNeo	AvrII	4032
	NcoI	3234 and 800
pBTBPPCas9	NcoI	7512
	EcoRV	5073 and 2439
	SacI	5397 and 2115

pBTBPPCas9 (7512 bp) was linearised using the restriction enzyme Acc65I (Figure 54) and followed by cleavage with ClaI to generate 4582 bp + 2930 bp fragments (Figure 55).

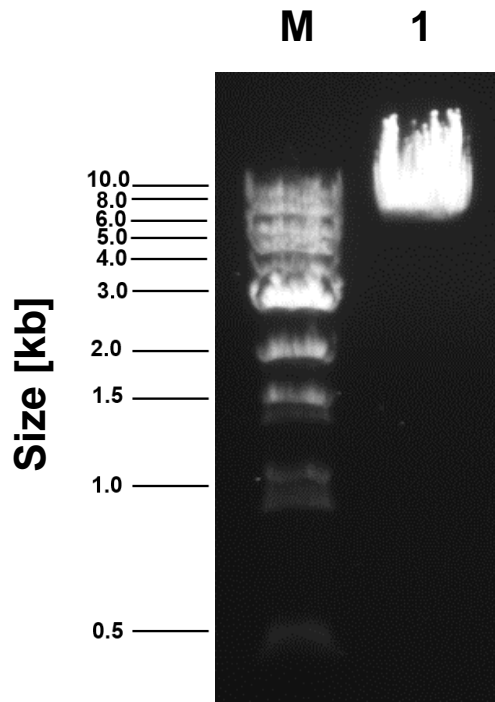


Figure 54. Restriction cleavage of pBTBPPcas9 with Acc65I.

M, 1 kb DNA ladder; lane 1, pBTBPPcas9 was cleaved with Acc65I (7512 bp) to be linearised. 0.8% agarose gel prepared with 0.5x TBE after electrophoresis stained with ethidium bromide.

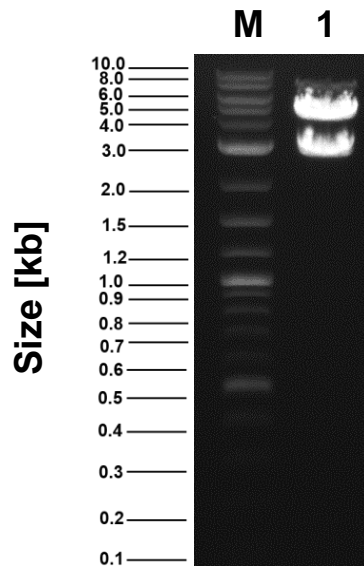


Figure 55. Restriction cleavage of pBTBPPcas9 with Acc65I and ClaI.

M, 1 kb Plus DNA ladder; lane 1, pBTBPPcas9 previously digested with Acc65I was further digested with ClaI generating the 4582 bp and 2930 bp DNA fragments. 0.8% agarose gel prepared with 0.5x TBE after electrophoresis stained with ethidium bromide.

The 4582 bp fragment containing the TBP promoter, 3xFLAG Cas9 and PolyA was gel isolated, filled-in using Klenow polymerase and purified. The plasmid pRFPSV40 was linearised with BamHI expecting a band of 5948 bp. This band was purified, filled-in, purified again and SAP-treated (Figure 56).

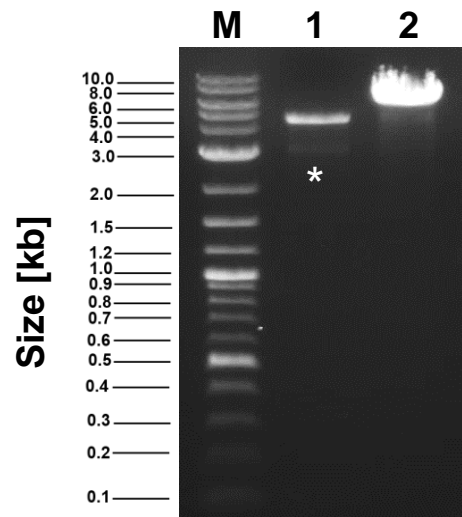


Figure 56. Agarose gel showing purified pBTBPPCas9 fragment and linearised pRFPSV40

M, 1 kb Plus DNA ladder; lane 1, Gel isolation of pBTBPPCas9 fragment (4582 bp) after Klenow polymerase and PCR-clean up, however, the presence of the smallest DNA fragment (2930 bp) was present (marked with *); lane 2, the pRFPSV40 5948 bp DNA fragment was linearised with BamHI and SAP-treated. 0.8% agarose gel prepared with 0.5x TBE after electrophoresis stained with ethidium bromide.

Isolation of pBTBPPCas9 DNA fragment (4582 bp) was achieved (Figure 57). The 4582 bp DNA fragment from pBTBPPCas9 and the 5948 bp DNA fragment from pRFPSV40 were ligated, transformed into *E. coli* DH5 α to generate pBRFPNeoCas9 (10536 bp) (Figure 58).

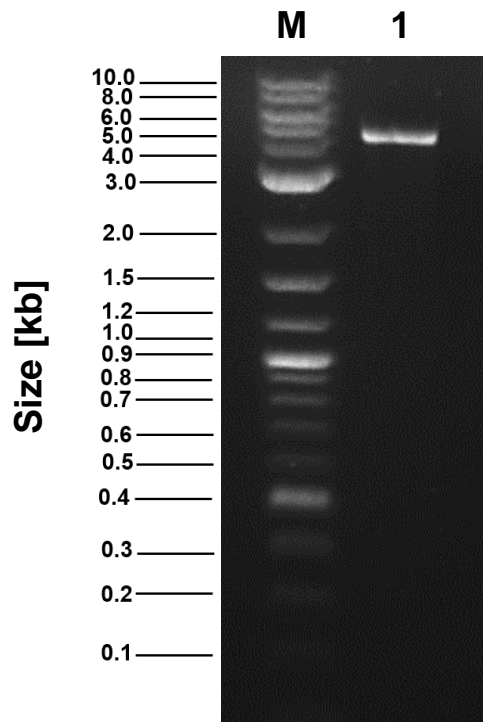


Figure 57. Agarose gel showing purified pBTBPPCas9 fragment (4582 bp).

M, 1 kb Plus DNA ladder; lane 1, region (4582 bp) containing the TBP promoter, 3xFLAG Cas9 and PolyA tail was isolated, filled-in using Klenow polymerase and purified. 0.8% agarose gel prepared with 0.5x TBE after electrophoresis stained with ethidium bromide.

Following on from analysing plasmid DNA from 17 individual colonies more DNA was isolated in a “MIDIPREP”, and the identity of the plasmid was confirmed by restriction cleavage with i) BamHI+KpnI: 5701 bp and 4835 bp; ii) EcoRI 5081: bp, 4314 bp, 1101 bp, 20 bp, 20 bp; iii) EcoRV: 10536 bp (pBRFPNeoCas9 linearised), iv) BglII: 6831 bp + 3706 bp (Figure 59 and Table 25).

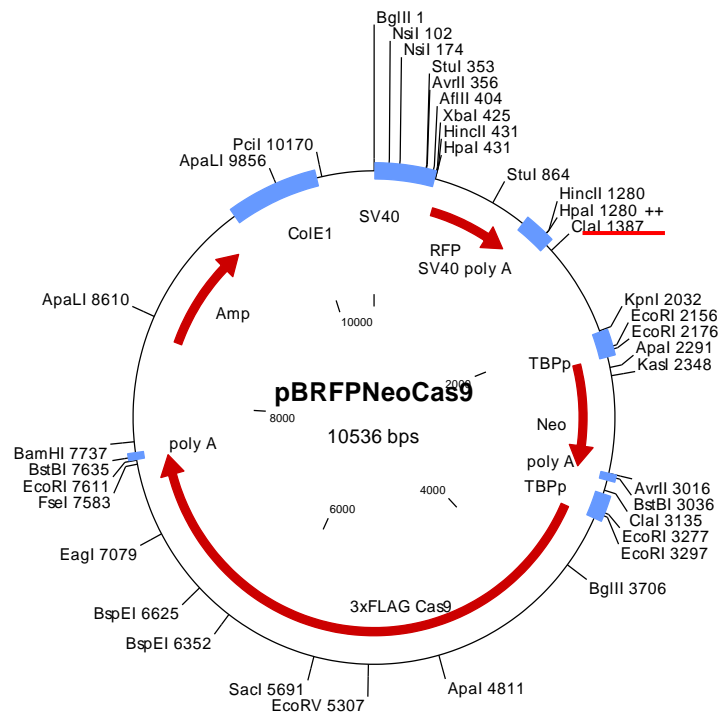


Figure 58. Plasmid map of pBRFPNeoCas9 (10536 bp).

AMP, ampicillin resistance gene; ColE1, origin of replication; SV40, simian virus 40 promoter; poly A, poly A tail addition site; RFP, Red Fluorescent Protein; SV40 poly A, poly A tail addition site; TBPP, TATA box binding-protein promoter; Neo, Neomycin resistance gene; poly A, poly A tail addition site; 3xFLAG Cas9, three FLAG tandem peptides (DYKDHD-G-DYKDHD-I-DYKDDDDKRFP) fused to Cas9; poly A, poly A tail addition site. The Cla site localised at 1387 bp is dam-methylase sensitive (underlined in red). The plasmid map was generated in Clone Manager 9.

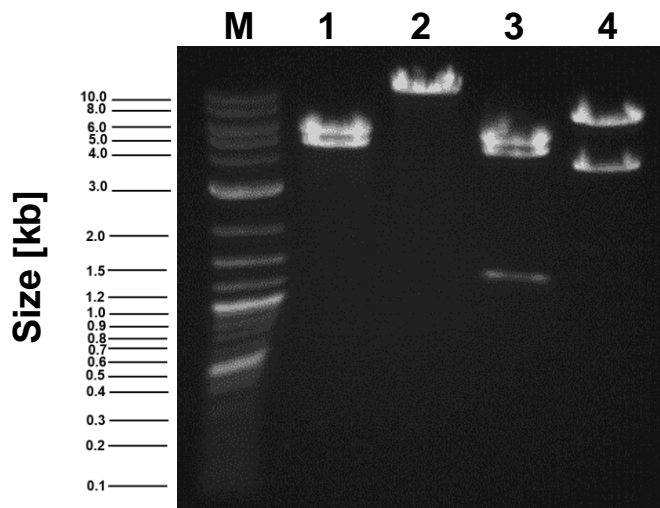


Figure 59. Restriction cleavage of pBRFPNeoCas9 with BamHI, EcoRV, EcoRI and BglII

M, 1 kb Plus DNA ladder; lane 1, BamHI and KpnI: 5701 bp and 4835 bp; lane 2, EcoRV: 10536 bp; lane 3, EcoRI: 5081 bp, 4314 bp and 1101 bp; lane 4, BglII: 6831 bp and 3706 bp. 0.6% agarose gel prepared with 0.5x TBE after electrophoresis stained with ethidium bromide.

Table 25. Restriction cleavage of pBTBPPCas9, pRFPSV40 and pBRFPNeoCas9

A table to illustrate the expected fragment sizes, in base pairs, after pBTBPPCas9, pRFPSV40 and pBRFPNeoCas9 cleavage utilising various restriction enzymes.

Plasmid	Restriction enzymes	Fragment sizes [bp]
pBTBPPCas9	ACC65I+Clal	4582 and 2930
pRFPSV40	BamHI	5948
pBRFPNeoCas9	BamHI+KpnI	5701 and 4835
	EcoRI	5081, 4314, 1101, 20 and 20
	EcoRV	10536
	BglII	6831 and 3706

5.4.8 Analysis of *Acanthamoeba castellanii* trophozoites transfected with pBRFPNeoCas9 using Xfect and Polyplus.

Transfection of pBRFPNeoCas9 was carried out as described in the Chapter 2 section 2.2.8.2 utilising two different reagents: Xfect and Polyplus. Polyplus was used because although Xfect displayed a successful expression with pRFPSV40, it showed slow growth of potential positive transfected cells (see section 5.4.6).

The transfection efficiency of pBRFPNeoCas9 using Xfect reagent was poor showing only a small number of transfected trophozoites when grown for six days (Figure 60).

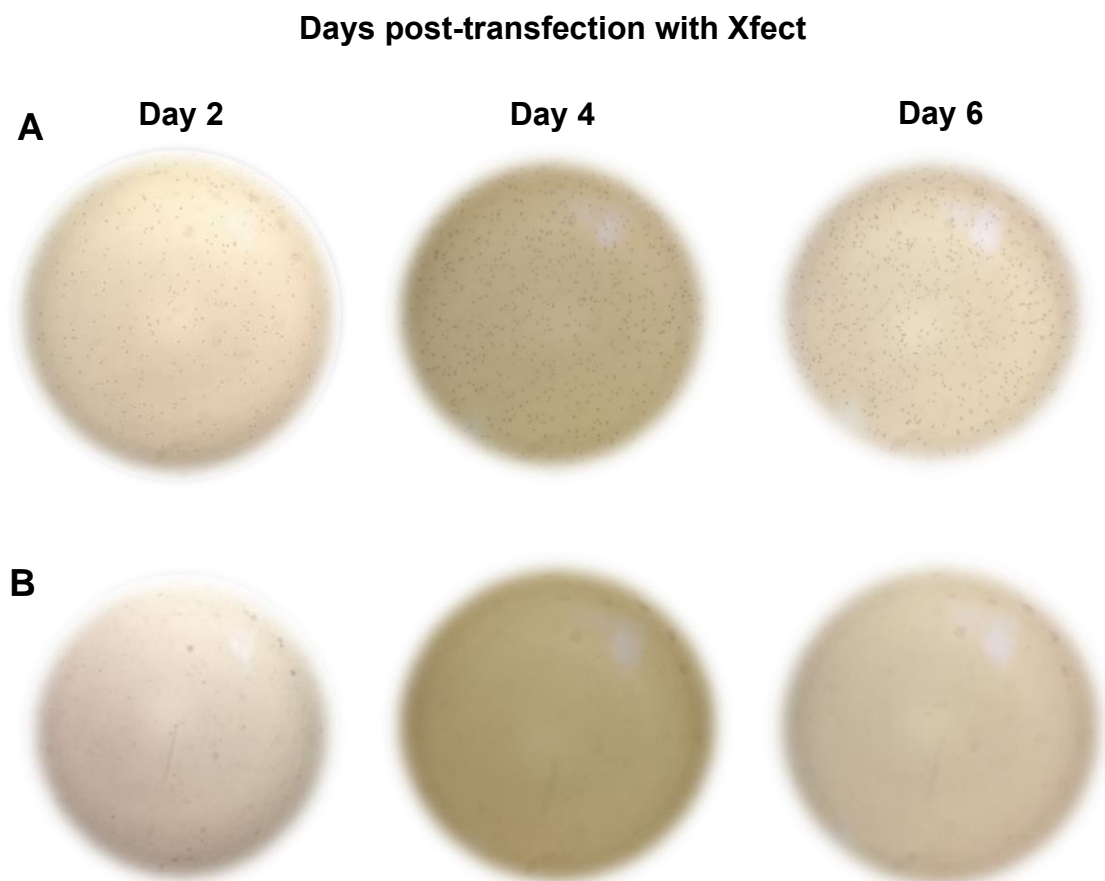
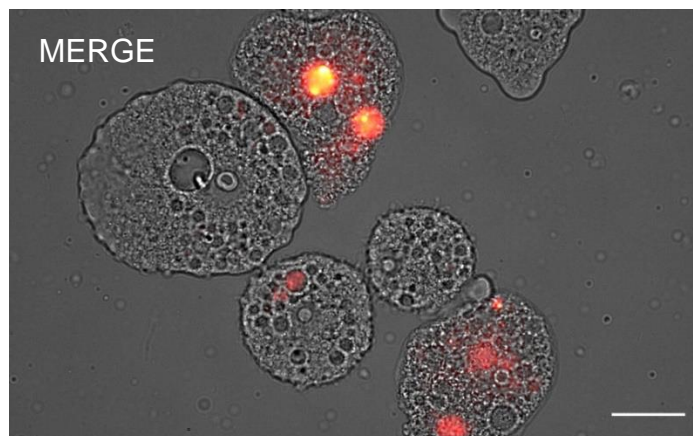
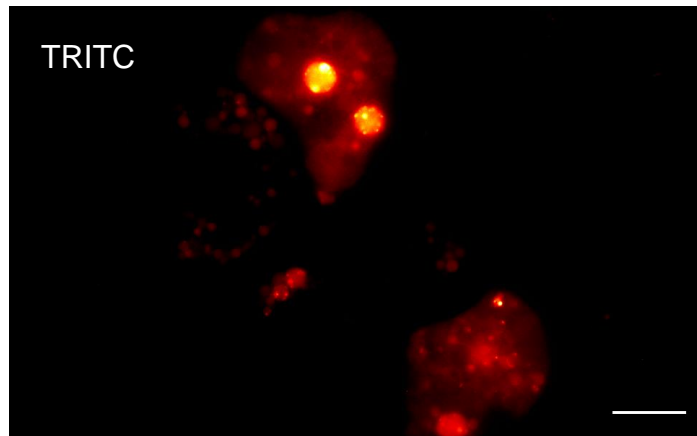
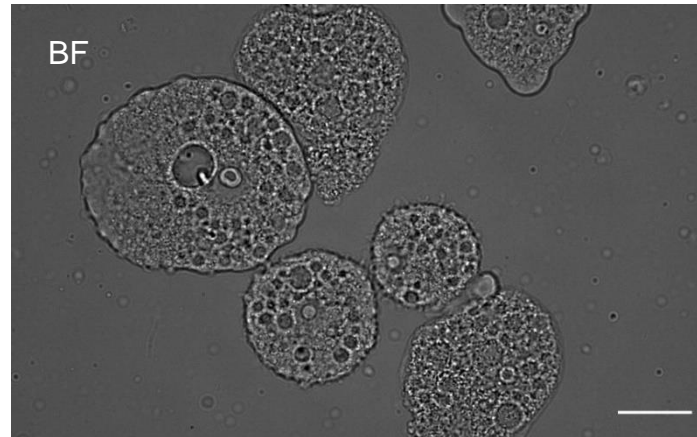


Figure 60. Transfection efficiency of pBRFPNeoCas9 using Xfect reagent.

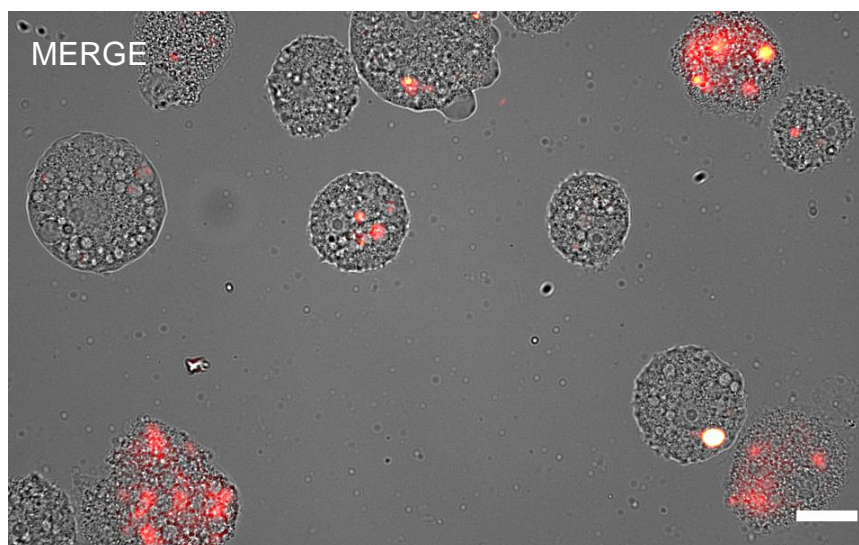
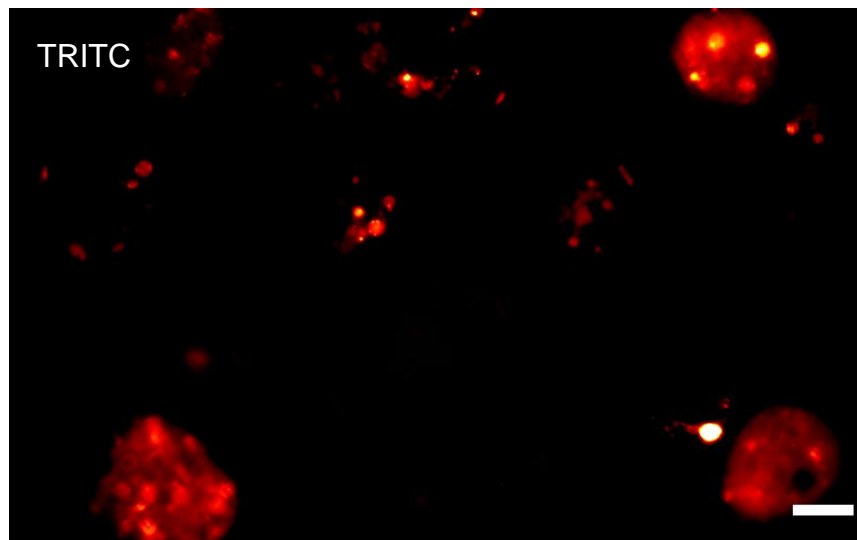
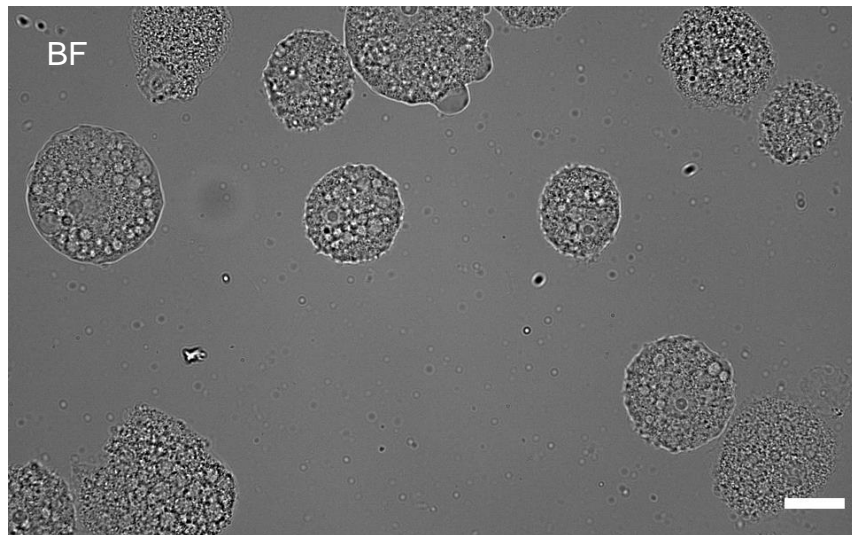
(A), Low number of potentially positive, transfected trophozoites. (B), Control group, trophozoites treated with Xfect polymer and buffer without pBRFPNeoCas9. The comparative study was carried out for 6 days and the drug selection marker G418 was added at day 1. The pictures were taken at 40x magnification using an Axiovert Zeiss 25 light microscope.

Only few trophozoites showed red fluorescence indicative for being positively transfected cells. The trophozoites display a clear rounded shape implying a stress condition due to the presence of a harsh environment caused by the reagent mix and foreign plasmid DNA (Figure 61).

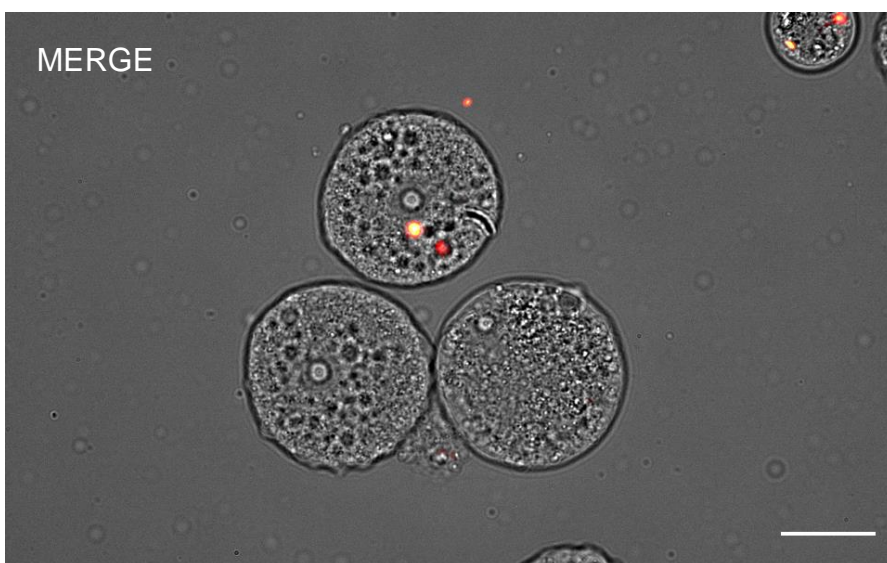
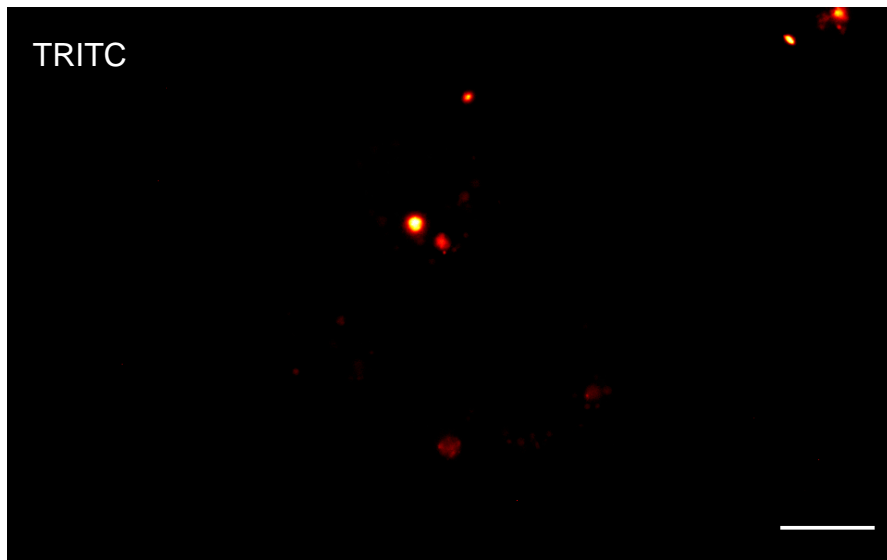
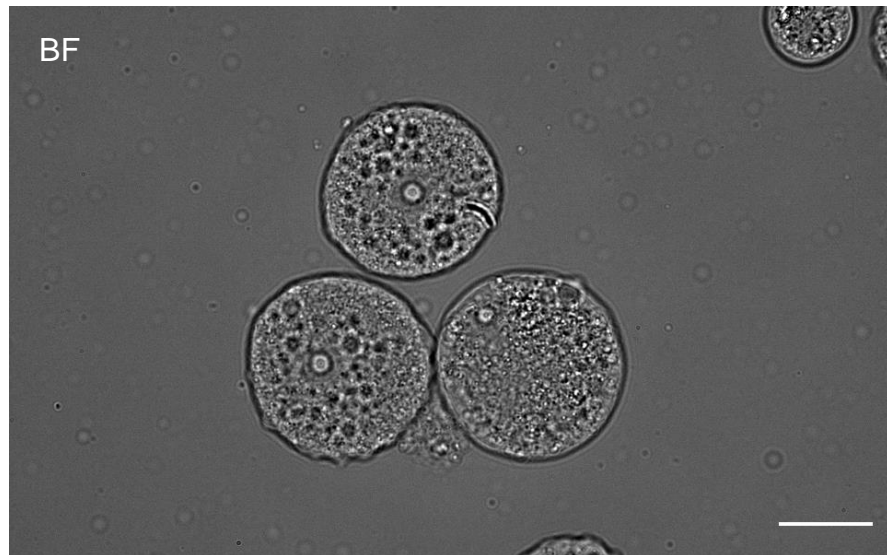
A.



B.



C.



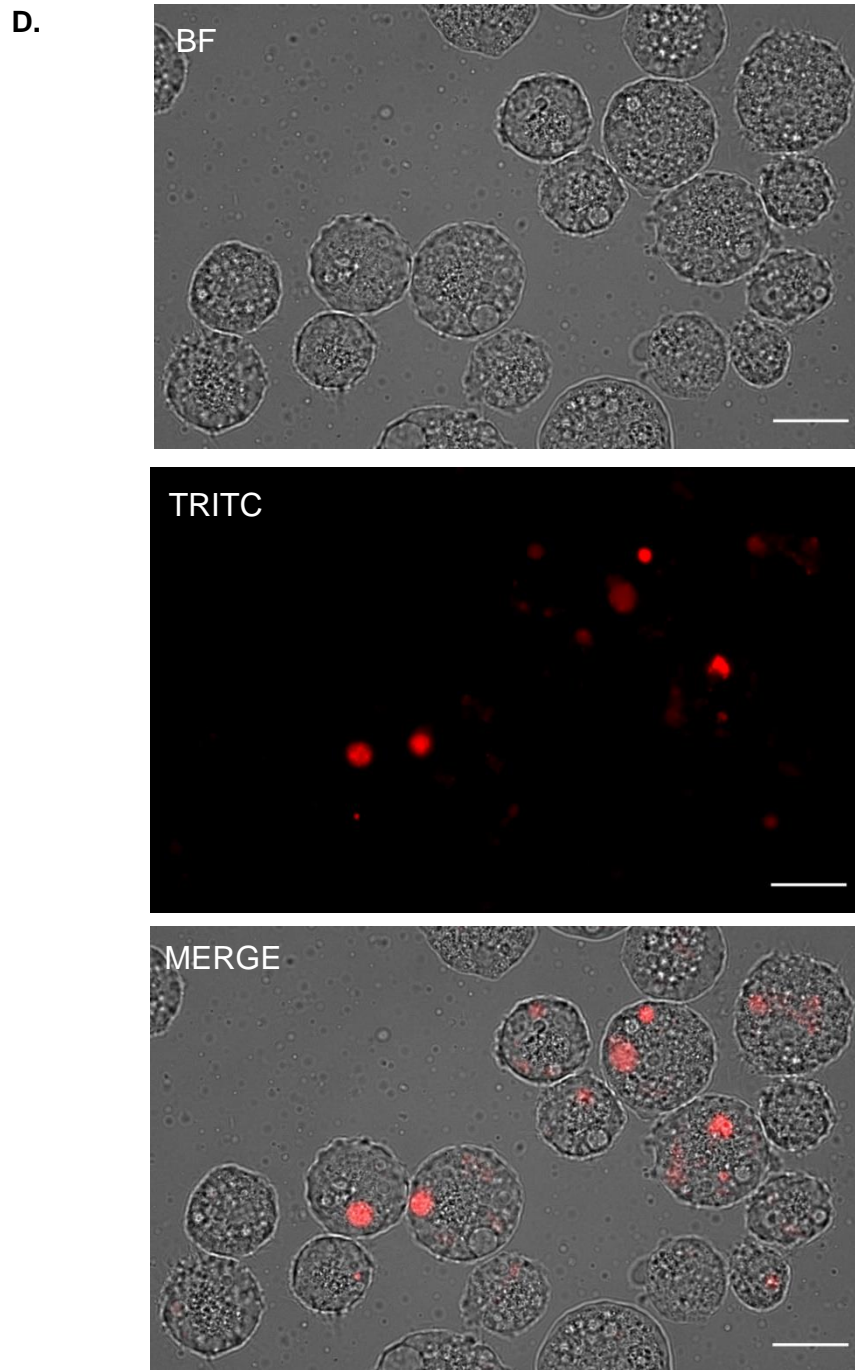


Figure 61. Efficiency of pBRFPNeoCas9 expression in *A. castellanii* trophozoites using Xfect reagent.

A. and **B.** Positive expression of RFP protein in pBRFPNeoCas9 is displayed by the bright red fluorescence observed in trophozoites at 60x and 40x, respectively. **C.** Negative control: Trophozoites treated with Xfect mix without pBRFPNeoCas9 observed at 60x; **D.** Positive control: *A. castellanii* wild trophozoites observed at 60x. The analysis was carried out utilising a Nikon Eclipse 600 Epifluorescent Upright Microscope (Nikon, USA) under TRITC filter with $E_{x_{max}}$. 540 nm/DM 565 and $E_{m_{max}}$. 605/55. Scale bar: 20 μ m.

5.4.9 *Acanthamoeba castellanii* trophozoites transfected with pBRFPNeoCas9 utilising Polyplus.

Polyplus was considered as an alternative transfection reagent to improve efficiency and expression of RFP from pBRFPNeoCas9. Interestingly, the number of potentials positively transfected trophozoites was significantly increased as observed in figure 62 (also compare with Figure 60).

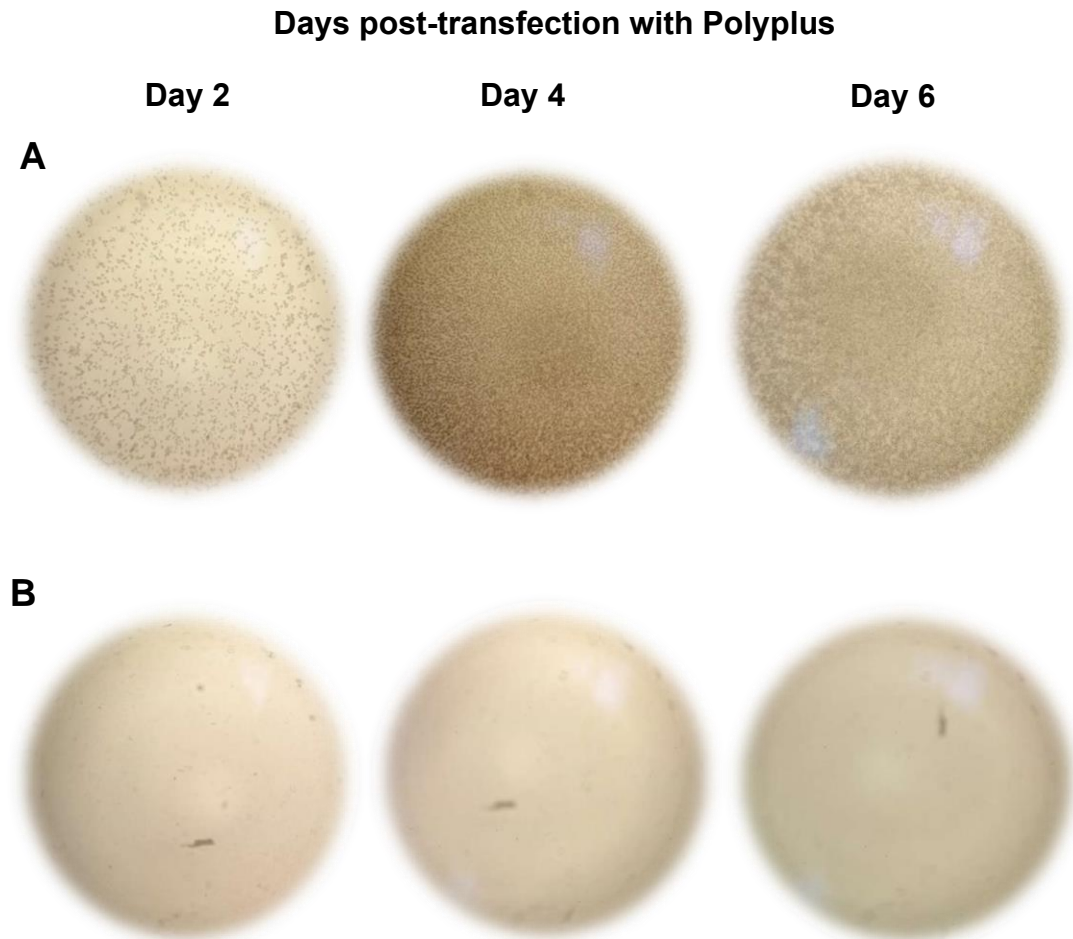
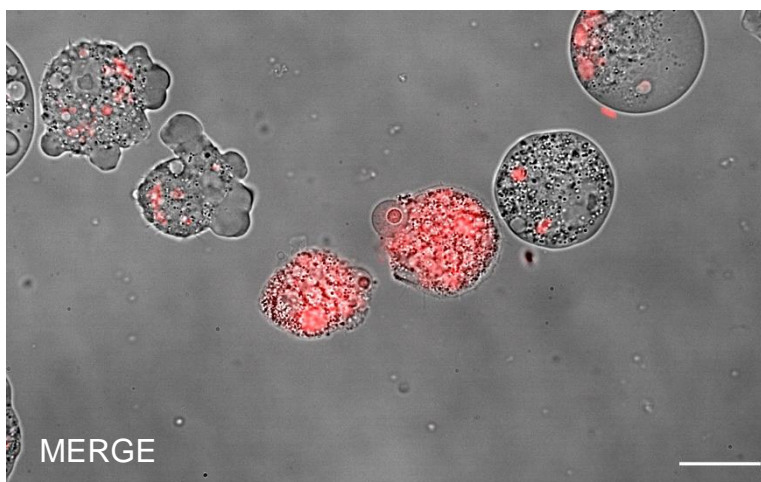
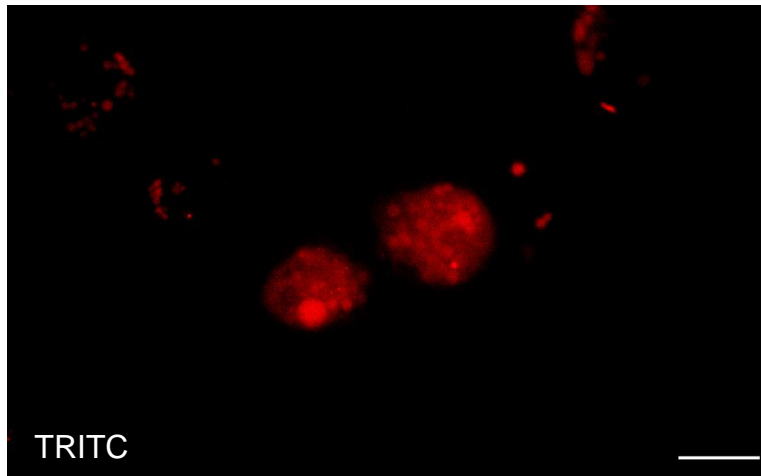
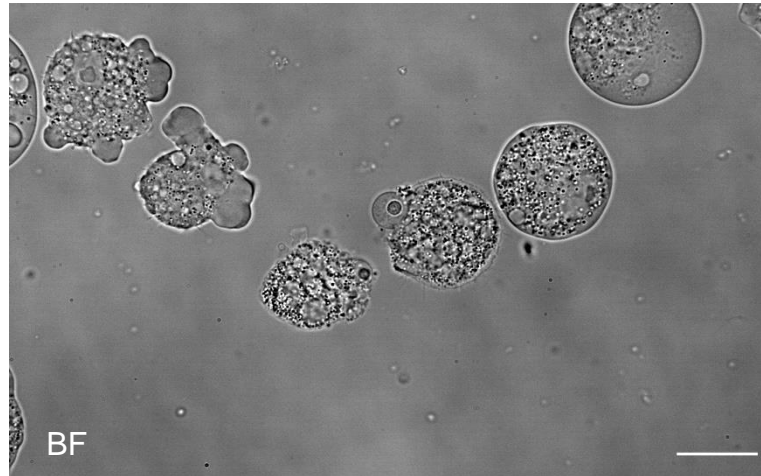


Figure 62. Transfection efficacy of pBRFPNeoCas9 using Polyplus reagent.

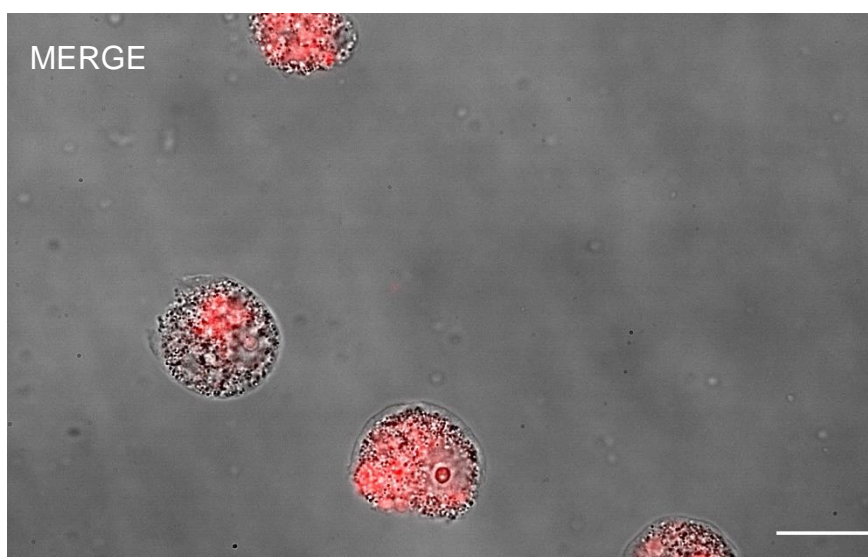
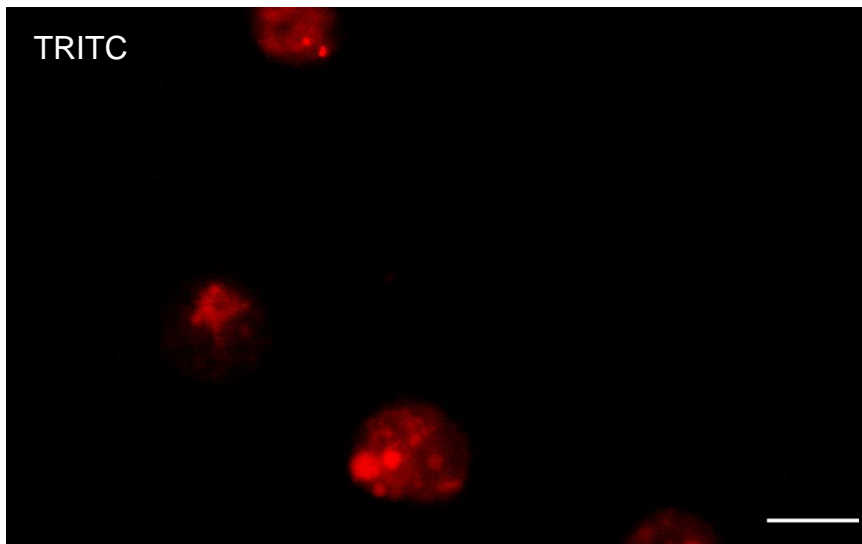
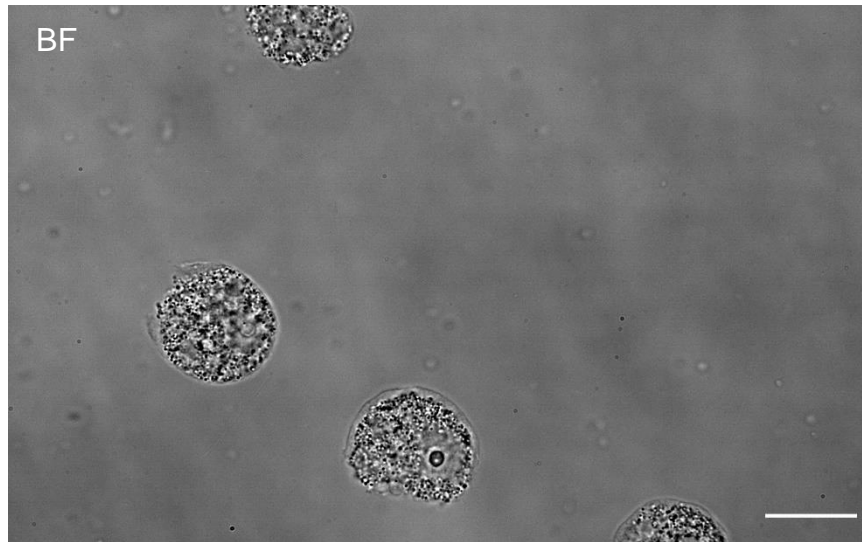
(I) High number of potential positive transfected trophozoites. (II). Trophozoites treated with Polyplus polymer and buffer without the plasmid used as control. The comparative study was carried out for 6 days and the drug selection marker G418 was added according to Chapter 2 only at day 1. Images were taken at 40x utilising Axiovert Zeiss 25 Light microscope.

However, again only few trophozoites showed red fluorescence indicating expression of RFP from pBRFPNeoCas9, a similar result as previously observed with Xfect reagent (Figure 63).

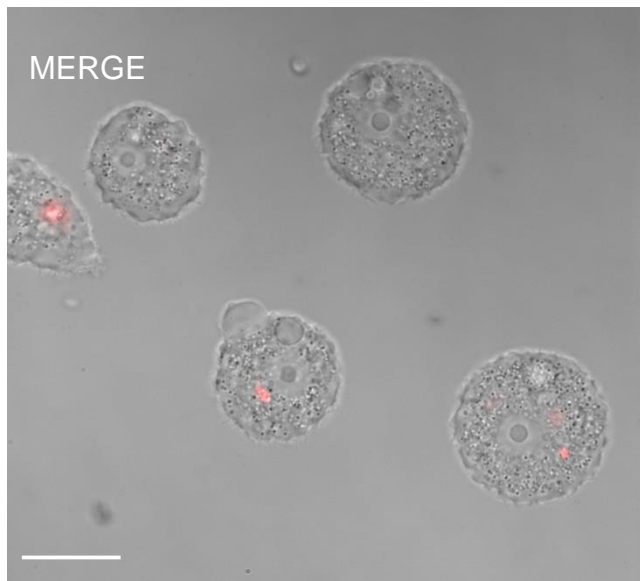
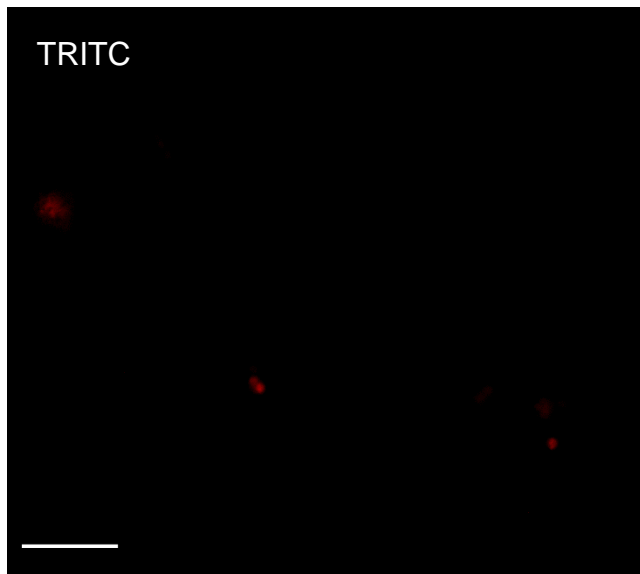
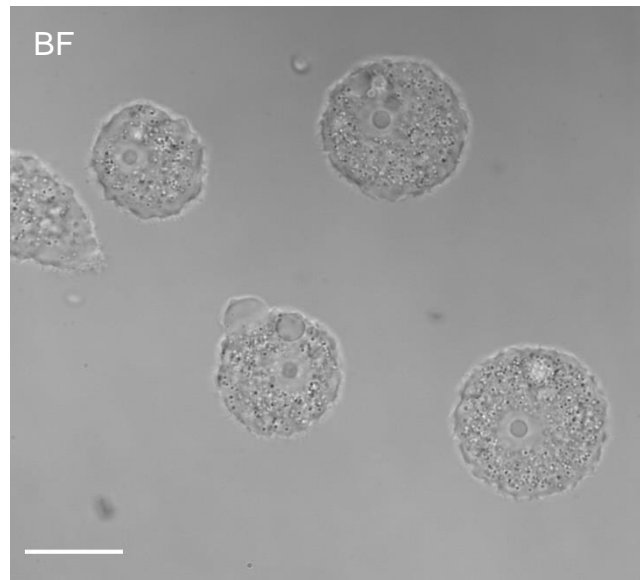
A.



B.



C.



D.

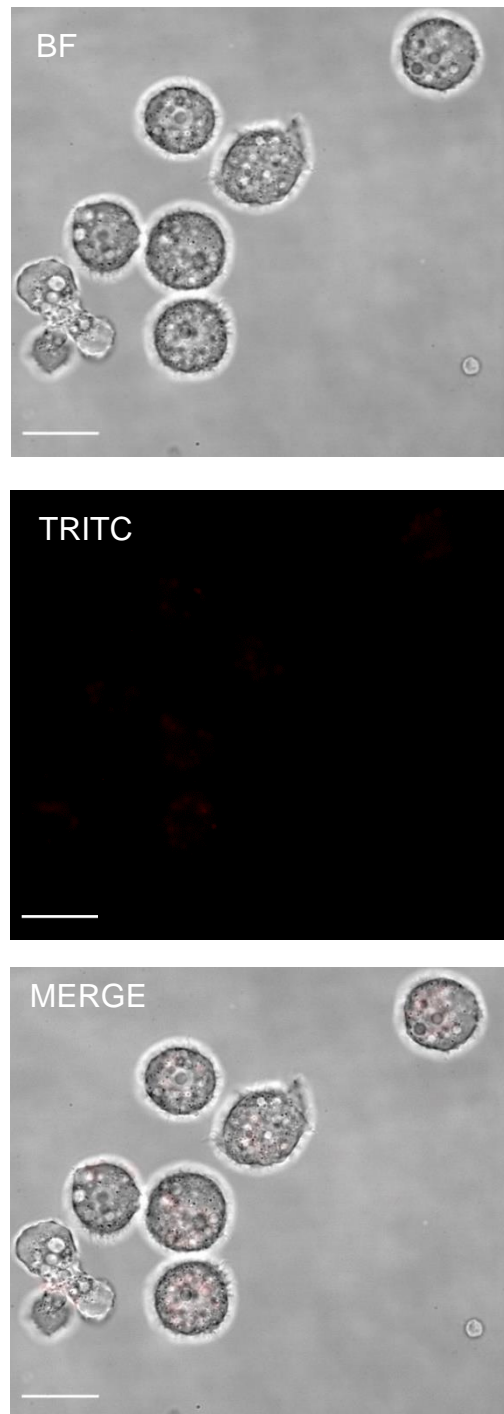


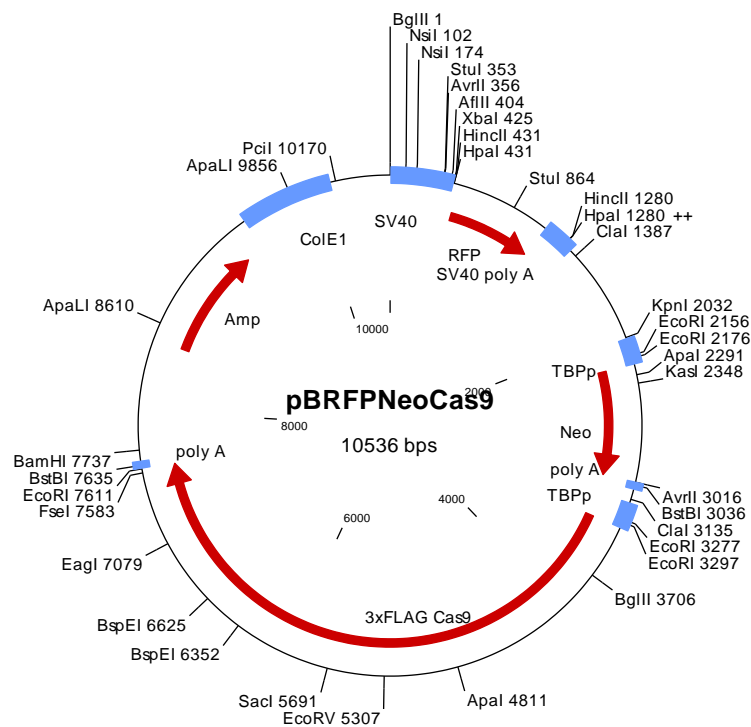
Figure 63. Transfection efficiency of pBRFPNeoCas9 expression in *A. castellanii* trophozoites utilising Polyplus reagent.

A. and **B.** Positive expression of RFP in pBRFPNeoCas9 is displayed by the red fluorescence observed in some trophozoites observed at 60x; **C.** Negative control: trophozoites treated with Polyplus mix without pBRFPNeoCas9 observed at 60x; **D.** Positive control: *A. castellanii* wild type trophozoites. 40x. The analysis was carried out utilising a Nikon Eclipse 600 Epifluorescent Upright Microscope (Nikon, USA) under TRITC filter with Ex_{max} . 540 nm/DM 565 and Em_{max} . 605/55. Scale bar: 20 μ m.

5.4.10 Change of Neo resistance gene to Phleo resistance gene in pBRFPNeoCas9.

As observed in table 18, G418 (Geneticin) has been the only drug selection marker to be used for transfection processes in the past. Previously in this chapter, alternative drug selection markers such as phleomycin, hygromycin B, puromycin and blasticidin were analysed against *A. castellanii* Neff in vitro (see section 5.4.2). The minimum inhibitory concentration (IC_{50s}) results showed phleomycin and hygromycin B to be potently effective against *A. castellanii* Neff strain, therefore the generation of a host strain with Phleo resistance as part of the CRISPR-Cas9 system was performed.

pBRFPNeoCas9 (10536 bp) (see below) was cleaved with ClaI+KpnI to generate fragments of 9436 bp and 1100 bp (Figure 64). The second ClaI restriction site is dam-methylase sensitive and not cleaved in a plasmid isolated from *E. coli* DH5 α .



Plasmid map of pBRFPNeoCas9 (10536 bp)

AMP, ampicillin resistance gene; ColE1, origin of replication; SV40, simian virus 40 promoter; poly A, poly A tail addition site; RFP, Red Fluorescent Protein; SV40 poly A, poly A tail addition site; TBPP, TATA box binding-protein promoter, Neo, Neomycin resistant gene; poly A, poly A tail addition site 3xFLAG Cas9, three FLAG tandem peptides (DYKDHD-G-DYKDHD-I-DYKDDDDKRFP) fused to Cas9; poly A, poly A tail addition site. The ClaI site localised at 1387 bp is dam-methylase sensitive (underlined in red). The plasmid map was generated in Clone Manager 9.

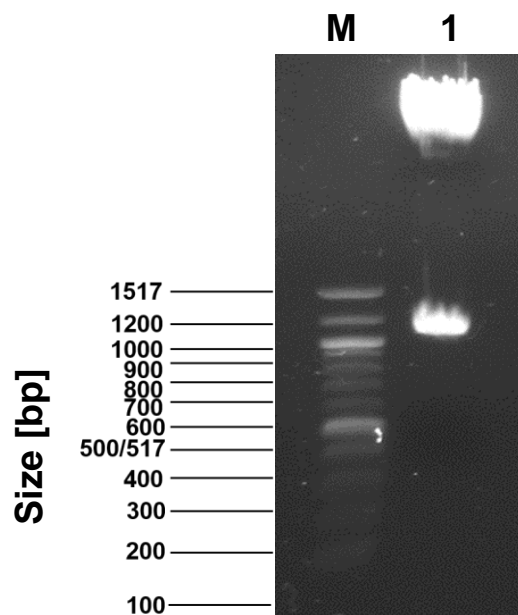


Figure 64. Restriction cleavage of pBRFPNeoCas9 with Clal and KpnI

M, Quick-Load® Purple 100 bp DNA Ladder; lane 1, pBRFPNeoCas9 was cleaved with Clal+KpnI resulting in 9436 bp and 1100 bp DNA fragments. 0.8% agarose gel prepared with 0.5x TBE after electrophoresis stained with ethidium bromide.

The 9436 bp fragment containing the three regions: (i) SV40 promoter+RFP gene sequence+PolyA tail addition site, (ii) TBP promoter+3xFLAG Cas9+PolyA tail and (iii) TBP promoter+Neo resistance marker+PolyA tail was gel purified (Figure 65).

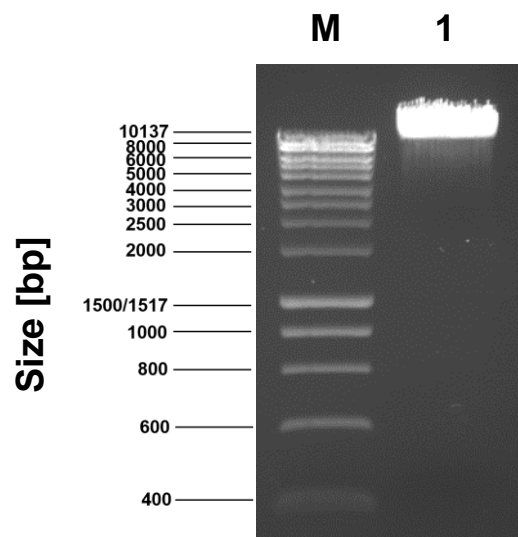


Figure 65. Agarose gel showing purified pBRFPNeoCas9 (9436 bp) fragment.

M, HyperLadder 1kb; lane 1; the fragment 9436 bp was gel isolated. 0.8% agarose gel prepared with 0.5x TBE after electrophoresis stained with ethidium bromide.

pCR2.1Phleo (4298 bp) (Figure 66) was linearised with NcoI and AvrII generating the 2349 bp, 1572 bp and 377 bp DNA fragments. pBKCTBPpNeo (4034 bp) was also cleaved with NcoI and AvrII generating the 3234 bp + 800 bp DNA fragments (Figure 67).

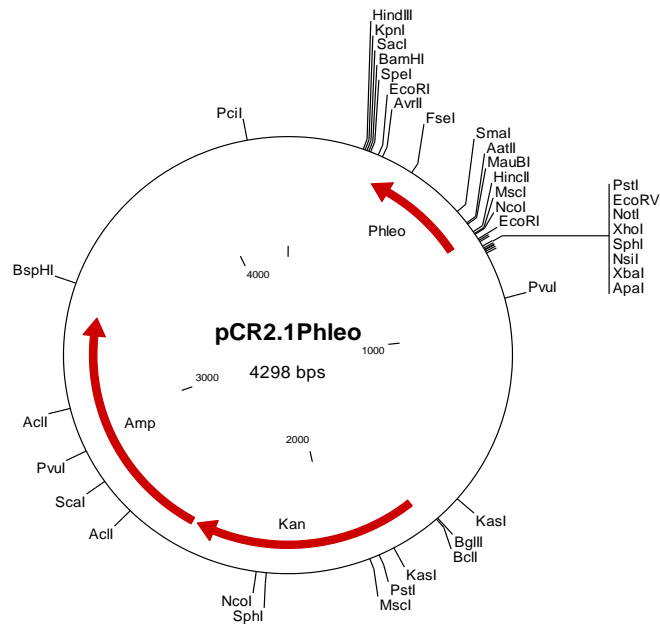


Figure 66. Plasmid map of pCR2.1phleo (4298 bp).

AMP, ampicillin resistance gene; Phleo, phleomycin resistant gene; Kan, kanamycin resistance gene. The plasmid map was generated in Clone Manager 9.

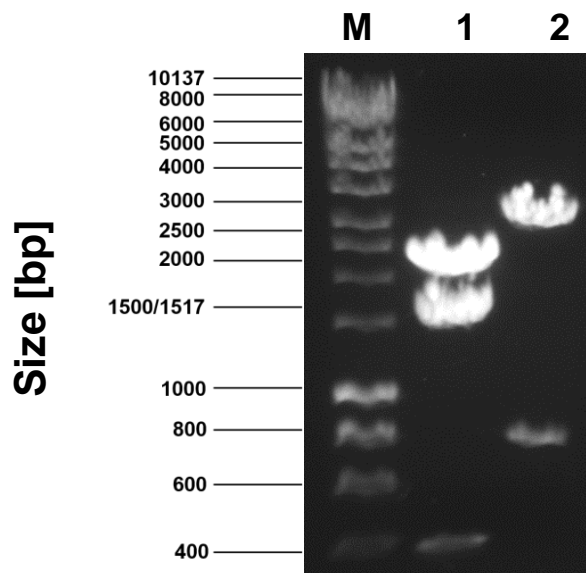


Figure 67. Restriction cleavage of pCR2.1Phleo and pBKCTBPpNeo with NcoI and AvrII.

M, HyperLadder 1kb; lane 1, pCR2.1Phleo (2349 bp+1572 bp+377 bp); lane 2, pBKCTBPpNeo (3234 bp+800 bp) were cleaved with NcoI + AvrII. 0.8% agarose gel prepared with 0.5x TBE after electrophoresis stained with ethidium bromide.

The smaller fragment 377 from pCR2.1Phleo and the biggest fragment 3234 bp from pBKCTBPpNeo were gel isolated and purified using PCR-clean up method. Then, pBRFPNeoCas9 fragment 9436 bp was SAP treated. (Figure 68).

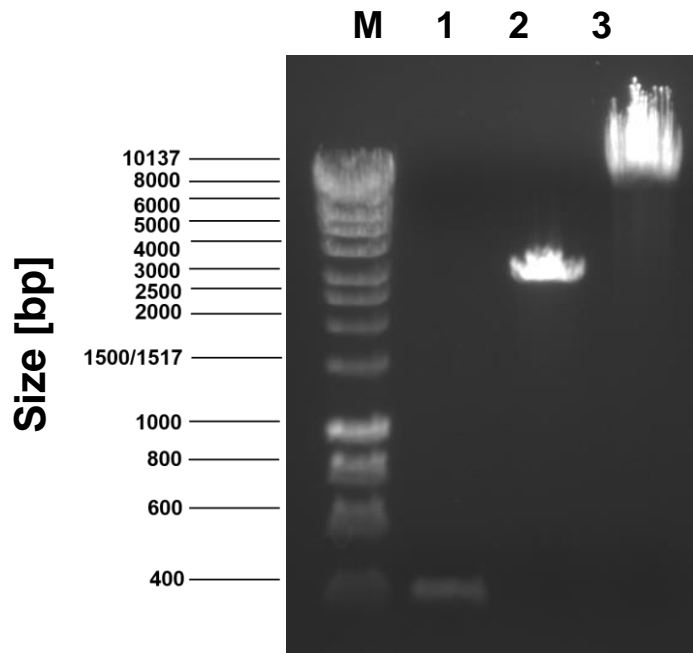


Figure 68. Agarose gel showing purified pCR2.1Phleo and pBKCTBPpNeo fragments and Shrimp Alkaline Phosphatase (SAP) treatment to pBRFPNeoCas9 fragment.

M, Hyperladder 1kb; lane 1, pCR2.1Phleo smallest fragment (377 bp) and lane 2, pBKCTBPpNeo biggest fragment (3234 bp) were gel isolated and purified; lane 3, after gel purification, pBRFPNeoCas9 fragment (9436bp) was SAP-treated. 0.8% agarose gel prepared with 0.5x TBE after electrophoresis stained with ethidium bromide.

Fragments 3234 bp and 377 bp were ligated, transformed into *E. coli* DHα to generate the product pBTBPPhleopolyA (3611 bp) (Figure 69). Following on from analysing plasmid DNA from 10 individual colonies more DNA was isolated in a “MIDIPREP” and the identity of the plasmid was confirmed by restriction cleavage with ApaLI: 1246 bp, 1184 bp, 933 bp and SmaI: 3175 bp + 436 bp (Figure 70 and Table 26).

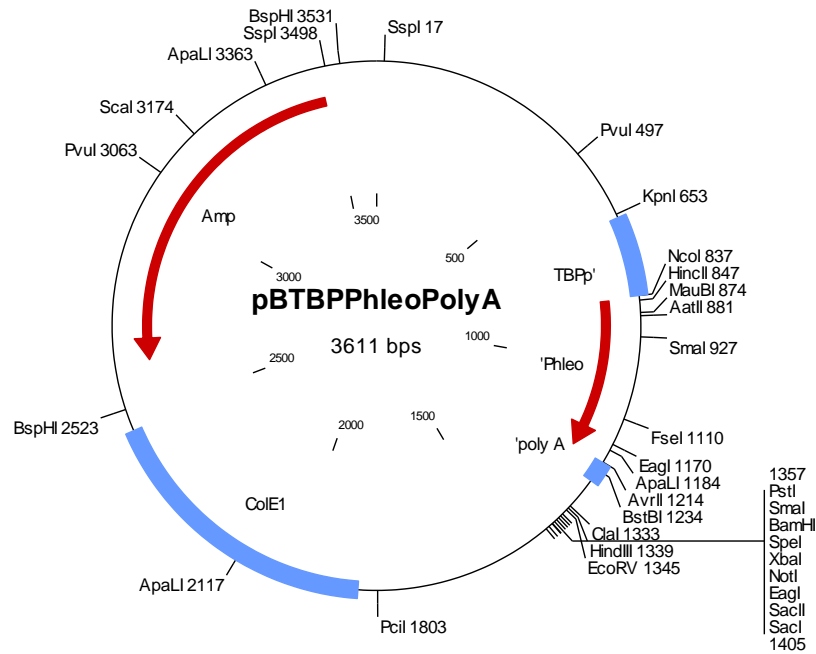


Figure 69. Plasmid map of pBTBPPhleopolyA (3611 bp).

AMP, ampicillin resistance gene; TBPp, TATA box binding-protein promoter; Phleo, Phleomycin resistance gene; poly A, poly A tail addition site; ColE1, origin of replication. The plasmid map was generated in Clone Manager 9.

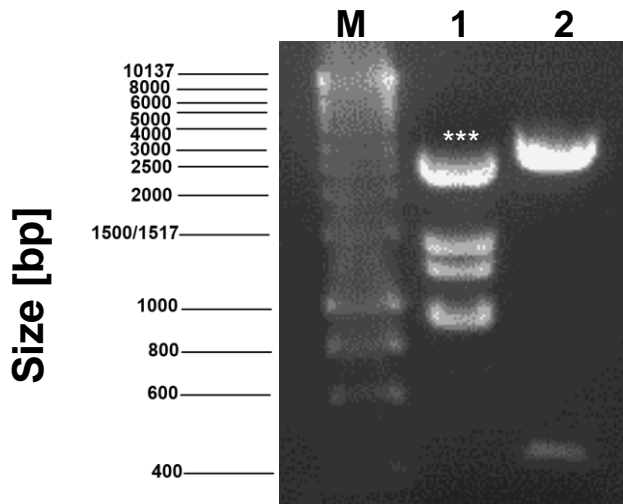


Figure 70. Restriction cleavage of pBTBPPhleopolyA

M, Hyperladder 1kb; lane 1, ApaLI: 1246 bp, 1184 bp and 933 bp. A higher band marked with *** indicates incomplete cleavage by this enzyme; lane 2, SmaI: 3175 bp and 436 bp. 0.8% agarose gel prepared with 0.5x TBE after electrophoresis stained with ethidium bromide.

Table 26. Restriction cleavage of pBRFPNeoCas9, pCR2.1Phleo and pBKCTBPpNeo

A table to illustrate the expected fragment sizes, in base pairs, after pBRFPNeoCas9, pCR2.1Phleo, and pBKCTBPpNeo cleavage utilising various restriction enzymes.

Plasmid	Restriction enzymes	Fragment sizes [bp]
pBRFPNeoCas9	Clal+KpnI	9436 and 1100
pCR2.1Phleo	NcoI-HF+ AvrII	2349, 1572 and 377
pBKCTBPpNeo	NcoI-HF+ AvrII	3234 and 800

pBTBPPhleopolyA (3611 bp) was cleaved with Clal+KpnI to generate the 2934 bp and 677 bp DNA fragments (Figure 71) followed by isolation of the 677 bp DNA fragment.

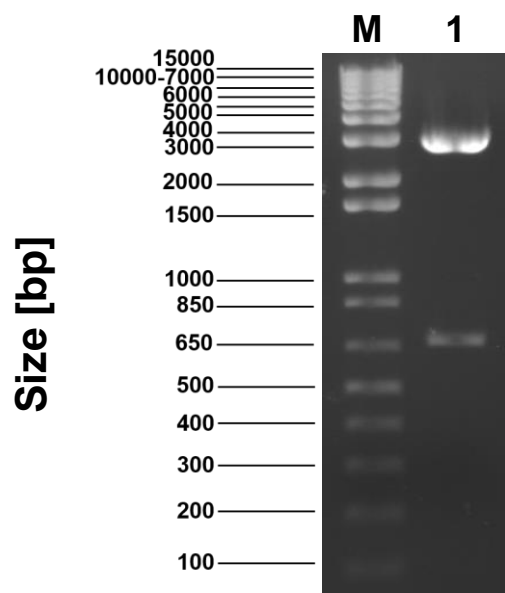


Figure 71. Restriction cleavage of pBTBPPhleopolyA with Clal and KpnI.

M, 1kb Plus DNA ladder; lane 1, pBTBPPhleopolyA was cleaved with Clal+KpnI resulting in 2934 bp and 677 bp DNA fragments. 0.8% agarose gel prepared with 0.5x TBE after electrophoresis stained with ethidium bromide.

The 9436 bp from pBRFPNeoCas9 and 677 bp from pBTBPPhleopolyA were ligated, transformed into *E. coli* DH5 α to generate pBRFPPhleocCas9 (10113 bp) (Figure 72). Following on from analysing plasmid DNA from 16 individual colonies more DNA was isolated in a "MIDIPREP" and the identity of the plasmid was confirmed by restriction cleavage with ClaI: 10113 bp (linearised plasmid), NcoI: 7462 bp + 1953 bp + 698 bp and EcoRI: 5081 bp + 4314 bp + 678 bp + 20 bp were carried out (Figure 73 and Table 27).

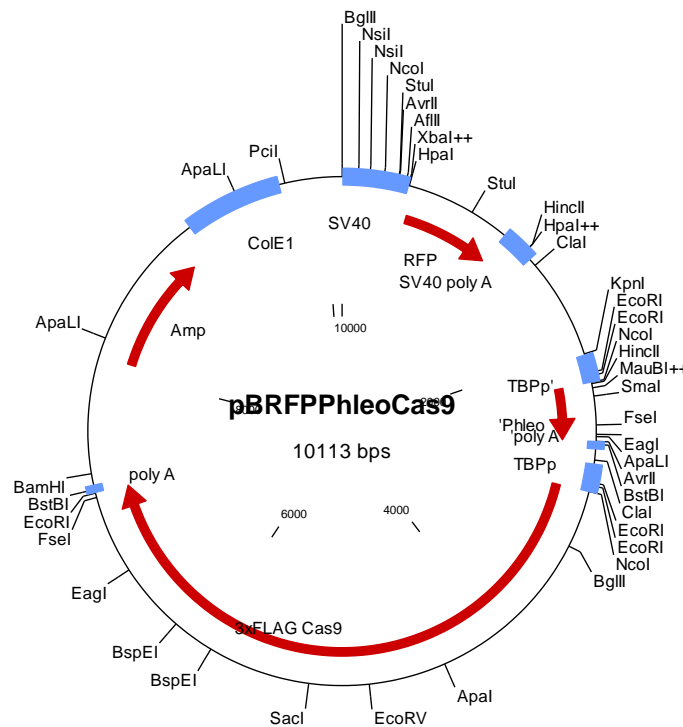


Figure 72. Plasmid map of pBRFPPhleocCas9 (10113 bp)

AMP, ampicillin resistance gene; ColE1, origin of replication; SV40, simian virus 40 promoter; RFP, Red Fluorescent Protein; SV40 poly A, poly A tail addition site; TBPP', TATA box binding-protein promoter; Phleo, Phleomycin resistance gene; poly A, poly A tail addition site; TBPP, TATA box binding-protein promoter; 3xFLAG Cas9, three FLAG tandem peptides (DYKDHD-G-DYKDHD-I-DYKDDDDKRFP) fused to Cas9; poly A, poly A tail addition site. The plasmid map was generated in Clone Manager 9.

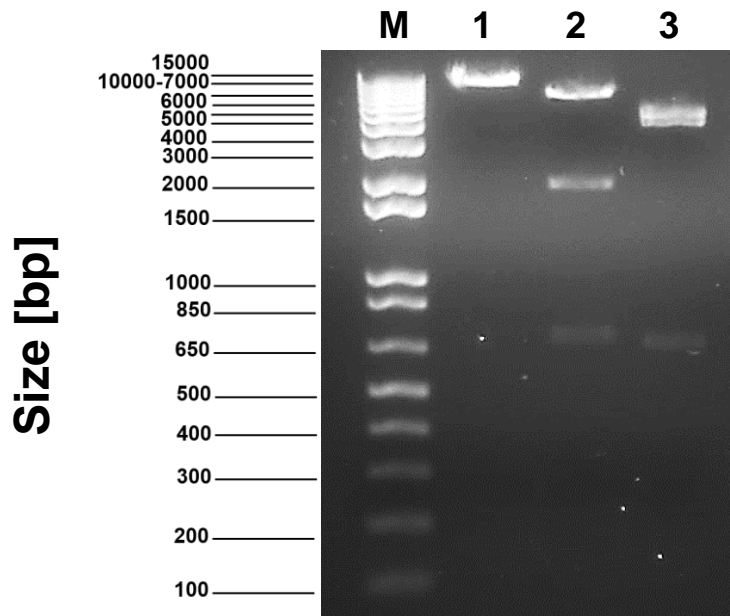


Figure 73. Restriction cleavage of pBRFPPhleCas9 with Clal, NcoI, EcoRI

M, 1kb Plus DNA ladder; lane 1, pBRFPPhleCas9 was cleaved with Clal: 10113 bp; lane 2, NcoI: 7462 and 1953 bp, and lane 3, EcoRI: 5081 bp, 4314 bp, 678 bp and 20 bp DNA fragments. 0.8% agarose gel prepared with 0.5x TBE after electrophoresis stained with ethidium bromide.

Table 27. Restriction cleavage of pBTBPPhlePolyA and pBRFPPhleCas9

A table to illustrate the expected fragment sizes, in base pairs, after pBTBPPhlePolyA and pBRFPPhleCas9 cleavage utilising various restriction enzymes.

Plasmid	Restriction enzymes	Fragment sizes [bp]
pBTBPPhlePolyA	ApaLI	1246, 1184 and 933
	SmaI	3175 and 436
	Clal+KpnI	2934 and 677
pBRFPPhleCas9	Clal	10113 (linearised)
	NcoI	7462, 1953 and 698
	EcoRI	5081, 4314, 678 and 20

5.4.11 Addition of T7 RNA polymerase gene sequence to pBRFPNeoCas9 and pBRFPPhleCas9 to generate pBRFPT7NeoCas9 and pBRFPT7PhleoCas9.

The integration of a T7 RNA polymerase gene into pBRFPNeoCas9 and pBRFPPhleCas9 will allow the *in vivo* sgRNA transcription in *Acanthamoeba castellanii* Neff strain. pBRFPNeoCas9 (10563 bp) and pBRFPPhleCas9 (10113 bp) were linearised with MfeI (isoschizomer of MunI) (Figure 74).

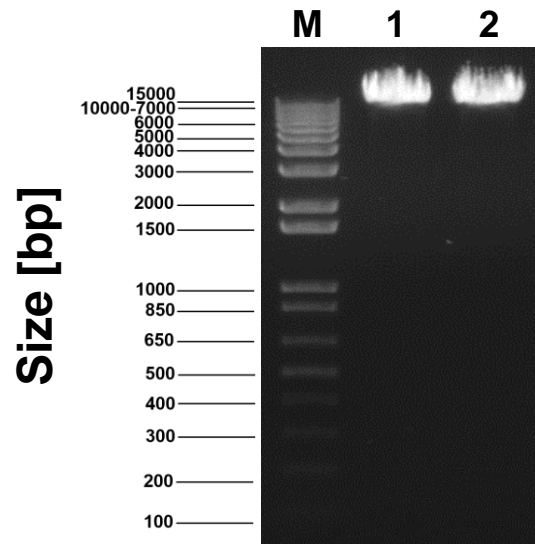


Figure 74. Restriction cleavage of pBRFPNeoCas9 and pBRFPPhleCas9 with MfeI

M, 1kb Plus DNA ladder; both lane 1, pBRFPNeoCas9 (10563 bp); lane 2, pBRFPPhleCas9 (10113 bp) were cleaved with MfeI. 0.8% agarose gel prepared with 0.5x TBE after electrophoresis stained with ethidium bromide.

The plasmid pUCSV40T7PolyA (6544 bp) (Figure 75) was generated by gene synthesis to contain the T7 RNA polymerase gene. To generate more DNA a "MIDIPREP" was performed, and the identity of the plasmid was confirmed by restriction cleavage with NdeI+NcoI: 3188 bp, 2542 bp, 649 bp and 165 bp; KpnI+ApaI: 4217 bp, 2100 bp and 227 bp; XbaI+EcoRI: 3038 bp, 2912 bp, 522 bp, 36 bp and 36 bp; and MunI+ApaI: 3392 bp, 2100 bp, 725 bp and 327 bp (Figure 76).

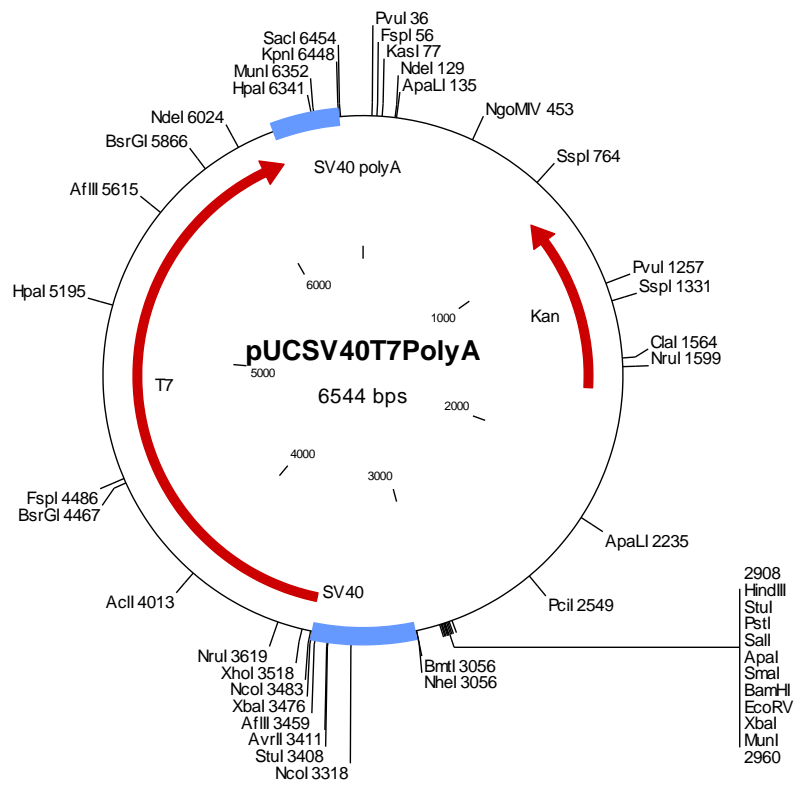


Figure 75. Plasmid map of pUCSV40T7PolyA (6544 bp)

Kan, kanamycin resistance gene; SV40, simian virus 40 promoter; T7, T7 RNA polymerase gene; poly A, poly A tail addition site. The plasmid map was generated in Clone Manager 9.

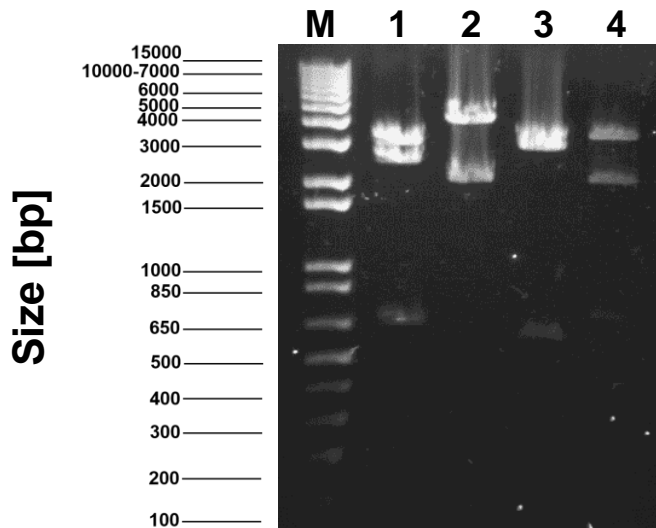


Figure 76. Restriction cleavage of pUCSV40T7PolyA.

The identity of the plasmid was confirmed by restriction analysis. M, 1kb Plus DNA ladder; lane 1, NdeI and NcoI, 3188 bp and 2542 bp; lane 2, KpnI and ApaLI, 4217 bp and 2100 bp; lane 3, XbaI and EcoRI, 3038 bp and 2912 bp; lane 4, MnlI and ApaLI, 3392 bp and 2100 bp DNA fragments. 0.8% agarose gel prepared with 0.5x TBE after electrophoresis stained with ethidium bromide.

Subsequently, pUCSV40T7PolyA was cleaved with MfeI to yield 3392 bp and 3152 bp DNA fragments. The DNA fragments were PCR cleaned up and the fragment 3392 bp was gel purified. Afterwards, pBRFPNeoCas9 (10563 bp) and pBRFPPhleoCas9 (10113 bp) linearized plasmids were SAP treated (Figure 77).

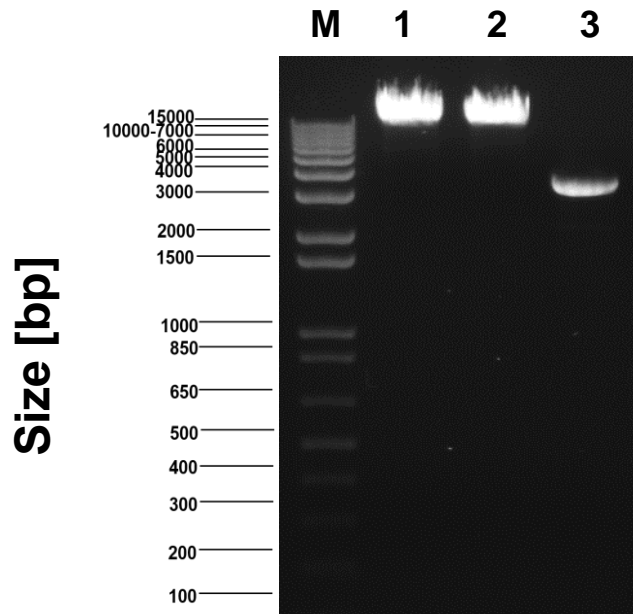


Figure 77. Agarose gel showing Shrimp Alkaline Phosphatase (SAP) treated fragments of pBRFPNeoCas9 and pBRFPPhleoCas9 and purified pUCSV40T7PolyA fragment.

M, 1kb Plus DNA ladder; lane 1, pBRFPNeoCas9 linearised with MfeI and SAP-treated (10536 bp); lane 2, pBRFPPhleoCas9 linearised with MfeI and SAP-treated (10113 bp); lane 3, pUCSV40T7PolyA 3392 bp DNA fragment purified using an agarose gel. 0.8% agarose gel prepared with 0.5x TBE after electrophoresis stained with ethidium bromide.

Linearised pBRFPNeoCas9 (10563 bp) was ligated with the 3392 bp fragment from pUCSV40T7, transformed into *E. coli* DH5 α to generate pBRFPT7sNeoCas9 (13928 bp) (Figure 78). Following on from analysing plasmid DNA from 2 individual colonies more DNA was isolated in a “MIDIPREP” and the identity of the plasmid pBRFPT7sNeoCas9 (13928 bp) was confirmed by double restriction cleavage with NdeI and KpnI to generate 12856 bp and 1072 bp, and XbaI+XhoI to generate 12504 bp and 1424 bp (Figure 79).

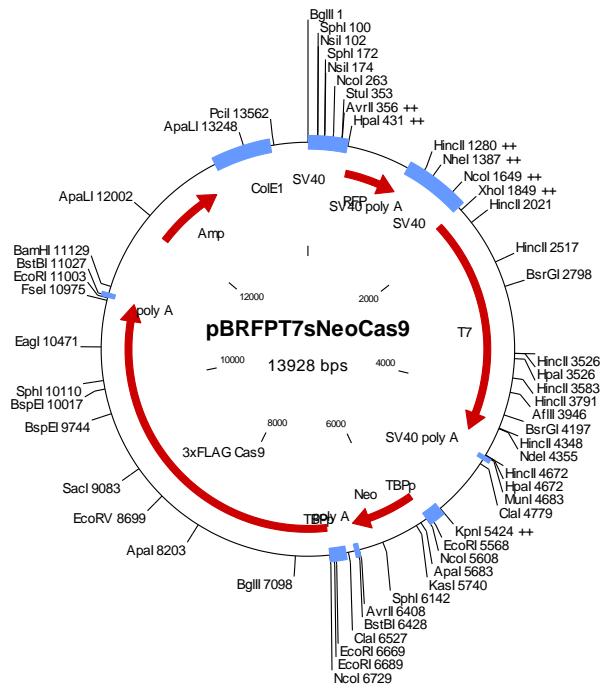


Figure 78. Plasmid map of pBRFPT7sNeoCas9 (13928 bp).

Amp, ampicillin resistance gene; ColE1, origin of replication; SV40, simian virus 40 promoter; RFP, Red Fluorescent Protein; SV40 poly A tail, polyA tail addition site; SV40, simian virus 40 promoter; T7, T7 RNA polymerase gene sequence; SV40 poly A tail, polyA tail addition site; TBpp, TATA box binding-protein, Neo, Neomycin resistance gene; poly A tail, polyA tail addition site; TBpp, TATA box binding-protein; 3xFLAG Cas9, three FLAG tandem peptides (DYKDHD-G-DYKDHD-I-DYKDDDDKRFP) fused to Cas9; poly A tail, polyA tail addition site. The plasmid map was generated in Clone Manager 9.

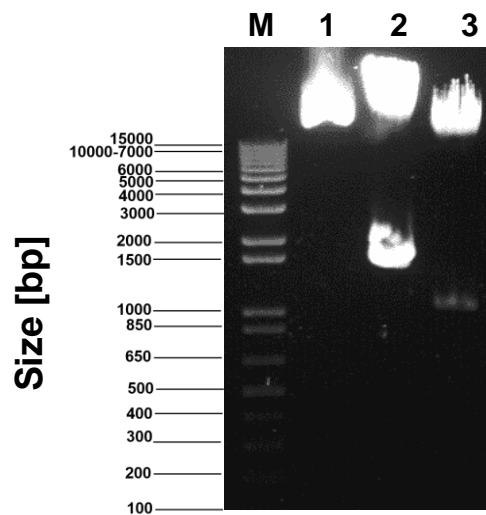


Figure 79. Restriction cleavage of pBRFPT7sNeoCas9 with XbaI and XhoI, NdeI and KpnI

Confirmation of pBRFPT7sNeoCas9. M, 1kb Plus DNA ladder; lane 1, pBRFPT7sNeoCas9 not cleaved; lane 2, XbaI and XhoI, 12504 bp and 1424 bp; lane 3, NdeI and KpnI, 12856 bp and 1072 bp DNA fragments. 0.8% agarose gel prepared with 0.5x TBE after electrophoresis stained with ethidium bromide.

Linearised pBRFPPhleoCas9 (10113 bp) was ligated with pUCSV40T7PolyA (3392 bp) fragment, transformed into *E. coli* DH5 α to generate pBRFPT7sPhleoCas9 (13505 bp) (Figure 80). Following on from analysing plasmid DNA from 12 individual colonies more DNA was isolated in a “MIDIPREP” and the identity of the plasmid pBRFPT7sPhleoCas9 (13505 bp) was confirmed by double restriction cleavage with Xba+XhoI 12081 bp and 1424 bp and NdeI+KpnI 1072 bp and 12433 bp (Figure 81).

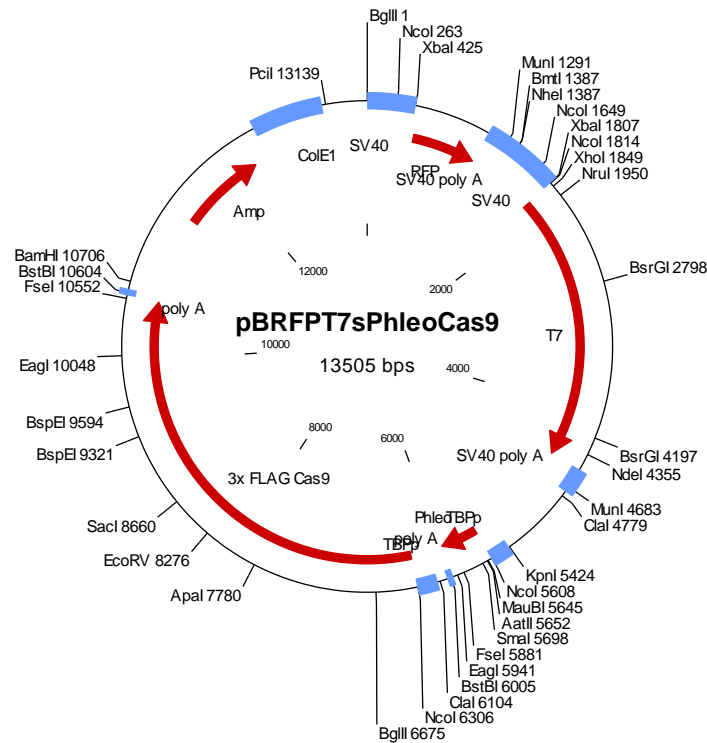


Figure 80. Plasmid map of pBRFPT7sPhleoCas9 (13505 bp).

Amp, ampicillin resistance gene; ColE1, origin of replication; SV40, simian virus 40 promoter; RFP, Red Fluorescent Protein; SV40 poly A tail, polyA tail addition site; SV40, simian virus 40 promoter; T7, T7 RNA polymerase gene sequence; SV40 poly A tail, polyA tail addition site; TBPP, TATA box binding-protein promoter, Phleo, Phleomycin resistance gene; poly A tail, polyA tail addition site; TBPP, TATA box binding-protein; 3xFLAG Cas9, three FLAG tandem peptides (DYKDHD-G-DYKDHD-I-DYKDDDDKRFP) fused to Cas9; poly A tail, polyA tail addition site. The plasmid map was generated in Clone Manager 9.

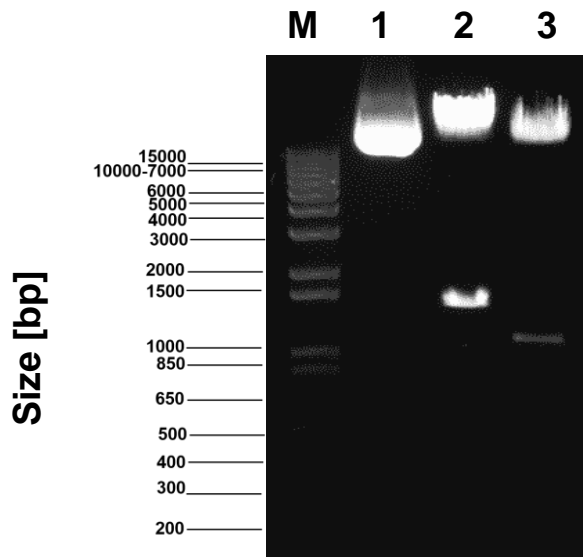


Figure 81. Restriction cleavage of pBRFPT7sPhleoCas9 with XbaI and XhoI, NdeI and KpnI.

Confirmation of pBRFPT7sPhleoCas9. M, 1kb Plus DNA ladder; lane 1, pBRFPT7sNeoCas9 not cleaved; lane 2, Xba and XhoI, 12081 bp and 1424 bp; lane 3, NdeI and KpnI, 12433 bp and 1072 bp DNA fragments. 0.8% agarose gel prepared with 0.5x TBE after electrophoresis stained with ethidium bromide.

pUCSV40T7PolyA (6544 bp) was cleaved with NdeI+KpnI generating 5895 bp, 427 bp and 222 bp DNA fragments. The 427 bp DNA fragment was purified using an agarose gel (Figure 82).

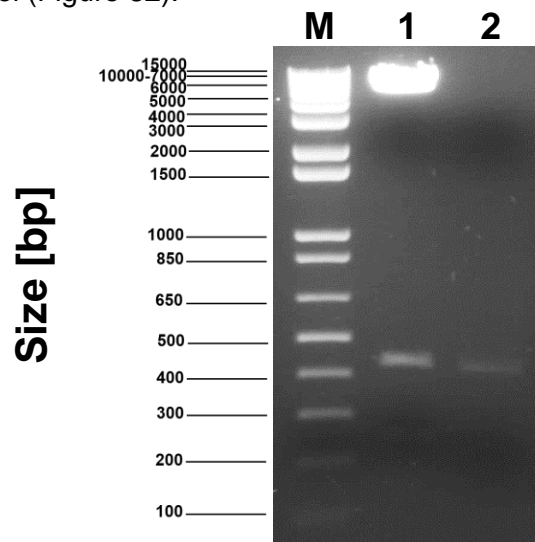


Figure 82. Restriction cleavage of pUCSV40T7PolyA with NdeI and KpnI and purified fragment.

M, 1kb Plus DNA ladder; lane 1, pUCSV40T7PolyA cleaved with NdeI+KpnI (5895 bp + 427 bp); lane 2, the 427 bp DNA fragment was purified. 0.8% agarose gel prepared with 0.5x TBE after electrophoresis stained with ethidium bromide.

The 12856 bp DNA fragment of pBRFPT7sNeoCas9 and the 12433 bp DNA fragment of pBRFPT7sPhleoCas9 were isolated and SAP treated. Each of these fragments was ligated with the 427 bp DNA fragment isolated from pUCSV40T7PolyA, transformed into *E. coli* DH5 α to generate the final constructs pBRFPT7NeoCas9 and pBRFPT7PhleoCas9. Following on from analysing plasmid DNA from 7 individual colonies carrying the potential ligation pBRFPT7NeoCas9 and 5 individual colonies carrying the potential ligation pBRFPT7PhleoCas9, more DNA was isolated in a "MIDIPREP" and the identity of the plasmid was confirmed by restriction cleavages for pBRFPT7NeoCas9 with NcoI+NdeI (7462 bp, 2541 bp, 1386 bp, 1121 bp and 608 bp), EcoRI (4768 bp, 4314 bp, 3024 bp, 1101 bp), and ApaLI+EcoRV (8734 bp, 3303 bp and 1246 bp); and for pBRFPT7PhleoCas9 with NcoI+NdeI (7462 bp, 2541 bp, 1386 bp, 698 bp and 608 bp), EcoRI (4768 bp, 4314 bp, 3024 bp and 678 bp), and ApaLI+EcoRV (5590 bp, 3303 bp, 2321 bp and 1246 bp) (Figure 83).

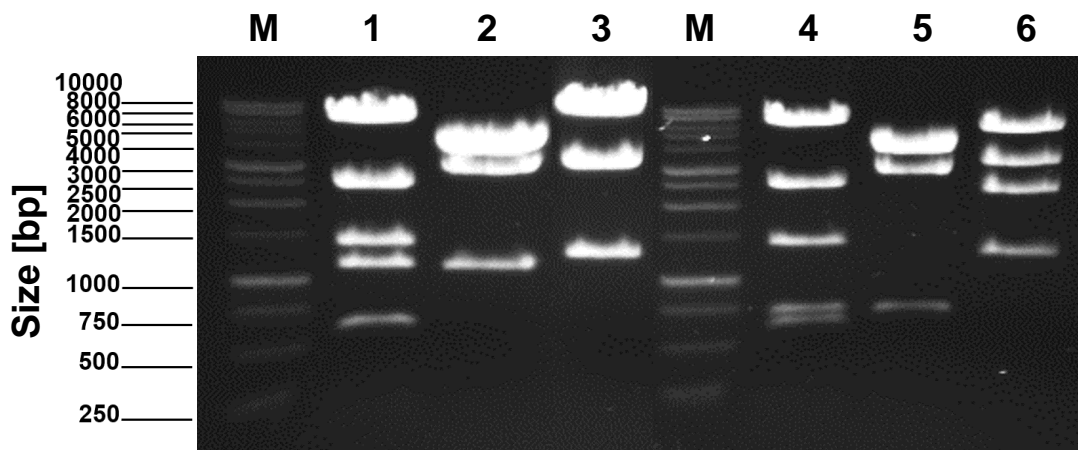


Figure 83. Restriction cleavage of pBRFPT7NeoCas9 and pBRFPT7PhleoCas9 with NcoI and NdeI, EcoRI, ApaLI and EcoRV.

M, 1 kb DNA ladder; pBRFPT7NeoCas9 cleaved with lane 1, NcoI+NdeI (7462 bp, 2541 bp, 1386 bp, 1121 bp and 608 bp); lane 2, EcoRI (4768 bp, 4314 bp, 3024 bp, 1101 bp); lane 3, ApaLI+EcoRV (8734 bp, 3303 bp and 1246 bp); pBRFPT7PhleoCas9 cleaved with lane 4, NcoI+NdeI (7462 bp, 2541 bp, 1386 bp, 698 bp and 608 bp); lane 5, EcoRI (4768 bp, 4314 bp, 3024 bp, 678 bp); lane 6, ApaLI+EcoRV (5590 bp, 3303 bp, 2321 bp and 1246 bp). 0.8% agarose gel prepared with 0.5x TBE after electrophoresis stained with ethidium bromide.

Therefore, the results shown in figure 83 confirm the correct identity of pBRFPT7NeoCas9 (13283 bp) (Figure 84) and pBRFPT7PhleoCas9 (12860 bp) (Figure 85), which contain the T7 RNA polymerase and Cas9 gene sequences, as part of the CRISPR-Cas9 system development for *A. castellanii* Neff strain trophozoites.

A review of all the restriction cleavage process to add T7 RNA polymerase in pBRFPNeoCas9 and pBRFPPhleoCas9 to generate pBRFPT7NeoCas9 and pBRFPT7PhleoCas9 is summarised in table 28.

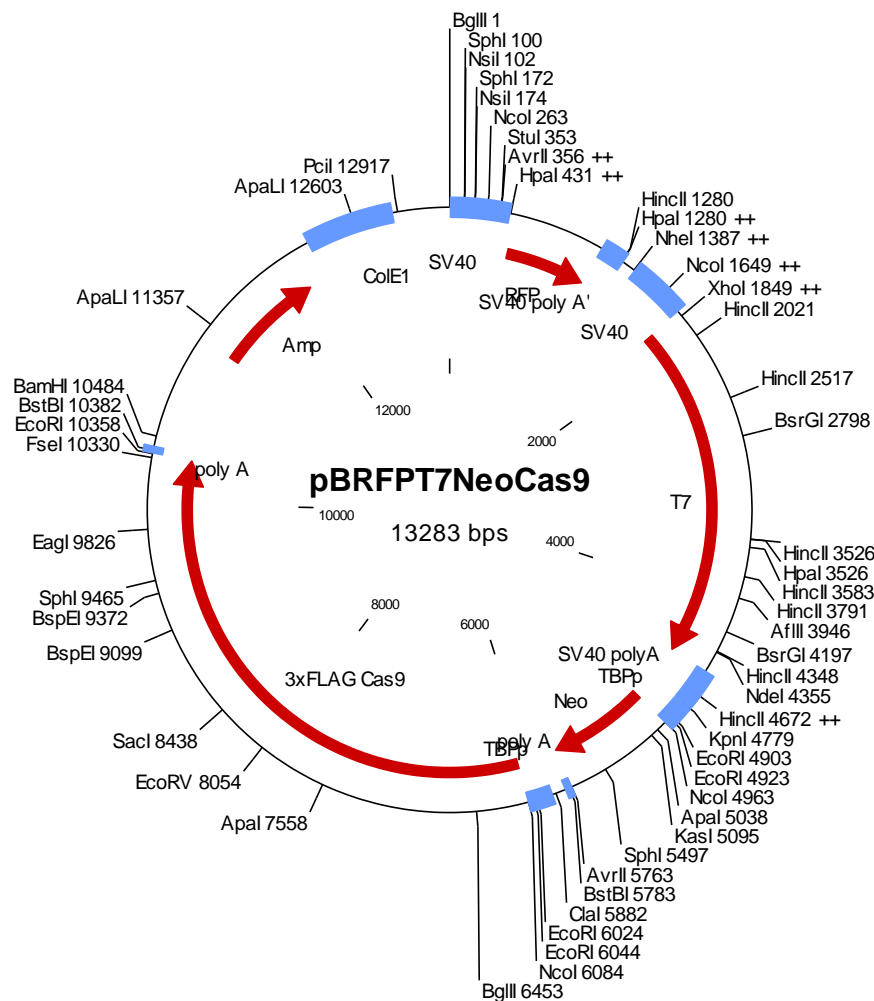


Figure 84. Plasmid map of pBRFPT7sNeoCas9 (13283 bp)

Amp, ampicillin resistance gene; ColE1, origin of replication; SV40, simian virus 40 promoter; RFP, Red Fluorescent Protein; SV40 poly A tail, polyA tail addition site; SV40, simian virus 40 promoter; T7, T7 RNA polymerase gene sequence; SV40 poly A tail, polyA tail addition site; TBPP, TATA box binding-protein promoter, Neo, Neomycin resistance gene; poly A tail, polyA tail addition site; TBPP, TATA box binding-protein; 3xFLAG Cas9, three FLAG tandem peptides (DYKDHD-G-DYKDHD-I-DYKDDDDKRFP) fused to Cas9; poly A tail, polyA tail addition site. The plasmid map was generated in Clone Manager 9.

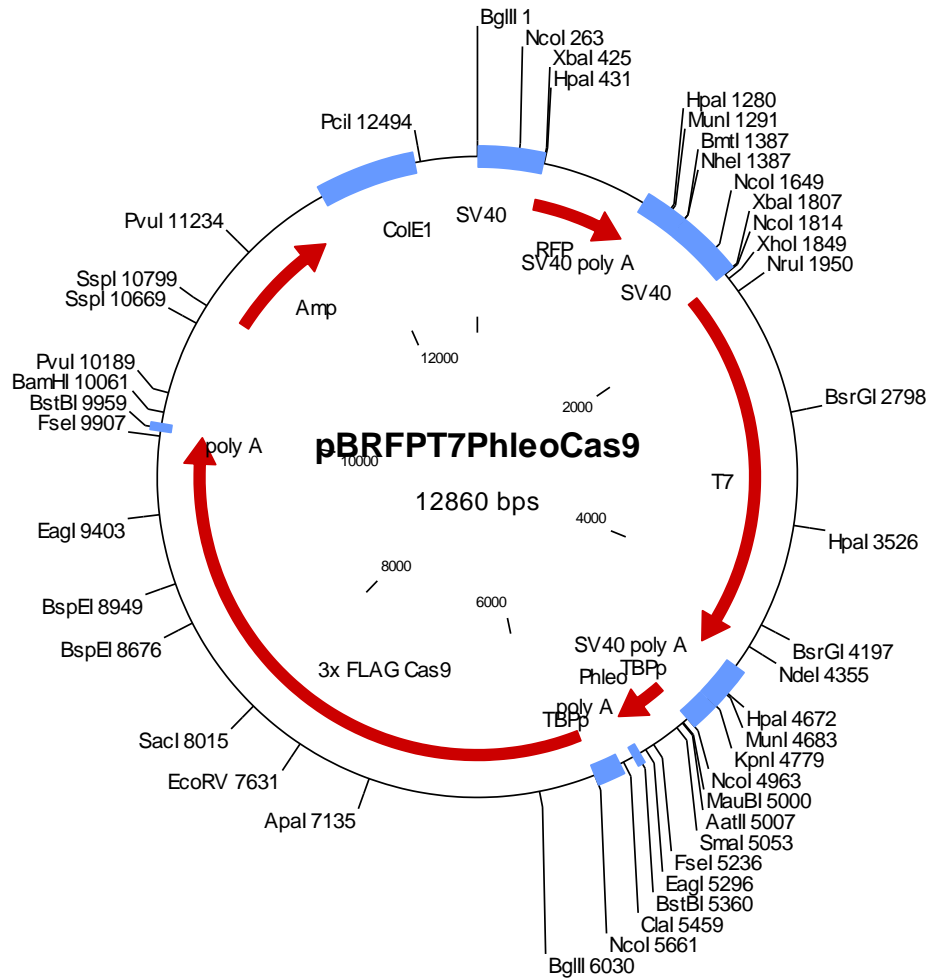


Figure 85. Plasmid map of pBRFPT7sPhleoCas9 (12860 bp)

Amp, ampicillin resistance gene; ColE1, origin of replication; SV40, simian virus 40 promoter; RFP, Red Fluorescent Protein; SV40 poly A tail, polyA tail addition site; SV40, simian virus 40 promoter; T7, T7 RNA polymerase gene sequence; SV40 poly A tail, polyA tail addition site; TBPP, TATA box binding-protein promoter, Phleo, Phleomycin resistance gene; poly A tail, polyA tail addition site; TBPP, TATA box binding-protein; 3xFLAG Cas9, three FLAG tandem peptides (DYKDHD-G-DYKDHD-I-DYKDDDDKRFP) fused to Cas9; poly A tail, polyA tail addition site. The plasmid map was generated in Clone Manager 9.

Table 28. Restriction analysis of pBRFPNeoCas9, pBRFPPhleCas9, pUCSV40T7PolyA, pBRFPT7sNeoCas9, pBRFPT7sPhleoCas9, pBRFPT7NeoCas9, and pBRFPT7PhleoCas9

A table to illustrate the expected fragment sizes, in base pairs, after pBRFPNeoCas9, pBRFPPhleCas9, pUCSV40T7PolyA, pBRFPT7sNeoCas9, pBRFPT7sPhleoCas9, pBRFPT7NeoCas9, and pBRFPT7PhleoCas9 cleavage utilising various restriction enzymes.

Plasmid	Restriction enzymes	Fragment sizes [bp]
pBRFPNeoCas9	MfeI	10563 (linearized)
pBRFPPhleCas9	MfeI	10113 (linearized)
pUCSV40T7PolyA	NdeI+NcoI	3188, 2542, 649 and 165
	KpnI+ApaLI	4217, 2100 and 227
	XbaI+EcoRI	3038, 2912, 522, 36 and 36
	MfeI	3392 and 3152
	NdeI+KpnI	5895, 427 and 222
pBRFPT7sNeoCas9	Xba+XhoI	1424 and 12504
	NdeI+KpnI	12856 and 1072
pBRFPT7sPhleoCas9	XbaI+XhoI	1424 and 12081
	NdeI+KpnI	12433 and 1072
pBRFPT7NeoCas9	NcoI+NdeI	7462, 2541, 1386, 1121, and 608
	EcoRI	4768, 4314, 3024 and 1101
	ApaLI+EcoRV	8734, 3303 and 1246
pBRFPT7PhleoCas9	NcoI+NdeI	7462, 2541, 1386, 698 and 608
	EcoRI	4768, 4314, 3024 and 678
	ApaLI+EcoRV	5590, 3303, 2321 and 1246

5.4.12 PCR amplification of CS-Neo-CS, CS-Phleo-CS, and CS-Hyg-CS

To generate repair cassettes that allow directed deletion by CRISPR-Cas9, resistance marker genes were PCR-amplified using the oligonucleotides (CSCRupneo.for, CSCRdsneo.rev, CSCRupphleo.for, CSCRdspheo.rev, CSCRuphyg.for, CSCRdsneo.rev) to add short flanking sequences of the chorismate synthase gene before and after the respective resistance gene using pCR2.1Neo, pCR2.1Phleo and pCR2.1Hyg. The amplicons CS-Neo-CS (897 bp), CS-Phleo-CS (468 bp), CS-Hyg-CS (1174 bp) (Figure 86) were purified using the PCR-clean up method (Figure 88).

A description of CS-Neo-CS (897 bp), CS-Phleo-CS (468 bp), CS-Hyg-CS (1174 bp) sequences is described in figure 87.

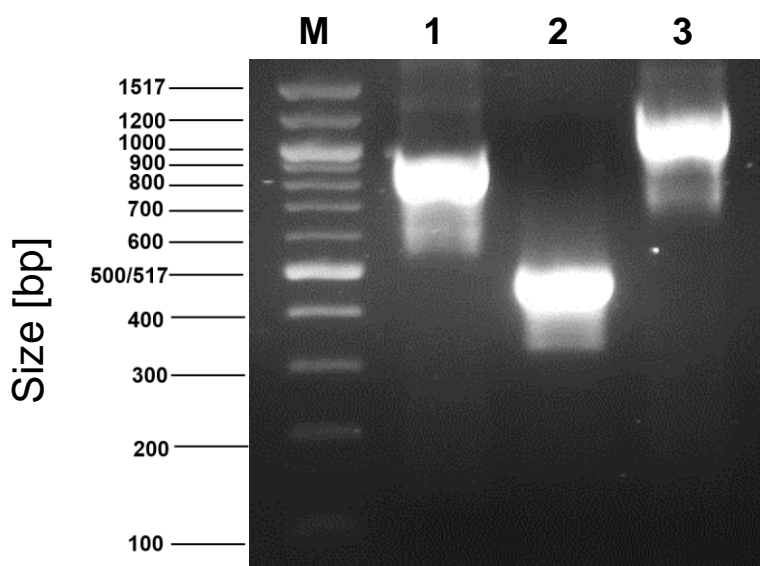


Figure 86. Agarose gel showing CS-Neo-CS, CS-Phleo-CS, and CS-Hyg-CS DNA repair cassette amplicons.

M, Quick-Load® Purple 100 bp DNA Ladder; small flanking sequences of chorismate synthase gene upstream and downstream were annealed to Neomycin, Phleomycin and Hygromycin drug resistance genes to yield lane 1, CS-Neo-CS (897 bp); lane 2, CS-Phleo-CS (468 bp); lane 3, CS-Hyg-CS (1174 bp). The amplicons were utilised as insertion repair cassettes. 1% agarose gel prepared with 0.5x TBE after electrophoresis stained with ethidium bromide.

A. CS-Neo-CS (897 bp)

GGCGTTAGAGCTTGAAGAAGACGCGACATCAATTTCGGCTTGCCATCATGAGCTCGGCCA
TTGAACAAGATGGATTGCACGCAGGTTCTCCGGCCGCTTGGGTGGAGAGGCTATTTCG
GCTATGACTGGGCACAACAGACAATCGGCTGCTCTGATGCCGCCGTGTTCCGGCTGT
CAGCGCAGGGGCGCCCGGTTCTTTTTGTCAAGACCGACCTGTCCGGTGCCCTGAATG
AACTGCAGGACGAGGCAGCGCGGCTATCGTGGCTGGCCACGACGGGCGTTCCTTGCG
CAGCTGTGCTCGACGTTGTCACTGAAGCGGAAGGACTGGCTGCTATTGGGCGAAG
TGCCGGGGCAGGATCTCCTGTCATCTCACCTTGCTCCTGCCGAGAAAGTATCCATCA
TGGCTGATGCAATGCGGCGGCTGCATACGCTTGATCCGGCTACCTGCCATTCGACC
ACCAAGCGAAACATCGCATCGAGCGAGCACGTA CTCCGATGGAAGCCGGTCTTGTCG
ATCAGGATGATCTGGACGAAGAGCATCAGGGGCTCGCGCCAGCCGA ACTGTTCCGCA
GGCTCAAGGCGCGCATGCCCGACGGCGAGGATCTCGTCGTGACCCATGGCGATGCCT
GCTTGCCGAATATCATGGTGGAAAATGGCCGCTTTTCTGGATTCATCGACTGTGGCC
GGCTGGGTGTGGCGGACCGCTATCAGGACATAGCGTTGGCTACCCGTGATATTGCTG
AAGAGCTTGGCGGCGAATGGGCTGACCGCTTCCTCGTGCTTTACGGTATCGCCGCTC
CCGATTCGCAGCGCATCGCCTTCTATCGCCTTCTTGACGAGTTCTTCTGAGCTAGCC
GGCAAAGCCGCGTGCGCCAAACAGAGCAAGAAGCGCGCTG

B. CS-Phleo-CS (468 bp)

GGCGTTAGAGCTTGAAGAAGACGCGACATCTTCGGCTTAGATCACCATGGCCAAGTTGA
CCAGTGCCGTTCCGGTGCTCACCGCGCGGACGTCGCCGGAGCGGTTCGAGTTCTGGA
CCGACCGGCTCGGGTTCTCCCGGGACTTCGTGGAGGACGACTTCGCCGGTGTGGTCC
GGGACGACGTGACCCTGTTTCATCAGCGCGGTCCAGGACCAGGTGGTGCCGGACAACA
CCCTGGCCTGGGTGTGGGTGCGCGGCCTGGACGAGCTGTACGCCGAGTGGTCCGAGG
TCGTGTCCACGAACTTCCGGGACGCTCCGGGCCGGCCATGACCCGAGATCGGCGAGC
AGCCGTGGGGGCGGGAGTTCCGCCCTGCGCGACCCGGCCGGCAACTGCGTGCACCTTCG
TGGCCGAGGAGCAGGACTGACCTAGGCCGAAGCCGAAAGCGTGCGCCAAACAGAGCAAGA
AGCGCGCTG

C. CS-Hyg-CS (1174 bp)

GGCGTTAGAGCTTGAAGAAGACGCGACATCAATTGGGCCCTCTAGATGCATGCTCGAGCG
GCCGCCAGTGTGATGGATATCTGCAGAATTCGGCTTCTAGTCATGAAAAGCCTGAA
CTCACCGCGACGTCTGTCGAGAAGTTTCTGATCGAAAAGTTCGACAGCGTCTCCGAC
CTGATGCAGCTCTCGGAGGGCGAAGAATCTCGTGCTTTCAGCTTCGATGTAGGAGGG
CGTGGATATGTCCTGCGGGTAAATAGCTGCGCCGATGGTTTCTACAAAGATCGTTAT
GTTTATCGGCACTTTGCATCGGCCGCGCTCCCGATTCCGGAAGTGCTTGACATTGGG
GAATTCAGCGAGAGCCTGACCTATTGCATCTCCCGCCGTGCACAGGGTGTACAGTTG
CAAGACCTGCCTGAAACCGAACTGCCCGCTGTTCTGCAGCCGGTCGCGGAGGCCATG
GATGCGATCGCTGCGGCCGATCTTAGCCAGACGAGCGGGTTCGGCCATTCGGACCG
CAAGGAATCGGTCAATACTACTACATGGCGTGATTTTCATATGCGCGATTGCTGATCCC
CATGTGTATCACTGGCAA ACTGTGATGGACGACACCGTCAGTGCGTCCGTCGCGCAG
GCTCTCGATGAGCTGATGCTTTGGGCCGAGGACTGCCCCGAAGTCCGGCACCTCGTG

CACGCGGATTTTCGGCTCCAACAATGTCCTGACGGACAATGGCCGCATAACAGCGGTC
ATTGACTGGAGCGAGGCGATGTTTCGGGGATTCCCAATACGAGGTCGCCAACATCTTC
TTCTGGAGGCCGTGGTTGGCTTGTATGGAGCAGCAGACGCGCTACTTCGAGCGGAGG
CATCCGGAGCTTGCAGGATCGCCGCGGCTCCGGGCGTATATGCTCCGCATTGGTCTT
GACCAACTCTATCAGAGCTTGGTTGACGGCAATTTTCGATGATGCAGCTTGGGCGCAG
GGTCGATGCGACGCAATCGTCCGATCCGGAGCCGGGACTGTCGGGCGTACACAAATC
GCCCGCAGAAGCGCGGCCGTCTGGACCGATGGCTGTGTAGAAGTACTCGCCGATAGT
GGAAACCGACGCCCCAGCACTCGTCCGAGGGCAAAGGAA**TAG**GCTAGCTGCCGAAGC
CG**CGTGCGCCAAACAGAGCAAGAAGCGCGCTG**

Figure 87. Sequence of donor DNA repair cassettes CS-Neo-CS, CS-Phleo-CS and CS-Hyg-CS.

Insertion of the donor DNA **A.** CS-Neo-CS; **B.** CS-Phleo-CS or **C.** CS-Hyg-CS will result in replacement of the wild-type CS gene. Highlighted in **blue** the position of 30 nucleotide homology flanks used to PCR-generate the donor repair cassettes. The start (ATG) and stop (TGA/TAG) codons are in **bold**.

5.4.13 Single-guide RNA template construction.

To replace the CS gene sequence in *A. castellanii* Neff trophozoites, a double-stranded template was necessary to form single guide RNA (sgRNA) and direct the Cas9 enzyme to cleave around targeted CS gene sequence. Generation of template was accomplished by annealing and filling-in of G00 and sgRNA oligomers (sgRNACSup and sgRNACSDs). The fragments either CS-Neo-CS, CS-Phleo-CS or CS-Hyg-CS could be inserted until the formation of two double-stranded breaks and removal of wild type CS gene. The sgRNA PCR-generated resulted in small fragments roughly 100 bp (Figure 88).

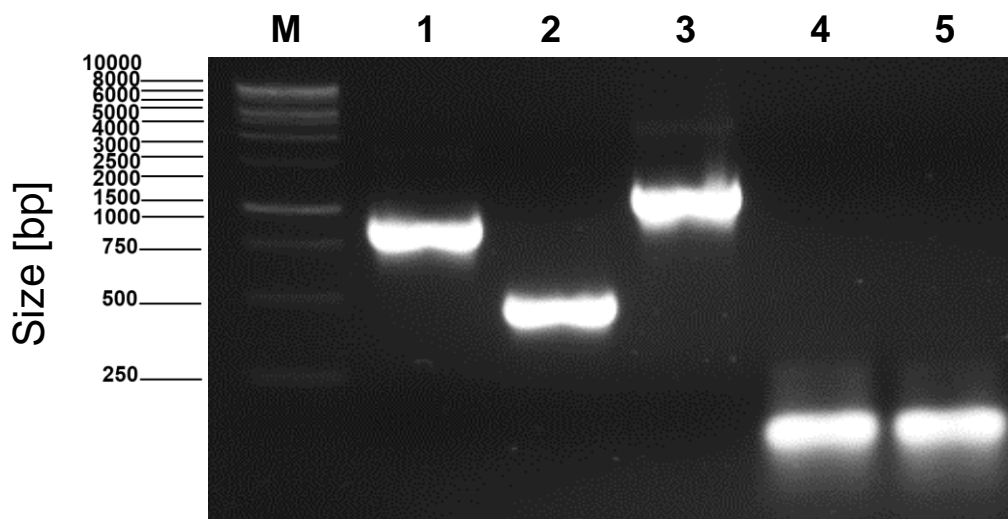


Figure 88. Agarose gel showing sgRNA templates for CRISPR-Cas9 system.

M, 1 kb DNA ladder; gel purification in sterile conditions of lane 1, CS-Neo-CS (897 bp); lane 2, CS-Phleo-CS (468 bp) and lane 3, CS-Hyg-CS (1174 bp). Lane 4, sgRNAup 5, sgRNAd primers were annealed with scaffold G00 sequence to generate ~100 bp amplicons each, further gel purified in sterile conditions. 1% agarose gel prepared with 0.5x TBE after electrophoresis 1.5, run at 120 V and dyed with ethidium bromide.

5.4.14 Robust fluorescence of *A. castellanii* Neff strain trophozoites transfected with pBRFPT7NeoCas9 compared to trophozoites transfected with pBRFPT7PhleoCas9.

Transfection using SuperFect by Qiagen® was intended with both pBRFPT7NeoCas9 and pBRFPT7PhleoCas9 constructs. However, the reagent was discontinued. The transfection assay was performed with Xfect instead using three different concentrations of G418 and phleomycin for selection (Table 19). Wild type trophozoites were transfected with Xfect polymer with either pBRFPT7NeoCas9 or pBRFPT7PhleoCas9. G418 or phleomycin was added at selection day and the addition of drug was repeated every day with a change of media every three days for the next 2-3 weeks until fluorescence microscopy analysis. Wild type trophozoites without plasmid and without Xfect polymer treatment were used as a negative control with the drug added as previously described. pBRFPNeoCas9 was used in a transfection as a positive control.

Transfected trophozoites with pBRFPT7NeoCas9 and pBRFPT7PhleoCas9 treated with high, optimal or low concentrations of G418 and phleomycin were analysed by light microscopy at 40x at 24 h, 48 h and 1 week after selection day to assess morphological changes. Trophozoites treated either with G418 or phleomycin lost their normal pleomorphic state and became rounded cells during the first 24 h with visible loss of movement at 48 h. The time of conversion from trophozoites to rounded cells depended on the concentration of the drug (low drug concentrations lead to a delay of the change in morphology and loss of mobility). A significant feature of trophozoites treated with phleomycin is that they become globular, extended cells without refraction over the granuloplasm (Figure 89 and Figure 90). Surprisingly, the WT control did not show a decline in cell number or significant cell death compared to the transfected cells, making it challenging to discern if cells were truly selected by the addition of the drugs.

Around week 3 post-transfection, fluorescence microscopy analysis was carried out with parasites selected at high, optimal and low dose of G418 or phleomycin. The parasites treated with a high dose of G418 or phleomycin showed a robust fluorescence signal compared to those treated with the medium and low dose (data not shown).

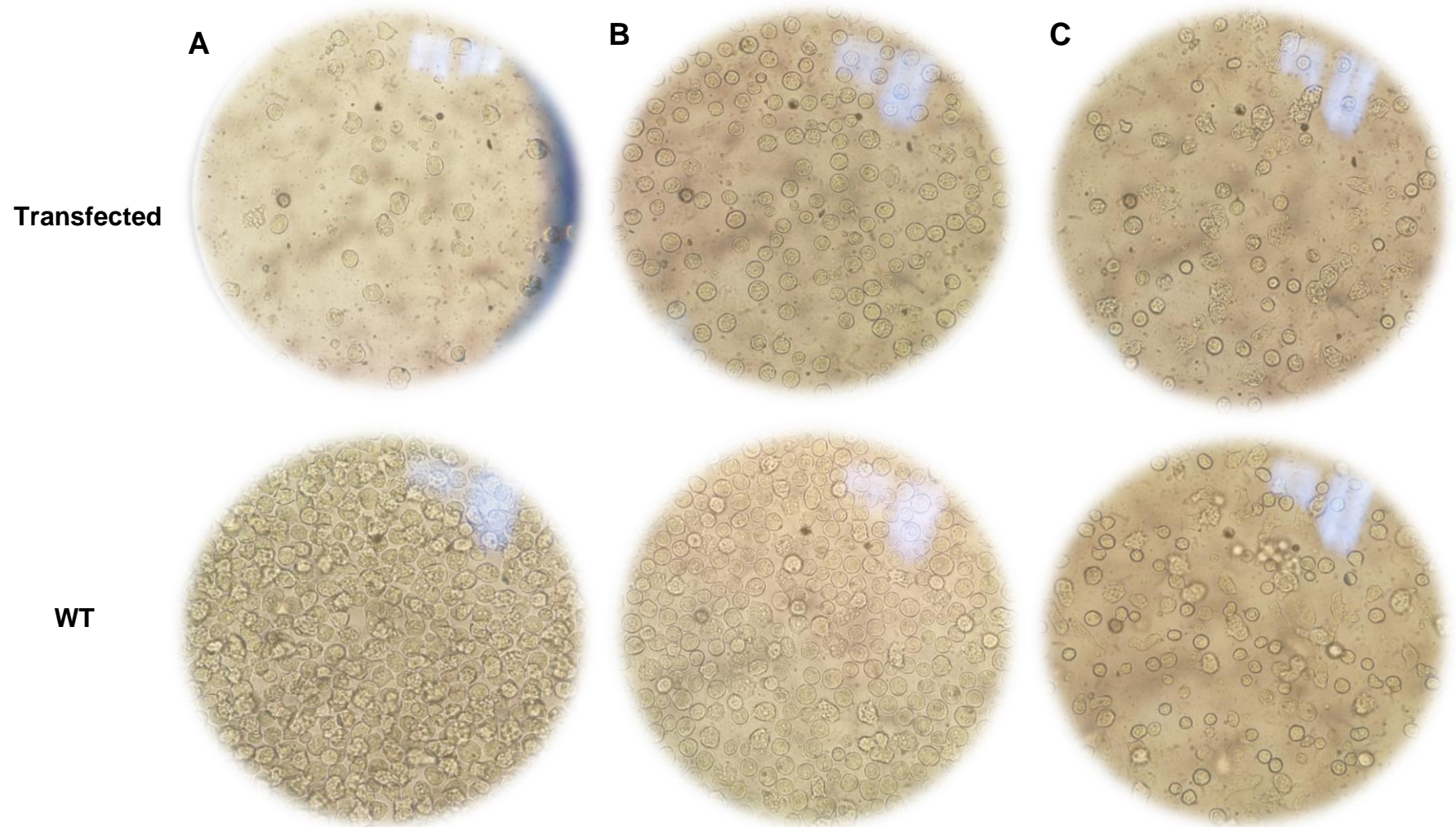
Notably, all the images in the TRITC channel in Figure 91 A, B and C shows a higher fluorescence intensity of RFP in *A. castellanii* Neff trophozoites transfected with

pBRFPT7NeoCas9 than trophozoites transfected with pBRFPT7PhleoCas9. Additionally, these images clearly display a dark nucleus and a robust fluorescence throughout the cytoplasm. Opposite, in Figure 91 D, the nucleus is not visible, the red fluorescence intense is dim with dark background distribution through the whole cytoplasm and the fluorescence seems concentrated in the contractile vacuoles as red spots, suggesting a poor expression.

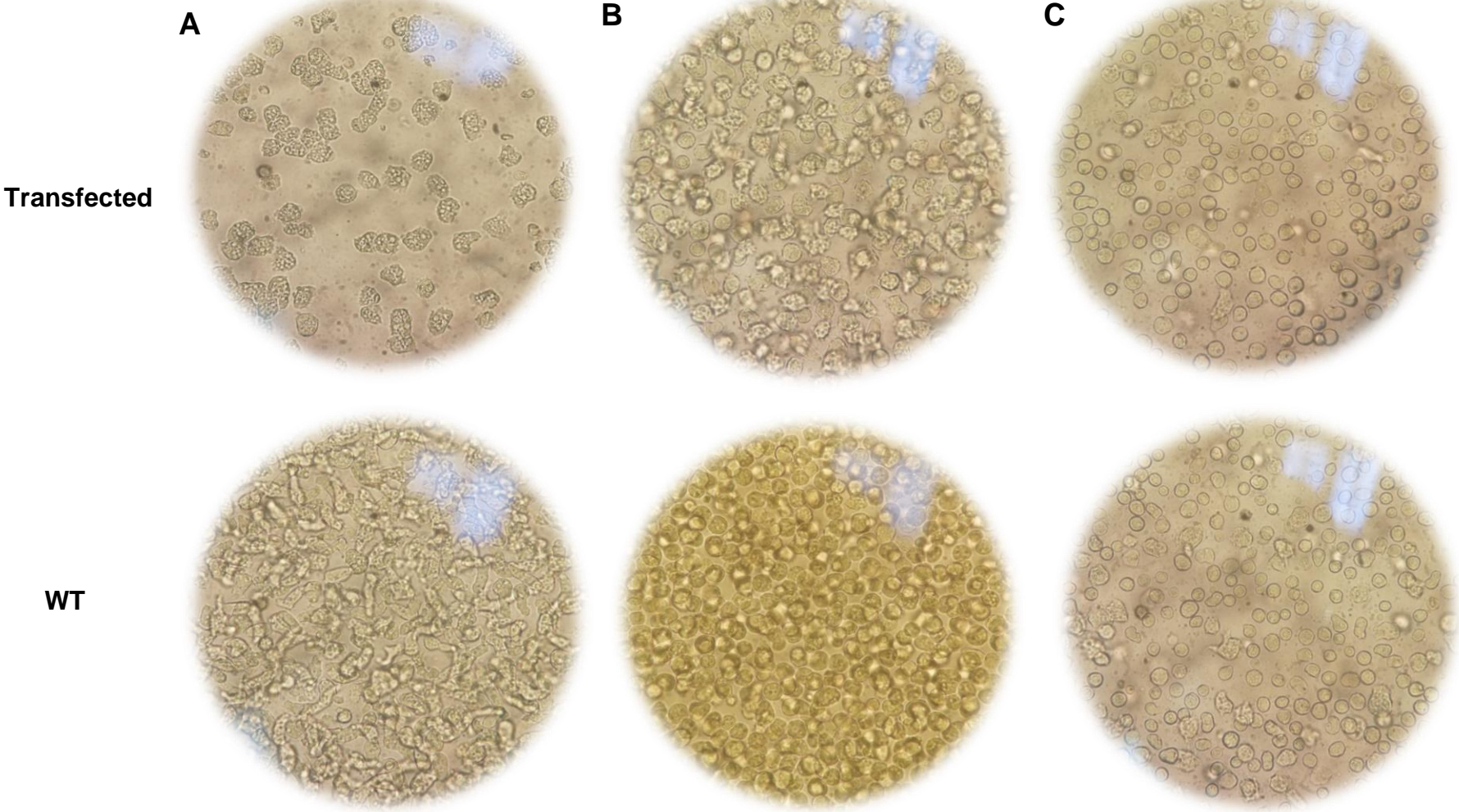
The negative control (trophozoites treated with G418) in figure 91 E and F show a complete dark background with low signal of red fluorescence, which suggests potential autofluorescence. The positive control pBRFPNeoCas9 was not analysed.

The results confirm expression of RFP driven by the SV40 promoter from both pBRFPT7NeoCas9 and pBRFPT7PhleoCas9, however the construct carrying the Neo resistance gene offers a strong fluorescent signal in some cells compared to a low fluorescence in cells carrying the Phleo gene.

Transfection with pBRFPT7NeoCas9 treated with High dose (6.2 µg/ml) of G418



Transfection with pBRFPT7NeoCas9 treated with Optimal dose (3.1 µg/ml) of G418



Transfection with pBRFPT7NeoCas9 treated with Low dose (1.55 µg/ml) of G418

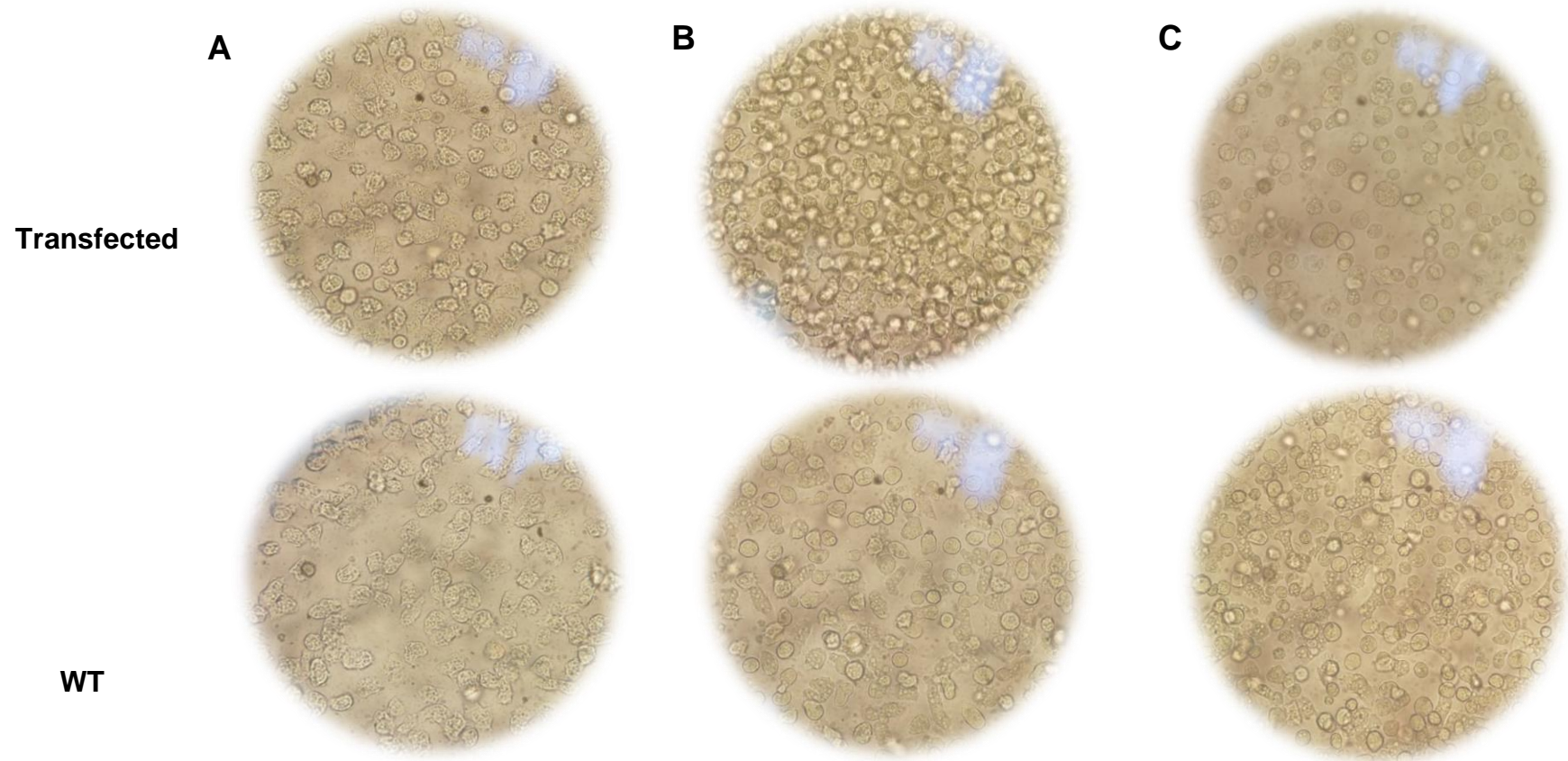
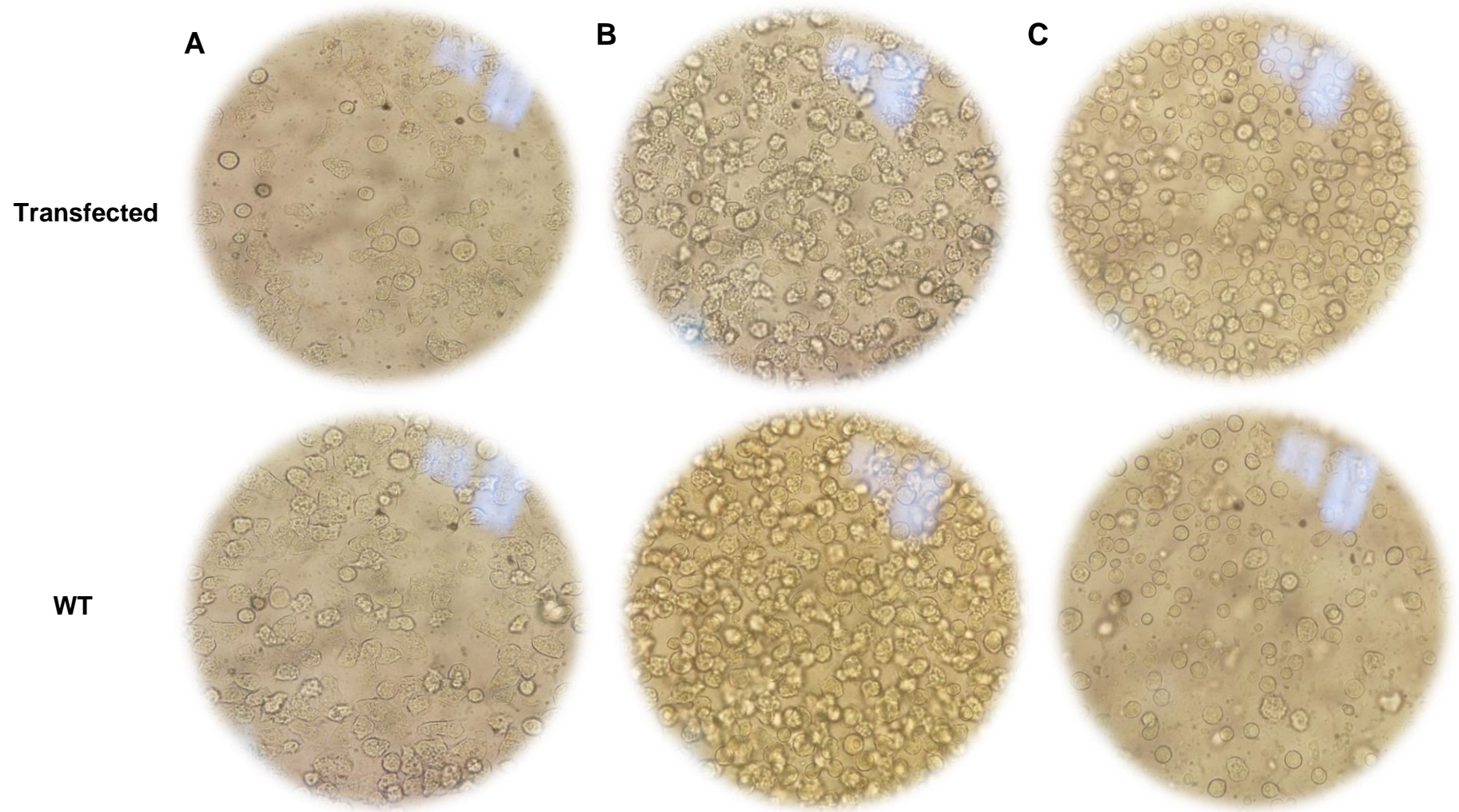


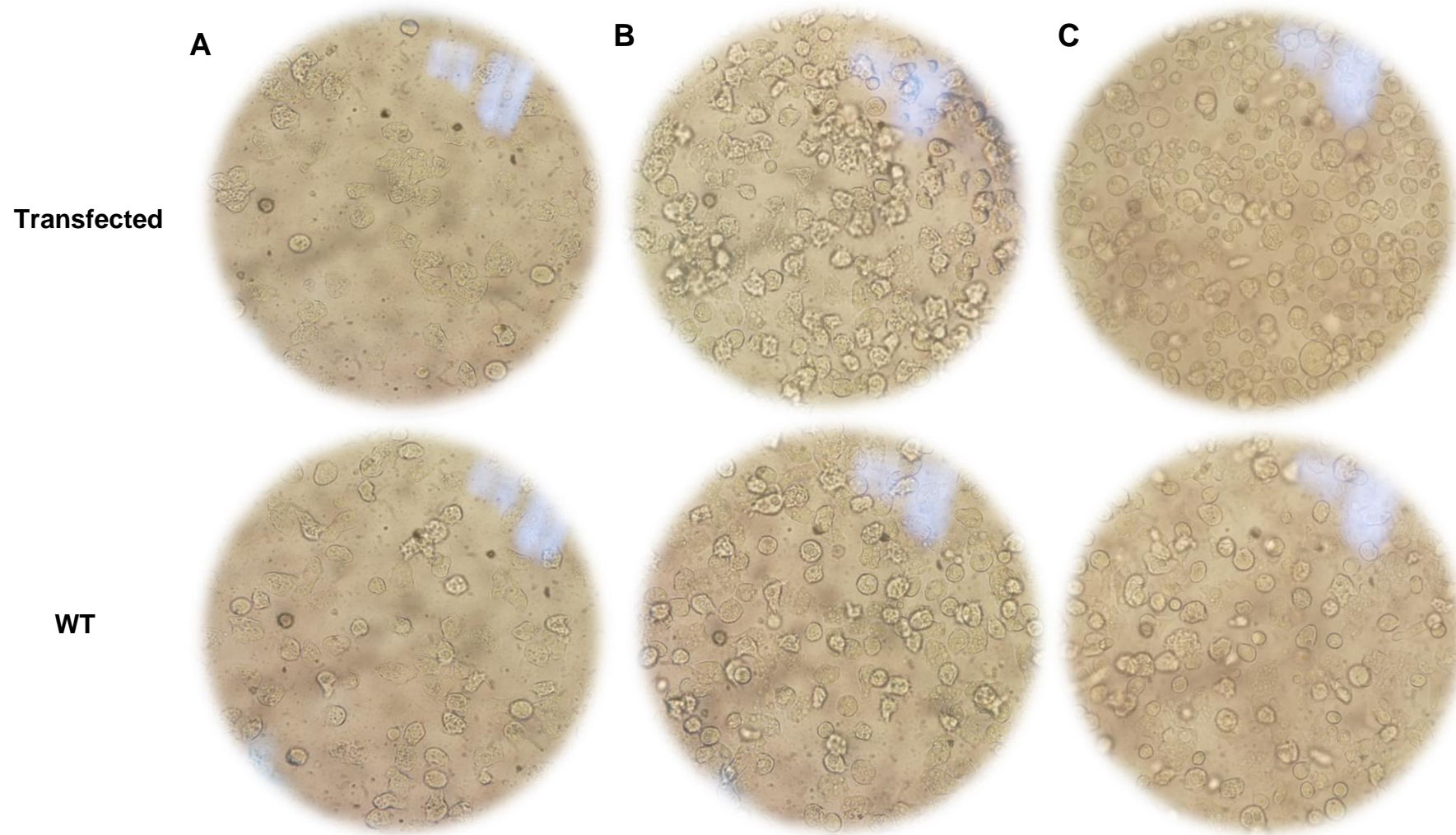
Figure 89. Transfection efficiency of *A. castellanii* Neff trophozoites with pBRFPT7NeoCas9

Differences in cell number and shape post transfection utilising high, optimal and low doses of G418 for one week are observed. A. 1 day; B. 3 days; C. 7 days post transfection. WT: Wild type cells (Negative control). Images were taken at 40x utilising Axiovert Zeiss 25 Light microscope.

Transfection with pBRFPT7PhleoCas9 treated with High dose (0.53 $\mu\text{g/ml}$) of Phleomycin



Transfection with pBRFPT7PhleoCas9 treated with Optimal dose (0.26 $\mu\text{g/ml}$) of Phleomycin



Transfection with pBRFPT7PhleoCas9 treated with Low dose (0.13 µg/ml) of Phleomycin

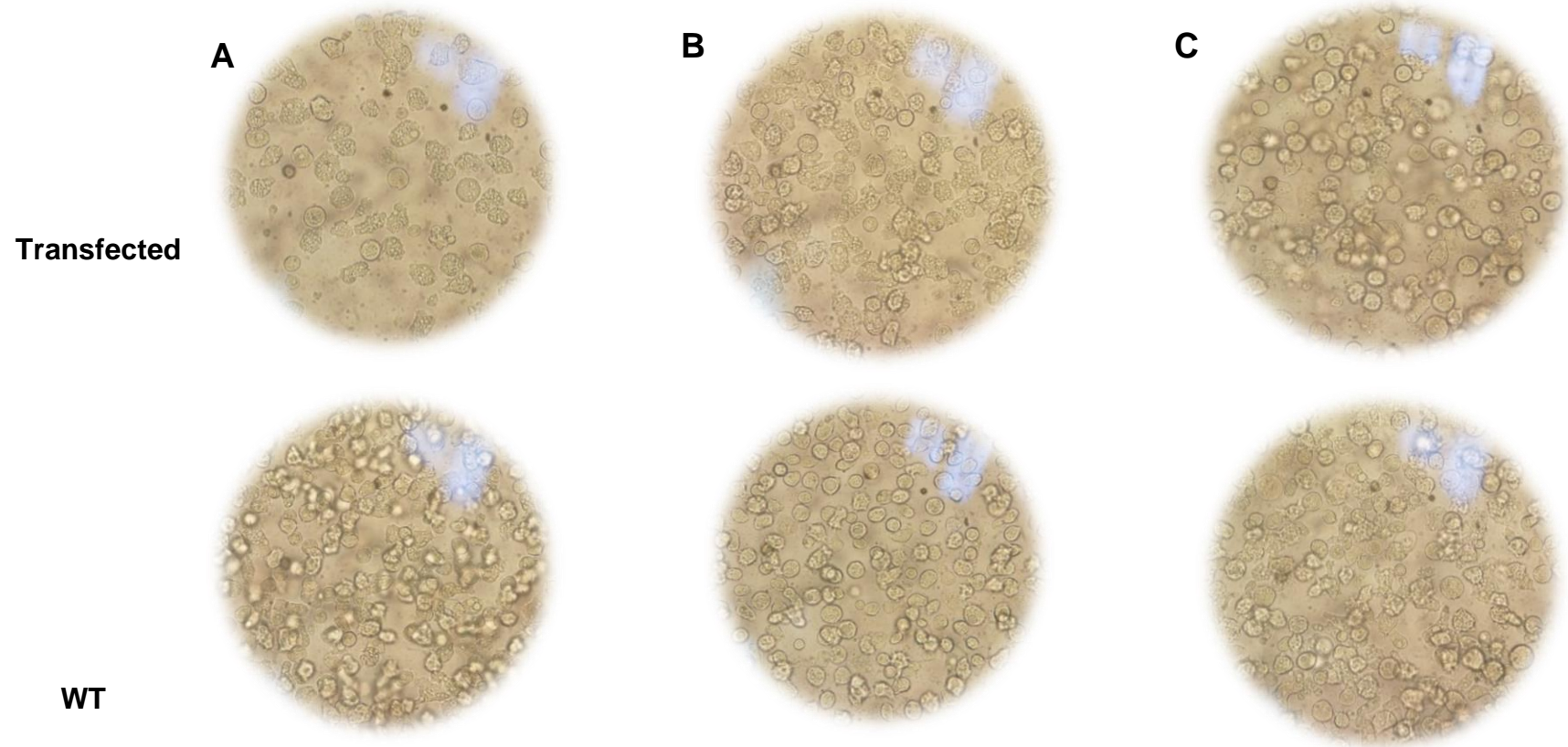
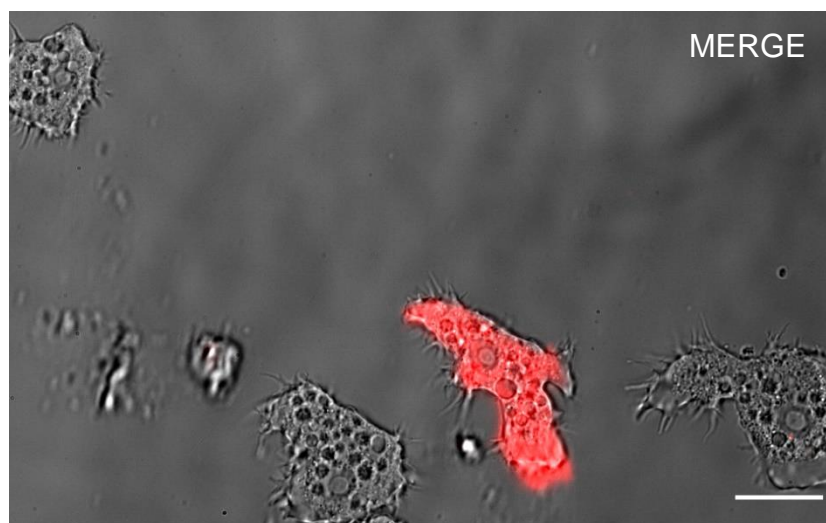
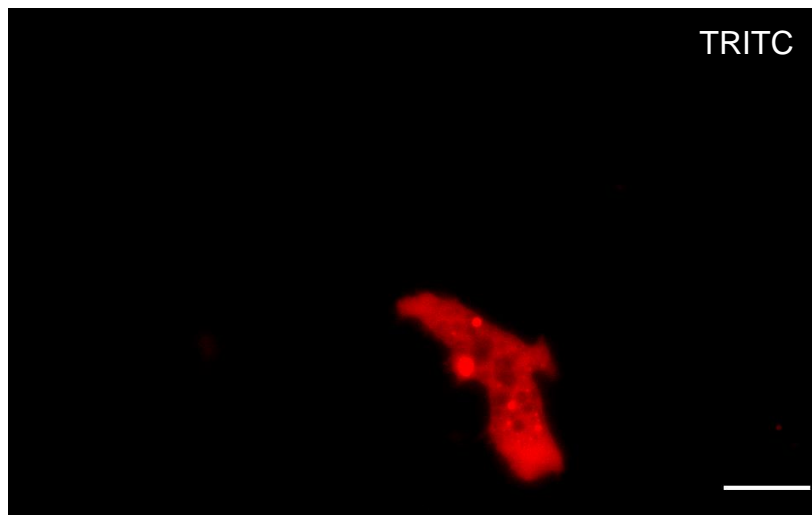
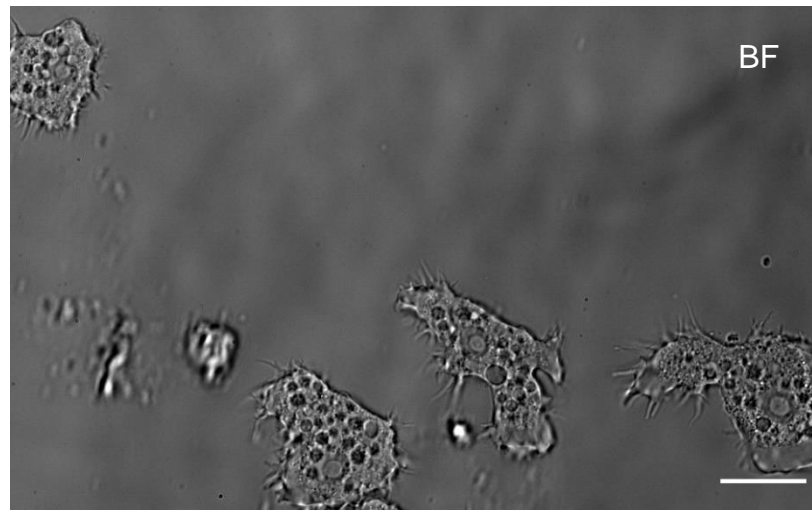


Figure 90. Transfection efficiency of *A. castellanii* Neff trophozoites with pBRFPT7PhleoCas9

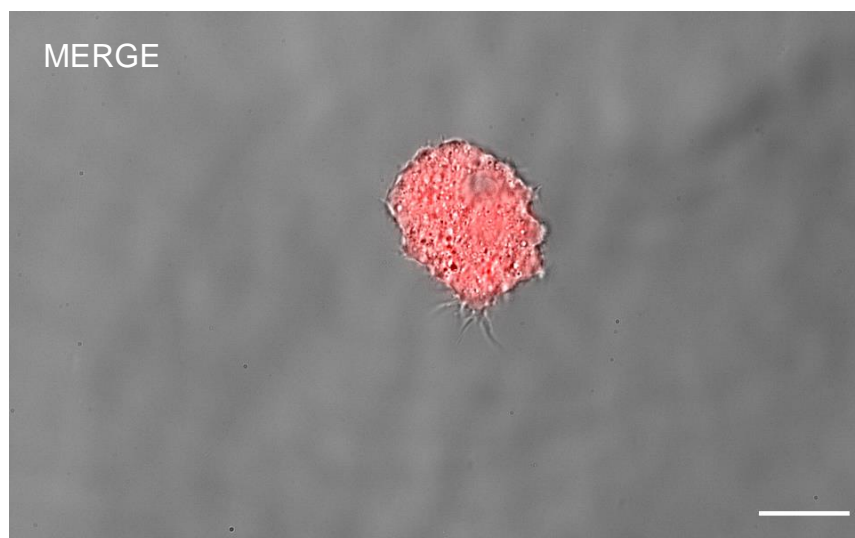
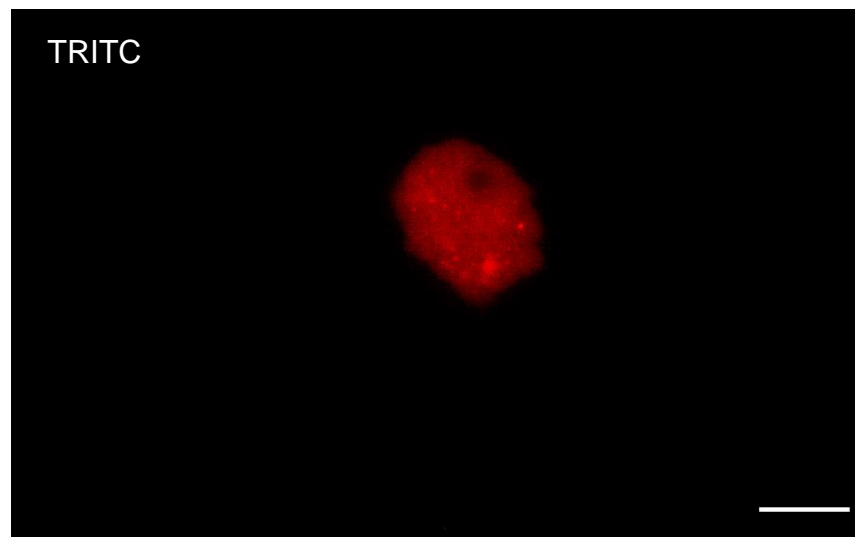
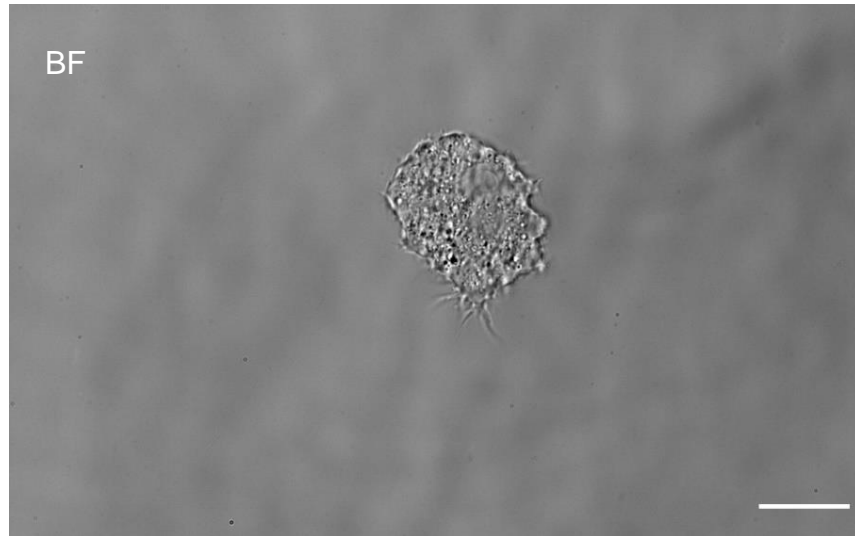
Differences in cell number and shape post transfection utilising high, optimal and low doses of Phleomycin for one week are observed. A representative image was taken for each culture. **A.** 1 day; **B.** 3 days; **C.** 7 days post transfection. WT: Wild type cells (Negative control). Images were taken at 40x utilising Axiovert Zeiss 25 Light microscope.

pBRFPT7NeoCas9

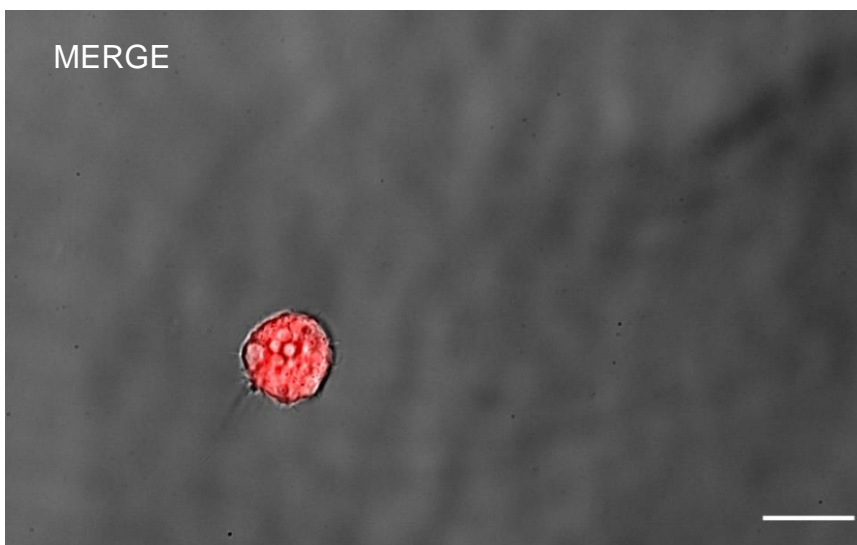
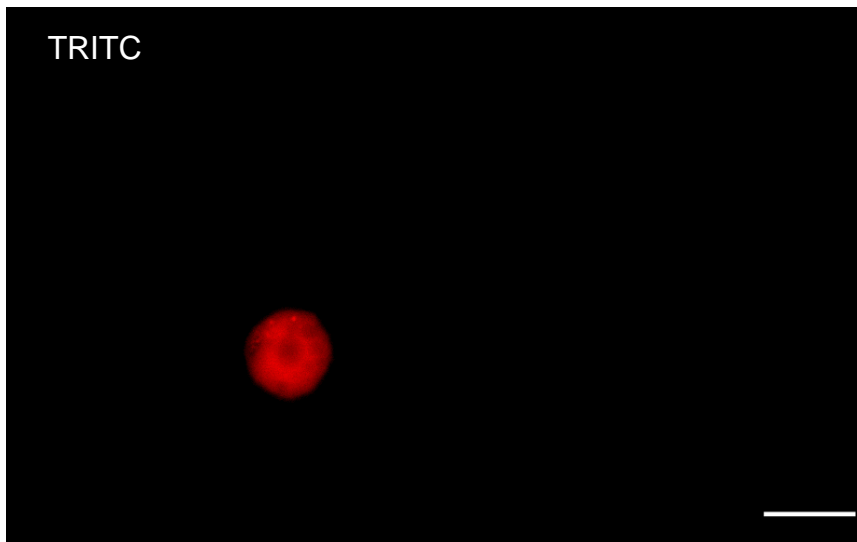
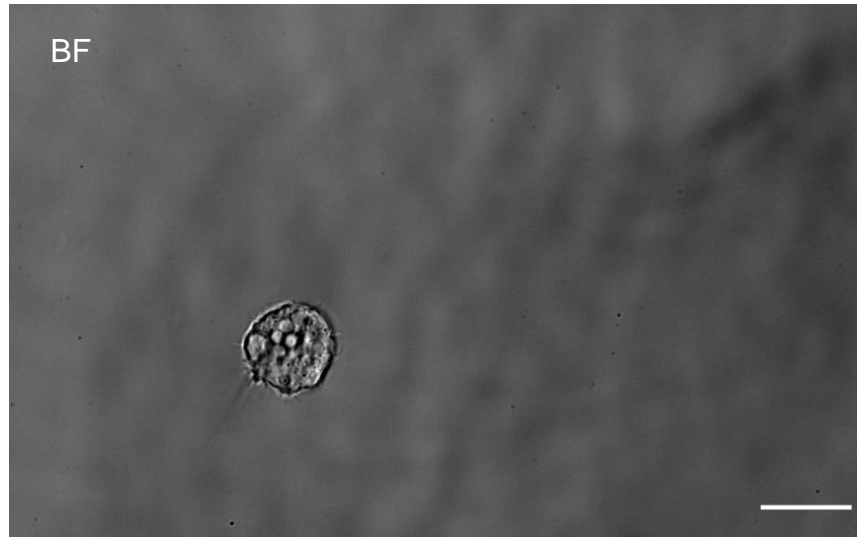
A.



B.

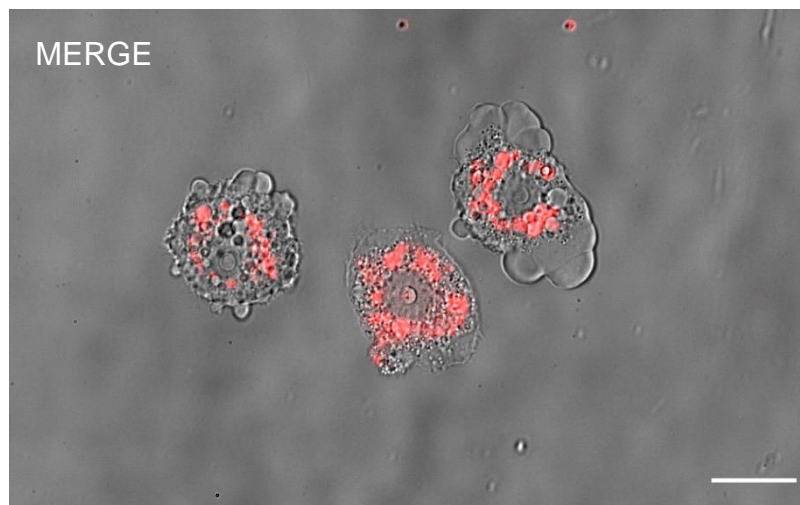
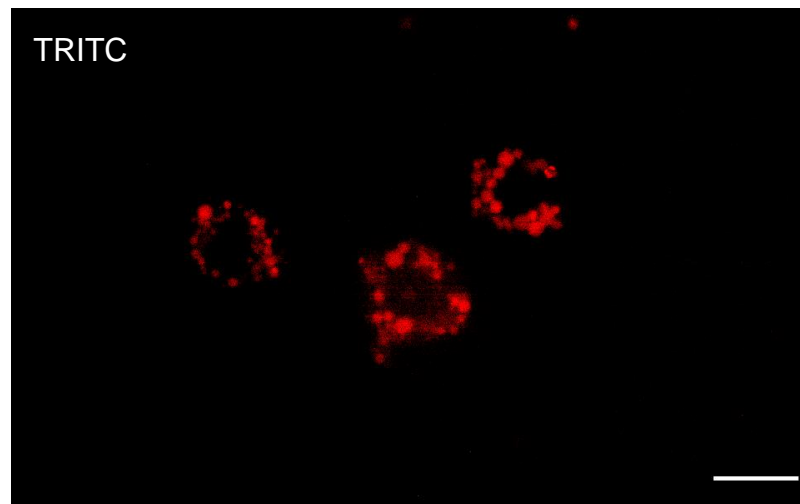
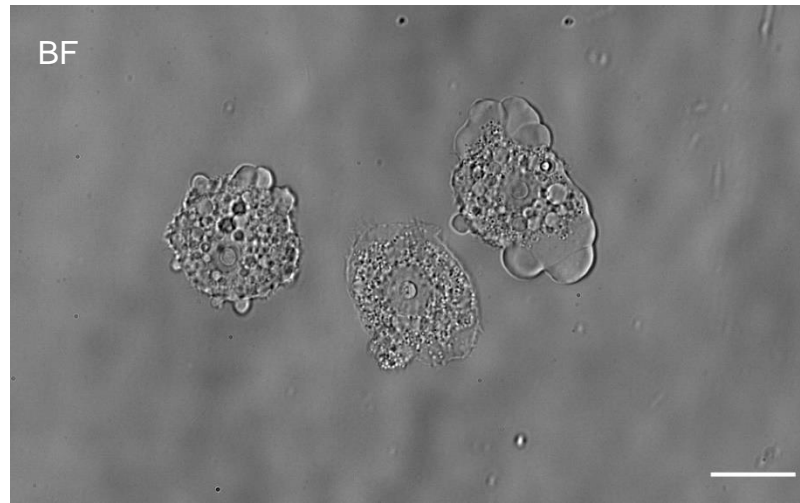


C.



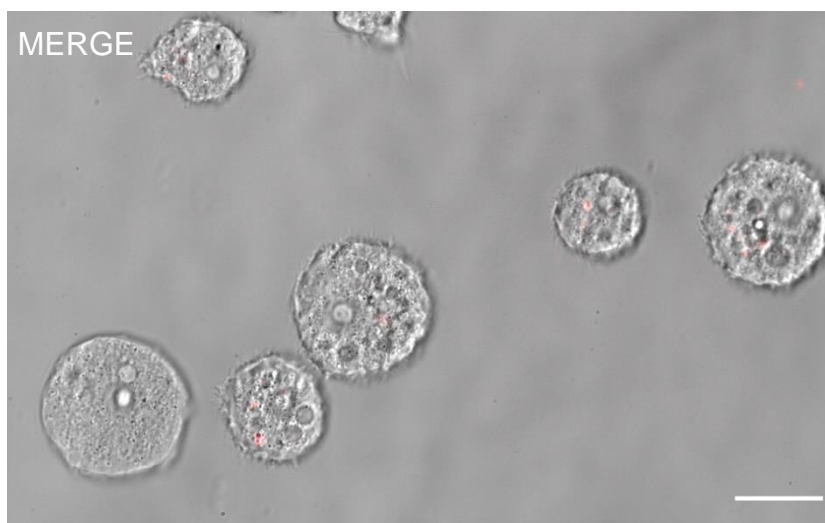
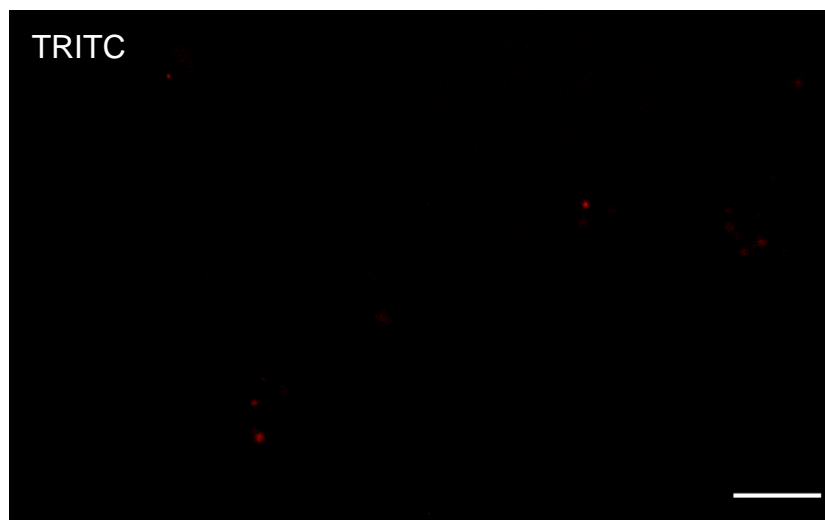
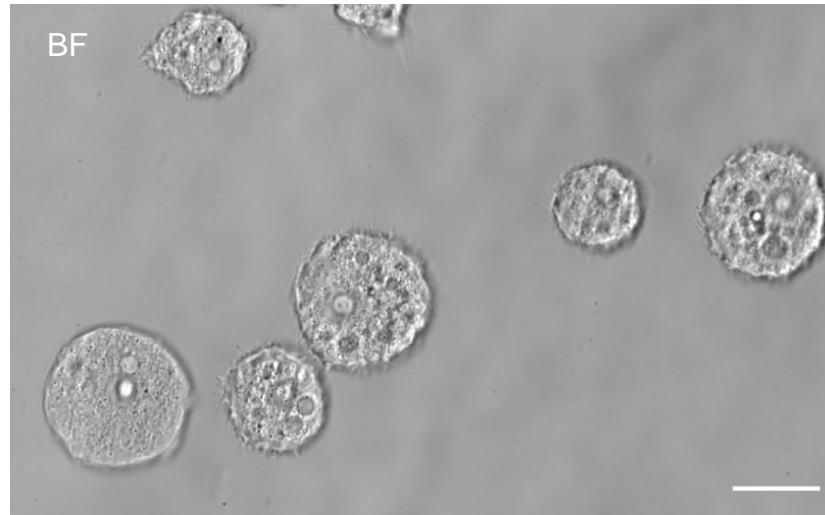
pBRFPPhleCas9

D.



Wild type (Negative control)

E.



F.

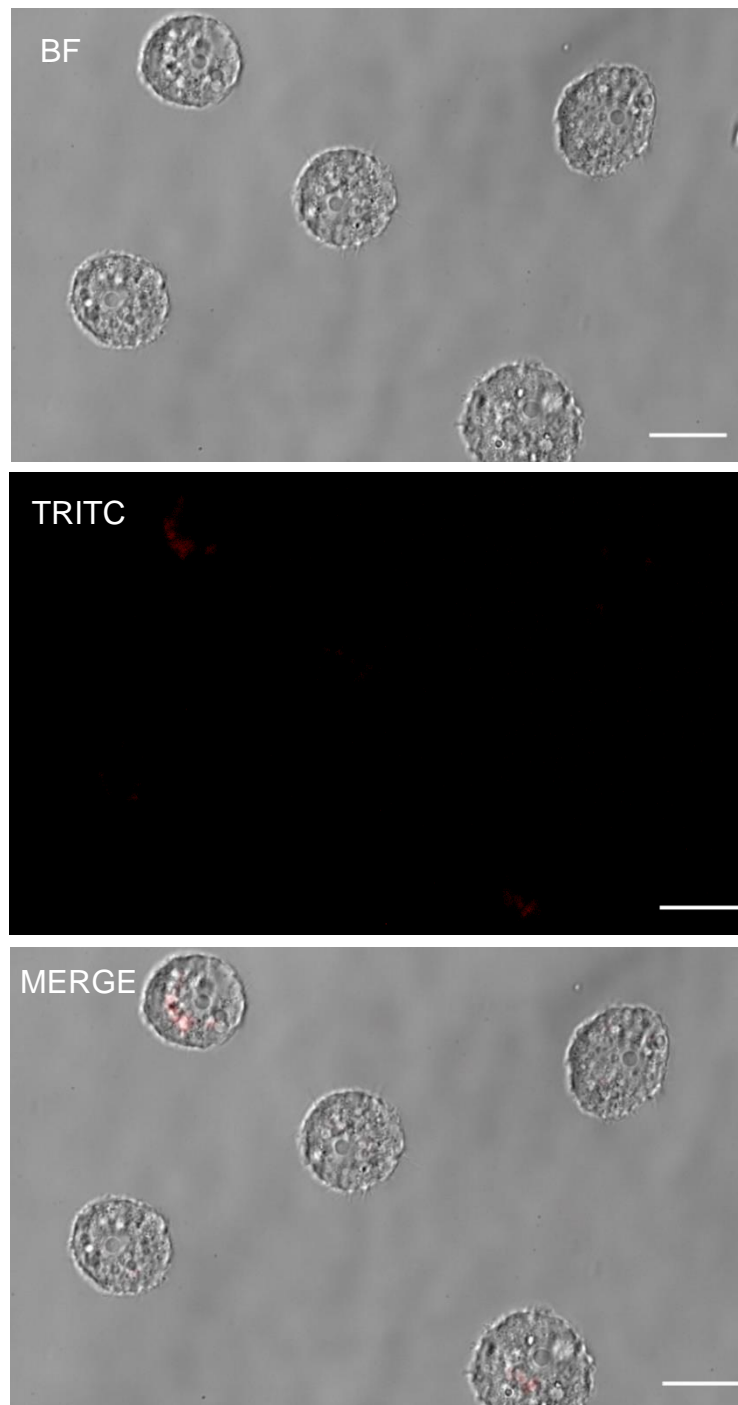


Figure 91. Transfection efficiency of pBRFPT7NeoCas9 and pBRFPPhleCas9 expression in *A. castellanii* trophozoites utilising Xfect reagent analysed by confocal microscopy

A., B., and C. Trophozoites transfected with pBRFPT7NeoCas9 treated with high dose (6.2 $\mu\text{g/ml}$) of G418. **D.** Trophozoites transfected with pBRFPT7PhleoCas9 treated with 0.53 $\mu\text{g/ml}$ of Phleomycin. **E. and F.** Wild type trophozoites treated with high dose (6.2 $\mu\text{g/ml}$) of G418. Magnification: 60x. The analysis was carried out utilising a Nikon Eclipse 600 Epifluorescent Upright Microscope (Nikon, USA) under TRITC filter with Ex_{max} . 540 nm/DM 565 and Em_{max} . 605/55. Scale bar: 20 μm .

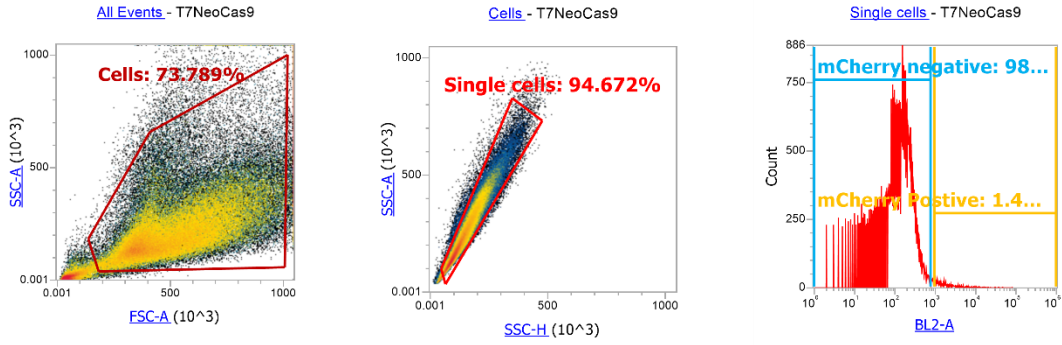
5.4.15 Red fluorescent protein (RFP) expression in *A. castellanii* Neff trophozoites transfected with pBRFPT7NeoCas9 and pBRFPPhleCas9 confirmed by Flow Cytometry.

The expression of RFP in Neff trophozoites transfected with pBRFPT7NeoCas9 and pBRFPPhleCas9 and treated with a high dose of G418 (6.2 µg/ml) or Phleomycin (0.53 µg/ml) respectively, was confirmed using an AttuneNxt flow cytometer (Invitrogen).

The fluorescence pattern was determined by flow cytometry detected by spectra of $E_{x_{max}}$. 587 nm and $E_{m_{max}}$. 610 nm. Even though the percentage of cells showing red fluorescence is low in trophozoites transfected with pBRFPT7NeoCas9 (1.462% gated) (Figure 92, A.), it is almost 100-fold higher than for those transfected with pBRFPT7PhleoCas9 (0.016% gated) (Figure 92, B.) but twofold lower than the positive control pBRFPNeoCas9 (3.255% gated) (Figure 92, C.). The red fluorescence signal displayed by cells transfected with pBRFPT7PhleoCas9 is comparable to the autofluorescence signal detected in the negative control, wild type trophozoites (0.015% gated) (Figure 92, D.). The results are summarised as overlay in Figure 92, E.

These results confirm the level of fluorescence expression previously observed in confocal microscopy comparing pBRFPT7NeoCas9 and pBRFPT7PhleoCas9 (see Figure 91).

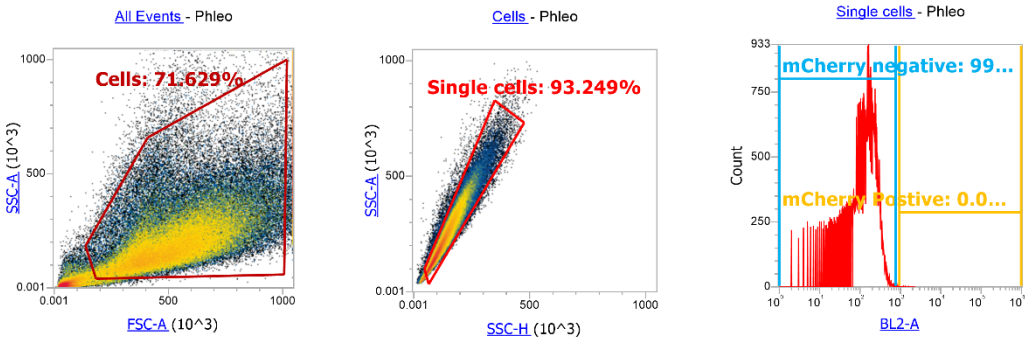
A.



Experiment: **Experiment(1)**
 Group: **Group**
 Sample: **T7NeoCas9**
 Time Recorded: **14:52:20**

Name	Gate	X Parameter	Y Parameter	Count	%Total	%Gated
▣ All Events	All Events	N/A	N/A	135,522	100.000	100.000
▣ Cells	Cells	FSC - FSC-A	SSC - SSC-A	100,000	73.789	73.789
▣ Single cells	Single cells	SSC - SSC-H	SSC - SSC-A	94,672	69.857	94.672
▣ mCherry Postive	mCherry Postive	BL2 - BL2-A		1,384	1.021	1.462
▣ mCherry negative	mCherry negative	BL2 - BL2-A		92,794	68.472	98.016

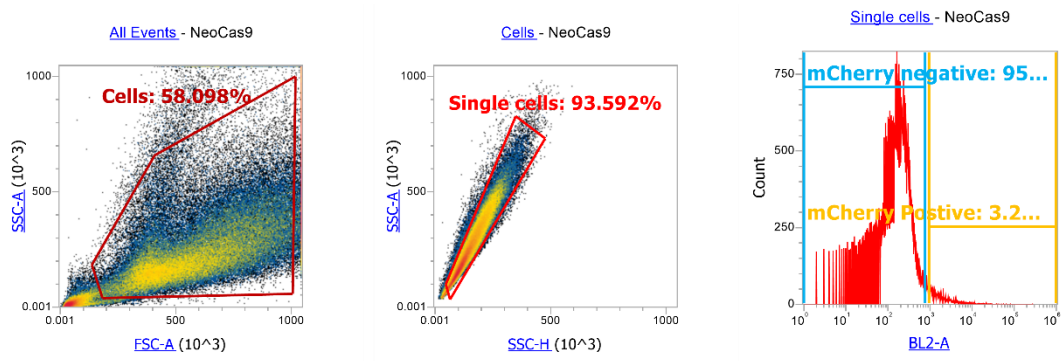
B.



Experiment: **Experiment(1)**
 Group: **Group**
 Sample: **Phleo**
 Time Recorded: **14:50:17**

Name	Gate	X Parameter	Y Parameter	Count	%Total	%Gated
▣ All Events	All Events	N/A	N/A	139,608	100.000	100.000
▣ Cells	Cells	FSC - FSC-A	SSC - SSC-A	100,000	71.629	71.629
▣ Single cells	Single cells	SSC - SSC-H	SSC - SSC-A	93,249	66.793	93.249
▣ mCherry Postive	mCherry Postive	BL2 - BL2-A		15	0.011	0.016
▣ mCherry negative	mCherry negative	BL2 - BL2-A		93,205	66.762	99.984

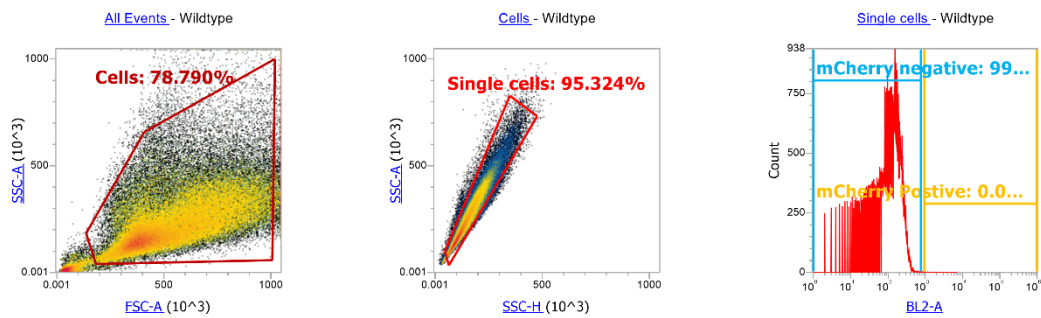
C.



Experiment: **Experiment(1)**
 Group: **Group**
 Sample: **NeoCas9**
 Time Recorded: **14:57:53**

Name	Gate	X Parameter	Y Parameter	Count	%Total	%Gated
▣ All Events	All Events	N/A	N/A	172,124	100.000	100.000
▣ Cells	Cells	FSC - FSC-A	SSC - SSC-A	100,000	58.098	58.098
▣ Single cells	Single cells	SSC - SSC-H	SSC - SSC-A	93,592	54.375	93.592
▣ mCherry Postive	mCherry Postive	BL2 - BL2-A		3,046	1.770	3.255
▣ mCherry negative	mCherry negative	BL2 - BL2-A		89,649	52.084	95.787

D.



Experiment: **Experiment(1)**
 Group: **Group**
 Sample: **Wildtype**
 Time Recorded: **15:00:03**

Name	Gate	X Parameter	Y Parameter	Count	%Total	%Gated
▣ All Events	All Events	N/A	N/A	126,920	100.000	100.000
▣ Cells	Cells	FSC - FSC-A	SSC - SSC-A	100,000	78.790	78.790
▣ Single cells	Single cells	SSC - SSC-H	SSC - SSC-A	95,324	75.106	95.324
▣ mCherry Postive	mCherry Postive	BL2 - BL2-A		14	0.011	0.015
▣ mCherry negative	mCherry negative	BL2 - BL2-A		95,302	75.088	99.977

E.

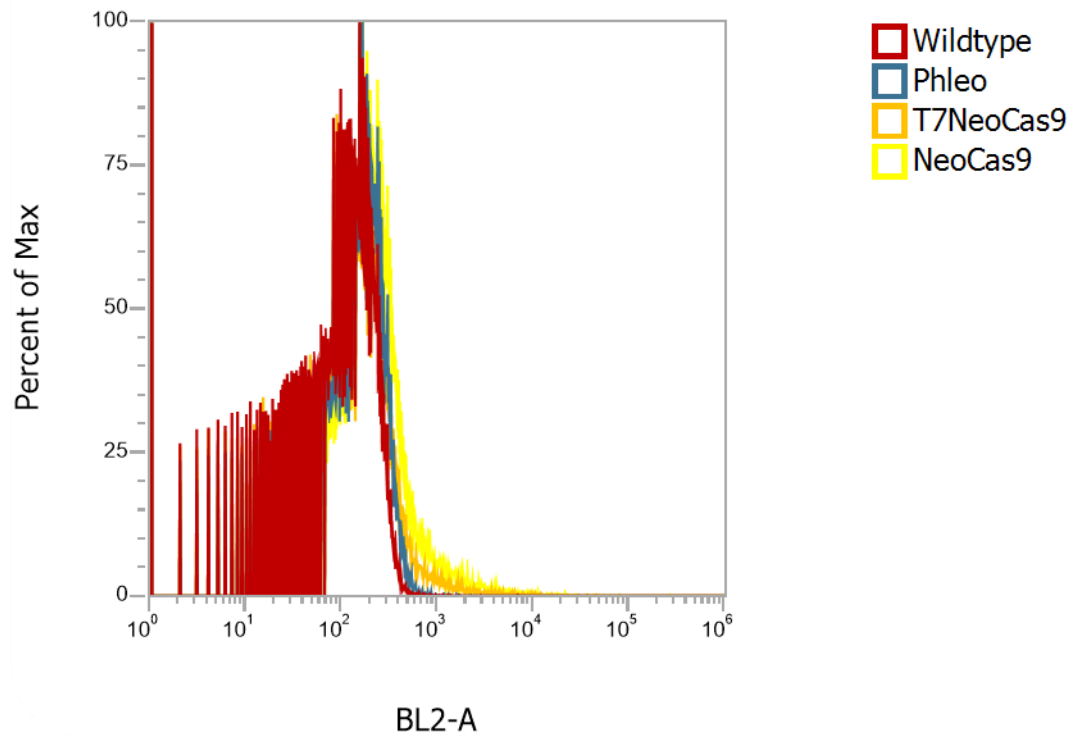


Figure 92. Flow cytometry analysis of trophozoites transfected with pBRFPT7NeoCas9 and pBRFPT7PhleoCas9

A. Trophozoites transfected with pBRFPT7NeoCas9; **B.** Trophozoites transfected with pBRFPT7PhleoCas9; **C.** Positive control (trophozoites transfected with pBRFPNeoCas9); and **D.** Negative control (Wild type trophozoites); **E.** Overlay. Abbreviations: FSC: forward scatter, SSC: side scatter, BL2 channel for blue excitation laser-488 nm and emission filter 574/26 nm.

5.4.16 Different level of red fluorescent protein (RFP) expression in *A. castellanii* Neff trophozoites transfected with pBRFPT7NeoCas9 observed in Fluorescence microscopy after Fluorescence-activated cell sorting (FACS).

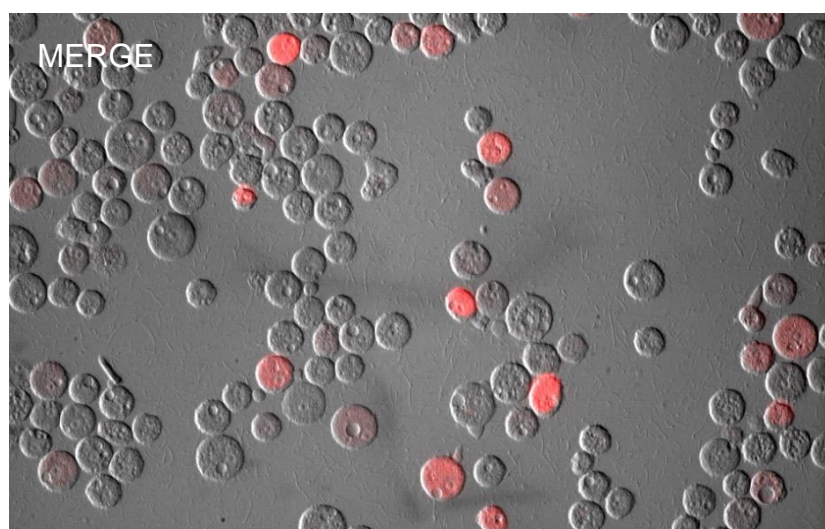
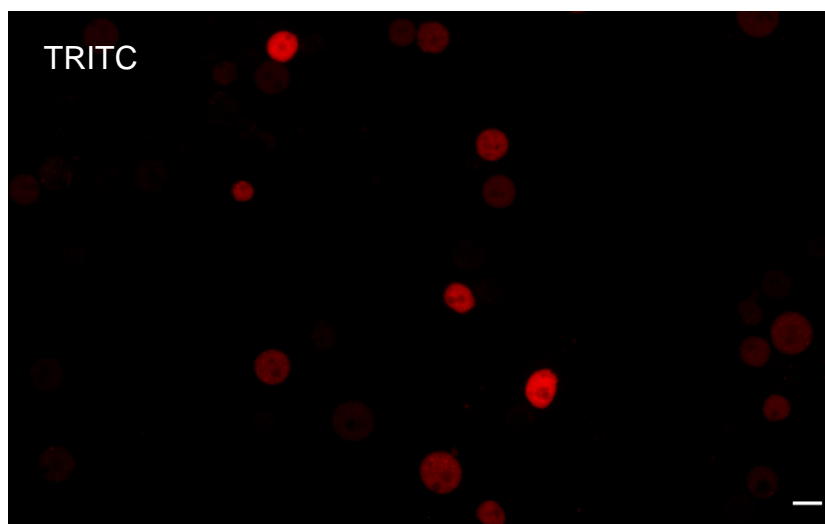
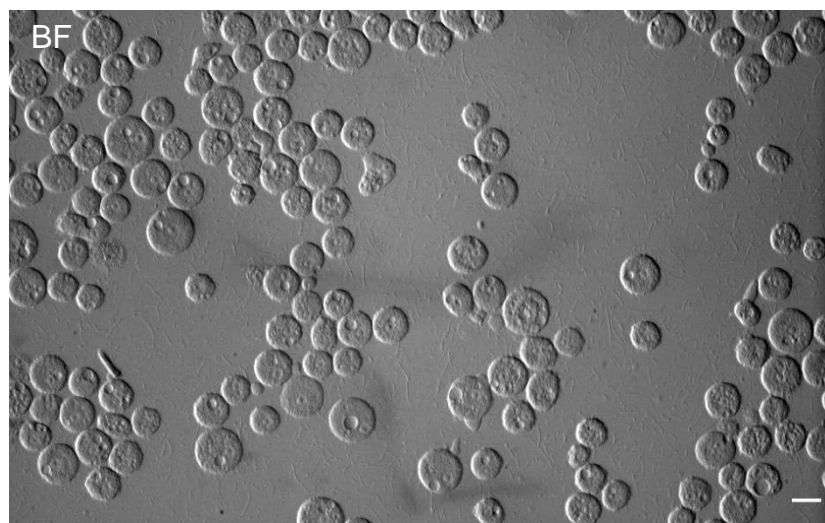
The red fluorescent protein (RFP) expression was visually analysed by fluorescence microscopy after FACS.

Figure 93, A and B show a considerable number of positive transfectants pooled together by FACS which displayed different levels of red fluorescence intensity.

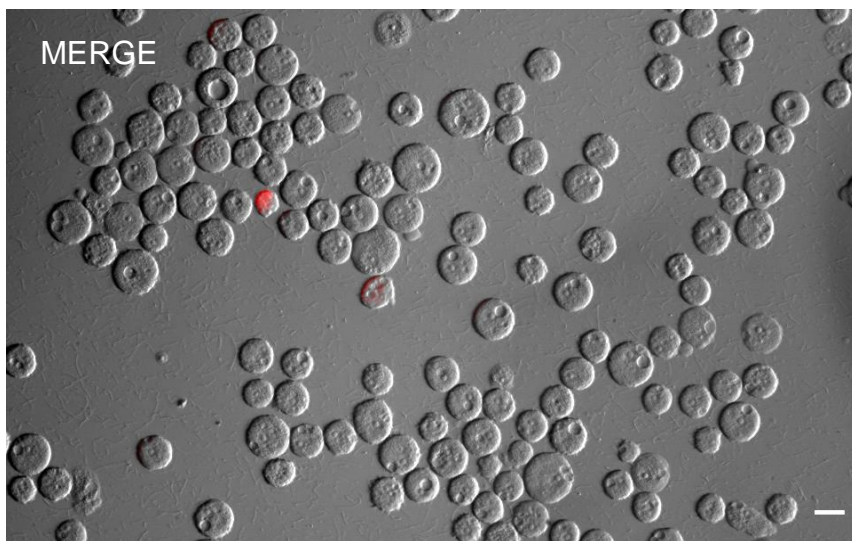
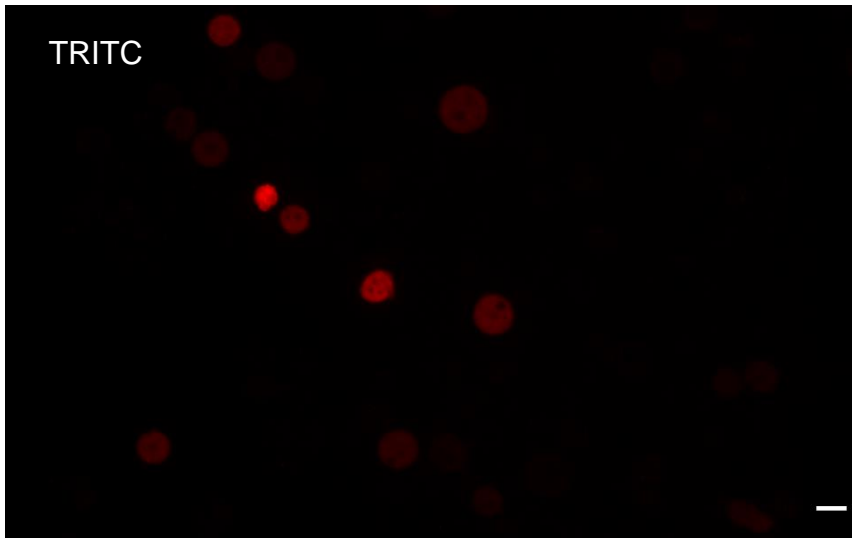
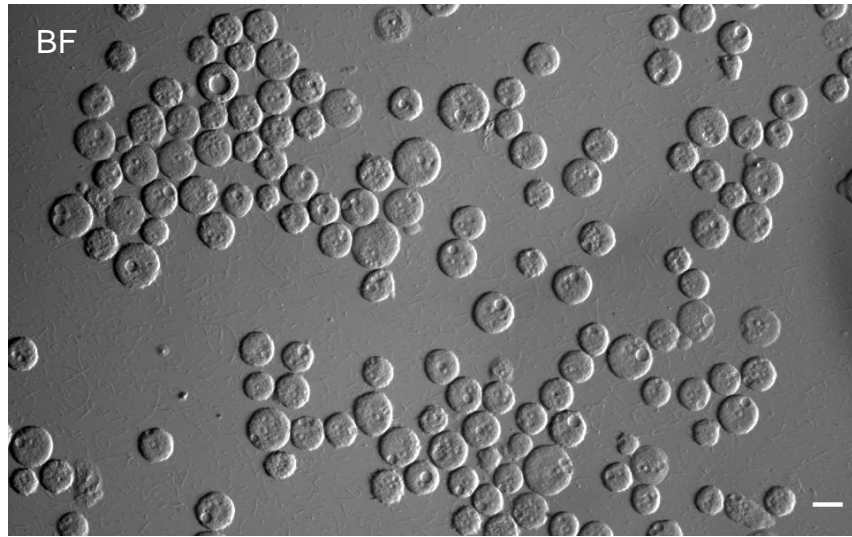
Figure 93 C displays the wild type trophozoites with no apparent red fluorescence.

Transfected Neff trophozoites with pBRFPT7NeoCas9 and treated with high dose of G418 post-FACS.

A.



B.



Wild type Neff trophozoites treated with G418 post-FACS

C.

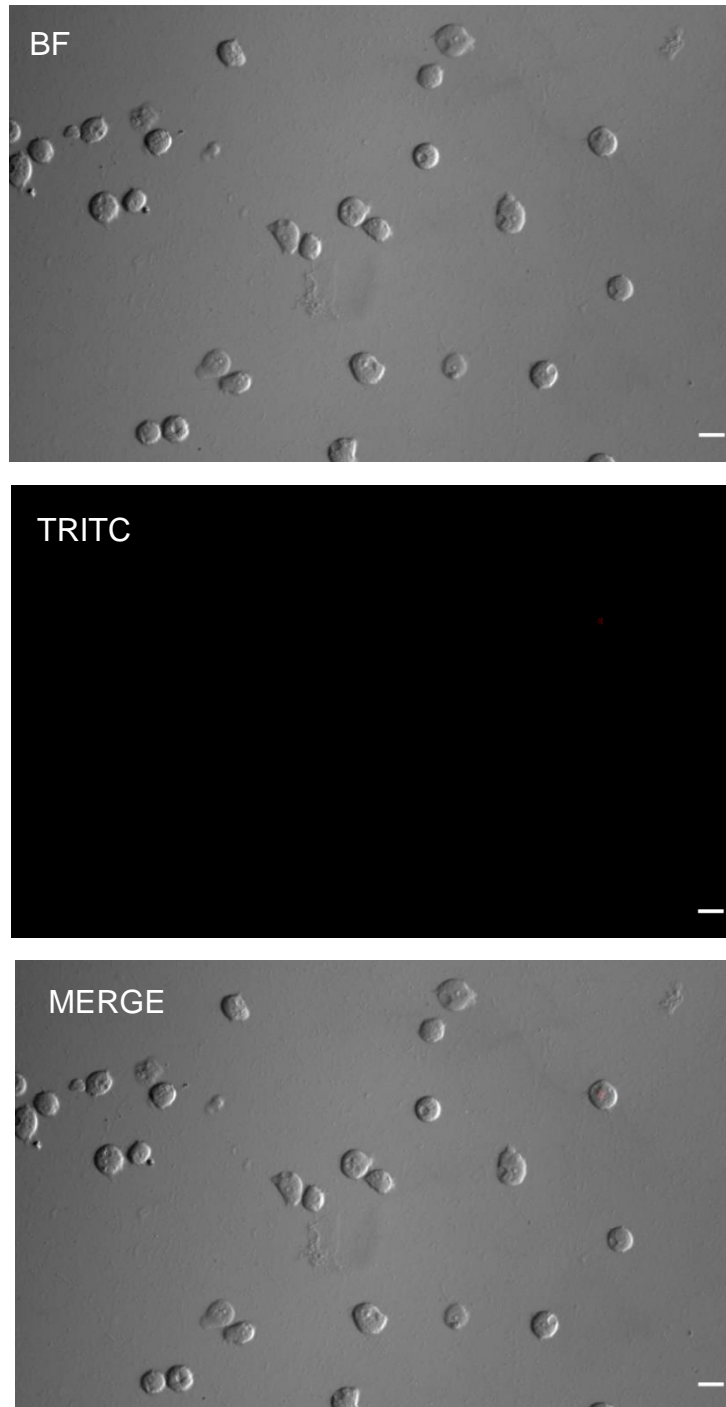


Figure 93. Analysis of FACS-sorted *A. castellanii* Neff trophozoites transfected with pBRFPT7NeoCas9 analysed by fluorescence microscopy

A. and **B.** Trophozoites transfected with pBRFPT7NeoCas9 treated with high dose (6.2 $\mu\text{g/ml}$) of G418 observed post-FACS. **C.** Wild type trophozoites treated with high dose (6.2 $\mu\text{g/ml}$) of G418 observed post-FACS. Magnification: 20 \times . The analysis was carried out utilising a Nikon Eclipse 600 Epifluorescent Upright Microscope (Nikon, USA) under TRITC filter with Ex_{max} . 540 nm/DM 565 and Em_{max} . 605/55. Scale bar: 20 μm .

5.4.17 Red fluorescent protein (RFP) expression in *A. castellanii* Neff trophozoites transfected with pBRFPT7NeoCas9 confirmed by Flow Cytometry post-FACS.

Trophozoites were cultured, harvested, and counted to reach a concentration of 1×10^7 cells/ml to perform a second FACS Purity type (Figure 94) with MoFlo XDP Cell Sorter (Beckman Coulter Life Sciences).

Flow cytometry analysis using Ex_{max} . 587 nm and Em_{max} . 610 nm verified a robust increase of gated cells (26.044%) (Figure 95, A), which shows a successful FACS sorting when compared with non-sorted cell populations (positive 0.201 % and negative 0.064% gated) (Figure 95, B and C).

The wild type (Figure 95, D) population of trophozoites treated with G418 did not show any signal when analysed, confirming any fluorescence signal in the previous fluorescence microscopy analysis (Figure 91, E and F).

A substantial increase of positive transfectants sorted carrying pBRFPT7NeoCas9 expressing RFP is observed in the overlay (Figure 95, E).

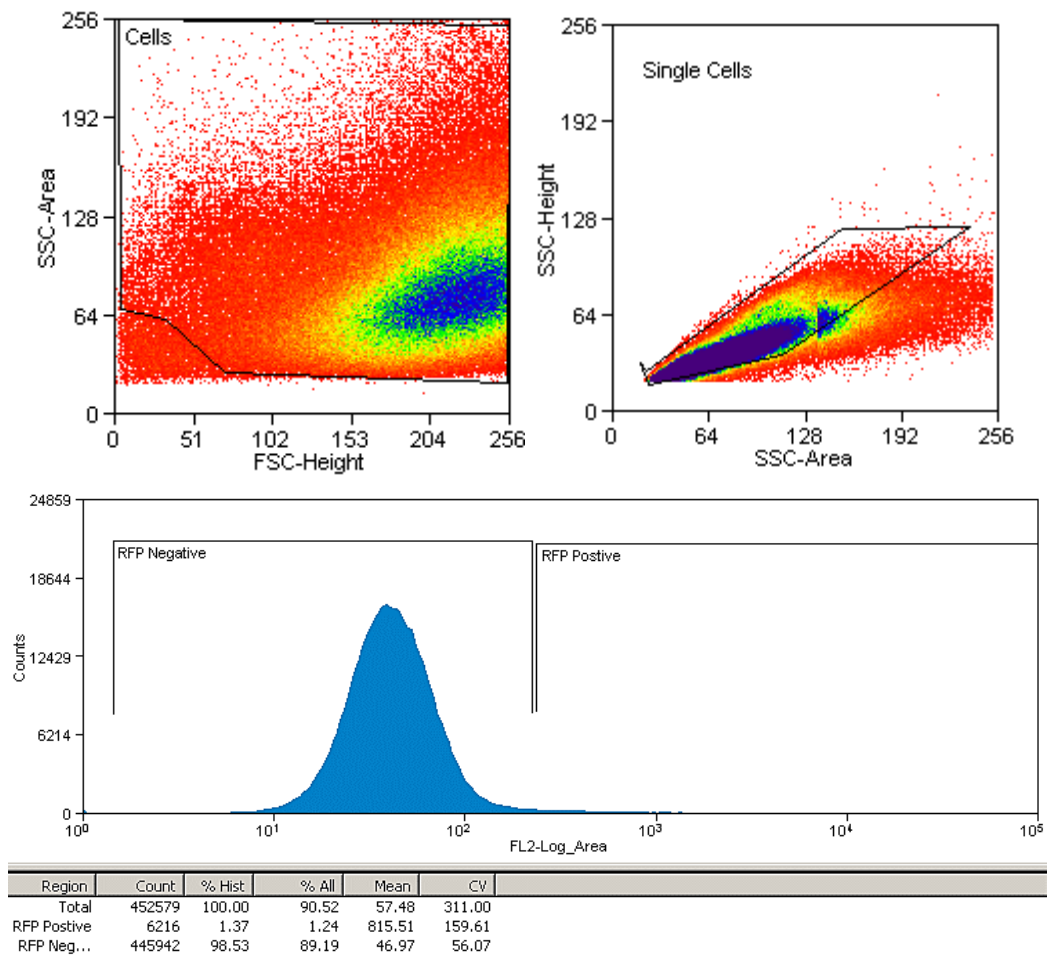
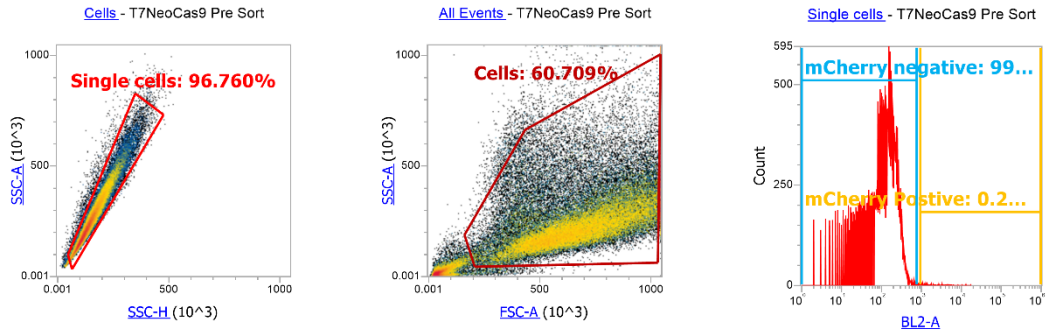


Figure 94. FACS profile of *Acanthamoeba* Neff trophozoites transfected with pBRFPT7NeoCas9

1.37% RFP positive cells of 10×10^6 trophozoites/ml sorted in mode Purity is depicted. The FSC and SSC discriminate single trophozoites in a whole population. Analysis was carried out on a Moflo Xdp (Beckman Coulter). Abbreviations: FSC: forward scatter, SSC: side scatter, FL2-Log_Area: total cell fluorescence.

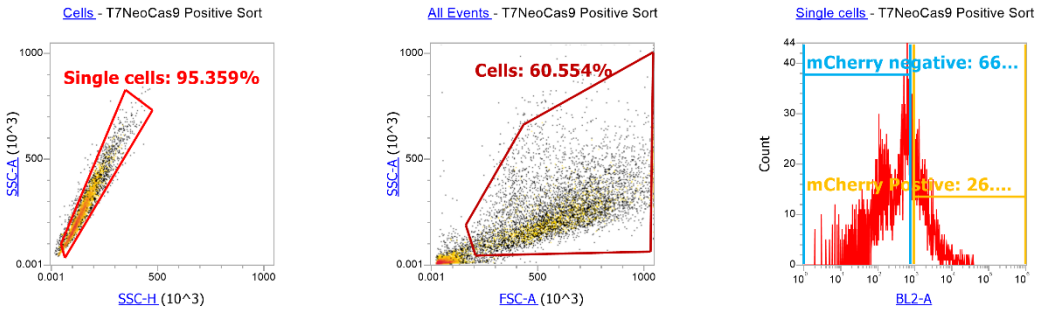
A.



Experiment: **Post sort 3**
 Group: **Group**
 Sample: **T7NeoCas9 Pre Sort**
 Time Recorded: **15:58:32**

Name	Gate	X Parameter	Y Parameter	Count	%Total	%Gated
▢ All Events	All Events	N/A	N/A	100,000	100.000	100.000
▢ Cells	Cells	FSC - FSC-A	SSC - SSC-A	60,709	60.709	60.709
▢ Single cells	Single cells	SSC - SSC-H	SSC - SSC-A	58,742	58.742	96.760
▢ mCherry Positive	mCherry Positive	BL2 - BL2-A		118	0.118	0.201
▢ mCherry negative	mCherry negative	BL2 - BL2-A		58,577	58.577	99.719

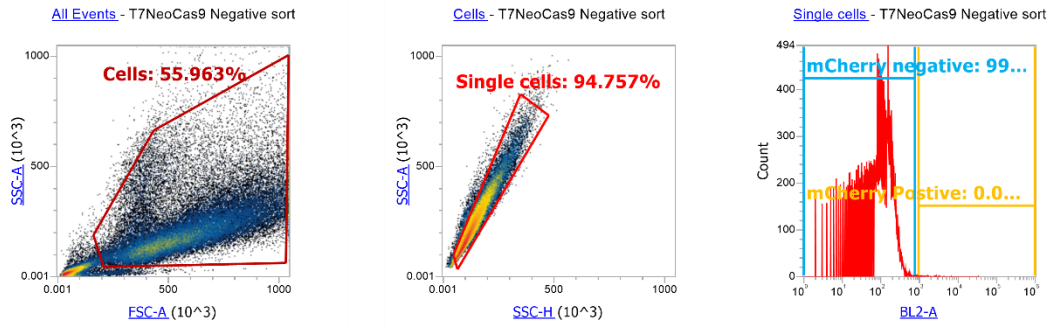
B.



Experiment: **Post sort 3**
 Group: **Group**
 Sample: **T7NeoCas9 Positive Sort**
 Time Recorded: **16:00:40**

Name	Gate	X Parameter	Y Parameter	Count	%Total	%Gated
▢ All Events	All Events	N/A	N/A	10,247	100.000	100.000
▢ Cells	Cells	FSC - FSC-A	SSC - SSC-A	6,205	60.554	60.554
▢ Single cells	Single cells	SSC - SSC-H	SSC - SSC-A	5,917	57.744	95.359
▢ mCherry Positive	mCherry Positive	BL2 - BL2-A		1,541	15.039	26.044
▢ mCherry negative	mCherry negative	BL2 - BL2-A		3,962	38.665	66.960

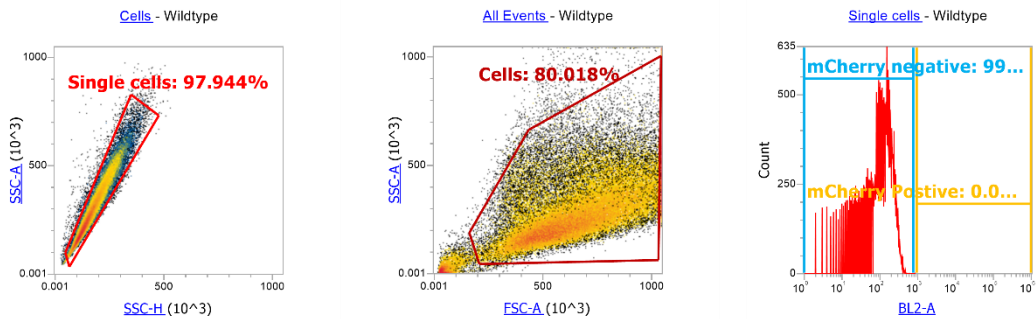
C.



Experiment: **Post sort 3**
 Group: **Group**
 Sample: **T7NeoCas9 Negative sort**
 Time Recorded: **15:56:25**

Name	Gate	X Parameter	Y Parameter	Count	%Total	%Gated
All Events	All Events	N/A	N/A	100,000	100.000	100.000
Cells	Cells	FSC - FSC-A	SSC - SSC-A	55,963	55.963	55.963
Single cells	Single cells	SSC - SSC-H	SSC - SSC-A	53,029	53.029	94.757
mCherry Positive	mCherry Positive	BL2 - BL2-A		34	0.034	0.064
mCherry negative	mCherry negative	BL2 - BL2-A		52,975	52.975	99.898

D.



Experiment: **Post sort 3**
 Group: **Group**
 Sample: **Wildtype**
 Time Recorded: **15:52:09**

Name	Gate	X Parameter	Y Parameter	Count	%Total	%Gated
All Events	All Events	N/A	N/A	78,840	100.000	100.000
Cells	Cells	FSC - FSC-A	SSC - SSC-A	63,086	80.018	80.018
Single cells	Single cells	SSC - SSC-H	SSC - SSC-A	61,789	78.373	97.944
mCherry Positive	mCherry Positive	BL2 - BL2-A		0	0.000	0.000
mCherry negative	mCherry negative	BL2 - BL2-A		61,788	78.371	99.998

E.

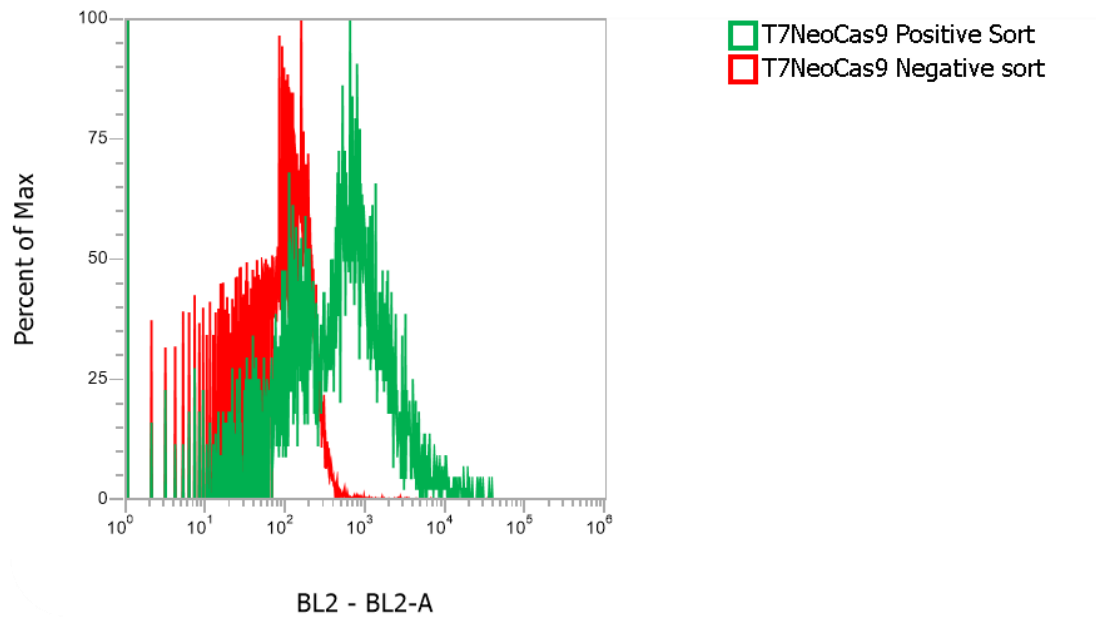


Figure 95. Flow cytometry analysis of trophozoites transfected with pBRFPT7NeoCas9 expressing plasmids post-fluorescence-activated cell sorting (FACS)

A. Trophozoites transfected with pBRFPT7NeoCas9; **B.** Positive sorted trophozoites transfected with pBRFPT7NeoCas9; **C.** Negative sorted trophozoites transfected with pBRFPT7NeoCas9; and **D.** Negative control (Wild type trophozoites); **E.** Overlay. Abbreviations: FSC: forward scatter, SSC: side scatter, BL2 channel for blue excitation laser-488 nm and emission filter 574/26 nm.

PCR using the oligonucleotides (T7NeoCas9.for, T7NeoCas9.rev, T7PhleoCas9.for) was intended using primers and genomic DNA from sorted positive trophozoites transfected with pBRFPT7NeoCas9 to confirm the presence of the plasmid.

Due to the outbreak of COVID-19, experimental proceedings were delayed hindering their completion.

5.5 Discussion

Despite to be ubiquitous in the environment and the capacity to cause serious AK and rare but lethal GAE in humans and animals, molecular aspects of *Acanthamoeba* have been poorly explored. The unavailability of a complete genome sequence, the lack of expression vectors and the uncertain ploidy number make the development of genetic editing approaches such as CRISPR-Cas9 to manipulate *Acanthamoeba spp.* challenging (Anderson *et al.*, 2005; Clarke *et al.*, 2013b; Clarke *et al.*, 2013a; Maciver, 2016; Muramoto *et al.*, 2019). In addition, these limitations impede the possibilities to improve the understanding of biological mechanisms of life cycle stage conversion, pathogenesis processes, symbiosis with other microorganisms, drug therapeutic target exploitation, etc.

During the last decade, few efforts to manipulate *Acanthamoeba* through gene silencing have been carried out. Small interfering RNAs (siRNA) have been synthesised to understand the role of cysteine proteases as a pathogenic mechanism and its role on the encystment process, to target an essential protein of the contractile vacuole to interfere with the osmotic balance and to provoke the downregulation of cellulose synthase protein to inhibit the encystment (Martín-Navarro *et al.*, 2014; Wang *et al.*, 2020). However, there is no report of a full description of the use of CRISPR-Cas9 to dissect molecular processes in *Acanthamoeba spp.*

In this chapter, we shared advances in the attempt to design, develop and implement a CRISPR-Cas9 system as a powerful approach for the study of *Acanthamoeba* biology through targeted deletion of the chorismate synthase gene coding for a protein required for the novo synthesis of aromatic compounds and a plausible target for antiparasitics.

The system relied on the development of a cell line that carries pBRFPT7NeoCas9 or pBRFPT7PhleoCas9, plasmids containing G418 or Phleomycin resistance genes, the red fluorescent protein gene (RFP), the Cas9 nuclease gene and the T7 RNA polymerase gene. The latter allows the *in vivo* transcription of transfected sgRNA templates carrying a T7 promoter (sgRNA_{up} and sgRNAs). Donor DNA constructs containing 30 nucleotides homology flanks that match the target locus (CS-Neo-CS, CS-Phleo-CS and CS-Hyg-CS) and drug selectable marker genes can be amplified from plasmid templates.

Based on fluorescence microscopy, all the CRISPR-Cas9 related plasmids showed red fluorescence indicating RFP expression in some trophozoites transfected either with Xfect or Polyplus reagents. Further, a significant number of cells were enriched using FACS resulting in a higher number of fluorescent trophozoites carrying pBRFPT7NeoCas9 compared to those ones transfected with pBRFPT7PhleoCas9. Both cell lines were treated with the highest dose of G418 or phleomycin. These results confirmed previous fluorescence intensities observations. It is likely that Cas9 and T7 RNA polymerase are also expressed, however, confirmation through RT-PCR amplification using specific primers or immunoblot analysis using an anti-FLAG antibody to detect the triple FLAG-tagged Cas9 or anti-T7 RNA polymerase antibodies (commercially available) to detect T7 RNA polymerase must be carried out to confirm expression.

The difference of fluorescence intensities in a population of transfected *Acanthamoeba* trophozoites with pGAPDH-EGFP and pTPBF-EGFP treated with G418 (10 and 50 µg/ml) had been previously described due to the differences in expression levels driven by GAPDH and TPBF promoters (Bateman, 2010). In this study, a robust green fluorescence caused by EGFP as well as an increase in the growth rate in trophozoites transfected with pGAPDH-EGFP driven by the GAPDH promoter and treated with 10 µg/ml of G418 was observed compared to cells carrying pTPBF-EGFP treated with the same concentration of drug. To note, this phenomenon was only observed when the cells transfected with pGAPDH-EGFP were selected with a higher concentration of G418 (50 µg/ml), but then sub-cultured in media containing 10 µg/ml. The authors hypothesised that due to G418 being a potent inhibitor of the function of 80S ribosomes and protein synthesis in eukaryotic cells, all the translation in trophozoites is inhibited to some extent leading to a potential balance of how protein synthesis efficiency is dependent on the neomycin concentration (Stepanenko and Heng, 2017). This is in some way reflected on the selection pressure with cultures containing initially highest concentration of G418 where the translation machinery of the cells is inhibited (50 µg/ml) and passaged to a lower concentration where this constraint is removed, and protein production is resumed. However, sensitivity of untransfected *A. castellanii* trophozoites to G418 analysed by toxicity screenings are not shown and a WT control to rule out the possibility of autofluorescence is missing in this study. In fact, in a previous work it was stated that concentrations of G418 above 10 µg/ml inhibited trophozoites growth (cell density not

reported) and treatment with G418 for long periods lead to cell lysis and loss of viable cells (Peng, Omaruddin and Bateman, 2005). This chapter reports sensitivity screenings of 4×10^4 cells/ml of *A. castellanii* Neff trophozoites treated with to G418 which showed an IC_{50} of 6.25 μ M, we designated this value as the “optimal” concentration. Twofold the optimal concentration (12.5 μ M) and half the optimal concentration (3.125 μ M) were analysed to demonstrate which one generated the best transfection efficiency. Based on our fluorescence microscopy results, cells treated with the highest concentration of 12.5 μ M showed the strongest fluorescence.

According to Peng *et al.*, 2005, viral promoters like the SV40 promoter are not functional in *Acanthamoeba* because in their hands either stable or transient transfection did not lead to G418 resistance, however this data is not shown in the publication. In contrast, our results suggest a robust expression based on fluorescence level of RFP driven by the SV40 promoter in pBRFPT7NeoCas9 compared with the WT control.

To our understanding, this is the first time that sensitivity of *A. castellanii* Neff trophozoites for different drug selection markers such as Phleomycin, Hygromycin B and Puromycin has been tested. Phleomycin turned out to be a potent inhibitor of trophozoites *in vitro* with an IC_{50} below 0.20 μ M. However, the expression of RFP was low according to the poor level of fluorescence observed in trophozoites transfected with pBRFPT7PhleoCas9 in fluorescence microscopy analysis. This was also confirmed by the low level of fluorescence signal detected in cells in flow cytometry.

In *Acanthamoeba* spp., it has not been determined if plasmids are integrated into chromosomal DNA or whether they remain episomal. Recently, an episomal CRISPR-Cas9 system was successfully developed for *Entamoeba histolytica*. On this study, stable transfectant *Entamoeba* cell lines expressing Cas9 were achieved when fused to a dihydrofolate reductase (DHFR) destabilisation domain and a myc-tag in the presence of trimethoprim (TMP) and carrying Luc-sgRNA which were driven by U6 promoter (Eh-Cas9-gLuc). Eh-Cas9-gLuc cell line were transiently transfected with either a mutated luciferase gene (pDeadLuc) targeted by Luc-gRNA and another plasmid with a truncated luciferase gene (pDonorLuc) to restore luciferase expression. Luminiscence signal was increased in those cell lines expressing Luc-gRNA, suggesting DNA repair was carried out by homologous recombination. The

specific DNA recombination sites were confirmed by PCR detecting the presence of chimeric DNA and sequencing (Kangussu-Marcolino *et al.*, 2021). Several meiotic gene homologues in eukaryotes necessary for sexual reproduction have also been found in some protists with non-related sexual functions. Despite *Acanthamoeba* spp. reproduces by binary fission and there is no evidence of sexual processes, some core meiotic genes i.e., Rad50, Spo11, Hop1, Mnd1, Dmc1, etc have been found to be constitutively expressed in exponentially growing *Acanthamoeba* GS-336 and SB-53 (closely related with Neff strain ATCC30010). These have been speculated to be involved in homologous recombination of multicopy genomic elements in the polyploid nucleus to avoid accumulation of mutations as already shown in *Entamoeba histolytica* (Maciver, Koutsogiannis and de Obeso Fernández Del Valle, 2019; Kangussu-Marcolino *et al.*, 2021).

An attempt to generate an M28 aminopeptidase (M28AP) mutant strain of *Acanthamoeba* Neff ATCC 30010 using CRISPR-Cas9 to prove M28AP prevented complement-mediated lysis was carried out (Huang *et al.*, 2019). Synthesised sgRNAs combined with the Cas9 protein formed an RNP complex and were transfected via electroporation. Transfectants were plated in 96-well plates and two “clones” were analysed using PCR, annealing of mutant and wild type PCR fragments followed by digestion utilising T7 endonuclease I to confirm the presence of the mutation. A successful mutation would lead to a difference of molecular weight in the mutated M28AP proteins of “clones” 2 and 10 compared to the WT control. However, we carried out BLAST searches using the sgRNA sequence to identify the regions they chose to generate the mutation without finding a match. Further BLAST using the partial gene sequence provided in the supplementary data was done on AmoebaDB and NCBI to look for the M28AP full-length genomic DNA sequence without success. A gene accession number was not provided by the authors (Huang *et al.*, 2019). Taken together, this publication does not constitute a successful application of CRISPR-Cas9.

CRISPR-Cas9 is very useful for microorganisms with genome plasticity or polyploidy like *Leishmania* or *Acanthamoeba*. It might make it possible to achieve a deletion of multicopy genes. This is the main reason we applied the method developed by Beneke in 2017 for *Leishmania* in *Acanthamoeba*. These results encourage to fully establish CRISPR-Cas9 in *Acanthamoeba*.

Chapter 6. General Discussion

6.1 Overview

Over the last few decades, there have been increasing numbers of *Acanthamoeba* keratitis (AK) cases among healthy individuals, especially in those who wear contact lenses; and the progressive and mostly lethal Granulomatous Amoebic Encephalitis (GAE) in immunocompromised patients. A lack of awareness of these infections, poor diagnosis, and failure of successful patient prognosis due to the side effects and not fully effective therapies emphasises the importance of the quest for new antiamoebic agents (Ahmed *et al.*, 2021).

This chapter summarizes the work in this thesis which has aimed to: (i) provide alternative active antiamoebic agents to the those used in current therapies, (ii) establish *Galleria mellonella* larvae as a consolidated *in vivo* infection model for testing novel drugs and progressing those identified in (aim i) and (iii) to develop a CRISPR-Cas9 mutagenesis system for genetic manipulation of *Acanthamoeba* and drug target validation in this organism. The overall aim of the work is to provide tools that can help the development of new drugs that can overcome the unmet medical needs for the diseases caused by *Acanthamoeba*.

6.2 New anti-amoebic Strathclyde Minor Binding Groove *in vitro* screening

Throughout Chapter 3 I have examined various compounds synthesized at University of Strathclyde with divergence from Distamycin A that exert their biological effect through binding to the minor groove of the double helix DNA (S-MGBs). I established *in vitro* experimental conditions allowing the screening of S-MGB compounds to determine their effectiveness against *Acanthamoeba* spp. trophozoites by means of the alamarBlue assay. Previous data have proven this technique is suitable, sensitive, and non-subjective and has been widely used in drug discovery against this pathogenic amoeba (Martín-Navarro *et al.*, 2008; Sifaoui *et al.*, 2017; Thomson *et al.*, 2017). Our data shows that from 42 S-MGBs analysed, those with amidinylethyl tail produced a robust effect *in vitro* against *Acanthamoeba* Neff strain in comparison with their analogues with morpholine tails, hence a Structure-Activity relationship (SAR) was achieved. In addition, I was able to define a library of eight S-MGBs with great inhibitory activity from which S-MGB 235 displayed the most potent active inhibitory effect at 24 hours and 96 hours against five different *Acanthamoeba* species,

including clinical and environmental isolates. Prior studies using other compounds with such amidinyl groups such as propamidine and pentamidine, believed to also target the minor groove of DNA, have reported severe morphological changes and cell lysis of *Acanthamoeba* trophozoites (Perris et al., 1995; Jenkins and Lane, 1997). Of particular interest, these severe effects were also observed in our Confocal microscopy results when trophozoites were labelled with S-MGBS 363, a fluorescent analogue of S-MGB 235. The present results in Chapter 3 are significant because any of the compounds in the library could be potential candidates to substitute or complement propamidine isethionate, a diamidine widely used in combination with PHMB or chlorhexidine as therapy against AK (Sangkanu *et al.*, 2021) .

Despite the success of these studies and significant milestones, certain limitations were also faced throughout the analysis of S-MGBs. The availability of these compounds depends on a third party and guarantee of the purity and quality of these experimental compounds when they are resynthesized in different batches must be controlled and confirmed. Whilst the 96 well-plate alamarBlue technique is not a limitation *per se*, other similar assays are available and have been used successfully such as CellTiter-Glo, which measures ATP production has shown to be equally reliable to determine cell viability. This has been particularly useful for scaling into 384 well plates and higher throughput assays. If combinatorial chemistry was used to develop more S-MGBs this assay could prove beneficial in screening higher number of S-MGBs utilizing high-throughput automated worktables (Martín-Navarro *et al.*, 2014; Rice *et al.*, 2020a).

6.3 Novel *in vivo* infection model

In Chapter 4 I have standardised a protocol to employ *Galleria mellonella* larvae as a new *in vivo* infection model to determine the efficacy of S-MGB 235 against *Acanthamoeba* spp. As mentioned before, during the last years insects such as *Drosophila melanogaster*, *Locusta migratoria* and *Galleria mellonella* have become a golden standard alternative to mammals as models to for initial drug-screening tools for infectious diseases (Piatek, Sheehan and Kavanagh, 2020; Harnish, Link and Yamamoto, 2021; Siddiqui, Muhammad and Khan, 2021). *G. mellonella* is a consolidated infection model for bacteria and fungi (Jemel *et al.*, 2020; Pereira *et al.*, 2020). To date no study has been conducted for parasites and much less for free-living amoebas.

In this chapter, initial assays demonstrated a dose-time dependant relationship between infectious dose of *A. castellanii* Neff trophozoites and susceptibility of *G. mellonella* larvae. As well established before, the inoculum size of *Acanthamoeba* trophozoites/cysts is crucial for the onset and severity of AK symptoms (Khan, 2006a). Further studies found that contrary to the expectations, voriconazole and miltefosine, two of the drugs routinely used in clinical cases against AK and GAE did not show significant protection of infected *G. mellonella*. However, S-MGB 235 was found to be protective and non-toxic specifically at 25 mg/kg in groups with larvae infected with 1×10^7 amoebae. However, the larvae were not completely protected by S-MGB 235 and ultimately most did succumb to infection. The inability of S-MGB 235 to fully protect larvae and indeed voriconazole and miltefosine to have any beneficial effect on infected *G. mellonella* larvae might represent a deficiency in the model as currently used. Potentially the relatively high infectious dose might not allow the larvae to recover. In future, studies *G. mellonella* should be inoculated with lower concentrations of trophozoites to determine if this is better able to distinguish the potential protective effects of drugs. These studies were not possible in the timeframe which was curtailed due to the ongoing pandemic.

One of the main limitations is the unknown health conditions of the larvae when transited to the laboratory and the possibility of any underlying natural infection of these insects. In addition, different batches of purchased larvae with “small variations” such as age, size and nutritional status could be critical in the course of the infection and consequently different results among independent experiments might be obtained (Desbois and Coote, 2012). Another important issue using *G. mellonella* like any other model is toxicity testing since toxicity cannot be directly evaluated in humans and mechanisms of toxicity are poorly understood in *G. mellonella*. Another major issue previously reported in the procedure is the use of DMSO as vehicle. In this study, 50% DMSO was lethal to wax moths above 100 mg/kg body weight. It was difficult to correctly assign median lethal dose (LD_{50}) when 50% of DMSO was used in mildly toxic (ciprofloxacin, chloramphenicol) and non-toxic compounds (glutamic acid, glucose, sodium chloride) (Ignasiak and Maxwell, 2017). In our study, toxicity was also observed in those groups of non-infected larvae, treated with 125 mg/kg voriconazole or 125 mg/kg of S-MGB 235 solubilised with DMSO at 100%. In the case of larva treated with this dose of voriconazole, 50% of the non-infected larvae survived for the last day of observation (day 15) and for larva treated with this dose of S-MGB

235 just the 20% survived until day 25. We managed to overcome this limitation without compromising the test procedure by decreasing DMSO to 11% (the minimum required to solubilise S-MGB 235).

6.4 Gene editing tools as therapeutic options

The findings in Chapter 5 demonstrate *Acanthamoeba* spp. is a challenging model to develop and apply the CRISPR-Cas9 gene editing tool. We chose to follow the successful protocol applied in *Leishmania* spp. by Beneke *et al.*, 2017. The basis of this protocol is to provide the cells with DNA templates containing a T7 RNA polymerase promoter for *in vivo* transcription to form sgRNAs. In addition, a resistance marker gene flanked by 30 nucleotide sequences homologous to the flanking regions of the target gene are generated by PCR and used for transfection into *Acanthamoeba* trophozoites along with the sgRNA DNA templates. T7 RNA polymerase is expressed along with the Cas9 protein and RFP as a reporter from a plasmid introduced into the parasites. In this chapter, besides G418, I established for the very first time the inhibition efficacy of phleomycin, hygromycin B, and puromycin against *A. castellanii* Neff trophozoites to establish their use as drug selection markers. I constructed a series of expression plasmids to generate pBRFPNeoT7Cas9 and pBRFPT7PhleoCas9, which contain the genes coding for Cas9, T7 RNA polymerase and RFP. These plasmids were transfected into trophozoites using Xfect reagent. Additionally, I generated sgRNA DNA templates and DNA donor repair sequences for the chorismate synthase gene. The data described in this chapter show positive transfection of pBRFPNeoT7Cas9 trophozoites with different levels of red fluorescent protein expression when selected with a high dose of G418, which suggests expression RFP from the plasmid along with Cas9 and T7 RNA polymerase.

The main challenge throughout the development of this system was trophozoites in the positive control group (wild type cells) were not killed even with the highest concentration of G418/phleomycin despite the fact a standardisation of these drugs was carried out. This raises the possibility *Acanthamoeba* trophozoites have an unknown resistance mechanism such as an efflux pump to avoid cell death. However, a similar plasmid system approach for the application of CRISPR-Cas9 system performed well for *Entamoeba histolytica* and *Dictyostelium discoideum* where DNA repair of double strand breaks generated by Cas9 occurred by homologous recombination in both protists (Muramoto *et al.*, 2019; Kangussu-Marcolino *et al.*,

2021). As Superfect (Qiagen) used in previous research (Kong and Pollard, 2002; Peng, Omaruddin and Bateman, 2005; Moon *et al.*, 2011) was not available any longer I used Xfect and Polyplus. In accordance with our results Xfect was the reagent that displayed a better transfection efficiency compared with Polyplus (see Chapter 5, Results section). Regardless of evidence of the presence of meiotic genes potentially involved in homologous recombination in *Acanthamoeba* spp., a major limitation for the application of CRISPR-Cas9 is the current unknown status of the DNA double strand repair machinery utilised by *Acanthamoeba* spp. (Maciver, Koutsogiannis and de Obeso Fernández Del Valle, 2019). A recent and flexible editing tool named Retron Library Recombineering (RLR) overcomes this and other disadvantages of CRISPR. With this technique each progeny inherits the same modification, and it is an alternative in cases where there is no endogenous repair system in which Cas9 cuts unintended and off-target sites resulting in toxicity (Schubert *et al.*, 2021).

Despite these promising results, questions remain unanswered at present; nevertheless, the results of this thesis represent a contribution to the potential applications of S-MGBs or CRISPR-Cas9 gene editing tool in therapeutic strategies that improve the prognosis of patients suffering from AK and GAE.

6.5 Future work

The work developed in the present thesis could be extended as follows:

- © The findings obtained with S-MGB 235 could be followed up by investigating its potential inhibitory effect as cysticidal against all the five strains of *Acanthamoeba* we managed in our laboratory. This would be fascinating since most of the drugs evaluated so far in the literature are unable to penetrate the double cyst layer.
- © Preliminary evidence indicates drug combination therapy is widely used by clinicians to treat AK and GAE. Thus, further research is required to evaluate the potential synergistic effect of S-MGB 235 with polyhexamethylene biguanide (PHMB), voriconazole and miltefosine against *Acanthamoeba* spp. trophozoites and cysts.

- © RNA extractions of both wild and treated S-MGB 235 samples of *A. castellanii* Neff strain and *A. polyphaga* trophozoites were performed (Appendix) for RNA Sequencing Transcriptome analysis. This would enable a better understanding of the gene expression changes over the metabolic pathways because of the effect of S-MGB 235 on these amoeba species.
- © Along with RNA-seq, additional techniques such as qPCR melt analysis, phenotypic microarrays, DNase I foot printing and potassium permanganate foot printing will allow the identification of promoters that are sensitive to S-MGB 235 which elucidate the mode of action against *Acanthamoeba* spp.
- © Further assays to explore the active library of S-MGBs with $IC_{50} < 1 \mu M$ utilising *G. mellonella* larvae will be performed to assess *in vivo* efficacy and toxicity.
- © Standardise a method that allows the recovery of trophozoites or cysts from infected *G. mellonella* larvae to be grown in PG medium and evaluate their viability.
- © Preliminary evidence of the expression of Cas9 and T7 RNA polymerase due to the red fluorescence expression could be followed up by RT-PCR and immunoblot analysis.
- © Deletion of the chorismate synthase gene using the generated sgRNA DNA templates, the replacement constructs and the *Acanthamoeba* cell line expressing Cas9 and T7 RNA polymerase.

Overall, the work undertaken and described in this thesis has made progress in the 3 main aims intimated in Chapter 1. Firstly, I have successfully screened a number of S-MGBs for activity against *Acanthamoeba* and identified a lead candidate with low nanomolar activity. Secondly, I have developed a *G. mellonella* model for testing antimicrobials against *Acanthamoeba* and demonstrated its utility using the lead S-MGB. Thirdly I have made a number of genetic tools that with refinement to procedures should prove useful for CRISPR-mediated gene replacement in *Acanthamoeba*. In addition, the above section identifies strategies to advance and exploit these 3 lines of research.

References

- Abbasoglu, Ö. E., Hoşal, B. M., Şener, B., Erdemoglu, N. and Gürsel, E. (2001) 'Penetration of Topical Fluconazole into Human Aqueous Humor', *Experimental Eye Research*, 72(2), pp. 147-151.
- Adl, S. M., Simpson, A. G., Farmer, M. A., Andersen, R. A., Anderson, O. R., Barta, J. R., Bowser, S. S., Brugerolle, G., Fensome, R. A., Fredericq, S., James, T. Y., Karpov, S., Kugrens, P., Krug, J., Lane, C. E., Lewis, L. A., Lodge, J., Lynn, D. H., Mann, D. G., McCourt, R. M., Mendoza, L., Moestrup, O., Mozley-Standridge, S. E., Nerad, T. A., Shearer, C. A., Smirnov, A. V., Spiegel, F. W. and Taylor, M. F. (2005) 'The new higher level classification of eukaryotes with emphasis on the taxonomy of protists', *J Eukaryot Microbiol*, 52(5), pp. 399-451.
- Ahmad, G. and Amiji, M. (2018) 'Use of CRISPR/Cas9 gene-editing tools for developing models in drug discovery', *Drug Discov Today*, 23(3), pp. 519-533.
- Ahmed, U., Anwar, A., Ong, S. K. and Khan, N. A. (2021) 'Applications of medicinal chemistry for drug discovery against Acanthamoeba infections', *Med Res Rev*.
- Akins, R. A. and Byers, T. J. (1980) 'Differentiation promoting factors induced in Acanthamoeba by inhibitors of mitochondrial macromolecule synthesis', *Developmental biology*, 78(1), pp. 126-140.
- Alafag, J. I.-i., Moon, E.-K., Hong, Y.-C., Chung, D.-I. and Kong, H.-H. (2006) 'Molecular and biochemical characterization of a novel actin bundling protein in Acanthamoeba', *Korean J Parasitol*, 44(4), pp. 331-341.
- Alizadeh, H., Apte, S., El-Agha, M. S., Li, L., Hurt, M., Howard, K., Cavanagh, H. D., McCulley, J. P. and Niederkorn, J. Y. (2001) 'Tear IgA and serum IgG antibodies against Acanthamoeba in patients with Acanthamoeba keratitis', *Cornea*, 20(6), pp. 622-7.
- Alizadeh, H., He, Y., McCulley, J. P., Ma, D., Stewart, G. L., Via, M., Haehling, E. and Niederkorn, J. Y. (1995) 'Successful immunization against Acanthamoeba keratitis in a pig model', *Cornea*, 14(2), pp. 180-186.
- Alizadeh, H., Li, H., Neelam, S. and Niederkorn, J. Y. (2008) 'Modulation of corneal and stromal matrix metalloproteinase by the mannose-induced Acanthamoeba cytolytic protein', *Experimental eye research*, 87(3), pp. 286-291.
- Alizadeh, H., Neelam, S. and Cavanagh, H. D. (2009) 'Amoebicidal Activities of Alexidine Against 3 Pathogenic Strains of Acanthamoeba', *Eye & Contact Lens*, 35(1).
- Alizadeh, H., Neelam, S., Hurt, M. and Niederkorn, J. Y. (2005) 'Role of contact lens wear, bacterial flora, and mannose-induced pathogenic protease in the pathogenesis of amoebic keratitis', *Infection and immunity*, 73(2), pp. 1061-1068.
- Alizadeh, H., Neelam, S. and Niederkorn, J. Y. (2007) 'Effect of immunization with the mannose-induced Acanthamoeba protein and Acanthamoeba plasminogen activator in mitigating Acanthamoeba keratitis', *Investigative ophthalmology & visual science*, 48(12), pp. 5597-5604.
- Alizadeh, H., Silvany, R. E., Meyer, D. R., Dougherty, J. M. and McCulley, J. P. (1997) 'In Vitro Amoebicidal Activity of Propamidine and Pentamidine Isethionate Against Acanthamoeba Species and Toxicity to Corneal Tissues', *Cornea*, 16(1).

- Alizadeh, H., Tripathi, T., Abdi, M. and Smith, A. D. (2014) 'Pathogenic strains of *Acanthamoeba* are recognized by TLR4 and initiated inflammatory responses in the cornea', *PLoS One*, 9(3), pp. e92375.
- Alsam, S., Kim, K. S., Stins, M., Rivas, A. O., Sissons, J. and Khan, N. A. (2003) 'Acanthamoeba interactions with human brain microvascular endothelial cells', *Microbial pathogenesis*, 35(6), pp. 235-241.
- Amoils, S. P. and Heney, C. (1999) 'Acanthamoeba keratitis with live isolates treated with cryosurgery and fluconazole', *American Journal of Ophthalmology*, 127(6), pp. 718-720.
- Anaya-Velázquez, F., Martínez-Palomo, A., Tsutsumi, V. and González-Robles, A. (1985) 'Intestinal invasive amebiasis: an experimental model in rodents using axenic or monoxenic strains of *Entamoeba histolytica*', *Am J Trop Med Hyg*, 34(4), pp. 723-30.
- Anderson, I. J., Watkins, R. F., Samuelson, J., Spencer, D. F., Majoros, W. H., Gray, M. W. and Loftus, B. J. (2005) 'Gene discovery in the *Acanthamoeba castellanii* genome', *Protist*, 156(2), pp. 203-214.
- Anwar, A., Numan, A., Siddiqui, R., Khalid, M. and Khan, N. A. (2019) 'Cobalt nanoparticles as novel nanotherapeutics against *Acanthamoeba castellanii*', *Parasites & Vectors*, 12(1), pp. 280.
- Anwar, A., Siddiqui, R., Hussain, M. A., Ahmed, D., Shah, M. R. and Khan, N. A. (2018) 'Silver nanoparticle conjugation affects antiacanthamoebic activities of amphotericin B, nystatin, and fluconazole', *Parasitology Research*, 117(1), pp. 265-271.
- Anwar, A., Ting, E. L. S., Anwar, A., Ain, N. u., Faizi, S., Shah, M. R., Khan, N. A. and Siddiqui, R. (2020) 'Antiamoebic activity of plant-based natural products and their conjugated silver nanoparticles against *Acanthamoeba castellanii* (ATCC 50492)', *AMB Express*, 10(1), pp. 24.
- Aparicio, D. V., Bejarano, J. I. C., de Los Santos, A. M., Ramírez-Cortinas, S. and de la O Cavazos, M. (2021) 'Case Report: Granulomatous Amebic Encephalitis due to *Acanthamoeba* spp. in an Immunocompetent Pediatric Patient', *Am J Trop Med Hyg*.
- Aqeel, Y., Siddiqui, R. and Khan, N. A. (2013) 'Silencing of xylose isomerase and cellulose synthase by siRNA inhibits encystation in *Acanthamoeba castellanii*', *Parasitology research*, 112(3), pp. 1221-1227.
- Aqeel, Y., Siddiqui, R., Manan, Z. and Khan, N. A. (2015) 'The role of G protein coupled receptor-mediated signaling in the biological properties of *Acanthamoeba castellanii* of the T4 genotype', *Microbial pathogenesis*, 81, pp. 22-27.
- Arcuri, H. A. and Palma, M. S. (2011) 'Understanding the structure, activity and inhibition of chorismate synthase from *Mycobacterium tuberculosis*', *Curr Med Chem*, 18(9), pp. 1311-7.
- Arnalich-Montiel, F., Lumbreras-Fernández, B., Martín-Navarro, C. M., Valladares, B., Lopez-Velez, R., Morcillo-Laiz, R. and Lorenzo-Morales, J. (2014) 'Influence of *Acanthamoeba* genotype on clinical course and outcomes for patients with *Acanthamoeba* keratitis in Spain', *Journal of clinical microbiology*, 52(4), pp. 1213-1216.
- Atalay, H. T., Uysal, B. S., Sarzhanov, F., Usluca, S., Yeşilirmak, N., Özmen, M. C., Erganiş, S., Tefon, A. B., Dogruman-Al, F. and Bilgihan, K. (2020) 'Rose Bengal-Mediated Photodynamic Antimicrobial Treatment of *Acanthamoeba* Keratitis', *Current Eye Research*, 45(10), pp. 1205-1210.

- Austin, A., Lietman, T. and Rose-Nussbaumer, J. (2017) 'Update on the Management of Infectious Keratitis', *Ophthalmology*, 124(11), pp. 1678-1689.
- Avdagic, E., Chew, H. F., Veldman, P., Tu, E. Y., Jafri, M., Doshi, R., Boggild, A. K., Reidy, J. J. and Farooq, A. V. (2021) 'Resolution of Acanthamoeba Keratitis with Adjunctive Use of Oral Miltefosine', *Ocular Immunology and Inflammation*, 29(2), pp. 278-281.
- Awwad, S. T., Heilman, M., Hogan, R. N., Parmar, D. N., Petroll, W. M., McCulley, J. P. and Cavanagh, H. D. (2007) 'Severe reactive ischemic posterior segment inflammation in acanthamoeba keratitis: a new potentially blinding syndrome', *Ophthalmology*, 114(2), pp. 313-320.
- Badenoch, P. R., Johnson, A. M., Christy, P. E. and Coster, D. J. (1990) 'Pathogenicity of Acanthamoeba and a Corynebacterium in the rat cornea', *Archives of Ophthalmology*, 108(1), pp. 107-112.
- Baig, A. M. (2014) 'Granulomatous amoebic encephalitis: ghost response of an immunocompromised host?', *Journal of medical microbiology*, 63(12), pp. 1763-1766.
- Baig, A. M. (2015) 'Pathogenesis of amoebic encephalitis: Are the amoebae being credited to an 'inside job' done by the host immune response?', *Acta Trop*, 148, pp. 72-6.
- Baig, A. M., Iqbal, J. and Khan, N. A. (2013) '*In Vitro* Efficacies of Clinically Available Drugs against Growth and Viability of an Acanthamoeba castellanii Keratitis Isolate Belonging to the T4 Genotype', *Antimicrobial Agents and Chemotherapy*, 57(8), pp. 3561-3567.
- Baig, A. M. and Khan, N. A. (2015) 'A proposed cascade of vascular events leading to granulomatous amoebic encephalitis', *Microbial pathogenesis*, 88, pp. 48-51.
- Baldo, E. T., Moon, E.-K., Kong, H.-H. and Chung, D.-I. (2005) 'Acanthamoeba healyi: Molecular cloning and characterization of a coronin homologue, an actin-related protein', *Experimental Parasitology*, 110(2), pp. 114-122.
- Baraldi, P. G., Bovero, A., Fruttarolo, F., Preti, D., Tabrizi, M. A., Pavani, M. G. and Romagnoli, R. (2004) 'DNA minor groove binders as potential antitumor and antimicrobial agents', *Medicinal research reviews*, 24(4), pp. 475-528.
- Barchiesi, F., Poeta, M. D., Morbiducci, V., Ancarani, F. and Scalise, G. (1994) 'Effect of pentamidine on the growth of Cryptococcus neoformans', *Journal of Antimicrobial Chemotherapy*, 33(6), pp. 1229-1232.
- Barrett, M. P. and Croft, S. L. (2012) 'Management of trypanosomiasis and leishmaniasis', *British Medical Bulletin*, 104(1), pp. 175-196.
- Barrett, M. P., Gemmell, C. G. and Suckling, C. J. (2013) 'Minor groove binders as anti-infective agents', *Pharmacology & therapeutics*, 139(1), pp. 12-23.
- Bateman, E. (2010) 'Expression plasmids and production of EGFP in stably transfected Acanthamoeba', *Protein Expr Purif*, 70(1), pp. 95-100.
- Behnke Michael, S., Khan, A. and Sibley, L. D. (2015) 'Genetic Mapping Reveals that Sinefungin Resistance in Toxoplasma gondii Is Controlled by a Putative Amino Acid Transporter Locus That Can Be Used as a Negative Selectable Marker', *Eukaryotic Cell*, 14(2), pp. 140-148.
- Behnke, M. S., Khan, A., Lauron, E. J., Jimah, J. R., Wang, Q., Tolia, N. H. and Sibley, L. D. (2015) 'Rhoptry Proteins ROP5 and ROP18 Are Major Murine Virulence Factors in Genetically

Divergent South American Strains of *Toxoplasma gondii*', *PLOS Genetics*, 11(8), pp. e1005434.

Beneke, T., Madden, R., Makin, L., Valli, J., Sunter, J. and Gluenz, E. (2017) 'A CRISPR Cas9 high-throughput genome editing toolkit for kinetoplastids', *R Soc Open Sci*, 4(5), pp. 170095.

Bentley, R. (1990) 'The shikimate pathway--a metabolic tree with many branches', *Crit Rev Biochem Mol Biol*, 25(5), pp. 307-84.

Bergin, D., Reeves, E. P., Renwick, J., Wientjes, F. B. and Kavanagh, K. (2005) 'Superoxide production in *Galleria mellonella* hemocytes: identification of proteins homologous to the NADPH oxidase complex of human neutrophils', *Infect Immun*, 73(7), pp. 4161-70.

Bhaduri, S., Ranjan, N. and Arya, D. P. (2018) 'An overview of recent advances in duplex DNA recognition by small molecules', *Beilstein J Org Chem*, 14, pp. 1051-1086.

Bhaya, D., Davison, M. and Barrangou, R. (2011) 'CRISPR-Cas systems in bacteria and archaea: versatile small RNAs for adaptive defense and regulation', *Annu Rev Genet*, 45, pp. 273-97.

Bikard, D., Euler, C. W., Jiang, W., Nussenzweig, P. M., Goldberg, G. W., Duportet, X., Fischetti, V. A. and Marraffini, L. A. (2014) 'Exploiting CRISPR-Cas nucleases to produce sequence-specific antimicrobials', *Nat Biotechnol*, 32(11), pp. 1146-50.

Bikard, D., Jiang, W., Samai, P., Hochschild, A., Zhang, F. and Marraffini, L. A. (2013) 'Programmable repression and activation of bacterial gene expression using an engineered CRISPR-Cas system', *Nucleic Acids Research*, 41(15), pp. 7429-7437.

Biopharma, M. (2013) *Bringing true novelty to the anti-infectives space*: MGB, Biopharma. Available at: <https://www.mgb-biopharma.com/wp-content/uploads/MGB-Biopharma-Bio-Europe-Presentation-6th-Nov-2013.pdf> (Accessed).

Blondel, C. J., Park, J. S., Hubbard, T. P., Pacheco, A. R., Kuehl, C. J., Walsh, M. J., Davis, B. M., Gewurz, B. E., Doench, J. G. and Waldor, M. K. (2016) 'CRISPR/Cas9 Screens Reveal Requirements for Host Cell Sulfation and Fucosylation in Bacterial Type III Secretion System-Mediated Cytotoxicity', *Cell Host Microbe*, 20(2), pp. 226-37.

Bohnert, H. J. and Herrmann, R. G. (1974) 'The genomic complexity of *Acanthamoeba castellanii* mitochondrial DNA', *The FEBS Journal*, 50(1), pp. 83-90.

Boman, H. G. and Hultmark, D. (1987) 'Cell-free immunity in insects', *Annu Rev Microbiol*, 41, pp. 103-26.

Bora, N. S., Jha, P. and Bora, P. S. 'The role of complement in ocular pathology'. *Seminars in immunopathology*: Springer, 85-95.

Borad, A. and Ward, H. (2010) 'Human immune responses in cryptosporidiosis', *Future Microbiol*, 5(3), pp. 507-19.

Borman, A. M., Szekely, A. and Johnson, E. M. (2016) 'Comparative Pathogenicity of United Kingdom Isolates of the Emerging Pathogen *Candida auris* and Other Key Pathogenic *Candida* Species', *mSphere*, 1(4).

Bouheraoua, N., Labbé, A., Chaumeil, C., Liang, Q., Laroche, L. and Borderie, V. (2014) '*Acanthamoeba keratitis*', *Journal francais d'ophtalmologie*, 37(8), pp. 640-652.

- Bouyer, S., Rodier, M.-H., Guillot, A. and Héchard, Y. (2009) 'Acanthamoeba castellanii: proteins involved in actin dynamics, glycolysis, and proteolysis are regulated during encystation', *Experimental parasitology*, 123(1), pp. 90-94.
- Bowers, B. and Korn, E. D. (1968) 'The fine structure of Acanthamoeba castellanii: I. The Trophozoite', *The Journal of Cell Biology*, 39(1), pp. 95-111.
- Bowers, B. and Korn, E. D. (1969) 'The fine structure of Acanthamoeba castellanii (Neff Strain): II. Encystment', *The Journal of cell biology*, 41(3), pp. 786-805.
- Bowers, B. and Olszewski, T. E. (1972) 'Pinocytosis in Acanthamoeba castellanii. Kinetics and morphology', *J Cell Biol*, 53(3), pp. 681-94.
- Brasseur, G., Favennec, L., Perrine, D., Chenu, J. and Brasseur, P. (1994) 'Successful treatment of Acanthamoeba keratitis by hexamidine', *Cornea*, 13(5), pp. 459-462.
- Brindley, N., Matin, A. and Khan, N. A. (2009) 'Acanthamoeba castellanii: high antibody prevalence in racially and ethnically diverse populations', *Exp Parasitol*, 121(3), pp. 254-6.
- Brunet, K., Eestermans, R., Rodier, M.-H. and Cateau, E. (2020) 'In vitro activity of isavuconazole against three species of Acanthamoeba', *Journal Français D'Ophtalmologie*, 43(4), pp. 330-333.
- Bryant, J. M., Baumgarten, S., Glover, L., Hutchinson, S. and Rachidi, N. (2019) 'CRISPR in Parasitology: Not Exactly Cut and Dried!', *Trends Parasitol*, 35(6), pp. 409-422.
- Buerano, C. C., Trinidad, A. D., Fajardo, L. S. N., Cua, I. Y., Baclig, M. O. and Natividad, F. F. (2014) 'Isolation of Acanthamoeba genotype T4 from a non-contact lens wearer from the Philippines', *Tropical medicine and health*, 42(4), pp. 145-147.
- Burger, G., Plante, I., Lonergan, K. M. and Gray, M. W. (1995) 'The mitochondrial DNA of the amoeboid protozoon, Acanthamoeba castellanii: complete sequence, gene content and genome organization', *Journal of molecular biology*, 245(5), pp. 522-537.
- Byers, T. J. (1986) 'Molecular Biology of DNA in Acanthamoeba, Amoeba, Entamoeba, and Naegleria', *International Review of Cytology*, 99, pp. 311-341.
- BYERS, T. J., HUGO, E. R. and STEWART, V. J. (1990) 'Genes of Acanthamoeba: DNA, RNA and protein sequences (a review)', *Journal of Eukaryotic Microbiology*, 37(4).
- Byers, T. J., Hugo, E. R. and Stewart, V. J. (1990) 'Genes of Acanthamoeba: DNA, RNA and protein sequences (a review)', *J Protozool*, 37(4), pp. 17S-25S.
- Byers, T. J., Kim, B. G., King, L. E. and Hugo, E. R. (1991) 'Molecular aspects of the cell cycle and encystment of Acanthamoeba', *Reviews of infectious diseases*, 13(Supplement_5), pp. S373-S384.
- Callicott, J. H., Nelson, E. C., Jones, M. M., dos Santos, J. G., Utz, J. P., Duma, R. J. and Morrison, J. V. (1968) 'Meningoencephalitis due to pathogenic free-living amoebae: report of two cases', *Jama*, 206(3), pp. 579-582.
- Cao, Z., Jefferson, D. M. and Panjwani, N. (1998) 'Role of carbohydrate-mediated adherence in cytopathogenic mechanisms of Acanthamoeba', *Journal of Biological Chemistry*, 273(25), pp. 15838-15845.

- Carrijo-Carvalho, L. C., Sant'ana, V. P., Foronda, A. S., de Freitas, D. and de Souza Carvalho, F. R. (2017) 'Therapeutic agents and biocides for ocular infections by free-living amoebae of Acanthamoeba genus', *Survey of Ophthalmology*, 62(2), pp. 203-218.
- Carter, R. F., Cullity, G., Ojeda, V., Silberstein, P. and Willaert, E. (1981) 'A fatal case of meningoencephalitis due to a free-living amoeba of uncertain identity—probably Acanthamoeba sp', *Pathology*, 13(1), pp. 51-68.
- Carvalho-Kelly, L. F., Pralon, C. F., Rocco-Machado, N., Nascimento, M. T., Carvalho-de-Araújo, A. D. and Meyer-Fernandes, J. R. (2020) 'Acanthamoeba castellanii phosphate transporter (AcPHS) is important to maintain inorganic phosphate influx and is related to trophozoite metabolic processes', *J Bioenerg Biomembr*, 52(2), pp. 93-102.
- Cerva, L. (1989) 'Acanthamoeba culbertsoni and Naegleria fowleri: occurrence of antibodies in man', *Journal of hygiene, epidemiology, microbiology, and immunology*, 33(1), pp. 99-103.
- Chao, M., Thongseesuksai, T., Boonmars, T. and Laummaunwai, P. (2020) 'Investigation of the in vitro cysticidal activity of miltefosine against Acanthamoeba spp', *Journal of Parasitic Diseases*, 44(2), pp. 491-495.
- Charret, K. S., Lagrota-Cândido, J., Carvalho-Pinto, C. E., Hottz, C. F., Lira, M. L., Rodrigues, R. F., Gomes, A. O., Bernardino, A. M., Canto-Cavalheiro, M. M., Leon, L. L. and Amaral, V. F. (2013) 'The histopathological and immunological pattern of CBA mice infected with Leishmania amazonensis after treatment with pyrazole carbohydrazide derivatives', *Exp Parasitol*, 133(2), pp. 201-10.
- Chatelain, E. and Konar, N. (2015) 'Translational challenges of animal models in Chagas disease drug development: a review', *Drug Des Devel Ther*, 9, pp. 4807-23.
- Chen, L., Orfeo, T., Gilmartin, G. and Bateman, E. (2004) 'Mechanism of cyst specific protein 21 mRNA induction during Acanthamoeba differentiation', *Biochimica et Biophysica Acta (BBA)-Molecular Cell Research*, 1691(1), pp. 23-31.
- Chen, Z., Xuguang, S., Zhiqun, W. and Ran, L. (2008) 'In vitro amoebacidal activity of photodynamic therapy on Acanthamoeba', *British Journal of Ophthalmology*, 92(9), pp. 1283.
- Chew, H. F., Yildiz, E. H., Hammersmith, K. M., Eagle Jr, R. C., Rapuano, C. J., Laibson, P. R., Ayres, B. D., Jin, Y.-P. and Cohen, E. J. (2011) 'Clinical outcomes and prognostic factors associated with Acanthamoeba keratitis', *Cornea*, 30(4), pp. 435-441.
- Chlapowski, F. J. and Band, R. N. (1971) 'ASSEMBLY OF LIPIDS INTO MEMBRANES IN ACANTHAMOEBA PALESTINENSIS: II. The Origin and Fate of Glycerol³H-Labeled Phospholipids of Cellular Membranes', *The Journal of cell biology*, 50(3), pp. 634-651.
- Choudhary, E., Thakur, P., Pareek, M. and Agarwal, N. (2015) 'Gene silencing by CRISPR interference in mycobacteria', *Nat Commun*, 6, pp. 6267.
- Chua, K. B. and Gubler, D. J. (2013) 'Perspectives of public health laboratories in emerging infectious diseases', *Emerging microbes & infections*, 2(6), pp. e37.
- Citorik, R. J., Mimee, M. and Lu, T. K. (2014) 'Sequence-specific antimicrobials using efficiently delivered RNA-guided nucleases', *Nature biotechnology*, 32(11), pp. 1141.
- Clarke, D. W. and Niederkorn, J. Y. (2006a) 'The immunobiology of Acanthamoeba keratitis', *Microbes and infection*, 8(5), pp. 1400-1405.

- Clarke, D. W. and Niederkorn, J. Y. (2006b) 'The pathophysiology of Acanthamoeba keratitis', *Trends Parasitol*, 22(4), pp. 175-80.
- Clarke, D. W. and Niederkorn, J. Y. (2006c) 'The pathophysiology of Acanthamoeba keratitis', *Trends in parasitology*, 22(4), pp. 175-180.
- Clarke, M., Lohan, A. J., Liu, B., Lagkouvardos, I., Roy, S., Zafar, N., Bertelli, C., Schilde, C., Kianianmomeni, A. and Bürglin, T. R. (2013a) 'Genome of Acanthamoeba castellanii highlights extensive lateral gene transfer and early evolution of tyrosine kinase signaling', *Genome biology*, 14(2), pp. R11.
- Clarke, M., Lohan, A. J., Liu, B., Lagkouvardos, I., Roy, S., Zafar, N., Bertelli, C., Schilde, C., Kianianmomeni, A., Bürglin, T. R., Frech, C., Turcotte, B., Kopec, K. O., Synnott, J. M., Choo, C., Paponov, I., Finkler, A., Heng Tan, C. S., Hutchins, A. P., Weinmeier, T., Rattei, T., Chu, J. S., Gimenez, G., Irimia, M., Rigden, D. J., Fitzpatrick, D. A., Lorenzo-Morales, J., Bateman, A., Chiu, C. H., Tang, P., Hegemann, P., Fromm, H., Raoult, D., Greub, G., Miranda-Saavedra, D., Chen, N., Nash, P., Ginger, M. L., Horn, M., Schaap, P., Caler, L. and Loftus, B. J. (2013b) 'Genome of Acanthamoeba castellanii highlights extensive lateral gene transfer and early evolution of tyrosine kinase signaling', *Genome Biol*, 14(2), pp. R11.
- Cope, J. (2014) 'CDC's Acanthamoeba Keratitis Investigations, 1985–2011 and Healthy Contact Lens Wear Initiative', *FDA*.
- Cornaby, C., Gibbons, L., Mayhew, V., Sloan, C. S., Welling, A. and Poole, B. D. (2015) 'B cell epitope spreading: mechanisms and contribution to autoimmune diseases', *Immunology letters*, 163(1), pp. 56-68.
- Cortes, A., Nequiz, M., Sandoval, J., Mendoza, E., Gudiño, M., López-Velázquez, G., Enríquez-Flores, S., Saavedra, E., Pérez-Tamayo, R. and Olivos-García, A. (2019) 'Mechanisms of natural resistance of Balb/c mice to experimental liver amoebiasis', *Biosci Rep*, 39(5).
- Craig, A. G., Grau, G. E., Janse, C., Kazura, J. W., Milner, D., Barnwell, J. W., Turner, G., Langhorne, J. and Malaria, p. o. t. H. R. m. o. A. M. f. R. o. S. (2012) 'The role of animal models for research on severe malaria', *PLoS Pathog*, 8(2), pp. e1002401.
- Crary, M. J. (2012) *Genetic variability and its relationship to Acanthamoeba pathogenesis*. The Ohio State University.
- Cristina, S., Cristina, V. and Mihaela, P. (2016) 'Acanthamoeba keratitis challenges a case report', *Romanian journal of ophthalmology*, 60(1), pp. 40.
- Cursons, R., Brown, T., Keys, E., Moriarty, K. and Till, D. (1980) 'Immunity to pathogenic free-living amoebae: role of cell-mediated immunity', *Infection and immunity*, 29(2), pp. 408-410.
- D'Incalci, M. and Galmarini, C. M. (2010) 'A review of trabectedin (ET-743): a unique mechanism of action', *Molecular cancer therapeutics*, 9(8), pp. 2157-2163.
- Dart, J. K., Saw, V. P. and Kilvington, S. (2009) 'Acanthamoeba keratitis: diagnosis and treatment update 2009', *Am J Ophthalmol*, 148(4), pp. 487-499.e2.
- Davies, G. M., Barrett-Bee, K. J., Jude, D. A., Lehan, M., Nichols, W. W., Pinder, P. E., Thain, J. L., Watkins, W. J. and Wilson, R. G. (1994) '(6S)-6-fluoroshikimic acid, an antibacterial agent acting on the aromatic biosynthetic pathway', *Antimicrob Agents Chemother*, 38(2), pp. 403-6.

- De Niz, M., Meibalan, E., Mejia, P., Ma, S., Brancucci, N. M. B., Agop-Nersesian, C., Mandt, R., Ngotho, P., Hughes, K. R., Waters, A. P., Huttenhower, C., Mitchell, J. R., Martinelli, R., Frischknecht, F., Seydel, K. B., Taylor, T., Milner, D., Heussler, V. T. and Marti, M. (2018) 'gametocytes display homing and vascular transmigration in the host bone marrow', *Sci Adv*, 4(5), pp. eaat3775.
- De Obeso Fernandez Del Valle, A., Lorenzo-Morales, J. and Maciver, S. K. (2017) 'Leptomyxa valladaresi n. sp. (Amoebozoa, Tubulinea, Leptomyxida), from Mount Teide, Tenerife, Spain', *Exp Parasitol*, 183, pp. 85-91.
- Dearborn, D. G. and Korn, E. D. (1974) 'Lipophosphoglycan of the Plasma Membrane of Acanthamoeba castellanii FATTY ACID COMPOSITION', *Journal of Biological Chemistry*, 249(11), pp. 3342-3346.
- Debnath, A., Tunac, J. B., Silva-Olivares, A., Galindo-Gómez, S., Shibayama, M. and McKerrow, J. H. (2014) 'In Vitro Efficacy of Corifungin against Acanthamoeba castellanii Trophozoites and Cysts', *Antimicrobial Agents and Chemotherapy*, 58(3), pp. 1523-1528.
- del Buey, M. A., Cristóbal, J. A., Casas, P., Goñi, P., Clavel, A., Mínguez, E., Lanchares, E., García, A. and Calvo, B. (2012) 'Evaluation of In Vitro Efficacy of Combined Riboflavin and Ultraviolet A for Acanthamoeba Isolates', *American Journal of Ophthalmology*, 153(3), pp. 399-404.
- Del Poeta, M., Schell, W. A., Dykstra, C. C., Jones, S., Tidwell, R. R., Czarny, A., Bajic, M., Bajic, M., Kumar, A. and Boykin, D. (1998) 'Structure-in vitro activity relationships of pentamidine analogues and dication-substituted bis-benzimidazoles as new antifungal agents', *Antimicrobial agents and chemotherapy*, 42(10), pp. 2495-2502.
- Demirci, G., Ay, G. M., Karabas, L. V., Altintas, Ö., Tamer, G. S. and Çağlar, Y. (2006) 'Acanthamoeba Keratitis in a 5-Year-Old Boy Without a History of Contact Lens Usage', *Cornea*, 25(3).
- Derda, M., Hadaś, E. and Thiem, B. (2008) 'Plant extracts as natural amoebicidal agents', *Parasitology Research*, 104(3), pp. 705.
- Derrer, B., Macheroux, P. and Kappes, B. (2013) 'The shikimate pathway in apicomplexan parasites: implications for drug development', *Front Biosci (Landmark Ed)*, 18, pp. 944-69.
- Desbois, A. P. and Coote, P. J. (2011) 'Wax moth larva (*Galleria mellonella*): an in vivo model for assessing the efficacy of antistaphylococcal agents', *J Antimicrob Chemother*, 66(8), pp. 1785-90.
- Desbois, A. P. and Coote, P. J. (2012) 'Utility of Greater Wax Moth Larva (*Galleria mellonella*) for Evaluating the Toxicity and Efficacy of New Antimicrobial Agents', *Adv Appl Microbiol*, 78, pp. 25-53.
- Diamond, L. S., Tanimoto Weki, M. and Martínez-Palomo, A. (1978) 'Production of cecal lesions in newborn guinea pigs with axenically cultivated *Entamoeba histolytica*', *Arch Invest Med (Mex)*, 9 Suppl 1, pp. 223-8.
- Dias, M. V., Ely, F., Palma, M. S., de Azevedo, W. F., Basso, L. A. and Santos, D. S. (2007) 'Chorismate synthase: an attractive target for drug development against orphan diseases', *Curr Drug Targets*, 8(3), pp. 437-44.
- Doudna, J. A. and Charpentier, E. (2014) 'Genome editing. The new frontier of genome engineering with CRISPR-Cas9', *Science*, 346(6213), pp. 1258096.

- Driebe, W. T., Jr., Stern, G. A., Epstein, R. J., Visvesvara, G. S., Adi, M. and Komadina, T. (1988) 'Acanthamoeba Keratitis: Potential Role for Topical Clotrimazole in Combination Chemotherapy', *Archives of Ophthalmology*, 106(9), pp. 1196-1201.
- Du, Q., Schilde, C., Birgersson, E., Chen, Z.-h., McElroy, S. and Schaap, P. (2014) 'The cyclic AMP phosphodiesterase RegA critically regulates encystation in social and pathogenic amoebas', *Cellular signalling*, 26(2), pp. 453-459.
- Duarte, J. L., Furst, C., Klisiowicz, D. R., Klassen, G. and Costa, A. O. (2013) 'Morphological, genotypic, and physiological characterization of Acanthamoeba isolates from keratitis patients and the domestic environment in Vitoria, Espírito Santo, Brazil', *Experimental parasitology*, 135(1), pp. 9-14.
- Dudley, R., Jarroll, E. L. and Khan, N. A. (2009) 'Carbohydrate analysis of Acanthamoeba castellanii', *Experimental parasitology*, 122(4), pp. 338-343.
- Duggal, S. D., Rongpharpi, S. R., Duggal, A. K., Kumar, A. and Biswal, I. (2018) 'Role of Acanthamoeba in Granulomatous Encephalitis: A Review', *Journal of Infectious Diseases & Immune Therapies*, 2017.
- Duguid, I. G. M., Dart, J. K. G., Morlet, N., Allan, B. D. S., Matheson, M., Ficker, L. and Tuft, S. (1997) 'Outcome of Acanthamoeba Keratitis Treated with Polyhexamethyl Biguanide and Propamidine', *Ophthalmology*, 104(10), pp. 1587-1592.
- Duma, R. J. and Finley, R. (1976) 'In Vitro Susceptibility of Pathogenic *Naegleria* and *Acanthamoeba* Species to a Variety of Therapeutic Agents', *Antimicrobial Agents and Chemotherapy*, 10(2), pp. 370-376.
- Dwia Pertiwi, Y., Chikama, T., Sueoka, K., Ko, J.-A., Kiuchi, Y., Onodera, M. and Sakaguchi, T. (2021) 'Efficacy of Photodynamic Anti-Microbial Chemotherapy for Acanthamoeba Keratitis In Vivo', *Lasers in Surgery and Medicine*, 53(5), pp. 695-702.
- Dyatkina, N. B., Roberts, C. D., Keicher, J. D., Dai, Y., Nadherny, J. P., Zhang, W., Schmitz, U., Kongpachith, A., Fung, K. and Novikov, A. A. (2002) 'Minor groove DNA binders as antimicrobial agents. 1. Pyrrole tetraamides are potent antibacterials against vancomycin resistant Enterococci and methicillin resistant Staphylococcus aureus', *Journal of medicinal chemistry*, 45(4), pp. 805-817.
- Elsheikha, H. M., Siddiqui, R. and Khan, N. A. (2020) 'Drug Discovery against Acanthamoeba Infections: Present Knowledge and Unmet Needs', *Pathogens*, 9(5).
- Ertabaklar, H., Türk, M., Dayanir, V., Ertuğ, S. and Walochnik, J. (2007) 'Acanthamoeba keratitis due to Acanthamoeba genotype T4 in a non-contact-lens wearer in Turkey', *Parasitology research*, 100(2), pp. 241-246.
- Fanselow, N., Sirajuddin, N., Yin, X. T., Huang, A. J. W. and Stuart, P. M. (2021) 'Keratitis, Pathology, Diagnosis and Treatment', *Pathogens*, 10(3).
- Farboud, B. and Meyer, B. J. (2015) 'Dramatic Enhancement of Genome Editing by CRISPR/Cas9 Through Improved Guide RNA Design', *Genetics*, 199(4), pp. 959-971.
- Feng, X., Zheng, W., Wang, Y., Zhao, D., Jiang, X. and Lv, S. (2015) 'A rabbit model of Acanthamoeba keratitis that better reflects the natural human infection', *The Anatomical Record*, 298(8), pp. 1509-1517.
- Ferrante, A. and Rowan-Kelly, B. (1983) 'Activation of the alternative pathway of complement by Acanthamoeba culbertsoni', *Clinical and experimental immunology*, 54(2), pp. 477.

Fichtner, F., Urrea Castellanos, R. and Ülker, B. (2014) 'Precision genetic modifications: a new era in molecular biology and crop improvement', *Planta*, 239(4), pp. 921-939.

Fini, M. E., Girard, M. T. and Matsubara, M. (1992) 'Collagenolytic/gelatinolytic enzymes in corneal wound healing', *Acta ophthalmologica*, 70(S202), pp. 26-33.

Firacative, C., Khan, A., Duan, S., Ferreira-Paim, K., Leemon, D. and Meyer, W. (2020) 'Rearing and Maintenance of', *J Fungi (Basel)*, 6(3).

Fonseca-Berzal, C., Arán, V. J., Escario, J. A. and Gómez-Barrio, A. (2018) 'Experimental models in Chagas disease: a review of the methodologies applied for screening compounds against *Trypanosoma cruzi*', *Parasitol Res*, 117(11), pp. 3367-3380.

Fouque, E., Trouilhé, M.-C., Thomas, V., Hartemann, P., Rodier, M.-H. and Héchard, Y. (2012) 'Cellular, biochemical, and molecular changes during encystment of free-living amoebae', *Eukaryotic cell*, 11(4), pp. 382-387.

Fuchs, B. B., O'Brien, E., Houry, J. B. and Mylonakis, E. (2010) 'Methods for using *Galleria mellonella* as a model host to study fungal pathogenesis', *Virulence*, 1(6), pp. 475-82.

Fučíková, K. and Lahr, D. J. (2016) 'Uncovering cryptic diversity in two amoebozoan species using complete mitochondrial genome sequences', *Journal of Eukaryotic Microbiology*, 63(1), pp. 112-122.

Gagnon, J. A., Valen, E., Thyme, S. B., Huang, P., Akhmetova, L., Ahkmetova, L., Pauli, A., Montague, T. G., Zimmerman, S., Richter, C. and Schier, A. F. (2014) 'Efficient mutagenesis by Cas9 protein-mediated oligonucleotide insertion and large-scale assessment of single-guide RNAs', *PLoS One*, 9(5), pp. e98186.

Galarza, C., Ramos, W., Gutierrez, E. L., Ronceros, G., Teran, M., Uribe, M., Navincopa, M. and Ortega-Loayza, A. G. (2009) 'Cutaneous acanthamebiasis infection in immunocompetent and immunocompromised patients', *Int J Dermatol*, 48(12), pp. 1324-9.

Garg, P., Kalra, P. and Joseph, J. (2017) 'Non-contact lens related *Acanthamoeba* keratitis', *Indian journal of ophthalmology*, 65(11), pp. 1079.

Gawryluk, R. M., Chisholm, K. A., Pinto, D. M. and Gray, M. W. (2014) 'Compositional complexity of the mitochondrial proteome of a unicellular eukaryote (*Acanthamoeba castellanii*, supergroup Amoebozoa) rivals that of animals, fungi, and plants', *Journal of proteomics*, 109, pp. 400-416.

Ge, Y., Difuntorum, S., Touami, S., Critchley, I., Bürli, R., Jiang, V., Drazan, K. and Moser, H. (2002) 'In vitro antimicrobial activity of GSQ1530, a new heteroaromatic polycyclic compound', *Antimicrobial agents and chemotherapy*, 46(10), pp. 3168-3174.

Geuthner, A. C., Koethe, M., Ludewig, M., Pott, S., Schares, G., Maksimov, P., Dausgies, A. and Bangoura, B. (2019) 'Development of an in vivo model for *Toxoplasma gondii* infections in chickens and turkeys simulating natural routes of infection', *Vet Parasitol*, 276, pp. 108956.

Ghorbal, M., Gorman, M., Macpherson, C. R., Martins, R. M., Scherf, A. and Lopez-Rubio, J. J. (2014) 'Genome editing in the human malaria parasite *Plasmodium falciparum* using the CRISPR-Cas9 system', *Nat Biotechnol*, 32(8), pp. 819-21.

Giannangelo, C. R., Ellis, K. M., Sexton, A. E., Stoessel, D. and Creek, D. J. (2016) 'The Role of Metabolomics in Antiparasitic Drug Discovery', *Comprehensive Analysis of Parasite Biology: From Metabolism to Drug Discovery*, 7, pp. 321.

Giordani, F., Khalaf, A. I., Gillingwater, K., Munday, J. C., de Koning, H. P., Suckling, C. J., Barrett, M. P. and Scott, F. J. (2019) 'Novel Minor Groove Binders Cure Animal African Trypanosomiasis in an in Vivo Mouse Model', *J Med Chem*, 62(6), pp. 3021-3035.

Goldschmidt, P., Degorge, S., Benallaoua, D., Saint-Jean, C., Batellier, L., Alouch, C., Laroche, L. and Chaumeil, C. (2009) 'New tool for the simultaneous detection of 10 different genotypes of *Acanthamoeba* available from the American Type Culture Collection', *British Journal of Ophthalmology*, 93(8), pp. 1096-1100.

Gomart, G., Denis, J., Bourcier, T., Dory, A., Abou-Bacar, A., Candolfi, E. and Sauer, A. (2018) 'In Vitro Amoebicidal Activity of Titanium Dioxide/UV-A Combination Against *Acanthamoeba*', *Investigative Ophthalmology & Visual Science*, 59(11), pp. 4567-4571.

González-Robles, A., Castañón, G., Hernández-Ramírez, V. I., Salazar-Villatoro, L., González-Lázaro, M., Omaña-Molina, M., Talamás-Rohana, P. and Martínez-Palomo, A. (2008) '*Acanthamoeba castellanii*: identification and distribution of actin cytoskeleton', *Experimental parasitology*, 119(3), pp. 411-417.

Gordon, D. J., Eisenberg, E. and Korn, E. D. (1976) 'Characterization of cytoplasmic actin isolated from *Acanthamoeba castellanii* by a new method', *Journal of Biological Chemistry*, 251(15), pp. 4778-4786.

Gordon, V. R., Asem, E. K., Vodkin, M. H. and McLaughlin, G. L. (1993) '*Acanthamoeba* binds to extracellular matrix proteins in vitro', *Investigative ophthalmology & visual science*, 34(3), pp. 658-662.

Greub, G. and Raoult, D. (2004) 'Microorganisms resistant to free-living amoebae', *Clin Microbiol Rev*, 17(2), pp. 413-33.

Griffin, J. L. (1972) 'Temperature tolerance of pathogenic and nonpathogenic free-living amoebas', *Science*, 178(4063), pp. 869-870.

Grimaldi, G. (2008) 'The utility of rhesus monkey (*Macaca mulatta*) and other non-human primate models for preclinical testing of *Leishmania* candidate vaccines', *Mem Inst Oswaldo Cruz*, 103(7), pp. 629-44.

Grzybek, M., Golonko, A., Górska, A., Szczepaniak, K., Strachecka, A., Lass, A. and Lisowski, P. (2018) 'The CRISPR/Cas9 system sheds new lights on the biology of protozoan parasites', *Applied Microbiology and Biotechnology*, 102(11), pp. 4629-4640.

Grün, A.-L., Stemplewitz, B. and Scheid, P. (2014) 'First report of an *Acanthamoeba* genotype T13 isolate as etiological agent of a keratitis in humans', *Parasitology research*, 113(6), pp. 2395-2400.

Gubbels, M. J. and Striepen, B. (2004) 'Studying the cell biology of apicomplexan parasites using fluorescent proteins', *Microsc Microanal*, 10(5), pp. 568-79.

Guedes, P. M., Veloso, V. M., Tafuri, W. L., Galvão, L. M., Carneiro, C. M., Lana, M., Chiari, E., Ataíde Soares, K. and Bahia, M. T. (2002) 'The dog as model for chemotherapy of the Chagas' disease', *Acta Trop*, 84(1), pp. 9-17.

Gueudry, J., Le Goff, L., Compagnon, P., Lefevre, S., Colasse, E., Aknine, C., Duval, F., François, A., Razakandrainibe, R., Ballet, J. J., Muraine, M. and Favennec, L. (2018) 'Evaluation of voriconazole anti-*Acanthamoeba polyphaga* in vitro activity, rat cornea penetration and efficacy against experimental rat *Acanthamoeba* keratitis', *Journal of Antimicrobial Chemotherapy*, 73(7), pp. 1895-1898.

- Guimaraes, A. J., Gomes, K. X., Cortines, J. R., Peralta, J. M. and Peralta, R. H. (2016) 'Acanthamoeba spp. as a universal host for pathogenic microorganisms: One bridge from environment to host virulence', *Microbiol Res*, 193, pp. 30-38.
- Hadas, E. and Mazur, T. (1997) 'Biosynthesis of prostaglandins in pathogenic and nonpathogenic strains of Acanthamoeba spp', *Parasitology research*, 83(3), pp. 296-299.
- Hafiz, S. and Kyriakopoulos, C. (2021) *Pentamidine*. Treasure Island (FL): StatPearls Publishing. Available at: <https://www.ncbi.nlm.nih.gov/books/NBK557586/> (Accessed).
- Hamilton, P. L. and Arya, D. P. (2012) 'Natural product DNA major groove binders', *Natural product reports*, 29(2), pp. 134-143.
- Hargrave, S. L., McCulley, J. P. and Hussein, Z. (1999) 'Results of a trial of combined propamidine isethionate and neomycin therapy for acanthamoeba keratitis', *Ophthalmology*, 106(5), pp. 952-957.
- Harnish, J. M., Link, N. and Yamamoto, S. (2021) 'as a Model for Infectious Diseases', *Int J Mol Sci*, 22(5).
- Harrison, P. T. and Hart, S. (2018) 'A beginner's guide to gene editing', *Experimental Physiology*, 103(4), pp. 439-448.
- Hau, S. C., Dart, J. K., Vesaluoma, M., Parmar, D. N., Claerhout, I., Bibi, K. and Larkin, D. F. (2010) 'Diagnostic accuracy of microbial keratitis with in vivo scanning laser confocal microscopy', *British Journal of Ophthalmology*, 94(8), pp. 982-987.
- He, Y. G., McCulley, J. P., Alizadeh, H., Pidherney, M., Mellon, J., Ubelaker, J. E., Stewart, G. L., Silvany, R. E. and Niederkorn, J. Y. (1992) 'A pig model of Acanthamoeba keratitis: transmission via contaminated contact lenses', *Investigative Ophthalmology & Visual Science*, 33(1), pp. 126-133.
- Heaselgrave, W., Hamad, A., Coles, S. and Hau, S. (2019) 'In Vitro Evaluation of the Inhibitory Effect of Topical Ophthalmic Agents on Acanthamoeba Viability', *Translational Vision Science & Technology*, 8(5), pp. 17-17.
- Hemady, R. K., Chu, W. and Foster, C. S. (1992) 'Intraocular Penetration of Ketoconazole in Rabbits', *Cornea*, 11(4).
- Henriquez, F. L., Campbell, S. J., Sundararaj, B. K., Cano, A., Muench, S. P. and Roberts, C. W. (2015) 'The Acanthamoeba shikimate pathway has a unique molecular arrangement and is essential for aromatic amino acid biosynthesis', *Protist*, 166(1), pp. 93-105.
- Henriquez, F. L., Mooney, R., Bandel, T., Giammarini, E., Zeroual, M., Fiori, P. L., Margarita, V., Rappelli, P. and Dessi, D. (2020) 'Paradigms of Protist/Bacteria Symbioses Affecting Human Health:' *Front Microbiol*, 11, pp. 616213.
- Herrmann, K. M. (1995) 'The shikimate pathway as an entry to aromatic secondary metabolism', *Plant Physiol*, 107(1), pp. 7-12.
- Hirabayashi, K. E., Lin, C. C. and Ta, C. N. (2019) 'Oral miltefosine for refractory Acanthamoeba keratitis', *American Journal of Ophthalmology Case Reports*, 16, pp. 100555.
- Hirst, L. W., Green, W. R., Merz, W., Kaufmann, C., Visvesvara, G. S., Jensen, A. and Howard, M. (1984) 'Management of Acanthamoeba Keratitis: A Case Report and Review of the Literature', *Ophthalmology*, 91(9), pp. 1105-1111.

- Hlaka, L., Rosslee, M. J., Ozturk, M., Kumar, S., Parihar, S. P., Brombacher, F., Khalaf, A. I., Carter, K. C., Scott, F. J., Suckling, C. J. and Guler, R. (2017) 'Evaluation of minor groove binders (MGBs) as novel anti-mycobacterial agents and the effect of using non-ionic surfactant vesicles as a delivery system to improve their efficacy', *J Antimicrob Chemother*, 72(12), pp. 3334-3341.
- Horáčková, V., Voleman, L., Petrů, M., Vinopalová, M., Weisz, F., Janowicz, N., Marková, L., Motyčková, A., Tůmová, P. and Doležal, P. (2021) 'Cas9-mediated genome editing in *Giardia intestinalis*', *bioRxiv*, pp. 2021.04.21.440745.
- Hryhorowicz, M., Lipiński, D., Zeyland, J. and Słomski, R. (2017) 'CRISPR/Cas9 Immune System as a Tool for Genome Engineering', *Archivum Immunologiae et Therapiae Experimentalis*, 65(3), pp. 233-240.
- Hu, Q. and Henney, H. R. (1997) 'An Acanthamoeba polyubiquitin gene and application of its promoter to the establishment of a transient transfection system', *Biochimica et Biophysica Acta (BBA) - Gene Structure and Expression*, 1351(1), pp. 126-136.
- Huang, J. M., Chang, Y. T., Shih, M. H., Lin, W. C. and Huang, F. C. (2019) 'Identification and characterization of a secreted M28 aminopeptidase protein in Acanthamoeba', *Parasitol Res*, 118(6), pp. 1865-1874.
- Huang, T. L., Mayence, A. and Vanden Eynde, J. J. (2014) 'Some non-conventional biomolecular targets for diamidines. A short survey', *Bioorganic & Medicinal Chemistry*, 22(7), pp. 1983-1992.
- Hugo, E. R. and Byers, T. J. (1993) 'S-adenosyl-L-methionine decarboxylase of Acanthamoeba castellanii (Neff): purification and properties', *Biochemical Journal*, 295(1), pp. 203-209.
- Hurt, M., Apte, S., Leher, H., Howard, K., Niederkorn, J. and Alizadeh, H. (2001) 'Exacerbation of Acanthamoeba keratitis in animals treated with anti-macrophage inflammatory protein 2 or antineutrophil antibodies', *Infection and immunity*, 69(5), pp. 2988-2995.
- Hurt, M., Neelam, S., Niederkorn, J. and Alizadeh, H. (2003) 'Pathogenic Acanthamoeba spp. secrete a mannose-induced cytolytic protein that correlates with the ability to cause disease', *Infection and immunity*, 71(11), pp. 6243-6255.
- Ignasiak, K. and Maxwell, A. (2017) 'Galleria mellonella (greater wax moth) larvae as a model for antibiotic susceptibility testing and acute toxicity trials', *BMC Res Notes*, 10(1), pp. 428.
- Illingworth, C., Cook, S., Karabatsas, C. and Easty, D. (1995) 'Acanthamoeba keratitis: risk factors and outcome', *British journal of ophthalmology*, 79(12), pp. 1078-1082.
- Illingworth, C. D. and Cook, S. D. (1998) 'Acanthamoeba keratitis', *Surv Ophthalmol*, 42(6), pp. 493-508.
- Indiani de Oliveira, C., Teixeira, M. J., Teixeira, C. R., Ramos de Jesus, J., Bomura Rosato, A., Santa da Silva, J., Brodskyn, C., Barral-Netto, M. and Barral, A. (2004) 'Leishmania braziliensis isolates differing at the genome level display distinctive features in BALB/c mice', *Microbes Infect*, 6(11), pp. 977-84.
- Iovieno, A., Gore, D. M., Carnt, N. and Dart, J. K. (2014a) 'Acanthamoeba sclerokeratitis: epidemiology, clinical features, and treatment outcomes', *Ophthalmology*, 121(12), pp. 2340-2347.
- Iovieno, A., Ledee, D. R., Miller, D. and Alfonso, E. C. (2010) 'Detection of bacterial endosymbionts in clinical Acanthamoeba isolates', *Ophthalmology*, 117(3), pp. 445-452. e3.

- Iovieno, A., Miller, D., Ledee, D. R. and Alfonso, E. C. (2014b) 'Cysticidal Activity of Antifungals against Different Genotypes of Acanthamoeba', *Antimicrobial Agents and Chemotherapy*, 58(9), pp. 5626-5628.
- Ishibashi, Y., Matsumoto, Y., Kabata, T., Watanabe, R., Hommura, S., Yasuraoka, K. and Ishii, K. (1990) 'Oral Itraconazole and Topical Miconazole With Debridement for Acanthamoeba Keratitis', *American Journal of Ophthalmology*, 109(2), pp. 121-126.
- Ishino, Y., Shinagawa, H., Makino, K., Amemura, M. and Nakata, A. (1987) 'Nucleotide sequence of the iap gene, responsible for alkaline phosphatase isozyme conversion in Escherichia coli, and identification of the gene product', *J Bacteriol*, 169(12), pp. 5429-33.
- Jager, B. V. and Stamm, W. P. (1972) 'Brain abscesses caused by free-living amoeba probably of the genus Hartmannella in a patient with Hodgkin's disease', *Lancet*, 2(7791), pp. 1343-5.
- Janjigian, Y. Y., Lee, W., Kris, M. G., Miller, V. A., Krug, L. M., Azzoli, C. G., Senturk, E., Calcutt, M. W. and Rizvi, N. A. (2010) 'A phase I trial of SJG-136 (NSC#694501) in advanced solid tumors', *Cancer Chemother Pharmacol*, 65(5), pp. 833-8.
- Janssen, B. D., Chen, Y.-P., Molgora, B. M., Wang, S. E., Simoes-Barbosa, A. and Johnson, P. J. (2018) 'CRISPR/Cas9-mediated gene modification and gene knock out in the human-infective parasite Trichomonas vaginalis', *Scientific Reports*, 8(1), pp. 270.
- Jantzen, H., Schulze, I. and Stohr, M. (1988) 'Relationship between the timing of DNA replication and the developmental competence in Acanthamoeba castellanii', *Journal of cell science*, 91(3), pp. 389-399.
- Jemel, S., Guillot, J., Kallel, K., Botterel, F. and Dannaoui, E. (2020) 'for the Evaluation of Antifungal Efficacy against Medically Important Fungi, a Narrative Review', *Microorganisms*, 8(3).
- Jenkins, T. C. and Lane, A. N. (1997) 'AT selectivity and DNA minor groove binding: modelling, NMR and structural studies of the interactions of propamidine and pentamidine with d(CGCGAATTCGCG)₂', *Biochimica et Biophysica Acta (BBA) - Gene Structure and Expression*, 1350(2), pp. 189-204.
- Jha, B. K., Jung, H.-J., Seo, I., Kim, H. A., Suh, S.-I., Suh, M.-H. and Baek, W.-K. (2014) 'Chloroquine Has a Cytotoxic Effect on Acanthamoeba Encystation through Modulation of Autophagy', *Antimicrobial Agents and Chemotherapy*, 58(10), pp. 6235-6241.
- Jha, B. K., Seo, I., Kong, H.-H., Suh, S.-I., Suh, M.-H. and Baek, W.-K. (2015) 'Tigecycline inhibits proliferation of Acanthamoeba castellanii', *Parasitology Research*, 114(3), pp. 1189-1195.
- Jiang, W., Bikard, D., Cox, D., Zhang, F. and Marraffini, L. A. (2013) 'RNA-guided editing of bacterial genomes using CRISPR-Cas systems', *Nat Biotechnol*, 31(3), pp. 233-9.
- Johnston, S. P., Sriram, R., Qvarnstrom, Y., Roy, S., Verani, J., Yoder, J., Lorick, S., Roberts, J., Beach, M. J. and Visvesvara, G. (2009) 'Resistance of Acanthamoeba cysts to disinfection in multiple contact lens solutions', *Journal of clinical microbiology*, 47(7), pp. 2040-2045.
- Jones, D., Visvesvara, G. and Robinson, N. (1975) 'Acanthamoeba polyphaga keratitis and Acanthamoeba uveitis associated with fatal meningoencephalitis', *Trans Ophthalmol Soc UK*, 95(2), pp. 221-232.

- Joo, S. Y., Aung, J. M., Shin, M., Moon, E. K., Kong, H. H., Goo, Y. K., Chung, D. I. and Hong, Y. (2020) 'The role of the *Acanthamoeba castellanii* Sir2-like protein in the growth and encystation of *Acanthamoeba*', *Parasit Vectors*, 13(1), pp. 368.
- Joslin, C. E., Tu, E. Y., McMahon, T. T., Passaro, D. J., Stayner, L. T. and Sugar, J. (2006) 'Epidemiological characteristics of a Chicago-area *Acanthamoeba* keratitis outbreak', *American journal of ophthalmology*, 142(2), pp. 212-217. e2.
- Joslin, C. E., Tu, E. Y., Shoff, M. E., Booton, G. C., Fuerst, P. A., McMahon, T. T., Anderson, R. J., Dworkin, M. S., Sugar, J. and Davis, F. G. (2007) 'The association of contact lens solution use and *Acanthamoeba* keratitis', *American journal of ophthalmology*, 144(2), pp. 169-180. e2.
- Juárez, M., Tártara, L., Cid, A., Real, J., Bermúdez, J., Rajal, V. and Palma, S. (2017) '*Acanthamoeba* in the eye, can the parasite hide even more? Latest developments on the disease', *Contact Lens and Anterior Eye*.
- Kamal, F., Peters, D. L., McCutcheon, J. G., Dunphy, G. B. and Dennis, J. J. (2019) 'Use of Greater Wax Moth Larvae (*Galleria mellonella*) as an Alternative Animal Infection Model for Analysis of Bacterial Pathogenesis', *Methods Mol Biol*, 1898, pp. 163-171.
- Kangussu-Marcolino, M. M., Morgado, P., Manna, D., Yee, H. and Singh, U. (2021) 'Development of a CRISPR/Cas9 system in *Entamoeba histolytica*: proof of concept', *Int J Parasitol*, 51(2-3), pp. 193-200.
- Kassab, K., Dei, D., Roncucci, G., Jori, G. and Coppellotti, O. (2003) 'Phthalocyanine-photosensitized inactivation of a pathogenic protozoan, *Acanthamoeba palestinensis*', *Photochemical & Photobiological Sciences*, 2(6), pp. 668-672.
- Kaufman, S. C., Musch, D. C., Belin, M. W., Cohen, E. J., Meisler, D. M., Reinhart, W. J., Udell, I. J. and Van Meter, W. S. (2004) 'Confocal microscopy: a report by the American Academy of Ophthalmology', *Ophthalmology*, 111(2), pp. 396-406.
- Kaur, I. P., Rana, C. and Singh, H. (2008) 'Development of Effective Ocular Preparations of Antifungal Agents', *Journal of Ocular Pharmacology and Therapeutics*, 24(5), pp. 481-494.
- Kenawy, E.-R., Worley, S. D. and Broughton, R. (2007) 'The Chemistry and Applications of Antimicrobial Polymers: A State-of-the-Art Review', *Biomacromolecules*, 8(5), pp. 1359-1384.
- Kennett, M. J., Hook, R. R., Franklin, C. L. and Riley, L. K. (1999) '*Acanthamoeba castellanii*: characterization of an adhesin molecule', *Exp Parasitol*, 92(3), pp. 161-9.
- Khalaf, A. I. (2009) 'Minor groove binders: Some recent research in drug development', *Current Trends in Medicinal Chemistry*, 6, pp. 53-63.
- Khalaf, A. I., Waigh, R. D., Drummond, A. J., Pringle, B., McGroarty, I., Skellern, G. G. and Suckling, C. J. (2004) 'Distamycin analogues with enhanced lipophilicity: synthesis and antimicrobial activity', *Journal of medicinal chemistry*, 47(8), pp. 2133-2156.
- Khan, N. A. (2006a) '*Acanthamoeba*: biology and increasing importance in human health', *FEMS microbiology reviews*, 30(4), pp. 564-595.
- Khan, N. A. (2006b) '*Acanthamoeba*: biology and increasing importance in human health', *FEMS Microbiol Rev*, 30(4), pp. 564-95.
- Khan, N. A. (2010) 'Novel in vitro and in vivo models to study central nervous system infections due to *Acanthamoeba* spp', *Experimental Parasitology*, 126(1), pp. 69-72.

- Khan, N. A. (2015) *Acanthamoeba*. Caister Academic Press.
- Khan, N. A. and Siddiqui, R. (2009) 'Acanthamoeba affects the integrity of human brain microvascular endothelial cells and degrades the tight junction proteins', *International journal for parasitology*, 39(14), pp. 1611-1616.
- Khan, N. A. and Siddiqui, R. (2015) 'Is there evidence of sexual reproduction (meiosis) in Acanthamoeba?', *Pathogens and global health*, 109(4), pp. 193-195.
- Khan, Y. A., Kashiwabuchi, R. T., Martins, S. A., Castro-Combs, J. M., Kalyani, S., Stanley, P., Flikier, D. and Behrens, A. (2011) 'Riboflavin and ultraviolet light a therapy as an adjuvant treatment for medically refractive Acanthamoeba keratitis: report of 3 cases', *Ophthalmology*, 118(2), pp. 324-331.
- Khunkitti, Hann, Lloyd, Furr and Russell (1998) 'Biguanide-induced changes in Acanthamoeba castellanii: an electron microscopic study', *Journal of Applied Microbiology*, 84(1), pp. 53-62.
- Kitagawa, K., Nakamura, T., Takahashi, N., Oikawa, Y. and Ikeda, T. (2003) 'A novel combination treatment of chlorhexidine gluconate, natamycin (pimaricin) and debridement for a Acanthamoeba keratitis', *Japanese Journal of Ophthalmology*, 47(6), pp. 616-617.
- Kliescikova, J., Kulda, J. and Nohynkova, E. (2011) 'Propylene glycol and contact-lens solutions containing this diol induce pseudocyst formation in acanthamoebae', *Experimental parasitology*, 127(1), pp. 326-328.
- Koike-Yusa, H., Li, Y., Tan, E. P., Velasco-Herrera, M. e. C. and Yusa, K. (2014) 'Genome-wide recessive genetic screening in mammalian cells with a lentiviral CRISPR-guide RNA library', *Nat Biotechnol*, 32(3), pp. 267-73.
- Kokot, J., Dobrowolski, D., Lyssek-Boroń, A., Milka, M., Smedowski, A., Wowra, B. and Wyligala, E. (2012) 'New approach to diagnosis and treatment of Acanthamoeba keratitis--systematic review of literature', *Klinika oczna*, 114(4), pp. 311-316.
- Kong, H.-H. and Pollard, T. D. (2002) 'Intracellular localization and dynamics of myosin-II and myosin-IC in live Acanthamoeba by transient transfection of EGFP fusion proteins', *Journal of Cell Science*, 115(24), pp. 4993-5002.
- Konkel, M. E. and Tilly, K. (2000) 'Temperature-regulated expression of bacterial virulence genes', *Microbes Infect*, 2(2), pp. 157-66.
- Korn, E. D. and Weisman, R. A. (1967) 'Phagocytosis of Latex Beads by Acanthamoeba: II. Electron Microscopic Study of the Initial Events', *The Journal of cell biology*, 34(1), pp. 219-227.
- Kowalski, R. P., Melan, M. A., Karenchak, L. M. and Mammen, A. (2015) 'Comparison of validated polymerase chain reaction and culture isolation for the routine detection of Acanthamoeba from ocular samples', *Eye & contact lens*, 41(6), pp. 341-343.
- Kristensson, K., Masocha, W. and Bentivoglio, M. (2013) 'Mechanisms of CNS invasion and damage by parasites', *Handbook of clinical neurology*: Elsevier, pp. 11-22.
- Kwadha, C. A., Ong'amo, G. O., Ndegwa, P. N., Raina, S. K. and Fombong, A. T. (2017) 'The Biology and Control of the Greater Wax Moth, Galleria mellonella', *Insects*, 8(2).
- Kwiatkowski, S., Knap, B., Przystupski, D., Saczko, J., Kędzierska, E., Knap-Czop, K., Kotlińska, J., Michel, O., Kotowski, K. and Kulbacka, J. (2018) 'Photodynamic therapy –

mechanisms, photosensitizers and combinations', *Biomedicine & Pharmacotherapy*, 106, pp. 1098-1107.

Köhler, M., Leitsch, D., Fürnkranz, U., Duchêne, M., Aspöck, H. and Walochnik, J. (2008) 'Acanthamoeba strains lose their abilities to encyst synchronously upon prolonged axenic culture', *Parasitology research*, 102(5), pp. 1069-1072.

La Rosa, S. L., Diep, D. B., Nes, I. F. and Brede, D. A. (2012) 'Construction and application of a luxABCDE reporter system for real-time monitoring of Enterococcus faecalis gene expression and growth', *Appl Environ Microbiol*, 78(19), pp. 7003-11.

La Rosa, S. L., Leanti La Rosa, S., Casey, P. G., Hill, C., Diep, D. B., Nes, I. F. and Brede, D. A. (2013) 'In vivo assessment of growth and virulence gene expression during commensal and pathogenic lifestyles of luxABCDE-tagged Enterococcus faecalis strains in murine gastrointestinal and intravenous infection models', *Appl Environ Microbiol*, 79(13), pp. 3986-97.

Lalitha, P., Lin, C. C., Srinivasan, M., Mascarenhas, J., Prajna, N. V., Keenan, J. D., McLeod, S. D., Acharya, N. R., Lietman, T. M. and Porco, T. C. (2012) 'Acanthamoeba keratitis in South India: a longitudinal analysis of epidemics', *Ophthalmic epidemiology*, 19(2), pp. 111-115.

Lamb, D. C., Warrilow, A. G. S., Rolley, N. J., Parker, J. E., Nes, W. D., Smith, S. N., Kelly, D. E. and Kelly, S. L. (2015) 'Azole Antifungal Agents To Treat the Human Pathogens Acanthamoeba castellanii and Acanthamoeba polyphaga through Inhibition of Sterol 14 α -Demethylase (CYP51)', *Antimicrobial Agents and Chemotherapy*, 59(8), pp. 4707-4713.

Lamy, R., Chan, E., Good, S. D., Cevallos, V., Porco, T. C. and Stewart, J. M. (2016) 'Riboflavin and ultraviolet A as adjuvant treatment against Acanthamoeba cysts', *Clinical & Experimental Ophthalmology*, 44(3), pp. 181-187.

Lander, N., Li, Z.-H., Niyogi, S., Docampo, R. and Sibley, L. D. (2015) 'CRISPR/Cas9-Induced Disruption of Paraflagellar Rod Protein 1 and 2 Genes in Trypanosoma cruzi Reveals Their Role in Flagellar Attachment', *mBio*, 6(4), pp. e01012-15.

Lau, D., Fedinands, M., Leung, L., Fullinfaw, R., Kong, D., Davies, G. and Daniell, M. (2008) 'Penetration of Voriconazole, 1%, Eyedrops Into Human Aqueous Humor: A Prospective Open-Label Study', *Archives of Ophthalmology*, 126(3), pp. 343-346.

Lee, J.-E., Oum, B. S., Choi, H. Y., Yu, H. S. and Lee, J. S. (2007) 'Cysticidal Effect on Acanthamoeba and Toxicity on Human Keratocytes by Polyhexamethylene Biguanide and Chlorhexidine', *Cornea*, 26(6).

Lee, J.-Y., Song, S.-M., Moon, E.-K., Lee, Y.-R., Jha Bijay, K., Danne Dinzouna-Boutamba, S., Cha, H.-J., Yu Hak, S., Kong, H.-H., Chung, D.-I. and Hong, Y. (2013) 'Cysteine Protease Inhibitor (AcStefin) Is Required for Complete Cyst Formation of Acanthamoeba', *Eukaryotic Cell*, 12(4), pp. 567-574.

Lee, J. Y., Yu, I. K., Kim, S. M., Kim, J. H. and Kim, H. Y. (2021) 'Fulminant Disseminating Fatal Granulomatous Amebic Encephalitis: The First Case Report in an Immunocompetent Patient in South Korea', *Yonsei Med J*, 62(6), pp. 563-567.

Leher, H., Kinoshita, K., Alizadeh, H., Zaragoza, F. L., He, Y. and Niederkorn, J. (1998a) 'Impact of oral immunization with Acanthamoeba antigens on parasite adhesion and corneal infection', *Invest Ophthalmol Vis Sci*, 39(12), pp. 2337-43.

- Leher, H., Silvany, R., Alizadeh, H., Huang, J. and Niederkorn, J. Y. (1998b) 'Mannose induces the release of cytopathic factors from *Acanthamoeba castellanii*', *Infection and immunity*, 66(1), pp. 5-10.
- Lepelletier, D., Maillard, J. Y., Pozzetto, B. and Simon, A. (2020) 'Povidone Iodine: Properties, Mechanisms of Action, and Role in Infection Control and *Staphylococcus aureus* Decolonization', *Antimicrobial Agents and Chemotherapy*, 64(9), pp. e00682-20.
- Lim, L., Coster, D. J. and Badenoch, P. R. (2000) 'Antimicrobial susceptibility of 19 Australian corneal isolates of *Acanthamoeba*', *Clinical & Experimental Ophthalmology*, 28(2), pp. 119-124.
- Lim, N., Goh, D., Bunce, C., Xing, W., Fraenkel, G., Poole, T. R. and Ficker, L. (2008) 'Comparison of polyhexamethylene biguanide and chlorhexidine as monotherapy agents in the treatment of *Acanthamoeba keratitis*', *American journal of ophthalmology*, 145(1), pp. 130-135.
- Lin, H.-C., Hsiao, C.-H., Ma, D. H.-K., Yeh, L.-K., Tan, H.-Y., Lin, M.-Y. and Huang, S. C.-M. (2009) 'Medical treatment for combined *Fusarium* and *Acanthamoeba keratitis*', *Acta Ophthalmologica*, 87(2), pp. 199-203.
- Lindsay, D., Blagburn, B., Hall, J. and Tidwell, R. (1991) 'Activity of pentamidine and pentamidine analogs against *Toxoplasma gondii* in cell cultures', *Antimicrobial agents and chemotherapy*, 35(9), pp. 1914-1916.
- Lino, C. A., Harper, J. C., Carney, J. P. and Timlin, J. A. (2018) 'Delivering CRISPR: a review of the challenges and approaches', *Drug Deliv*, 25(1), pp. 1234-1257.
- Lionakis, M. S., Lewis, R. E., Samonis, G. and Kontoyiannis, D. P. (2003) 'Pentamidine is active in vitro against *Fusarium* species', *Antimicrobial agents and chemotherapy*, 47(10), pp. 3252-3259.
- List, W., Glatz, W., Riedl, R., Mossboeck, G., Steinwender, G. and Wedrich, A. (2021) 'Evaluation of *Acanthamoeba keratitis* cases in a tertiary medical care centre over 21 years', *Sci Rep*, 11(1), pp. 1036.
- Liu, C. (2013) 'Strategies for Designing Transgenic DNA Constructs', in Freeman, L.A. (ed.) *Lipoproteins and Cardiovascular Disease: Methods and Protocols*. Totowa, NJ: Humana Press, pp. 183-201.
- Loh, J. M., Adenwalla, N., Wiles, S. and Proft, T. (2013) '*Galleria mellonella* larvae as an infection model for group A streptococcus', *Virulence*, 4(5), pp. 419-28.
- Lorenzo-Morales, J., Kliescikova, J., Martinez-Carretero, E., De Pablos, L. M., Profotova, B., Nohynkova, E., Osuna, A. and Valladares, B. (2008) 'Glycogen phosphorylase in *Acanthamoeba* spp.: determining the role of the enzyme during the encystment process using RNA interference', *Eukaryotic cell*, 7(3), pp. 509-517.
- Lorenzo-Morales, J., Marciano-Cabral, F., Lindo, J. F., Visvesvara, G. S. and Maciver, S. K. (2010) 'Pathogenicity of amoebae', *Exp Parasitol*, 126(1), pp. 2-3.
- Loureiro, A. and da Silva, G. J. (2019) 'CRISPR-Cas: Converting A Bacterial Defence Mechanism into A State-of-the-Art Genetic Manipulation Tool', *Antibiotics*, 8(1), pp. 18.
- Lu, A., Zhang, Q., Zhang, J., Yang, B., Wu, K., Xie, W., Luan, Y. X. and Ling, E. (2014) 'Insect prophenoloxidase: the view beyond immunity', *Front Physiol*, 5, pp. 252.

- Maciver, S. K. (2016) 'Asexual Amoebae Escape Muller's Ratchet through Polyploidy', *Trends Parasitol*, 32(11), pp. 855-862.
- Maciver, S. K., Koutsogiannis, Z. and de Obeso Fernández Del Valle, A. (2019) 'Meiotic genes' are constitutively expressed in an asexual amoeba and are not necessarily involved in sexual reproduction', *Biol Lett*, 15(3), pp. 20180871.
- Maeda, H. and Dudareva, N. (2012) 'The shikimate pathway and aromatic amino Acid biosynthesis in plants', *Annu Rev Plant Biol*, 63, pp. 73-105.
- Marciano-Cabral, F. and Cabral, G. (2003) 'Acanthamoeba spp. as agents of disease in humans', *Clin Microbiol Rev*, 16(2), pp. 273-307.
- Marciano-Cabral, F. and Toney, D. M. (1998) 'The interaction of Acanthamoeba spp. with activated macrophages and with macrophage cell lines', *Journal of Eukaryotic Microbiology*, 45(4), pp. 452-458.
- Martinez, A. and Janitschke, K. (1985) 'Acanthamoeba, an opportunistic microorganism: a review', *Infection*, 13(6), pp. 251-256.
- Martinez, A. J. (1991) 'Infection of the central nervous system due to Acanthamoeba', *Rev Infect Dis*, 13 Suppl 5, pp. S399-402.
- Martín-Navarro, C. M., Lorenzo-Morales, J., Cabrera-Serra, M. G., Rancel, F., Coronado-Álvarez, N. M., Piñero, J. E. and Valladares, B. (2008) 'The potential pathogenicity of chlorhexidine-sensitive Acanthamoeba strains isolated from contact lens cases from asymptomatic individuals in Tenerife, Canary Islands, Spain', *J Med Microbiol*, 57(Pt 11), pp. 1399-1404.
- Martín-Navarro, C. M., Lorenzo-Morales, J., López-Arencibia, A., Reyes-Batlle, M., Piñero, J. E., Valladares, B. and Maciver, S. K. (2014) 'Evaluation of Acanthamoeba myosin-IC as a potential therapeutic target', *Antimicrob Agents Chemother*, 58(4), pp. 2150-5.
- Martín-Navarro, C. M., López-Arencibia, A., Sifaoui, I., Reyes-Batlle, M., Valladares, B., Martínez-Carretero, E., Piñero, J. E., Maciver, S. K. and Lorenzo-Morales, J. (2015) 'Statins and Voriconazole Induce Programmed Cell Death in Acanthamoeba castellanii', *Antimicrobial Agents and Chemotherapy*, 59(5), pp. 2817-2824.
- Massilamany, C., Marciano-Cabral, F., Rocha-Azevedo, B., Jamerson, M., Gangaplara, A., Steffen, D., Zabad, R., Illes, Z., Sobel, R. A. and Reddy, J. (2014) 'SJL mice infected with Acanthamoeba castellanii develop central nervous system autoimmunity through the generation of cross-reactive T cells for myelin antigens', *PLoS One*, 9(5), pp. e98506.
- Matsunaga, S., Endo, T., Yagita, K., Hirukawa, Y., Tomino, S., Matsugo, S. and Tsuruhara, T. (1998) 'Chromosome size polymorphisms in the genus acanthamoeba electrokaryotype by pulsed-field gel electrophoresis', *Protist*, 149(4), pp. 323-340.
- Mattana, A., Biancu, G., Alberti, L., Accardo, A., Delogu, G., Fiori, P. L. and Cappuccinelli, P. (2004) 'In Vitro Evaluation of the Effectiveness of the Macrolide Rokitamycin and Chlorpromazine against *Acanthamoeba castellanii*', *Antimicrobial Agents and Chemotherapy*, 48(12), pp. 4520-4527.
- Mattana, A., Cappai, V., Alberti, L., Serra, C., Fiori, P. L. and Cappuccinelli, P. (2002) 'ADP and other metabolites released from Acanthamoeba castellanii lead to human monocytic cell death through apoptosis and stimulate the secretion of proinflammatory cytokines', *Infection and immunity*, 70(8), pp. 4424-4432.

- Mattana, A., Tozzi, M. G., Costa, M., Delogu, G., Fiori, P. L. and Cappuccinelli, P. (2001) 'By releasing ADP, *Acanthamoeba castellanii* causes an increase in the cytosolic free calcium concentration and apoptosis in wish cells', *Infection and immunity*, 69(6), pp. 4134-4140.
- Mattar, F. E. and Byers, T. J. (1971) 'Morphological changes and the requirements for macromolecule synthesis during excystment of *Acanthamoeba castellanii*', *The Journal of cell biology*, 49(2), pp. 507-519.
- Maurer, E., Browne, N., Surlis, C., Jukic, E., Moser, P., Kavanagh, K., Lass-Flörl, C. and Binder, U. (2015) 'Galleria mellonella as a host model to study *Aspergillus terreus* virulence and amphotericin B resistance', *Virulence*, 6(6), pp. 591-8.
- Maycock, N. J. and Jayaswal, R. (2016) 'Update on *Acanthamoeba* Keratitis: Diagnosis, Treatment, and Outcomes', *Cornea*, 35(5), pp. 713-20.
- McAllum, P., Bahar, I., Kaiserman, I., Srinivasan, S., Slomovic, A. and Rootman, D. (2009) 'Temporal and seasonal trends in *Acanthamoeba* keratitis', *Cornea*, 28(1), pp. 7-10.
- McBride, J., Ingram, P. R., Henriquez, F. L. and Roberts, C. W. (2005) 'Development of colorimetric microtiter plate assay for assessment of antimicrobials against *Acanthamoeba*', *Journal of clinical microbiology*, 43(2), pp. 629-634.
- McBride, J., Mullen, A. B., Carter, K. C. and Roberts, C. W. (2007) 'Differential cytotoxicity of phospholipid analogues to pathogenic *Acanthamoeba* species and mammalian cells', *J Antimicrob Chemother*, 60(3), pp. 521-5.
- McClellan, K., Howard, K., Mayhew, E., Niederkorn, J. Y. and Alizadeh, H. (2002) 'Adaptive immune responses to *Acanthamoeba* cysts', *Experimental eye research*, 75(3), pp. 285-293.
- Mead, J. R. (2014) 'Prospects for immunotherapy and vaccines against *Cryptosporidium*', *Hum Vaccin Immunother*, 10(6), pp. 1505-13.
- Mears, E. R., Modabber, F., Don, R. and Johnson, G. E. (2015) 'A Review: The Current In Vivo Models for the Discovery and Utility of New Anti-leishmanial Drugs Targeting Cutaneous Leishmaniasis', *PLoS Negl Trop Dis*, 9(9), pp. e0003889.
- Medzhitov, R., Preston-Hurlburt, P., Kopp, E., Stadlen, A., Chen, C., Ghosh, S. and Janeway Jr, C. A. (1998) 'MyD88 is an adaptor protein in the hToll/IL-1 receptor family signaling pathways', *Molecular cell*, 2(2), pp. 253-258.
- Mewara, A., Khurana, S., Yoonus, S., Megha, K., Tanwar, P., Gupta, A. and Sehgal, R. (2017) 'Evaluation of loop-mediated isothermal amplification assay for rapid diagnosis of *Acanthamoeba* keratitis', *Indian journal of medical microbiology*, 35(1), pp. 90.
- Michalek, M., Sönnichsen, F. D., Wechselberger, R., Dingley, A. J., Hung, C.-W., Kopp, A., Wienk, H., Simanski, M., Herbst, R. and Lorenzen, I. (2013) 'Structure and function of a unique pore-forming protein from a pathogenic *acanthamoeba*', *Nature chemical biology*, 9(1), pp. 37.
- Miletti, K. E. and Leibowitz, M. J. (2000) 'Pentamidine inhibition of group I intron splicing in *Candida albicans* correlates with growth inhibition', *Antimicrobial agents and chemotherapy*, 44(4), pp. 958-966.
- Millan, C. R., Acosta-Reyes, F. J., Lagartera, L., Ebiloma, G. U., Lemgruber, L., Nué Martínez, J. J., Saperas, N., Dardonville, C., de Koning, H. P. and Campos, J. L. (2017) 'Functional and structural analysis of AT-specific minor groove binders that disrupt DNA-protein interactions and cause disintegration of the *Trypanosoma brucei* kinetoplast', *Nucleic Acids Res*, 45(14), pp. 8378-8391.

- Miller, R. F., Le Noury, J., Corbett, E. L., Felton, J. M. and De Cock, K. M. (1996) 'Pneumocystis carinii infection: current treatment and prevention', *Journal of Antimicrobial Chemotherapy*, 37(suppl_B), pp. 33-53.
- Misteli, T. and Spector, D. L. (1997) 'Applications of the green fluorescent protein in cell biology and biotechnology', *Nat Biotechnol*, 15(10), pp. 961-4.
- Mito, T., Suzuki, T., Kobayashi, T., Zheng, X., Hayashi, Y., Shiraishi, A. and Ohashi, Y. (2012) 'Effect of Photodynamic Therapy with Methylene Blue on Acanthamoeba In Vitro', *Investigative Ophthalmology & Visual Science*, 53(10), pp. 6305-6313.
- Miyawaki, A., Shcherbakova, D. M. and Verkhusha, V. V. (2012) 'Red fluorescent proteins: chromophore formation and cellular applications', *Curr Opin Struct Biol*, 22(5), pp. 679-88.
- Moiseev, R. V., Morrison, P. W. J., Steele, F. and Khutoryanskiy, V. V. (2019) 'Penetration Enhancers in Ocular Drug Delivery', *Pharmaceutics*, 11(7).
- Moon, E.-K., Chung, D.-I., Hong, Y. and Kong, H.-H. (2011) 'Expression levels of encystation mediating factors in fresh strain of Acanthamoeba castellanii cyst ESTs', *Experimental parasitology*, 127(4), pp. 811-816.
- Moon, E.-K., Chung, D.-I., Hong, Y.-C., Ahn, T.-I. and Kong, H.-H. (2008a) 'Acanthamoeba castellanii: gene profile of encystation by ESTs analysis and KOG assignment', *Experimental parasitology*, 119(1), pp. 111-116.
- Moon, E.-K., Chung, D.-I., Hong, Y.-C. and Kong, H.-H. (2008b) 'Characterization of a Serine Proteinase Mediating Encystation of Acanthamoeba', *Eukaryotic Cell*, 7(9), pp. 1513-1517.
- Moon, E.-K., Chung, D.-I., Hong, Y.-C. and Kong, H.-H. (2009) 'Autophagy protein 8 mediating autophagosome in encysting Acanthamoeba', *Molecular and biochemical parasitology*, 168(1), pp. 43-48.
- Moon, E.-K., Hong, Y., Chung, D.-I. and Kong, H.-H. (2012) 'Cysteine protease involving in autophagosomal degradation of mitochondria during encystation of Acanthamoeba', *Molecular and biochemical parasitology*, 185(2), pp. 121-126.
- Moon, E.-K., Lee, S.-T., Chung, D.-I. and Kong, H.-H. (2006) 'Intracellular Localization and Trafficking of Serine Proteinase AhSub and Cysteine Proteinase AhCP of Acanthamoeba healyi', *Eukaryotic Cell*, 5(1), pp. 125-131.
- Moon, E. K., Hong, Y., Chung, D. I., Goo, Y. K. and Kong, H. H. (2016) 'Identification of Protein Arginine Methyltransferase 5 as a Regulator for Encystation of Acanthamoeba', *Korean J Parasitol*, 54(2), pp. 133-8.
- Moon, E. K., Kong, H. H., Hong, Y., Lee, H. A. and Quan, F. S. (2017) 'Identification and Characterization of Protein Arginine Methyltransferase 1 in', *Korean J Parasitol*, 55(2), pp. 109-114.
- Morgan, S. R., Pilia, N., Hewitt, M., Moses, R. L., Moseley, R., Lewis, P. N., Morrison, P. W. J., Kelly, S. L., Parker, J. E., Whitaker, D., Quantock, A. J. and Heard, C. M. (2020) 'Controlled in vitro delivery of voriconazole and diclofenac to the cornea using contact lenses for the treatment of Acanthamoeba keratitis', *Int J Pharm*, 579, pp. 119102.
- Morrison, A. O., Morris, R., Shannon, A., Lauer, S. R., Guarner, J. and Kraft, C. S. (2016) 'Disseminated Acanthamoeba Infection Presenting With Cutaneous Lesions in an

Immunocompromised Patient: A Case Report, Review of Histomorphologic Findings, and Potential Diagnostic Pitfalls', *Am J Clin Pathol*, 145(2), pp. 266-70.

Mortazavi, P. N., Goldsworthy, G., Kirk, R. and Khan, N. A. (2010) 'Acanthamoeba produces disseminated infection in locusts and traverses the locust blood-brain barrier to invade the central nervous system', *BMC Microbiol*, 10, pp. 186.

Morén, H., Malmjö, M., Mortensen, J. and Öhrström, A. (2010) 'Riboflavin and Ultraviolet A Collagen Crosslinking of the Cornea for the Treatment of Keratitis', *Cornea*, 29(1).

Moura, H., Wallace, S. and Visvesvara, G. S. (1992) 'Acanthamoeba healyi n. sp. and the isoenzyme and immunoblot profiles of Acanthamoeba spp., groups 1 and 3', *J Protozool*, 39(5), pp. 573-83.

Mrva, M., Garajová, M., Lukáč, M. and Ondriska, F. (2011) 'Weak Cytotoxic Activity of Miltefosine Against Clinical Isolates of *Acanthamoeba* spp.', *Journal of Parasitology*, 97(3), pp. 538-540.

Muramoto, T., Iriki, H., Watanabe, J. and Kawata, T. (2019) 'Recent Advances in CRISPR/Cas9-Mediated Genome Editing in', *Cells*, 8(1).

Murti, C. K. and Shukla, O. (1984) 'Differentiation of pathogenic amoebae: encystation and excystation of *Acanthamoeba culbertsoni*—A model', *Journal of Biosciences*, 6(4), pp. 475-489.

Müller, W. G., Rieder, D., Karpova, T. S., John, S., Trajanoski, Z. and McNally, J. G. (2007) 'Organization of chromatin and histone modifications at a transcription site', *The Journal of Cell Biology*, 177(6), pp. 957-967.

Nagington, J. and Richards, J. E. (1976) 'Chemotherapeutic compounds and Acanthamoebae from eye infections', *Journal of Clinical Pathology*, 29(7), pp. 648.

Nagington, J., Watson, P., Playfair, T., McGill, J., Jones, B. and Steele, A. M. (1974) 'Amoebic infection of the eye', *The Lancet*, 304(7896), pp. 1537-1540.

Naranjo, A., Martinez, J. D., Miller, D., Tonk, R. and Amescua, G. (2020) 'Systemic Miltefosine as an Adjunct Treatment of Progressive Acanthamoeba Keratitis', *Ocular Immunology and Inflammation*, pp. 1-9.

Naranjo, A., Pelaez, D., Arrieta, E., Salero-Coca, E., Martinez, J. D., Sabater, A. L., Amescua, G. and Parel, J.-M. (2019) 'Cellular and molecular assessment of rose bengal photodynamic antimicrobial therapy on keratocytes, corneal endothelium and limbal stem cell niche', *Experimental Eye Research*, 188, pp. 107808.

Naveed, A. K. 2015. *Acanthamoeba: Biology and Pathogenesis*. Second Edition ed. Karachi, Pakistán: Caister Academic Press.

Neelam, S. and Niederkorn, J. Y. (2017) 'Focus: Infectious Diseases: Pathobiology and Immunobiology of Acanthamoeba Keratitis: Insights from Animal Models', *The Yale journal of biology and medicine*, 90(2), pp. 261.

Nerad, T. A., Sawyer, T. K., Lewis, E. J. and McLaughlin, S. M. (1995) 'Acanthamoeba pearcei n. sp. (Protozoa: Amoebida) from sewage contaminated sediments', *J Eukaryot Microbiol*, 42(6), pp. 702-5.

Nguyen, R., Khanna, N. R., Safadi, A. O. and ., Y. S. (2021) *Bacitracin Topical*: StatPearls Publishing. Available at: <https://www.ncbi.nlm.nih.gov/books/NBK536993/> (Accessed).

Nieder Korn, J., Alizadeh, H., Leher, H., Apte, S., El Agha, S., Ling, L., Hurt, M., Howard, K., Cavanagh, H. and McCulley, J. (2002) 'Role of tear anti-acanthamoeba IgA in Acanthamoeba keratitis', *Lacrimal Gland, Tear Film, and Dry Eye Syndromes 3*: Springer, pp. 845-850.

Nieder Korn, J. Y. (2002) 'The role of the innate and adaptive immune responses in Acanthamoeba keratitis', *ARCHIVUM IMMUNOLOGIAE ET THERAPIAE EXPERIMENTALIS-ENGLISH EDITION*-, 50(1), pp. 53-60.

Nieder Korn, J. Y., Alizadeh, H., Leher, H. and McCulley, J. P. (1999) 'The pathogenesis of Acanthamoeba keratitis', *Microbes and Infection*, 1(6), pp. 437-443.

Nomura, H., Isshiki, Y., Sakuda, K., Sakuma, K. and Kondo, S. (2015) 'Effects of Oakmoss and its Components on *Acanthamoeba castellanii* ATCC 30234 and the Uptake of *Legionella pneumophila* JCM 7571 (ATCC 33152) into *A. castellanii*', *Biocontrol Science*, 20(1), pp. 59-65.

O'Day, D. M., Foulds, G., Williams, T. E., Robinson, R. D., Allen, R. H. and Head, W. S. (1990) 'Ocular Uptake of Fluconazole Following Oral Administration', *Archives of Ophthalmology*, 108(7), pp. 1006-1008.

Obaji, J., Lee-Pack, L. R., Gutierrez, C. and Chan, C. K. (2003) 'The Pulmonary Effects of Long-term Exposure to Aerosol Pentamidine: A 5-Year Surveillance Study in HIV-Infected Patients', *Chest*, 123(6), pp. 1983-1987.

Ong, T. Y. Y., Khan, N. A. and Siddiqui, R. (2017) 'Brain-eating amoebae: predilection sites in the brain and disease outcome', *Journal of clinical microbiology*, pp. JCM. 02300-16.

Onichandran, S., Kumar, T., Salibay, C. C., Dungca, J. Z., Tabo, H. A., Tabo, N., Tan, T. C., Lim, Y. A., Sawangjaroen, N., Phiriyasamith, S., Andiappan, H., Ithoi, I., Lau, Y. L. and Nissapatorn, V. (2014) 'Waterborne parasites: a current status from the Philippines', *Parasit Vectors*, 7, pp. 244.

Orfeo, T. and Bateman, E. (1998) 'Transcription by RNA polymerase II during Acanthamoeba differentiation', *Biochimica et Biophysica Acta (BBA)-Gene Structure and Expression*, 1443(3), pp. 297-304.

Page, F. C. (1987) 'The classification of 'naked' amoebae (Phylum Rhizopoda)', *Archiv für Protistenkunde*, 133(3-4), pp. 199-217.

Page, M. A. and Mathers, W. D. (2013) 'Acanthamoeba keratitis: a 12-year experience covering a wide spectrum of presentations, diagnoses, and outcomes', *Journal of ophthalmology*, 2013.

Paix, A., Wang, Y., Smith, H. E., Lee, C.-Y. S., Calidas, D., Lu, T., Smith, J., Schmidt, H., Krause, M. W. and Seydoux, G. (2014) 'Scalable and Versatile Genome Editing Using Linear DNAs with Microhomology to Cas9 Sites in *Caenorhabditis elegans*', *Genetics*, 198(4), pp. 1347-1356.

Panjwani, N. (2010) 'Pathogenesis of Acanthamoeba keratitis', *The ocular surface*, 8(2), pp. 70-79.

Payne, D. J., Wallis, N. G., Gentry, D. R. and Rosenberg, M. (2000) 'The impact of genomics on novel antibacterial targets', *Curr Opin Drug Discov Devel*, 3(2), pp. 177-90.

Pelletier, J. S., Miller, D., Liang, B. and Capriotti, J. A. (2011) 'In vitro efficacy of a povidone-iodine 0.4% and dexamethasone 0.1% suspension against ocular pathogens', *Journal of Cataract & Refractive Surgery*, 37(4).

- Peng, D., Kurup Samarchith, P., Yao Phil, Y., Minning Todd, A., Tarleton Rick, L. and Johnson Patricia, J. (2014) 'CRISPR-Cas9-Mediated Single-Gene and Gene Family Disruption in *Trypanosoma cruzi*', *mBio*, 6(1), pp. e02097-14.
- Peng, Z., Omaruddin, R. and Bateman, E. (2005) 'Stable transfection of *Acanthamoeba castellanii*', *Biochim Biophys Acta*, 1743(1-2), pp. 93-100.
- Pereira, M. F., Rossi, C. C., da Silva, G. C., Rosa, J. N. and Bazzolli, D. M. S. (2020) 'Galleria mellonella as an infection model: an in-depth look at why it works and practical considerations for successful application', *Pathog Dis*, 78(8).
- Perrine, D., Chenu, J. P., Georges, P., Lancelot, J. C., Saturnino, C. and Robba, M. (1995) 'Amoebicidal efficiencies of various diamidines against two strains of *Acanthamoeba polyphaga*', *Antimicrob Agents Chemother*, 39(2), pp. 339-42.
- Pertiwi, Y. D., Chikama, T., Sueoka, K., Ko, J.-A., Kiuchi, Y., Onodera, M. and Sakaguchi, T. (2019) 'Antimicrobial Photodynamic Therapy with the photosensitizer TONS504 eradicates *Acanthamoeba*', *Photodiagnosis and Photodynamic Therapy*, 28, pp. 166-171.
- Peters, J. M., Colavin, A., Shi, H., Czarny, T. L., Larson, M. H., Wong, S., Hawkins, J. S., Lu, C. H. S., Koo, B. M., Marta, E., Shiver, A. L., Whitehead, E. H., Weissman, J. S., Brown, E. D., Qi, L. S., Huang, K. C. and Gross, C. A. (2016) 'A Comprehensive, CRISPR-based Functional Analysis of Essential Genes in Bacteria', *Cell*, 165(6), pp. 1493-1506.
- Piatek, M., Sheehan, G. and Kavanagh, K. (2020) 'Utilising *Galleria mellonella* larvae for studying in vivo activity of conventional and novel antimicrobial agents', *Pathog Dis*, 78(8).
- Pietrucha-Dilanchian, P., Chan, J. C., Castellano-Sanchez, A., Hirzel, A., Laowansiri, P., Tuda, C., Visvesvara, G. S., Qvarnstrom, Y. and Ratzan, K. R. (2012) '*Balamuthia mandrillaris* and *Acanthamoeba* amebic encephalitis with neurotoxoplasmosis coinfection in a patient with advanced HIV infection', *Journal of clinical microbiology*, 50(3), pp. 1128-1131.
- Por, Y. M., Mehta, J. S., Chua, J. L., Koh, T.-H., Khor, W. B., Fong, A. C., Lim, J. W., Heng, W. J., Loh, R. S. and Lim, L. (2009) '*Acanthamoeba* keratitis associated with contact lens wear in Singapore', *American journal of ophthalmology*, 148(1), pp. 7-12. e2.
- Prescott, D. M. (1959) 'Nuclear synthesis of cytoplasmic ribonucleic acid in *Amoeba proteus*', *The Journal of Cell Biology*, 6(2), pp. 203-206.
- Preston, T. and King, C. (1984) 'Amoeboid locomotion of *Acanthamoeba castellanii* with special reference to cell-substratum interactions', *Microbiology*, 130(9), pp. 2317-2323.
- Price Marianne, O., Tenkman Lawrence, R., Schrier, A., Fairchild Kelly, M., Trokel Stephen, L. and Price Francis, W. (2012) 'Photoactivated Riboflavin Treatment of Infectious Keratitis Using Collagen Cross-linking Technology', *Journal of Refractive Surgery*, 28(10), pp. 706-713.
- Pumidonming, W., Koehsler, M. and Walochnik, J. (2010) '*Acanthamoeba* strains show reduced temperature tolerance after long-term axenic culture', *Parasitology research*, 106(3), pp. 553-559.
- Pussard, M. 1977. Morphologies de la paroi kystique et taxonomie du genre *Acanthamoeba* (Protozoa, Amoebida). In: Pons, R. (ed.). Protistologica.
- Putaporntip, C., Kuamsab, N., Nuprasert, W., Rojrung, R., Pattanawong, U., Tia, T., Yanmanee, S. and Jongwutiwes, S. (2021) 'Analysis of *Acanthamoeba* genotypes from public freshwater sources in Thailand reveals a new genotype, T23 *Acanthamoeba bangkokensis* sp. nov', *Sci Rep*, 11(1), pp. 17290.

- Pérez-Santonja, J. J., Kilvington, S., Hughes, R., Tufail, A., Matheson, M. and Dart, J. K. (2003) 'Persistently culture positive Acanthamoeba keratitis: in vivo resistance and in vitro sensitivity', *Ophthalmology*, 110(8), pp. 1593-1600.
- Radford, C., Minassian, D. and Dart, J. (2002) 'Acanthamoeba keratitis in England and Wales: incidence, outcome, and risk factors', *British Journal of Ophthalmology*, 86(5), pp. 536-542.
- Rahman, K. M., Thompson, A. S., James, C. H., Narayanaswamy, M. and Thurston, D. E. (2009) 'The pyrrolobenzodiazepine dimer SJG-136 forms sequence-dependent intrastrand DNA cross-links and monoalkylated adducts in addition to interstrand cross-links', *Journal of the American Chemical Society*, 131(38), pp. 13756-13766.
- Ramarao, N., Nielsen-Leroux, C. and Lereclus, D. (2012) 'The insect *Galleria mellonella* as a powerful infection model to investigate bacterial pathogenesis', *J Vis Exp*, (70), pp. e4392.
- Ramirez, E., Robles, E., Bonilla, P., Sainz, G., Lopez, M., De La Cerda, J. and Warren, A. (2005) 'Occurrence of Pathogenic Free-Living Amoebae and Bacterial Indicators in a Constructed Wetland Treating Domestic Wastewater from a Single Household', *Engineering in life sciences*, 5(3), pp. 253-258.
- Ramirez, E., Robles, E., Martinez, B., Ayala, R., Sainz, G., Martinez, M. E. and Gonzalez, M. E. (2014) 'Distribution of free-living amoebae in a treatment system of textile industrial wastewater', *Experimental parasitology*, 145, pp. S34-S38.
- Ramjee, M. N., Balasubramanian, S., Abell, C., Coggins, J. R., Davies, G. M., Hawkes, T. R., Lowe, D. J. and Thorneley, a. R. N. F. (1992) 'Reaction of (6R)-6-fluoroEPSP with recombinant *Escherichia coli* chorismate synthase generates a stable flavin mononucleotide semiquinone radical', - *Journal of the American Chemical Society*, (8), pp. 3151.
- Ren, M. and Wu, X. (2011) 'Toll-like receptor 4 signalling pathway activation in a rat model of Acanthamoeba Keratitis', *Parasite immunology*, 33(1), pp. 25-33.
- Ren, X., Yang, Z., Xu, J., Sun, J., Mao, D., Hu, Y., Yang, S. J., Qiao, H. H., Wang, X., Hu, Q., Deng, P., Liu, L. P., Ji, J. Y., Li, J. B. and Ni, J. Q. (2014) 'Enhanced specificity and efficiency of the CRISPR/Cas9 system with optimized sgRNA parameters in *Drosophila*', *Cell Rep*, 9(3), pp. 1151-62.
- Renwick, J., Reeves, E. P., Wientjes, F. B. and Kavanagh, K. (2007) 'Translocation of proteins homologous to human neutrophil p47phox and p67phox to the cell membrane in activated hemocytes of *Galleria mellonella*', *Dev Comp Immunol*, 31(4), pp. 347-59.
- Retana-Moreira, L., Abrahams-Sandí, E., Castro-Artavia, E., Fernández-Sánchez, A., Castro-Castillo, A., Reyes-Batlle, M. and Lorenzo-Morales, J. (2015) 'Isolation and Molecular Characterization of Acanthamoeba Strains from Dental Units in Costa Rica', *J Eukaryot Microbiol*, 62(6), pp. 733-6.
- Rice, C. A., Campbell, S. J., Bisson, C., Owen, H. J., Sedelnikova, S. E., Baker, P. J., Rice, D. W., Henriquez, F. L. and Roberts, C. W. (2018) 'Structural and functional studies of histidine biosynthesis in *Acanthamoeba* spp. demonstrates a novel molecular arrangement and target for antimicrobials', *PLOS ONE*, 13(7), pp. e0198827.
- Rice, C. A., Colon, B. L., Chen, E., Hull, M. V. and Kyle, D. E. (2020a) 'Discovery of repurposing drug candidates for the treatment of diseases caused by pathogenic free-living amoebae', *PLoS Negl Trop Dis*, 14(9), pp. e0008353.
- Rice, C. A., Troth, E. V., Russell, A. C. and Kyle, D. E. (2020b) 'Discovery of Anti-Amoebic Inhibitors from Screening the MMV Pandemic Response Box on', *Pathogens*, 9(6).

- Risler, A., Coupat-Goutaland, B. and Pélandakis, M. (2013) 'Genotyping and phylogenetic analysis of *Acanthamoeba* isolates associated with keratitis', *Parasitology research*, 112(11), pp. 3807-3816.
- Roberts, C. W. and Henriquez, F. L. (2010) 'Drug target identification, validation, characterisation and exploitation for treatment of *Acanthamoeba* (species) infections', *Exp Parasitol*, 126(1), pp. 91-6.
- Roberts, C. W., Roberts, F., Lyons, R. E., Kirisits, M. J., Mui, E. J., Finnerty, J., Johnson, J. J., Ferguson, D. J., Coggins, J. R., Krell, T., Coombs, G. H., Milhous, W. K., Kyle, D. E., Tzipori, S., Barnwell, J., Dame, J. B., Carlton, J. and McLeod, R. (2002) 'The shikimate pathway and its branches in apicomplexan parasites', *J Infect Dis*, 185 Suppl 1, pp. S25-36.
- Robin, J. B., Chan, R. and Andersen, B. R. (1988) 'Rapid visualization of *Acanthamoeba* using fluorescein-conjugated lectins', *Archives of Ophthalmology*, 106(9), pp. 1273-1276.
- Rocha-Azevedo, B., Jamerson, M., Cabral, G. A. and Marciano-Cabral, F. (2010) '*Acanthamoeba culbertsoni*: analysis of amoebic adhesion and invasion on extracellular matrix components collagen I and laminin-1', *Experimental parasitology*, 126(1), pp. 79-84.
- Rodriguez-Zaragoza, S., Mayzlish, E. and Steinberger, Y. (2005) 'Vertical distribution of the free-living amoeba population in soil under desert shrubs in the Negev desert, Israel', *Appl Environ Microbiol*, 71(4), pp. 2053-60.
- Romero, L. and Vela, J. M. (2014) 'Alternative Models in Drug Discovery and Development Part II: In Vivo Nonmammalian and Exploratory/Experimental Human Models', *In Vivo Models for Drug Discovery*, pp. 59-90.
- Rugarabamu, G., Marq, J.-B., Guérin, A., Lebrun, M. and Soldati-Favre, D. (2015) 'Distinct contribution of *Toxoplasma gondii* rhomboid proteases 4 and 5 to micronemal protein protease 1 activity during invasion', *Molecular Microbiology*, 97(2), pp. 244-262.
- Rusciano, G., Capriglione, P., Pesce, G., Del Prete, S., Cennamo, G., Di Cave, D., Cerulli, L. and Sasso, A. (2013) 'Raman Microspectroscopy Analysis in the Treatment of *Acanthamoeba* Keratitis', *PLOS ONE*, 8(8), pp. e72127.
- Salameh, A., Bello, N., Becker, J. and Zangeneh, T. 'Fatal granulomatous amoebic encephalitis caused by *Acanthamoeba* in a patient with kidney transplant: a case report'. *Open forum infectious diseases*: Oxford University Press.
- Salvador, R.-Z. and Soledad, G. (1997) 'Species Richness and Abundance of Naked Amebae in the Rhizoplane of the Desert Plant *Escontria chiotilla* (Cactaceae)', *Journal of Eukaryotic Microbiology*, 44(2), pp. 122-126.
- Sampson, T. R., Saroj, S. D., Llewellyn, A. C., Tzeng, Y. L. and Weiss, D. S. (2019) 'Author Correction: A CRISPR/Cas system mediates bacterial innate immune evasion and virulence', *Nature*, 570(7760), pp. E30-E31.
- Sangkanu, S., Mitsuwan, W., Mahabusarakam, W., Jimoh, T. O., Wilairatana, P., Girol, A. P., Verma, A. K., de Lourdes Pereira, M., Rahmatullah, M., Wiart, C., Siyadatpanah, A., Norouzi, R., Mutombo, P. N. and Nissapatorn, V. (2021) 'Anti-*Acanthamoeba* synergistic effect of chlorhexidine and *Garcinia mangostana* extract or α -mangostin against *Acanthamoeba triangularis* trophozoite and cyst forms', *Sci Rep*, 11(1), pp. 8053.
- Saraf, P., Shwab, E. K., Dubey, J. P. and Su, C. (2017) 'On the determination of *Toxoplasma gondii* virulence in mice', *Exp Parasitol*, 174, pp. 25-30.

- Sateriale, A., Šlapeta, J., Baptista, R., Engiles, J. B., Gullicksrud, J. A., Herbert, G. T., Brooks, C. F., Kugler, E. M., Kissinger, J. C., Hunter, C. A. and Striepen, B. (2019) 'A Genetically Tractable, Natural Mouse Model of Cryptosporidiosis Offers Insights into Host Protective Immunity', *Cell Host Microbe*, 26(1), pp. 135-146.e5.
- Sato, A., McNulty, L., Cox, K., Kim, S., Scott, A., Daniell, K., Summerville, K., Price, C., Hudson, S. and Kiakos, K. (2005) 'A novel class of in vivo active anticancer agents: achiral seco-amino-and seco-hydroxycyclopropylbenz [e] indolone (seco-CBI) analogues of the duocarmycins and CC-1065', *Journal of medicinal chemistry*, 48(11), pp. 3903-3918.
- Saunders, P. P. R., Proctor, E. M., Rollins, D. F. and Richards, J. S. F. (1992) 'Enhanced Killing of Acanthamoeba Cysts in vitro Using Dimethylsulfoxide', *Ophthalmology*, 99(8), pp. 1197-1200.
- Scheid, P. (2014) 'Relevance of free-living amoebae as hosts for phylogenetically diverse microorganisms', *Parasitol Res*, 113(7), pp. 2407-14.
- Schiller, B., Makrypidi, G., Razzazi-Fazeli, E., Paschinger, K., Walochnik, J. and Wilson, I. B. (2012) 'Exploring the unique N-glycome of the opportunistic human pathogen Acanthamoeba', *Journal of Biological Chemistry*, 287(52), pp. 43191-43204.
- Schmitz-Esser, S., Toenshoff, E. R., Haider, S., Heinz, E., Hoenninger, V. M., Wagner, M. and Horn, M. (2008) 'Diversity of bacterial endosymbionts of environmental Acanthamoeba isolates', *Applied and environmental microbiology*, 74(18), pp. 5822-5831.
- Schubert, M. G., Goodman, D. B., Wannier, T. M., Kaur, D., Farzadfard, F., Lu, T. K., Shipman, S. L. and Church, G. M. (2021) 'High-throughput functional variant screens via in vivo production of single-stranded DNA', *Proc Natl Acad Sci U S A*, 118(18).
- Schuster, F. L. and Jacob, L. S. (1992) 'Effects of magainins on ameba and cyst stages of Acanthamoeba polyphaga', *Antimicrob Agents Chemother*, 36(6), pp. 1263-71.
- Scott, F. J., Khalaf, A. I., Duffy, S., Avery, V. M. and Suckling, C. J. (2016a) 'Selective anti-malarial minor groove binders', *Bioorg Med Chem Lett*, 26(14), pp. 3326-3329.
- Scott, F. J., Khalaf, A. I., Giordani, F., Wong, P. E., Duffy, S., Barrett, M., Avery, V. M. and Suckling, C. J. (2016b) 'An evaluation of Minor Groove Binders as anti-Trypanosoma brucei brucei therapeutics', *European journal of medicinal chemistry*, 116, pp. 116-125.
- Seal, D. (2003) 'Treatment of Acanthamoeba keratitis', *Expert review of anti-infective therapy*, 1(2), pp. 205-208.
- Shah, S. A., Erdmann, S., Mojica, F. J. and Garrett, R. A. (2013) 'Protospacer recognition motifs: mixed identities and functional diversity', *RNA Biol*, 10(5), pp. 891-9.
- Sharma, R., Jhanji, V., Satpathy, G., Sharma, N., Khokhar, S. and Agarwal, T. (2013) 'Coinfection with Acanthamoeba and Pseudomonas in Contact Lens-Associated Keratitis', *Optometry and Vision Science*, 90(2), pp. e53-e55.
- Sharma, S., Kunimoto, D. Y., Gopinathan, U., Athmanathan, S., Garg, P. and Rao, G. N. (2002) 'Evaluation of corneal scraping smear examination methods in the diagnosis of bacterial and fungal keratitis: a survey of eight years of laboratory experience', *Cornea*, 21(7), pp. 643-647.
- Shcherbakova, D. M., Hink, M. A., Joosen, L., Gadella, T. W. and Verkhusha, V. V. (2012) 'An orange fluorescent protein with a large Stokes shift for single-excitation multicolor FCCS and FRET imaging', *J Am Chem Soc*, 134(18), pp. 7913-23.

Sheehan Daniel, J., Hitchcock Christopher, A. and Sibley Carol, M. (1999) 'Current and Emerging Azole Antifungal Agents', *Clinical Microbiology Reviews*, 12(1), pp. 40-79.

Shen, B., Brown, K. M., Lee, T. D. and Sibley, L. D. (2014) 'Efficient Gene Disruption in Diverse Strains of *Toxoplasma gondii* Using CRISPR/CAS9', *mBio*, 5(3), pp. e01114-14.

Shi, L., Muthukumar, V., Stachon, T., Latta, L., Elhawy, M. I., Gunaratnam, G., Orosz, E., Seitz, B., Kiderlen, A. F., Bischoff, M. and Szentmáry, N. (2020) 'The Effect of Anti-Amoebic Agents and Ce6-PDT on', *Transl Vis Sci Technol*, 9(12), pp. 29.

Shibayama, M., Navarro-García, F., López-Revilla, R., Martínez-Palomo, A. and Tsutsumi, V. (1997) 'In vivo and in vitro experimental intestinal amebiasis in Mongolian gerbils (*Meriones unguiculatus*)', *Parasitol Res*, 83(2), pp. 170-6.

Shing, B., Balen, M., McKerrow, J. H. and Debnath, A. (2021) 'Keratitis: an update on amebicidal and cysticidal drug screening methodologies and potential treatment with azole drugs', *Expert Rev Anti Infect Ther*, pp. 1-15.

Shoff, M., Rogerson, A., Schatz, S. and Seal, D. (2007) 'Variable responses of *Acanthamoeba* strains to three multipurpose lens cleaning solutions', *Optometry and Vision Science*, 84(3), pp. 202-207.

Siddiqui, R., Aqeel, Y. and Khan, N. A. (2016) 'The Development of Drugs against *Acanthamoeba* Infections', *Antimicrob Agents Chemother*, 60(11), pp. 6441-6450.

Siddiqui, R. and Khan, N. A. (2012a) 'Biology and pathogenesis of *Acanthamoeba*', *Parasites & vectors*, 5(1), pp. 6.

Siddiqui, R. and Khan, N. A. (2012b) 'Photochemotherapeutic strategies against *Acanthamoeba* keratitis', *AMB Express*, 2(1), pp. 47.

Siddiqui, R., Muhammad, J. S. and Khan, N. A. (2021) 'Locust as an', *ACS Chem Neurosci*, 12(9), pp. 1469-1471.

Siddiqui, R., Roberts, S. K., Ong, T. Y. Y., Mungroo, M. R., Anwar, A. and Khan, N. A. (2019) 'Novel insights into the potential role of ion transport in sensory perception in *Acanthamoeba*', *Parasit Vectors*, 12(1), pp. 538.

Siddiqui, R., Syed, A., Tomas, S., Prieto-Garcia, J. and Khan, N. A. (2009) 'Effect of free versus liposomal-complexed pentamidine isethionate on biological characteristics of *Acanthamoeba castellanii* in vitro', *J Med Microbiol*, 58(Pt 3), pp. 327-30.

Sidik, S. M., Hackett, C. G., Tran, F., Westwood, N. J. and Lourido, S. (2014) 'Efficient Genome Engineering of *Toxoplasma gondii* Using CRISPR/Cas9', *PLOS ONE*, 9(6), pp. e100450.

Sifaoui, I., Reyes-Battle, M., López-Arencibia, A., Wagner, C., Chiboub, O., De Agustino Rodríguez, J., Rocha-Cabrera, P., Valladares, B., Piñero, J. E. and Lorenzo-Morales, J. (2017) 'Evaluation of the anti-*Acanthamoeba* activity of two commercial eye drops commonly used to lower eye pressure', *Exp Parasitol*, 183, pp. 117-123.

Singh, A. K., Carette, X., Potluri, L.-P., Sharp, J. D., Xu, R., Prisic, S. and Husson, R. N. (2016) 'Investigating essential gene function in *Mycobacterium tuberculosis* using an efficient CRISPR interference system', *Nucleic Acids Research*, 44(18), pp. e143-e143.

- Singkum, P., Suwanmanee, S., Pumeesat, P. and Luplertlop, N. (2019) 'A powerful in vivo alternative model in scientific research: *Galleria mellonella*', *Acta Microbiol Immunol Hung*, 66(1), pp. 31-55.
- Sissons, J., Alsam, S., Jayasekera, S. and Khan, N. A. (2004) 'Ecto-ATPases of clinical and non-clinical isolates of *Acanthamoeba*', *Microbial pathogenesis*, 37(5), pp. 231-239.
- Skarin, A., Florén, I., Kiss, K., Miörner, H. and Stenevi, U. (1996) '*Acanthamoeba* keratitis in the south of Sweden', *Acta Ophthalmologica Scandinavica*, 74(6), pp. 593-597.
- Smith, T. L. (1965) 'External Morphology of the Larva, Pupa, and Adult of the Wax Moth, *Galleria mellonella* L', *Journal of the Kansas Entomological Society*, 38(3), pp. 287-310.
- Smoot, L. M., Smoot, J. C., Graham, M. R., Somerville, G. A., Sturdevant, D. E., Migliaccio, C. A., Sylva, G. L. and Musser, J. M. (2001) 'Global differential gene expression in response to growth temperature alteration in group A *Streptococcus*', *Proc Natl Acad Sci U S A*, 98(18), pp. 10416-21.
- Soeiro, M., Werbovetz, K., Boykin, D., Wilson, W., Wang, M. and Hemphill, A. (2013) 'Novel amidines and analogues as promising agents against intracellular parasites: a systematic review', *Parasitology*, 140(8), pp. 929-951.
- Soeiro, M. N., De Souza, E., Stephens, C. E. and Boykin, D. (2005) 'Aromatic diamidines as antiparasitic agents', *Expert opinion on investigational drugs*, 14(8), pp. 957-972.
- Sollelis, L., Ghorbal, M., MacPherson, C. R., Martins, R. M., Kuk, N., Crobu, L., Bastien, P., Scherf, A., Lopez-Rubio, J.-J. and Sterkers, Y. (2015) 'First efficient CRISPR-Cas9-mediated genome editing in *Leishmania* parasites', *Cellular Microbiology*, 17(10), pp. 1405-1412.
- Song, S.-M., Han, B.-I., Moon, E.-K., Lee, Y.-R., Yu, H. S., Jha, B. K., Danne, D.-B. S., Kong, H.-H., Chung, D.-I. and Hong, Y. (2012) 'Autophagy protein 16-mediated autophagy is required for the encystation of *Acanthamoeba castellanii*', *Molecular and biochemical parasitology*, 183(2), pp. 158-165.
- Soto-Arredondo, K. J., Flores-Villavicencio, L. L., Serrano-Luna, J. J., Shibayama, M. and Sabanero-López, M. (2014) 'Biochemical and cellular mechanisms regulating *Acanthamoeba castellanii* adherence to host cells', *Parasitology*, 141(4), pp. 531-41.
- Sowa-Jasiłek, A., Zdybicka-Barabas, A., Stączek, S., Wydrych, J., Skrzypiec, K., Mak, P., Deryło, K., Tchórzewski, M. and Cytryńska, M. (2016) '*Galleria mellonella* lysozyme induces apoptotic changes in *Candida albicans* cells', *Microbiological Research*, 193, pp. 121-131.
- Speijer, D., Lukeš, J. and Eliáš, M. (2015) 'Sex is a ubiquitous, ancient, and inherent attribute of eukaryotic life', *Proceedings of the National Academy of Sciences*, 112(29), pp. 8827-8834.
- Sponsel, W., Chen, N., Dang, D., Paris, G., Graybill, J., Najvar, L. K., Zhou, L., Lam, K.-W., Glickman, R. and Scribbick, F. (2006) 'Topical Voriconazole as a Novel Treatment for Fungal Keratitis', *Antimicrobial Agents and Chemotherapy*, 50(1), pp. 262-268.
- Sriram, R., Shoff, M., Booton, G., Fuerst, P. and Visvesvara, G. S. (2008) 'Survival of *Acanthamoeba* cysts after desiccation for more than 20 years', *Journal of clinical microbiology*, 46(12), pp. 4045-4048.
- Stelzer, S., Basso, W., Benavides Silván, J., Ortega-Mora, L. M., Maksimov, P., Gethmann, J., Conraths, F. J. and Schares, G. (2019) 'infection and toxoplasmosis in farm animals: Risk factors and economic impact', *Food Waterborne Parasitol*, 15, pp. e00037.

- Stepanenko, A. A. and Heng, H. H. (2017) 'Transient and stable vector transfection: Pitfalls, off-target effects, artifacts', *Mutat Res Rev Mutat Res*, 773, pp. 91-103.
- Suckling, C. (2012) 'From multiply active natural product to candidate drug? Antibacterial (and other) minor groove binders for DNA', *Future medicinal chemistry*, 4(8), pp. 971-989.
- Suckling, C. and Scott, F. (2017) 'Selectivity in Anti-infective Minor Groove Binders', *3rd International Electronic Conference on Medicinal Chemistry*.
- Sunada, A., Kimura, K., Nishi, I., Toyokawa, M., Ueda, A., Sakata, T., Suzuki, T., Inoue, Y., Ohashi, Y., Asari, S. and Iwatani, Y. (2014) 'In Vitro Evaluations of Topical Agents to Treat Acanthamoeba Keratitis', *Ophthalmology*, 121(10), pp. 2059-2065.
- Suresh, A. B., Rosani, A. and Wadhwa, R. (2021) *Rifampin*. Treasure Island (FL). Available at: <https://www.ncbi.nlm.nih.gov/books/NBK557488/> (Accessed).
- Suryawanshi, A., Cao, Z., Sampson, J. F. and Panjwani, N. (2015) 'IL-17A-Mediated Protection against Acanthamoeba Keratitis', *The Journal of Immunology*, 194(2), pp. 650-663.
- Swearengen, J. R. (2018) 'Choosing the right animal model for infectious disease research', *Animal Model Exp Med*, 1(2), pp. 100-108.
- Sánchez, A. G., Virginio, V. G., Maschio, V. J., Ferreira, H. B. and Rott, M. B. (2016) 'Evaluation of the immunodiagnostic potential of a recombinant surface protein domain from Acanthamoeba castellanii', *Parasitology*, 143(12), pp. 1656-64.
- Taketo, M. M. and Sonoshita, M. (2002) 'Phospholipase A 2 and apoptosis', *Biochimica et Biophysica Acta (BBA)-Molecular and Cell Biology of Lipids*, 1585(2), pp. 72-76.
- Talbott, M., Cevallos, V., Chen, M. C., Chin, S. A., Lalitha, P., Seitzman, G. D., Lietman, T. M. and Keenan, J. D. (2019) 'Synergy Testing of Antiamoebic Agents for Acanthamoeba: Antagonistic Effect of Voriconazole', *Cornea*, 38(10).
- Tao, L., Zhang, J., Meraner, P., Tovaglieri, A., Wu, X., Gerhard, R., Zhang, X., Stallcup, W. B., Miao, J., He, X., Hurdle, J. G., Breault, D. T., Brass, A. L. and Dong, M. (2016) 'Frizzled proteins are colonic epithelial receptors for C. difficile toxin B', *Nature*, 538(7625), pp. 350-355.
- Taravaud, A., Fechtali-Moute, Z., Loiseau, P. M. and Pomel, S. (2021) 'Drugs used for the treatment of cerebral and disseminated infections caused by free-living amoebae', *Clin Transl Sci*, 14(3), pp. 791-805.
- Taravaud, A., Loiseau, P. M. and Pomel, S. (2017) 'In vitro evaluation of antimicrobial agents on Acanthamoeba sp. and evidence of a natural resilience to amphotericin B', *Int J Parasitol Drugs Drug Resist*, 7(3), pp. 328-336.
- Tavassoli, S., Buckle, M., Tole, D., Chiodini, P. and Darcy, K. (2018) 'The use of miltefosine in the management of refractory Acanthamoeba keratitis', *Contact Lens and Anterior Eye*, 41(4), pp. 400-402.
- Thebpatiphat, N., Hammersmith, K. M., Rocha, F. N., Rapuano, C. J., Ayres, B. D., Laibson, P. R., Eagle Jr, R. C. and Cohen, E. J. (2007) 'Acanthamoeba keratitis: a parasite on the rise', *Cornea*, 26(6), pp. 701-706.
- Thomas, V., McDonnell, G., Denyer, S. P. and Maillard, J.-Y. (2010) 'Free-living amoebae and their intracellular pathogenic microorganisms: risks for water quality', *FEMS Microbiology Reviews*, 34(3), pp. 231-259.

Thomaz, L., García-Rodas, R., Guimarães, A. J., Taborda, C. P., Zaragoza, O. and Nosanchuk, J. D. (2013) 'Galleria mellonella as a model host to study Paracoccidioides lutzii and Histoplasma capsulatum', *Virulence*, 4(2), pp. 139-46.

Thomson, S. (2020) *Sterol Biosynthesis as an Antimicrobial Target in Acanthamoeba species*. PhD, University of West of Scotland, Paisley, Scotland.

Thomson, S., Rice, C. A., Zhang, T., Edrada-Ebel, R., Henriquez, F. L. and Roberts, C. W. (2017) 'Characterisation of sterol biosynthesis and validation of 14 α -demethylase as a drug target in Acanthamoeba', *Sci Rep*, 7(1), pp. 8247.

Thulasi, P., Saeed, H. N., Rapuano, C. J., Hou, J. H., Appenheimer, A. B., Chodosh, J., Kang, J. J., Morrill, A. M., Vyas, N., Zegans, M. E., Zuckerman, R. and Tu, E. Y. (2021) 'Oral Miltefosine as Salvage Therapy for Refractory Acanthamoeba Keratitis', *American Journal of Ophthalmology*, 223, pp. 75-82.

Thurtle-Schmidt, D. M. and Lo, T.-W. (2018) 'Molecular biology at the cutting edge: A review on CRISPR/CAS9 gene editing for undergraduates', *Biochemistry and Molecular Biology Education*, 46(2), pp. 195-205.

Toney, D. M. and Marciano-Cabral, F. (1998) 'Resistance of Acanthamoeba species to complement lysis', *The Journal of parasitology*, pp. 338-344.

Trabelsi, H., Dendana, F., Sellami, A., Sellami, H., Cheikhrouhou, F., Neji, S., Makni, F. and Ayadi, A. (2012) 'Pathogenic free-living amoebae: epidemiology and clinical review', *Pathol Biol (Paris)*, 60(6), pp. 399-405.

Tripathi, T., Abdi, M. and Alizadeh, H. (2014) 'Protease-activated receptor 2 (PAR2) is upregulated by Acanthamoeba plasminogen activator (aPA) and induces proinflammatory cytokine in human corneal epithelial cells', *Investigative ophthalmology & visual science*, 55(6), pp. 3912-3921.

Tripathi, T., Smith, A. D., Abdi, M. and Alizadeh, H. (2012) 'Acanthamoeba-cytopathic protein induces apoptosis and proinflammatory cytokines in human corneal epithelial cells by cPLA2 α activation', *Investigative ophthalmology & visual science*, 53(13), pp. 7973-7982.

Tsai, C. J., Loh, J. M. and Proft, T. (2016) 'Galleria mellonella infection models for the study of bacterial diseases and for antimicrobial drug testing', *Virulence*, 7(3), pp. 214-29.

Tsutsumi, V. and Shibayama, M. (2006) 'Experimental amebiasis: a selected review of some in vivo models', *Arch Med Res*, 37(2), pp. 210-20.

Tu, E. Y., Joslin, C. E., Sugar, J., Booton, G. C., Shoff, M. E. and Fuerst, P. A. (2008) 'The relative value of confocal microscopy and superficial corneal scrapings in the diagnosis of Acanthamoeba keratitis', *Cornea*, 27(7), pp. 764-772.

Tyagi, G., Mehrotra, P., Agarwal, S. and Mehrotra, R. (2017) 'DNA-Interacting Molecules and Cancer Treatments', in Z. Wang, U.W.a.E.J. (ed.) *Encyclopedia of Physical Organic Chemistry*.

Tyml, T., Skulinová, K., Kavan, J., Ditrich, O., Kostka, M. and Dyková, I. (2016) 'Heterolobosean amoebae from Arctic and Antarctic extremes: 18 novel strains of Allovahlkampfia, Vahlkampfia and Naegleria', *Eur J Protistol*, 56, pp. 119-133.

Ulsamer, A. G., Wright, P. L., Wetzel, M. G. and Korn, E. D. (1971) 'Plasma and phagosome membranes of Acanthamoeba castellanii', *The Journal of cell biology*, 51(1), pp. 193-215.

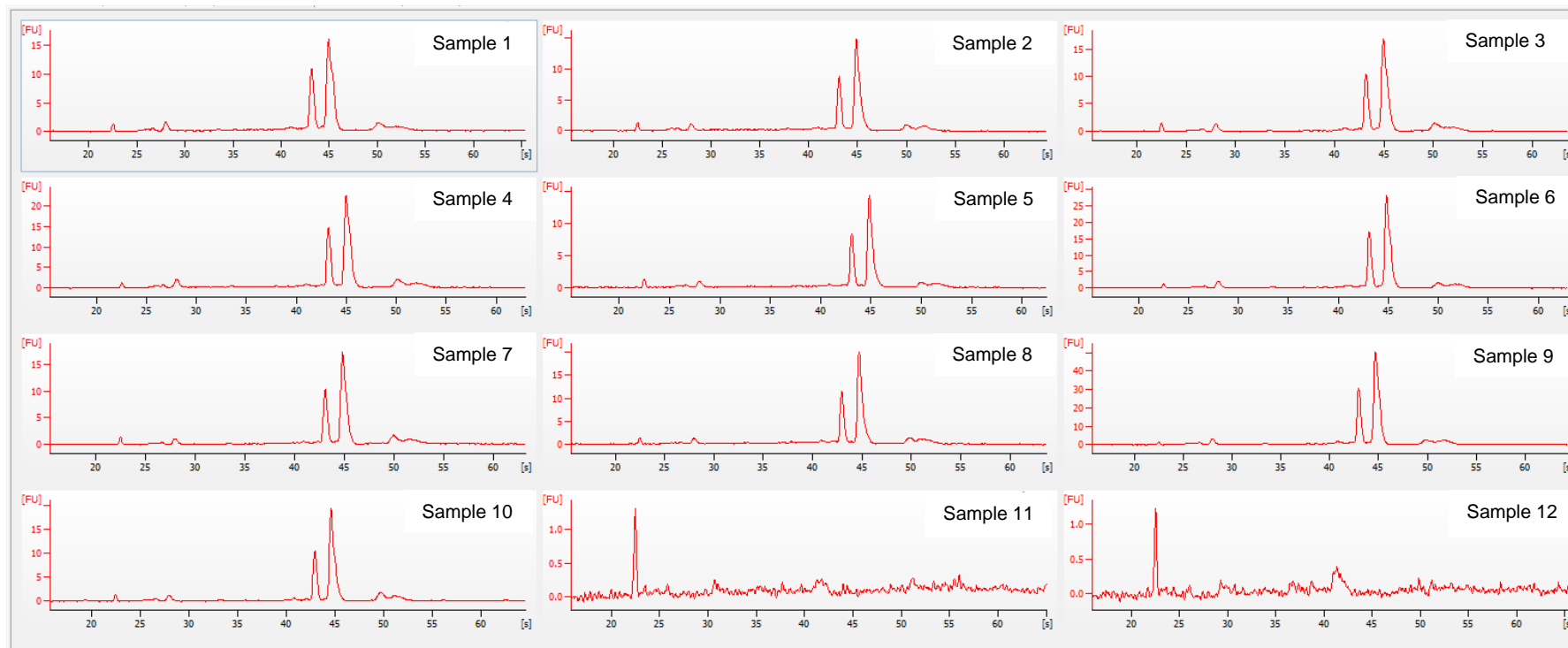
- van Klink, F., Taylor, W. M., Alizadeh, H., Jager, M. J., van Rooijen, N. and Niederkorn, J. Y. (1996) 'The role of macrophages in Acanthamoeba keratitis', *Investigative ophthalmology & visual science*, 37(7), pp. 1271-1281.
- Verma, A., Raizada, M., Shukla, O. and Murti, C. K. (1974) 'Degradation of cysts of Hartmannella culbertsoni by culture filtrates of Alternaria sp', *Microbiology*, 80(1), pp. 307-309.
- Vinayak, S., Pawlowic, M. C., Sateriale, A., Brooks, C. F., Studstill, C. J., Bar-Peled, Y., Cipriano, M. J. and Striepen, B. (2015) 'Genetic modification of the diarrhoeal pathogen Cryptosporidium parvum', *Nature*, 523(7561), pp. 477-480.
- Visvesvara, G. S. (1991) 'Classification of Acanthamoeba', *Rev Infect Dis*, 13 Suppl 5, pp. S369-72.
- Visvesvara, G. S. (2010) 'Amebic meningoencephalitis and keratitis: challenges in diagnosis and treatment', *Curr Opin Infect Dis*, 23(6), pp. 590-4.
- Visvesvara, G. S., Booton, G. C., Kelley, D. J., Fuerst, P., Sriram, R., Finkelstein, A. and Garner, M. M. (2007) 'In vitro culture, serologic and molecular analysis of Acanthamoeba isolated from the liver of a keel-billed toucan (Ramphastos sulfuratus)', *Vet Parasitol*, 143(1), pp. 74-8.
- Visvesvara, G. S., Moura, H. and Schuster, F. L. (2007) 'Pathogenic and opportunistic free-living amoebae: Acanthamoeba spp., Balamuthia mandrillaris, Naegleria fowleri, and Sappinia diploidea', *FEMS Immunol Med Microbiol*, 50(1), pp. 1-26.
- Vyas, S., Jain, V., Goyal, M., Radotra, B. and Khandelwal, N. (2013) 'Granulomatous amoebic meningoencephalitis', *Neurology India*, 61(5), pp. 530.
- Wagner, J. C., Platt, R. J., Goldfless, S. J., Zhang, F. and Niles, J. C. (2014) 'Efficient CRISPR-Cas9-mediated genome editing in Plasmodium falciparum', *Nature Methods*, 11(9), pp. 915-918.
- Walia, R., Montoya, J. G., Visvesvera, G. S., Booton, G. C. and Doyle, R. L. (2007) 'A case of successful treatment of cutaneous Acanthamoeba infection in a lung transplant recipient', *Transpl Infect Dis*, 9(1), pp. 51-4.
- Walochnik, J., Duchêne, M., Seifert, K., Obwaller, A., Hottkowitz, T., Wiedermann, G., Eibl, H. and Aspöck, H. (2002) 'Cytotoxic activities of alkylphosphocholines against clinical isolates of Acanthamoeba spp', *Antimicrob Agents Chemother*, 46(3), pp. 695-701.
- Walochnik, J., Obwaller, A. and Aspöck, H. (2000) 'Correlations between morphological, molecular biological, and physiological characteristics in clinical and nonclinical isolates of Acanthamoeba spp', *Appl Environ Microbiol*, 66(10), pp. 4408-13.
- Walochnik, J., Obwaller, A., Haller-Schober, E. M. and Aspöck, H. (2001) 'Anti-Acanthamoeba IgG, IgM, and IgA immunoreactivities in correlation to strain pathogenicity', *Parasitol Res*, 87(8), pp. 651-6.
- Wand, M. E., McCowen, J. W. I., Nugent, P. G. and Sutton, J. M. (2013) 'Complex interactions of Klebsiella pneumoniae with the host immune system in a Galleria mellonella infection model', *J Med Microbiol*, 62(Pt 12), pp. 1790-1798.
- Wang, J.-L., Huang, S.-Y., Li, T.-T., Chen, K., Ning, H.-R. and Zhu, X.-Q. (2016) 'Evaluation of the basic functions of six calcium-dependent protein kinases in Toxoplasma gondii using CRISPR-Cas9 system', *Parasitology Research*, 115(2), pp. 697-702.

- Wang, Z., Wu, D., Tachibana, H., Feng, M. and Cheng, X. J. (2020) 'Identification and biochemical characterisation of *Acanthamoeba castellanii* cysteine protease 3', *Parasit Vectors*, 13(1), pp. 592.
- Watt, K. G. and Swarbrick, H. A. (2007) 'Trends in microbial keratitis associated with orthokeratology', *Eye & contact lens*, 33(6, Part 2 of 2), pp. 373-377.
- Weber-Lima, M. M., Prado-Costa, B., Becker-Finco, A., Costa, A. O., Billilad, P., Furst, C., de Moura, J. F. and Alvarenga, L. M. (2020) 'spp. monoclonal antibody against a CPA2 transporter: a promising molecular tool for acanthamoebiasis diagnosis and encystment study', *Parasitology*, 147(14), pp. 1678-1688.
- Weir, C. and Le, J. (2021) *Pentamidine*. StatPearls Publishing. Available at: <https://www.ncbi.nlm.nih.gov/books/NBK539728/> (Accessed).
- Weisman, R. A. (1976) 'Differentiation in *Acanthamoeba castellanii*', *Annual Reviews in Microbiology*, 30(1), pp. 189-219.
- Wilhelmus, K. R., Osato, M. S., Font, R. L., Robinson, N. M. and Jones, D. B. (1986) 'Rapid diagnosis of *Acanthamoeba* keratitis using calcofluor white', *Archives of ophthalmology*, 104(9), pp. 1309-1312.
- Winchester, K., Mathers, W. D., Sutphin, J. E. and Daley, T. E. (1995) 'Diagnosis of *Acanthamoeba* keratitis in vivo with confocal microscopy', *Cornea*, 14(1), pp. 10-17.
- Wojda, I. (2017) 'Immunity of the greater wax moth *Galleria mellonella*', *Insect Sci*, 24(3), pp. 342-357.
- Woodruff, T. M., Ager, R. R., Tenner, A. J., Noakes, P. G. and Taylor, S. M. (2010) 'The role of the complement system and the activation fragment C5a in the central nervous system', *Neuromolecular medicine*, 12(2), pp. 179-192.
- Wright, P., Warhurst, D. and Jones, B. R. (1985) '*Acanthamoeba* keratitis successfully treated medically', *Br J Ophthalmol*, 69(10), pp. 778-82.
- Wu, M. and Li, R. (2016) 'A novel role of the Type I CRISPR-Cas system in impairing host immunity by targeting endogenous genes', *The Journal of Immunology*, 196(1 Supplement), pp. 200.14-200.14.
- Wynter-Allison, Z. O. E., Morales, J. L., Calder, D., Radlein, K., Ortega-Rivas, A. and Lindo, J. F. (2005) 'ACANTHAMOEBA INFECTION AS A CAUSE OF SEVERE KERATITIS IN A SOFT CONTACT LENS WEARER IN JAMAICA', *The American Journal of Tropical Medicine and Hygiene Am J Trop Med Hyg*, 73(1), pp. 92-94.
- Yamamoto, M., Sato, S., Mori, K., Hoshino, K., Takeuchi, O., Takeda, K. and Akira, S. (2002) 'Cutting edge: a novel Toll/IL-1 receptor domain-containing adapter that preferentially activates the IFN- β promoter in the Toll-like receptor signaling', *The Journal of Immunology*, 169(12), pp. 6668-6672.
- Yanow, S. K., Purcell, L. A., Pradel, G., Sato, A., Rodriguez, A., Lee, M. and Spithill, T. W. (2008) 'Potent antimalarial and transmission-blocking activities of centanamycin, a novel DNA-binding agent', *The Journal of infectious diseases*, 197(4), pp. 527-534.
- Yin, J. and Henney Jr, H. R. (1997) 'Stable transfection of *Acanthamoeba*', *Canadian Journal of Microbiology*, 43(3), pp. 239-244.

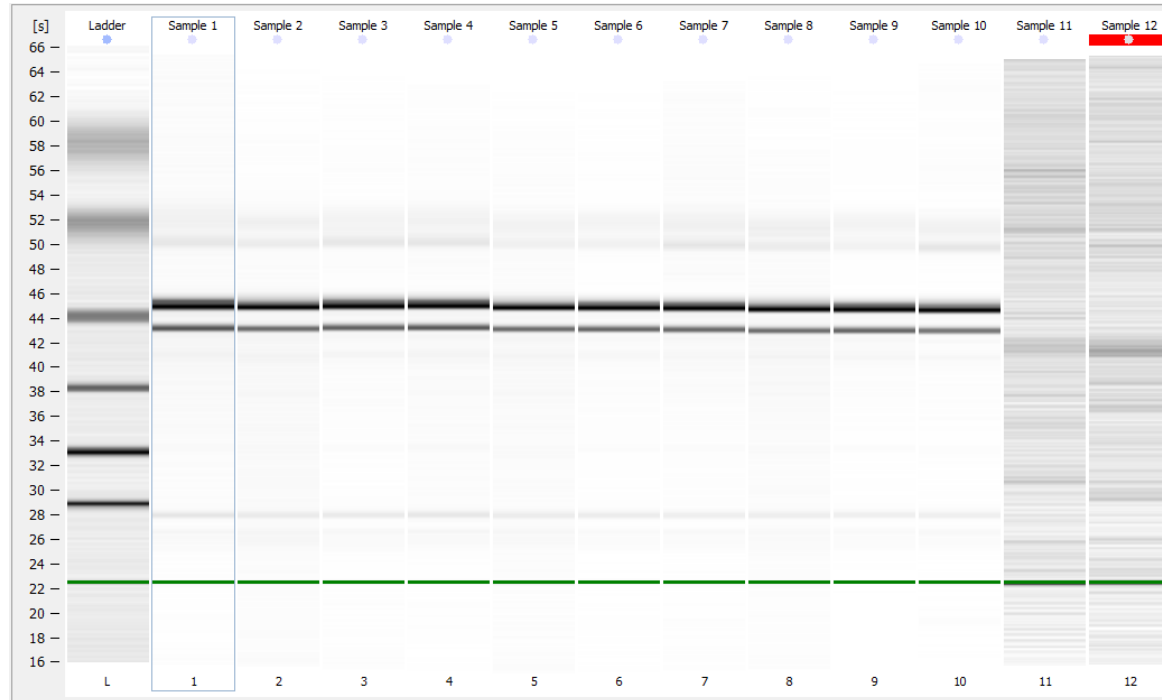
- Yousuf, F. A., Siddiqui, R., Subhani, F. and Khan, N. A. (2013) 'Status of free-living amoebae (*Acanthamoeba* spp., *Naegleria fowleri*, *Balamuthia mandrillaris*) in drinking water supplies in Karachi, Pakistan', *J Water Health*, 11(2), pp. 371-5.
- Zdybicka-Barabas, A., Mak, P., Jakubowicz, T. and Cytryńska, M. (2014) 'Lysozyme and defense peptides as suppressors of phenoloxidase activity in *Galleria mellonella*', *Arch Insect Biochem Physiol*, 87(1), pp. 1-12.
- Zhang, C., Xiao, B., Jiang, Y., Zhao, Y., Li, Z., Gao, H., Ling, Y., Wei, J., Li, S., Lu, M., Su, X.-z., Cui, H., Yuan, J. and Sibley, L. D. (2014) 'Efficient Editing of Malaria Parasite Genome Using the CRISPR/Cas9 System', *mBio*, 5(4), pp. e01414-14.
- Zhang, H. and Cheng, X. (2021) 'Various brain-eating amoebae: the protozoa, the pathogenesis, and the disease', *Frontiers of Medicine*.
- Zhang, J.-P., Li, X.-L., Li, G.-H., Chen, W., Arakaki, C., Botimer, G. D., Baylink, D., Zhang, L., Wen, W., Fu, Y.-W., Xu, J., Chun, N., Yuan, W., Cheng, T. and Zhang, X.-B. (2017) 'Efficient precise knockin with a double cut HDR donor after CRISPR/Cas9-mediated double-stranded DNA cleavage', *Genome Biology*, 18(1), pp. 35.
- Zhang, W.-W., Matlashewski, G. and Sibley, L. D. (2015) 'CRISPR-Cas9-Mediated Genome Editing in *Leishmania donovani*', *mBio*, 6(4), pp. e00861-15.
- Zheng, J., Jia, H. and Zheng, Y. (2015) 'Knockout of leucine aminopeptidase in *Toxoplasma gondii* using CRISPR/Cas9', *International Journal for Parasitology*, 45(2), pp. 141-148.
- Zimmer, M. (2002) 'Green fluorescent protein (GFP): applications, structure, and related photophysical behavior', *Chem Rev*, 102(3), pp. 759-81.

Appendix

A.



B.



Appendix 1. Electropherograms of wild-type and S-MGB 235 treated *Acanthamoeba* spp. trophozoites RNA extracted.

Samples 1,4,7: wild-type *A. castellanii* Neff strain; Samples 2,5,8: wild-type *A. polyphaga*; Samples 3,6,9: *A. castellanii* Neff trophozoites treated with 0.20 μ M S-MGB 235 for 24 hours. Sample 10: Second aliquot of Sample 1; Sample 11 & 12: RNase-free water. Fluorescence units (FU) are positively correlated with the RNA concentration. The first peak indicates the marker, second peak at ~28 seconds indicates 5S rRNA, third peak at ~43 seconds indicates 18S rRNA, fourth peak at ~45 seconds indicates 28S rRNA. RIN as follows: Sample 1= 7.1; Sample 2= 6.3; Sample 3= 7.3; Sample 4= 6.8; Sample 5= 6.3, Sample 6= 7.1; Sample 7= 7.2; Sample 8= 6.2; Sample 9= 7.1. RNA extractions were performed in triplicate using RNeasy Plus Mini Kit (Qiagen). Raw data was generated using Agilent 2100 Bioanalyzer and analysed with Agilent 2100 Expert software. Abbreviations: FU: fluorescence units; S: seconds; RIN: RNA Integrity number.